THE EFFECTS OF HIGH-FREQUENCY CYCLICITY ON RESERVOIR CHARACTERISTICS OF THE "MISSISSIPPIAN LIMESTONE", ANADARKO BASIN, KINGFISHER COUNTY, OKLAHOMA

By

KELLER CHARLES FLINTON

Bachelor of Science in Geology

Oklahoma State University

Stillwater, OK

2012

Submitted to the Faculty of the
Graduate College of the
Oklahoma State University
in partial fulfillment of
the requirements for
the Degree of
MASTER OF SCIENCE
May, 2016

THE EFFECTS OF HIGH-FREQUENCY CYCLICITY

ON RESERVOIR CHARACTERISTICS

OF THE “MISSISSIPPIAN LIMESTONE”,

ANADARKO BASIN, KINGFISHER COUNTY, OKLAHOMA

Thesis Advisor:

Dr. G. Michael Grammer

Committee Members:

Dr. James Puckette

Dr. Jay M. Gregg

Mr. Doug Pethoud

ACKNOWLEDGEMENTS

I would first like to thank Dr. Michael Grammer for sharing his knowledge and expertise with me throughout my research. His approach has helped me learn far more than I thought possible during my graduate studies and I would not be the geologist I am today without having the opportunity to work with him. I would also like to thank Dr. Jim Puckette for the lasting impact he has had on my career. From my first experiences at OSU as an undergraduate student to the final stages of my graduate research, Dr. Puckette's unrelenting enthusiasm for teaching has made an indelible mark on my career, and I am forever thankful.

I would like to thank Maverick Brothers Resources, specifically Mr. Doug Pethoud, for allowing me the opportunity to gain invaluable industry experience in conjunction with my research. Their selflessness, support, and work ethic set an example that I will follow throughout my career. I would also like to thank my new colleagues at American Energy Partners for their encouragement and understanding during the final stages of my research.

The support and encouragement I received from Dr. Grammer's group in Stillwater was tremendous. Buddy Price, Miranda Childress, Stephanie LeBlanc, Taylor Thompson, Lara Jaeckel, Ahmed Elbelasy, Yulun Wang, Ashley Dupont and Scott Shelley were all beyond willing to help me in my research and made my time in Stillwater a pleasure. I would also like to thank Dr. Mohammed Abdel Salam for his assistance throughout graduate school.

Lastly, I would like to thank my family for their love and support throughout my education. During the long nights and early mornings, commuting to Stillwater and Enid, and times I thought I couldn't make it while working full time, the constant love and encouragement from my wife, Emma Flinton, gave me the motivation to make it through and to her I owe my deepest gratitude. I would also like to thank my parents, Peggy and Terry Flinton, for always believing in me and supporting my career. This work was done in hopes to make my family proud.

Name: Keller Charles Flinton

Date of Degree: May, 2016

Title of Study: THE EFFECTS OF HIGH-FREQUENCY CYCLICITY ON RESERVOIR CHARACTERISTICS OF THE "MISSISSIPPIAN LIMESTONE", ANADARKO BASIN, KINGFISHER COUNTY, OKLAHOMA

Major Field: GEOLOGY

Abstract:

Mississippian-aged limestones along the northern edge of the Anadarko basin in north-central Oklahoma and southern Kansas store considerable amounts of hydrocarbons and have been exploited through vertical drilling for more than 50 years. A shift to horizontal exploitation in this unconventional resource play has not yielded consistent well performance due to a lack of understanding of the controlling factors responsible for production-scale reservoir distribution.

The "Mississippian limestone" is characterized by a hierarchical stratigraphy of sequences (100s of meters thick), high-frequency sequences (10s of meters thick) and high-frequency cycles (few meters thick) caused by fluctuations in eustatic and relative sea level due in part to Milankovitch-band cyclicity. Detailed facies analysis using cored intervals of the "Mississippian limestone" suggests deposition occurred along a distally-steepened mixed carbonate-siliciclastic ramp. The vertical stacking patterns of depositional facies defines high-frequency sequences and cycles (probable 4th and 5th-Order) within a shoaling-upward succession. From base to top within an ideal sequence, the shoaling-upward succession of facies consists of argillaceous and calcareous and slightly burrowed mudstones and wackestones followed by progressively higher-energy environments of deposition indicated by traction-laminated and more heavily bioturbated wackestones, packstones and grainstones. Incomplete development of this ideal vertical succession marked by a landward shift in facies belts established stacking patterns of hierarchical sea level cyclicity. High-frequency, Milankovitch-band sea level cyclicity ultimately controls the fundamental flow units of production-scale hydrocarbon reservoirs.

Reservoir development is a function of the primary depositional facies and the sequence stratigraphic hierarchy. The primary reservoir is controlled by exposure associated with 3rd-Order regression and is vertically compartmentalized by 4th & 5th-Order high-frequency flooding surfaces. The abundance of detrital sedimentation is thought to improve the quality of secondary reservoir development. Guard resistivity curves are most useful at extrapolating the cyclostratigraphy throughout the subsurface. The core-defined, high-frequency sequence stratigraphy improves production-scale predictability of hydrocarbon reservoirs of the "Mississippian limestone".

TABLE OF CONTENTS

LIST OF TABLES

LIST OF FIGURES

Figure Page

CHAPTER I

INTRODUCTION

Summary of the Problem

The Mississippian Subsystem of northwest and north-central Oklahoma and southern Kansas is an "unconventional resource play" that historically was targeted for vertical drilling (Figure 1). Unconventional resource plays are regionally pervasive accumulations of hydrocarbons that, unlike conventional resource plays, generally are not buoyancy-driven and are independent of structural and stratigraphic traps. These low-permeability (average <0.1 mD) reservoirs often require horizontal drilling and completion techniques to be economically viable targets (Law and Curtis, 2002; Roundtree et al., 2010; Grieser and Pinkerton, 2013). The economics of this developing resource play depend on the ability to predict and accurately target hydrocarbon-bearing reservoirs.

Reservoirs in carbonate rocks are commonly multiple-porosity systems that impart petrophysical heterogeneity to the reservoirs (Mazzullo, 2004). Lucia (1995) and Martin et al. (1997) demonstrated that petrophysical flow units are independent of total volume porosity. The distribution of specific types of pores exert strong control on the stimulation and subsequent production characteristics of carbonate reservoirs (Mazzullo, 2004). Also, much of the production from these rocks must be associated with permeability pathways along natural fractures and joints, thus locating areas that contain a high fracture density is of prime exploration concern (Harris, 1987; Mazzullo et al., 2011a). Whether the ultimate economic goal is to predict the distribution of porous and permeable reservoirs and impermeable seals or fractured reservoirs and ductile seals, the ability to accurately characterize hydrocarbon-bearing reservoirs is dependent upon the construction of an accurate sequence stratigraphic framework (Kerans and Tinker, 1997).

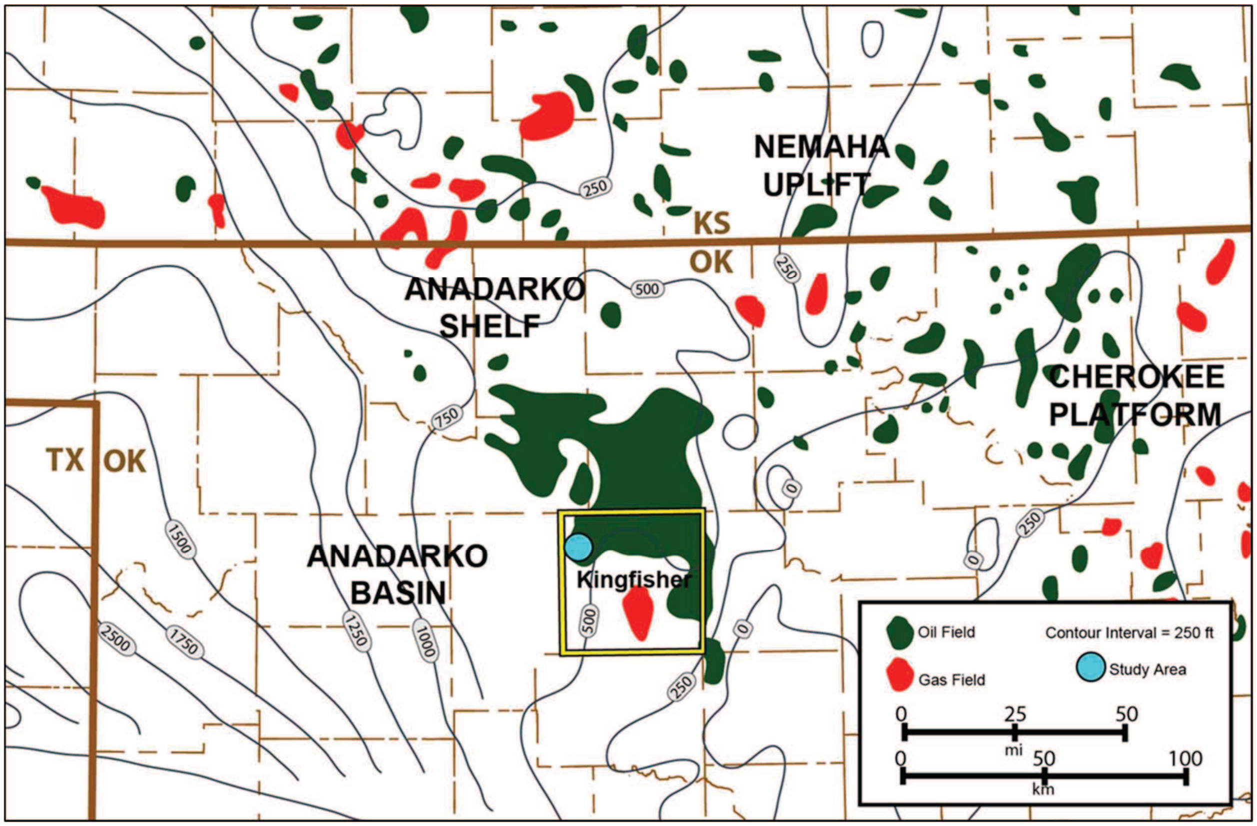

Figure 1. Historical play map showing the distribution of vertically targeted "Mississippian limestone" oil (green) and gas (red) fields in north-central Oklahoma and southern Kansas. Thickness of the "Mississippian limestone" is shown in gray contours with a contour interval of 250 feet. Kingfisher County outlined in yellow and study area noted by light blue circle located in northwest Kingfisher County. Note this location in the southwest corner of the Sooner Trend which is historically the largest contiguous "Mississippian limestone" oil field (large green outline) approximately 20 miles (32 km) wide and 60 miles (96 km) long) while having an approximate thickness of 500 ft. (152 m). Modified from Harris, 1987.

The Mississippian Subsystem limestone has been termed by industry as "Miss Lime", "Mississippian Chat", "Mississippian limestone", and variations thereof, but will be referred to as the "Mississippian limestone" for the remainder of this study. Research of the "Mississippian limestone" reservoirs has been conducted from the outcrop belt in northeast Oklahoma, northwest Arkansas, southwest Missouri and southeast Kansas (Figure 2; Shoeia, 2012; Price, 2014; Childress, 2015; Childress and Grammer, 2015); as well as subsurface studies from cores and cuttings in north-central and northeastern Oklahoma and southern Kansas (Beebe, 1959; Jordan and Rowland, 1959; Rowland, 1961; Mikkelson, 1966; Withrow, 1972; Harris, 1987; Montgomery et al., 1998; Rogers, 2001; Watney et al., 2001; Mazzullo et al., 2009a, 2009b; Yenugu et al., 2010; Evans et al., 2011; Mazzullo et al., 2011a, 2011b; Zhao, 2011; Friesenhahn, 2012; Shoeia, 2012; Boardman et al., 2013; LeBlanc, 2014).

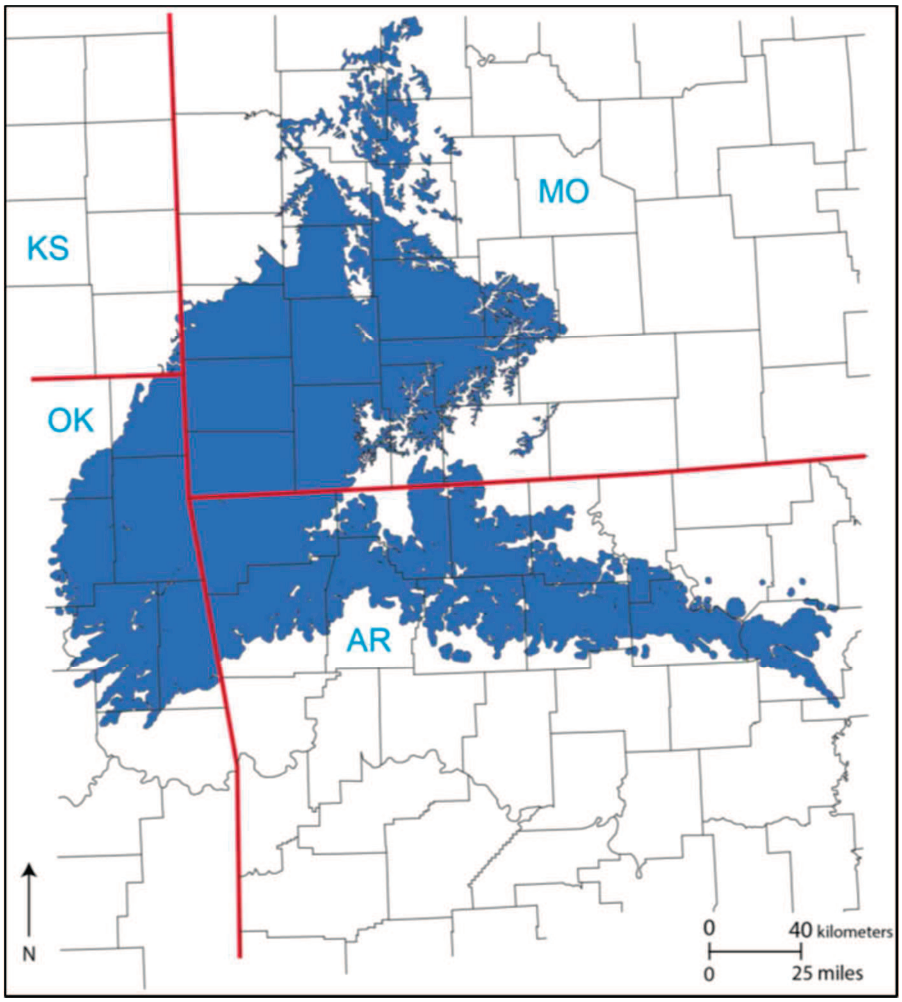

Figure 2. Mississippian Outcrop Belt. Aerial extent of outcrops shown in blue. Note the location of the outcrop belt in northeast Oklahoma, northwest Arkansas, southeast Missouri and southeast Kansas. Deposits become younger to the south and west and are absent to the east and northeast due to erosion. Modified from Mazzullo et al., 2011a.

In the vicinity of the study area, Withrow (1972) describes the oil and gas development and Rowland (1961) defines the lithostratigraphic relationships of likely Mississippian-aged rocks. However, the sequence-stratigraphic hierarchy has not been accurately defined, and production results show signs of localized heterogeneity that are not accounted for with lithostratigraphic subsurface mapping techniques. Modifying these techniques through petrophysical core research tied to subsurface wireline logs will result in an accurate sequence-stratigraphic hierarchy that can then be used to predict lateral and vertical heterogeneities controlling the reservoir distribution within the “Mississippian limestone”.

Fundamental Questions and Hypothesis

To determine the effects of high-frequency eustatic sea level changes and their impact on reservoir development in the “Mississippian limestone” this investigation will focus on a group of three “Mississippian limestone” cores (Table 1) from within the current play area (Figure 1). Wells were chosen because each has (1) a continuous or near-continuous cored interval of the “Mississippian limestone”, 2) conventional wireline log suites, 3) close proximity (< 3 miles (5 km)) to one another to accurately correlate units, yet (4) dissimilarities in both a strike and dip direction and dissimilar well performance.

Historical Operator	Lease Name	Legal Location	County	"Mississippian limestone" Thickness
Pan American	Effie B York #1	13-18N-09W	Kingfisher	525 ft. (160 m)
Pan American	Moore Unit #D1	12-18N-09W	Kingfisher	518 ft. (158 m)
Pan American	Droke Unit #1	04-18N-09W	Kingfisher	504 ft. (154 m)

Table 1. List of cored “Mississippian limestone” wells selected for research. Well information obtained from well log headers and the Oklahoma Petroleum Information Center database. All wells are located in T18N-R9W of Kingfisher County, Oklahoma. Average thickness of the cored “Mississippian limestone” interval is 516 ft. (157 m).

The hypothesis of this study is that the "Mississippian limestone" reservoirs of northwest Kingfisher County, Oklahoma are controlled by the effects of overarching high-frequency, 4th- and 5th-Order (20-400 thousand year) eustatic sea-level cyclicity. This set of cores (Table 1) will provide sedimentological indications of relative sea level change. A hierarchy of sea level cyclicity, observed through the stacking patterns of these sedimentological changes, will reveal the controlling mechanism for reservoir development. Production-scale distribution of these reservoirs can then be precisely mapped when tied to discrete subsurface wireline log signatures and will result in a more accurate reservoir characterization of the "Mississippian limestone" with respect to the defined sequence stratigraphic architecture.

Objectives

The goal of this research is to define the production- and enhanced production-scale reservoir architecture in the "Mississippian limestone" in northwest Kingfisher County, Oklahoma. The primary objectives of this investigation are to:

(1) determine the local depositional topography of the "Mississippian limestone" in northwest Kingfisher County, Oklahoma - the antecedent bathymetry being the basis for subsequent cyclostratigraphic distribution;

(2) define the sequence-stratigraphic hierarchy of the "Mississippian limestone";

(3) identify ideal hydrocarbon-bearing units on the basis of defined lithofacies within a defined stratigraphic hierarchy;

(4) tie these units to the available suite of subsurface wireline log signatures to accurately map the trend of potential hydrocarbon-bearing reservoirs;

(5) compare and contrast the results to modern and ancient analogs to make more reasonable geometrical assumptions of facies variability within the study area.

Production-scale reservoir distribution and variability cannot be accurately predicted without a sequence stratigraphic framework that captures the chronostratigraphic relationships of rock units in the subsurface (Rowland 1961; Kerans et al., 1994). The wireline log expressions of the bounding surfaces of the sequence stratigraphic hierarchy can be used to map the lateral and vertical heterogeneity and ultimately identify production-scale reservoir or flow units. This approach can then be applied to other areas of the "Mississippian limestone" play to improve economic success.

GEOLOGIC BACKGROUND

The Anadarko Basin is a deep to moderately deep, asymmetrical foreland basin covering approximately 58,000 square miles (150,000 square kilometers) in western Oklahoma, the northern portion of the Texas Panhandle, southwestern Kansas and southeastern Colorado (Beebe, 1959; Lane and De Keyser, 1980; Gutschick and Sandberg, 1983; Ball et al., 1991). Along its structurally deepest southern margin it contains more than 40,000 ft. (12 km) of Cambrian through Permian sediments (Ham et al., 1965). The northwesterly trending basin is bound by the Amarillo-Wichita Uplift to the south-southwest, the Arbuckle Uplift to the south, the Nemaha Uplift to the east, and the basin gradually shallows northward onto the Central Kansas Uplift and northwestward into the Hugoton Embayment and Las Animas Arch (Figure 3; Ball et al., 1991; Perry, 1990; Lane and De Keyser, 1980). The northwest trending structural events of the southern North American craton that were established during the middle Proterozoic affected the entire subsequent tectonic history of Oklahoma (Ham et al., 1965; Perry, 1990; Gallardo and Blackwell, 1999).

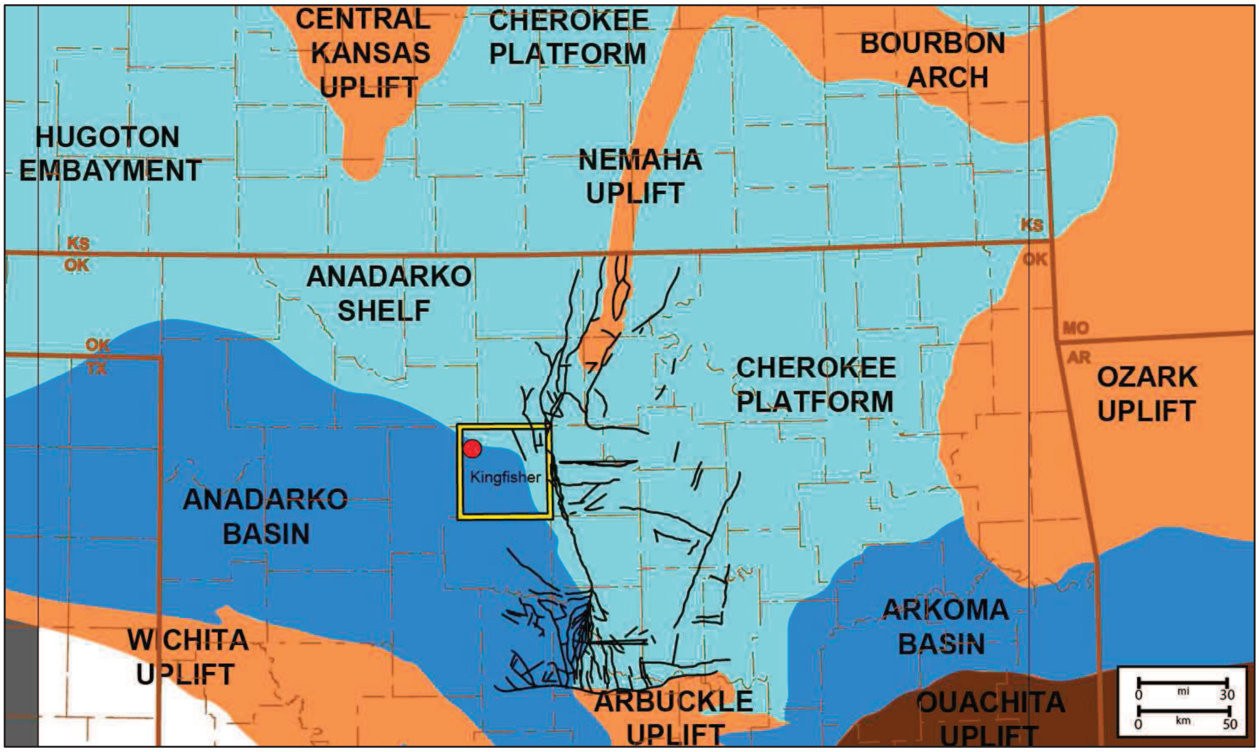

Figure 3. Geologic provinces of the Mid-Continent and faults associated with the Nemaha Uplift. Shelves/shallow basins/platforms denoted by light blue. Deep basins denoted by dark blue. Basement-rooted uplifts denoted by light brown. Detachment uplifts denoted by dark brown. Nemaha faults denoted by black lines. Study area denoted by red circle in the northwest corner of Kingfisher County (yellow outline). Note the location of the study area at the present day transition between the shallow Anadarko Shelf and deeper Anadarko Basin. Also note the proximity to the Nemaha Uplift and associated faults approximately 30 miles east of the study. Geologic Provinces modified from Northcutt and Campbell, 1995 (Oklahoma), and Ramondetta, 1990 (Kansas). Nemaha faults from Gay, 2003.

Tectonic History

The formation of the southern Oklahoma aulacogen during the Early to Middle Cambrian contributed to the inundation of the continent. This rifting in southern Oklahoma is possibly coincident with the deepest part of the Anadarko Basin (Perry, 1990). At the close of the rifting phase, the aulacogen began to cool and subside to form the southern Oklahoma geosyncline (Perry, 1990; Ham et al., 1965). From the Cambrian through the Early Mississippian, the subsidence rate decreased and a passive continental margin existed outward from the trough (Perry, 1990). The Anadarko Basin was a fairly stable region through the end of the Ordovician, while the Acadian orogeny during the Silurian and Devonian caused broad warping of the Anadarko area (Hill, 1984).

Throughout Mississippian time the Iapetus Ocean and the Rheic Ocean to the south were closing, and by the Late Mississippian the initial phase of the Ouachita orogeny resulted in the positive feature of the Wichita Uplift and structural inversion of the Anadarko Basin on its northern flank (Gallardo and Blackwell, 1999; Ball et al., 1991; Perry, 1990; Evans, 1979; Wheeler, 1955). From the Early to Late Pennsylvanian, continued uplift of the Wichitas caused rapid isostatic subsidence resulting in the accumulation of more than 40,000 ft. (12 km) of Post-Mississippian sediments to be deposited in the Anadarko Basin (Ham et al., 1965; Hill, 1984; Perry, 1990; Gallardo and Blackwell, 1999). The basin has essentially been dormant since the Early Permian, yet minor tilting occurred during the middle and late Permian as well as the late Mesozoic and possibly Holocene (Beebe, 1959; Perry, 1990; Gay, 2003).

The Nemaha Uplift is a north-south trending structural high that extends from northern Kansas south into north-central Oklahoma (Figure 3). The timing of the structural events associated with the Nemaha Uplift is still disputed. Gay (2003) concluded that while periods of lesser movement occurred during the mid-Ordovician and mid-Devonian, the onset of the main uplift occurred during the Late Mississippian to Early Pennsylvanian, contemporaneous with the Appalachian Mountains in the east and possibly the Ancestral Rocky Mountains in the west. Thrusting resulted in high-angle reverse faulting in north-central Oklahoma (Figure 4; Gay, 2003). More recently, the timing of the Ouachita orogeny is believed to have begun in Early Mississippian time due to syndepositional tectonism observed in outcrop research from the outcrop region and subsurface studies from southern Kansas (Mazzullo et al., 2011c; Wilhite et al., 2011).

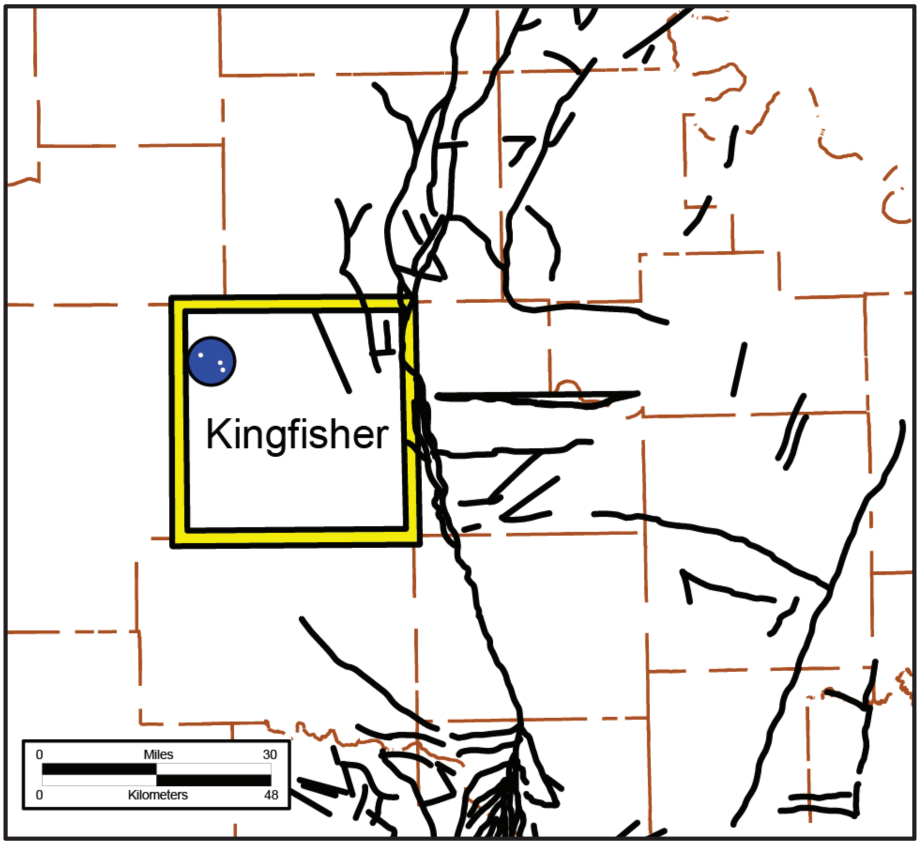

Figure 4. Faults associated with the Nemaha Uplift as described by Gay, 2003. Faults denoted by black lines. Kingfisher County outlined in yellow with the study area denoted by blue circle and location of cores denoted by white dots. Note the location of cores approximately 30 mi (48 km) west of the primary fault system and 15-20 miles (24-32 km) west of a fault located in the northeast corner of Kingfisher County. Modified from Gay (2003).

The study area is located in what is perceived to be a transitional geological province between the shallow Anadarko shelf and deeper Anadarko Basin (Figure 3). The Nemaha Uplift and associated faults are located approximately 30 miles east of the study area (Figure 4; Gay, 2003). While it is unclear whether this local tectonism resulted in a positive feature or bathymetric high during the Early Mississippian System, it should be noted that the timing and nature of tectonism can have a substantial effect on carbonate depositional lithofacies and stacking patterns (Drummond and Wilkinson, 1993).

Paleogeography and Climate

Carbonate production is inherently dependent on climate. Autochthonous production of carbonate sediment distinctly differentiates the carbonate sequence-stratigraphic model from the siliciclastic model (Kerans and Tinker, 1997). While cool-water carbonates are evident in the rock record (James and Clarke, 1997), carbonate production and preservation is closely tied to tropical environments (Tucker and Wright, 1997). Within low-latitude environments a number of geometrical settings might occur that range from platforms to broad shelves. Architectural distribution of facies can be markedly different as these settings and climates evolve through time. The climate and depositional topography of the study area during the Mississippian Subsystem has pronounced effects on the sequence stratigraphy when subjected to hierarchical fluctuations in relative sea level.

During the Mississippian Subsystem (365 to 310 mya) of the Kaskaskia sequence, a 2nd-Order sequence from Sloss (1963), the southern part of the North American craton was covered by a broad carbonate platform and carbonate foreslopes that gradually descended into elongate foreland troughs, including the Anadarko Basin (Gutschick and Sandberg, 1983). At the end of Woodford Shale deposition (latest Devonian, earliest Kinderhookian) the sea withdrew and then transgressed again, establishing a shallow, well-oxygenated environment during the Early Mississippian (Figure 5; Frezon and Jordan, 1979).

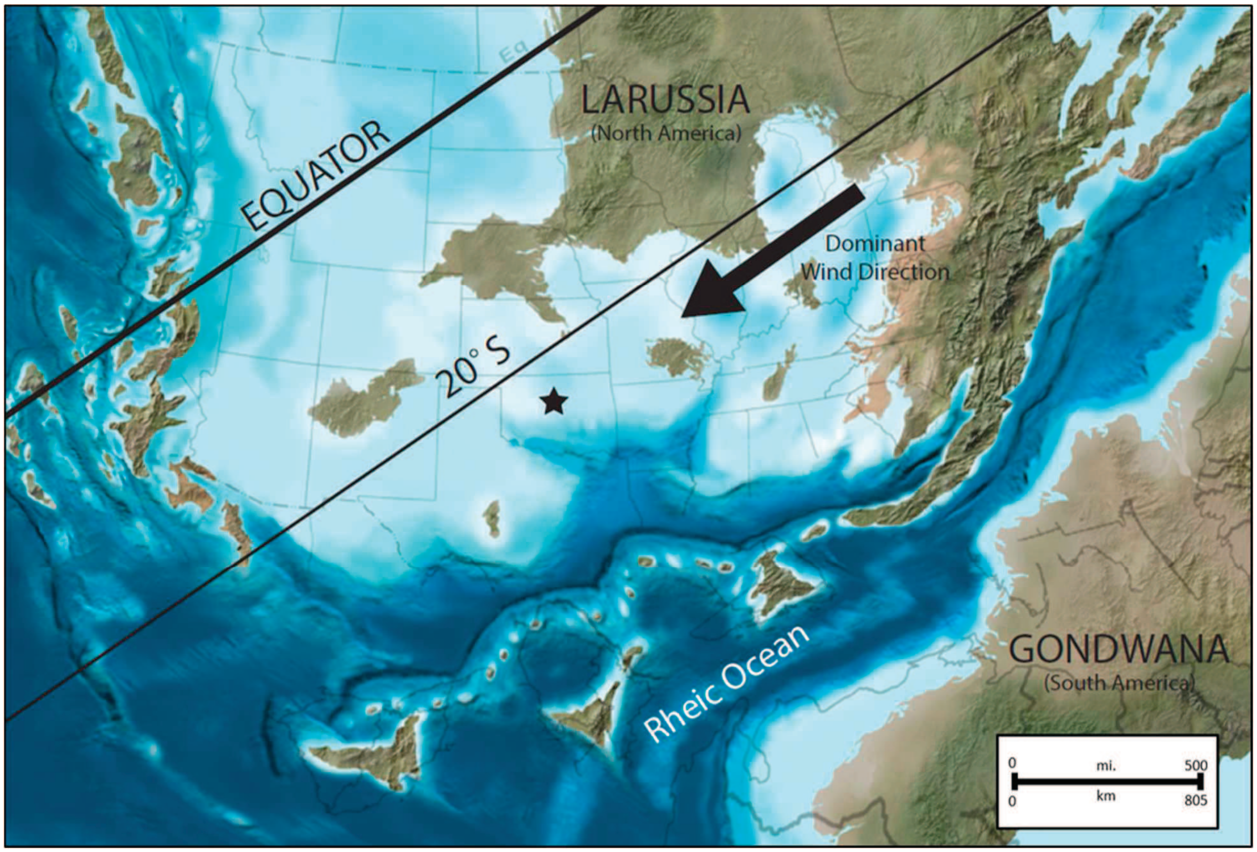

Figure 5. Early Mississippian (345 Ma) paleogeographic time-slice. The study area (indicated by the black star) is located between 20-30°S of the paleoequator with prevailing winds coming from the present day northeast. Water depth is indicated by color contrast with dark blue indicating deep water and light blue indicating relatively shallow water depths. Land masses are indicated by brown and green colors. Note the location of the study area in relatively shallow water depths on the North American craton and leeward of the Ozark Uplift to the present day northeast. Modified from Blakey, 2014.

Paleogeographic studies place the study area between 20°-30° S latitude (Figure 5), within the tropical to subtropical latitudinal belt. Humid, warm-temperate to subtropical conditions existed throughout Mississippian time with rare, minor arid conditions locally (Curtis and Champlin, 1959; Franseen, 2006; Buggisch et al., 2008). The Carboniferous through the Permian was a time of globally low carbon dioxide concentrations and the Mississippian

Subsystem was a transitional period between greenhouse conditions of the Devonian and icehouse conditions of the Pennsylvanian Subsystem (Figure 6; Read and Horbury, 1993; Read, 1995). Glaciation events occurred in the Visean (Middle Mississippian) and Serpukhovian (Late Mississippian) with a very warm interval between (Pfefferkorn et al., 2014; Buggisch et al., 2008). Ocean surface temperatures were also transitional throughout Mississippian time (Haq and Schutter, 2008). Through analysis of carbon isotopes of whole rock and oxygen isotopes of conodont apatite it was determined that ocean surface temperatures fell from initially 30°C (˜85°F) during the Early Mississippian to approximately 15°C (˜60°F) by the Late Mississippian (Buggisch et al., 2008).

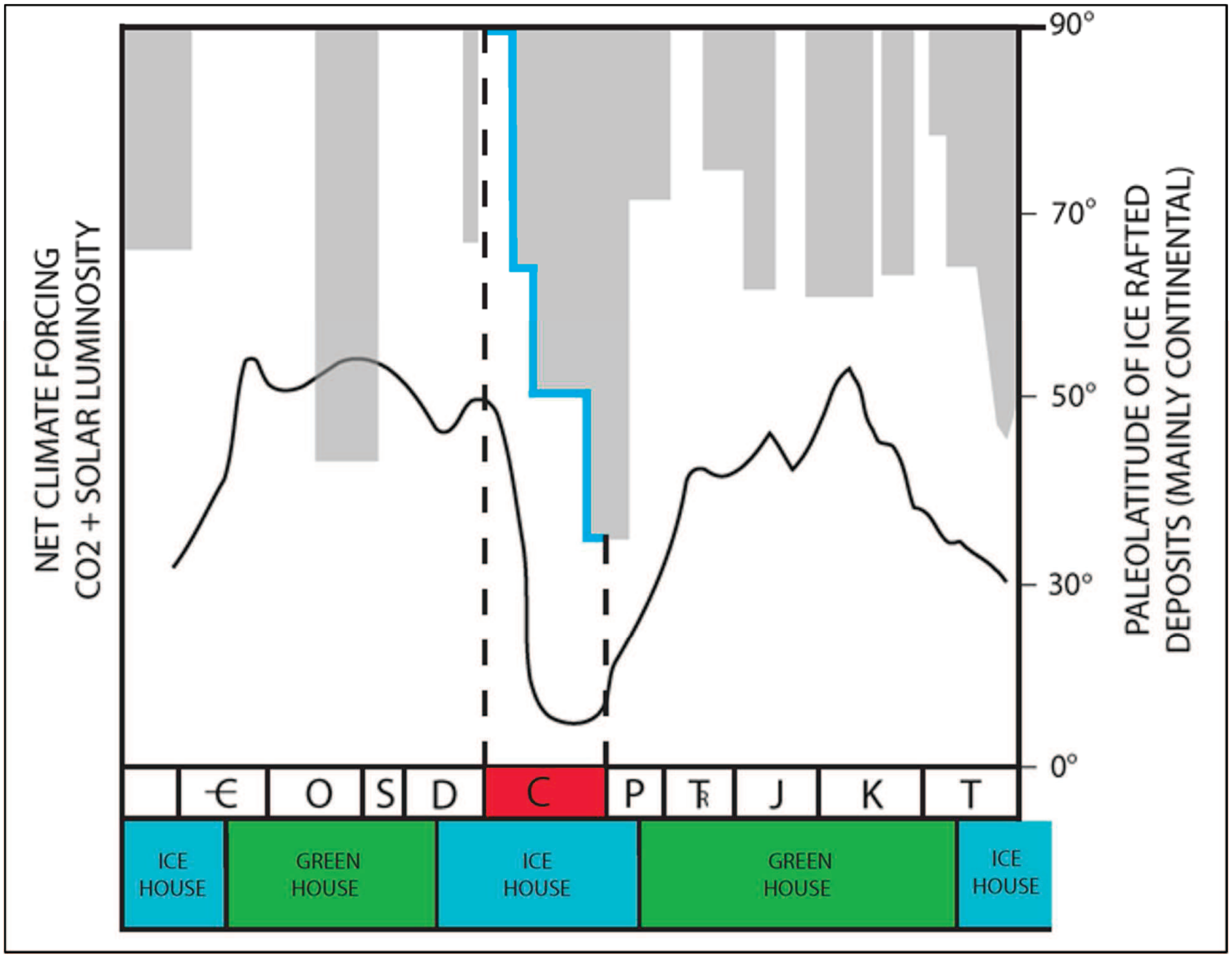

Figure 6. Diagram illustrating icehouse and greenhouse climate conditions that existed throughout the Phanerozoic. Paleo-latitude of ice-rafted deposits (gray boxes) combined with climate change due to variations in carbon dioxide and solar intensity (black curve) illustrates the transitional nature of the Mississippian Subsystem. Carboniferous highlighted in red. Note the change in ice-rafted deposits occurring during the Carboniferous (blue trace) from no ice-rafted deposits to ice-rafted deposits at approximately 35° paleo-latitude at the Carboniferous-Permian boundary. Modified from Read, 1995.

Upwelling from the south-southeast was an important factor along the margins of much of the carbonate shelf for the nourishment of benthic faunas, especially echinoderms and bryozoans and for the development of build-ups, bioherms, banks and Waulsortian-type mounds (Gutschick and Sandberg, 1983; Mazzullo et al., 2009a). Surface sea currents are interpreted to be controlled by southeast paleo-trade winds to conform to the counterclockwise Coriolis effect of the southern hemisphere (Figure 7; Gutschick and Sandberg, 1983).

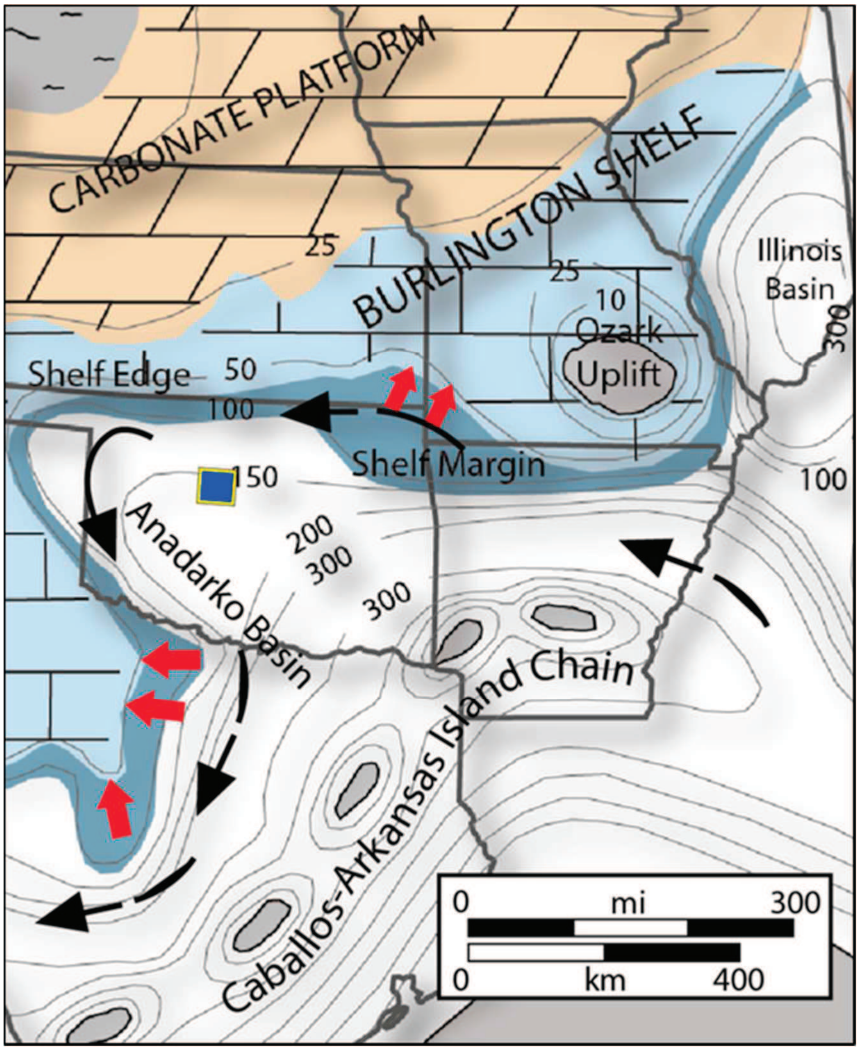

Figure 7. Regional paleogeographic time-slice map during deposition of the *anchoralis-latus* conodont Zone, Latest Tournaisian, Middle Osagean. Estimated water depth indicated by gray contours with a contour interval of 50 m (164 ft.). Inferred surface sea current direction denoted by black arrows. Inferred areas of upwelling denoted by red arrows. Approximate location of study area denoted by yellow outline and blue infill of Kingfisher County, OK. Note the location of the study area in an estimated water depth of approximately 150 m (492 ft.) at this time. Also note that this diagram is modeled as a carbonate shelf/platform whereas this study (and other recent research) models the Mississippian as a ramp setting. Modified from Gutschick and Sandberg, 1983.

During Mississippian time the dominant wind direction in study area was primarily out of the present day northeast. Approximately 450 mi (725 km) east-northeast of the study area, the Ozark Uplift was an emergent feature during the Mississippian (Figures 5 & 7). This relatively large (approximately 5,000-7,000 mi^2 [13,000-18,000 km^2]) landmass in the southeast corner of present day Missouri might have potentially provided large volumes of subangular to subrounded quartz silt and very fine sand with lesser amounts of feldspars, possibly of Pre-Cambrian, Cambrian, and Early Ordovician origin (Koenig, 1967), westward into the shallow carbonate ramp environment of present day northern Oklahoma and southern Kansas.

Depending on the degree of deformation and timing of the Nemaha Uplift, deposition approximately 30 mi (48 km) west of this feature would also be characteristic of a downwind position in the event of exposure during Mississippian time. While this potential feature is considerably smaller in size (approximately 500-1,000 mi^2 [1,300-2,600 km^2]) compared to the Ozark Uplift, its close proximity to the study area provides the possibility of affecting local deposition by providing quartz silt and minor quantities of detrital feldspar grains like that previously described for the Ozark Uplift. Although the definitive occurrence of such an emergent feature is not yet proven, the Nemaha Uplift likely contributed to bathymetric relief during deposition of the "Mississippian limestone". Such relief may either restrict the study area from the inferred southeast surface sea currents and/or provide additional siliciclastic sediment for transport westward.

The study area during the Mississippian was characterized by a well-oxygenated, humid and tropical to subtropical climate during a time of a transitional global climate from greenhouse to icehouse. While characterized as being located downwind of the emergent Ozark Uplift, and potentially downwind of an emergent feature associated with the Nemaha Uplift, the antecedent topography of the study area is still unknown. Detailed facies analysis within the sequence-stratigraphic architecture will aid in determining the local paleoceanography of the "Mississippian limestone" and attempts to attribute the likely mechanisms responsible for reservoir distribution through the establishment of a depositional model and the identification of hierarchical sea level cyclicity.

REGIONAL STRATIGRAPHY

The "Mississippian limestone" and its lateral equivalents are widely distributed across Oklahoma, southern Kansas, northwest Arkansas and southwest Missouri. Laterally equivalent outcrops are found in northeast Oklahoma, southeast Kansas, southwest Missouri and northwest Arkansas (Figure 6; Mazzullo et al., 2011a). It is in these outcrop areas where the majority of research has been conducted and the nomenclature defined and tied to subsurface studies in northeast Oklahoma and southern Kansas. However, previous attempts to tie the stratigraphic nomenclature to subsurface data west of the Nemaha Ridge are limited and have been unsatisfactory (Hoffman, Jr., 1964; Rowland, 1961). This is due to a general lack of well control at the time this research was conducted combined with lithostratigraphic correlations that do not accurately capture the chronostratigraphic relationships.

Recent outcrop research by Mazzullo et al. (2013) developed accurate terminology and correlations, particularly between differences in local and state nomenclature (Figure 8) and, while changes to historical nomenclature have not as yet been formally accepted by the Stratigraphic Commission of North America or the USGS, the new terminology will be referred to throughout this study. Biostratigraphic research by Thompson and Fellows (1970) and recently by Boardman et al. (2013) determined the various conodont zonations within the

Mississippian strata in the outcrop belt (Figure 7). Details and implications of this will not be summarized in this paper due to the absence of biostratigraphic data for this study coupled with the study area being located approximately 250 mi (400 km) west of the outcrop belt. It is, however, important to note that in light of the biostratigraphic research, the Mississippian Subsystem is interpreted to be time-transgressive. The occurrence of a specific or unique lithology, often used as a lithostratigraphic marker, does not indicate a specific moment in geologic time, but rather a unique environment of deposition. By understanding this relationship, a high-frequency sequence stratigraphic approach can accurately define the likely chronostratigraphic correlations that inevitably control the fundamental flow units within hydrocarbon reservoirs.

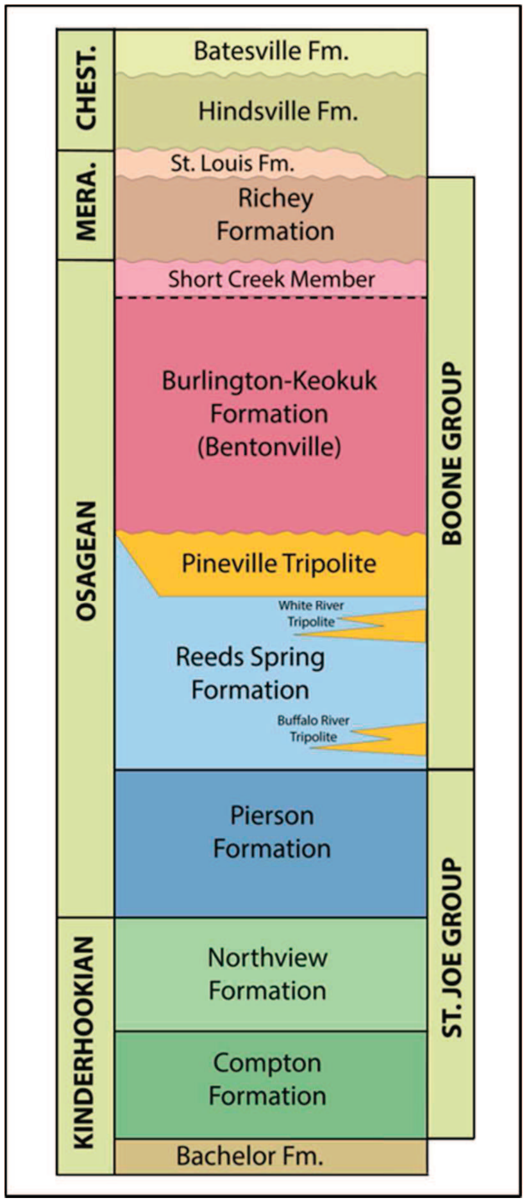

Figure 8. Stratigraphic column of the Mississippian Subsystem. From Mazzullo et al., 2013.

Kinderhookian Strata

Kinderhookian strata in the study area are characterized by gray-green silty calcareous shale and finely-crystalline, dark gray to greenish-gray slightly silty and slightly dolomitic limestone that overlies the Woodford Shale of likely Devonian age and variably displays a visible disconformity (Curtis and Champlin, 1959; Rowland, 1961; Harris, 1987). The

Kinderhookian strata are composed of the Bachelor Formation and the lower units of the St. Joe Group, the Compton Formation and the Northview Formation in outcrop (Figure 8; Mazzullo et al., 2013). A maximum thickness of approximately 150 ft. (45 m) is reached in the Oklahoma panhandle and thins eastward where the unit is approximately 80 ft. (25 m) in northwestern and northern Oklahoma (Curtis and Champlin, 1959). In the study area the Kinderhookian Strata varies in thickness from absent to approximately 10 ft. (3 m) thick (Rowland, 1961).

Bachelor Formation

The Bachelor Formation is characterized by a thin basal sandstone unit that grades upward into a calcareous, light to dark green silty shale (Shoeia, 2012). This basal unit marks the initial flooding of the transgressive systems tract between the Woodford Shale of likely Devonian age and the overlying Mississippian strata (Evans et al., 2011). As defined from outcrop research, the basal sandstone is not present west of a north-south trending line from Springfield, Missouri to St. Joe, Arkansas (Boardman et al., 2013). In the study area, it is assumed that the basal sandstone is absent and that the thin upper shale unit might only be present locally (Rowland, 1961).

Compton Formation

The Compton Formation is the lowermost unit of the St. Joe Group and is characterized by thinly bedded, grey to greenish grey, very finely crystalline crinoidal mudstones to packstones with interbedded dark green shale wisps (Shoeia, 2012). In the outcrop region the Formation varies in thickness from 5 to 30 ft. (1.5-9 m) with a “normal” thickness occurring between 5 and 15 ft. (1.5-4.5 m) and a maximum thickness of about 20 to 30 ft. (6-9 m) occurring where “mud mounds” are present. This unit thins to the southwestern portions of Delaware and Adair counties of northeastern Oklahoma (Shoeia, 2012) and its presence in the study area in north-central Oklahoma is unknown. The lower Compton Limestone is interpreted to be part of the transgressive systems tract and the upper Compton Limestone is attributed to the highstand systems tract (Evans et al., 2011).

Northview Formation

The Northview Formation is characterized by variable greenish-brown siltstone to green silty calcareous shale as well as bluish-gray and grayish-green dolomitic siltstone (Shoeia, 2012). Outcrop research determined that truncation below the Northview Formation created a sequence boundary between the Compton Formation and Northview Formation (Evans et al., 2011). Approximately 80 ft. (25 m) at its maximum thickness, the Northview Formation thins to the north and south of this northwest to southeast thick trend and in northeast Oklahoma thins to a pinch-out. Its occurrence in the study area is unknown but is important to note that its lithology varies with its thickness (Shoeia, 2012).

Osagean Strata

Osagean strata in the study area are characterized by interbedded brownish gray, finely-crystalline cherty limestone containing variable amounts of chert, dolomite and silt as well as gray to brown, blocky, calcareous shale (Curtis and Champlin, 1959; Rowland, 1961). Osagean strata are composed of the uppermost unit of the St. Joe Group, the Pierson Formation, and the Boone Group, excluding the uppermost unit of the Boone Group, the Richey Formation, which is assigned to Meramecian age (Figure 8; Mazzullo et al., 2013). The maximum thickness of the Osagean occurs in western Oklahoma where approximately 700 ft. (213 m) of Osagean rock is present. In the study area, approximately 300 ft. (91 m) of Osagean rock is present (Rowland, 1961). Here, the Osagean strata unconformably overlie either Kinderhookian strata or the Devonian Woodford Shale (Rowland, 1961). Osagean rocks thin to the southeast, indicating a probable northeast-southwest depositional strike paralleling the northeast-southwest trending Transcontinental Arch (Lane and DeKeyser, 1980; Curtis and Champlin, 1959).

Pierson Formation

The Pierson Formation is the uppermost member of the St. Joe Group and is characterized by buff-colored, thinly-bedded and finely crystalline echinodermal and bryozoan mudstones to packstones that are variably dolomitic (Wilhite et al., 2011; Shoeia, 2012). Due to its lithologic similarities with the stratigraphically older Compton Formation (Figure 8), the Pierson Formation can become indiscernible from the Compton Formation in east-central Oklahoma where the underlying Northview Formation is absent (Shoeia, 2012). The typical thickness of the Pierson Formation ranges from 4 to 18 ft. (1-5.5 m) in the outcrop belt but can reach anomalous thicknesses of 75 ft. (23 m) or greater (Wilhite et al., 2011). The Pierson Formation is absent in extreme northeast Oklahoma (Thompson and Fellows, 1970) and is assumed to be absent in the immediate study area.

Reeds Spring Formation

The Reeds Spring Formation, the lowermost member of the Boone Group, conformably and locally unconformably overlies the Pierson Formation and is characterized by cherty lime mudstones variably exposed during Mississippian time resulting in substantial tripolite to develop (Figure 8; Wilhite et al., 2011; Mazzullo et al., 2013). Dolomite is present at the top of the Reeds Spring in the subsurface of south-central Kansas where it locally forms oil reservoirs (Mazzullo et al., 2013). At the type locality and other exposures in the outcrop belt the Reeds Spring shows preferential silicification of burrows and white chert-filled fractures suggesting that initial chert nucleation was syndepositional (Mazzullo et al., 2013).

The Pineville Tripolite facies of the Reeds Spring in the outcrop belt is characterized as a conspicuous unit of micro-porous tripolite with a gradational lower contact and a sharp upper contact (Mazzullo et al., 2013). This facies, approximately 50 ft. (15 m) thick, is interpreted to have formed during the middle Osagean as a result of subaerial weathering and diagenetic alteration of earlier-formed chert in the formation and along an unconformity of sub-regional extent (Mazzullo et al., 2013). Older, thinner tripolites in the Reeds Spring Formation (e.g. Buffalo River Tripolite and White River Tripolite) appear to be of limited areal extent and are likely related to local subaerial exposure along structural uplifts related to the Ouachita fore-bulge system that were active at these times (Mazzullo et al., 2013).

Bentonville Formation

The Bentonville Formation, formerly named Burlington-Keokuk, is characterized by beds and cross-stratified lenses of coarse and medium-grained crinoidal packstone and grainstone with interbeds of mudstone to wackestone that may be locally dolomitic (Thompson, 1986; Mazzullo et al., 2013). As indicated by Gutschick and Sandberg (1983), the Burlington Limestone and time-equivalent strata represent the *anchoralis-latus* conodont Zone. Brachiopods, bryozoans and rugose corals are present locally, but the excellent preservation of echinoderms is characteristic of the Burlington Limestone (Gutschick and Sandberg, 1983). It unconformably overlies the Pineville tripolite facies of the Reeds Spring Formation and is capped by the Short Creek Member characterized by cross-bedded, oolitic grainstone lithology (Figure 8; Mazzullo et al., 2013).

Meramecian Strata

"Meramecian" strata in the study area are characterized by calcareous siltstone and silty argillaceous limestones interbedded with silty calcareous shale and variable amounts of chert, glauconite and dolomite (Curtis and Champlin, 1959; Jordan and Rowland, 1959). This is lithologically identical to the "Meramecian" strata east of the Nemaha Uplift.

The Meramecian strata unconformably overlie the Osagean strata and are composed of the Richey Formation and the St. Louis Formation (Figure 8; Mazzullo et al., 2013). In north-central Oklahoma, approximately 300 ft. (91 m) of "Meramecian" rocks are present that thin shoreward to the north-northeast and thicken basinward to the west-southwest where approximately 900 ft. (274 m) of Meramecian rocks are present in western and southwestern Oklahoma and the Texas panhandle (Curtis and Champlin, 1959). This northwest-southeast depositional strike contrasts with the northeast-southwest depositional strike suggested by Rowland (1961) for the underlying Osagean strata.

The Ritchey Formation, formerly Warsaw Formation, is the uppermost member of the Boone Group and unconformably overlies the top of the Osagean Series (Figure 8; Mazzullo et al., 2013). In the outcrop belt the formation is characterized by slightly glauconitic, interbedded crinoidal packstone-grainstone and mudstone-wackestone with locally variable brachiopods, bryozoans, rugose corals, and discontinuous lenses, nodules and beds of white, light gray, bluish-gray and brownish-gray fossiliferous chert (Mazzullo et al., 2013). The St. Louis Formation, where present, unconformably overlies the Ritchey Formation and unconformably lies beneath the Hindsville Formation of Chesterian age (Figure 8; Mazzullo et al., 2013).

Chesterian Strata

Chesterian strata in north-central Oklahoma are characterized by interbedded gray shales and gray to brown, sublithographic to finely crystalline, fossiliferous limestone (Curtis and Champlin, 1959; Rowland, 1961). They unconformably overlie the Meramecian strata and are composed of the Hindsville Formation and Batesville Formation (Figure 8; Mazzullo et al., 2013). In the study area, the "Chesterian" strata are approximately 500 ft. (152 m) thick and thicken basinward to the south and southwest while thinning shoreward to the north and northeast resulting in a similar depositional strike to that of the underlying Meramecian Strata (Curtis and Champlin, 1959; Jordan and Rowland, 1959).

SEA LEVEL

Sea level is a crucial element in carbonate environments. Shallowing-upward carbonate cycles result from the interplay of allogenic and autogenic processes controlling accommodation and sediment accumulation (Kerans and Tinker, 1997; Yang and Lehrmann, 2014). Allogenic processes are controlled by eustasy and subsidence while autogenic processes are controlled by carbonate productivity and sediment redistribution and are commonly due to factors such as water depth, biota, salinity, oxygenation, nutrients and current energy (Yang and Lehrmann, 2014). Fluctuations in relative sea level disrupt the delicate relationships between these factors and alter the distribution and characteristics of lithofacies. Changes in eustatic sea level are dominantly a function of global tectonics and changes in ice volume related to Milankovitch orbital variability.

Eustatic Sea Level Cycles

First order (1st-Order) cycles (commonly referred to as "supersequences", Table 2) occur on the order of 200 to 300 million years (m.y.) and commonly relate to plate reorganization, starting with the breakup of supercontinents, opening of ocean basins, and ultimate closure. These cause the long term cratonic onlap and offlap signatures observed in the rock record (Read, 1995). Second order (2nd-Order) supersequences occur on the order of 10 to 100 m.y. and are driven by tectonics and change in ocean basin volumes, and to a lesser extent by ice-volume. These cycles form widespread major depositional sequences with thicknesses commonly hundreds to a few thousand meters and include stacks of seismically resolvable depositional sequences (Read, 1995; Kerans and Tinker, 1997). At this order of cyclicity, the condensed section at the supersequence scale typically forms the key regional hydrocarbon source bed (Kerans and Tinker, 1997).

Third order (3rd-Order) sequences are typically 1-10 m.y. in duration and develop units that are representative of the classic Exxon-type depositional sequences (Kerans and Tinker, 1997). The mechanisms controlling 3rd-Order sequences are changing rates of sea-floor spreading and/or long-term climatic/glacio-eustatic variations (Kerans and Tinker, 1997). A biostratigraphic technique is necessary to accurately resolve which of these mechanisms is dominant and such a technique is often limited or absent, as is the case for this study.

Cycle Hierarchy				
Tectono-Eustatic/ Eustatic Cycle Order	**Sequence Stratigraphic Unit**	**Duration (m.y.)**	**Relative Sea Level Amplitude (m)**	**Relative Sea Level Rise/Fall Rate (cm/1,000 yr)**
First	Supersequence	> 100		< 1
Second	Supersequence	10-100	50-100	1-3
Third	Depositional Sequence, Composite Sequence	1-10	50-100	1-10
Fourth	High-Frequency Sequence, Parasequence Set, Cycle Set	0.1-1	1-150	40-500
Fifth	High-Frequency Cycle, Parasequence	0.01-0.1	1-150	60-700

Table 2: Cycle Hierarchy chart demonstrating the characteristics between first- through fifth-order sea level cycles. Note the relatively high sea level amplitude and rate of sea level rise/fall of 4^{th}- and 5^{th}-Order cycles. Modified from Kerans and Tinker, 1997.

Climate-driven, high-frequency sea level sequences, cycle sets and cycles (4^{th} and 5^{th}-Order) result from cyclic changes in the orbital variability of the earth as well as the tilt and wobble of the earth's axis, all of which control the global ice volume and thus control sea level. (Table 2; Figure 9). Forced by Milankovitch-band glacio-eustasy, these changes in eustatic sea level occur on the order of less than 20 to 400 thousand years (k.y) and cause rapid flooding of platforms (Read, 1995; Kerans and Tinker, 1997). Eccentricity is the change in the shape of the earth's orbit around the sun that occurs on the order of 100 to 400 k.y. (Read, 1995). Obliquity is the variation of the tilt of the earth's axis and occurs on the order of approximately 40 k.y. (Read, 1995). Precession is the wobble of the earth and occurs on the order of 19 to 23 k.y. Furthermore, sub-Milankovitch cycles on the order of 10 k.y or less have been recognized in the stratigraphic record (Read, 1995; Grammer et al., 1996).

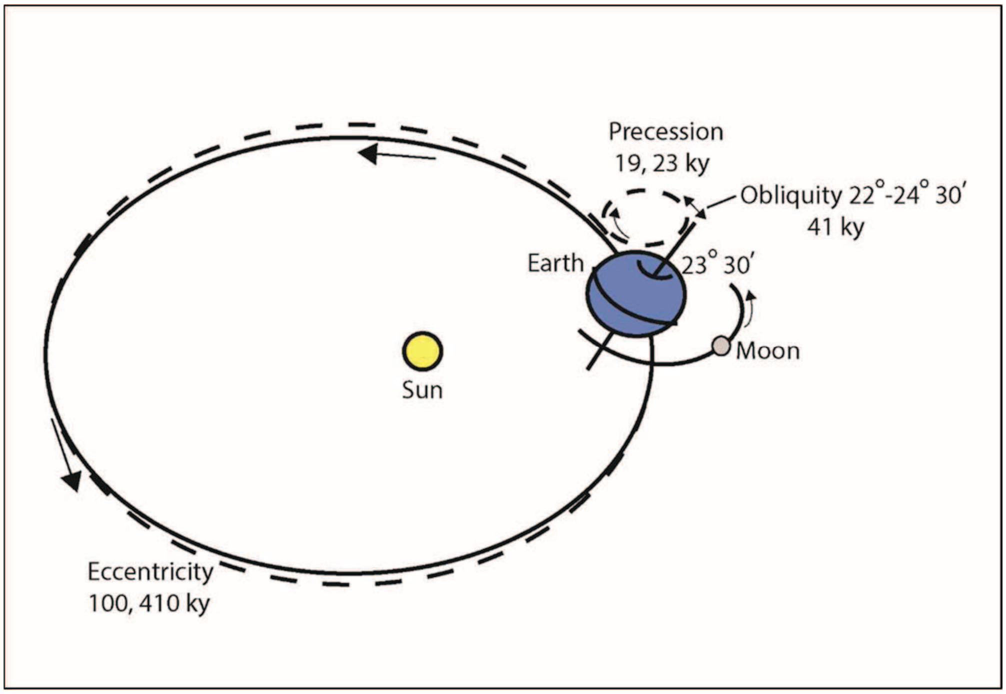

Figure 9. Illustration of the Milankovitch orbital patterns controlling glacioeustacy from Kerans and Tinker, 1997. Eccentricity, the change in shape of the earth's orbit, occurs on a duration of approximately 100,000 to 400,000 years. Obliquity, the tilt of the earth's axis, occurs on a duration of approximately 40,000 years. Precession, the wobble of the earth's axis, occurs on a duration of approximately 19,000 to 23,000 years. Modified from Kerans and Tinker (1997).

During greenhouse times, sea level changes are commonly small (less than 10 m (32.8 ft.)) and may be dominated by precessional cycles and possibly low amplitude 40, 100 and 400 k.y. cycles which generate bundles of cycles (Read, 1995; Kerans and Tinker, 1997; Yang and Lehrmann, 2014). Greenhouse cyclic carbonates typically show well-defined intermediate-scale cyclicity and lack well-resolved high-frequency cycles as a result of the low amplitude of the high-frequency signal (Kerans and Tinker, 1997). Autocycles reflecting local shoaling events may be commonly associated with greenhouse climatic conditions (Read, 1995).

During icehouse times, sea level gradually falls during glaciations and rapidly rises during deglaciations, resulting in rapid transgressions that far exceed most sedimentation rates

(Read, 1995). These changes are large (up to 100 m (328 ft.)) and are probably dominated by 100 and 400 k.y. eccentricity cycles (Read, 1995; Kerans and Tinker, 1997). Although apparently evident during greenhouse times, obliquity may be more important during transitional and icehouse times (Read, 1995). Icehouse cycles are a complex mix of both high-amplitude 4th- and 5th-Order signals resulting in complex stacking patterns, common exposure surfaces, and cycle and high-frequency sequence scale onlap and offlap (Kerans and Tinker, 1997).

Mississippian Sea Level

As indicated by Read and Horbury (1993), Milankovitch sea level fluctuations were generally large (up to 100 m (328 ft.) or more) during Mississippian time. Sea level reached a maximum highstand at the time of the *anchoralis-latus* conodont Zone, Latest Tournaisian, Middle Osagean (Figure 7; Gutschick and Sandberg, 1983). A long-term decline in sea level began in mid-Mississippian (mid-Visean), and reached a low in the late Mississippian near the Mississippian/Pennsylvanian boundary (Figure 10; Haq and Schutter, 2008). Accompanying this long-term sea-level decline, the Mississippian Subsystem represents a transition from greenhouse to icehouse, and with that, a change in the duration of dominant Milankovitch cyclicity observed in the strata (Figure 10; Read, 1995; Kerans and Tinker, 1997).

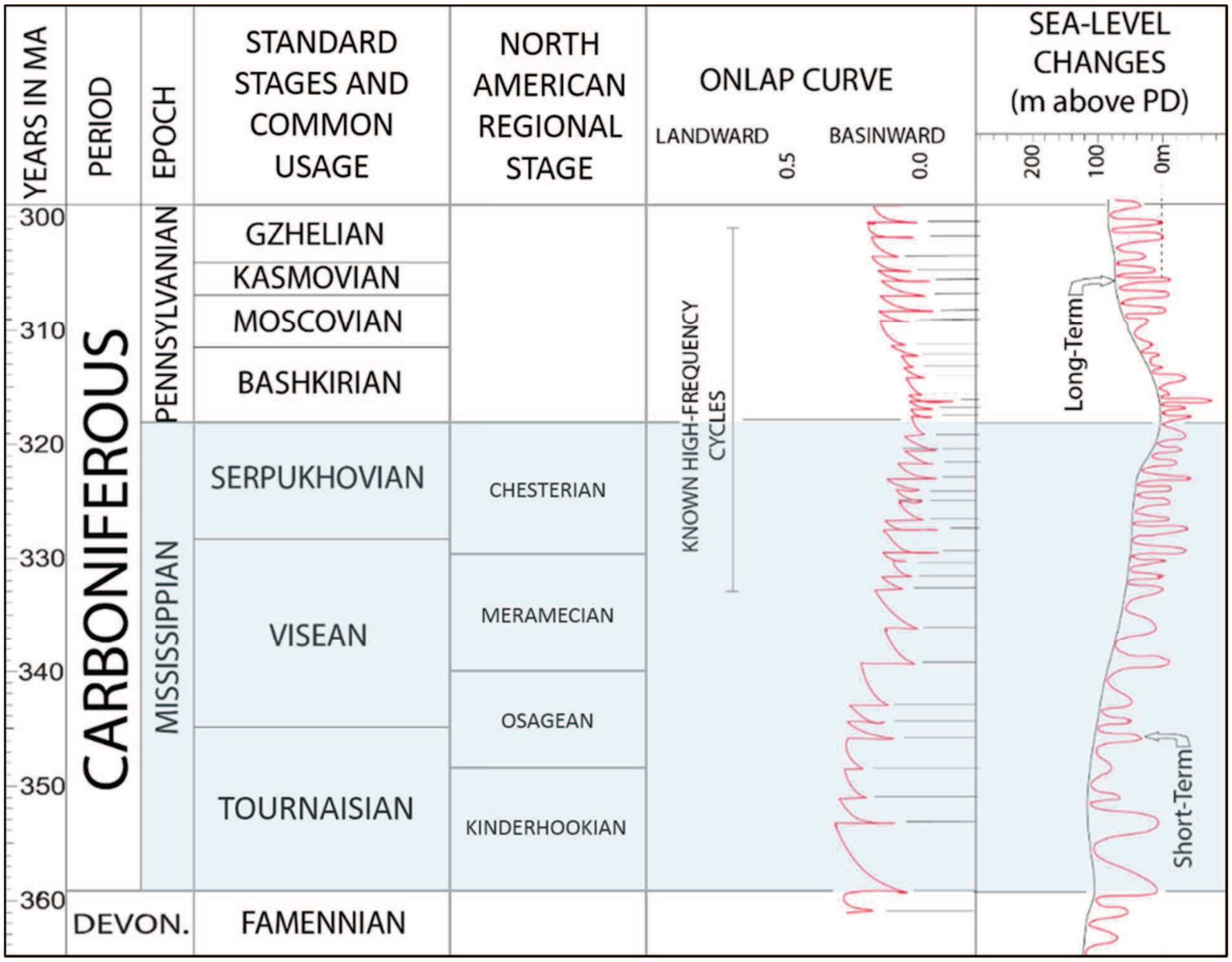

Figure 10. Mississippian sea level curve. Duration of 3rd-Order composite sequences decreases from approximately 2.9 m.y. during the Kinderhookian through Middle to Upper Meramecian to 1.3 m.y. during the Upper Meramecian through Chesterian and is believed to be the result of the transition from greenhouse to icehouse conditions. Modified from Haq and Schutter, 2008.

During transitional periods between greenhouse and icehouse, the stratigraphic record suggests that sea-level changes show little evidence of precessional (19-23 k.y.) forcing, and are dominated by eccentricity (100-400 k.y.) and obliquity (40 k.y.) forcing (Read, 1995). Stratigraphic attributes during such a transition are characterized by high-frequency cyclicity with well-defined stacked rock-fabric units that are commonly dominated by primary interparticle porosity and karst at intermediate-scale cycle boundaries (Kerans and Tinker, 1997).

A marked difference in high-frequency cyclicity in the cored intervals of the "Mississippian limestone" is expected from base to top due the overall transition from greenhouse to icehouse.

PROBLEMS IN DELINEATING HIGH-FREQUENCY CYCLICITY

Problems in delineating high-frequency sea level cyclicity from the sequence-stratigraphic hierarchy are common for a variety of reasons. Some problems stem from the Milankovitch cycles themselves, whereas others are external to the high-frequency cyclic nature of the system. Also, classifying the primary rock fabric to confidently interpret the depositional environment can prove difficult in units having intense diagenetic alteration. Lastly, correlating high-frequency cycles in the subsurface can prove problematic. Diagnostically identifying the effects of these potential problems in the study area is necessary to accurately define the role of high-frequency sea level cyclicity in the composite sequence-stratigraphic hierarchy.

Problems Associated with Milankovitch Cyclicity

Problems can be encountered when trying to delineate high-frequency cyclicity from the rock record that stem from the nature of the Milankovitch cycles themselves. Milankovitch periods are the dominant cycles but it is unlikely that simple 20, 40, 100 and 400 k.y. fluctuations will be observed in the rock record (Read, 1995). The interplay of the Milankovitch cycles creates errors associated with their durations of periodicity (Figure 11). There are numerous quasi-periods within the precession, obliquity and eccentricity bands (Read, 1995). Orbital eccentricity and obliquity are physically independent, whereas the precessional index is modulated by the eccentricity index (Yang and Lehrmann, 2014). The orbital forcing-climate-glaciation-sea level response is complex and non-linear (Read, 1995). Also, sub-Milankovitch cycles or 6th-Order cycles are likely to be present in the stratigraphy (Read, 1995; Grammer et al., 1996).

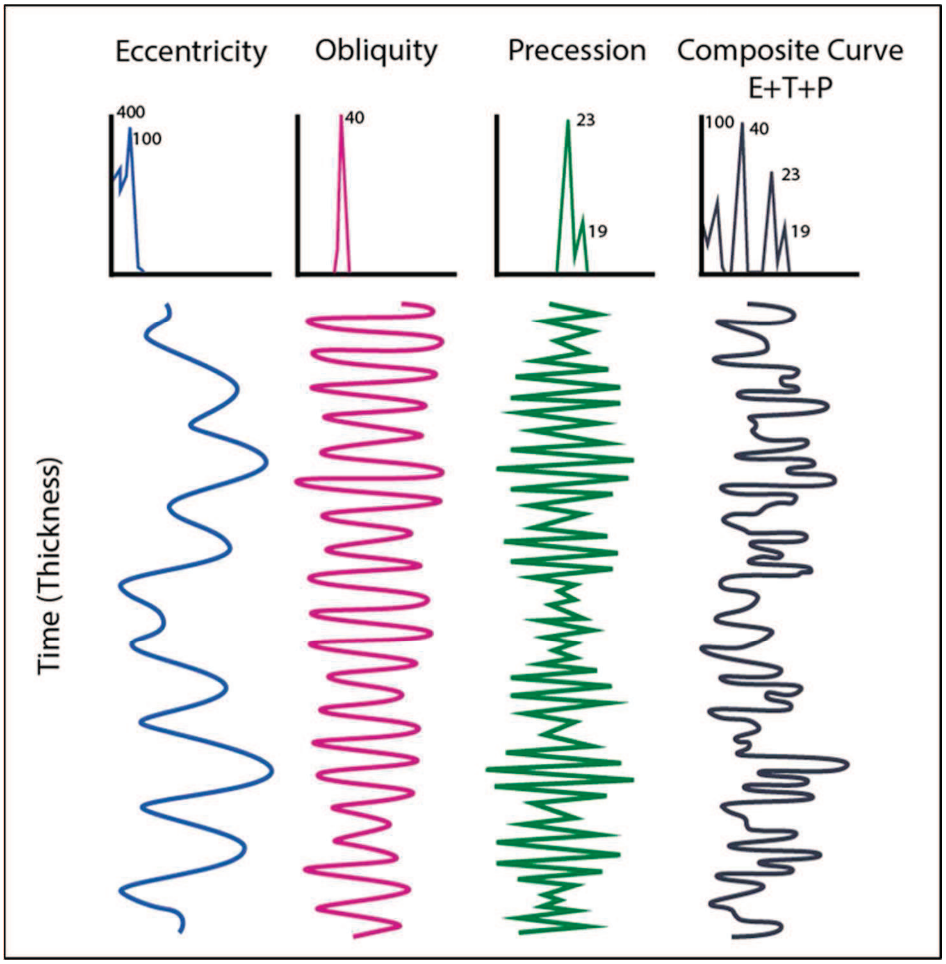

Figure 11: Composite sea level curve showing the constructive and destructive nature of the Milankovitch cycles. Modified from Read, 1995.

Other problems are external to Milankovitch cyclicity such as tectonism, rate of sedimentation and sediment body migration. Varying rates of sedimentation and sediment body migration hinder the delineation of high-frequency cyclicity and differential subsidence will not generate high-frequency cycle hierarchy (Drummond and Wilkinson, 1993; Handford and Loucks, 1993; Read, 1995). These potential problems are of importance due to their ability to produce meter-scale packages similar to those produced by high-frequency Milankovitch cyclicity (Drummond and Wilkinson, 1993). With regards to tectonism and local subsidence, Gay (2003) describes tectonic loading resulting in downwarping in front of the thrust of the Nemaha Uplift. Considering this interpretation, as well as recent work from Mazzullo et al. (2011c) and Wilhite et al. (2011) noting syndepositional tectonism within the "Mississippian limestone", the effects of local tectonism in the study area may prove problematic in attempting to delineate high-frequency cyclicity.

Problems in Facies Classification

Correctly characterizing rock fabrics in both core and thin section is required for the interpretation of depositional environments as they relate to high-frequency sea level fluctuations. Siliciclastic sedimentation can disrupt carbonate production and subsequent diagenetic alterations can completely destroy the primary rock fabric. Not only do these potential problems make lithofacies classifications more difficult, they can directly affect vertical stacking patterns and lateral distribution with respect to Milankovitch-band sea level cyclicity.

Mixed Carbonate-Siliciclastic System

While typically referred to as a limestone, core and thin section analyses revealed a significant influence of quartz silt within the "Mississippian limestone". Paleotopography in carbonates can have a direct influence on subsequent siliciclastic sedimentation and vice versa (McNeill et al., 2004). Sedimentation can alternate both vertically and laterally from siliciclastic to carbonate and might be temporally separated or contemporaneously deposited (McNeill et al., 2004). The exact origin of the siliciclastic sediment in the study area is currently unknown but its occurrence should be noted due to its ability to disrupt the inherently delicate carbonate environment (Yancey, 1991; McNeill et al., 2004). Siliciclastic "poisoning" due to turbidity reducing light or suffocating filter feeders can reduce or terminate carbonate production (Read, 1995). Clastic influx can also alter salinities that would likely reduce carbonate production rates (Read, 1995).

Chert: Origins and Implications

Diagenesis affects rock fabrics and reservoirs throughout the geologic record and the "Mississippian limestone" has prevalent accumulations of diagenetic chert both regionally and within the study area. As previously stated, chert is not diagnostic of a specific geologic time or a specific rock unit. While chert has close ties to carbonate environments it should be noted that its origins are ambiguous and a consensus for the origin of chert throughout the "Mississippian limestone" has yet to be reached. Chert may be deposited penecontemporaneously (Manger, 2014) or may be the product of post-depositional diagenetic alteration (Rogers et al., 1995; Montgomery et al., 1998; Franseen, 2006; Mazzullo et al., 2009a, 2009b; Mazzullo and Wilhite, 2010).

Chert is a hard, semi-vitreous, dense rock composed largely or entirely of several forms of silica – opal-CT, chalcedony or microcrystalline quartz. It has a tough, splintery to conchoidal fracture and varies in color (Folk and Weaver, 1952; Gary et al., 1974; Pettijohn, 1975; Friedman and Sanders, 1978). Most chert replaces pre-existing rocks such as limestone or dolomite, and some cherts are recrystallized accumulations of biogenic amorphous silica (opal-A) sourced initially from siliceous spicules, diatoms or radiolarians (Mazzullo and Wilhite, 2010). However, the presence of chert does not automatically suggest the presence of siliceous spicules in rocks and the source of silica in such deposits may be from silica-rich marine or meteoric waters that drained upland sources with abundant chert or siltstone (Mazzullo, 2009; Mazzullo and Wilhite, 2010).

Spiculite refers to a rock composed primarily of the siliceous spicules of invertebrates, including sponge spicules, with few to no other allochems (Gary et al., 1974; Pettijohn, 1975; Mazzullo, et al., 2009). Spiculites have been studied regionally in the Osagean and Meramecian strata, most notably the Cowley Formation in the subsurface of southern Kansas (Rogers et al., 1995; Franseen, 2006; Mazzullo et al., 2009a, 2009b). Tripolite is chert that has been highly-weathered by meteoric fluids along and for some distance beneath unconformities and is light-weight due to the high micro-porosity that formed during subaerial exposure (Mazzullo and Wilhite, 2010). This diagenetic alteration may be spicule-rich or spicule-poor depending on the original source of silica prior to weathering. Spiculitic tripolite has been described in subsurface studies from southern Kansas and north-central Oklahoma (Rogers et al., 1995; Montgomery et al., 1998; Watney et al., 2001).

Core descriptions and thin section analyses revealed the presence of both detrital and diagenetic quartz throughout the "Mississippian limestone" of the study area. Varying amounts of angular to subrounded quartz silt-very fine sand, lenticular chert nodules, cm-scale chert beds, and massively-bedded weathered cherts affect the lithofacies classification and interpreted depositional environments of the "Mississippian limestone". Further delineation of the role of high-frequency sea level cyclicity can be attained by correctly identifying the origin of these features in the study area.

Problems in Subsurface Correlating

Correlating carbonate cycles in the subsurface can lead to inaccuracies in various ways. Cycles that quickly onlap or downlap might only be known with sufficient well control. As observed from Rowland (1961), correlations based strictly on lithology, such as the presence of chert, tied to petrophysical log signatures can lead to inaccurate chronostratigraphic correlations.

High-frequency sequences and cycles have the potential to form relatively short-lived units that vertically compartmentalize relatively longer-lived reservoir units. These thin units may be smaller than the vertical resolution of wireline logs and would therefore be unrecognizable in subsurface correlations. This is a possible explanation for the lack of understanding of production-scale variability within "Mississippian limestone" reservoirs.

Potential problems in delineating high-frequency cyclicity from the rock record were expected for this study. As discussed, Milankovitch cycles represent a complex interplay of several variables that rarely yield a simple 20, 40, 100 and 400 k.y. cyclic rock record. This "limestone" is a mixed carbonate-siliciclastic system with significant distributions of chert that make this resource play attractive. Conversely, these characteristics make the play difficult to understand and predict. These problems make correlating the true cyclostratigraphic framework in the subsurface difficult.

"MISSISSIPPIAN LIMESTONE" PLAY HISTORY

Advancements in horizontal drilling and hydraulic fracturing completion techniques have reinvigorated the "Mississippian limestone" play in northern Oklahoma and southern Kansas since 2008 (Grieser and Pinkerton, 2013). As of 2013, there were +/- 18,000 historical Mississippian producing wells in Oklahoma and Kansas and +/- 5,500 active producing Mississippian wells, most of which were vertical completions (Grieser and Pinkerton, 2013). Due to its overlying relationship with the organic-rich Devonian Woodford Shale source rock, vast lateral distribution and characteristically high calcite and chert content that provides brittleness, the "Mississippian limestone" is a viable unconventional resource candidate.

The location of this study is in the Southwest Lacey field (Figure 12; Withrow, 1972). This field produces hydrocarbons from the Hunton (Silurian-Devonian) and Mississippian limestones (Withrow, 1972). During the early and mid-1950s, production from the Hunton was attributed to structural anomalies and updip pinchouts at the top of the Hunton limestone. In 1961, Calvert Exploration completed the No. 1 River Unit in Sec. 2, T. 18N, R. 9W. The "Meramec" limestone in this well produced nearly 500 barrels of oil in 7.5 hours, accelerating exploration of the "Mississippian limestone" in the field (Withrow, 1972).

Initial production from the "Mississippian limestone" in northern Oklahoma and southern Kansas was from the upper 100 ft. (30 m) of the "Mississippian limestone" and was often thought to be "Meramecian" in age (Mogharabi, 1964). Conventional vertical exploitation targeted structural traps, and initially operators would only drill through the top of the "Mississippian limestone" (Mogharabi, 1964; Withrow, 1972). Seismic exploration found potential within the underlying Hunton limestone that provided complete penetrations through the "Mississippian limestone" section (Mogharabi, 1964).

The primary Mississippian producing interval of the Southwest Lacey field is a 50 ft. (15 m) zone with primary intergranular porosity approximately 100-150 ft. (30-46 m) below the top of the "Meramec" that "apparently produces oil wherever it is found" (Withrow, 1972). This zone has been a prolific oil producer in the Southwest Lacey field and is the most significant "Mississippian limestone" reservoir (Withrow, 1972). There are zones of primary porosity throughout the "Mississippian limestone" interval and in the lower one-half there are fractured zones that form a productive reservoir of fair quality throughout the field (Withrow, 1972). Unconventional reservoirs are characterized by relatively low porosity and permeability values and may occur within or adjacent to the primary historical reservoirs. The high-resolution approach to sequence stratigraphy identifies the vertical and lateral distribution of both primary and secondary reservoirs.

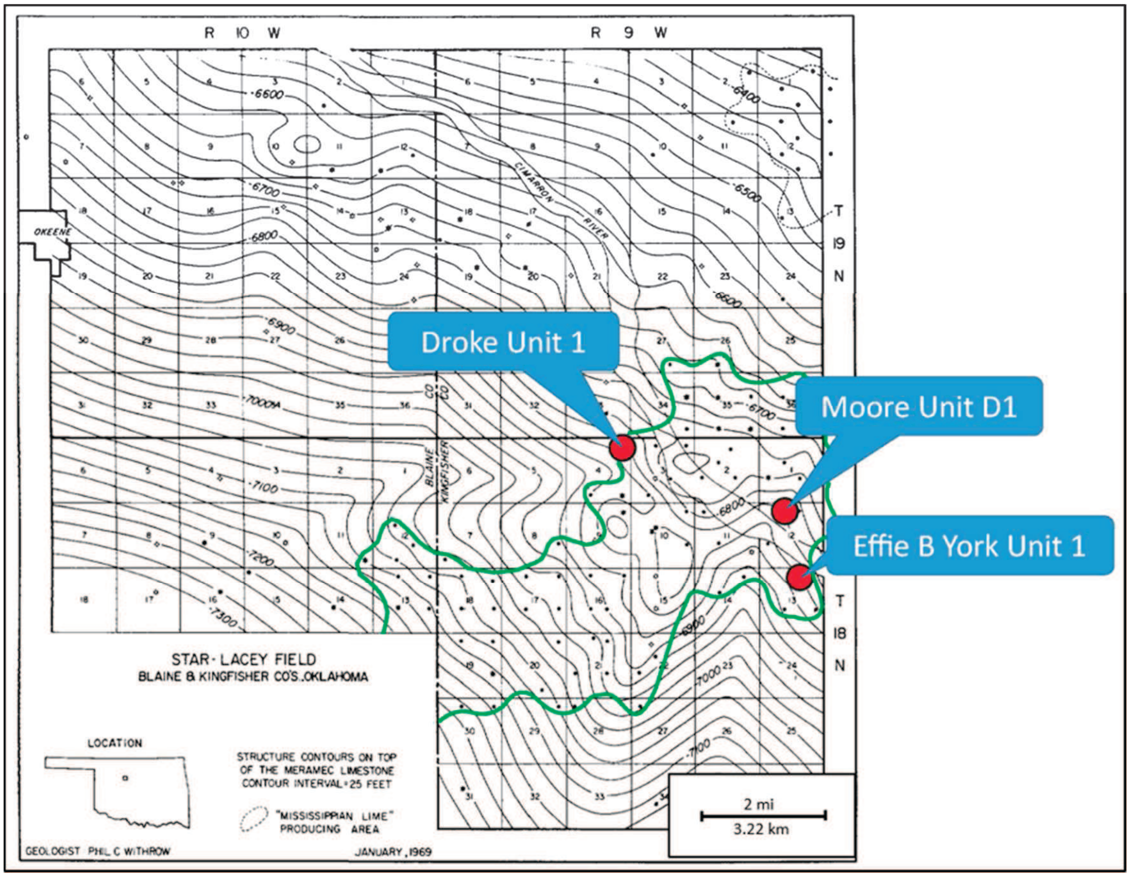

Figure 12. Star-Lacey Field and location of cores. Structure contour map on the top of the "Meramec Limestone" with a contour interval of 25 ft. (7.62 m). Location of cores evaluated in this study denoted by red circles. Note the structural features associated with the top of the "Meramec Limestone" in the immediate vicinity of the cores evaluated as well as their location within the "Mississippian Lime Producing Area" (green outline). Modified from Withrow, 1972.

DATA AND METHODS

The goal of this research is to define the sequence-stratigraphic hierarchy to characterize and predict the productive potential of the "Mississippian limestone" in the subsurface. By defining the sequence-stratigraphic framework through core descriptions (centimeter- through meter-scale), more accurately defining the depositional facies through thin section analyses (micrometer- through millimeter-scale), and correlating this framework throughout the study area, (kilometer-scale) accurate prediction of "Mississippian limestone" reservoir geometries in the subsurface can be attained.

Core Descriptions

A foot-by-foot description of the three cores of the "Mississippian limestone" (Table 1) was performed using the Dunham (1962) classification of carbonate rocks (Figure 13). From these descriptions, numerical values were assigned to similar lithofacies based on lithology, texture, grain size and shape, allochems, color, sedimentary structures and the degree and type of bioturbation. Visible fractures and pore types were also noted along with key surfaces/event boundaries. Depositionally significant packages were established using the described lithofacies and key surfaces to develop a preliminary cycle hierarchy.

Core plugs were taken throughout each shoaling upward succession of the "Mississippian limestone" to capture ideal and/or unique lithofacies and key surfaces. Core plugs provide the ability to further define lithofacies on a microscopic scale and accurately measure reservoir properties. From these precise descriptions, the lithologic and petrophysical characteristics of each lithofacies, both within their respective cycles and between cycles themselves, can be compared and contrasted.

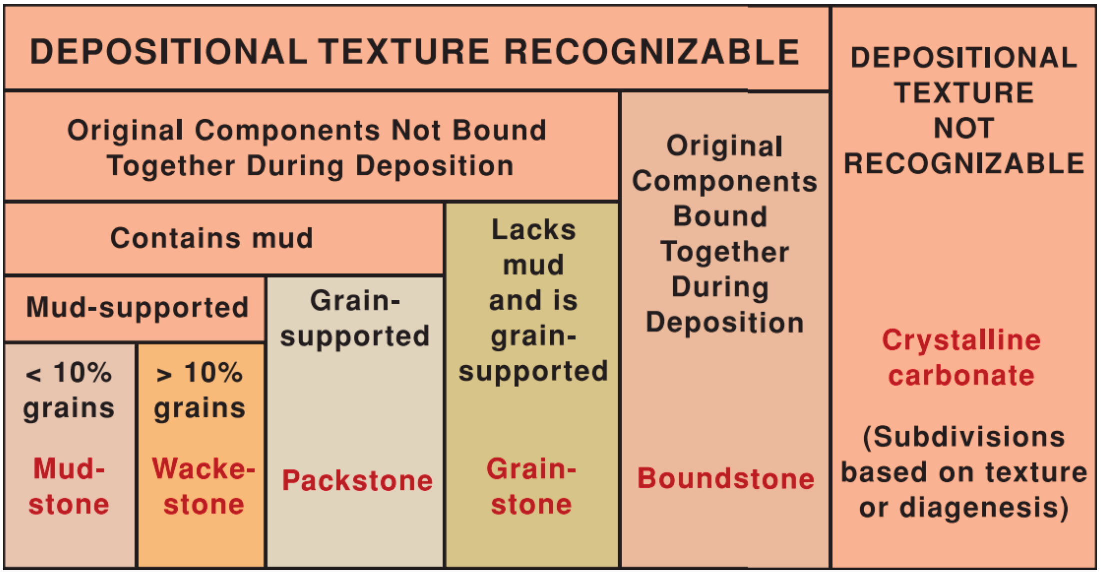

Figure 13**.** Diagram showing the Dunham (1962) classification of carbonate rocks according to depositional textures. From Scholle and Ulmer-Scholle, 2003.

Thin Section Analysis

Not all of the necessary information can be obtained from the core description alone and thin section analysis of carbonates is needed (Kerans and Tinker, 1997). Thin sections for the Droke Unit #1 and Effie B York #1 were prepared by Tulsa Thin Sections. Thin sections for the Moore Unit #D1 were prepared by CoreLab Petroleum Services and were stained with Alizarin Red-S on one half of the slide to reveal calcium carbonate.

Thin sections reveal more precise lithofacies descriptions using the Dunham (1962) classification method by further identifying environmental indicators that are unrecognizable in core. Mineralogy, diagenesis, porosity, microfractures, biota and grain composition, size and shape were identified. Visual estimation charts were used to estimate total volume porosity and key pore types using the Choquette and Pray (1970) classification scheme (Figure 14).

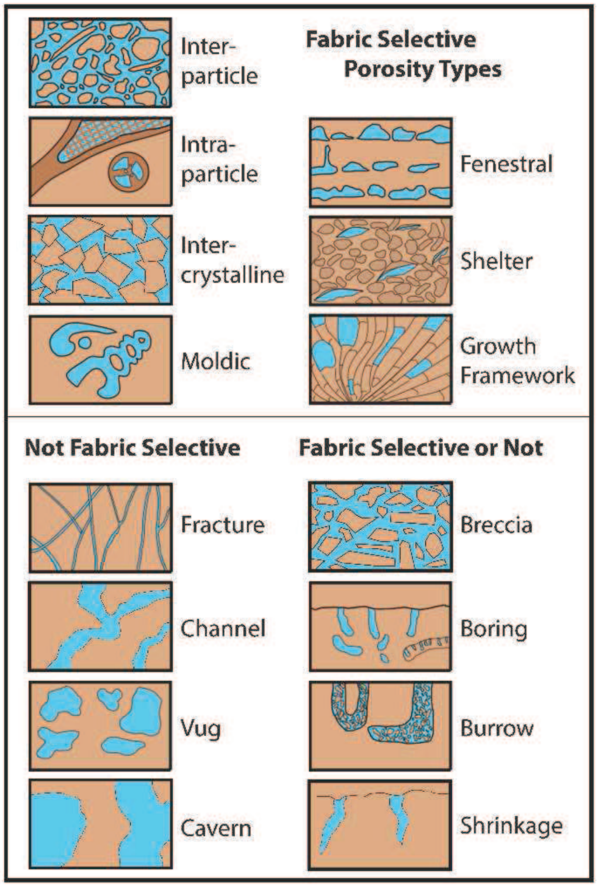

Figure 14. Diagrammatic representation of the Choquette and Pray (1970) classification of fabric selective and non-fabric selective porosity types observed in carbonate rocks. Modified from Scholle and Ulmer-Scholle, 2003.

Core Plug Analysis

Accurate hydrocarbon reservoir calculations are necessary due to the characteristically high water-cuts and low-permeability nature of the "Mississippian limestone" play in the Mid-Continent (Law and Curtis, 2002; Roundtree et al., 2010). Core plug analysis was performed on selected lithofacies to accurately define reservoir characteristics. "Shale Core Analysis" was performed on every selected core plug from the Moore Unit #D1 by CoreLab Petroleum Services via Marathon Oil Corporation. Porosity and permeability data integrated into the defined stratigraphic hierarchy quantitatively defines flow units allowing for the characterization of hydrocarbon-bearing reservoirs.

Subsurface Correlation

Wireline logs measure formation properties in a well and are used in exploration to correlate zones and evaluate their reservoir potential. These electrical, nuclear and acoustic logs help define lithology, porosity, pore geometry and permeability (Asquith and Krygowski, 2004). Asquith and Krygowski (2004) give a detailed description of these logging tools as well as the basic relationships of well log interpretation methods and Archie (1950) provides an introduction to the petrophysics of reservoir rocks. Conventional wireline logs were run on all three wells drilled. All three wells have gamma ray, neutron, resistivity, conductivity, SP, and acoustic curves. The Droke Unit #1 and Moore Unit #D1 have caliper logs. Droke Unit #1 logs were run by Schlumberger Oilfield Services Company. Moore Unit #D1 logs were run by Welex Jet Services. Effie B York #1 logs were run by Lane-Wells Company.

Petrophysical characteristics from the above analyses were tied to the suite of wireline logs for each respective core, as well as to the laboratory measured spectral-gamma ray performed on the Moore Unit #D1 core. The accuracy of these log signatures was compared to the measured characteristics from the core to determine the most reliable signatures for subsurface mapping. Subsurface correlation using the cyclostratigraphic approach combined with accurate quantitative petrophysical data results in geometrically precise reservoir units. The interpreted reservoir units can be defined 3-dimensionally in the study area to explain the inconsistencies seen in historical well performance and predict the distribution of potential unconventional reservoir targets.

Modern and Ancient Analog Analysis

Comparison of results obtained in this research to both modern and ancient analogs provide more reasonable spatial approximations. Modern analogs are valuable for conceptualizing the geometrical attributes of a single time-slice of a reservoir facies (Grammer et al., 2004). Shortcomings of modern analog analysis include, but are not limited to, diagenetic complexity, climatic and tectonic variability, and, particularly for carbonates, age-dependent faunal variability (Grammer et al., 2004). Ancient analogs help relate these interpreted reservoir geometries to a commonly known and researched geological setting, either from outcrop or subsurface studies. Comparison of both modern and ancient analogs will alleviate assumptions made in subsurface mapping of the sequence stratigraphic architecture.

LIMITATIONS

Limitations to this study range from the location and scope of the study area, incomplete and/or inaccurate data from subsurface logs and core laboratory procedures, as well as constraining the research within a budget. This study of the "Mississippian limestone" integrates data from three representative wells located in close proximity to one another (less than 3 mi (4.8 km)). While this provides the ability to witness heterogeneities on a production-scale, its location in a regional sense might not be representative of the aggregate "Mississippian limestone" play. This problem was alleviated by extrapolating the data away from the cored area using wireline logs until correlations were not reliable enough to be considered "ground-truthed".

There are limitations associated with wireline logs in a general sense and specifically in the study area. Wireline logs record the physical attributes of rocks and the fluids they contain and are only accurate to a certain extent. As previously mentioned, Lucia (1995) and Martin et al. (1997) demonstrated that petrophysical flow units are independent of total volume porosity. This suggests that porosity logs do not necessarily capture the true petrophysical characteristics of a reservoir unit. Interpretations of reservoir characteristics will become increasingly limited the farther they are extrapolated away from the cores studied. In the study area, the Southwest Lacey field was primarily discovered and developed in the 1960s resulting in a limited number of modern logs in a majority of the wells. All three cores were logged by different service companies and a one-to-one comparison of quantitative data was pursued with caution.

When dealing with carbonates, formation resistivities tend to vary widely with changing rock types, and commonly there are few shales against which to measure changes (Asquith and Krygowski, 2004). While the porosity log is the primary reconnaissance measurement, subsurface correlations revealed that the gamma ray log appears reliable in the study area as well as regionally within the "Mississippian limestone". Gamma ray logs were run on each of the cores (Table 1) and a laboratory measured spectral-gamma ray scan was performed by the Oklahoma Petroleum Information Center on the Moore Unit #D1. This scan comes with a disclaimer stating "the Total Gamma values are reliably reproducible, however the Total Gamma – Uranium should not be trusted," and was used instead to confirm the core-to-log tie.

Marathon Oil Corporation has generously provided extensive data for the Moore Unit #D1. Including the spectral-gamma ray measurements, they also provided "Mineralogy Determined by X-ray Diffraction" and "Shale Core Analysis" performed by CoreLab Petroleum Services. While this data set for the Moore Unit #D1 is greatly appreciated and helps quantitatively define reservoir architecture, the Droke Unit #1 and Effie B York #1 cores (Table 1) have limited data sets in comparison due to budget constraints.

This research is limited in a regional sense by the location and narrow scope of the study area in that it may only capture an anomalous portion of the “Mississippian limestone”. Incomplete and/or inaccurate data from subsurface logs and core laboratory procedures and subsequent interpretations are equally limited. Correlating and extrapolating quantitative data throughout the subsurface was done with caution and various inconsistencies in wireline logging data were thoroughly noted. Robust 3-dimensional reservoir modeling of the study area was not defined yet the sequence stratigraphic architecture is sufficiently mapped to the extent that reservoir characteristics can be confidently estimated.

CHAPTER II

THE EFFECTS OF HIGH-FREQUENCY CYCLICITY ON RESERVOIR CHARACTERISTICS OF THE "MISSISSIPPIAN LIMESTONE", ANADARKO BASIN, KINGFISHER COUNTY, OKLAHOMA

INTRODUCTION

"Mississippian limestone" reservoirs store significant volumes of hydrocarbons throughout the Mid-Continent and have historically been targeted for vertical drilling. Advancements in horizontal drilling and completion techniques renewed industry attention of these reservoirs. The widespread regional extent of this unconventional resource play, covering approximately 25,000 mi^2 (65,000 km^2) in northern Oklahoma and southwestern Kansas, is often accompanied by highly variable well performance. Inconsistent exploitation results are commonly experienced at the field or production-scale and are believed to be attributed to an overall lack of understanding of the factors controlling reservoir development and distribution. Historical studies and current subsurface mapping techniques have not been focused on development of the sequence stratigraphic architecture which is likely responsible for production-scale reservoir heterogeneities.

The uniqueness of this research lies in its observation of production-scale reservoir distribution between three closely spaced (avg. < 2 mi. (3.2 km)), dip-oriented cores of the entire "Mississippian limestone" with adequate (avg. 80-acre spacing (1,320 ft. / 402 m)) intervening well control. The goal of this study was to characterize the distribution of hydrocarbon-bearing reservoirs in the "Mississippian limestone" to improve predictability of well performance. The primary objectives were to: 1.) identify hydrocarbon-bearing reservoirs within a core-defined, high-resolution sequence stratigraphic framework; and 2.) characterize and predict reservoir distribution by extrapolating the core-defined wireline log signatures of the stratigraphic hierarchy throughout the study area. High-resolution sequence stratigraphic analysis increases the accuracy of reservoir characterization by identifying vertical and lateral heterogeneities of flow units. The resulting reservoir development and distribution within the sequence stratigraphic architecture can be applied regionally to the "Mississippian limestone" and serve as a template for other similar carbonate reservoirs.

Geologic Setting

Carbonate production and deposition occurred in a relatively shallow ramp setting throughout Mississippian time in north-central Oklahoma. The study area, located in northwest Kingfisher County (Figure 15) and covering approximately 160 mi^2 (415 km^2), was positioned in a tropical to subtropical and humid climate approximately 20-25° south of the paleoequator (Gutschick and Sandberg, 1983; Lane and De Keyser, 1980). Inferred paleo-trade winds were out of the present day east-northeast during the Mississippian (Mazzullo et al., 2009a). This relatively shallow ramp setting progressively deepened south toward the ancestral Anadarko Basin and shallowed north toward the Central Kansas Uplift and Transcontinental Arch (Curtis and Champlin, 1959). The main structural movement of the north-south trending Nemaha Uplift, located approximately 25 mi. (32.2 km) west of the study area, is believed to be constrained to the Late Mississippian or Early Pennsylvanian, yet more recent research suggests movement may have occurred during the Middle Mississippian, potentially affecting deposition of the "Mississippian limestone" in the study area (Figure 15; Gay, 2003). The Ozark Uplift, located approximately 250 mi (725 km) east of the study area, was emergent and active during the Mississippian (Figure 15; Lane and De Keyser, 1980). Carbonate deposition occurred regionally throughout this tectonically bound, low inclination (approximately 1° or less) ramp setting, resulting in numerous hydrocarbon-bearing reservoirs collectively referred to as the "Mississippian limestone" (Ahr, 1973; Price, 2014; LeBlanc, 2014; Childress and Grammer, 2015).

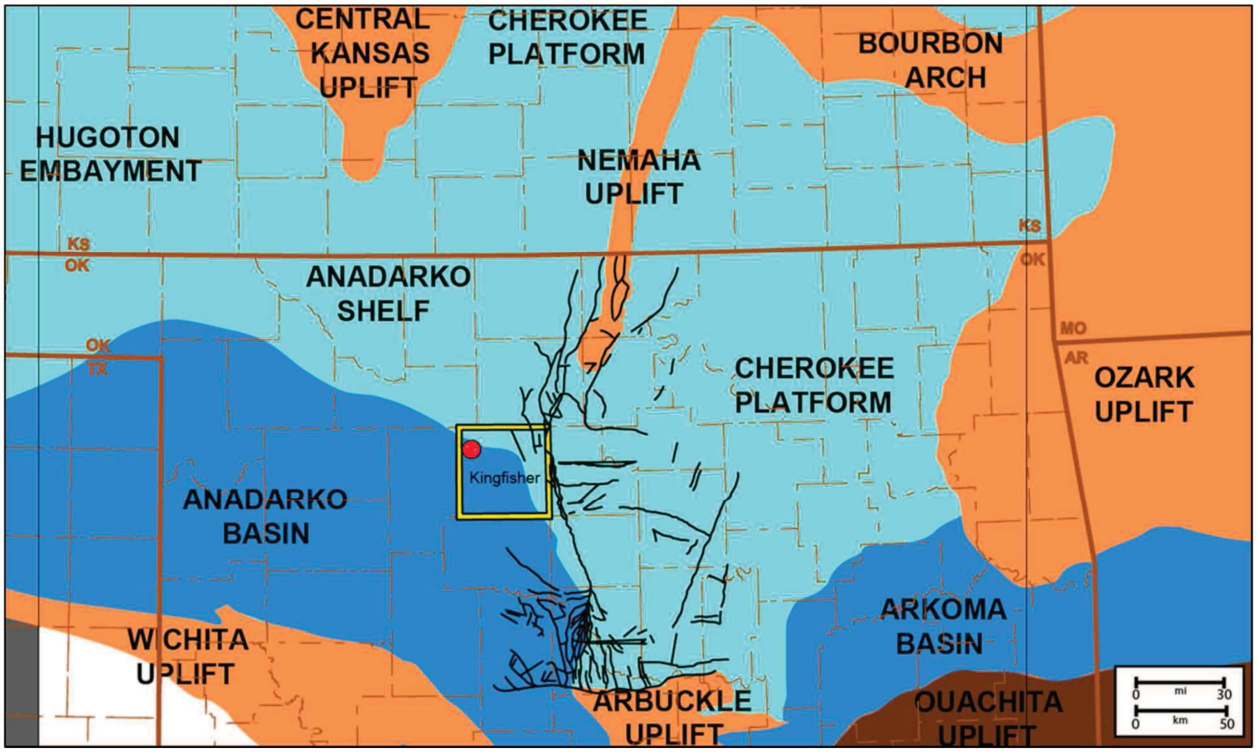

Figure 15. Geologic provinces of the Mid-Continent and faulting associated with the Nemaha Uplift. Shelves/shallow basins/platforms denoted by light blue. Deep basins denoted by dark blue. Basement-rooted uplifts denoted by light brown. Detachment uplifts denoted by dark brown. Faults associated with the Nemaha and Arbuckle Uplifts denoted by black lines. Location of cores utilized in this study denoted by red circle in the northwest corner of Kingfisher County (yellow outline). Note the location of the study area at the present day transition between the shallow Anadarko Shelf and deeper Anadarko Basin. Also note the proximity to the Nemaha Uplift and associated faults located approximately 25 mi. east of the study area. Geologic Provinces modified from Northcutt and Campbell, 1996 (Oklahoma), and Ramondetta, 1990 (Kansas). Nemaha faults from Gay, 2003.

Stratigraphy

The regional stratigraphy and primary nomenclature of the "Mississippian limestone" was developed and modified from outcrop data in the Ozark Uplift region (Mazzullo et al., 2011a). Hydrocarbon production from this grossly correlative system in Oklahoma and southern Kansas resulted in the transference of the original nomenclature westward into the subsurface. Application of this nomenclature is largely lithology-based and results in inaccurate chronostratigraphic associations that cloud regional and sub-regional production trends.

The Mississippian Subsystem is bound below by the Woodford Shale of likely Devonian age and above by an unconformity with Pennsylvanian strata. While informally the name "Mississippian limestone" suggests carbonate strata, it is more accurately characterized as a mixed carbonate-siliciclastic system. Lithology-based industry terms (i.e. "Miss Solid" or "Miss Chat") and the improper use of formal North American Regional Stage names (i.e. "Kinderhook", "Osage", "Meramec" and "Chester") often results in inaccurate subsurface correlations. Historical lithostratigraphic correlations in the vicinity of the study area are now insufficient with in-fill well control (Rowland, 1961; Hoffman, Jr., 1964; Withrow, 1972).

Recent biostratigraphic outcrop-based research of conodont zonations within the "Mississippian limestone" developed new nomenclature to facilitate accurate use of terminology in the subsurface (Mazzullo et al., 2013). While this approach captures the time-transgressive nature of the Mississippian Subsystem, the approximately 1-3 million year maximum temporal resolution of the depositional units does not provide adequate resolution to define production-scale flow units which were likely deposited in response to higher frequency sea level changes. This study defines production-scale variability of "Mississippian limestone" reservoirs by correlating genetically related rock units defined through the application of high-resolution sequence stratigraphy.

Sea Level

Identifying the depositional effects of sea level fluctuations is fundamental to carbonate reservoir characterization (Kerans and Tinker, 1997). Cyclic fluctuations of eustatic and relative sea level results in the hierarchical vertical stacking of carbonate facies mosaics (Read, 1995). High-frequency, glacio-eustatic processes (approximately 20-400 k.y. cycle duration) are superimposed on long-term, tectono-eustatic processes (approximately 1-300 m.y. cycle duration) and are the result of orbitally-forced, Milankovitch-band cyclicity (Read, 1995; Kerans and Tinker, 1997). These high-frequency sequences (4^{th}-Order) and high-frequency cycles (5^{th}-Order) impart lateral and vertical heterogeneity into the composite sequence (3^{rd}-Order) and control production-scale flow units (Kerans et al., 1994; Read, 1995; Grammer et al., 2004).

The Mississippian Subsystem is characterized as a transitional global climate between a greenhouse of the Devonian and an icehouse of the Pennsylvanian (Read, 1995), resulting in a decrease in the duration of 3^{rd}-Order composite sequences during the Middle and Late Mississippian (Figure 16; Haq and Schutter, 2008). The stratigraphic record suggests that such a transition typically results in stacked-rock fabric units dominated by primary interparticle porosity and karst at intermediate-scale cycle boundaries (Kerans and Tinker, 1997). Milankovitch-band sea level amplitudes during the Mississippian System are estimated to be approximately 75-100 m (246-328 ft.) (Read and Horbury, 1993). Due to the nature of the low inclination ramp setting, smaller amplitudes than those suggested would still result in widespread areal migration of facies belts. Core analysis was required to define production-scale variability of the “Mississippian limestone”, hypothesized to be the result of high-frequency eustatic sea level fluctuations.

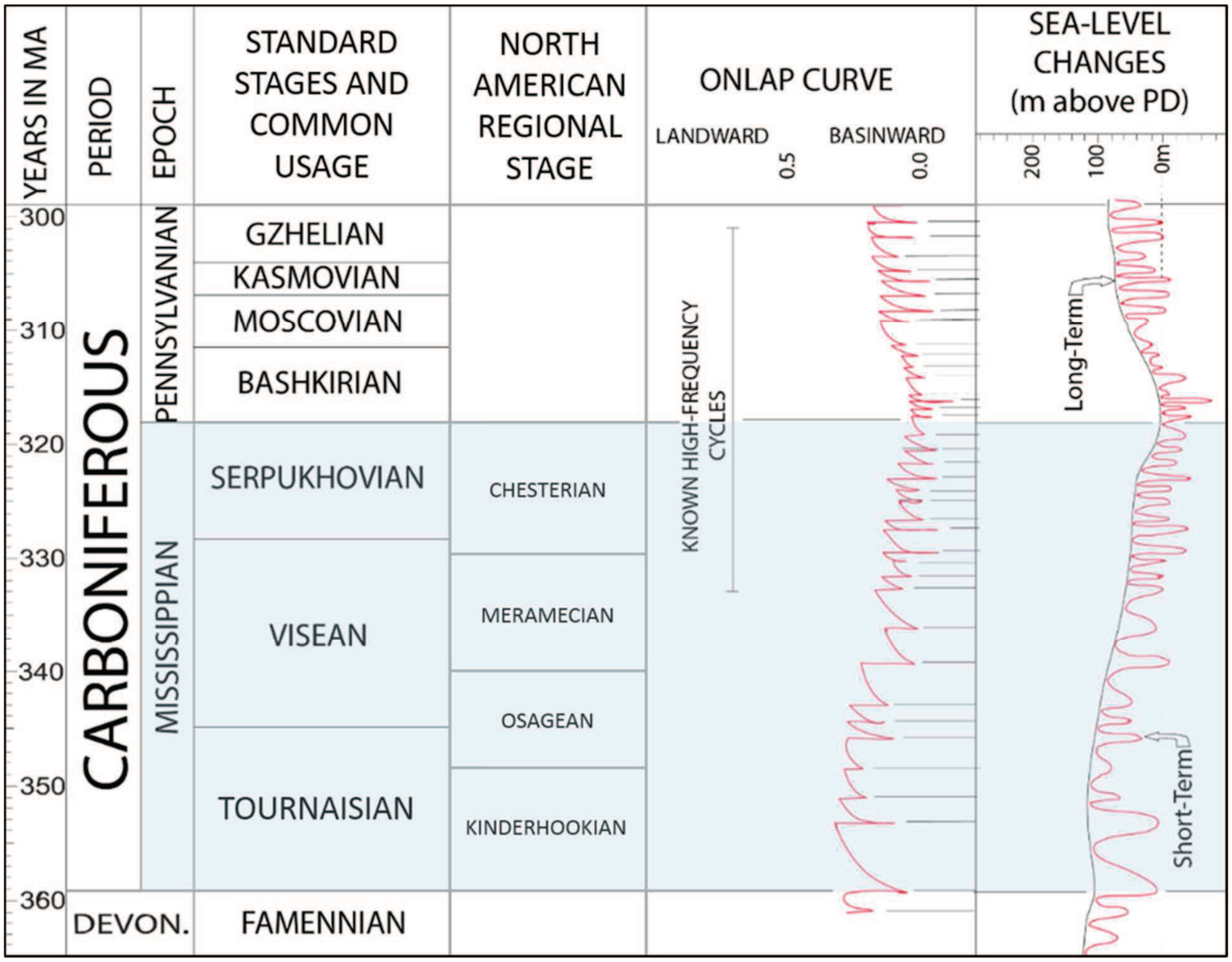

Figure 16. Global sea level and onlap curve of the Carboniferous Period. Duration of 3rd-Order composite sequences decreases from approximately 2.9 m.y. during the Kinderhookian through Middle to Upper Meramecian to 1.3 m.y. during the Upper Meramecian through Chesterian and is believed to be the result of the transition from greenhouse to icehouse conditions. Modified from Haq and Schutter, 2008.

DATA AND METHODS

The primary focus of this study was to analyze the reservoir characteristics of the "Mississippian limestone" through the application of high-resolution sequence stratigraphic analysis. Three cores of the entire "Mississippian limestone" ranging from 504-525 ft. (154-160 m) in length were selected for analysis (Table 3). These cores were ideal for observing the effects of high-frequency sea level cyclicity due to their orientation nearly perpendicular to depositional-strike with an average spacing of less than 2 mi (3.2 km). Seventy-seven core plugs, cylindrical samples of rock cut perpendicular to the axis of the core and typically 1-1.5 in (2.5 to 3.8 cm) in diameter and 2-3 in (5-7.6 cm) long, were taken from the 3 cored intervals (Figure 17). The sequence stratigraphic hierarchy was identified through core analysis (centimeter to meter-scale) and refined and quantified through petrographic analysis (micrometer to centimeter-scale). X-ray diffraction (XRD), scanning electron microscopy (SEM) and "Shale Core" analyses (micro to nanometer-scale) were performed on core plugs from the Moore Unit #D1 to identify mineralogical and petrophysical properties not observable through core and thin section analyses. Reservoir units were analyzed with respect to their hierarchical position to determine their likely causal mechanism. Subsurface wireline logs were tied to the bounding surfaces of the stratigraphic hierarchy and extrapolated within the study area (kilometer-scale), establishing the sequence stratigraphic architecture. The vertical and lateral reservoir distribution that this study defines exemplifies the heterogeneities commonly experienced throughout the "Mississippian limestone" and other ancient systems deposited under similar conditions.

Historical Operator	Lease Name	Legal Location	County	"Mississippian limestone" Thickness
Pan American	Effie B York #1	13-18N-09W	Kingfisher	525 ft. (160 m)
Pan American	Moore Unit #D1	12-18N-09W	Kingfisher	518 ft. (158 m)
Pan American	Droke Unit #1	04-18N-09W	Kingfisher	504 ft. (154 m)

Table 3. List of cored "Mississippian limestone" wells selected for study. Well information obtained from well log headers and the Oklahoma Petroleum Information Center database. All wells are located in T18N-R9W of Kingfisher County, Oklahoma. Average thickness of the cored "Mississippian limestone" interval is 516 ft. (157 m).

<u>Core Descriptions</u>

Cores were described using the Dunham classification system for carbonate rocks. Abbreviations used to illustrate these descriptions are listed in Table 4. Similar lithofacies were grouped based on grain type, texture, allochems, sedimentary structures, the degree and geometrical scale of bioturbation, and color following the Goddard et al. (1951) Rock Color Chart (Table 8). Flooding surfaces and other depositionally significant features were noted to identify vertical stacking patterns and to define a preliminary cycle hierarchy. A finer-scale of analysis was required due to the fine-grained texture and diagenetic overprinting of the gross interval.

Core and Thin Section Image Labels									
Feature Key								Porosity Key	
BLANK	thin section blank (location)	HCS	hummocky cross stratification	PLUG	core plug (location)	FR	fracture
BR	brachiopod	K-spar	potassium feldspar	PPL	plane-polarized light	IP	interparticle
BU	burrow	L	lamination	PY	pyrite	IX	intercrystalline
BY	bryozoan	M	mud/mudstone	Q	quartz (detrital)	MO	moldic
Ca	calcite	MI	mica/detrital clays	Qm	quartz matrix	SH	shelter
CH	chert	Mic	micrite	Qo	quartz overgrowth	VU	vug
CON	conodont	MW	mud wisp	S	stylolite	WP	intraparticle
CR	crinoid	Mxl	mixed-layer illite/smectite	SK	undifferentiated skeletal fragment	WX	intracrystalline
D/Dol	dolomite	O	ostracode	SP	spicule		
EC	echinoderm	OIL	oil/dead oil/organics	TL	traction laminae		
FR	fracture	P	peloid	TS	truncation surface		
G	glauconite	PH	phosphate	XB	cross-bedding		
GB	grain bed	PL	plagioclase feldspar	XPL	cross-polarized light		

Table 4. Core and Thin Section Image Labels. Porosity types are based on the classification system of Choquette and Pray (1970).

<u>Petrographic Analysis</u>

Microscopic analysis of thin sections facilitated the characterization of depositional facies and provided semi-quantitative estimations of porosity. A total of 77 core plugs were selected from the three cored intervals to capture variability within the cycle hierarchy (Figure 17). Thin sections from the Effie B York #1 and Droke Unit #1 cores were prepared by Tulsa Sections, Inc. and were blue epoxy impregnated to show porosity (Appendix A-II and C-II, respectively). Thin sections for the Moore Unit #D1 were prepared by Core Laboratories, Inc.

and were blue epoxy impregnated and alizarin red stained to identify calcite content (Appendix B-II). The Dunham (1962) classification method was used again to further characterize and delineate lithofacies. Standard visual estimation charts provided semi-quantitative percentages of mineralogy, grain type and porosity, using the Choquette and Pray (1970) classification method. Facies were confirmed or corrected through thin section analysis (micrometer-scale) and subtleties within the cycle hierarchy were identified (see Table 4 for thin section abbreviations). Stacking patterns were redefined to establish a more accurate sequence stratigraphic hierarchy. Reservoir characteristics were observed in relation to their facies classification and position within the stratigraphic hierarchy. The petrographically defined stratigraphic framework allowed for subsequent correlation of facies when calibrated to subsurface wireline logs.

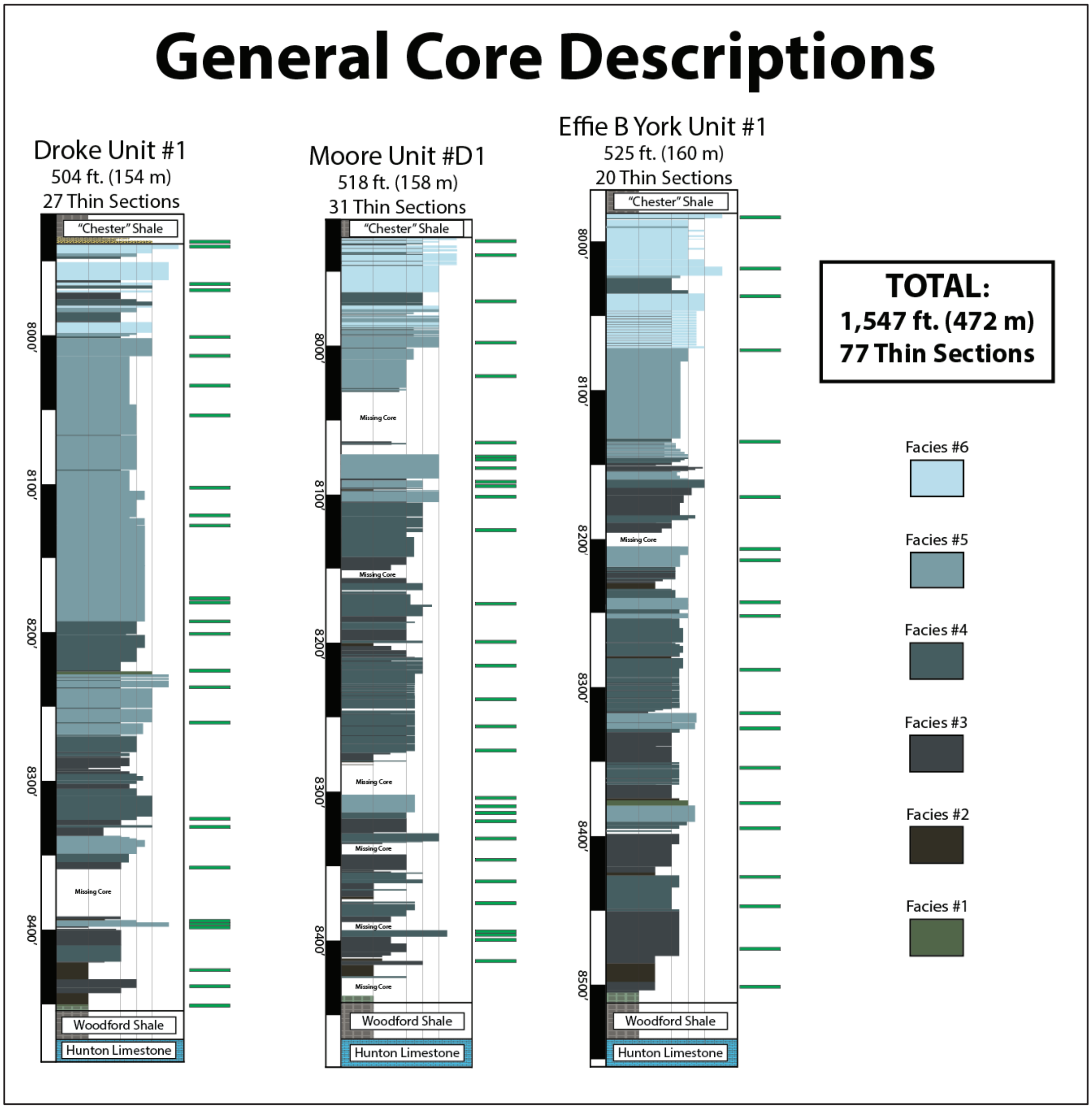

Figure 17. General Core Descriptions. The three cores included in this study range in thickness from 504-525 ft. (154-160 m). A total of 77 thin sections (green dash) were taken for petrographic analyses to capture variability within the gross "Mississippian limestone". Thin sections from the Droke Unit #1 and Effie B York #1 cores were prepared by Tulsa Sections, Inc. Thin sections from the Moore Unit #D1 core were prepared by Core Laboratories, Inc. in conjunction with XRD, SEM and "Shale Core" analyses of core plugs to quantitatively define reservoir petrophysical properties including porosity and permeability. Descriptions are color coded based on facies classification (also see Figure 26) and horizontally exaggerated to correspond to the Dunham classification.

Wireline Log Correlation

The sequence stratigraphic architecture was identified through subsurface wireline log correlation by extrapolating away from the "ground-truthed" rock data in the cores. Bounding surfaces of the defined stratigraphic hierarchy were tied to their respective log signatures (Appendix A-III-b, B-IV-b and C-III-b). All cored intervals were surveyed with gamma ray, neutron, resistivity, conductivity, SP and acoustic logs, and the Droke Unit #1 and Moore Unit #D1 possess caliper logs. Asquith and Krygowski (2004) and Pirson (1963) provide a detailed description of these logging tools and Archie (1950) provides an introduction to the petrophysics of reservoir rocks.

Of note, a Guard resistivity log was run on the Moore Unit #D1. Guard resistivity logs are typically used when formation resistivity values are significantly higher than borehole resistivity values. By focusing the current into the formation, this curve has a vertical resolution of approximately 3-6 in. (8-16 cm) (Pirson, 1963). Characteristically high resistivity values (typically 300-1,000 ohm/m) of the "Mississippian limestone" make the guard resistivity tool useful at identifying thin (1-6 in. (2.54-15 cm)) flooding surfaces commonly associated with high-frequency eustatic sea level fluctuations. Correlating discrete log signatures identified from the stratigraphic framework resulted in a more precise subsurface mapping technique for identifying the sequence stratigraphic architecture. This approach differs from the lithostratigraphic approach of forced extrapolation of arbitrary log signatures and results in a more accurate production-scale reservoir model.

FACIES ASSOCIATIONS

Six lithofacies were observed within the "Mississippian limestone" of the study area (Table 5). Interpreted depositional environments range from the distal outer ramp through the high-energy, shallow subtidal environments of the upper mid-ramp or lower ramp crest (Figure 18). Depositional facies range from glauconitic shales/sandstones deposited during initial transgression followed by argillaceous, suspension-laminated and infrequently burrowed mudstones-wackestones. Succeeding these relatively deep and/or restricted depositional facies are higher-energy environments of deposition indicated by an increase in bioturbation and a transition to traction-current lamination accompanied by an increasingly abundant and diverse faunal assemblage. Siliciclastic input and diagenesis results in a complex interplay of both pre- and post-depositional processes that collectively control reservoir development.

Depositional Facies		# of Samples	Porosity (%)	Permeability (mD)	Mineralogy (Avg. %)				Sedimentological Character	BI (0-6)	Primary Grain Constituents
					Carbonate	Quartz	Clays	Other			
6	Skeletal Packstone-Grainstone	8	3.6	2.8 E-06	58	29	4	9	Planar and ripple traction-current lamination & truncation surfaces	0.5	Crinoids, echinoids, peloids, brachiopods, bryozoan, sponge spicules, ostracodes & foraminifera
5	Traction-Current Wackestone-	11	5.6	3.3 E-05	53	42	2	3	Traction-current lamination; hummocky & swaley cross-stratification	1.4	Peloids, sponge spicules, bryozoan, crinoids, brachiopods, trace echinoids & trace foraminifera
4	Bioturbated Wackestone-	37	2.1	1.5 E-06	63	28	4	5	Horizontal and vertically bioturbated (cm-scale); dominant suspension, periodic traction-current lamination	2.5	Peloids, sponge spicules, brachiopods, crinoids, ostracodes, rare bryozoan & rare foraminifera
3	Burrowed Mudstone-Wackestone	14	1.7	3.4 E-07	79	13	4	4	Horizontally burrowed (mm-scale) & suspension-laminated	1.8	Brachiopods, trace sponge spicules, trace crinoids, trace ostracodes & rare foraminifera
2	Argillaceous Mudstone	3	<1	8.7 E-07	61	24	10	5	Traction-current mud wisps; suspension-laminated mudstone; rare horizontal burrows (mm-scale)	0.9	Brachiopods, trace sponge spicules & rare ostracodes
1	Glauconitic Silty Shale/ Sandstone	3	3	N/A	54	30	9	7	Poorly-sorted glauconitized sand grains	1.2	Rare brachiopods and undifferentiated carbonate skeletal fragments

Table 5. Depositional Facies. Average characteristics of the 6 depositional lithofacies observed from core and thin section analyses of the "Mississippian limestone". The Moore Unit #D1 core provided the most accurate quantitative data derived from XRD and porosity and permeability measurements. Porosity and mineralogy values for the Droke Unit #1 and Effie B York #1 were visually estimated from thin section analyses. Sedimentological characteristics were derived primarily from core descriptions. Grain types were derived from both core and thin section analyses and are listed in decreasing order of abundance. Bioturbation Index (BI) values were visually estimated from core and thin section data of all three cores using the Bann et al. (2008) classification method.

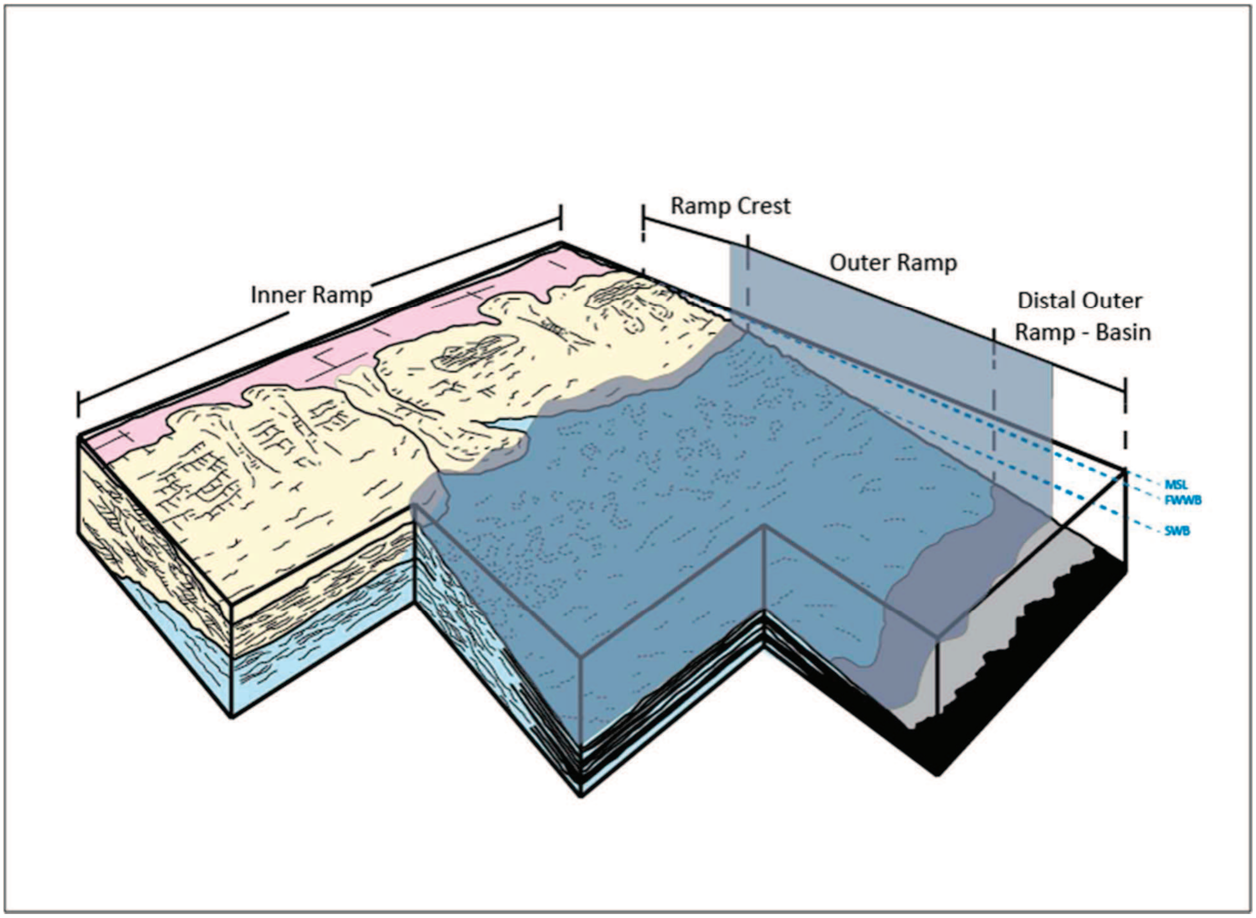

Figure 18: Illustration of a ramp environment. The facies observed from the cores of the "Mississippian limestone" in the study area are representative of the depositional lithofacies characteristic of a mixed carbonate-siliciclastic ramp setting. Blue overlay demarks the range of depositional facies observed in this study. Facies range from mudstones and wackestones of the distal outer ramp to relatively high energy environments of the mid-ramp and distal ramp crest indicated by skeletal packstones and grainstones. Modified from Handford, 1986.

Facies 1: Glauconitic Shale/Sandstone

The glauconitic shale/sandstone facies is composed of common (10-25%) sub-rounded and poorly sorted glauconitic (nascent to highly ordered) grains ranging from 75-400 µm. The matrix ranges from a carbonaceous shale unit (Figure 19) to a medium quartz sandstone unit (Figure 20) with rare (<1%) thin-shelled brachiopods and undifferentiated carbonate skeletal fragments of comparable size occurring in both members. The glauconitic shale unit, approximately 7 ft. (2.1 m) thick, occurs at the base of the cored intervals and is lithologically similar to the “Kinderhook Shale” (Rowland, 1961). The sandstone unit, approximately 0.5-3.0 ft. (15.2-91 cm) thick, is the stratigraphically highest/youngest expression of Facies 1. Mineralogically, Facies 1 averages 54% carbonate (52% calcite/ 2% dolomite), 30% quartz (15% chert/ 15% silt), 7% glauconite with the remainder (9%) attributable to feldspars and total clays. Minimal burrowing, likely *Zoophycos*-type, (avg. BI=1.2) and moderate silicification (20%) occur in the sandstone sample. Porosity values in the sandstone unit average 3% and seldom (1%) displays partial molds/vugular porosity after glauconite grains with very rare (<0.1%) shelter porosity after brachiopods (Figures 20 and 19, respectively).

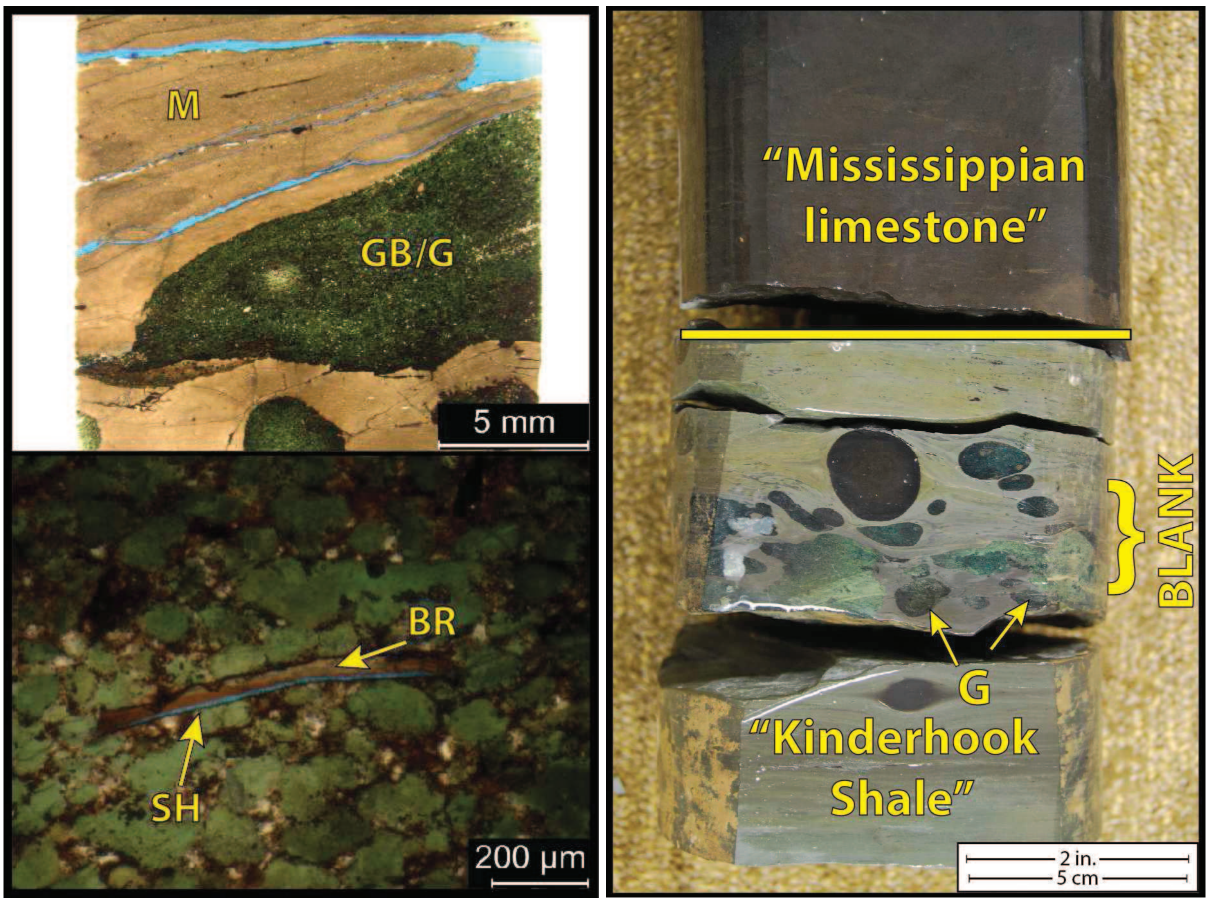

Figure 19. Facies 1: Glauconitic Shale/Sandstone: Shale unit (“Kinderhook Shale”). Figure illustrates thin section photomicrographs (left; plane polarized light (PPL)) from Droke Unit #1: 8,450’ and the corresponding core photograph (right) from that interval. Refer to Table 4 for abbreviations. Common (20%) subrounded, poorly sorted and highly evolved glauconitic grains

(avg. 200 µm) in a carbonaceous shale matrix. Displays very rare (<0.1%) shelter porosity (SH) beneath a thin-shelled brachiopod in thin section (bottom left).

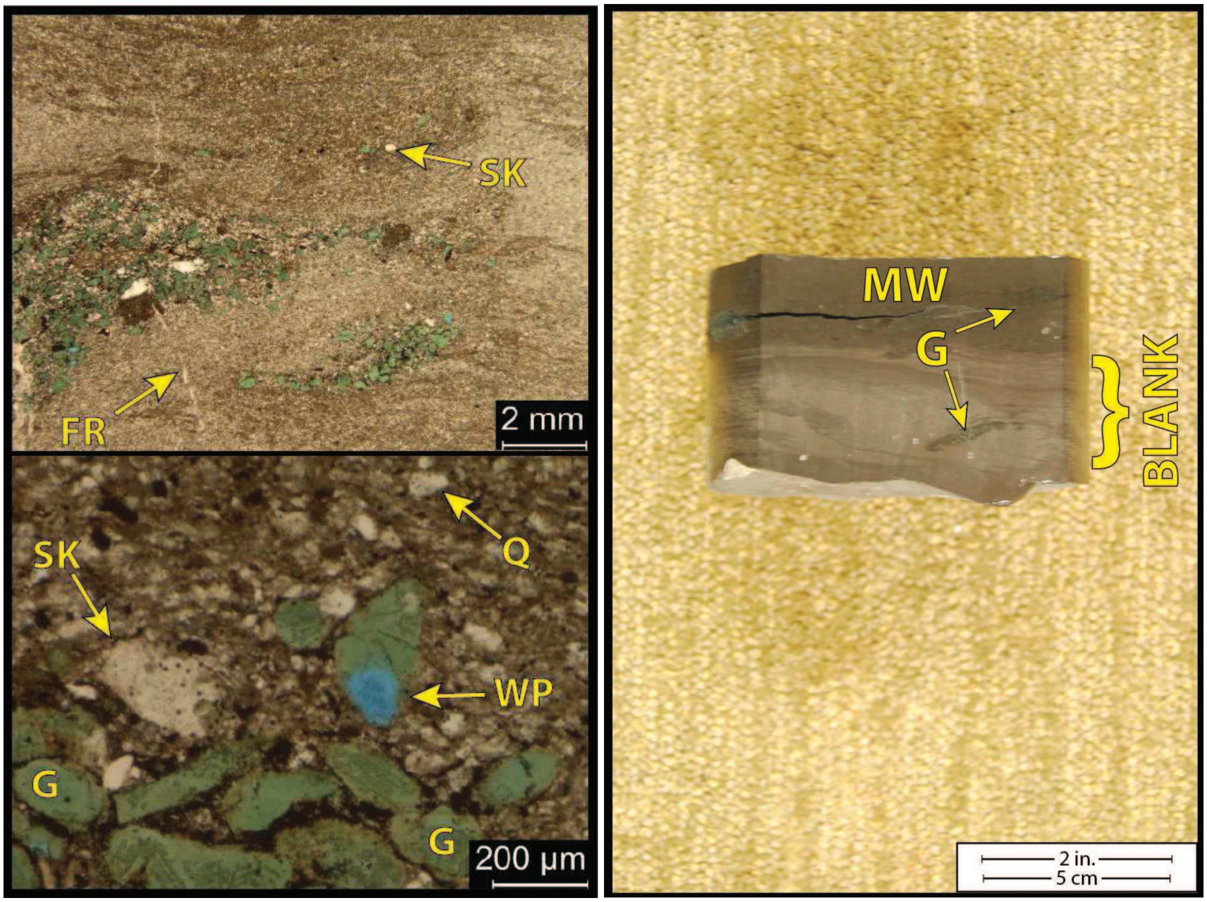

Figure 20. Facies 1: Glauconitic Shale/Sandstone: Sandstone unit. Figure illustrates thin section photomicrographs (left; PPL) from Effie B York #1: 8,377.7' and the corresponding core photograph (right) from that interval. Refer to Table 4 for abbreviations. Common (10-20%) subrounded, poorly sorted, and nascent to slightly evolved glauconitic grains in a micritic/siliciclastic matrix. Thin section seldom (1%) displays vugular porosity after glauconite dissolution. Detrital quartz silt (avg. 15%), undifferentiated carbonate skeletal grains and silicification (avg. 15%) are common in Facies 1.

Facies 1 is interpreted to have been deposited during initial transgression in a low-energy environment. Glauconitization requires plentiful supplies of iron and potassium and is generally thought to be authigenically formed in reducing environments (Burst, 1958; Bentor and Kastner, 1965). It is also interpreted that shallow seas extending over large areas with low sedimentation rates are suitable for the formation of glauconite (Bentor and Kastner, 1965; Middleton et al., 2003). In the stratigraphically higher sandstone end-member, the presence of likely *Zoophycos*-type burrows suggests a dysaerobic environment (Byers, 1977; Middleton et al., 2003). The interpretation of this environment is congruent with the presence of nascent glauconite in these samples. The presence of thin-shelled brachiopods and poorly sorted, subrounded glauconite grains suggests deposition in a relatively deep water setting below storm weather wave base (SWWB). A dysaerobic, reducing environment with low sedimentation rates is believed to have existed during the initial transgression across the widespread ramp setting of the study area.

Facies 2: Argillaceous Mudstone-Wackestone

The argillaceous mudstone to wackestone facies is composed of thin-shelled brachiopods (2.5-5%; up to 600 μm long), trace sponge spicules (1%; 100-200 μm long), rare ostracodes (<1%; avg. 200 μm) and undifferentiated carbonate skeletal grains (avg. 30 μm). Mineralogically, Facies 2 possesses the highest percentage of total clays (9.6%) out of all six facies to accompany its 61% carbonate, avg. 24% quartz (14% chert/ 10% silt) and 3% feldspars. Sedimentologically, Facies 2 is dominated by suspension lamination (Figure 21) and shows rare (avg. BI=0.9) mm-scale horizontal, likely *Zoophycos*-type burrows. Microboring of carbonate skeletal grains was also observed in trace amounts. Intergranular porosity between quartz silt grains as well as within the authigenic clay matrix average < 1% with permeability values averaging 8.7×10^{-08} mD, the lowest of all six facies. Observed continuous thickness of Facies 2 decreases vertically from approximately 11 ft. (3.4 m) in the lowermost portion of all three cores to approximately 3 in. (7.62 cm) or less in the middle and upper portions of all three cores.

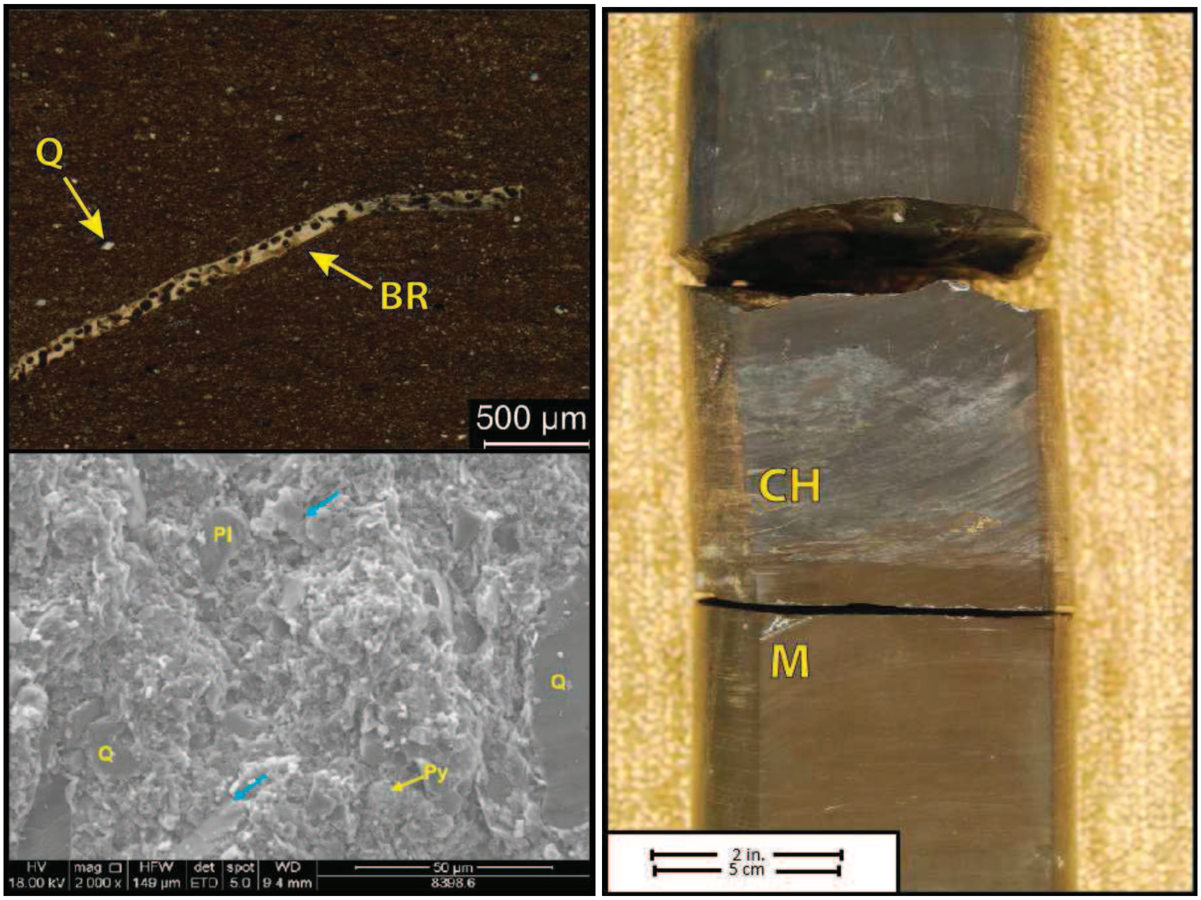

Figure 21. Facies 2: Argillaceous Mudstone-Wackestone. Figure illustrates thin section photomicrograph (top left; PPL), SEM analysis (bottom left; provided by CoreLab Petroleum Services) from Moore Unit #D1: 8,398.6' & core photograph from Effie B York Unit #1: 8,447'-8,448.5'. Refer to Table 4 for abbreviations. Thin section displays a microbored thin-shelled brachiopod within a mud-dominated matrix accompanied by minor amounts of detrital quartz silt. Facies 2 averages 10% detrital quartz silt. SEM photograph displays subhedral to anhedral quartz silt and trace anhedral plagioclase (Pl). Interparticle micropores (blue arrows) were observed within the mixed-layer illite/smectite matrix. Sample contains 44.5% quartz (24.5% quartz silt; 20% chert), 22.1% total clays, 4.3% feldspars & 2.9% pyrite. Core photograph displays a layer of chert within a mudstone facies.

Facies 2 is interpreted to represent continued transgression across the ramp environment, establishing carbonate production within a relatively deep and/or restricted environment below SWWB in the distal outer ramp (Figure 18). Suspension-laminated carbonate mud with common authigenic clays suggests deposition in a calm, low-energy setting. The low diversity and rare occurrence of organisms (sponge spicules, thin-shelled brachiopods and ostracodes) suggests a dysoxic to periodically slightly oxygenated environment (Finger, 1983). The presence of microbores observed on these carbonate organisms does not provide insight into the environment of deposition (Ekdale et al., 1984). Rare mud wisps containing quartz silt, clays and feldspars accompanied by horizontal, likely *Zoophycos*-type burrows (mm-scale) are interpreted to represent periodic oxygenation of bottom waters, possibly due to the influence of storms (Wehner et al., 2015).

Facies 3: Burrowed Mudstone-Wackestone

The burrowed mudstone to wackestone facies is composed of thin-shelled brachiopods (1-2.5%; up to 2 mm long and variably microbored), trace sponge spicules (1%; avg. 600 μm long; variably calcitic/siliceous), trace crinoids (1%; disaggregated avg. 1-1.5 mm), rare foraminifera (<1%; <60 μm), trace ostracodes (1%; avg. 400 μm) and undifferentiated carbonate skeletal grains (avg. 60 μm). Mineralogically, Facies 3 is comprised of 79% carbonate (76% calcite/ 3% dolomite), 13% quartz (8% silt/ 5% chert), 4% total clays and 4% feldspars. Sedimentologically, Facies 3 is suspension-laminated and commonly horizontally burrowed (mm-scale, likely *Cruziana*- or *Zoophycos*-type; BI=1.8) (Figure 22). It's average of 8% detrital quartz silt is the lowest of all six facies. Interparticle porosity (avg. 1.7%) and permeability (avg. 3.4×10^{-07} mD) are the second lowest of all six facies. Thickness ranges from approximately 5-25 ft. (1.5-7.6 m) and the facies is generally thicker in the lower and middle portions of all three cores.

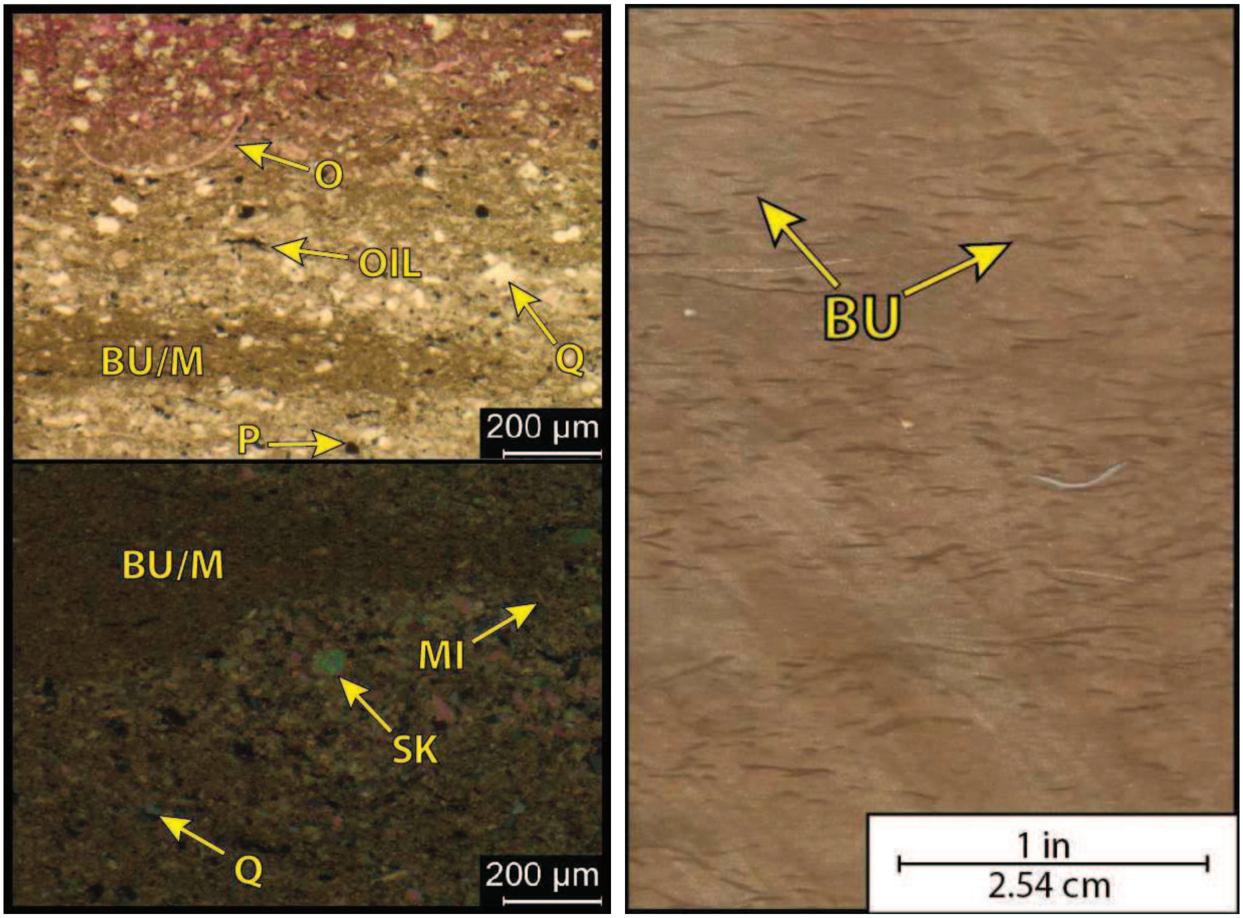

Figure 22. Facies 3: Burrowed Mudstone-Wackestone. Figure illustrates thin section photomicrographs (left; top=PPL, bottom= XPL) from Moore Unit #D1: 8,320.0' and a core photograph from Droke Unit #1: 8,310'-8,311'. Refer to Table 4 for abbreviations. Carbonate skeletal grains, ostracodes and quartz silt are supported by a micritic and clay-rich mud matrix. Detrital quartz silt comprises 8% of this facies, the lowest abundance of all 6 facies. Note the mm-scale, likely *Zoophycos*-type horizontal burrows in both thin section and core photograph (avg. BI = 1.8).

Facies 3 is interpreted to represent deposition in an oxygenated environment below SWWB in the distal outer ramp (Figure 18). Suspension lamination suggests a low-energy, relatively deep and/or restricted environment. The common occurrence of mm-scale, likely *Cruziana*- and *Zoophycos*- type, horizontal burrows (Figure 22) indicates an increase in oxygen levels from that of Facies 2. This inferred improvement of water quality is congruent with the increase in fossil diversity (thin-shelled brachiopods, sponge spicules, foraminifera, ostracodes and trace fragmented crinoids). The observed increase in carbonate skeletal grain size from that of Facies 2 also suggests a relatively higher energy depositional environment along the ramp setting (Figure 18) where improved biological living conditions occurred (Tucker and Wright, 1990).

<u>Facies 4: Bioturbated Wackestone-Packstone</u>

The bioturbated wackestone-packstone facies is composed of peloidal grains (10-25%; 30-100 μm), sponge spicules (10-15%; 0.3-1.0 mm long; variably calcitic/siliceous), brachiopods (5%; disaggregated and up to 1.5 mm), crinoids (5%; disaggregated and up to 1-3 mm), ostracodes (1-2%; 100-400 μm), rare bryozoa (<1%; up to 1.5 mm), rare foraminifera (<1%; 60-80 μm) and undifferentiated carbonate skeletal grains (avg. 65 μm). Mineralogically, Facies 4 is comprised of 63% carbonate (59% calcite/ 4% dolomite), 28% quartz (18% chert/ 10% silt), 4.5% total clays and 3% feldspars. Sedimentologically, variable traction-current and suspension-lamination is accompanied by horizontal and vertical, likely *Cruziana*- or *Skolithos*-type bioturbation (mm- and cm-scale, BI = 2.5) (Figure 23). Porosity and permeability values average 2.1% and 1.5 x 10^{-06} mD, respectively. Thickness ranges from approximately 12 in. (30.5 cm) or less to approximately 20 ft. (6.1 m) and is typically thickest and most prevalent in the middle portion of all three cores with less frequent, thinner units at the uppermost and lowermost portions of each core.

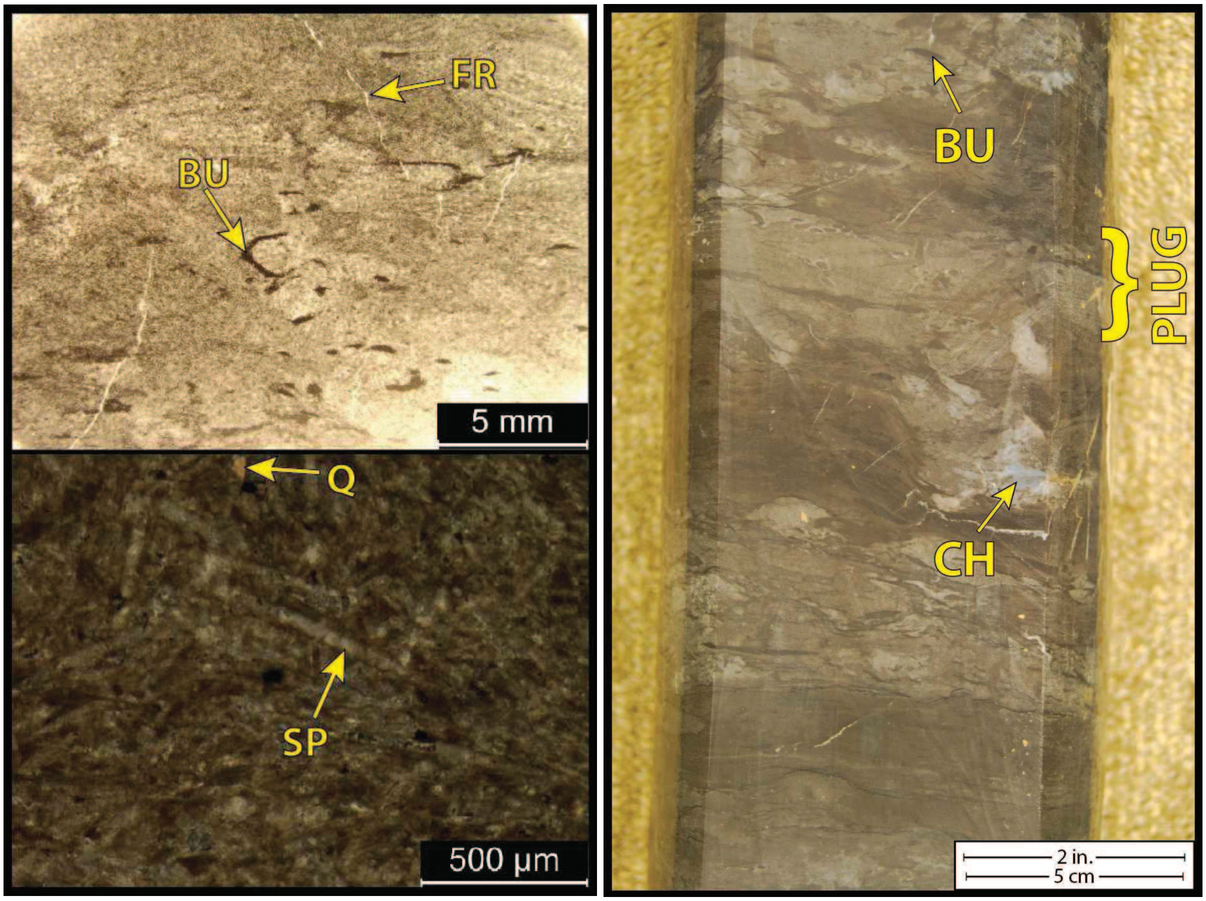

Figure 23. Facies 4: Bioturbated Wackestone-Packstone. Figure illustrates thin section photomicrographs (left; top=PPL; bottom=XPL) from Droke Unit #1: 8,437.6' and the corresponding core photograph (right) from that interval (right). Refer to Table 4 for abbreviations. Note the prevalent bioturbation (mm-cm-scales and horizontal/vertical orientation) and calcite-filled fractures. Sponge spicules are common throughout this facies and are variably siliceous and/or calcitic. Detrital quartz silt (avg. 9%) accompanies the carbonate skeletal grains. Microcrystalline quartz is also a common (18%) component.

Facies 4 is interpreted to represent deposition at or below SWWB in the distal outer ramp environment (Figure 18). Periodic traction-current laminations followed by subsequent suspension-laminated mud wisps are attributed to storm deposition (Kreisa, 1981**;** Appendix A-I-8,468' and Appendix C-I-8,193', among others)**.** An increase in frequency and scale of bioturbation, likely *Cruziana*- or *Skolithos*-type, suggests an increase in oxygen levels compared to that of Facies 3. Preservation of these cm-scale burrows is typically more common in suspension-laminated beds (MacEachern et al, 2009). A moderately diverse fauna of sponge (spicules), brachiopods, crinoids, ostracodes and rare bryozoan and foraminifera suggests a normal marine environment. Relatively larger (1-3 mm) and more abundant (5%) crinoid fragments and both thin- and thick-shelled brachiopods suggests a relatively higher energy environment of deposition than that of Facies 3.

Facies 5: Traction-Current Wackestone-Packstone

The traction-current wackestone-packstone facies (Figure 24) is composed of variably siliceous and/or calcitic sponge spicules (10-20%; avg. 500 μm), peloids (10-20%; avg. 75 μm), bryozoa (5-10%; avg. 100 μm), disaggregated crinoids (5%; avg. 80μm), brachiopods (2.5%; disaggregated debris and up to 3 mm), trace foraminifera (1-5%; 60-100 μm), trace echinoids (1%; avg. 80 μm) and undifferentiated carbonate skeletal grains (avg. 75 μm). Mineralogically, Facies 5 is comprised of 53% carbonate (50% calcite/ 3% dolomite), 42% quartz (31% chert/ 11% silt), 2% total clays and <2% feldspars. Sedimentologically, Facies 5 is moderately to well-sorted and dominated by traction-current lamination, displaying hummocky and swaley cross-stratification, ripple bedding, and truncation surfaces with less common planar laminations (Appendix A-I-8,106’, A-I-8,101’, C-I-8,263’& C-I-8,257’, among others). Variable bioturbation (mm- and cm-scale; likely *Cruziana*- or *Skolithos*-type) is observed in mud-rich interbeds. Porosity and permeability values average 5.6% and 3.3 x 10^{-05} mD, respectively, outperforming all other facies in reservoir quality. These relatively high porosity values are dominated by moldic and vugular porosity within a siliceous chert interval and will be discussed later in more detail. Thickness ranges from approximately 3 ft. (0.9 m) to upwards of 75-100 ft. (22.9-30.5 m). In the Droke Unit #1 core, Facies 5 makes up approximately 250 ft. (76.2 m) of the 504 ft. (154

m) gross “Mississippian limestone” section (or 50%) and is persistent from 8,000’-8,195’ with minor mud wisps/ organic compaction.

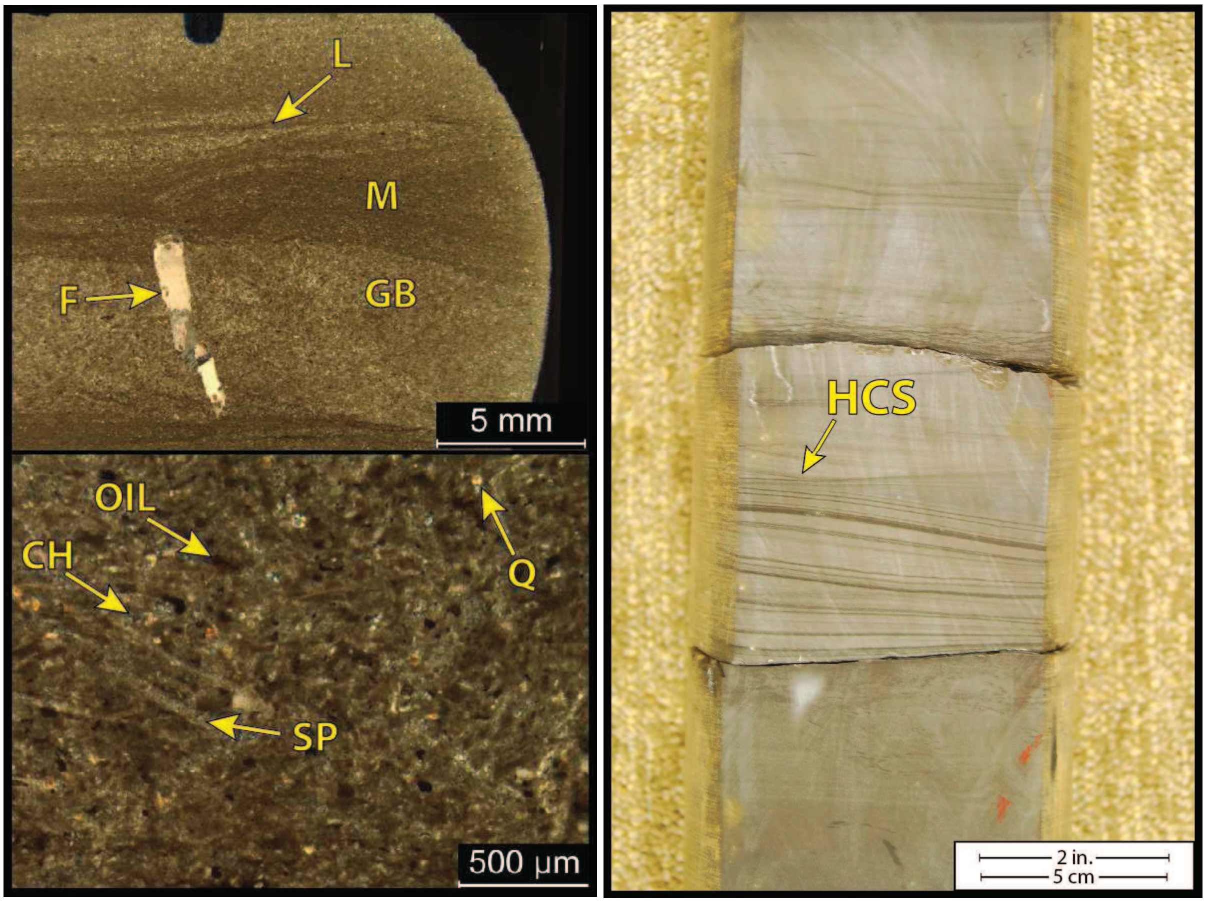

Figure 24. Facies 5: Traction-current Wackestone-Packstone. Thin section photomicrographs from Droke Unit #1: 8,127.7’ under PPL showing traction-current laminations and interbedded mud-rich and grain-rich beds with the latter displaying a higher tendency to fracture. Refer to Table 4 for abbreviations. Detrital quartz silt comprises an average of 11% of this facies. Spicules average 50x500 µm and are variably siliceous/calcitic. Dead oil/organics are also observed within the matrix. Core photograph from Effie B York #1: 8,284’-8,285’ (right) displays hummocky cross-stratification (See Appendix C-I-8,263’& C-I-8,257’, among others).

Facies 5 is interpreted to represent deposition between fair weather wave base (FWWB) and SWWB in the mid-ramp to outer ramp environment (Figure 18). The presence of traction-current laminations, particularly HCS, truncation surfaces and oscillation ripples, suggests an environment periodically reworked by storms (Dott and Bourgeois, 1982; Harms et al, 1982). A diverse fauna of sponge (spicules), bryozoan, foraminifera, crinoids, thick-shelled brachiopods and echinoid fragments suggests a well-oxygenated environment. Observed bioturbation (BI=4-5) displays cm-scale vertical burrows of likely *Cruziana*- or *Skolithos*-type but is commonly absent, indicating a lack of preservation due to the frequent reworking of sediment in the storm-dominated ramp (Howard and Reineck, 1980). Common peloids (10-20%) within Facies 5 are interpreted to represent deposition in a relatively shallow and restricted marine environment (Tucker and Wright, 1990).

<u>Facies 6: Skeletal Packstone-Grainstone</u>

The skeletal packstone-grainstone facies (Figure 25) is composed of crinoids (10%; up to 750 µm), echinoids (7.5%; avg. 800 µm plates), peloids (5%; avg. 70 µm), brachiopods (2.5%; avg. 800 µm and disaggregated), bryozoa (1-2.5%; avg. 800 µm), sponge spicules, (1%; avg. 100 µm), ostracodes (1%; avg. 500 µm) and undifferentiated carbonate skeletal grains (avg. 70 µm). Large skeletal grains, particularly brachiopods and crinoids, variably display calcite cementation, occluding primary porosity. Dissolution of these bioclasts was also variably observed. Mineralogically, Facies 6 is comprised of 58% carbonate (54% calcite/ 4% dolomite), 29% quartz (25% silt/ 4% chert), 8% feldspars, 4% total clays, and 1% other minerals. Its 25% quartz silt/very-fine sand is the highest out of all six facies. Sedimentologically, Facies 6 is traction-current laminated, displaying planar and ripple cross laminations and truncation surfaces. Bedforms range from thinly bedded wavy and flaser bedding to massive bedding. Porosity and permeability values average 3.6% and 2.8 x 10^{-06} mD, respectively. Thickness ranges from 6 in. (15.2 cm) to approximately 15 ft. (4.6 m). Facies 6 is only found in the uppermost portion of each core.

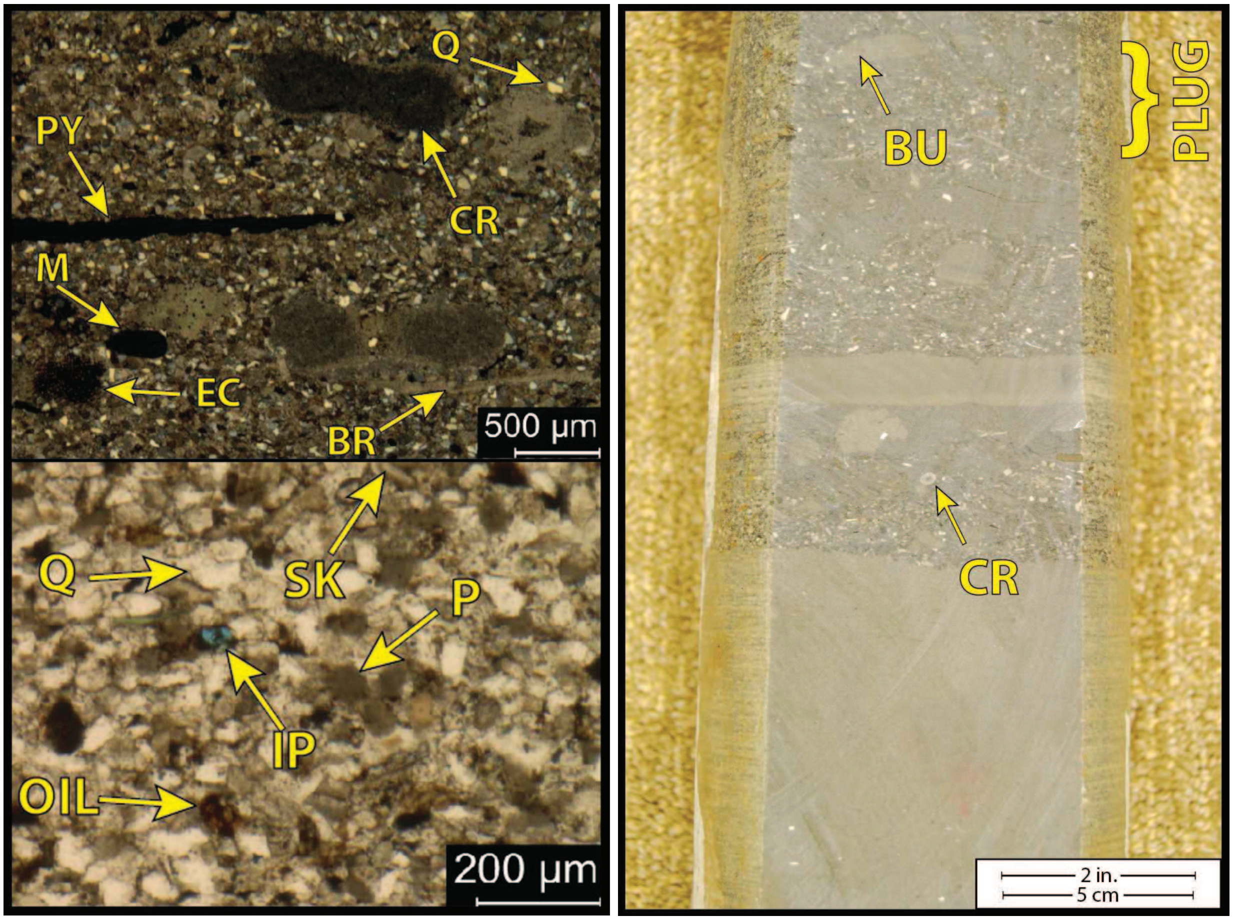

Figure 25. Facies 6: Skeletal Packstone-Grainstone. Thin section photomicrographs (left) from Effie B York #1: 7,983.2' and core photograph (right) of that interval. Photomicrographs taken under PPL (bottom) and XPL (top). Refer to Table 4 for abbreviations. Facies 6 consists of a more diverse carbonate skeletal grains of brachiopods, echinoids and crinoids, among others. Quartz silt-very fine sand (avg. 25%) and feldspars (avg. 4%) are most prevalent in this facies. Calcite cementation (avg. 9.6%) commonly occludes primary intergranular porosity. Note the interparticle porosity and dead oil/ oil staining between quartz and carbonate grains. Seldom (avg. BI=0.06) cm-scale horizontal burrows were observed.

Facies 6 is interpreted to represent deposition within the mid-ramp and distal ramp crest environment (Figure 18). Traction-current deposition indicated by planar laminations, truncation surfaces and flaser bedding suggests a relatively high-energy environment near or just below FWWB (Flügel, 2010). The variable presence of peloids suggests a somewhat restricted environment. A more diverse and generally larger faunal assemblage consisting of crinoids, echinoids (plates), thick-shelled brachiopods, bryozoan and rare sponge spicules and ostracodes indicates a well-oxygenated, normal marine environment. The increased abundance and relative size (up to very fine sand) of detrital quartz also suggests a higher-energy environment of deposition more proximal to a siliciclastic source.

"MISSISSIPPIAN LIMESTONE" SEQUENCE STRATIGRAPHY

Identifying the sequence stratigraphic framework of the "Mississippian limestone" is crucial to defining the controlling factors responsible for reservoir development and distribution. The ideal vertical succession of facies (Figure 26) is representative of one complete rise and fall of sea level. Incomplete regression of this ideal vertical succession and the initiation of a new transgression marked by a landward shift in facies revealed stacking patterns of hierarchical levels of sea level cyclicity. Four hierarchical levels of cyclicity were observed and are inferred to represent 2^{nd}-, 3^{rd}-, 4^{th}- and 5^{th}-Order as defined by Kerans and Tinker (1997) and Read et al. (1995). Correlating these genetically related sequences (3^{rd}-Order), high-frequency sequences (4^{th}-Order) and high-frequency cycles (5^{th}-Order) between their respective cores established the sequence stratigraphic framework. Distinct wireline log signatures that reliably captured sequence and high-frequency sequence boundaries were used to extrapolate the framework throughout the study area. This technique results in more accurate chronostratigraphic subsurface maps and identifies the likely mechanisms responsible for reservoir development, lateral distribution and vertical compartmentalization. While not all 4^{th}- and 5^{th}-Order high-frequency sequences and cycles were mapped, they impart considerable vertical heterogeneity into the composite sequence (3^{rd}-Order) and ultimately control production-scale reservoir flow units in carbonates and mixed carbonate/siliciclastic systems (Grammer et al, 2004).

Idealized Vertical Facies Succession

In the study area, six lithofacies were observed within the "Mississippian limestone" and have been interpreted to represent deposition within a carbonate ramp environment (Figures 18 & 26). According to Walther's Law of Facies successions (Middleton, 1973), these depositional facies occurred areally along the ramp setting at any one time during the Mississippian. Relative and eustatic sea level fluctuations are responsible for the areal migration of these distinct depositional environments and results in their vertical stacking. The ideal vertical succession of facies experienced during one complete rise and fall of sea level is representative of a relatively rapid transgression and a gradual, shallowing-upward regression (Figure 26). To represent this, transgressions are illustrated by upward pointing blue triangles and regressions are illustrated by downward pointing red triangles. Incomplete expressions of this ideal vertical succession in the form of a distinct landward shift in facies belts indicated by a return to lower-energy facies were interpreted to represent an incomplete regression (red triangle) and the initiation of a new transgression (blue triangle). Identifying these landward shifts in facies belts revealed stacking patterns indicative of hierarchical levels of relative cyclicity of sea level.

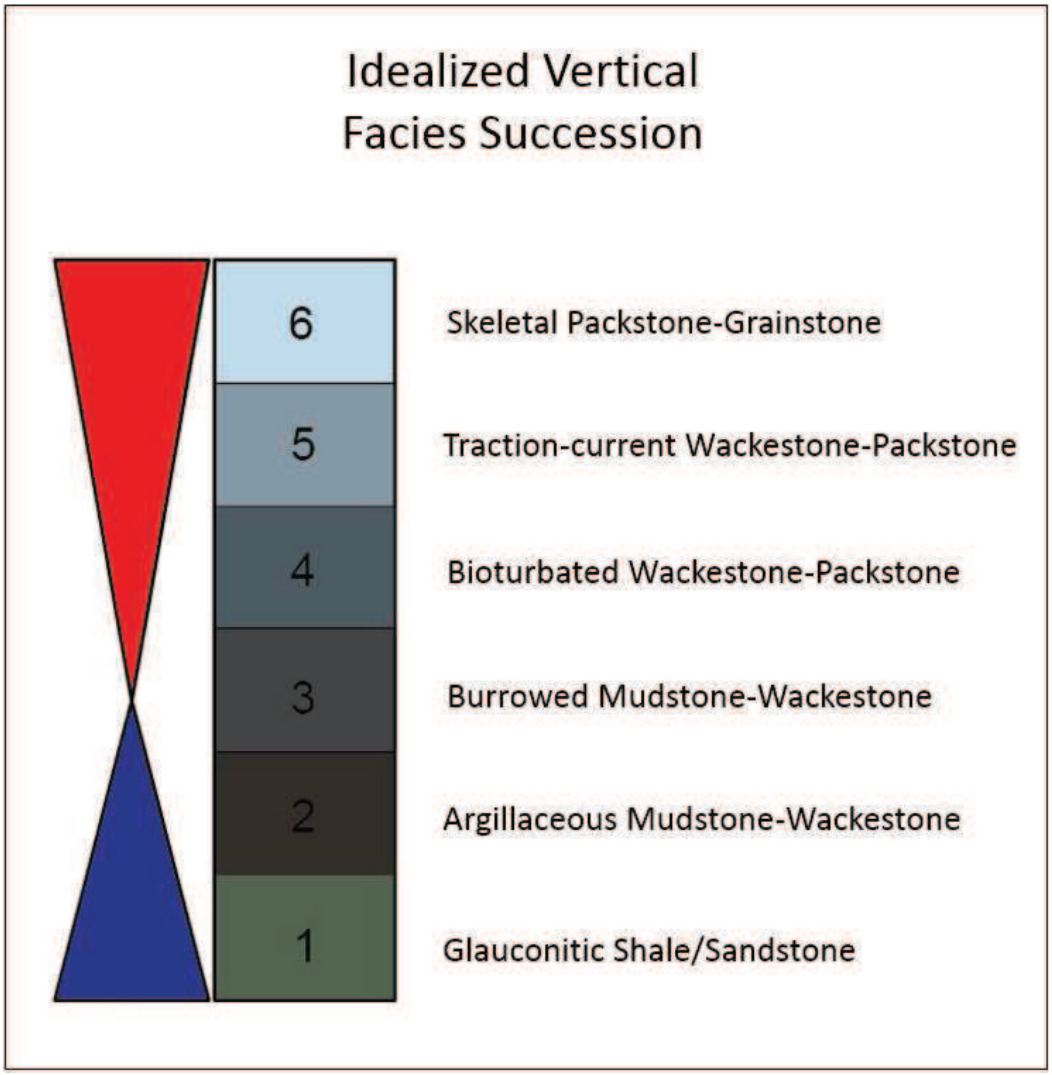

Figure 26. Idealized Vertical Facies Succession. The six facies identified through core and thin section analyses of the "Mississippian limestone" in the study area are representative of the depositional environments experienced during one complete rise and fall of base level. Relatively rapid transgression (blue triangle) resulted in the deposition of glauconitic shale/sandstone and argillaceous to burrowed mudstones and wackestones. Subsequent regression (red triangle) results in shallowing-upward lithofacies represented by bioturbated wackestones and packstones and traction-current laminated and variably fossiliferous packstones and grainstones. An increasing abundance of detrital quartz was also observed in the regressive phase of this ideal vertical facies succession.

The average abundance of detrital quartz shows trends related to their interpreted depositional environments (Figure 27). Facies 1 contains an average of 23% detrital quartz deposited during the initial transgression. This abundance decreases within Facies 2 and Facies 3 when carbonate productivity is established. During regression of the ideal vertical succession, the abundance of detrital quartz shows an increasing trend in Facies 4 through Facies 6. A general correlation between the abundance of detrital quartz and porosity is observed but it is unclear whether this siliciclastic component is the dominant driver of porosity in the observed facies (Figure 27).

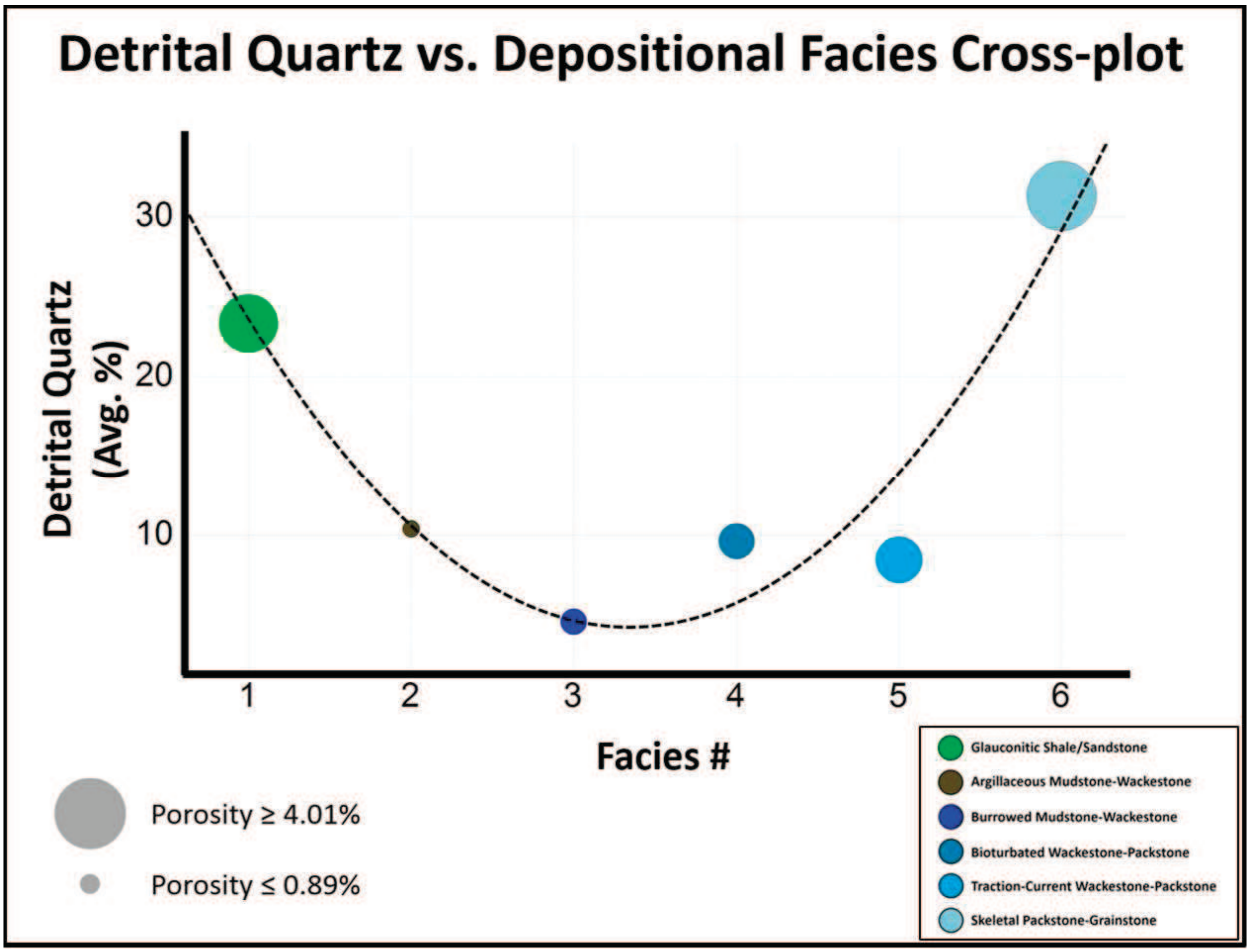

Figure 27. Cross-plot of the observed depositional facies (1-6) on the x-axis and average percentage of detrital quartz silt/ very-fine sand per depositional facies on the y-axis. Data points are sized by the average porosity for each facies and are color coded based on their facies classification. Intervals containing abundant diagenetic chert (within Facies 5) were excluded from the cross-plot. Detrital quartz is relatively high in Facies 1 (avg. 23%), decreases to 4.6% in Facies 3, and then increases to 31% in Facies 6. Average porosity is relatively high in Facies 1 (3.3%) and Facies 6 (4%) and is lowest in Facies 2 (0.89%) and Facies 3 (1.44%). A correlation between the average percentage of detrital quartz and average porosity was not observed in Facies 3 through Facies 5.

Sequence Stratigraphic Hierarchy

Four levels of cyclicity were observed in the cored intervals that demonstrate hierarchical controls on deposition revealed through the vertical stacking patterns of facies (Figure 28). These four levels have been termed "2nd-, 3rd-, 4th- and 5th-Order" to represent their nested position within the observed hierarchy and have not been biostratigraphically constrained to confirm their true durations and causal mechanisms. However, it is important to note that for the purpose of this study, the biostratigraphic resolution of the "Mississippian limestone" has a maximum temporal resolution of only 1-3 million years and thus can only differentiate sequences of a 3rd-Order scale at best. Such data would not provide the resolution required to correlate high-frequency sequences and cycles that may be responsible for production-scale reservoir heterogeneity.

In this study, the entire cored interval of the "Mississippian limestone" is interpreted to represent a 2nd-Order sequence and displays an overall shallowing-upward signature from the organic-rich Devonian Woodford Shale to silty skeletal packstones and grainstones (Facies 6) at the top of the "Mississippian limestone". An increase in the abundance of detrital grains was observed from bottom to top of the cored intervals. Approximately <2% to 12% quartz silt and 2% feldspars were observed at the base of the "Mississippian limestone" and increases to approximately 31% quartz silt/ very fine sand and 8.3% feldspars at the top. Four 3rd-Order sequences comprise this approximately 515 ft. (157 m) gross interval that each contain two more nested levels (frequencies) of sea level cyclicity. 4th-Order high-frequency sequences (HFSs) and 5th-Order high-frequency cycles (HFCs) are interpreted to be the result of Milankovitch-band sea level cyclicity and tend to control the fundamental reservoir flow units of many carbonate reservoirs (Grammer et al, 2004). Defining the hierarchical position of hydrocarbon reservoirs identifies the likely mechanisms responsible for their development.

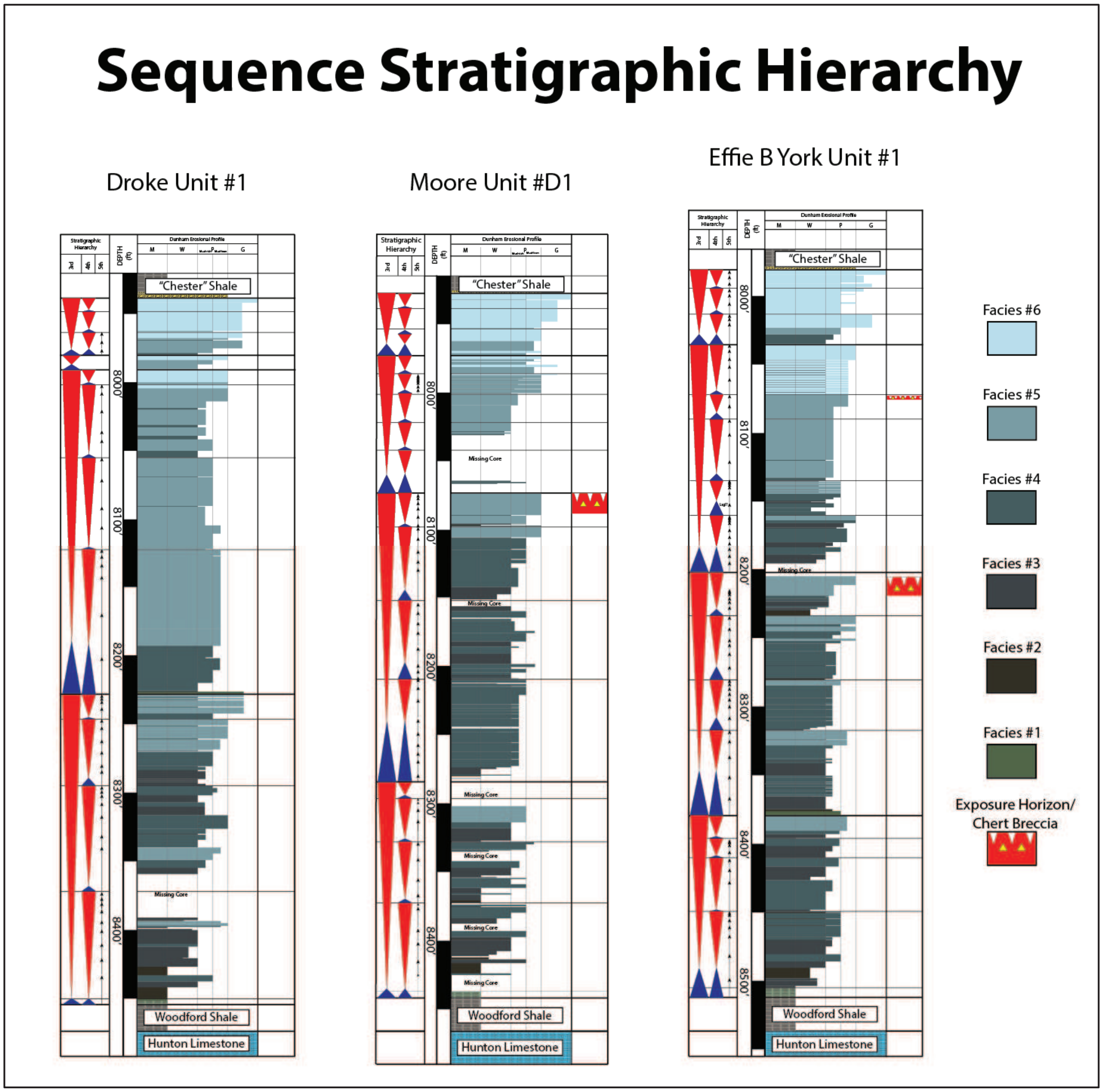

Figure 28. Sequence Stratigraphic Hierarchy. The "Mississippian limestone" of the study area displays four hierarchical levels of sea level cyclicity. The entire cored interval represents a 2nd-Order sequence and displays a shallowing-upward signature from the Devonian Woodford Shale below (above the Hunton limestone) to silty, and variably fossiliferous packstones and grainstones (Facies 6) at the top of the gross interval beneath the "Chester" Shale. Subaerial exposure horizons are indicated by the red figure in the right column of each cored interval. Four 3rd-Order sequences were observed that display a shallowing-upward signature (see Figure 26) and contain multiple 4th-Order HFSs within them. 5th-Order HFCs were variably observed (black arrows). HFSs and HFCs are interpreted to be the result of high-frequency, Milankovitch-band sea level cyclicity.

3^{rd}-Order Sequences

Four 3^{rd}-Order sequences (S1-S4) were observed that range in thickness from approximately 10 to 225 ft. (3-69 m). The base of each 3^{rd}-Order sequence is marked by a distinct deepening of facies types (Facies 1/2) relative to the underlying facies (Facies 5/6), indicative of a landward shift in facies belts due to a rise of relative sea level (Price, 2014; LeBlanc, 2014; Childress and Grammer, 2015). An overall shallowing-upward succession to higher-energy facies (Facies 5/6) was observed in the 3^{rd}-Order sequences indicative of a gradual decrease in relative sea level. These were assumed to be of probable 3^{rd}-Order due to the known occurrence of multiple 3^{rd}-Order sequences during the Mississippian Subsystem, their typical thickness and that they contain two hierarchical levels of cyclicity (4^{th}- and 5^{th}-Order) nested within them (Figure 28; Reid and Dorobek, 1991; Read, 1995; Sonnenfeld, 1996; Kerans and Tinker, 1997; Smith Jr., et al., 2004; Westphal et al., 2004; Haq and Schutter, 2008). Each 3^{rd}-Order sequence contains anywhere from three to five nested 4^{th}-Order high-frequency sequences (Figure 28).

Sequences 1 and 2 (S1 & S2) thicken to the northwest, or in an up-dip direction in relation to depositional strike whereas Sequences 3 and 4 (S3 & S4) thicken to the southeast in a down-dip, distal direction (Figures 12 & 28). Of note, S2 is capped by an exposure horizon in the Moore Unit #D1 and Effie B York Unit #1 cores indicated by dissolution pipes, vugs, chert breccia and trace terra rossa occurring within Facies 5, forming a potential hydrocarbon-bearing reservoir (Figure 28). These features were not observed in the Droke Unit #1 core and either were not subjected to the same diagenetic conditions during exposure or were not encountered by the specific placement of the borehole. The overlying 3^{rd}-Order sequence (S3) is abnormally thin (approximately 10 ft. (3 m)) in the Droke Unit #1 core and is interpreted to be the result of a decrease in accommodation following the S2 regression and progradation of S3 basinward to the southeast (Figures 12 & 28). S4 is characterized by the highest percentages of detrital quartz (avg. 30.5% quartz silt-very fine sand) and feldspars (avg. 8.3 %) of the four 3rd-Order sequences and is likely due to the long-term, 2nd-Order regression throughout the "Mississippian limestone". Intergranular porosity between detrital quartz grains of this sequence form the secondary reservoir within the study area.

High-Frequency Sequences (4th-Order)

4th-Order high-frequency sequences (HFSs) were recognized throughout the cored intervals, each displaying a shallowing-upward signature. A distinct landward shift in facies belts marks the base of HFSs where relatively lower energy facies (F2-F3) directly overlie higher energy facies (F4-F6) (Figure 28). HFSs range in thickness from approximately 10-100 ft. (3-30 m) and typically follow the depositional succession of their parent 3rd-Order sequence. High-frequency sequences thicken-upward during the transgressive phase of their parent 3rd-Order sequence and thin-upward during the regressive phase.

High-frequency sequences were not recognized within S3 of the Droke Unit #1 core where S3 was interpreted to be abnormally thin (10 ft. (3 m)). High-frequency sequences are thickest within S2 and thinnest at the bottom and top of each cored interval (S1 and S3-S4) and are interpreted to be the result of Milankovitch-band, eccentricity-driven glacioeustacy. Within S3, high-frequency sequence 4 (S3-HFS4) is characterized by a thin (2.5 ft. (0.76 m)) exposure horizon in the Effie B York Unit #1 core indicated by chert breccia, dissolution pipes and terra rossa that is similar in lithology to the previously described exposure horizon occurring at the top of S2. This interval contains partial molds and vugular porosity averaging 5-7% and was not observed in the more proximal Moore Unit #D1 and Effie B York Unit #1 cores (Figure 28).

High-Frequency Cycles (5th-Order)

5th-Order high-frequency cycles (HFCs) were variably observed throughout the cored intervals (Figure 28, black arrows). These highest frequency, sea-level driven cycles typically represent the fundamental reservoir flow units of many carbonate reservoirs (Grammer et al., 2004). HFCs were most often recognized by cm-scale flooding surfaces marked by mud wisps followed by a shallowing upward signature of facies types indicating a return to a relatively higher-energy environment of deposition. The likely occurrence of autocyclic and allocyclic processes clouds the interpretation of these cm-scale features.

High-frequency cycles range in thickness from approximately 1-30 ft. (0.3-9 m) and follow the trend and depositional succession of their parent HFS. Stacking patterns of HFCs, like that of HFSs, display a thickening-upward pattern during the transgressive phase of their parent HFS and a thinning-upward pattern during the regressive phase. High-frequency cycles are interpreted to be the result of Milankovitch-band glacioeustacy, likely related to precession and obliquity. The upper portion of each core included in this study, and specifically within S4, proved most problematic at identifying HFCs. In this upper portion of the "Mississippian limestone" the gross lithology is predominantly characterized as traction-current and variably fossiliferous packstones and grainstones with significant amounts (20-40%) of detrital quartz silt-very fine sand (Facies 5 & 6). The depositional processes responsible for such facies inherently have the potential to remove or rework cm-scale flooding surfaces. Identification of HFCs in areas of sparse core and/or thin section data was supplemented by wireline log signatures.

The boundaries of the observed stratigraphic hierarchy were first correlated between the cored intervals, developing the sequence stratigraphic framework. Boundaries were defined by the vertical stacking of nested high-frequency sequences and cycles and supplemented and/or confirmed by the nature or degree of the juxtaposed depositional facies. For example, a 4th-Order high-frequency sequence boundary is identified where 5th-Order cycles progressively thin upward and are overlain by an abrupt landward shift in facies belts (as defined above for 4th-Order HFSs) followed by a return to comparatively thicker 5th-Order cycles (Figure 28-Effie B York Unit #1: 8,450'-8,510'). Likewise, the vertical stacking patterns of 4th-Order HFSs define the boundaries of 3rd-Order sequences. These boundaries were correlated sequentially to the other cores studied, regardless of lithologic character. This approach developed a sequence stratigraphic framework that more accurately correlates the inferred genetically-related sequences and cycles that can then be tied to discrete wireline log signatures to extrapolate the framework throughout the study area.

Wireline Log Correlation

The boundaries between these hierarchical sequences and cycles of the stratigraphic framework were tied to their respective suites of wireline log signatures to extrapolate the stratigraphy in the subsurface (Figures 29, 30 & 31). The repetitive nature of the observed depositional lithofacies results in wireline log signatures that record relatively similar lithologies. Correlating sequence and cycle boundaries from the core-defined sequence stratigraphic framework results in more accurate extrapolation of chronostratigraphic units and ultimately defines the lateral connectivity of hydrocarbon reservoirs. The method used in this study directly contradicts the lithostratigraphic approach of forced extrapolation of arbitrary log signatures and is an essential step to identifying production-scale reservoir heterogeneities.

Gamma ray and resistivity curves were tied to sequence and cycle boundaries of the stratigraphic framework. This guard resistivity curve, run only on the Moore Unit #D1 core, proved most effective at identifying the boundaries of all hierarchical levels when compared to deep resistivity curves (Figures 29 & 30). The fine (approximately 3-6 in. (8-16 cm)) vertical resolution of this signature provided a sharp, readily identifiable change in resistivity values at sequence and cycle boundaries (Figure 29). This signature corresponds to the landward shift in facies belts and vertical stacking of lower-energy mudstones and wackestones (relatively low resistivity) on top of higher-energy packstones and grainstones (relatively high resistivity). The gamma ray curve, while effective at identifying boundaries of 2^{nd}- and 3^{rd}-Order sequences, did not reliably identify the more discrete boundaries of higher-frequency (4^{th}- and 5^{th}-Order) cycles and was therefore not as effective at identifying production-scale heterogeneities within the stratigraphy (Figure 30). Extrapolating these discrete log signatures with respect to the defined stratigraphic framework results in more precise subsurface correlations that identify production-scale variability (Figure 31).

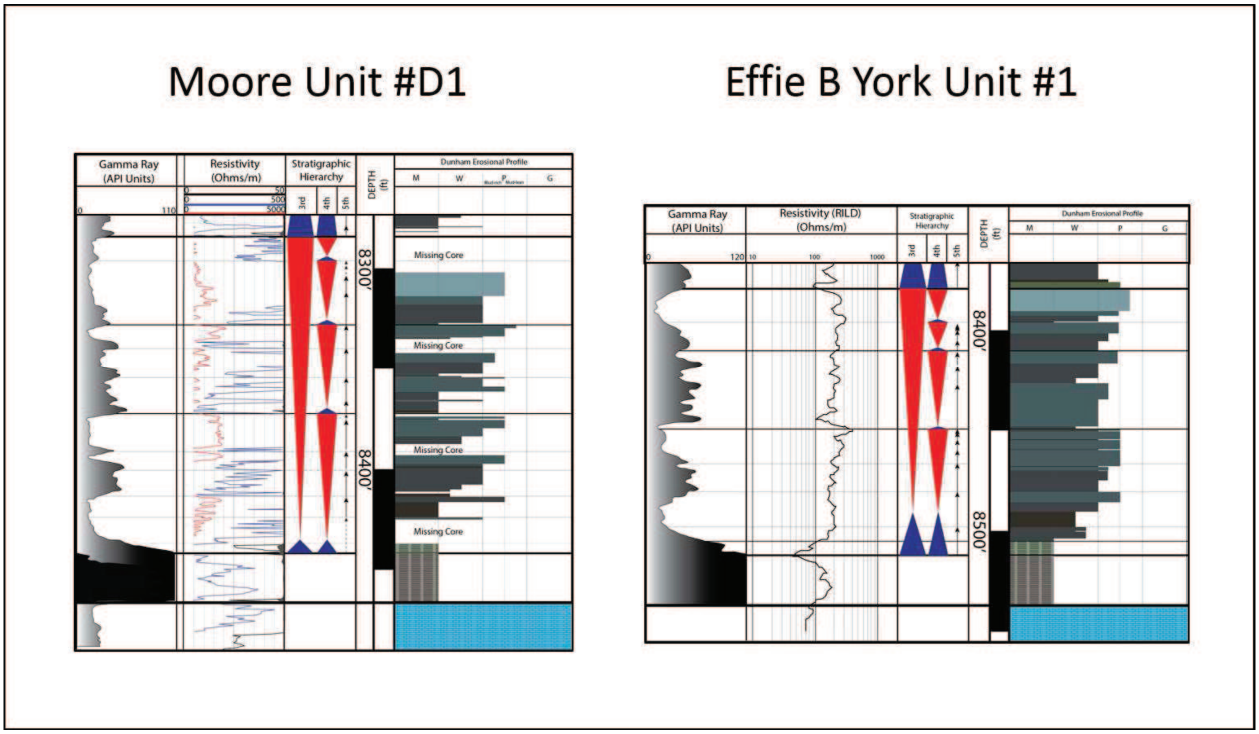

Figure 29. Wireline Log Signatures. Core-to-log example from S1 of both the Moore Unit #D1 and Effie B York #1 cores. Tracts from left to right in each core graphic: Gamma ray, resistivity, stratigraphic hierarchy (3rd-, 4th- and 5th-Order), depth (ft.) and horizontally-exaggerated Dunham classification (color-coded based on facies). Note the differences in identifying flooding surfaces between the guard resistivity curve (Moore Unit #D1) and the RILD resistivity curve (Effie B York #1). See Figure 30 for illustration of the core-to-log tie of the three cores included in this study.

RESULTS

The high-resolution sequence stratigraphic framework of the "Mississippian limestone" within the study area identifies the controlling factors responsible for reservoir development and distribution. Reservoir development is a function of the primary depositional facies and the sequence stratigraphic hierarchy. Primary reservoir development is controlled by 3rd-Order subaerial exposure of the S2 sequence and is dependent on the primary depositional facies (Facies 5). A lithologically similar, although thin, unit was also observed where Facies 5 was subaerially exposed at the top of S3-HFS4. Secondary reservoir development may be driven by the increased abundance of siliciclastic influx due to long-term, 2nd-Order regression throughout the Mississippian. Reservoirs are vertically compartmentalized by 4^{th}- and 5^{th}-Order high-frequency sequences and cycles that ultimately control production-scale reservoir flow units. When extrapolated, guard resistivity log signatures expressed sequence and cycle boundaries that were consistently more reliable than gamma-ray signatures. The high-resolution sequence stratigraphic analysis of the "Mississippian limestone" of the study area more accurately defines the mechanisms responsible for reservoir development and heterogeneities experienced on a sub-regional scale.

Sequence Stratigraphic Architecture

The sequence stratigraphic architecture of the "Mississippian limestone" observed in the study area displays strike-elongate geometries characteristic of a carbonate ramp environment (Ahr, 1973; Ward and Brady, 1979; Tucker and Wright, 1990). Sequence and high-frequency sequence gross isopach maps illustrate that any given contour is consistent for 10s to 100s of kilometers along depositional strike and displays relatively abrupt (few kilometers) variability in a depositional dip direction (Figures 32 & 33). Progradation of 3^{rd}-Order sequences was observed (S3 and S4 of Figures 30 & 31) and is a result of an overall decline in sea level throughout the Mississippian System (2^{nd}-Order), likely due to the transitional global climate from greenhouse to icehouse (Haq and Schutter, 2008). While HFCs were variably observed and difficult to correlate, their presence within the stratigraphic hierarchy suggests that they impart considerable vertical heterogeneity into the stratigraphy and ultimately compartmentalize reservoirs at the production-scale.

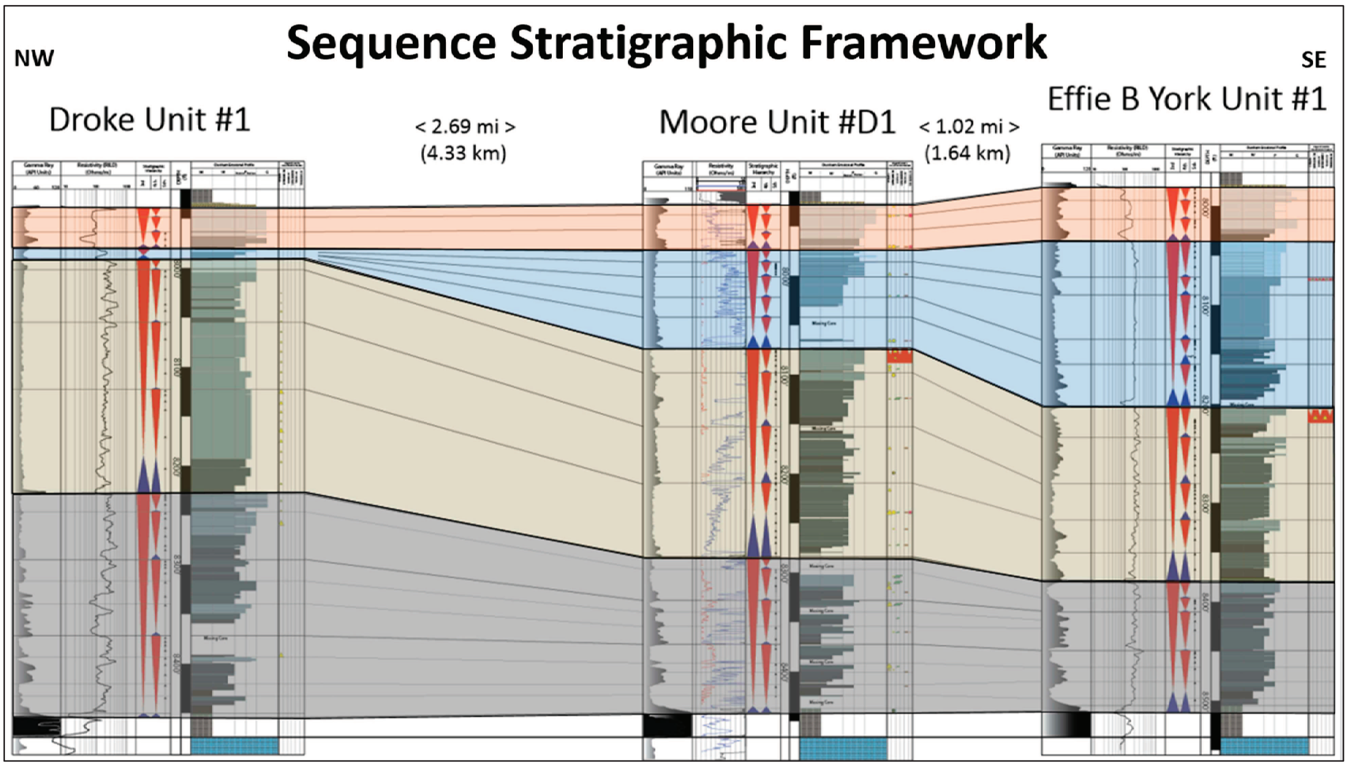

Figure 30. Scaled Sequence Stratigraphic Cross Section. Each cored interval from left to right displays: gamma ray curve, resistivity curve, sequence stratigraphic hierarchy (3rd-, 4th- and variably 5th-Order), the Dunham classification horizontally-exaggerated and color-coded for the observed depositional facies (see Figure 26). Sequences are shaded to illustrate their geometry (S1-gray; S2-tan; S3- light blue; S4- light orange). The sequence stratigraphic framework consistently ties to wireline logging signatures, particularly the Guard resistivity curve, at 3rd- and 4th-Order boundaries.

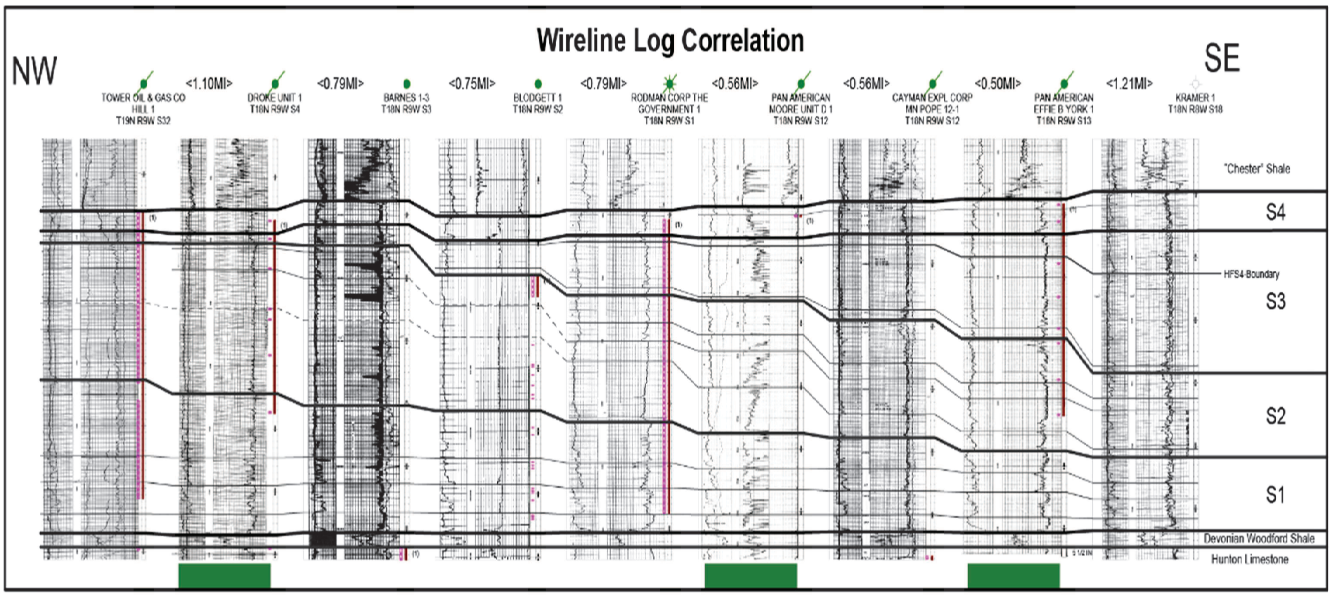

Figure 31. Wireline Log Correlation. Cross section is oriented nearly perpendicular to depositional strike (NW-SE) through the study area (See Figure 32). Green boxes indicate cores included in this research. Stratigraphic datum is the top of the Hunton Limestone/ base of the Devonian Woodford Shale. Bold correlation lines indicate sequence boundaries. Thinner correlation lines indicate variably correlative boundaries of higher-frequency HFSs and HFCs. Note the thickening of S1 and S2 to the NW (landward) and thickening of S3 and S4 to the SE (basinward). This progradation in a basinward direction is interpreted to be the result of the 2nd-Order decline in sea level throughout the Mississippian.

Sequence 1

Sequence 1 (S1) is bound by the contact between the underlying Woodford Shale of likely Devonian age and overlying glauconitic shale (Facies 1) at its base. In all three cores included in this study, S1 is recognized on wireline logs by a sharp change in gamma ray values from approximately 200 API Units to <100 API Units and a sharp change in resistivity values from approximately 125 ohm/m to 25 ohm/m (Figures 29 & 30). Sequence 1 displays an overall shallowing-upward signature to Facies 5 and contains four nested 4^{th}-Order HFSs.

Sequence 1 thickens from approximately 125 ft. (38 m) in the Effie B York Unit #1 core to approximately 227 ft. (69 m) in the more proximal Droke Unit #1 core due to aggradation (Figures 12, 30, 31 & 32). The uppermost 10-35 ft. (3-10.7 m) of S1 is characterized as a slightly dolomitic (avg. 8-10%) expression of Facies 5 and displays intergranular and intercrystalline porosities averaging from 2-5% accompanied by oil-staining in thin section (Appendix C-II-8,260' & 8,236.5'). The upper boundary of S1 is coincident with the base of the overlying S2 indicated by a landward shift of facies belts resulting in deposition of a glauconitic sandstone (Facies 1; Figure 30).

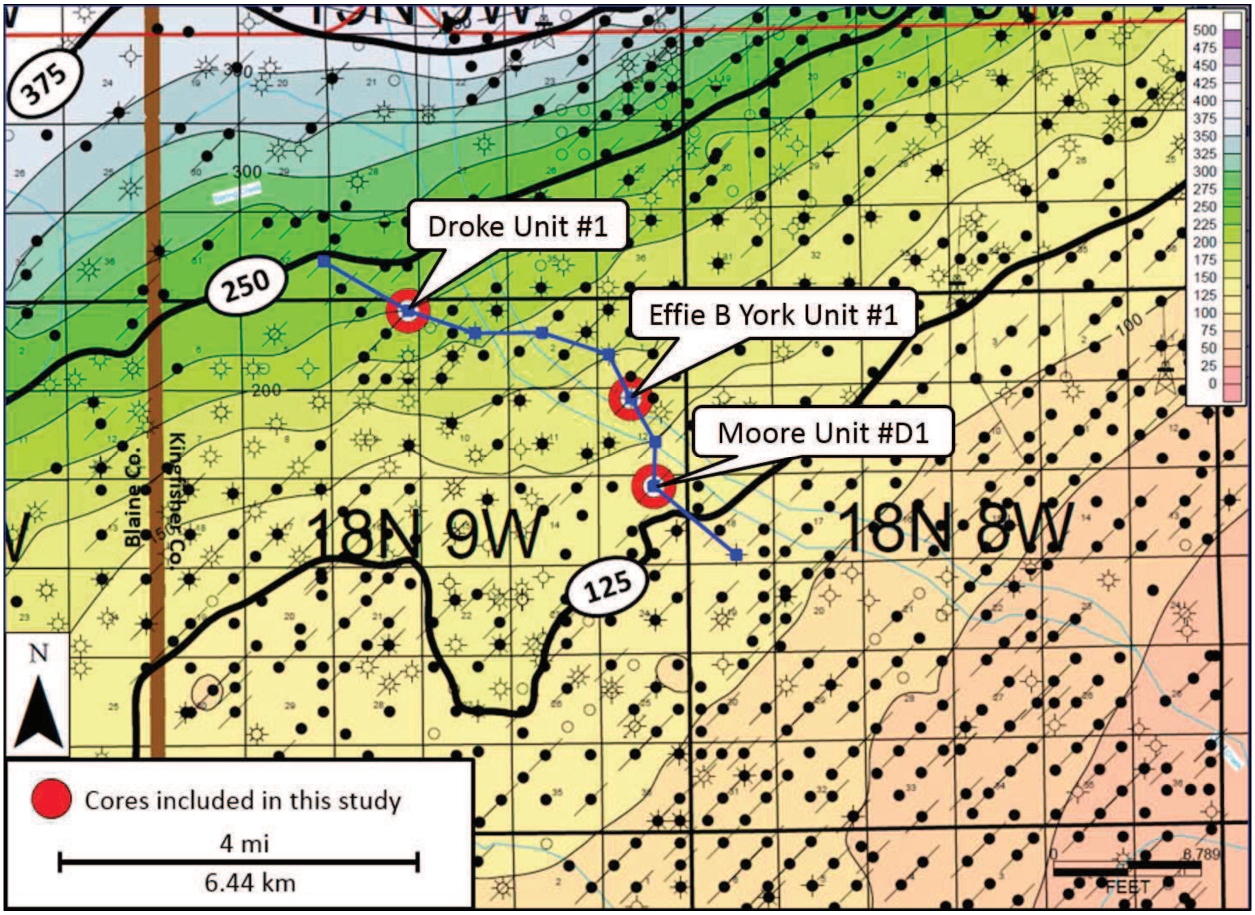

Figure 32. Sequence 1- Gross Isopach. Contour Interval = 25 ft. (7.6 m). Location of cores indicated by red circles. Cross-section (blue; Figure 31) oriented oblique to depositional-dip. Tan and yellow indicate relatively thin areas and green and light blue indicate thicker areas of S1. Note the thickening in a proximal direction to the northwest due to aggradation. Also note the strike-elongated geometry (NE-SW), a typical characteristic of carbonate ramp environments.

Sequence 2

Sequence 2 (S2) is bound by a glauconitic sandstone (Facies 1) at its base and displays an overall shallowing-upward signature to higher-energy facies (Facies 5 & 6). This boundary is consistently recognized on wireline log signatures by an increase in gamma ray values from approximately 10-15 API Units to 80-100 API Units and a decrease in resistivity values from approximately 200-300 ohm/m to 30-100 ohm/m (Figures 29, 30 & 31). Sequence 2 contains four nested 4th-Order HFSs that were consistently observed in the Effie B York Unit #1 and

Moore Unit #D1 cores. In the Droke Unit #1 core, these HFSs were not consistently observed where approximately 90 ft. (27 m) of S2 is dominated by centimeter to less common decimeter-scale amalgamated wavy and flaser bedding, and traction-current ripple laminations with variable HCS (Facies 5; Appendix C-I-8,193'-8,194') interpreted to have been deposited within the storm-dominated ramp.

Approximately 177 ft. (54 m) thick in the Effie B York Unit #1 core, S2 thickens to approximately 236 ft. (72 m) in the more proximal Droke Unit #1 core due to aggradation (Figures 12, 31, & 33). In the more distal Effie B York Unit #1 and Moore Unit #D1 cores, the uppermost 17-25 ft. (5-7.6 m) of S2 is characterized by a highly siliceous (60-80% chert) subaerial exposure horizon indicated by dissolution pipes, chert breccia and faint terra rossa occurring within Facies 5 (Estaban and Klappa, 1983; Figures 12, 30 & 35; Appendix B-I-8,096'-8,073'; A-I-8,214'-8,215'; Appendix A-I-8,205'-8,206'; A-II-8,206'; B-II-8,075.2'). Intergranular, moldic and vugular porosity averages from 4-12% with an average permeability of 3.46×10^{-6} mD. This characteristic lithology is absent in the more proximal Droke Unit #1 core where S2 culminates in a slightly silty (5-10% quartz silt) and fossiliferous packstone (Facies 6). The upper boundary of S2 (base of S3) was observed on wireline log signatures of the Effie B York Unit #1 and Moore Unit #D1 cores by an increase in gamma ray values from approximately 20 API Units to 40-60 API Units and a sharp decrease in resistivity values from approximately 200-1,000 ohms/m to 25-70 ohms/m (Figure 30). This signature is subdued in the Droke Unit #1 curves.

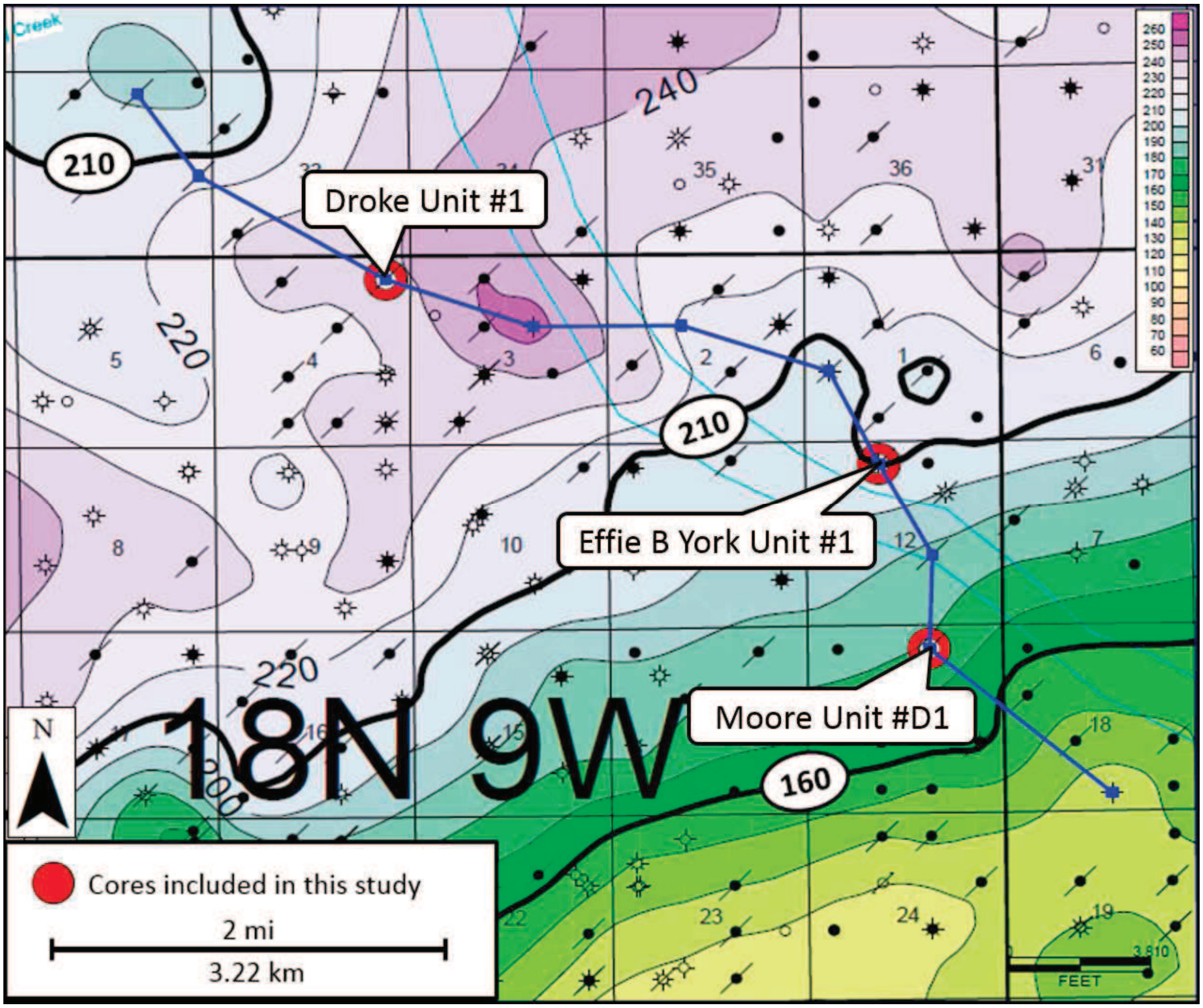

Figure 33. Sequence 2- Gross Isopach. Contour Interval = 10 ft. (3 m). Location of cores included in this study indicated by red circles. Cross-section (blue; Figure 31) oriented oblique to depositional-dip. Color bar displays yellow and green hues thinner than purple hues. The upper boundary of S2 is congruent with the top of an exposure surface (chert breccia, solution pipes) observed in the Effie B York Unit #1 (Sec. 13) and Moore Unit #D1 (Sec. 12) cores. Note the geometry of S2 elongated parallel to depositional strike (NE-SW) with dip-oriented (NW-SE) variability in the northwest corner of the study area (Sections 5 and 9 of T18N-R9W).

Sequence 3

Sequence 3 (S3) is bound by the contact between the underlying S2 and an interpreted landward shift in facies belts. This cored interval is missing in the Effie B York Unit #1 and Moore Unit #1 cores and is interpreted from wireline log signatures by an increase in gamma ray values from approximately 20 API Units to 40-60 API Units and a sharp decrease in resistivity values from approximately 200-1,000 ohms/m to 25-70 ohms/m (Figure 30). In the Droke Unit #1 core, the lower boundary of S3 is indicated by a cm-scale mud wisp followed by Facies 3 that directly overlies Facies 6 of S2 and displays a relatively similar wireline log signature as previously described for the Effie B York Unit #1 and Moore Unit #D1 cores. S3 displays an overall shallowing-upward signature to Facies 6 and contains five HFSs. High-frequency sequences were consistently observed in the Effie B York Unit #1 and Moore Unit #D1 cores yet were not observed in the Droke Unit #1 core (Figure 30).

Approximately 10 ft. (3 m) thick in the Droke Unit #1 core, S3 thickens to approximately 167 ft. (51 m) in the more distal Effie B York Unit #1 core and is interpreted to represent basinward progradation of the ramp system, likely due to long term, 2nd-Order regression of the gross “Mississippian limestone” interval (Figures 30 & 31). Of note, in the more distal Effie B York #1 core, a subaerial exposure horizon characteristically similar to that observed at the top of S2 was observed at the top of HFS4 within Facies 5 (Figure 37). This thin, approximately 2.5 ft. (0.76 m), chert breccia contains approximately 35% microcrystalline quartz and is absent in the proximal Moore Unit #D1 (1.02 miles (1.64 km) away) and Droke Unit #1 cores (Figure 30). Combined visual estimations of vugular, intergranular and moldic porosity values average between 5-7.5% (Figure 37). Although thin, S3-HFS4 is interpreted to be a result of high-frequency cyclicity directly effecting reservoir development. The upper boundary of S3 is observed as the contact between Facies 6 and the overlying Facies 3, indicating a landward shift in facies belts (Figure 30).

Sequence 4

Sequence 4 (S4) is bound at its base by a landward shift in facies (Facies 3 overlying Facies 6) in all three cores, indicating a new transgression. This surface is recognized on wireline log signatures as an increase in gamma ray values from approximately 25-30 API Units to 50-60 API Units and a marked decrease in resistivity values from approximately 200-250 ohms/m to 30-60 ohms/m (Figure 30). Sequence 4 displays an overall shallowing-upward signature to higher-energy facies (Facies 6) and contains three nested HFSs that were consistently observed in all three cores.

Approximately 39 ft. (11.9 m) in the Droke Unit #1 core, S4 thickens to approximately 55 ft. (16.8 m) in the Effie B York Unit #1 core (Figures 30, 31 & 34), representing continued progradation basinward to the southeast. Detrital quartz silt/ very fine sand and feldspars were observed in relatively higher amounts (average 30% & 8%, respectively) within S4 than in any other 3rd-Order sequence. Intergranular porosity between calcite crystals and quartz grains average 3-5%. The upper boundary of sequence 4 was observed as the contact between Facies 6 and the overlying shales and siltstones of likely "Chester" age and is recognized on wireline log signatures as a gradual increase in gamma ray vales from approximately 40 API Units to approximately 60-75 API Units and a relatively sharp decrease in resistivity values from approximately 100-200 ohms/m to less than 10 ohms/m (Figure 30).

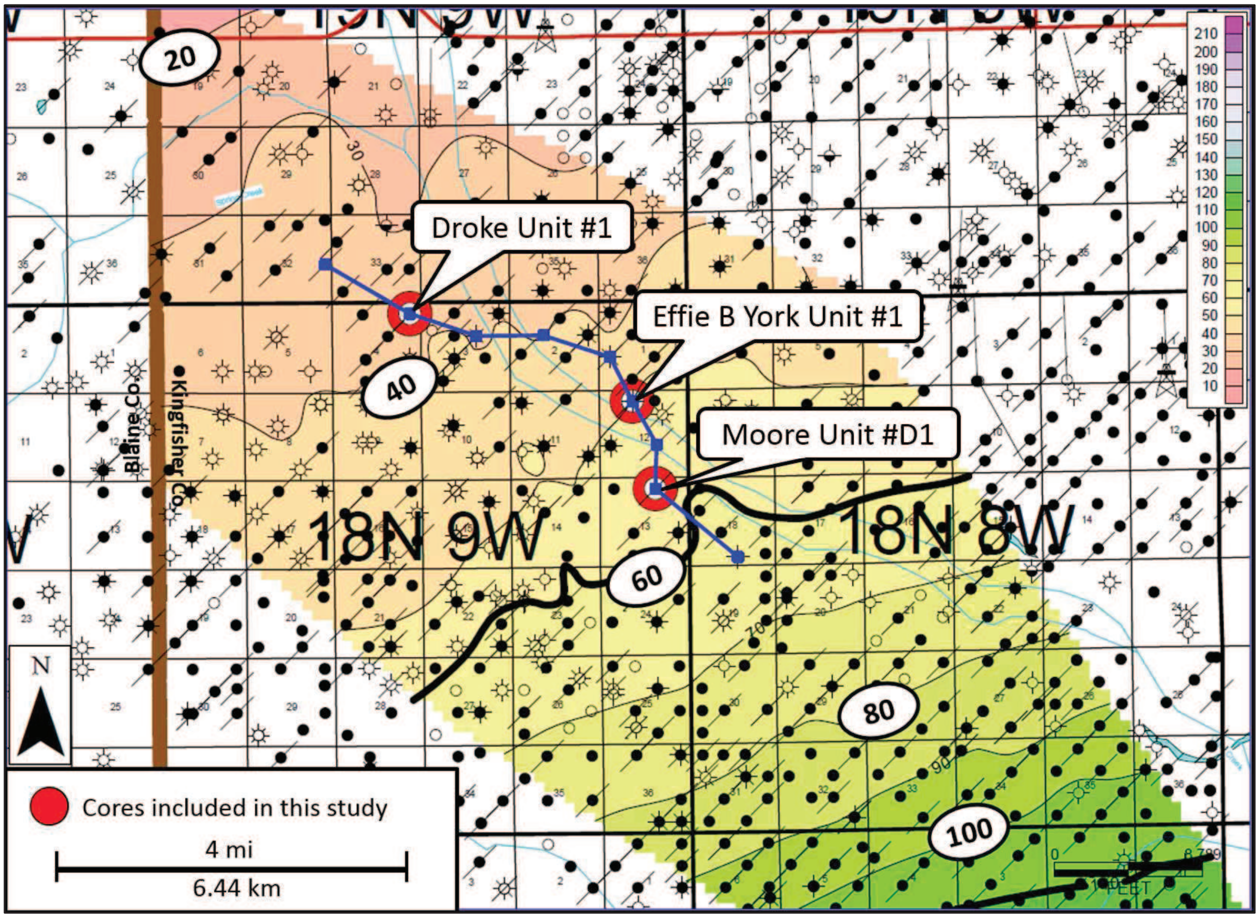

Figure 34**.** Sequence 4- Gross Isopach. Contour Interval = 10 ft. (3 m). Location of cores included in this study indicated by red circles. Cross-section (blue; Figure 31) oriented oblique to depositional-dip. Color bar displays colors and corresponding thickness. Note the geometry of S4 elongated parallel to depositional strike (NE-SW) and thickening to the SE (basinward) due to progradation.

Reservoir Characterization

High-frequency, Milankovitch-band sea level cyclicity is known to impart lateral and vertical variability in the rock record (Kerans et al., 1994; Grammer et al., 2004). Reservoir development within the "Mississippian limestone" of the study area is controlled by both the primary depositional facies and the sequence stratigraphic hierarchy. The primary reservoir occurs within Facies 5 at the top of the regressive phase of S2 in the Effie B York Unit #1 and Moore Unit #D1 cores (Figure 30). A lithologically similar reservoir, again occurring within

Facies 5, was observed at the top of the regressive phase of S3-HFS4 in the Effie B York Unit #1 core due to a high-frequency sequence subaerial exposure horizon (Figure 30). Secondary reservoir development occurs within Facies 6 of S4 of all three cores and may be controlled by an increase in siliciclastic sedimentation related to long-term, 2^{nd}-Order regression of the gross "Mississippian limestone" interval. In these reservoirs, authigenic quartz overgrowths are observed that occlude porosity. Reservoir distribution displays strike-elongated geometries that variably display dip-oriented heterogeneity, a characteristic of the ramp setting in which they were deposited (Ahr, 1973; Ward and Brady, 1979; Tucker and Wright, 1990). High-frequency sequence and cycle boundaries, expressed as Facies 2 and/or 3 that overlie higher energy facies (F4-6) and characterized by the lowest average porosity and permeability values (approximately 1-2% and 2.45×10^{-7} mD, respectively), are interpreted to vertically compartmentalize the observed reservoirs.

Primary Reservoir Development

Primary reservoir development occurs within Facies 5 in the Effie B York Unit #1 and Moore Unit #D1 cores where subaerial exposure at the top of the regressive phase of S2 resulted in a highly siliceous (avg. 77% microcrystalline quartz) chert breccia that displays dissolution pipes, vugs, and oil-staining in hand sample. This approximately 18-25 ft. (5.5-7.6 m) thick unit is characterized by moldic, vugular and intergranular porosity values averaging 6.2% with an average permeability of 2.8×10^{-6} mD, outperforming all other samples collected in this study in reservoir characteristics (Figure 35A & B).

Heterogeneities within the primary reservoir are attributed to both lateral and vertical changes in the primary depositional facies. The primary reservoir was not observed 2.69 miles (4.3 km) away in the more proximal Droke Unit #1 core at the top of S2 (Figure 30). In this locality, the particular wellbore placement may not have captured the brecciated exposure features observed in the two other cores. These unique features may have been completely removed by erosional processes or, alternatively, may never have been created in this precise location.

Vertical compartmentalization of the primary reservoir was observed in the Effie B York Unit #1 and Moore Unit #D1 cores by a HFC boundary that resulted in the deposition of Facies 3 & 4 (Figure 35C). While a sample was not taken from this interval (S2-HFS4-HFC1), the petrophysical characteristics of Facies 3 exhibit the lowest average porosity and permeability values (approximately 1-2% and 2.45 x 10^{-7} mD, respectively) of all six facies. This relatively impermeable and thin (approximately 1 ft. (0.3 m)) unit within the gross reservoir exemplifies the effects of high-frequency cyclicity on production-scale reservoir flow units.

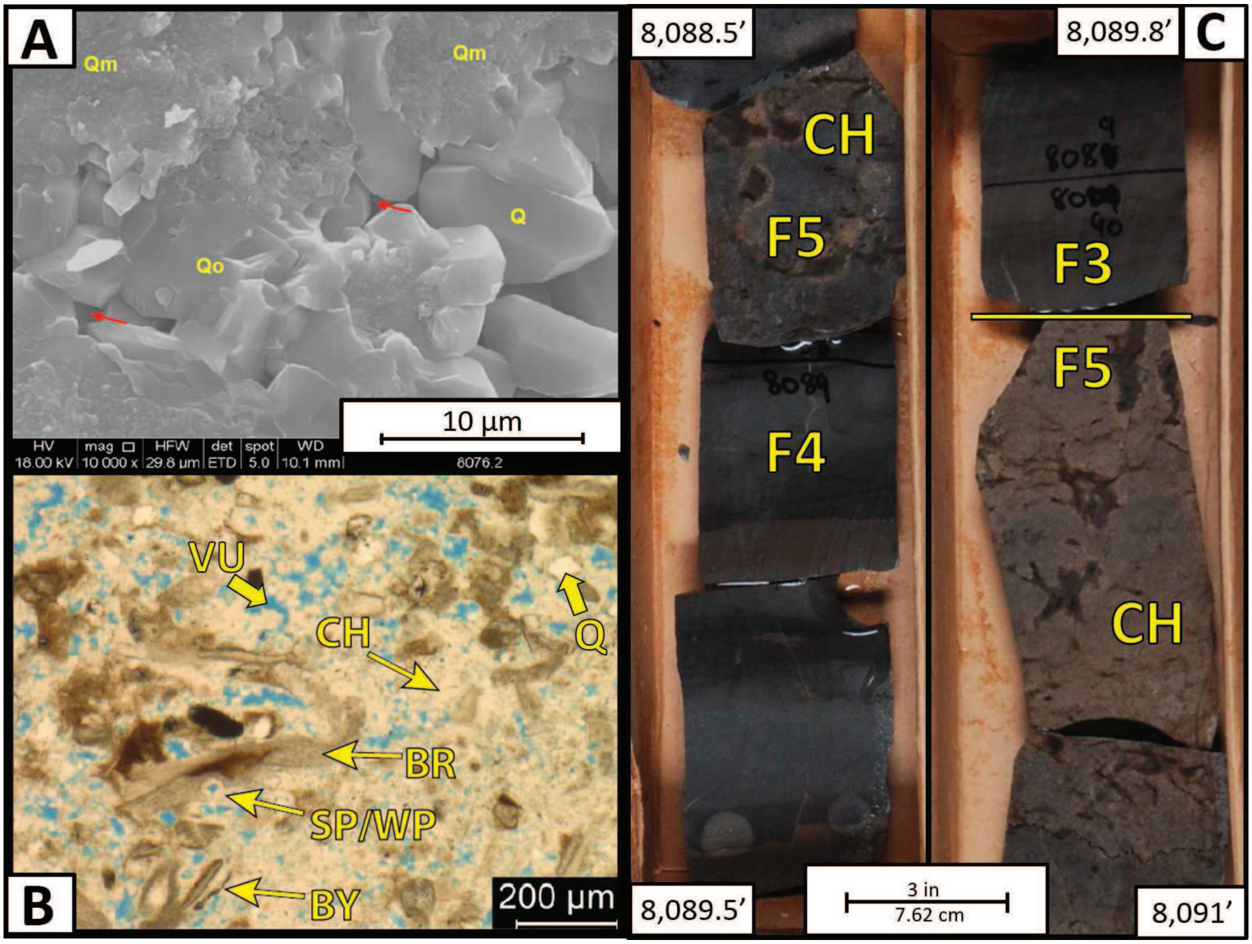

Figure 35. Primary Reservoir Characteristics. Figures illustrate: (A) SEM photograph from Moore Unit #D1 core at 8,076.2'; (B) Thin section photomicrograph from Moore Unit #D1 core at 8,091.4' under PPL and blue epoxy impregnated to show porosity; and (C) Core slab photograph from Moore Unit #D1 core from 8,091'- 8,088.5'. Refer to Table 4 for abbreviations. Note the intergranular porosity (A; red arrows) between euhedral to anhedral quartz grains within the silica-rich matrix (Qm). Also note the authigenic quartz overgrowths (Qo) occluding intergranular porosity (A). Intraparticle/partial moldic porosity after sponge spicules and vugular porosity within the chert matrix are also abundant (B). Primary reservoir development is controlled by both the primary depositional facies (Facies 5) and subaerial exposure in the late regressive phase of S2 (Figure 30) and possesses the highest porosity and permeability values (up to 12% and 9.29 x 10^{-6} mD, respectively) of all samples selected from the three cores researched. Core slab photograph (C) displays vertical compartmentalization (F3/F4) of the primary reservoir (F5/CH), interpreted to be the result of high-frequency, 5th-Order transgression.

The primary reservoir was mapped by the bounding surfaces of S2-HFS4 tied to distinct gamma ray and resistivity log signatures (Figure 30). The gross isopach contour map of this high-frequency sequence variably displays the expected northwest-southeast strike-elongated geometry (Figure 36). However, anomalous thickness trends occur. Thinning occurs to both the northwest and southeast that might be attributed to the clinoformal nature of this high-frequency sequence. A lack of subsurface control was encountered to the southeast (Figure 36) due to a substantial change in the wireline log signatures used for correlation. In general, S2-HFS4 thickens to the northeast to approximately 40 ft. (12 m) and displays variability oblique to depositional strike (trending WNW-ESE) through Section 12 of the study area. The observed lateral and vertical variability within the study area is expected when considering the primary reservoir was developed through subaerial exposure and the formation of a porous chert breccia within Facies 5.

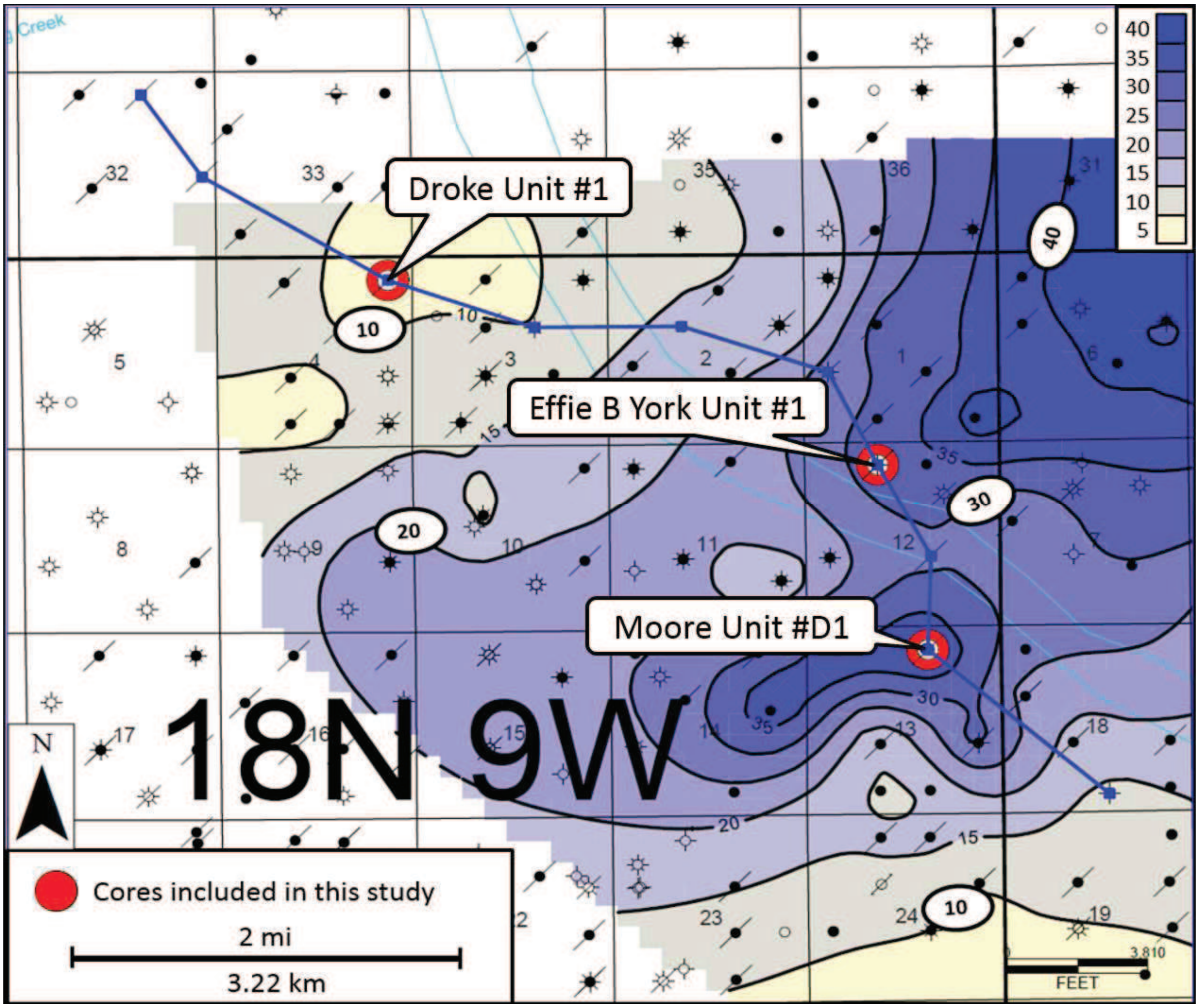

Figure 36. S2-HFS4 Gross Isopach Contour Map (Primary Reservoir Distribution). Contour interval = 5 ft. (1.52 m). Color fill displays thinner units in yellow/tan and thicker units in blue. 3 cores analyzed in this study indicated by the red well symbols. Cross section (Figure 31) denoted by blue lines between wells. Note the distribution elongated parallel to depositional strike (SW-NE) with thinning both to the SE and NW, due to the geometry of the S2-HFS4 clinoform. Also note the lack of control to the SW due to inconsistent wireline log signatures.

A lithologically similar reservoir, again developing within Facies 5, was observed in the Effie B York Unit #1 core where subaerial exposure at the top of the regressive phase of S3-HFS4 resulted in a thin, approximately 2.5 ft. (0.76 m), chert breccia (avg. 35% microcrystalline quartz) (Figure 37). This reservoir was not observed in the more proximal Moore Unit #D1 and Droke Unit #1 cores within S3-HFS4 (Figure 30). In the Moore Unit #D1 core, 1.02 miles (1.64

km) away, the uppermost 1-2 ft. (0.3-0.6 m) of S3-HFS4 is characterized as Facies 6 and displays an abrupt increase in the guard resistivity signature from approximately 250 ohms/m at 7,989’ to approximately 1,000 ohms/m at 7,987’, potentially due to a higher amount of chert in the gross HFS4 interval (Appendix B-II-7,998.7’ contains 37.2% chert). A correlation of S3-HFS4 to the Droke Unit #1 core was not observed; however, the gross 11 ft. (3.4 m) interval of S3 in this core displays a shallowing-upward signature from Facies 5 to Facies 6 and contains common chert in core photographs (Appendix C-I-7,985’). Visual estimations of vugular, intergranular and moldic porosity for this reservoir in the Effie B York Unit #1 core average between 5-7.5% (Figure 37). Although thin, and likely uneconomic in the study area, S3-HFS4 is interpreted to be a direct result of 4^{th}-Order, high-frequency cyclicity.

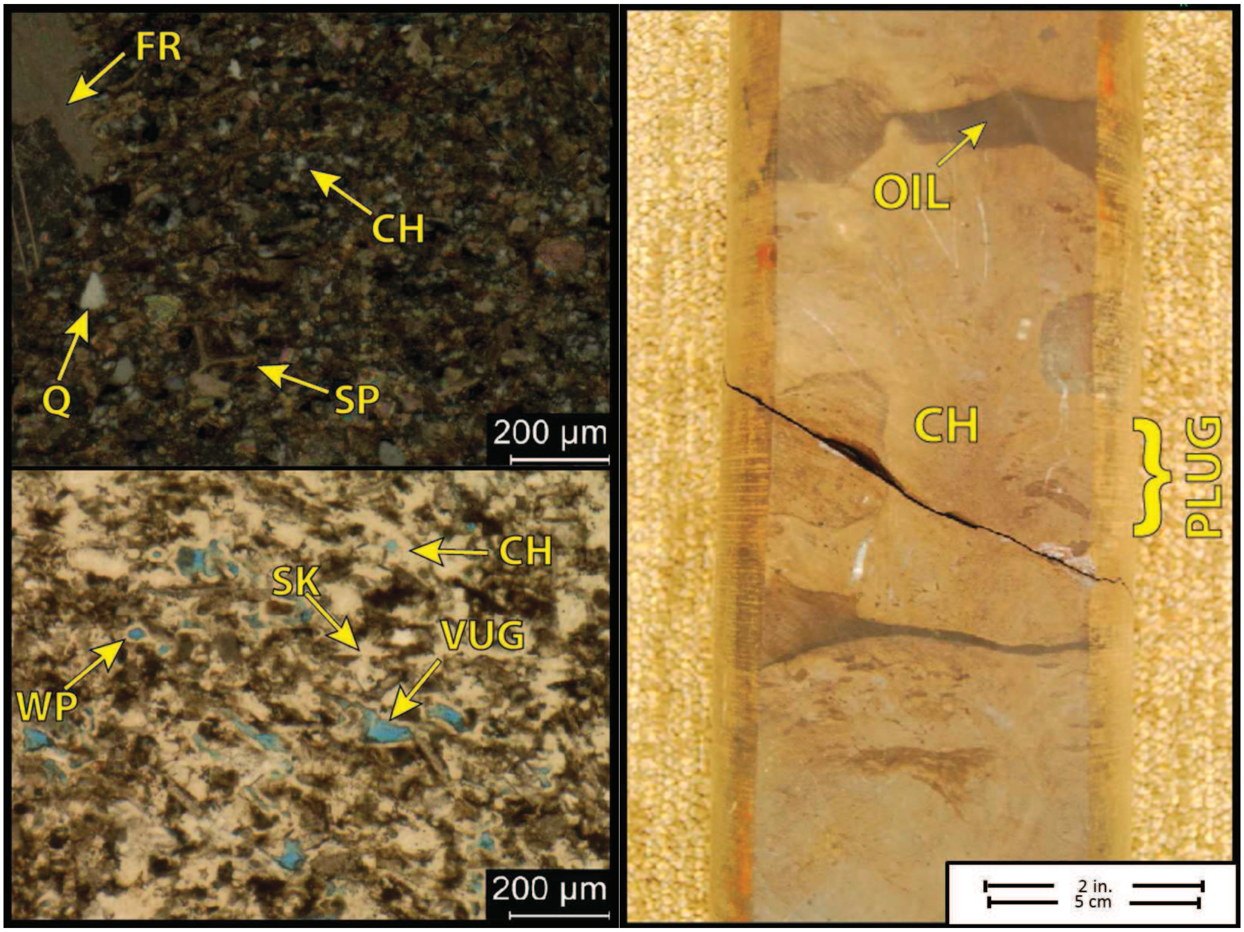

Figure 37. Sequence 3-High-frequency Sequence 4: Reservoir Characteristics. Figure illustrates thin section photomicrograph (left; top = XPL, bottom = PPL) from the Effie B York Unit #1 core at 8,072.5' and the corresponding core photograph (right) from that interval. Refer to Table 4 for abbreviations. Core photograph displays chert breccia and oil-staining. Thin section photomicrograph shows intraparticle/ partial moldic porosity after sponge spicules and vugular porosity within the chert matrix. Porosity values from this interval are visually estimated to be 5-7.5%. This reservoir develops within Facies 5 due to subaerial exposure at the top of S3-HFS4, interpreted to be a direct result of high-frequency cyclicity.

Secondary Reservoir Development

Secondary reservoir development occurs within Facies 6 of S4 and is characterized by an average of 31% detrital quartz silt/ very-fine sand and 8.2% feldspars. Intergranular porosity (avg. 3.5%) is observed between detrital quartz and calcite grains in both SEM and thin section photomicrographs (Figure 38A & B) while permeability averages 3.8 x 10^{-8} mD. Authigenic quartz is observed to occlude porosity (Figure 38A) and likely diminishes reservoir potential. Reservoir development within this approximately 47 ft. (14.3 m) gross sequence (Figure 34) is thought to be controlled by increased siliciclastic deposition due to late long-term, 2nd-Order regression at the top of the "Mississippian limestone". A relatively high abundance of detrital quartz (avg. 31%) within this sequence is accompanied by a relatively high percentage of plagioclase feldspar (avg. 6-8%). The secondary reservoir of the study area is also vertically compartmentalized by high-frequency sequences resulting in deposition of Facies 3 within the gross interval of Facies 6 (Figure 38C).

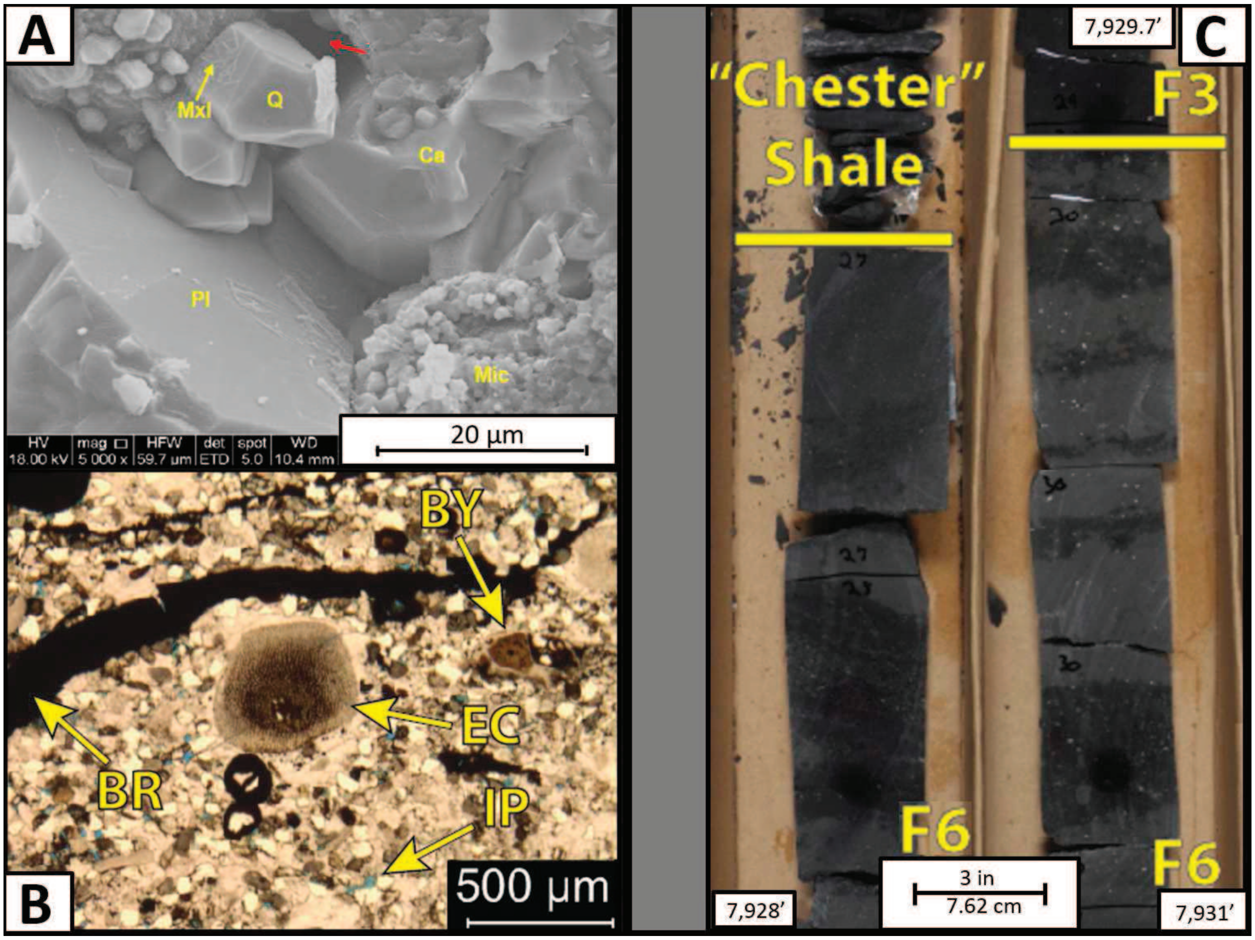

Figure 38. Secondary Reservoir Characteristics. Figure illustrates: (A) SEM photomicrograph and (B) thin section photomicrograph from the Moore Unit #D1 core at 7,930.9' and the corresponding core slab photograph. Refer to Table 4 for abbreviations. Intergranular porosity (red arrow in A and blue epoxy in B) between calcite crystals and euhedral to anhedral quartz grains average 4% with an average permeability of 3.5 x 10^{-8} mD. Note the presence of Facies 3 (F3) within the gross interval of Facies 6 (F6), interpreted to be the result of high-frequency cyclicity and imparting vertical heterogeneity into the reservoir. The uppermost portion of the cored interval is overlain by likely "Chester" shales and siltstones.

The secondary reservoir of the "Mississippian limestone" of the study area displays a relatively consistent, strike-elongated geometry and thickens basinward to the southeast due to progradation of the late S2 regression (Figures 30, 31 & 34). While this reservoir does not achieve the relatively high porosity and permeability values observed in the primary reservoir, its thickness, consistently observed intergranular porosity, and lateral continuity make this secondary reservoir a potential unconventional target.

Modern and Ancient Analogs

The stratigraphy of the "Mississippian limestone" in the study area is characterized as having been deposited along a distally-steepened, mixed carbonate-siliciclastic ramp environment. Modern and ancient analog comparison is used to make more realistic assumptions of the depositional processes and geometries observed in this study (Grammer et al., 2004). The Permian San Andres Formation has been interpreted as being deposited along a distally-steepened ramp and contains similar depositional facies to what was observed in this study (Kerans et al., 1994). Minimal bioturbation in the distal outer ramp is comparable to that of Facies 2 and 3 of this study, while bioclastic packstones and grainstones of the mid-ramp and distal ramp crest are similar to Facies 5 and 6 of this study (Kerans et al., 1994). Geometrical comparison of facies distribution in this study closely resembles that of the Persian Gulf. This modern carbonate ramp displays Holocene sediments that have accumulated over an area that is 310 miles (500 km) long and up to 37 miles (60 km) wide (Alsharhan and Kendall, 2005). Individual facies types observed in the Persian Gulf also display wide belts that parallel the shoreline (Alsharhan and Kendall, 2005). The types of facies observed in outcrop of the Permian San Andres distally-steepened ramp and the distribution of facies in the modern Persian Gulf ramp provide reasonable analogs for the facies types and architectural geometries observed in the "Mississippian limestone" of the study area.

DISCUSSION

The “Mississippian limestone” of the study area displays a complex interplay of depositional facies mosaics of a mixed carbonate-siliciclastic ramp setting and has been subjected to significant diagenesis throughout.. Integrating the effects of high-frequency, Milankovitch-band cyclicity in carbonate systems more accurately defines highly heterogeneous reservoir units. While the observed sequence stratigraphic hierarchy identifies the mechanisms responsible for primary reservoir development, the nature of the mixed carbonate-siliciclastic system inhibits the full understanding of this depositional system. Clearly defining the provenance of the siliciclastic sediment within the “Mississippian limestone” would improve reservoir characterization and would serve as a predictive exploratory tool to locate areas of highly concentrated siliciclastic reservoirs within the “Mississippian limestone”.

Primary Reservoir Development – Chert Formation

The observation that the primary reservoir and the thin chert breccia at the top of S3-HFS4 were both formed through subaerial exposure and are diagenetically altered expressions of Facies 5 established an important concept. Within these expressions of Facies 5 there are abundant sponge spicules or partial molds of sponge spicules. Moving up-dip in either of these units results in a lateral facies change to that of Facies 6 where the occurrence of siliceous sponge spicules is either absent or extremely diminished (Figure 30). The interpretation of this study is that the abundant quantities of silica required to form an approximately 20 ft. (6.1 m) thick chert were likely remobilized from siliceous sponge spicules deposited *in situ* within Facies 5. Following subaerial exposure, and dissolution of much of the remaining limestone, this chert breccia might be better classified as a spiculitic tripolite, similar to what has been described in subsurface studies from southern Kansas and north-central Oklahoma (Rogers et al., 1995; Montgomery et al., 1998; Watney et al., 2001).

This reservoir development is more accurately classified as conventional in the study area, displaying a stratigraphic trap attributed to the observed lateral facies change in a more proximal depositional dip direction. Understanding that the primary reservoir was subjected to subaerial exposure, dip-oriented variability observed in the gross isopach contour map (Figure 36) is more accurately interpreted. Furthermore, the wireline log signature of this interval was significantly different in character in the southwest portion of the study area and might indicate an area of incision (Figure 36). As an exploratory tool, if siliciclastic influx is shown to improve reservoir characteristics, these erosive features might be viable conventional targets where areas of detrital sediment accumulate.

Mixed Carbonate-Siliciclastic System

There is a fundamental disconnect between the sequence stratigraphic models of carbonate and siliciclastic systems. In carbonate systems, increased sediment production and deposition is achieved during highstand when the areal extent of the carbonate factory is greatest. Conversely, in siliciclastic systems, deposition increases during lowstand when the areal extent of an exposed landmass is greatest, providing a higher amount of detrital influx into the basin. Sedimentation can alternate both vertically and laterally from siliciclastic to carbonate and clastic poisoning may disrupt carbonate production (Yancey, 1991; Read, 1995; McNeill et al., 2004).

With these concepts in mind, S4 is interpreted to be the most viable candidate for unconventional targeting. This secondary reservoir within the “Mississippian limestone” of the study area displays the most consistent porosity and permeability values, both vertically within S4 (Figure 39) and between all three cores included in this study. Sequence 4 also displays the most laterally contiguous geometry, averaging approximately 50 ft. (15 m) in the study area and consistently thickens to the southeast where a thickness of over 100 ft. (30 m) is observed (Figure 34). While high-frequency sequences and cycles internally compartmentalize S4, and lateral facies changes are likely to occur, it does not appear as reliant on diagenetic alteration like that of the primary reservoir.

If the increased abundance of siliciclastics positively influences reservoir development, S4 would be the most viable candidate for unconventional targeting in the study area. The provenance of detrital grains observed in this sequence and throughout the cored intervals of this study are unknown. It is the opinion of this study that the detrital quartz observed throughout the "Mississippian limestone" is not eolian in origin due to the size (coarse silt to very-fine sand) and lack of frosted surfaces. Marine deposition suggests that potential sources of siliciclastic sediment might be the Transcontinental Arch, Central Kansas Uplift or the Nemaha Uplift. These features, both regional and local, could provide detrital quartz silt and feldspars to the region during periods of lowstand, either due to high-frequency sea level fluctuations or the overall 2^{nd}-Order regression. A detailed study of the provenance of detrital sedimentation within the "Mississippian limestone" and its effect on reservoir development could potentially identify a regional trend for future development in proximity to these ancient features.

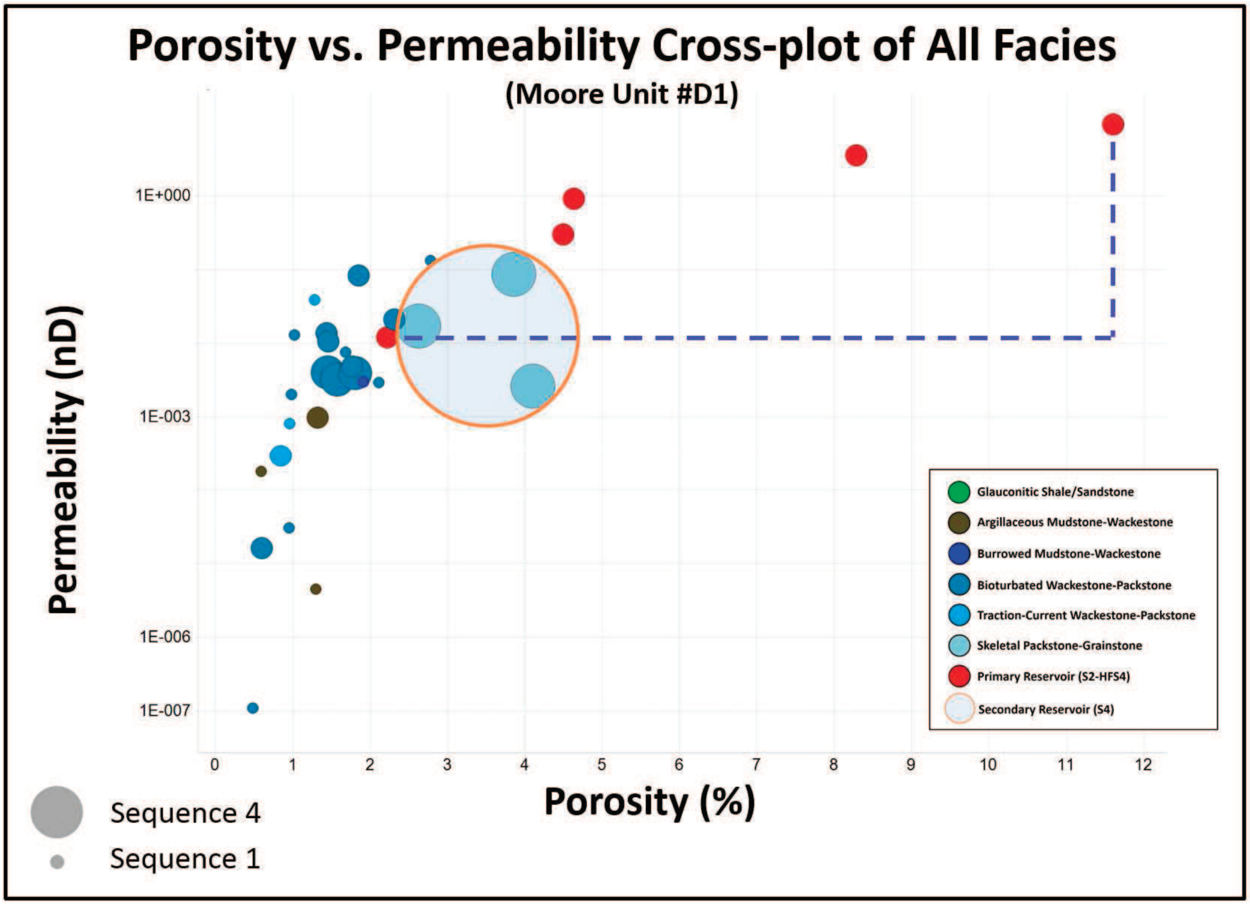

Figure 39. Porosity vs Permeability Cross-Plot of All Facies (Moore Unit #D1). Porosity (%) is plotted on the x-axis and permeability (nD) is plotted on the y-axis. Data points are sized (small to big) by their sequence classification (S1-S4) and are color coded based on their facies classification. The primary reservoir (S2-HFS4; chert breccia containing vugular, moldic and intergranular porosity) is separated from its facies classification (Facies 5) and displayed in red. Purple dashed lines illustrate the wide range of porosity (from 2.2% to 11.6%) and permeability (from 1.2 x 10^{-2} nD to 9.3 nD) values observed within the primary reservoir. Also note that the skeletal packstone-grainstone facies of Sequence 4, interpreted to be the secondary reservoir (orange circle with light blue shading) and characterized by increased siliciclastic abundance (22-40% detrital quartz and 4.5-10.9% feldspars) with intergranular porosity between quartz grains, displays a more consistent range of porosity (from 2.6% to 4.1%) and permeability values (from 0.3 x 10^{-2} nD to 1.7 x 10^{-2} nD).

Milankovitch Orbital Forcing

The nature of the mixed carbonate siliciclastic system in conjunction with significant diagenesis in the form of dense cherts and some dolomites, as discussed, can make identifying and correlating the chronostratigraphic surfaces difficult. Accurately tying the sequence stratigraphic hierarchy to the sea level fluctuations of the period might be a useful tool for identifying anomalies or unconformities. To do this, knowing the actual Milankovitch orbital forcing mechanism responsible for the hierarchy would be useful knowledge. For example, in sequence 1 of this study there are 5 HFSs within S1. During transitional global climates like that of the Mississippian, 3rd Order sequences are typically 1-3 million years in duration. Five HFSs would then be 200 to 600 thousand years in duration, and would most likely be due to the long-term eccentricity (400 k.y.) orbital mechanism. With this assumption, the 7-8 HFCs that are nested within each HFS within S1 would encompass approximately 50 k.y. in duration. This would most likely be due to the 40 k.y. obliquity orbital mechanism.

The validity of this hierarchical ratio of the controlling orbital mechanisms during the Mississippian would be a grand assumption considering the numerous mechanisms that can disrupt or distort the stacking patterns of high-frequency glacioeustacy. However, if this 8:5:1 ratio could be expected and identified throughout the Mississippian limestone it could be used as an exploration tool. For example, where this ratio is absent an unconformity might be identified that could lead to favorable reservoir conditions.

Chronostratigraphic Implications

The importance of the high-resolution approach to sequence stratigraphic analysis can be further justified when extrapolating the stratigraphic architecture away from the study area. The thin chert breccia that developed at the top of S3-HFS4 is interpreted to display thickening to the southeast due to progradation of the gross S3 interval (Figures 30 & 31). As another exploratory tool, assuming an adequate abundance of siliceous sponge spicules were deposited, this relatively thin (2.5 ft. (0.76 m)) interval may thicken basinward to form a potential reservoir. Furthermore, this unit might occur in a relatively similar portion of the gross “Mississippian limestone” interval (in relation to depth above the Woodford Shale or below the “Chester” shale) as S3 progrades basinward atop a progressively thinner S2. A regional subsurface map constructed through lithostratigraphic correlations without sufficient intervening well control would likely correlate these two intervals (Figures 30 & 31 – top of S2 and top of S3-HFS4), resulting in the inaccurate association of genetically-unrelated rock units.

CONCLUSION

The “Mississippian limestone” unconventional resource play possesses great potential, yet is accompanied by subpar well performance, often within the same field (production-scale). Ironically, the underlying mechanisms that result in ideal hydrocarbon-bearing reservoir units (i.e., chert and siliciclastic deposition) are also the primary cause for their frequent misunderstanding. The mixed carbonate-siliciclastic depositional system characteristic of the “Mississippian limestone” is a dynamic interplay of both pre- and post-depositional processes. Through detailed core analysis and the application of high-resolution sequence stratigraphy these often misunderstood heterogeneities were revealed. The key findings from this study are:

1. The “Mississippian limestone” of the study area is characterized by six depositional lithofacies encountered along a distally-steepened carbonate ramp environment.
2. Vertical stacking patterns of these six facies were observed that indicated 4 hierarchical durations of eustatic and relative sea level cyclicity that control the development and distribution of hydrocarbon reservoirs. The gross “Mississippian limestone” of the study area is interpreted to be a 2nd-Order supersequence that

contains four 3rd-Order sequences. Nested within 3rd-Order sequences are high-frequency sequences (4th-Order) and cycles (5th-Order).

3. Primary reservoir development is dependent on the depositional facies as well as its position within the sequence stratigraphic hierarchy. The primary reservoir developed within Facies 5 that contained abundant siliceous sponge spicules. A diagenetic chert (avg. 75% microcrystalline quartz) breccia was the result of subaerial exposure controlled by the late regressive phase of the second 3rd-Order sequence (S2).
4. A similarly porous chert breccia also developed within Facies 5 (also containing abundant sponge spicules) at the top of the regressive phase of the fourth high-frequency sequence of the third depositional sequence (S3-HFS4), confirming the requirements for porous chert development (sponge spicules and subaerial exposure) and exemplifying the effects of high-frequency cyclicity on reservoir development.
5. Secondary reservoir development occurs at the top of the "Mississippian limestone" within the fourth depositional sequence (S4) and is characterized as a moderately arenitic and variably fossiliferous packstone to grainstone (Facies 6). The increased abundance of detrital grains is thought to be a driver of interparticle porosity in this reservoir.
6. High-frequency, Milankovitch-band cyclicity was responsible for reservoir development and vertical compartmentalization. As described above, subaerial exposure of a high-frequency sequence (S3-HFS4) resulted in a porous chert breccia. Primary and secondary reservoirs are vertically compartmentalized by high-frequency sequences and cycles, forming the fundamental flow units at the production-scale.

7. Guard resistivity curves proved more effective at identifying the boundaries of the stratigraphic hierarchy than gamma ray curves, yet both tools were useful at extrapolating the sequence stratigraphic framework within the study area.
8. The high-resolution, high-frequency approach to sequence stratigraphy of the "Mississippian limestone" resulted in a more accurate subsurface mapping technique. The sequence stratigraphic architecture displayed strike-elongated geometries that are typical of carbonate ramp environments. Lateral and vertical heterogeneities were defined within this architecture that resulted in a more accurate representation of production-scale reservoir potential.

REFERENCES CITED

Ahr, W.M., 1973, The Carbonate Ramp: An Alternative to the Shelf Model, in S. Chuber, ed., Gulf Coast Association of Geological Societies Transactions, V. 23, p. 221-225.

Alsharhan, A.S., and Kendall, C.G.St.C., 2003, Holocene Coastal Carbonates and Evaporites of the Southern Arabian Gulf and Their Ancient Analogues, Elsevier Earth-Science Reviews 61, p. 191-243.

Archie, G.E., 1950, Introduction to Petrophysics of Reservoir Rocks, AAPG Bulletin, V. 34, No. 5, p. 943-961.

Asquith, G., and Krygowski, D., 2004, Basic Well Log Analysis, 2nd Edition, AAPG Methods in Exploration Series, No. 18, 244 p.

Ball, M.M., Henry, M.E., and Frezon, S.E., 1991, Petroleum Geology of the Anadarko Basin Region, Province (115), Kansas, Oklahoma and Texas, Department of the Interior, U.S. Geological Survey, Open-File Report 88-450W, 36 p.

Bann, K.L., Tye, S.C., MacEachern, J.A., Fielding, C.R., and Jones, B.G., 2008, Ichnological Signatures and Sedimentology of Mixed Wave- and Storm-dominated Deltaic Deposits: Examples from the Early Permian, Southern Sydney Basin of Southeastern Australia, in G. Hamson, R. Steel, P. Burgess, and R. Dalrymple, eds., Recent Advances in Models of Siliciclastic Shallow-Marine Stratigraphy, SEPM Special Publication 90, p. 293-332.

Beebe, B.W., 1959, Characteristics of Mississippian Production in the Northwestern Anadarko Basin, Tulsa Geological Society Digest, V. 27, p. 190-205.

Bentor, Y.K., and Kastner, M., 1965, Notes on the Mineralogy and Origin of Glauconite, Journal of Sedimentary Petrology, V. 35, No. 1, p. 155-166.

Blakey, R., 2014, Paleogeography and Geologic Evolution of North America, <http://www2.nau.edu/rcb7/nam.html> Accessed October, 2014.

Boardman, D.R., Thompson, T.L., Godwin, C., Mazzullo, S.J., Wilhite, B.W., and Morris, B.T., 2013, High-Resolution Conodont Zonation for Kinderhookian (Middle Tournaisian) and Osagean (Upper Tournaisian-Lower Visean) Strata of the Western Edge of the Ozark Plateau, North America, Oklahoma City Geological Society, The Shale Shaker Digest, V. 64, p. 98-151.

Buggisch, W., Joachimski, M.M., Sevastopulo, G., and Morrow, J.R., 2008, Mississippian $\delta^{13}C_{carb}$ and Conodont Apatite $\delta^{18}O$ Records – Their Relation to the Late Palaeozoic Glaciation, Palaeogeography, Palaeoclimatology, Palaeoecology, V. 268, p. 273-292.

Burst, J.F., 1958, "Glauconite" Pellets: Their Mineral Nature and Applications to Stratigraphic Interpretations, AAPG Bulletin, V. 42, No. 2, p. 310-327.

Byers, C.W., 1977, Biofacies Patterns in Euxinic Basins: A general model, in H.E. Cook and P. Enos, eds., Deep-Water Carbonate Environments, SEPM Special Publication 25, p. 5-17.

Childress, M., 2015, High Resolution Sequence Stratigraphic Architecture of a Mid-Continent Mississippian Outcrop in Southwest Missouri, M.S. Thesis, Oklahoma State University, Stillwater, Oklahoma, 272 p.

Childress, M. and Grammer, G.M., 2015, High Resolution Sequence Stratigraphic Architecture of a Mid-Continent Mississippian Outcrop in Southwest Missouri, Oklahoma City Geological Society, The Shale Shaker Digest, V. 66, No. 1, p. 206-234.

Choquette, P.W., and Pray, L.C., 1970, Geologic Nomenclature and Classification of Porosity in Sedimentary Carbonates, AAPG Bulletin, V. 54, No. 2, p. 207-250.

Curtis, D.M., and Champlin, S.C., 1959, Depositional Environments of Mississippian Limestones of Oklahoma, Tulsa Geological Society Digest, V. 27, No. 1, p. 90-103.

Dewey, C., and Puckette, T.M., 1993, Ostracodes as a Tool for Understanding the Distribution of Shelf-Related Environments in the Chesterian Strata of the Black Warrior Basin in Alabama, New Perspectives on the Mississippian system of Alabama, Alabama Geological Society, No. 30, p. 61-68.

Dott, R.H., Jr., and Bourgeois, J., 1982, Hummocky Stratification: Significance of its variable bedding sequences, Geological Society of America Bulletin, V. 93, p. 663-680.

Drummond, C.N., and Wilkinson, B.H., 1993, Carbonate Cycle Stacking Patterns and Hierarchies of Orbitally-Forced Eustatic Sea Level Change, Journal of Sedimentary Petrology, V. 63, p. 369-377.

Dunham, R.J., 1962, Classification of Carbonate Rocks According to Depositional Texture, in W.E. Ham, ed., Classification of Carbonate Rocks, AAPG Memoir 1, p. 108-121.

Ekdale, A.A., Bromley, R.G., and Pemberton, S.G., 1984, Ichnology: The Use of Trace Fossils in Sedimentology and Stratigraphy, SEPM Short Course Notes, V. 15, p 129-142.

Estaban, M., and Klappa, C.F., 1983, Subaerial Exposure Environment, in P.A Scholle, D.G. Bebout, and C.H., Moore, eds., Carbonate Depositional Environments, AAPG Memoir 33, p. 1-92.

Evans, K.R., Jackson, J.S., Mickus, K.L., Miller, J.F., and Cruz, D., 2011, Enigmas and Anomalies of the Lower Mississippian Subsystem in Southwestern Missouri, AAPG, Search and Discovery Article #50406, 47 p.

Evans, J.L., 1979, Major Structural Features of the Anadarko Basin, Tulsa Geological Society Special Publication No. 1, p. 97-114.

Finger, K.L., 1983, Observations on the Lower Cretaceous Ostracode Zone of Alberta, Bulletin of Canadian Petroleum Geology, V. 31, No. 4, p. 326-337.

Flügel, E., 2010, Microfacies of Carbonate Rocks: Analysis, Interpretation, and Application, 2nd Edition, Springer-Verlag, Berlin, Heidelberg, New York, 1007 p.

Friesenhahn, T.C., 2012, Reservoir Characterization and Outcrop Analog: The Osagean Reeds Spring Formation (Lower Boone), Western Osage and Eastern Kay County, Oklahoma, M.S. Thesis, University of Arkansas, Fayetteville, Arkansas, 86 p.

Folk, R.L., and Weaver, C.E., 1952, A Study of the Texture and Composition of Chert, American Journal of Science, V. 250, p. 498-510.

Franseen, E.K., 2006, Mississippian (Osagean) Shallow-Water, Mid-Latitude Siliceous Sponge Spicule and Heterozoan Carbonate Facies: An example from Kansas with implications for regional controls and distribution of potential reservoir facies, Kansas Geological Survey, Current Research in Earth Sciences, Bulletin 252, part 1, p. 1-23.

Frezon, S.E., and Jordan, L., 1979, Oklahoma, in L.C. Craig and C.W. Connor, eds., Paleotectonic Investigations of the Mississippian System in the United States: U.S. Geological Survey Professional Paper 1010, p. 146-159.

Friedman, G.M., and Sanders, J.E., 1978, Principles of Sedimentology, New York, John Wiley & Sons, 792 p.

Gallardo, J., and Blackwell, D.D., 1999, Thermal Structure of the Anadarko Basin, AAPG Bulletin, V. 83, No. 2, p. 333-361.

Gary, M., McAfee, R. Jr., and Wolf, C.L., eds., 1974, GI's Glossary of Geology, American Geological Institute, Falls Church, Virginia, 805 p. +52 page appendix A.

Gay, P.S. Jr., 2003, The Nemaha Trend – A System of Compressional Thrust-Fold, Strike-Slip Structural Features in Kansas and Oklahoma, Parts 1 & 2, Oklahoma City Geological Society, The Shale Shaker Digest, V. 54, Nos. 1 & 2, p. 9-49.

Grammer, G.M., Harris, P.M., and Eberli, G.P., 2004, Integration of Outcrop and Modern Analogs in Reservoir Modeling: Overview with Examples from the Bahamas, in G. M. Grammer, P.M. Harris, and G.P. Eberli, eds., Integration of Outcrop and Modern Analogs in Reservoir Modeling: AAPG Memoir 80, p. 1-22.

Grammer, G.M., Eberli, G.P., Van Buchem, F.S.P., Stevenson, G.M., and Homewood, P., 1996, Application of High-Resolution Sequence Stratigraphy to Evaluate Lateral Variability in Outcrop and Subsurface—Desert Creek and Ismay Intervals, Paradox Basin, in M.W. Longman and M.D. Sonnenfeld, eds., Paleozoic Systems of the Rocky Mountain Region, Rocky Mountain Section, SEPM, p. 235-266.

Grieser, B., and Pinkerton, H., 2013, Horizontal Mississippian Fracture Completions in Oklahoma and Kansas, Unconventional Resources Technology Conference, URTeC 1577780, p. 1-11.

Goddard, E.N., Trask, P.D., De Ford, R.K., Rove, O.N., Singewald, J.T., and Overbeck, R.M., 1951, Rock Color Chart, Geological Society of America, Boulder, Colorado.

Gutschick, R.C., and Sandberg, C.A., 1983, Mississippian Continental Margins of the Conterminous United States, in D.J. Stanley and G.T. Moore, The Shelfbreak: Critical Interface on Continental Margins, SEPM Special Publication 33, p. 79-96.

Ham, W.E., Denison, R.E., and Merritt, C.A., 1965, Basement Rocks and Structural Evolution of Southern Oklahoma-A Summary, AAPG Bulletin, V. 49, No. 7, p. 927-934.

Handford, C.R., and Loucks, R.G., 1993, Carbonate Depositional Sequences and Systems Tracts – Responses of Carbonate Platforms to Relative Sea-Level Changes, in R.G. Loucks, and F. Sarg, eds., Carbonate Sequence Stratigraphy: Recent Developments and Applications, AAPG Memoir 57, p. 3-42.

Handford, C.R., 1988, Review of Carbonate Sand-Belt Deposition of Ooid Grainstones and Application to Mississippian Reservoir, Damme Field, Southwestern Kansas, AAPG Bulletin, V. 72, No. 10, p. 118-1199.

Handford, C.R., 1986, Facies and Bedding Sequences in Shelf-Storm-Deposited Carbonates – Fayetteville Shale and Pitkin Limestone (Mississippian), Arkansas, Journal of Sedimentary Petrology, V. 56, No. 1, p 123-137.

Harms, J.C., Southard, J.B., and Walker, R.G., 1982, Structure and Sequence in Clastic Rocks, SEPM Short Course Notes, V. 9, 51 p.

Harris, S.A., 1987, Hydrocarbon Accumulation in "Meramec-Osage" (Mississippian) Rocks, Sooner Trend, Northwest-Central Oklahoma, in B. Rascoe, Jr., N.J. Hyne, eds., Tulsa Geological Society, Special Publication No. 3: Petroleum Geology of the Mid-Continent. P. 74-81

Haq, B.U., and Schutter, S.R., 2008, A Chronology of Paleozoic Sea-Level Changes, Science, V. 322, p. 64-68.

Hill, G.W., 1984, The Anadarko Basin: A Model for Regional Petroleum Accumulations, Technical Proceedings of the 1981 AAPG Mid-Continent Regional Meeting, p. 1-23.

Hoffman, E.A., Jr., 1964, Pre-Chester Mississippian Rocks of Northwestern Oklahoma, Oklahoma City Geological Society, The Shale Shaker Digest V. 14, p. 350-365.

Howard, J.D., and Reineck, H-E., Depositional Facies of High-Energy Beach-to-Offshore Sequence: Comparison with low-energy sequence, AAPG Bulletin, V. 65, p. 807-830.

James, N.P., and Clarke, J.A.D., eds., 1997, Cool-water Carbonates, SEPM Special Publication 56, p. 1-20.

Jordan, L., and Rowland, T.L., 1959, Mississippian Rocks in Northern Oklahoma, Tulsa Geological Society Digest, V. 27, p. 124-136.

Kerans, C., and Tinker, S.W., 1997, Sequence Stratigraphy and Characterization of Carbonate Reservoirs, SEPM Short Course No. 40, 130 p.

Kerans, C., Lucia, F.J., and Senger, R.K., 1994, Integrated Characterization of Carbonate Ramp Reservoirs Using Permian San Andres Formation Outcrop Analogs, AAPG Bulletin, V. 78, No. 2, p. 181-216.

Koenig, J.W., 1967, The Ozark Uplift and Midcontinent Silurian and Devonian Stratigraphy, Tulsa Geological Society, V. 35, p. 119-146.

Kreisa, R.D., 1981, Storm-Generated Sedimentary Structures in Subtidal Marine Facies with Examples from the Middle and Upper Ordovician of Southwestern Virginia, Journal of Sedimentary Petrology, V. 51, No. 3, p. 823-848.

Lane, H.R., and De Keyser, T.L., 1980, Paleogeography of the Late Early Mississippian (Tournaisian 3) in the Central and Southwestern United States, SEPM, Rocky Mountain Symposium 1, p. 149-162.

Law, B.E., and Curtis, J.B., 2002, Introduction to Unconventional Petroleum Systems, AAPG Bulletin, V. 86, No. 11, p. 1851-1852.

LeBlanc, S.E., 2014, High Resolution Sequence Stratigraphy and Reservoir Characterization of the “Mississippian Limestone” in North-Central Oklahoma, M.S. Thesis, Oklahoma State University, Stillwater, Oklahoma, 443 p.

Lucia, J.A., 1995, Rock-Fabric/Petrophysical Classification of Carbonate Pore Space for Reservoir Characterization, AAPG Bulletin, V. 79, No. 9, p. 1275-1300.

MacEachern, J.A., Bann, K.L., Gingras, M.K., and Pemberton, S.G., 2009, Applied Ichnology, SEPM Short Course Notes 52: Revised Edition, Tulsa, Oklahoma, SEPM, 145 p.

Manger, W.L., 2014, Tripolitic Chert Development in the Mississippian Lime: New Insights from SEM, Search and Discovery Article #50957, 39 p.

Martin, A.J., Solomon, S.T., and Hartmann, D.J., 1997, Characterization of Petrophysical Flow Units in Carbonate Reservoirs, AAPG Bulletin, V. 81, No. 5, p. 734-759.

Mazzullo, S.J., 2004, Overview of Porosity Evolution in Carbonate Reservoirs, Kansas Geological Society Bulletin, V. 79, Nos. 1 & 2, 19 p.

Mazzullo, S.J., Wilhite, B.W., and Woolsey, I.W., 2009a, Petroleum Reservoirs Within a Spiculite-Dominated Depositional Sequence: Cowley formation (Mississippian: Lower Carboniferous), south-central Kansas, AAPG Bulletin, V. 93, No. 12, p. 1649-1689.

Mazzullo, S.J., Wilhite, B.W., and Woolsey, I.W., 2009b, Rhythmic Carbonate Versus Spiculite Deposition in Mississippian Hydrocarbon Reservoirs in the Midcontinent USA: Causative factors and resulting reservoir petrophysical attributes, AAPG Search and Discovery Article #10209, 6 p.

Mazzullo, S.J., and Wilhite, B.W., 2010, Chert, Tripolite, Spiculite, Chat – What's in a Name?, KGS Bulletin, V. 85, No. 1, 32 p.

Mazzullo, S.J., Wilhite, B.W., and Boardman, D.R., 2011a, Lithostratigraphic Architecture of the Mississippian Reeds Spring Formation (Middle Osagean) in Southwest Missouri, Northwest Arkansas, and Northeast Oklahoma: Outcrop analog of subsurface petroleum reservoirs, Oklahoma City Geological Society, The Shale Shaker Digest, V. 61, No. 5, p. 254-269.

Mazzullo, S.J., Wilhite, B.W., and Morris, B.T., 2011b, Mississippian Oil Reservoirs in the Southern Midcontinent: New exploration concepts for a mature reservoir objective, AAPG Search and Discovery Article #10373, 34 p.

Mazzullo, S.J., Wilhite, B.W., Morris, B.T., and Boardman, D.R., 2011c, Syndepositional Tectonism and its Effects on Mississippian (Kinderhookian to Osagean) Lithostratigraphic Architecture: Part 2 – Subsurface Occurrences in the Midcontinent USA, AAPG Search and Discovery Article #30208, Tulsa, Oklahoma, 32 p.

Mazzullo, S.J., Boardman, D.R., Wilhite, B.W., Godwin, C., and Morris, B.T., 2013, Revisions of Outcrop Lithostratigraphic Nomenclature in the Lower to Middle Mississippian Subsystem (Kinderhookian to Basal Meramecian Series) Along the Shelf-Edge in Southwest Missouri, Northwest Arkansas, and Northeast Oklahoma, Oklahoma City Geological Society, The Shale Shaker Digest, V. 63, No. 6, p. 414-454.

McNeill, D.F., Cunningham, K.J., Guertin, L.A., and Anselmetti, F.S., 2004, Depositional Themes of Mixed-Carbonate-Siliciclastics in the South Florida Neogene: Application to ancient deposits, in G.M. Grammer, P.M. Harris, and G.P. Eberli, eds., Integration of Outcrop and Modern Analogs in Reservoir Modeling: AAPG Memoir 80, p. 23-43.

Middleton, G.V., 1973, Johannes Walther's Law of Correlation of Facies: Geological Society of America Bulletin, V. 38, p. 979-988.

Middleton, G.V., Church, M.J., Coniglio, M., Hardie, L.A., and Longstaffe, F.J., 2003, Encyclopedia of Sediments and Sedimentary Rocks, The Netherlands, Kluwer Academic Publishers, 821 p.

Mikkelson, D.H., 1966, The Origin and Age of the Mississippian "Chat" in North-Central Oklahoma, Oklahoma City Geological Society, The Shale Shaker Digest V, V. 15-17, p. 255-265.

Mogharabi, A., 1964, Petroleum Geology of T.19N., R.6W., Hennessey Area, Kingfisher County, Oklahoma, Oklahoma City Geological Society, The Shale Shaker Digest IV, V. 12-14, p. 336-349.

Montgomery, S.L., Mullarkey, J.C., Longman, M.W., Colleary, W.M., and Rogers, J.P., 1998, Mississippian "Chat" Reservoirs, South Kansas: Low-resistivity pay in a complex chert reservoir, AAPG Bulletin, V. 82, No. 2, p. 187-205.

Northcutt, R.A., and Campbell, J.A., 1995, Geologic Provinces of Oklahoma, Transactions of the 1995 AAPG Mid-Continent Section Meeting, 1996, p. 128-134.

Perry, Jr., W.J., 1990, Tectonic Evolution of the Anadarko Basin Region, Oklahoma, U.S. Geological Survey Bulletin 1866-A, p. A1-A19.

Pettijohn, F.J., 1975, Sedimentary Rocks (3rd edition), New York, Harper & Row, 628 p.

Pfefferkorn, H.W., Alleman, V, and Iannuzzi, R., 2014, A Greenhouse Interval Between Icehouse Times: climate change, long-distance plant dispersal, and plate motion in the Mississippian (late Visean-earliest Serpukhovian) of Gondwana, Gondwana Research V. 25, No. 4, p. 1338-1347.

Pirson, S.J., 1963, Handbook of Well Log Analysis: Modern well log interpretation techniques for oil and gas formation evaluation, Englewood Cliffs, New Jersey, Prentice Hall, 326 p.

Price, B., 2014, Sequence Stratigraphic Control on Distribution and Porosity Evolution in Cherts in the Mississippian of the Mid-Continent, M.S. Thesis, Oklahoma State University, Stillwater, Oklahoma, 144 p.

Ramondetta, P.J., 1990, El Dorado: an old field with potential, Oil and Gas Journal, V. 88, No. 13, p. 110-116.

Read, J.F., 1995, Overview of Carbonate Platform Sequences, Cycle Stratigraphy and Reservoirs in Greenhouse and Icehouse Worlds, in J.F. Read, C. Kerans, L.J. Weber, J.F. Sarg, and F.M. Wright, eds., Milankovitch Sea Level Changes, Cycles, and Reservoirs on Carbonate Platforms in Greenhouse and Ice-House Worlds: SEPM Short Course 35, p. 1-102.

Read, J.F., and Horbury, A.D., 1993, Eustatic and Tectonic Controls on Porosity Evolution Beneath Sequence-Bounding Unconformities and Parasequence Disconformities on Carbonate Platforms, in A.D. Horbury and A.G. Robinson, eds., Diagenesis and Basin Development: AAPG Studies in Geology 36, p. 155-197.

Reid, S.K., and Dorobek, S.L., 1991, Controls on Development of Third- and Fourth-Order Depositional Sequences in the Lower Mississippian Mission Canyon Formation and Stratigraphic Equivalents, Idaho and Montana, in J.D. Cooper and C.H. Stevens, eds., Paleozoic Paleogeography of the Western United States, pt. 2, SEPM Pacific Section, V. 67, p. 527-542.

Rogers, S.M., 2001, Deposition and Diagenesis of Mississippian Chat Reservoirs, North-Central Oklahoma, AAPG Bulletin, V. 85, No. 1, p. 115-129.

Rogers, J.P., Longman, M.W., and Lloyd, R.M., 1995, Spiculitic Chert Reservoir in Glick Field, South-Central Kansas, Rocky Mountain Association of Geologists, The Mountain Geologist, V. 32, No. 1, 22 p..

Roundtree, R., Wright, J., and Miskimins, J., 2010, Unconventional Resource Recovery Improvement Using Conventional Reservoir Engineering Strategies, AAPG Search and Discovery Article #80088, Tulsa, Oklahoma, 15 p.

Rowland, T.L., 1961, Mississippian Rocks in the Subsurface of the Kingfisher-Guthrie Area, Oklahoma, Oklahoma City Geological Society, The Shale Shaker Digest IV, V. 12-14, p. 145-162.

Scholle, P.A., and Ulmer-Scholle, D.S., 2003, A Color Guide to the Petrography of Carbonate Rocks: Grains, textures, porosity, diagenesis, AAPG Memoir 77, 474 p.

Shoeia, O.K., 2012, High Resolution Stratigraphy of Lower Mississippian Strata Near Jane, Missouri, M.S. Thesis, Oklahoma State University, Stillwater, Oklahoma, 262 p.

Sloss, L.L., 1963, Sequences in the Cratonic Interior of North America, Geological Society of America Bulletin, V. 74, No. 2, p 93-114.

Smith Jr., L.B., Eberli, G.P., and Sonnenfeld, M., 2004, Sequence Stratigraphic and Paleogeographic Distribution of Reservoir-quality Dolomite, Madison Formation, Wyoming and Montana, in G.M. Grammer, G.P. Eberli, and P.M. Harris, eds., Integration of Outcrop and Modern Analogues in Reservoir Modeling, AAPG Memoir 80, p. 94-188.

Sonnenfeld, M.D., 1996, Sequence Evolution and Hierarchy within the Lower Mississippian Madison Limestone of Wyoming, in M.W. Longman and M.D. Sonnenfeld, eds., 1996, Paleozoic Systems of the Rocky Mountain Region, Rocky Mountain Section, SEPM, p. 165-192.

Thompson, T.L., 1986, Paleozoic Succession in Missouri, Part 4, Mississippian System: Missouri Department of Natural Resources Report of Investigations, No. 70, 182 p.

Thompson, T.L., and Fellows, L.D., 1970, Stratigraphy and Conodont Biostratigraphy of Kinderhookian and Osagean (Lower Mississippian) Rocks of Southwestern Missouri and Adjacent Areas, Missouri Geological Survey and Water Resources Report of Investigations 45, 263 p.

Tucker, M.E., and Wright, V.P, 1990, Carbonate Sedimentology, Blackwell Science Ltd., London, Ch. 2.6: Carbonate Ramps, p. 47-52.

Ward, W.C., and Brady, M.J., 1979, Strandline Sedimentation of Carbonate Grainstones, Upper Pleistocene, Yucatan Peninsula, Mexico, AAPG Bulletin, V. 63, p. 362-369.

Watney, W.L., Guy, W.J., and Byrnes, A.P., 2001, Characterization of the Mississippian Chat in South-Central Kansas, AAPG Bulletin, V. 85, No. 1, p. 85-113.

Wehner, M., Gardner, P., Tice, M.M., Pope, M.C., Donovan, A.D., and Staerker, T.S., 2015, Anoxic, Storm Dominated Inner Carbonate Ramp Deposition of Lower Eagle Ford Formation, West Texas, URTeC, 16 p.

Westphal, H., Eberli, G.P., Smith, L.B., Grammer, G.M., Kislak, J., 2004, Reservoir Characterization of the Mississippian Madison Formation, Wind River Basin, Wyoming, AAPG Bulletin, V. 88, No. 4, p. 405-432.

Wheeler, R.R., 1955, Origin and Oil Possibilities of the Anadarko Basin, Oklahoma City Geological Society, The Shale Shaker Digest I, V. 1-4, p. 22-32.

Wilhite, B.W., Mazzullo, S.J., Morris, B.T., and Boardman, D.R. II, 2011, Syndepositional Tectonism and its Effects on Mississippian (Kinderhookian to Osagean) Lithostratigraphic Architecture: Part 1–Based on Exposures in the Midcontinent USA, AAPG Search and Discovery Article #30207.

Withrow, P.C., 1972, Star-Lacey Field, Blaine and Kingfisher Counties, Oklahoma, Oklahoma City Geological Society, The Shale Shaker Digest, V. 19, p. 78-88.

Yancey, T.E., 1991, Controls on Carbonate and Siliciclastic Sediment Deposition on a Mixed Carbonate-Siliciclastic Shelf (Pennsylvanian Eastern Shelf of north Texas), in Sedimentary Modeling: Computer simulations and methods for improved parameter definition, Kansas Geological Survey, Bulletin 233, p. 263-272.

Yang, W., and Lehrmann, D.J., 2014, Peritidal Carbonate Cycles Induced by Carbonate Productivity Variations: A Conceptual Model for an Isolated Early Triassic Greenhouse Platform in South China, Journal of Palaeogeography, V. 3, No. 2, p. 115-126.

Yenugu, M., Angelo, M., and Marfurt, K.J., 2010, Seismic Attribute Analysis of a Mississippian Chat, Osage County, Northeast Oklahoma, AAPG Search and Discovery Article #40605.

Zhao, M., 2011, Petrologic and Petrophysical Characteristics: Mississippian Chert, Oklahoma, M.S. Thesis, Oklahoma State University, Stillwater, Oklahoma, 85 p.

APPENDICES

Classifications and Abbreviations

Appendix A: Effie B York Unit #1

- I. **Core Photographs**
- II. **Thin Section Photomicrographs**
- III. **Core Descriptions**
  - a. **Preliminary/ Detailed**
  - b. **Wireline Log-tied/ Finalized**

Appendix B: Moore Unit D #1

- I. **Core Photographs**
- II. **Thin Section Photomicrographs**
- III. **SEM Photomicrographs**
- IV. **Core Descriptions**
  - a. **Preliminary/ Detailed**
  - b. **Wireline Log-tied/ Finalized**

Appendix C: Droke Unit #1

- I. **Core Photographs**
- II. **Thin Section Photomicrographs**
- III. **Core Descriptions**
  - a. **Preliminary/ Detailed**
  - b. **Wireline Log-tied/ Finalized**

Appendix D: Sequence Stratigraphic Architecture/ Subsurface Mapping

- I. **3rd-Order Gross Isopachs**
  - a. **S1**
  - b. **S2**
  - c. **S3**
  - d. **S4**
- II. **Reservoir Development and Distribution**
  - a. **Gross Chert interval (S2:HFS4)**

Classifications and Abbreviations

Bioturbation Index			
#	Characteristics	Mud-Dominated Facies	Grain-Dominated Facies
0	Bioturbation absent	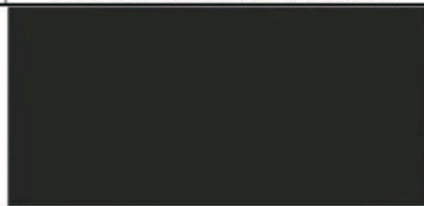	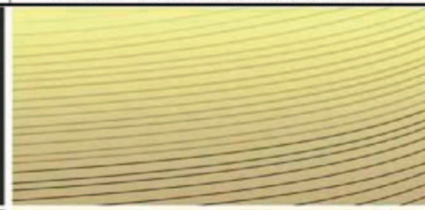
1	Sparse bioturbation, bedding distinct, few discrete traces	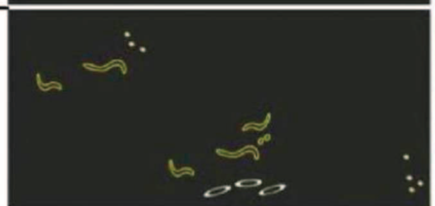	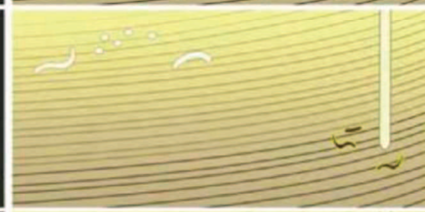
2	Uncommon bioturbation, bedding distinct, low trace density	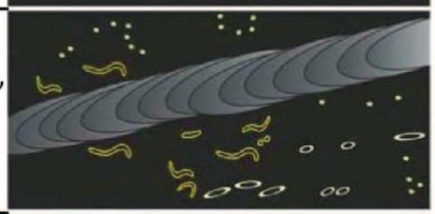	
3	Moderate bioturbation, bedding boundaries sharp, traces discrete, overlap rare	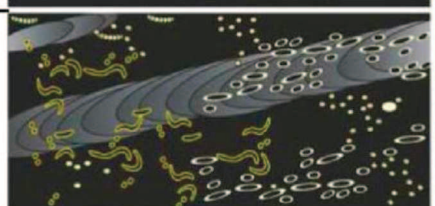	
4	Common bioturbation, bedding boundaries indistinct, high trace density with overlap common	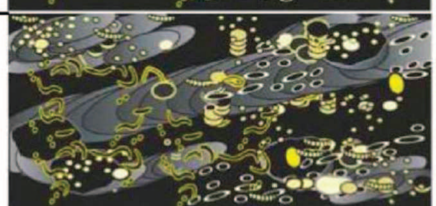	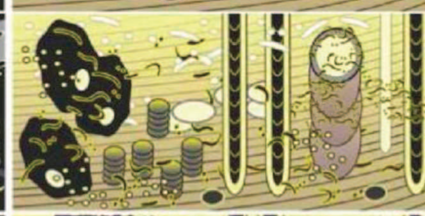
5	Abundant bioturbation, bedding completely disturbed (just visible)	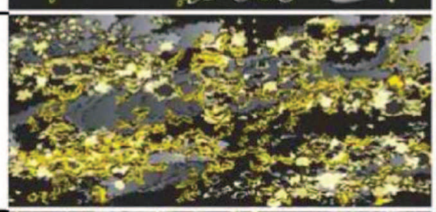	
6	Complete bioturbation, total biogenic homogenization of sediment	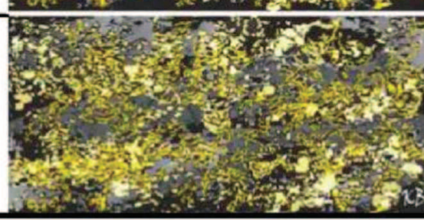	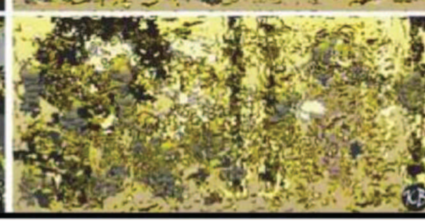

Table 6. Bioturbation Index (BI) used for core and thin section descriptions. From Bann et al., 2008.

Core and Thin Section Image Labels									
Feature Key								**Porosity Key**	
BLANK	thin section blank (location)	**HCS**	hummocky cross stratification	**PLUG**	core plug (location)	**FR**	fracture		
BR	brachiopod	**K-spar**	potassium feldspar	**PPL**	plane-polarized light	**IP**	interparticle		
BU	burrow	**L**	lamination	**PY**	pyrite	**IX**	intercrystalline		
BY	bryozoan	**M**	mud/mudstone	**Q**	quartz (detrital)	**MO**	moldic		
Ca	calcite	**MI**	mica/detrital clays	**Qm**	quartz matrix	**SH**	shelter		
CH	chert	**Mic**	micrite	**Qo**	quartz overgrowth	**VU**	vug		
CON	conodont	**MW**	mud wisp	**S**	stylolite	**WP**	intraparticle		
CR	crinoid	**Mxl**	mixed-layer illite/smectite	**SK**	undifferentiated skeletal fragment	**WX**	intracrystalline		
D/Dol	dolomite	**O**	ostracode	**SP**	spicule				
EC	echinoderm	**OIL**	oil/dead oil/organics	**TL**	traction laminae				
FR	fracture	**P**	peloid	**TS**	truncation surface				
G	glauconite	**PH**	phosphate	**XB**	cross-bedding				
GB	grain bed	**PL**	plagioclase feldspar	**XPL**	cross-polarized light				

Table 7. Core and Thin Section Image Labels.

Rock-Color Chart			
Color Name	**Numerical Designation**	**Color Name**	**Numerical Designation**
Black	N1	Medium Gray	N5
Brownish Black	5 YR 2/1	Moderate Yellowish Brown	10 YR 5/4
Dark Gray	N3	Olive Black	5 Y 2/1
Dark Yellowish Brown	10 YR 4/2	Olive Gray	5 Y 4/1
Dark Yellowish Orange	10 YR 6/6	Very Light Gray	N8
Dusky Yellowish Brown	10 YR 2/2	Yellowish Gray	5 Y 8/1
Grayish Black	N2		
Grayish Yellow Green	5 GY 7/2		
Greenish Black	5 GY 2/1		
Light Gray	N7		
Light Olive Gray	5 Y 6/1		
Medium Dark Gray	N4		

Table 8: Rock-Color Chart from Goddard et al., 1951.

APPENDIX A:

Effie B York Unit #1
Sec. 13 – T. 18N – R. 9W

I. Effie B York Unit #1 Core Photographs

Core butts of the Effie B York Unit #1 were oriented top (“younger”) up and are 3.5 inches wide. Please refer to Table 7 for abbreviations.

8,502-8,503’: Facies 3

8,483-8,483.5': Facies 4.

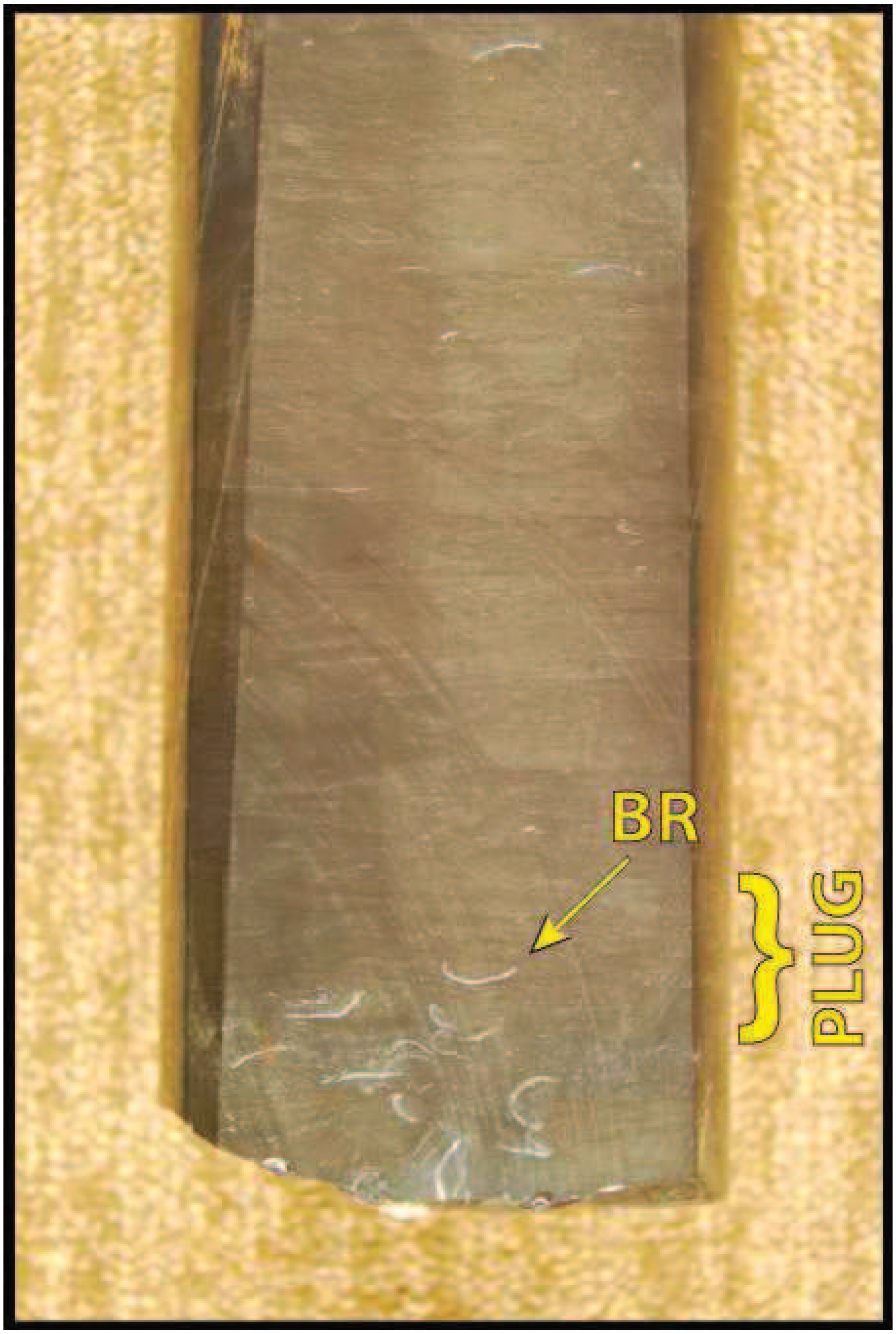

8,476-8,477’: Facies 3.

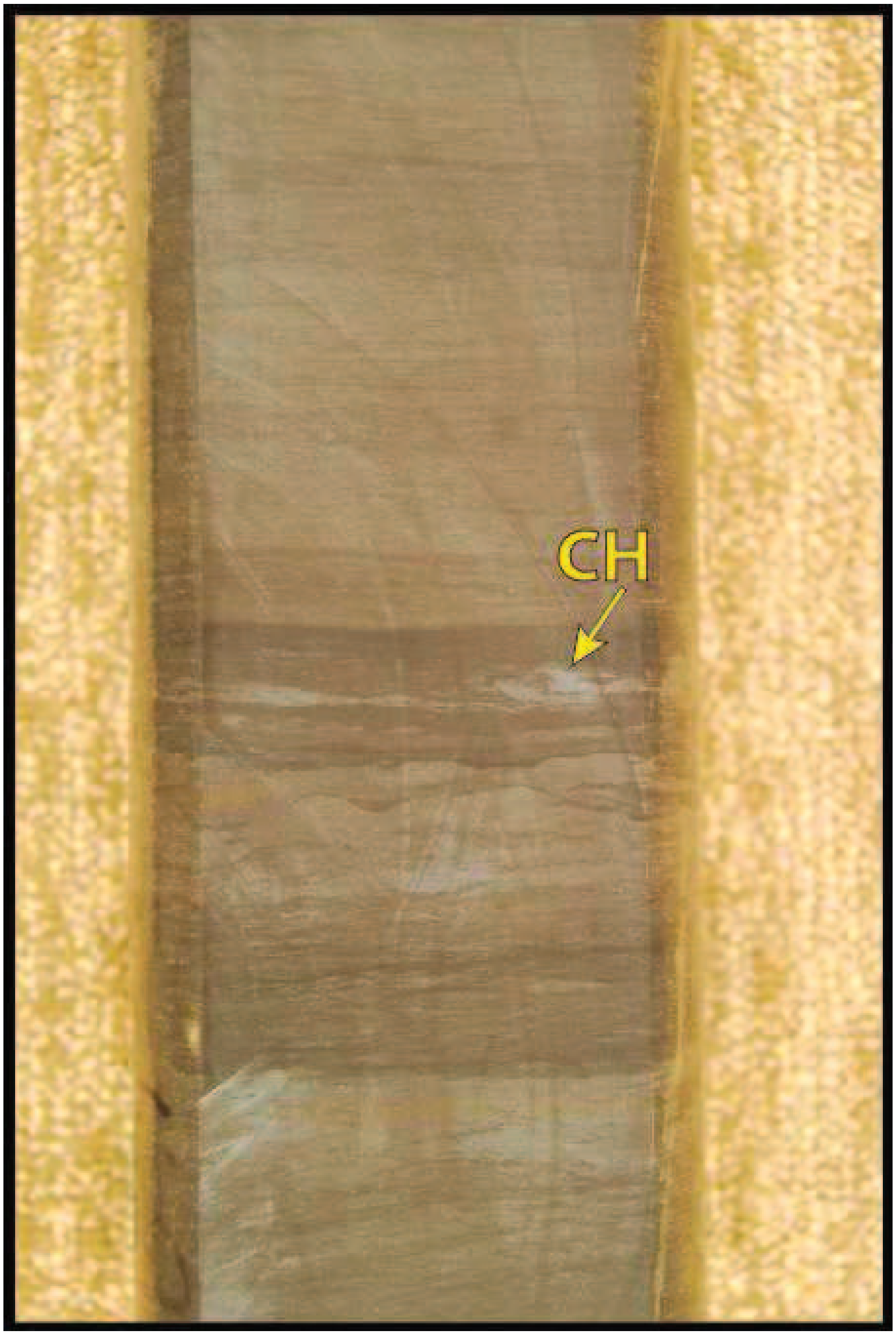

8,468’-8,469’: Facies 4.

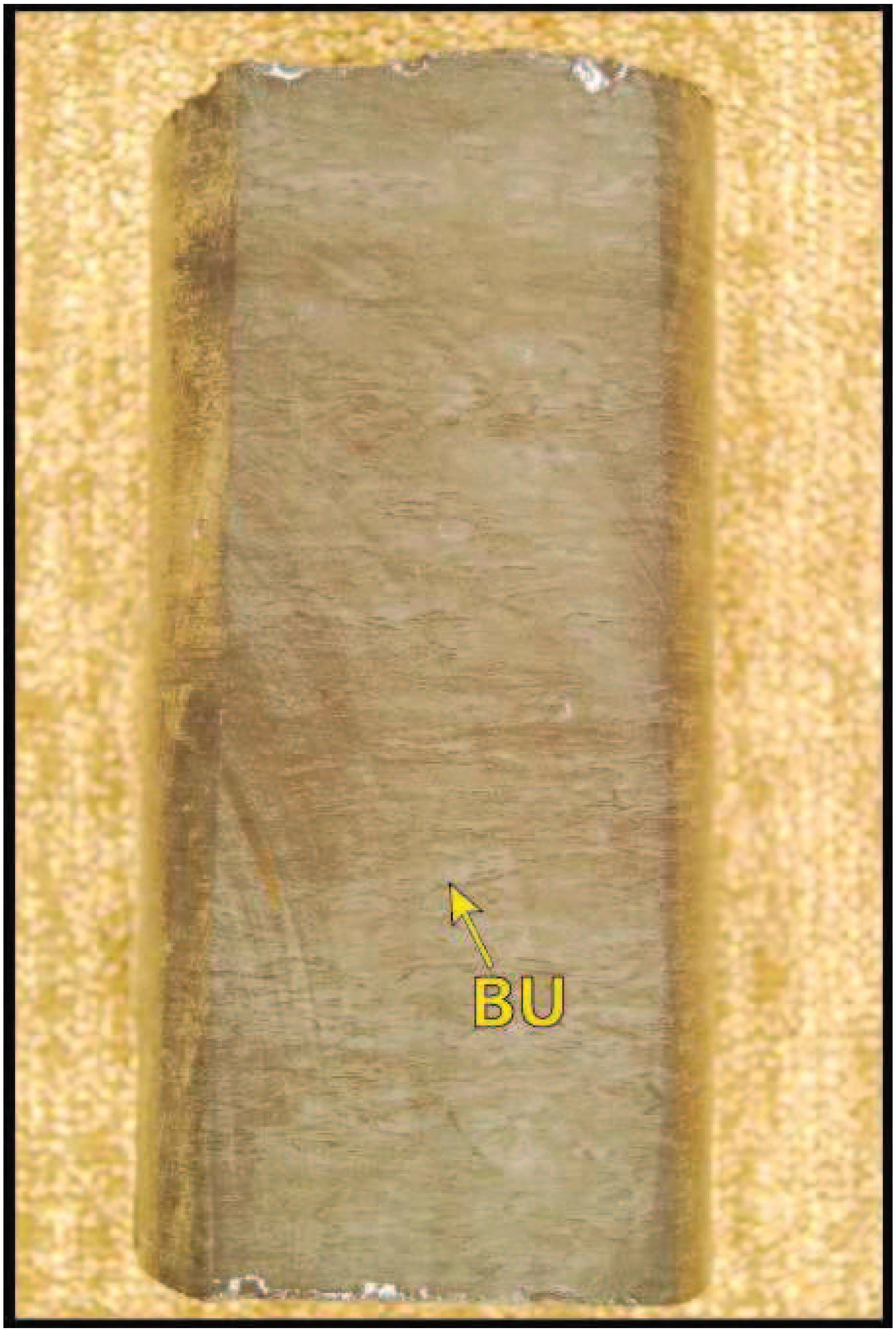

8,455'-8,456': Facies 3.

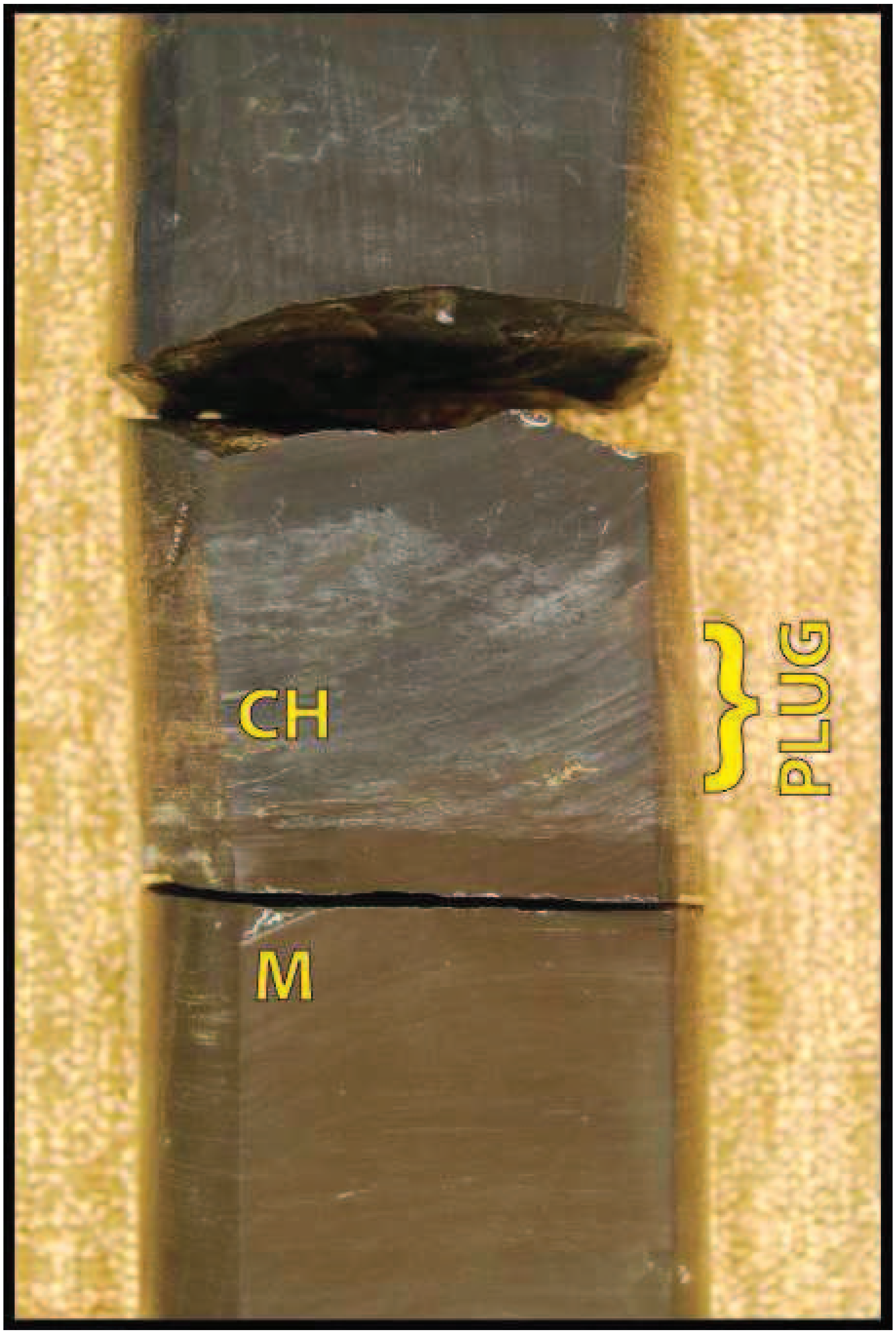

8,447’-8,448’: Facies 2

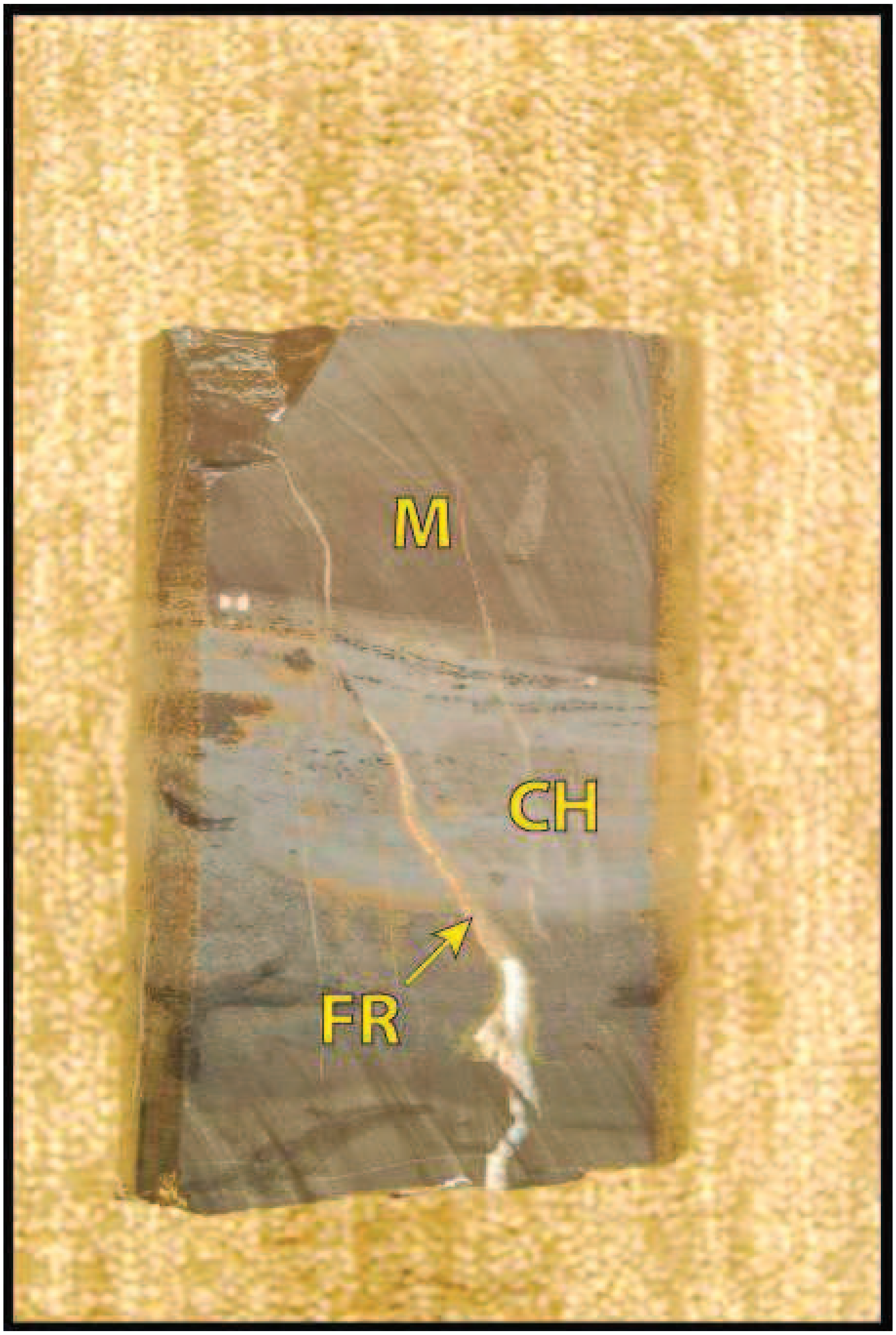

8,446-8,447': Facies 4.

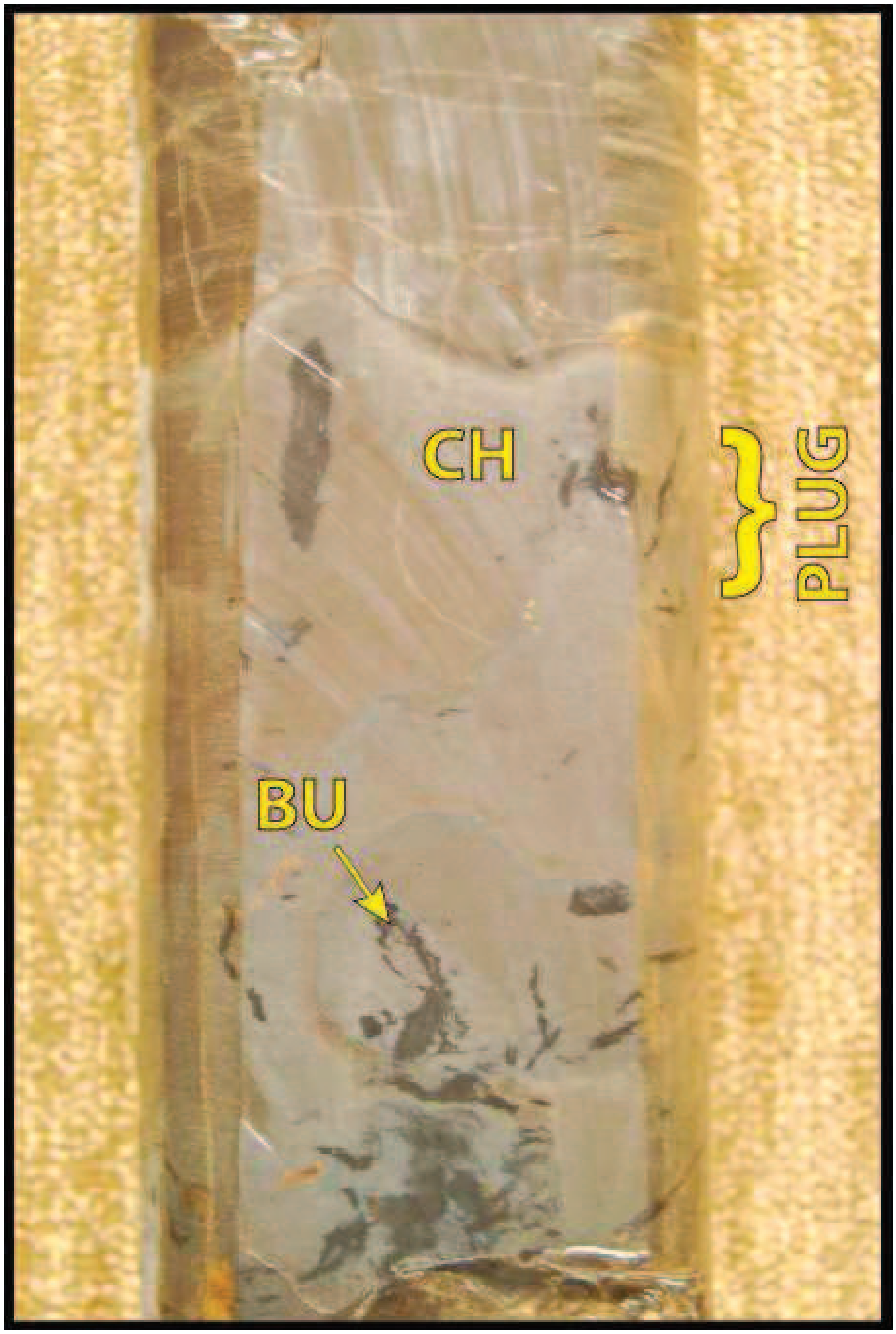

8,426'-8,427': Facies 4 (bottom) and Facies 3 (top).

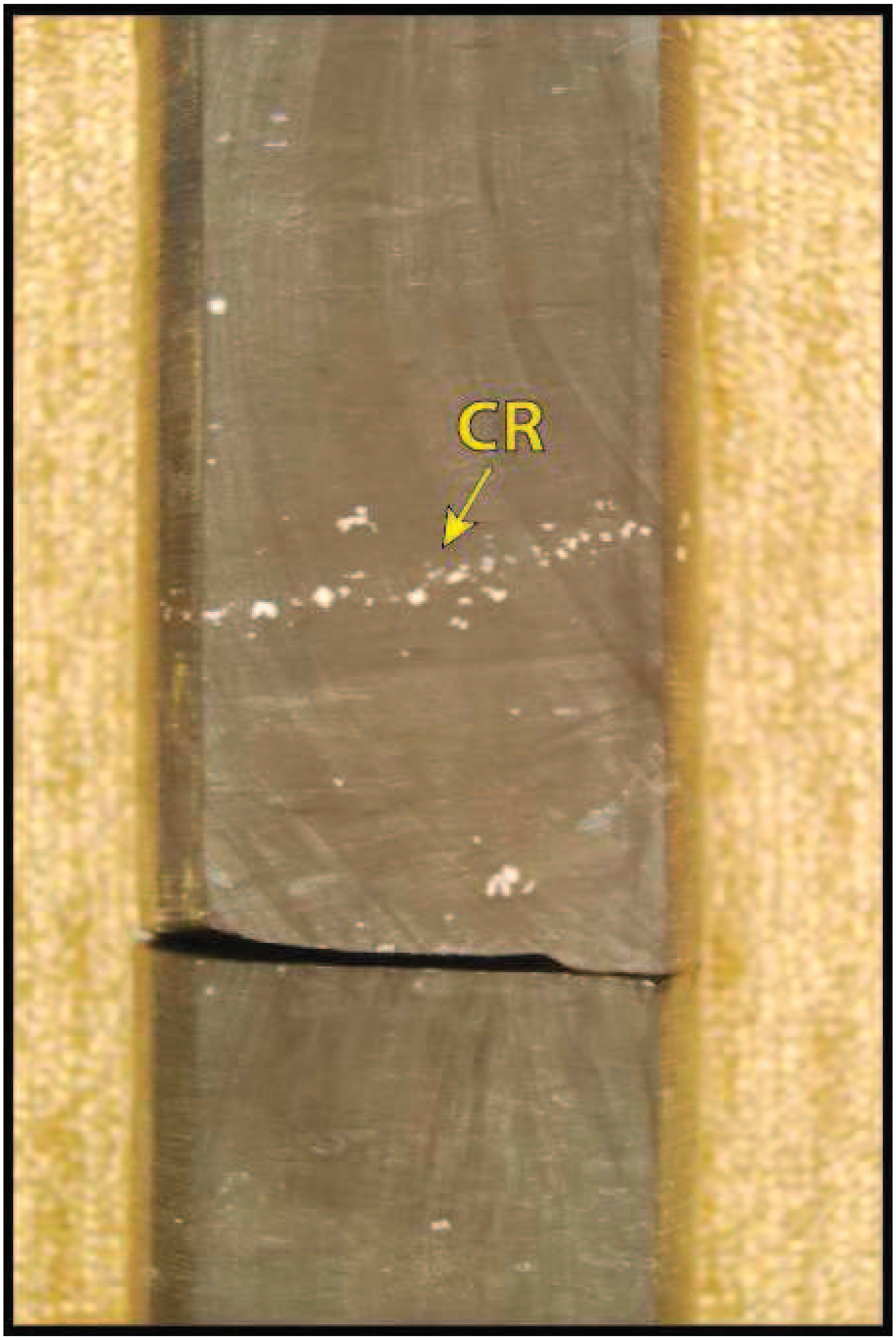

8,418’-8,419’: Facies 3.

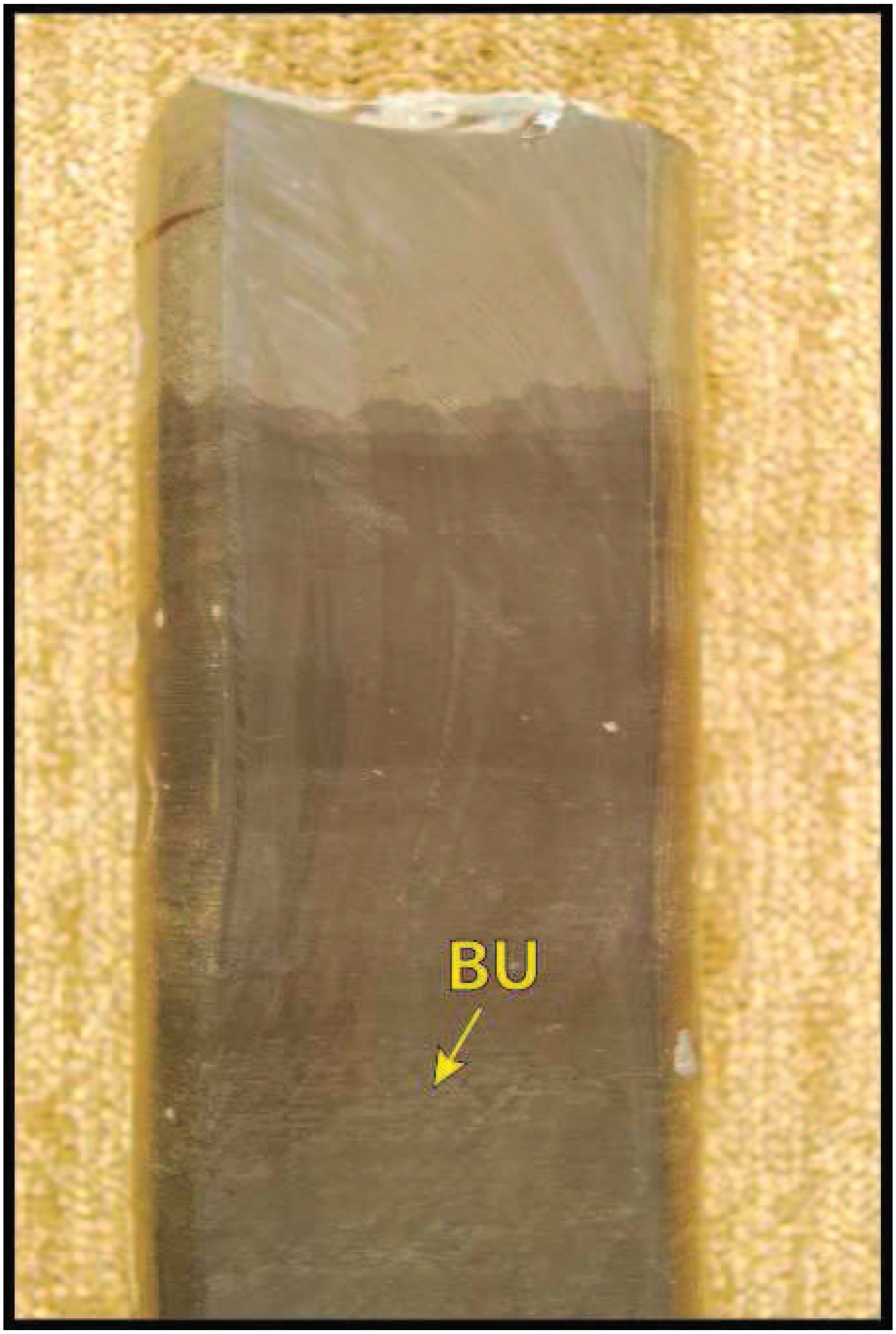

8,411'-8,412': Facies 3.

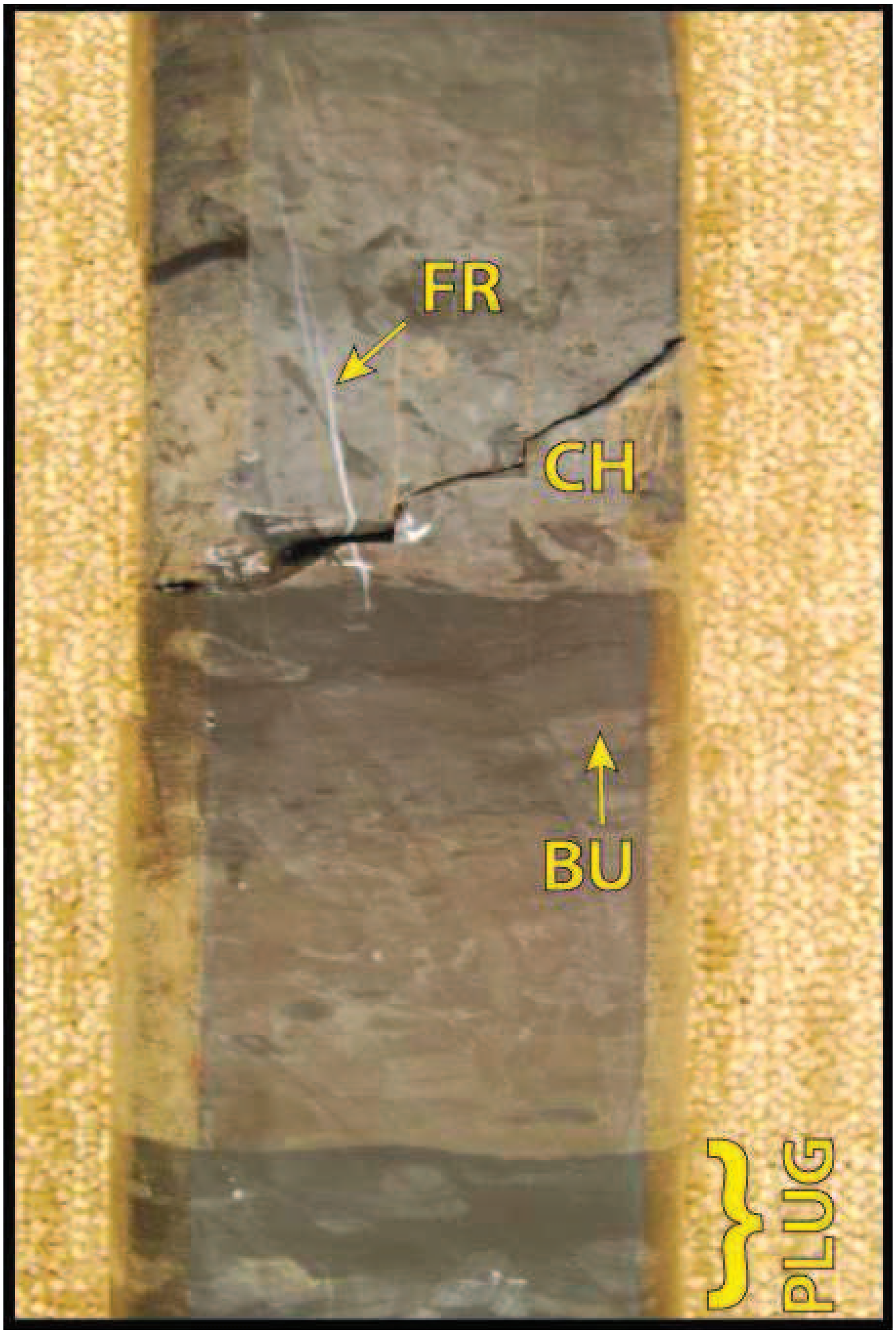

8,396'-8,397': Facies 4.

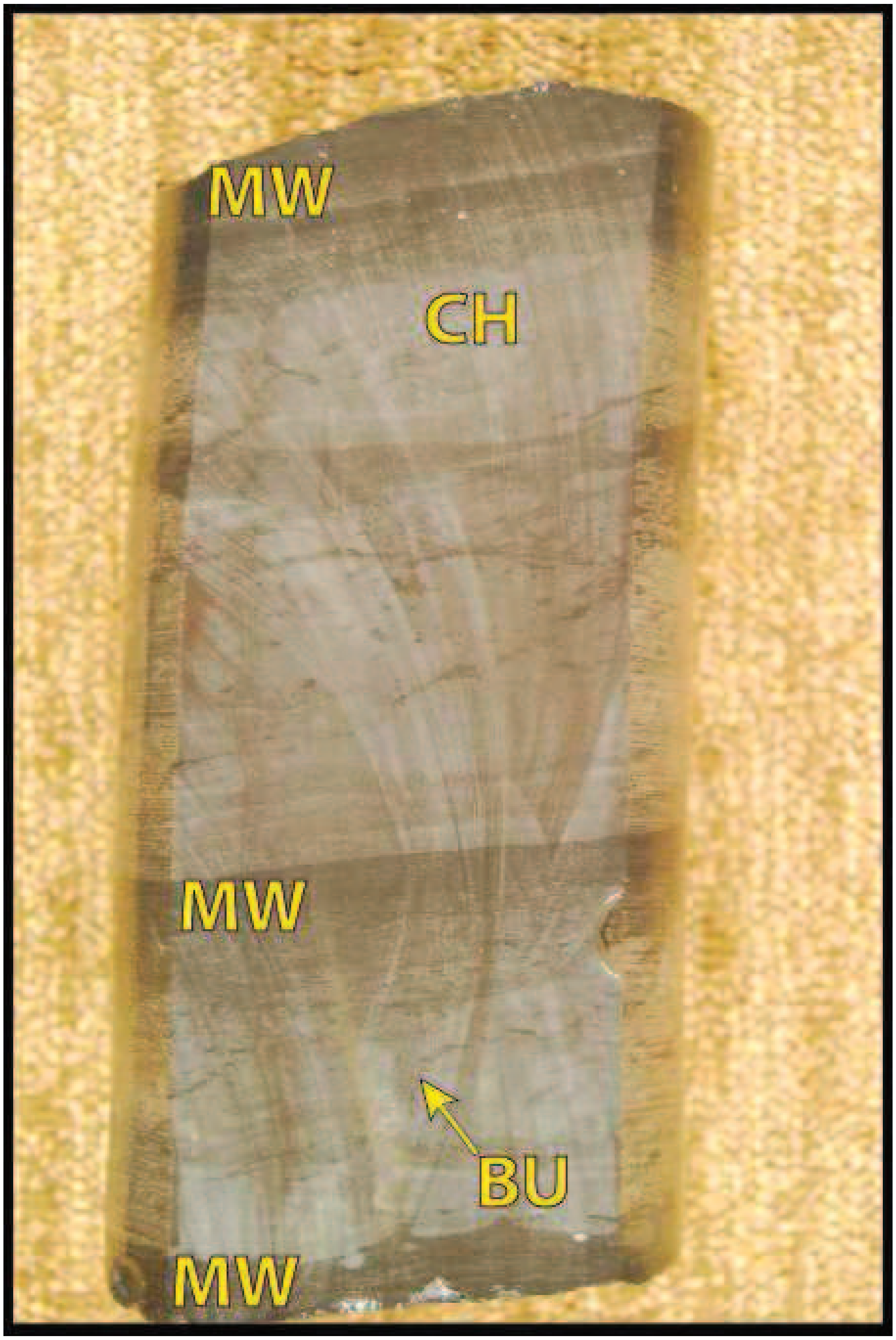

8,381': Facies 4/5.

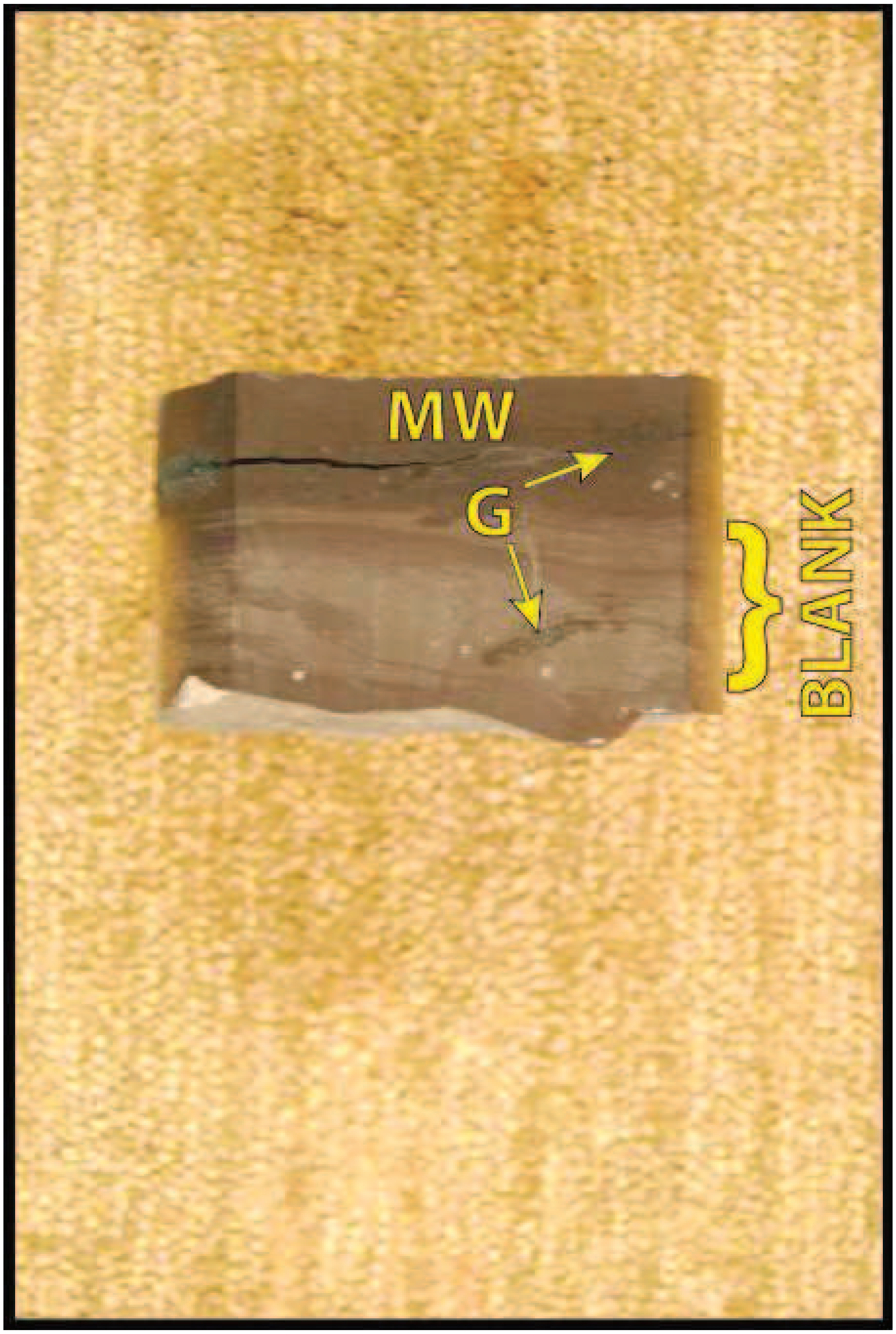

8,377': Facies 1.

8,361-8,362’: Facies 3/4.

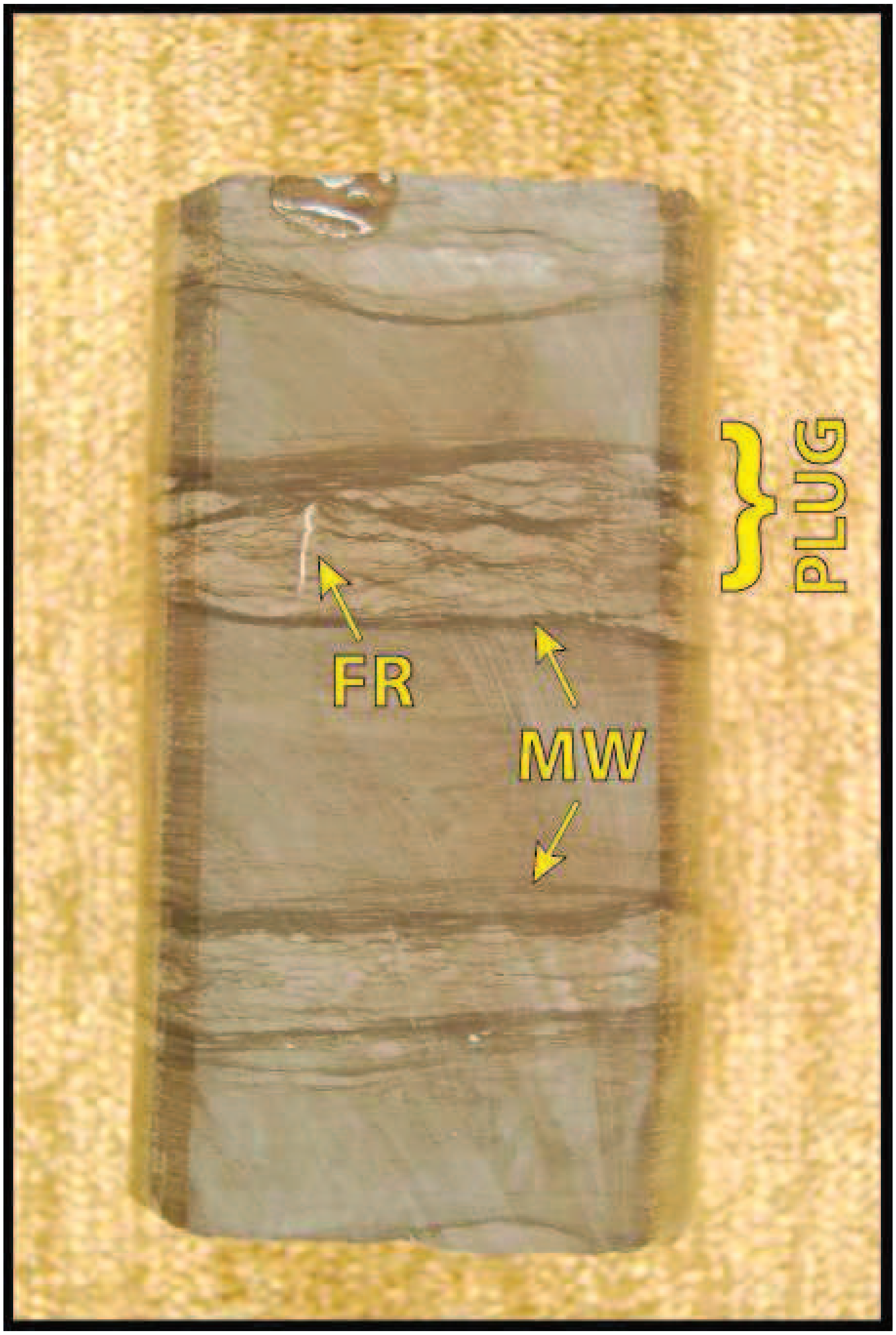

8,355-8,356’: Facies 4.

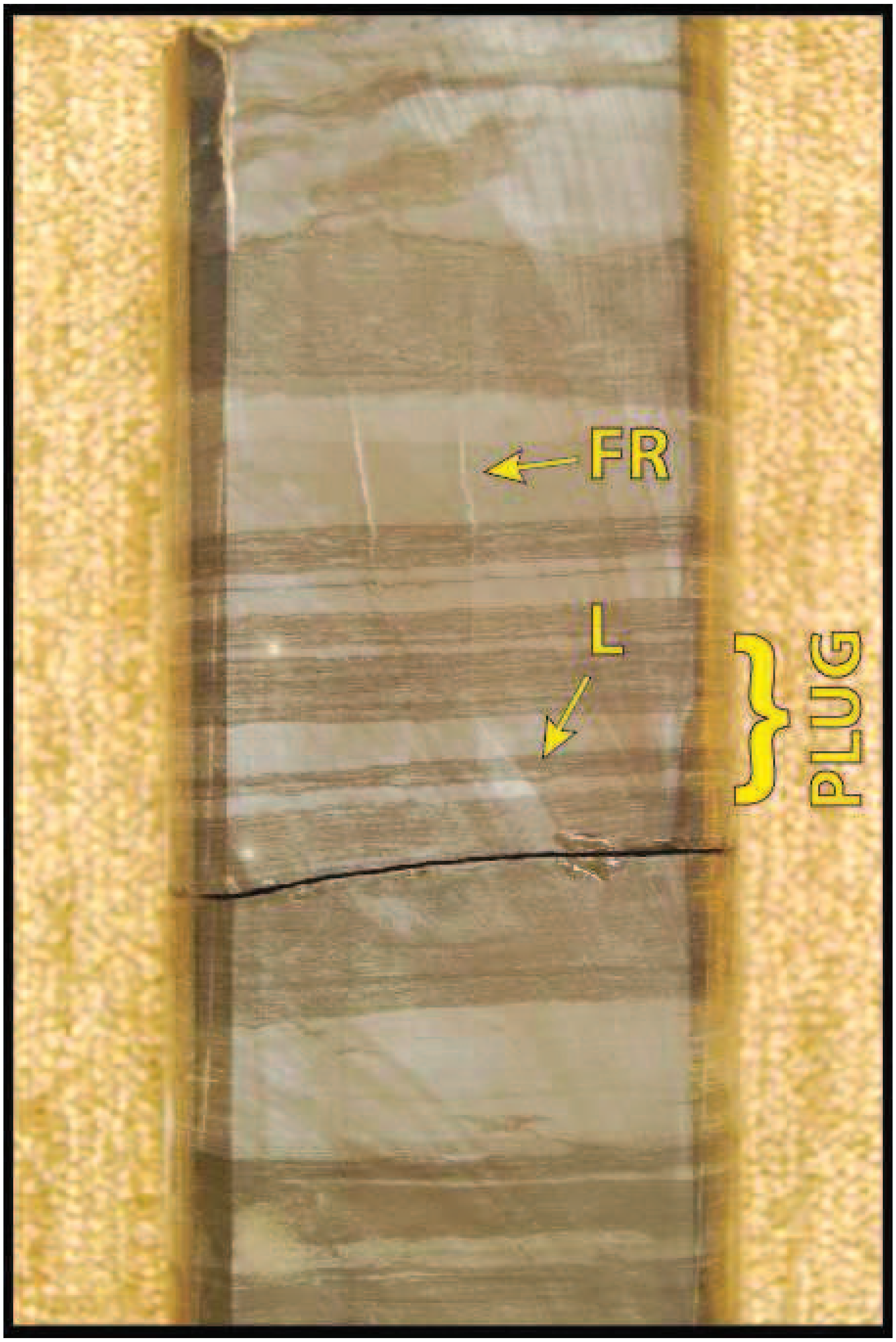

8,328-8,329’: Facies 5.

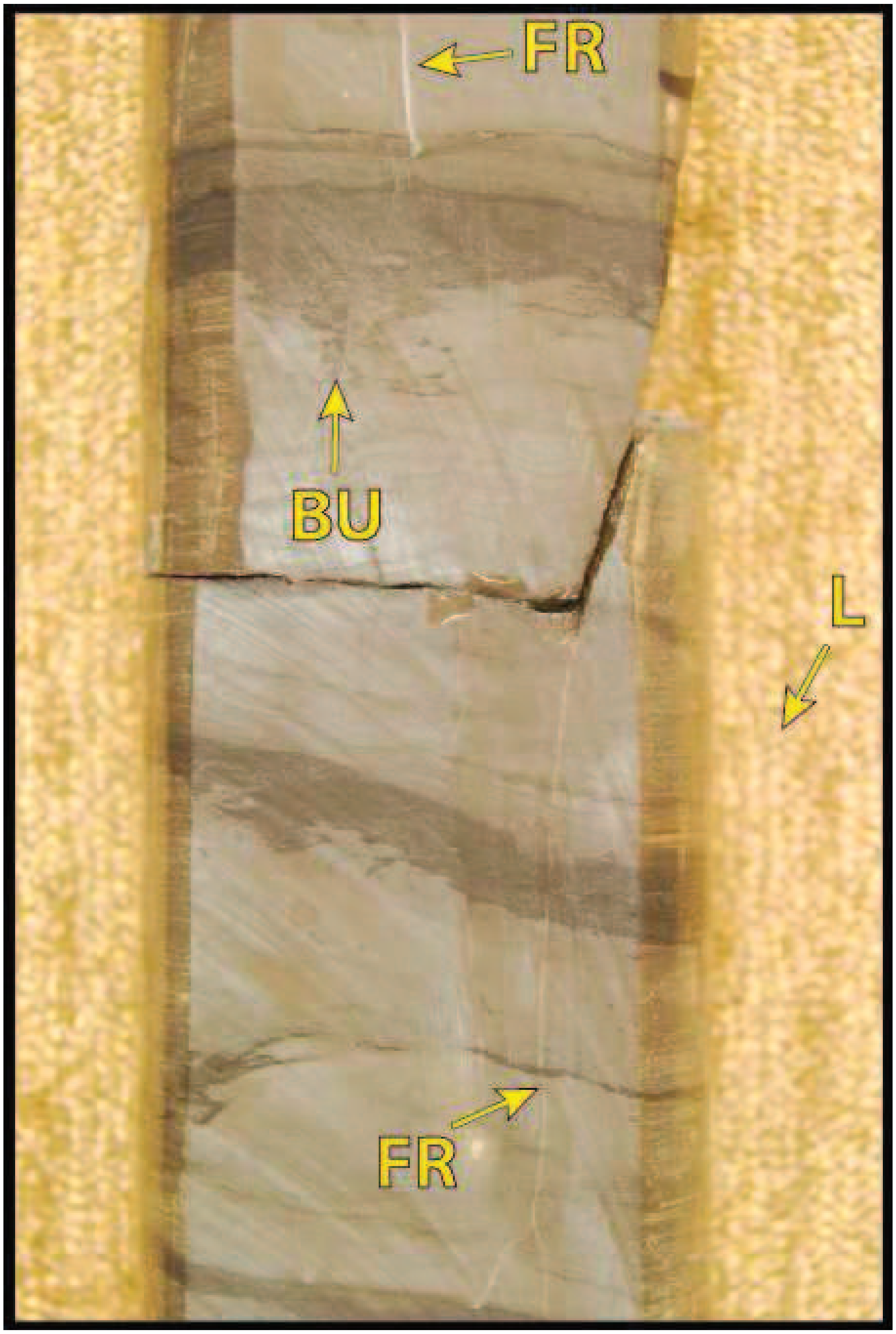

8,323-8,324': Facies 5.

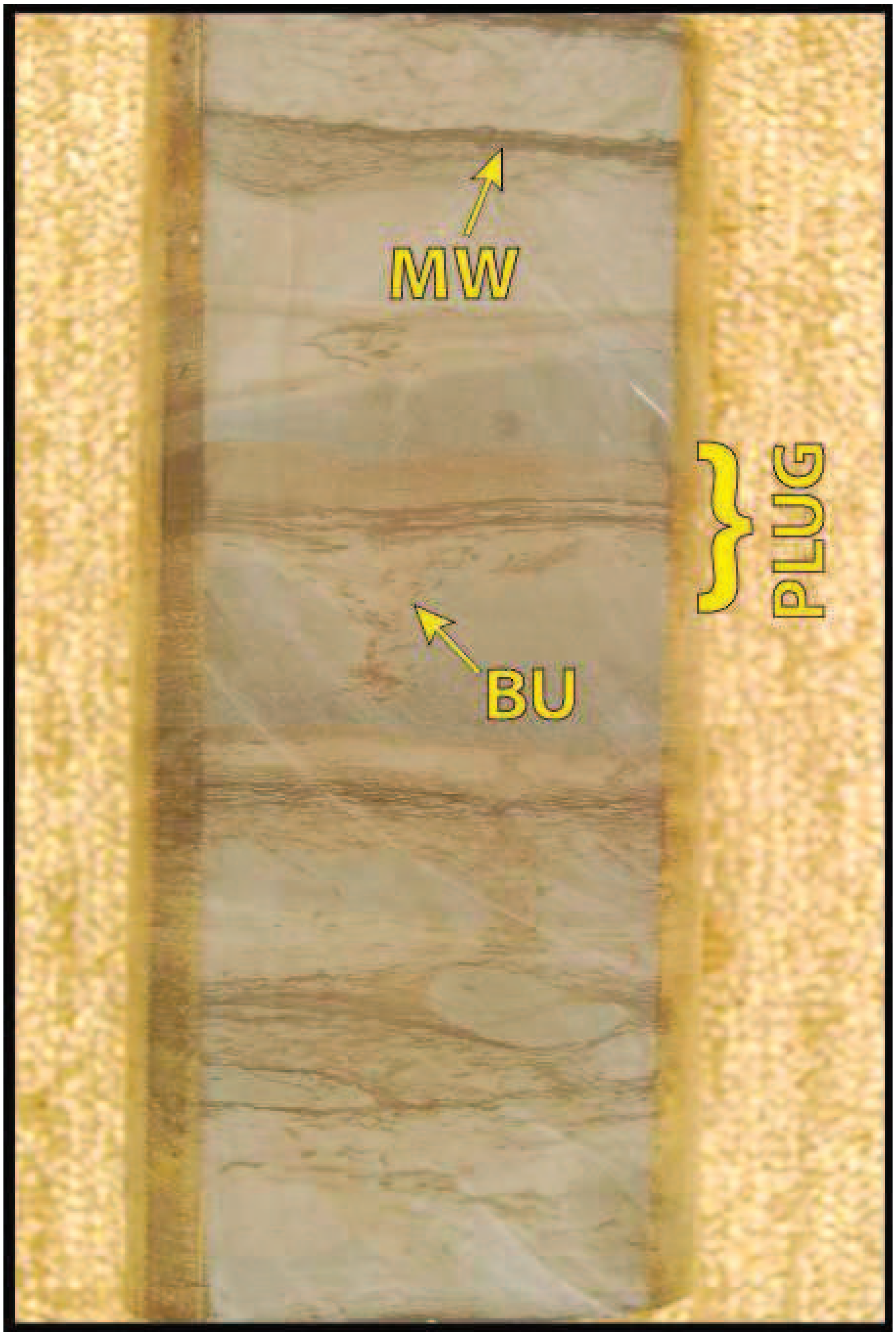

8,286.5-8,287.5’: Facies 4.

8,284-8,285’: Facies 5.

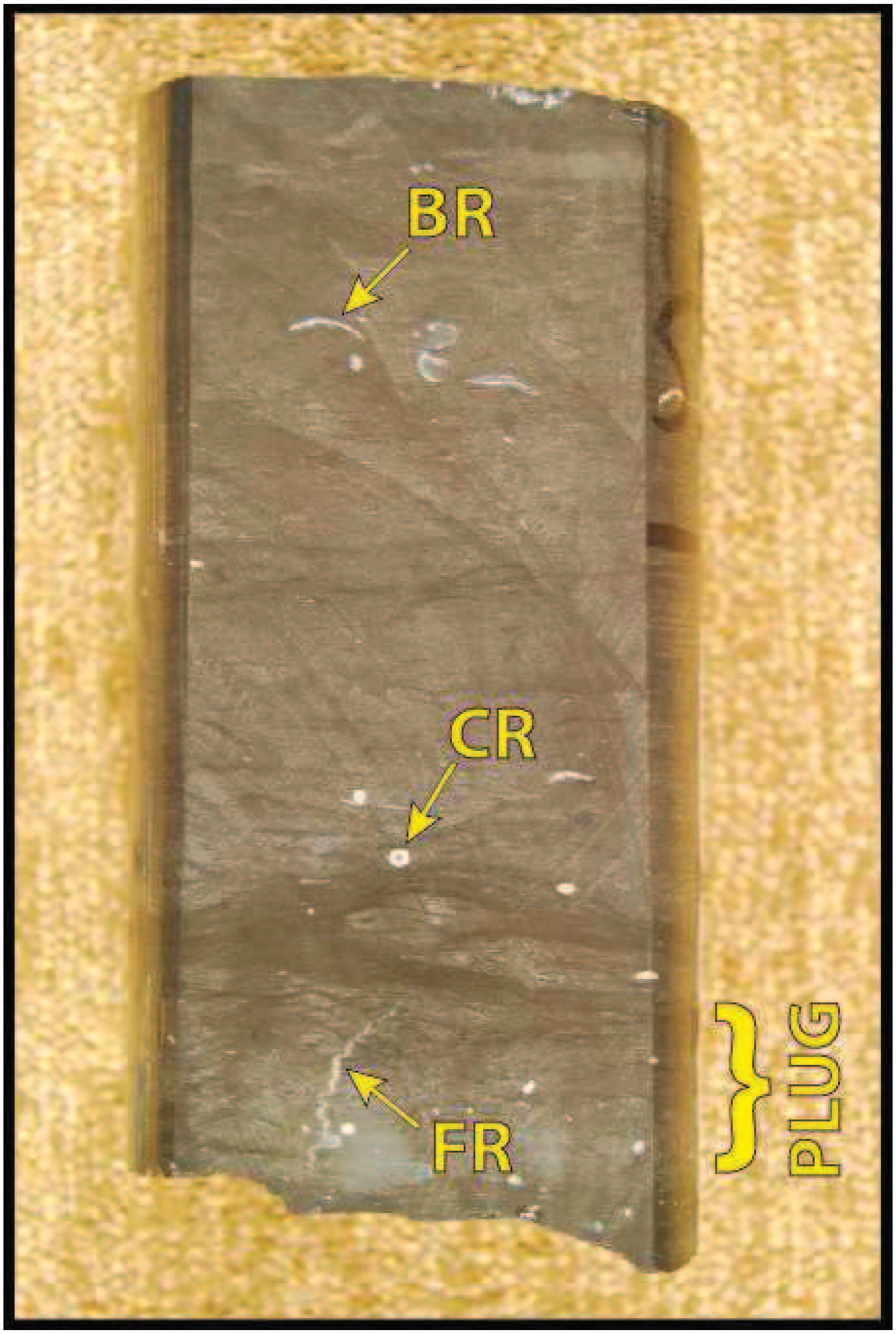

8,253-8,254’: Facies 4.

8,243-8,243.5’: Facies 4.

8,229-8,230’: Facies 2.

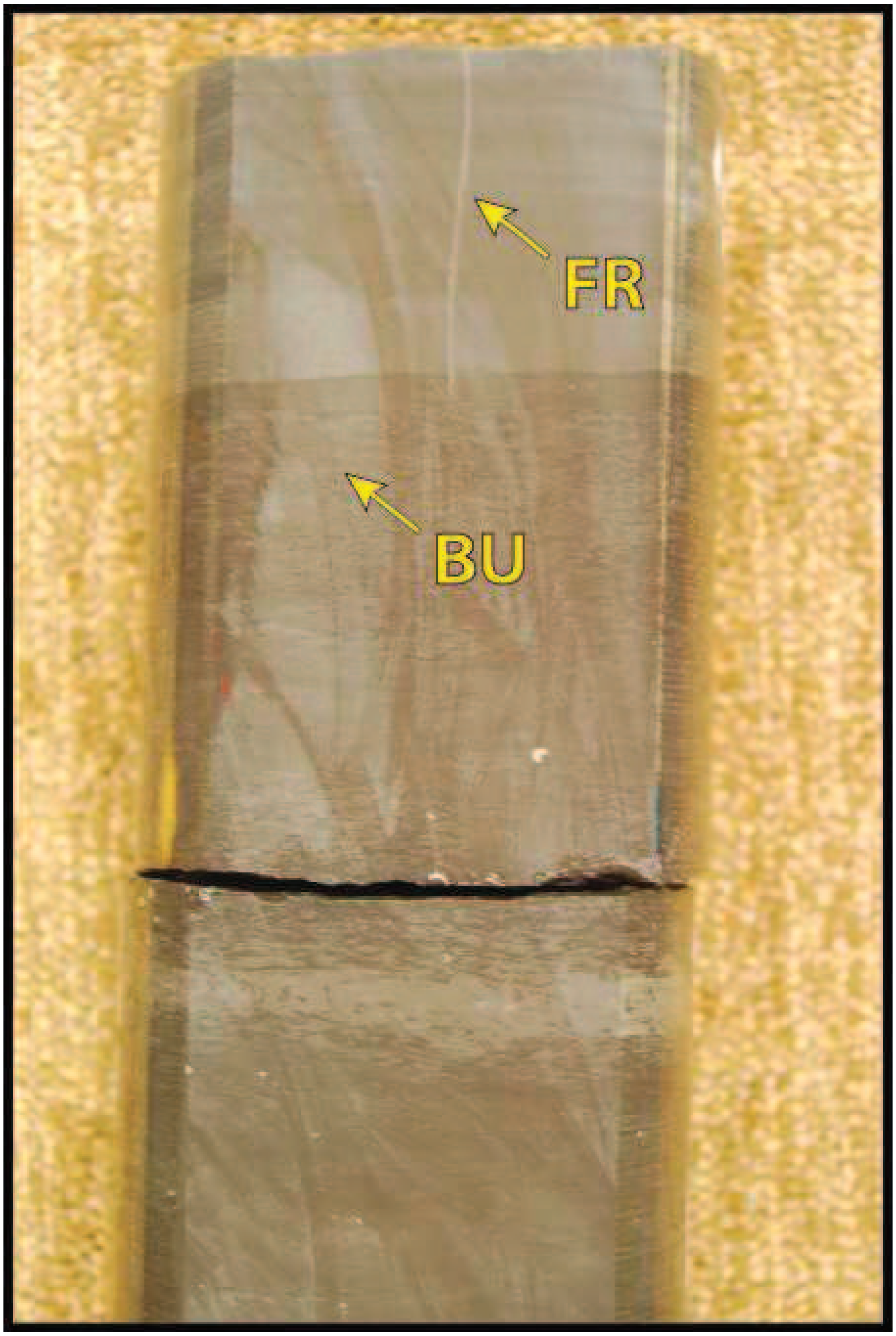

8,221-8,222': Facies 3.

8,214-8,215’: Facies 5.

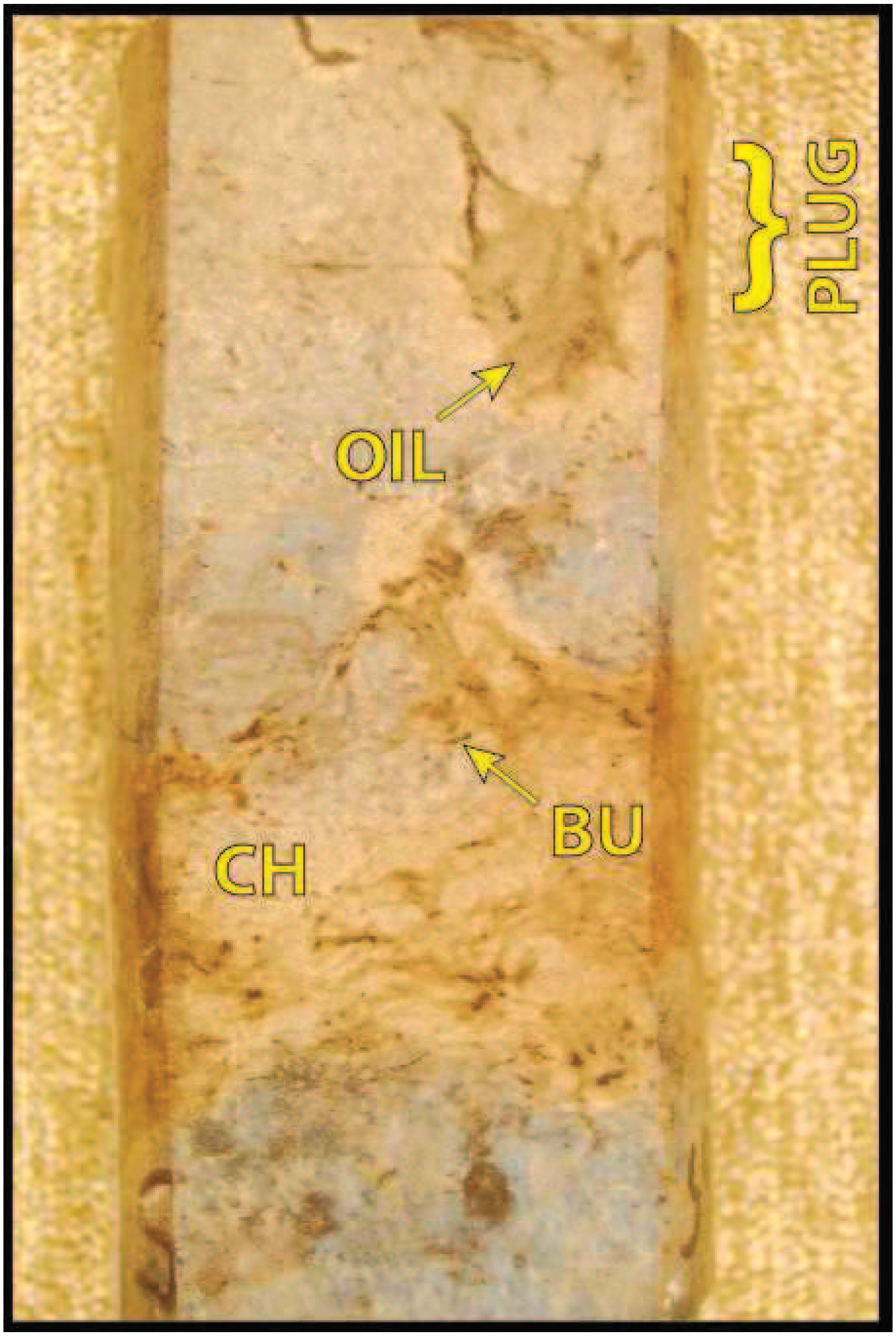

8,205-8,206’: Facies 5.

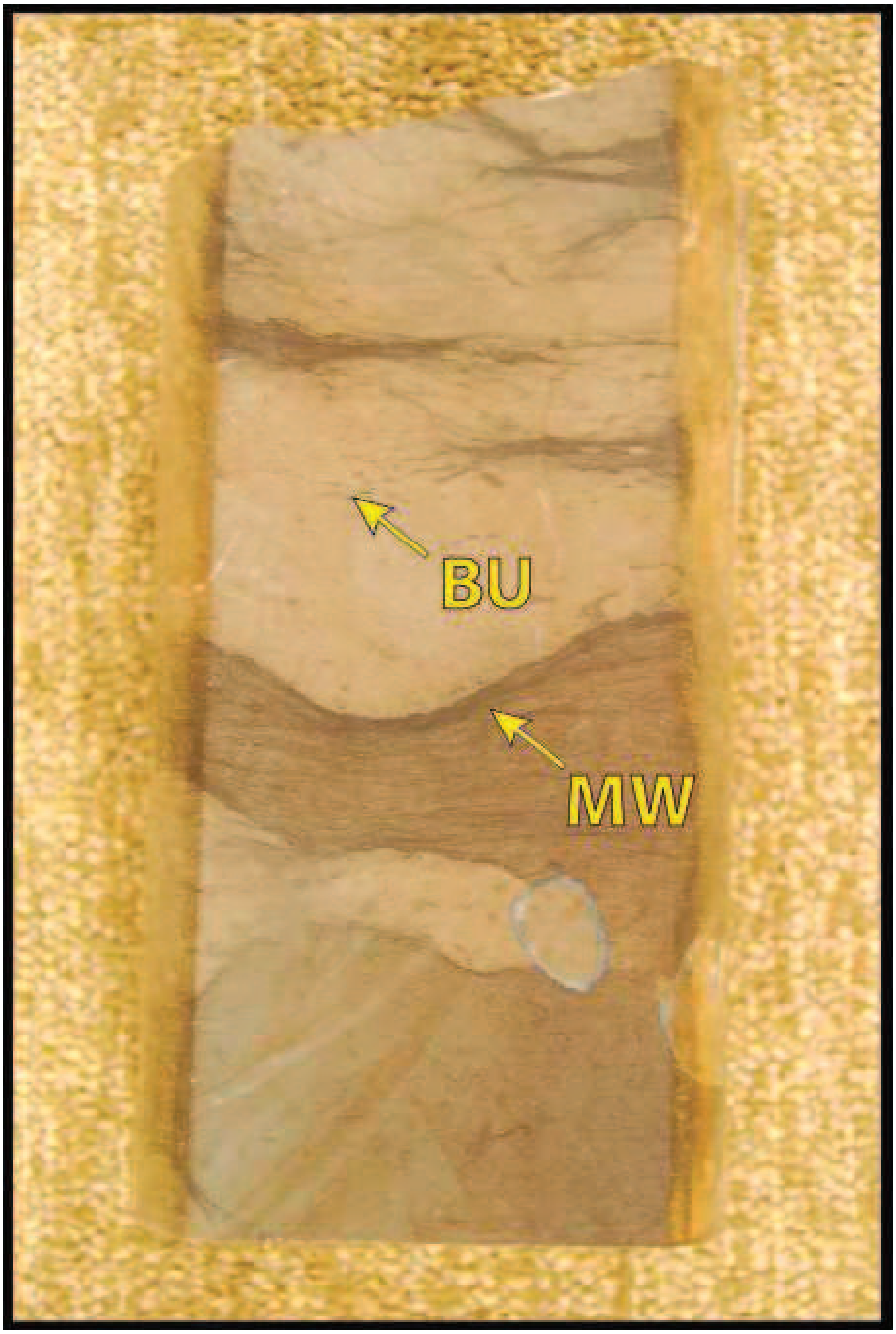

8,186-8,186.5’: Facies 4.

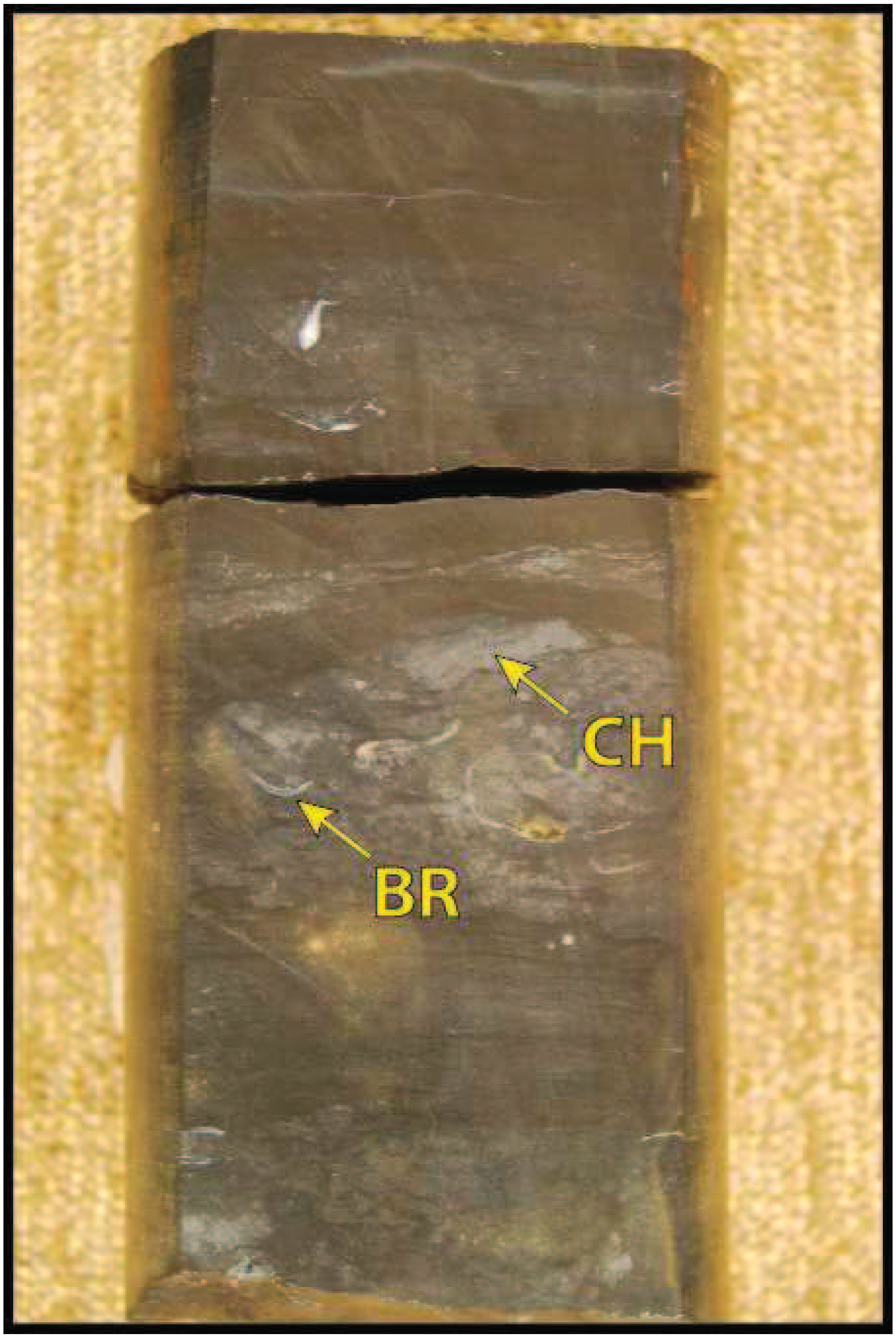

8,179-8,180’: Facies 3.

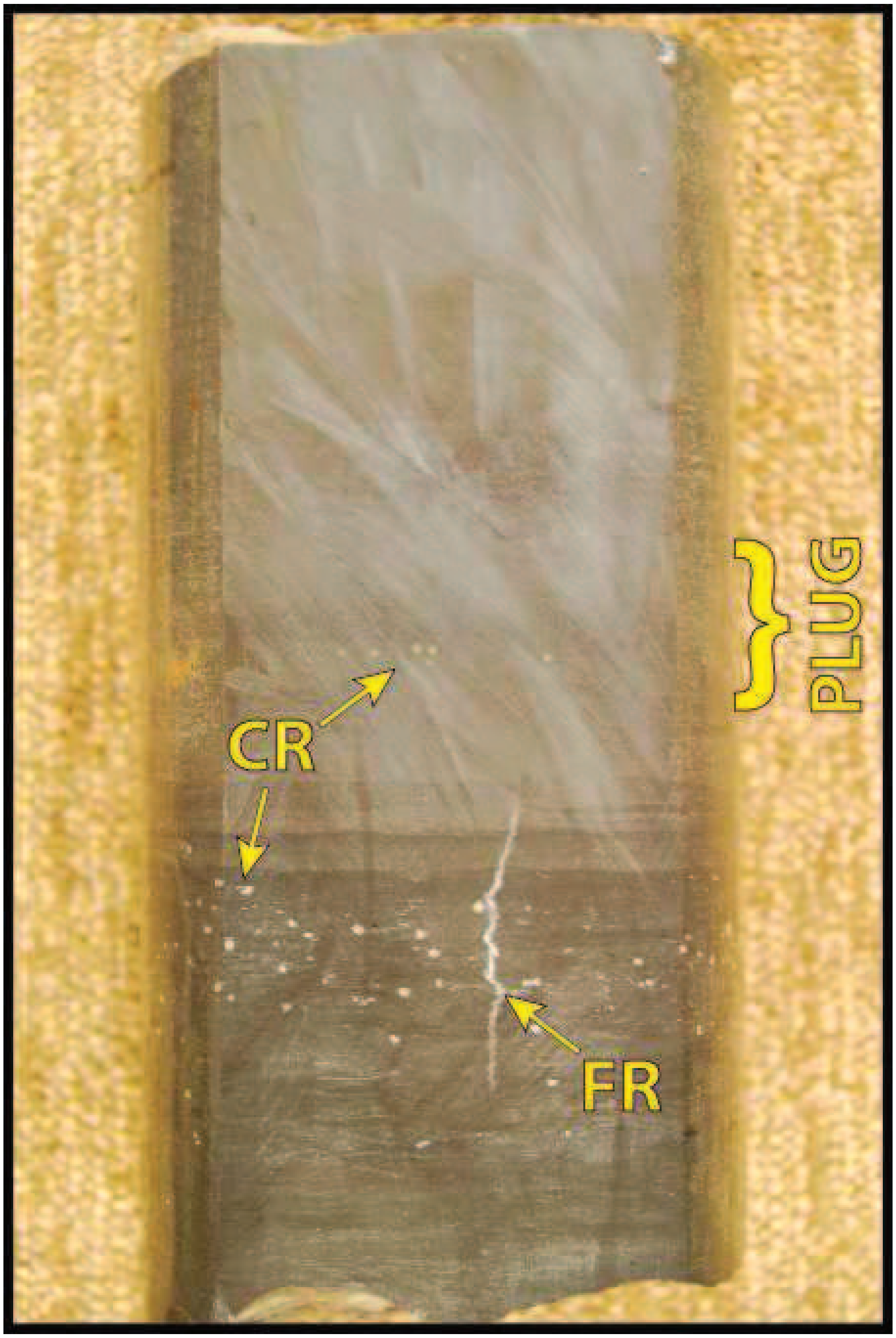

8,171-8,172’: Facies 4.

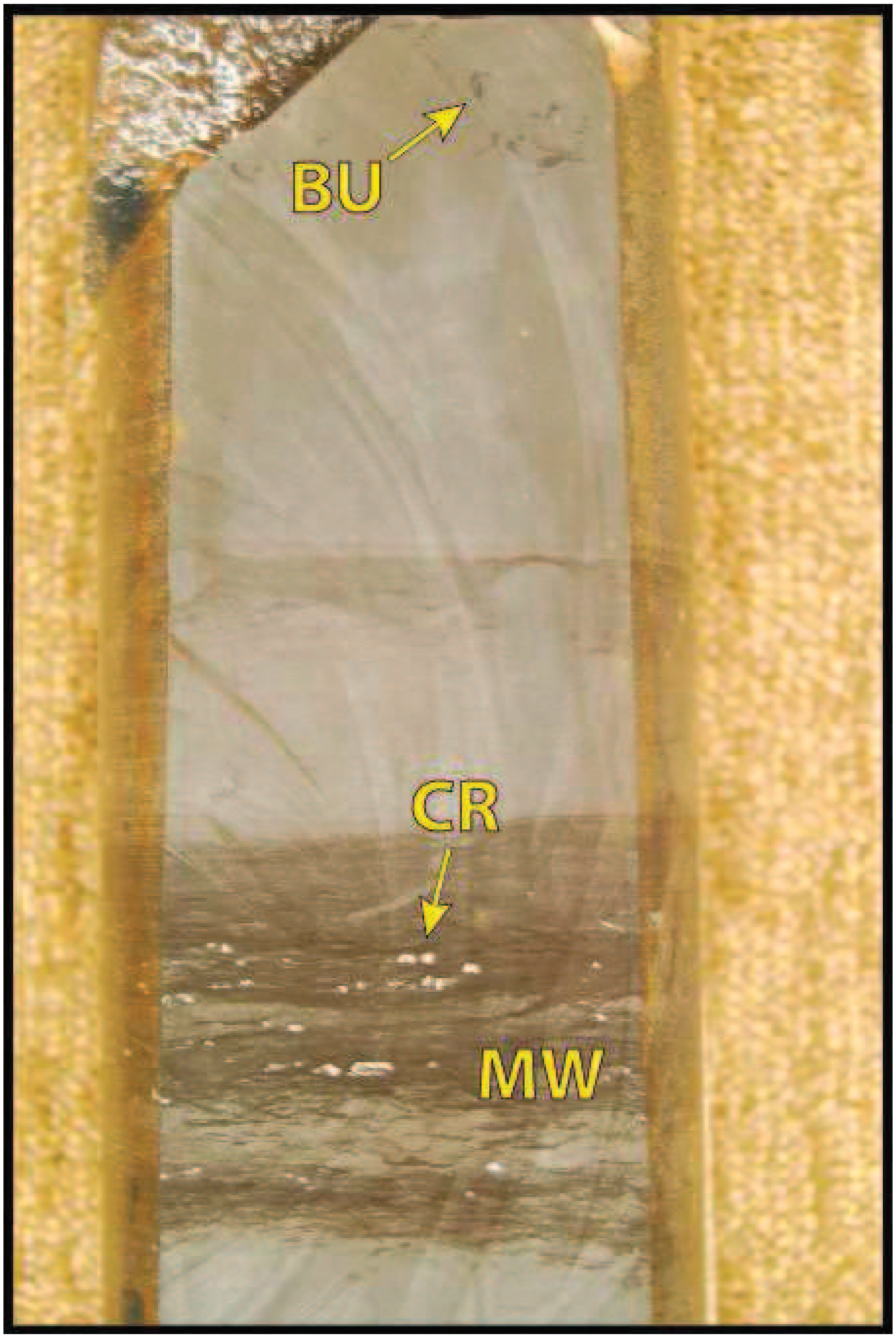

8,141.5-8,142.5’: Facies 4

8,134-8,134.5’: Facies 4.

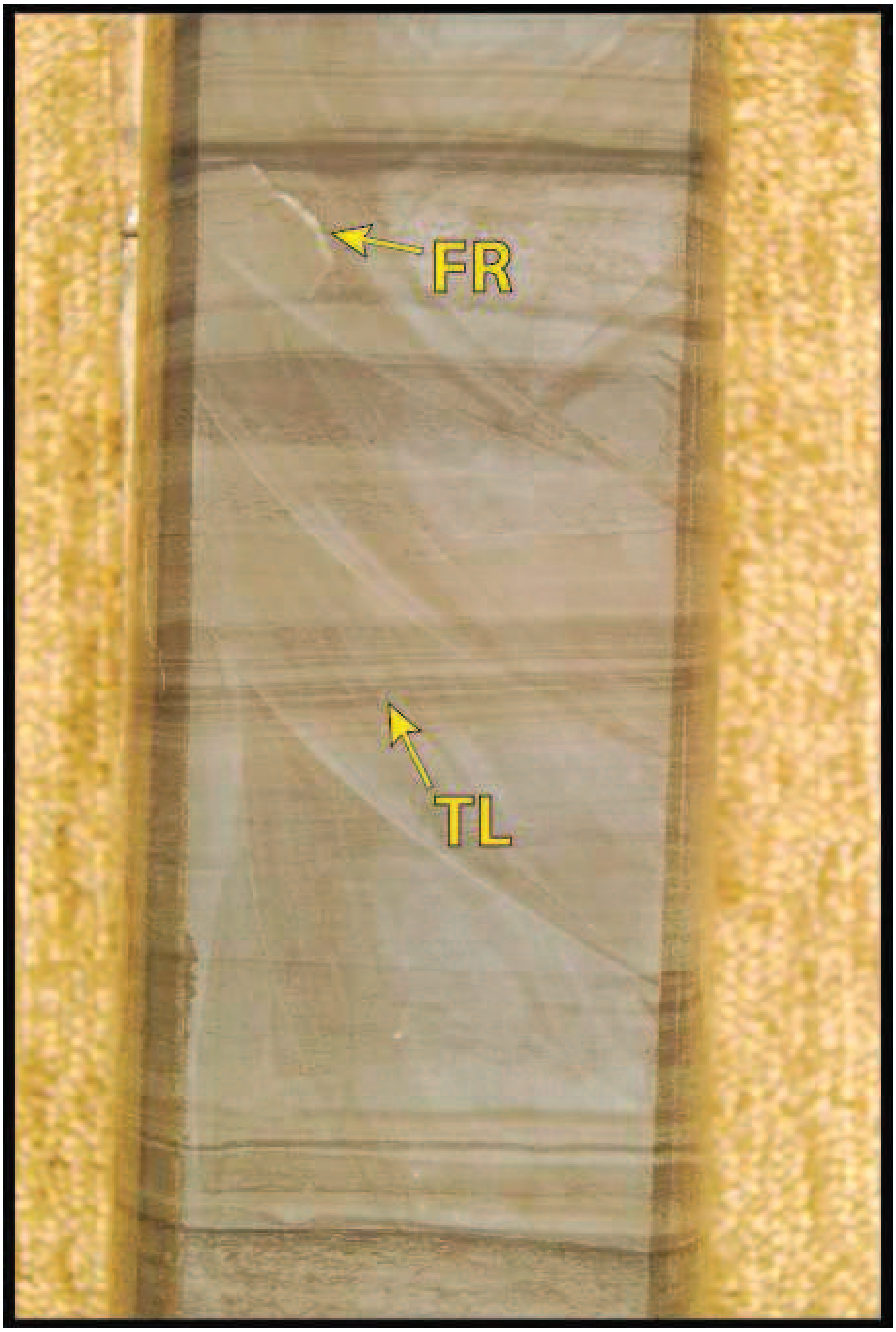

8,106-8,107': Facies 5.

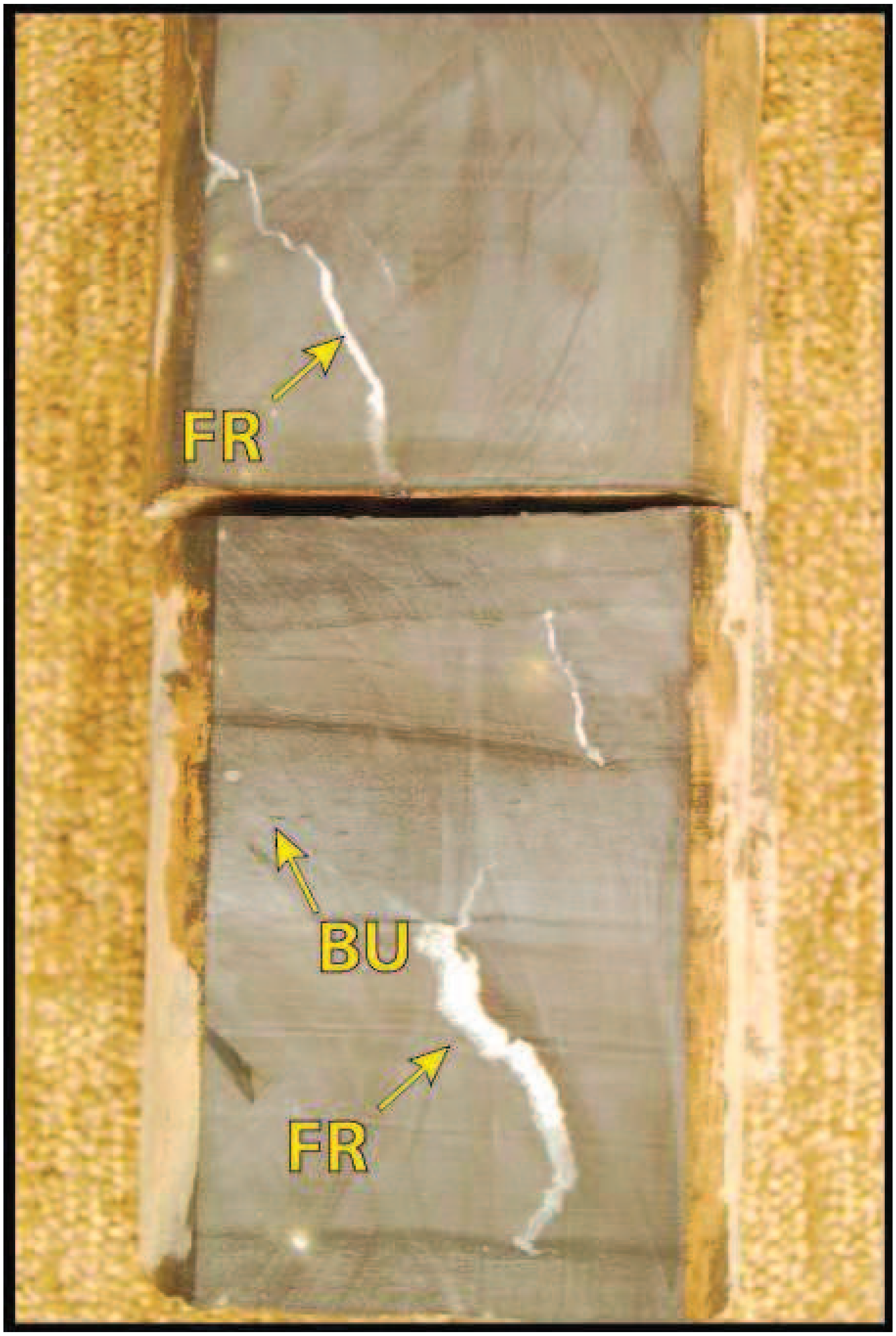

8,101-8,102’: Facies 5.

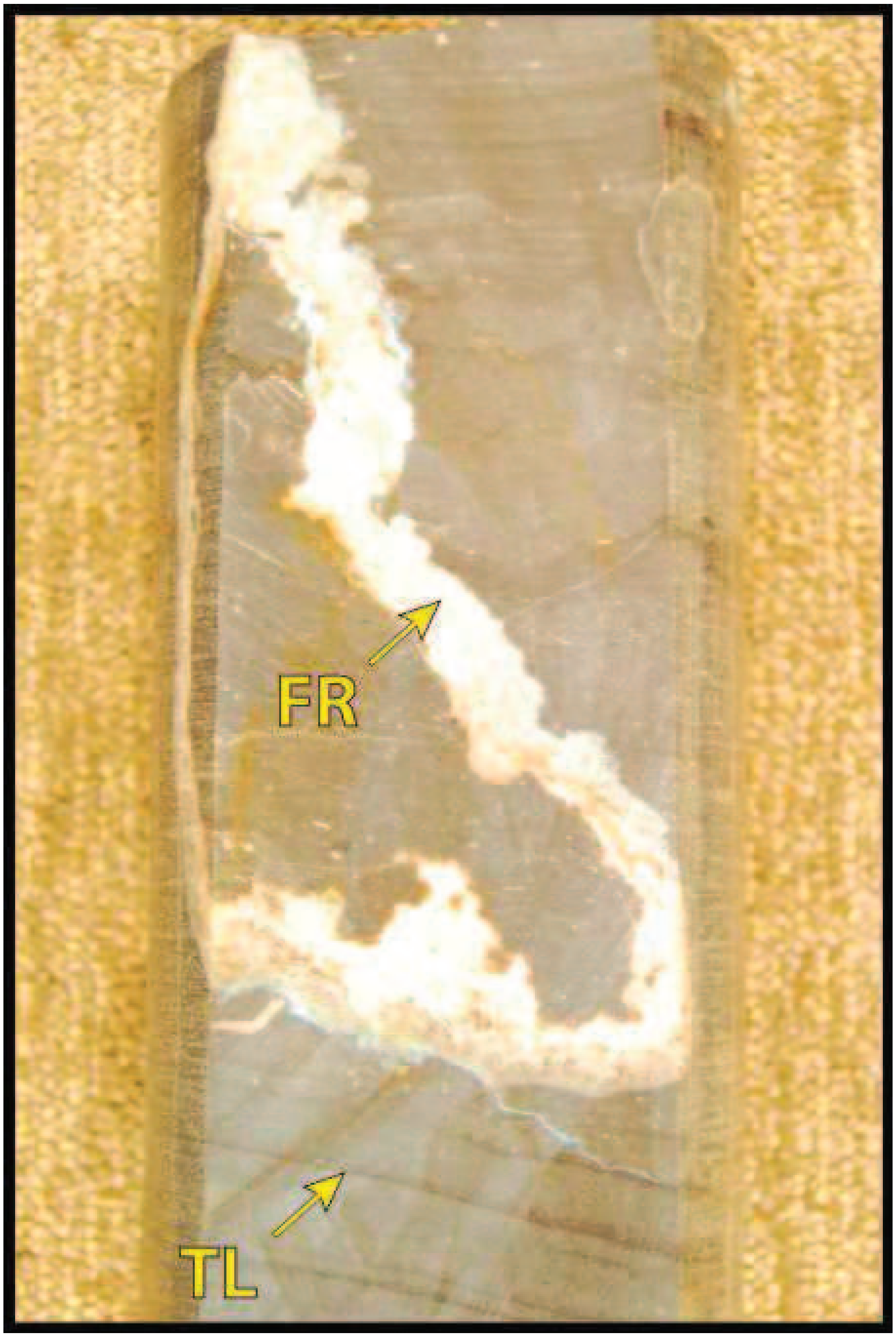

8,075-8,075.5': Facies 5.

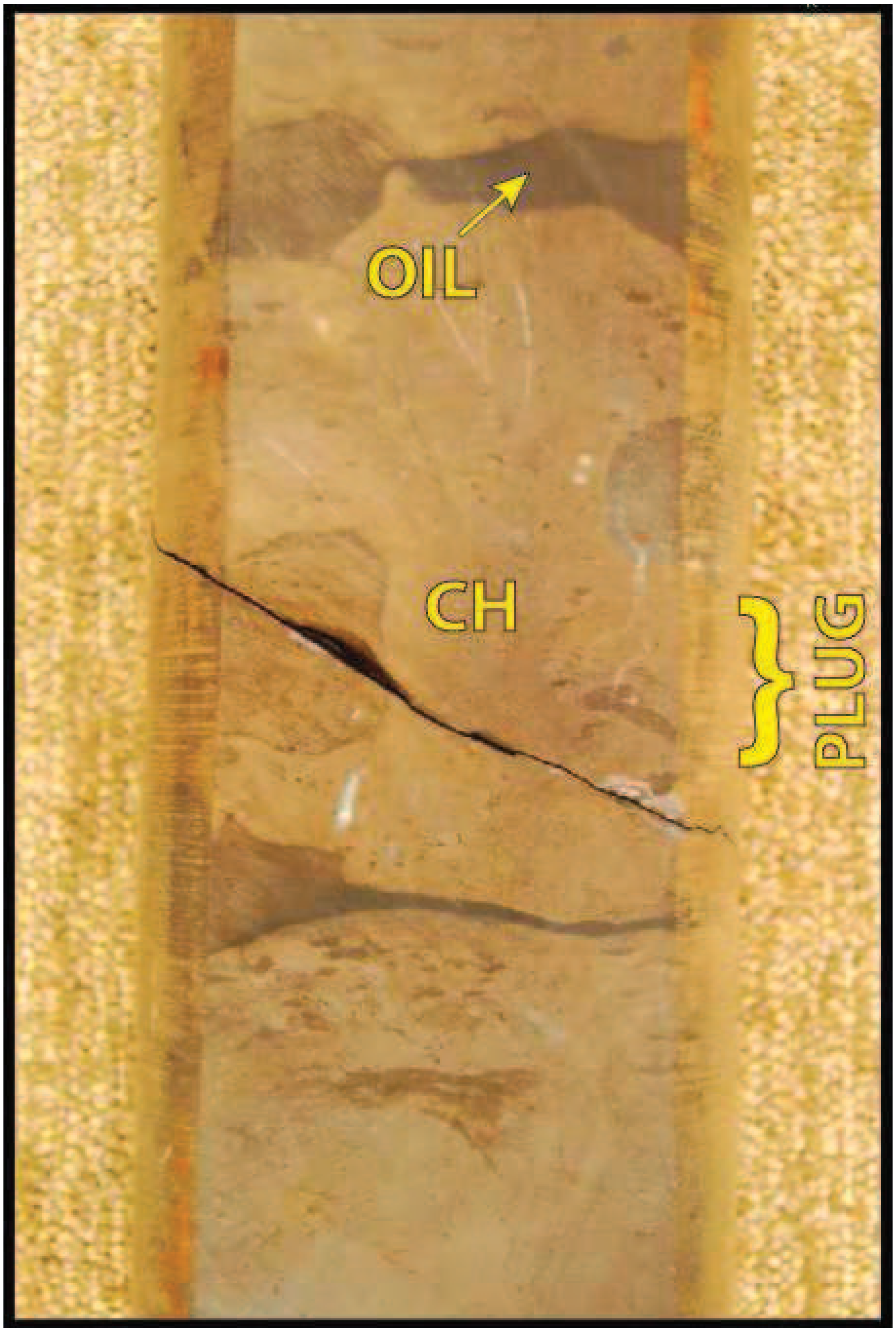

8,072’-8,073’: Facies 5.

8,064-8,065': Facies 6.

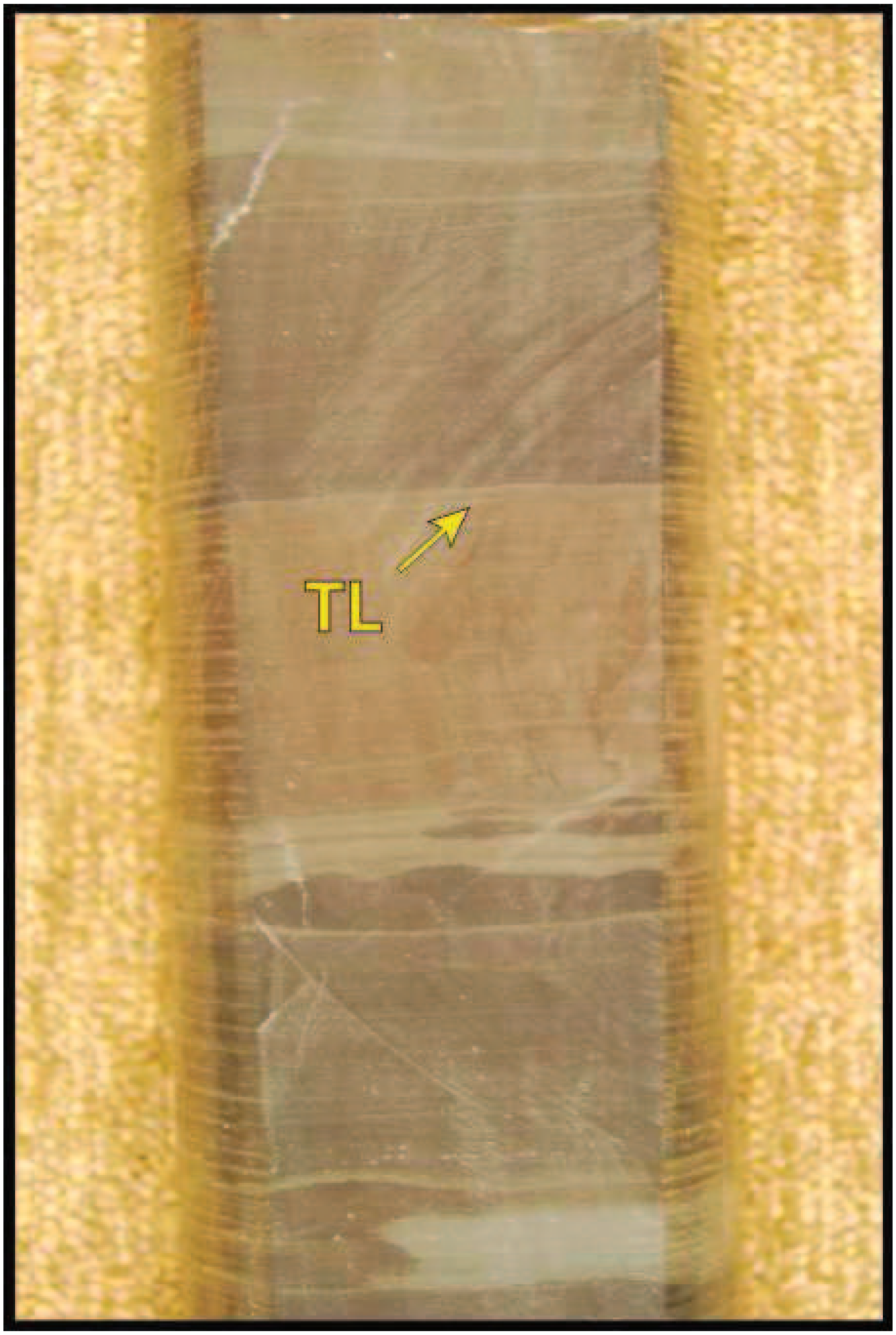

8,045-8,046’: Facies 5.

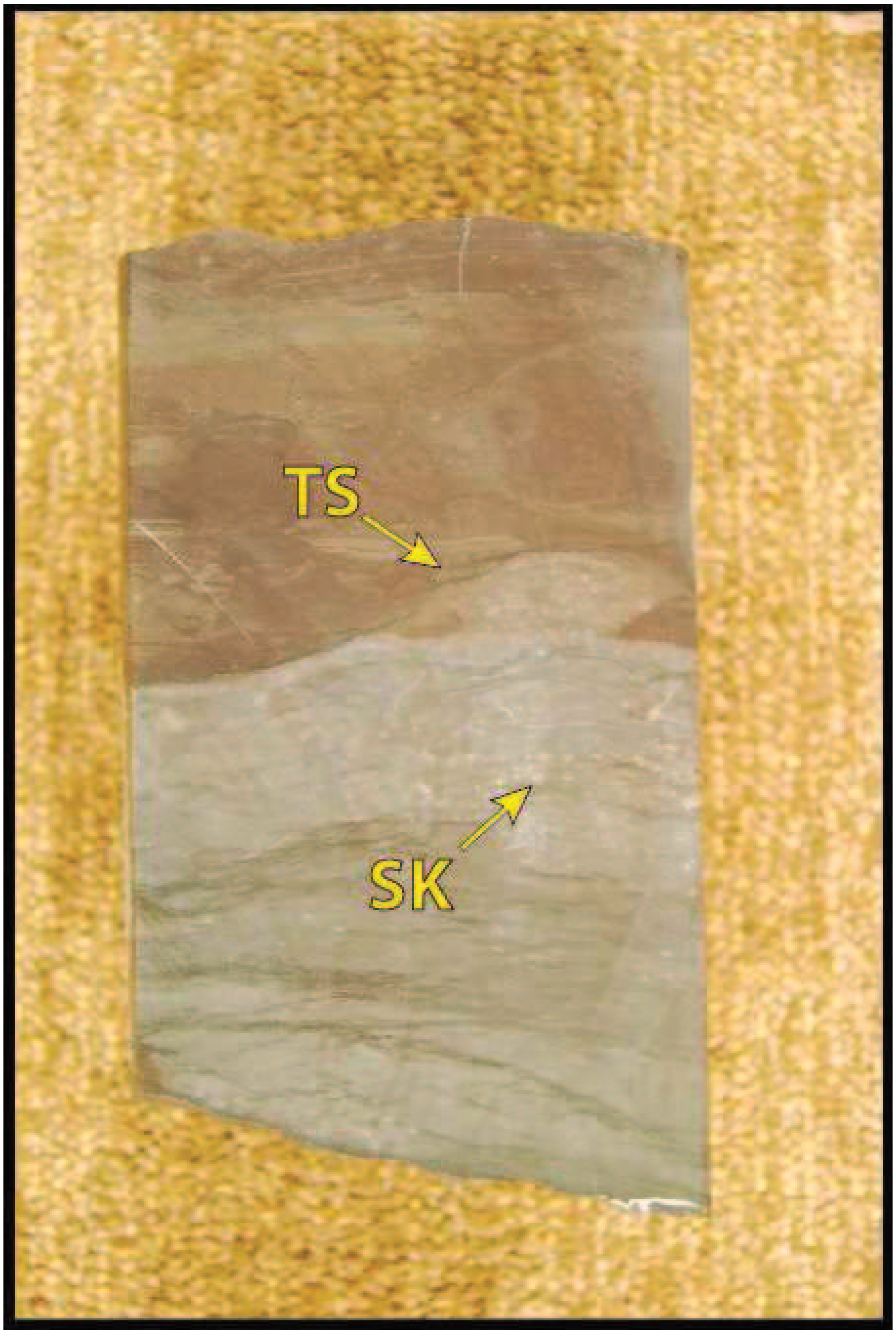

8,037-8,038’: Facies 6 (bottom) and Facies 5 (top).

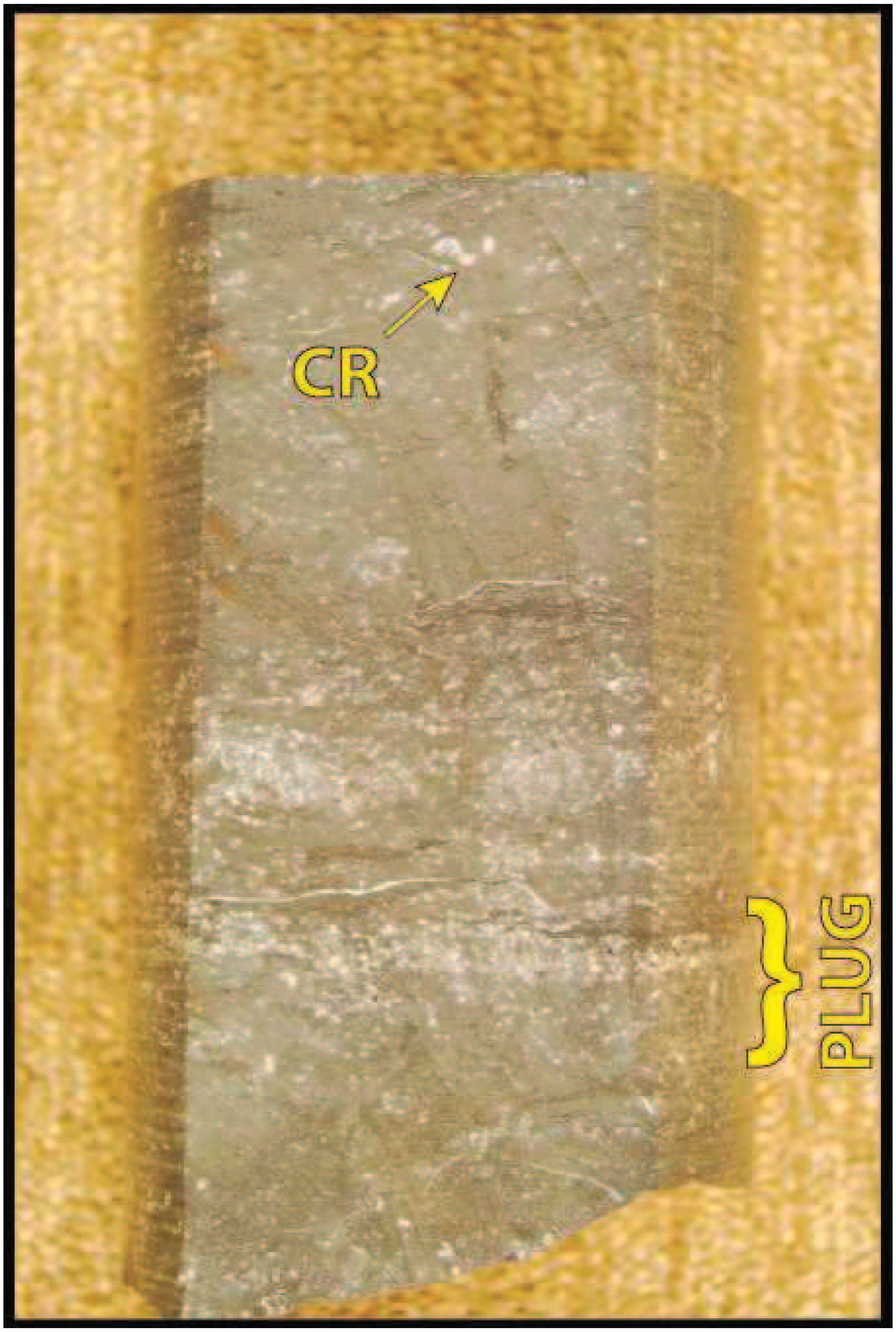

8,034-8,034.5’: Facies 6.

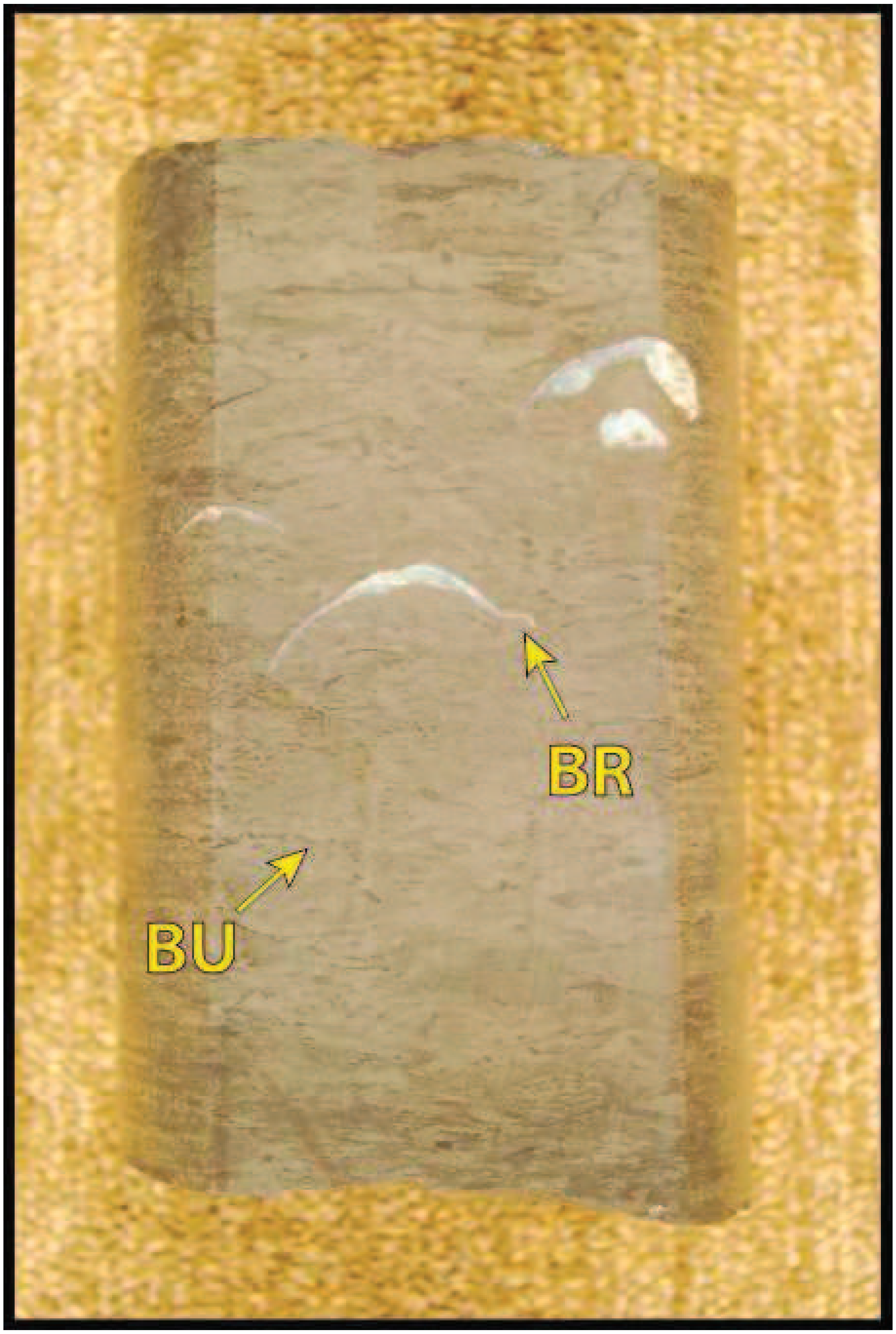

8,030-8,030.5’: Facies 3.

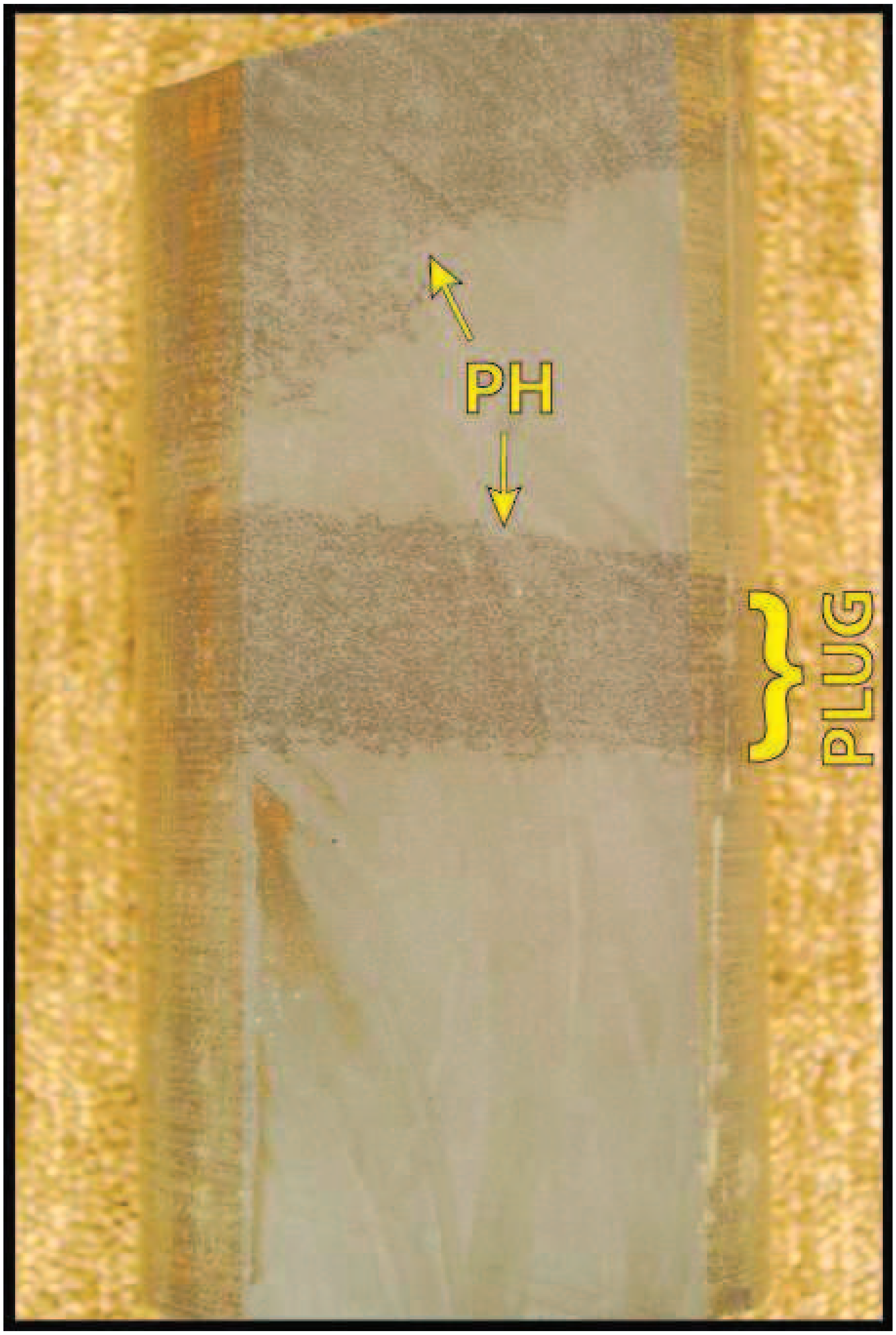

8,017-8,018’: Facies 6.

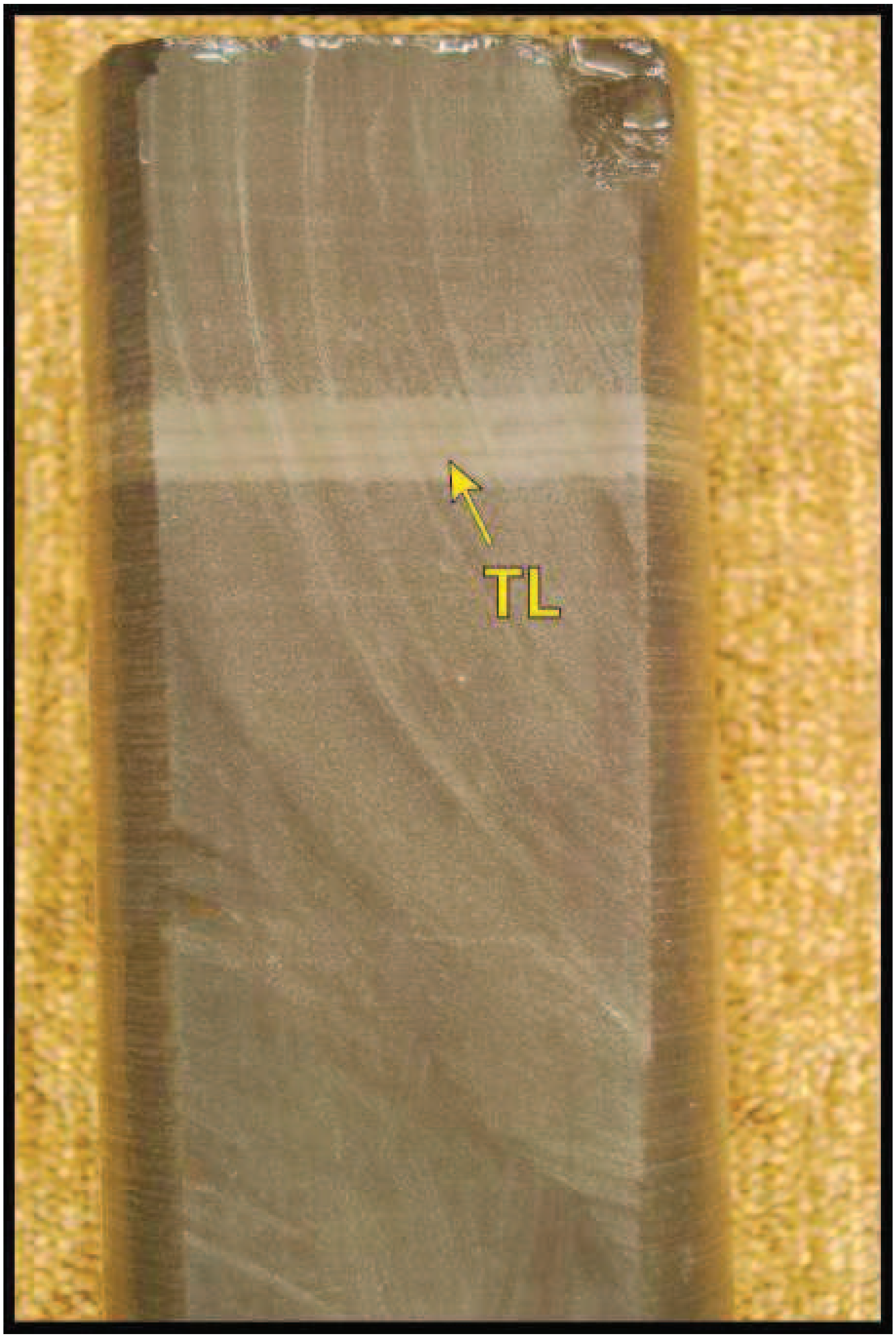

7,997-7,998': Facies 6.

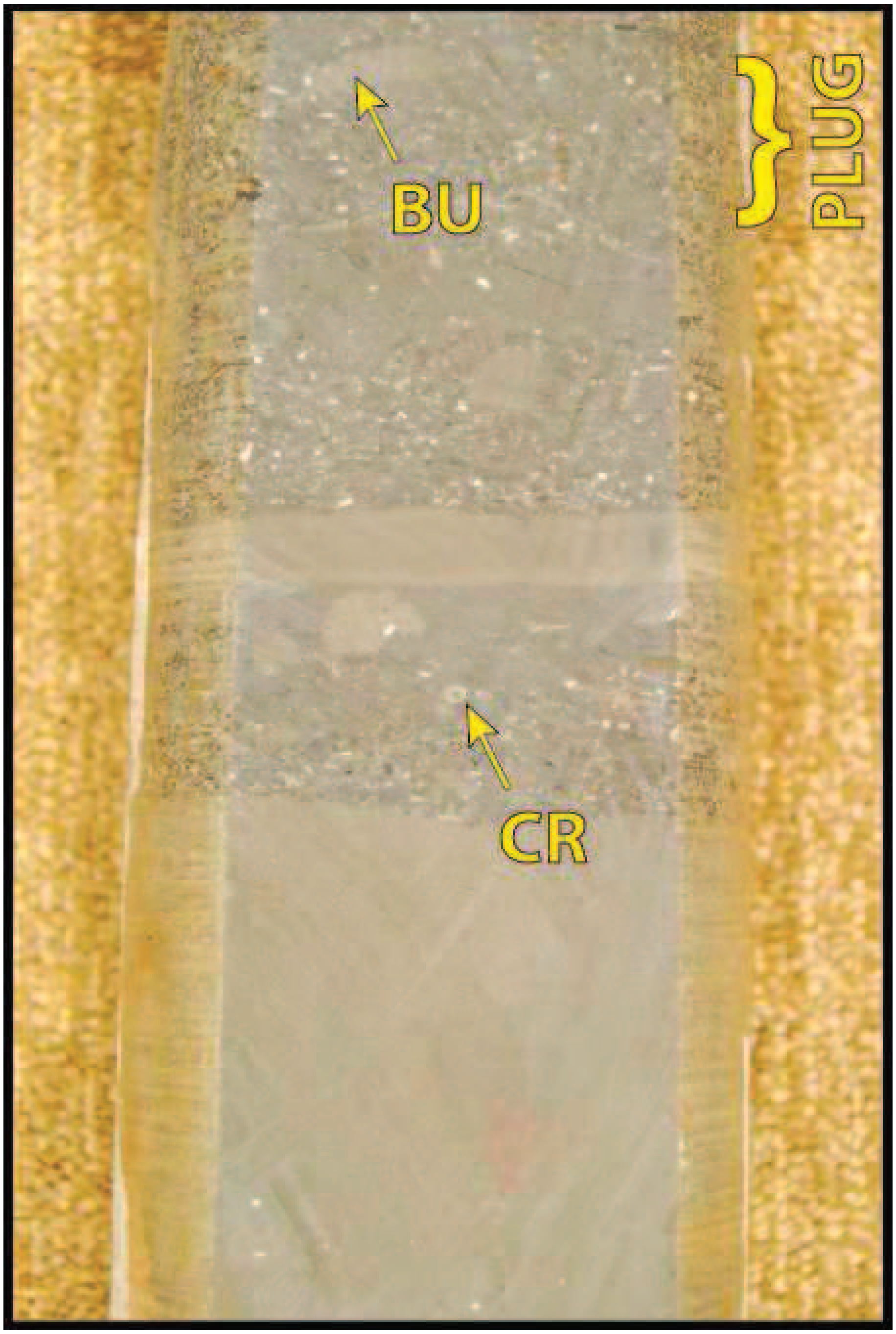

7,982-7,983': Facies 6.

II. Effie B York Unit #1 Thin Section Photomicrographs

Thin sections for the Effie B York Unit #1 were prepared by Tulsa Sections, Inc. and were blue epoxy impregnated to show porosity. All numerical quantifications were derived from visual estimation charts. Bioturbation Index (BI) was visually estimated using the guidelines outlined in Figure 1 of these appendices. Please refer to Table 6 for abbreviations.

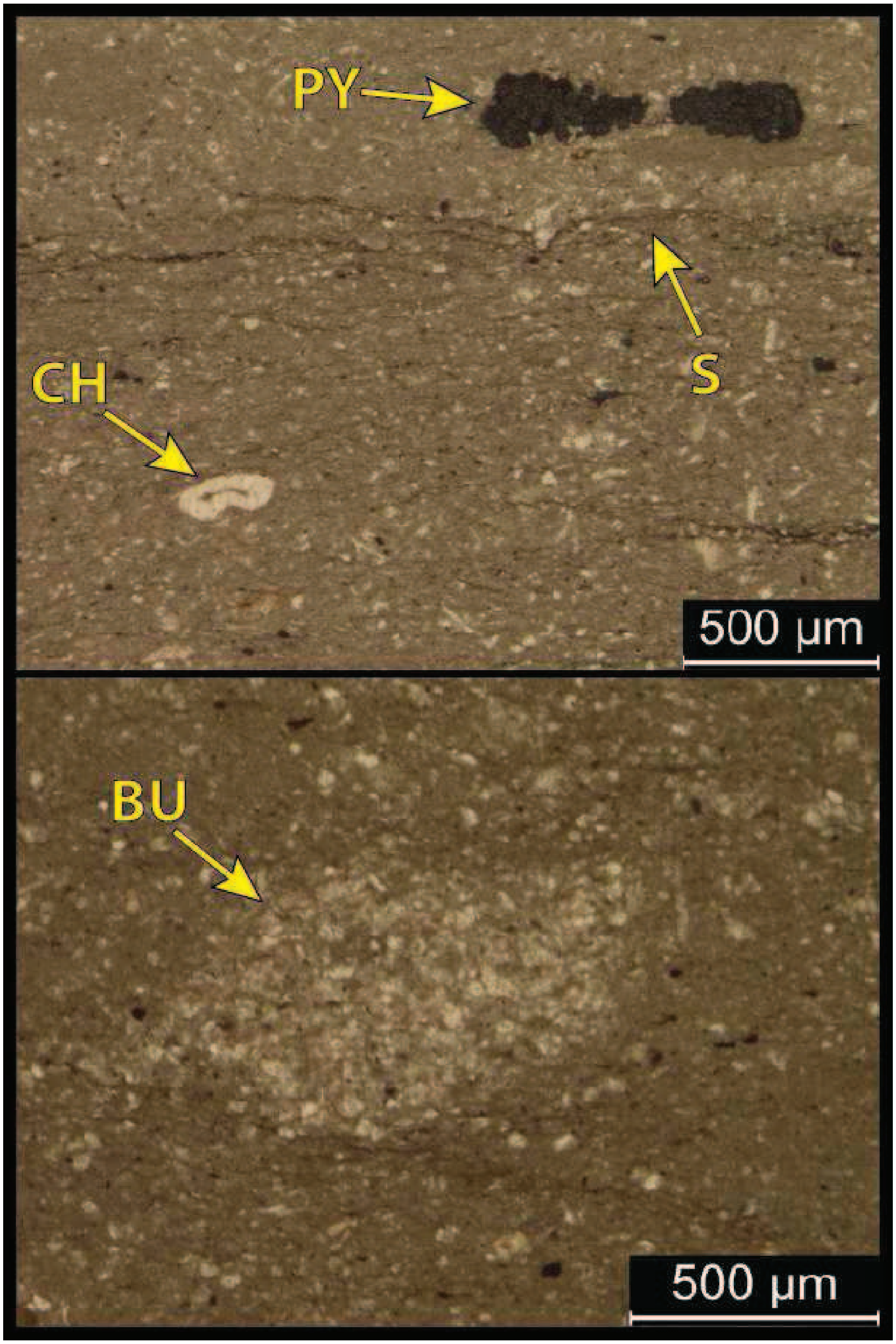

8,501.8': Mud-rich wackestone. Facies 3. Top & Bottom: PPL. Top & Bottom: PPL. Porosity= 1%. B.I.: 1-2. Mineralogy: 90% calcite, 2.5% chert, 1% pyrite, 1% clays, and 5% other minerals. Sample contains silt to very fine sand-sized undifferentiated bioclastic debris, variably preferential to mm-scale horizontal burrow within a micritic matrix. Suspension-laminated deposition exhibits nodular chert (2.5% and up to 300 µm diameter) and low-amplitude stylolites/organic compaction.

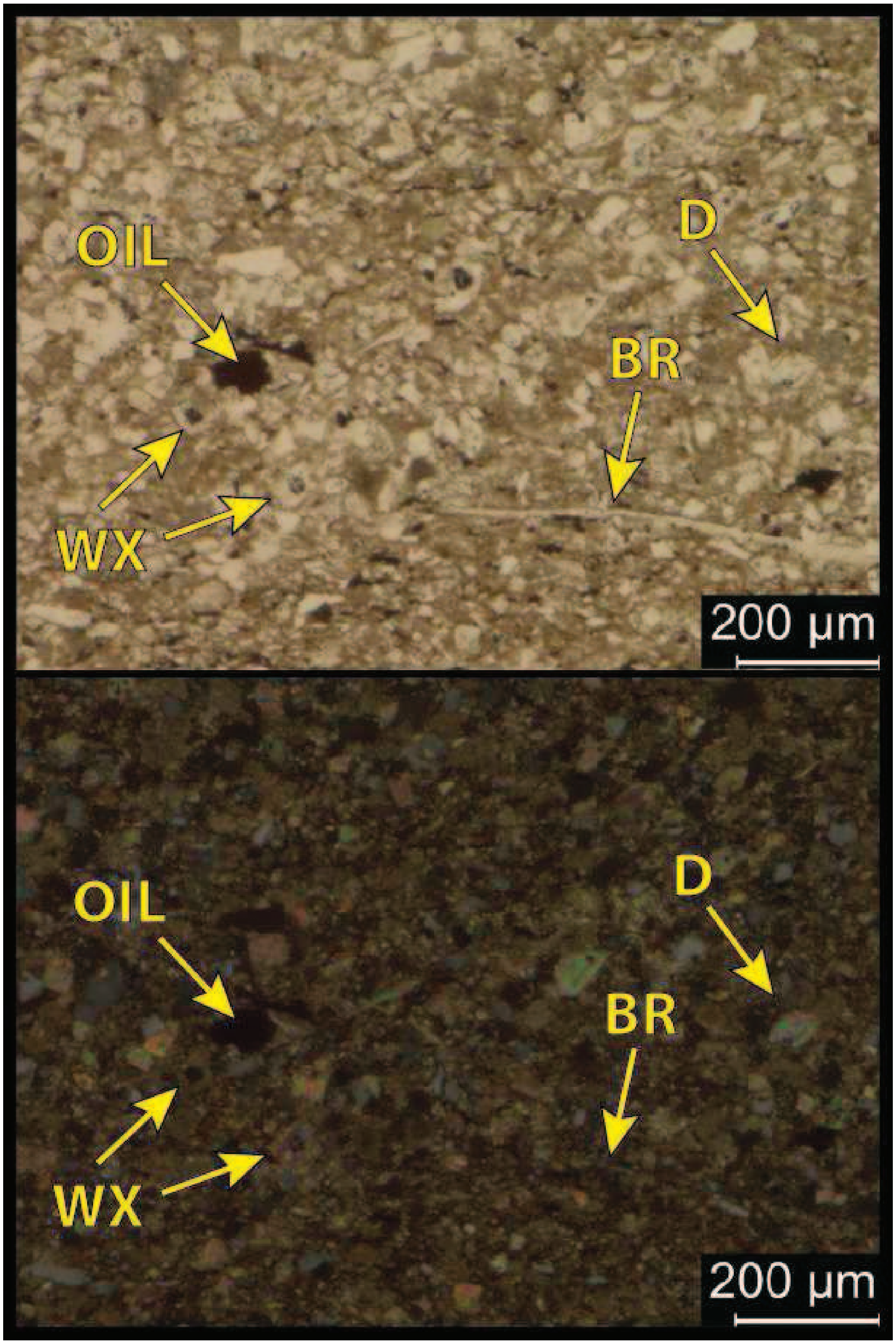

8,476.5': Mud-lean wackestone/ mud-rich packstone. Facies 3. Top: PPL. Bottom: XPL. Porosity: 1-2% associated with fractures, stylolites and dissolution as well as intracrystalline porosity variably after dolomite crystals. B.I.: 0. Mineralogy: 80% calcite, 10% chert, 5 % dolomite, 1.5% pyrite and 3.5% other minerals. Sample contains moderate to well-sorted calcareous grains (brachiopods, crinoids and seldom ostracodes) and displays moderate diagenesis (microcrystalline quartz, calcite cementation and dolomitization).

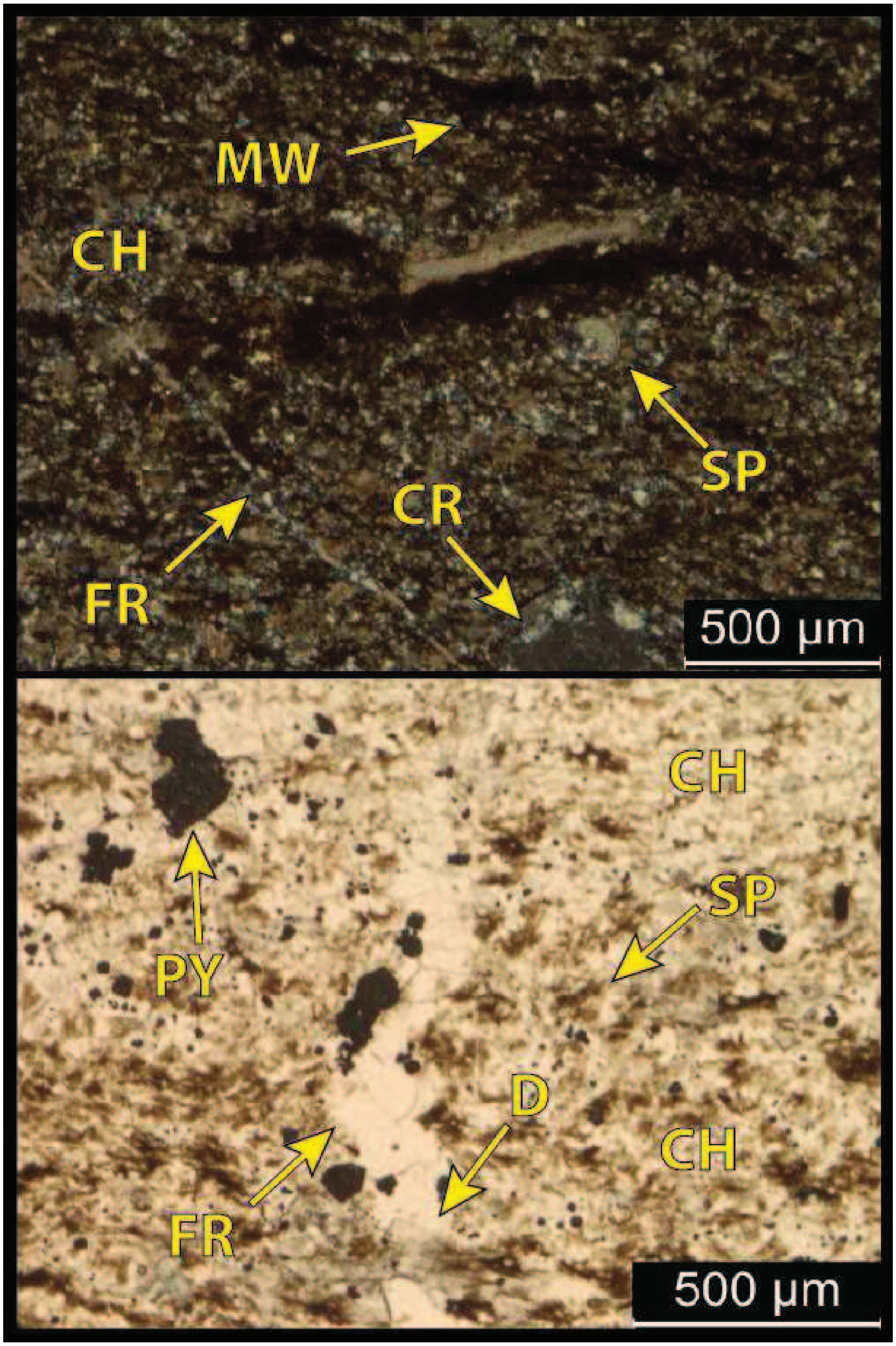

8,447.5': Siliceous wackestone. Facies 4. Top: XPL. Bottom: PPL. Minor porosity= <1%; associated with numerous fractures (1-2cm long). Significant diagenesis (chert, dolomite and pyrite) occludes primary porosity. Dead oil observed in muddier laminations. B.I.: 3-4. Mineralogy: 50% carbonates (45% calcite and 5% dolomite) 45% chert and 5% other minerals (2.5% pyrite). Grains are dominantly sponge spicules where recognizable with lesser amounts of undifferentiated calcareous fossil fragments.

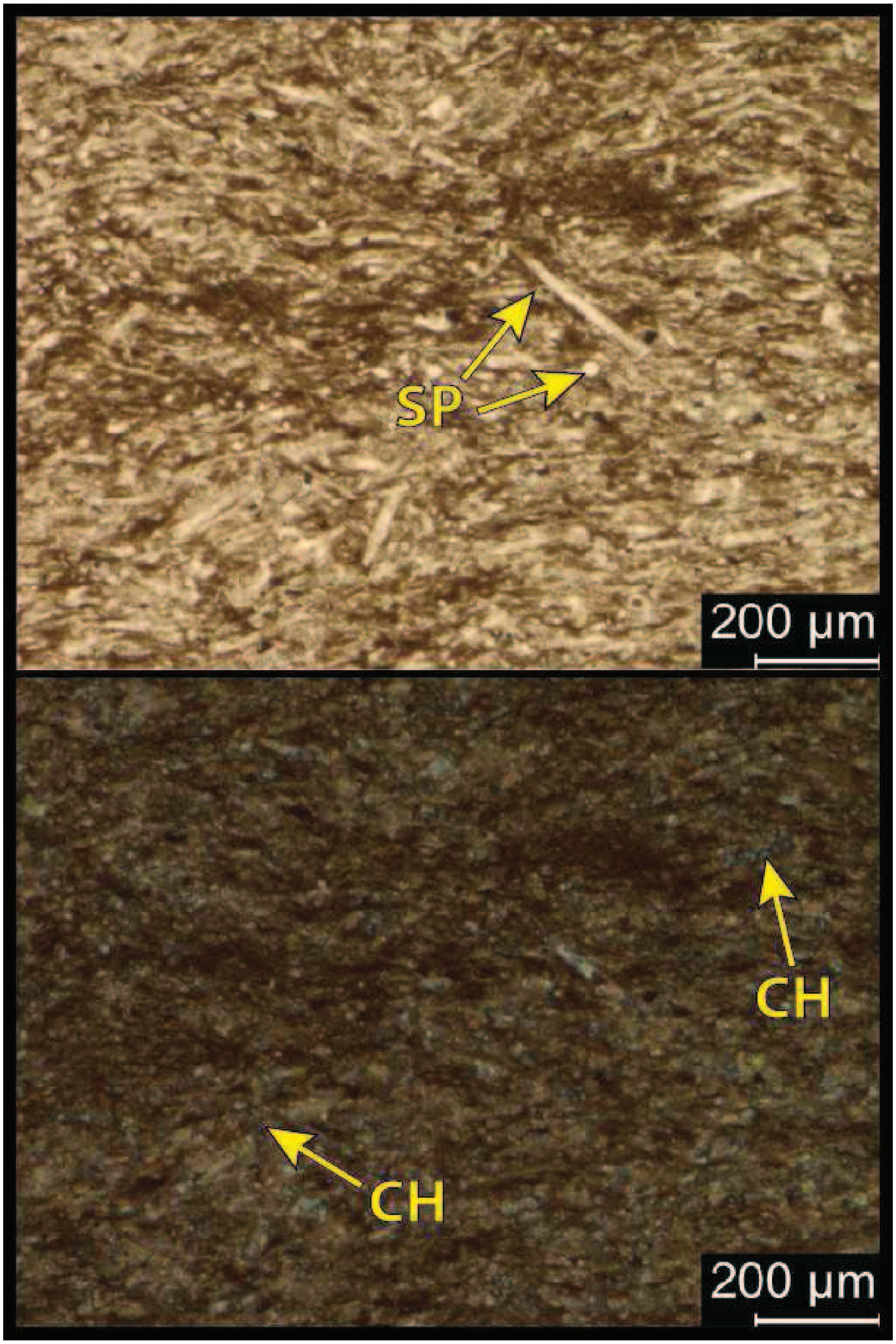

8,427.6': Siliceous, spiculitic mud-lean wackestone/ mud-rich packstone. Facies 4. Top: PPL. Bottom: XPL. Porosity= 1%. Mineralogy: 90% carbonate, 2.5% chert, 2% pyrite, 1% clays, and 5% other minerals. Grains are dominantly sponge spicules (95%, variably calcite/chert) with lesser amounts (5%) of silt-sized crinoid/undifferentiated fossil debris.

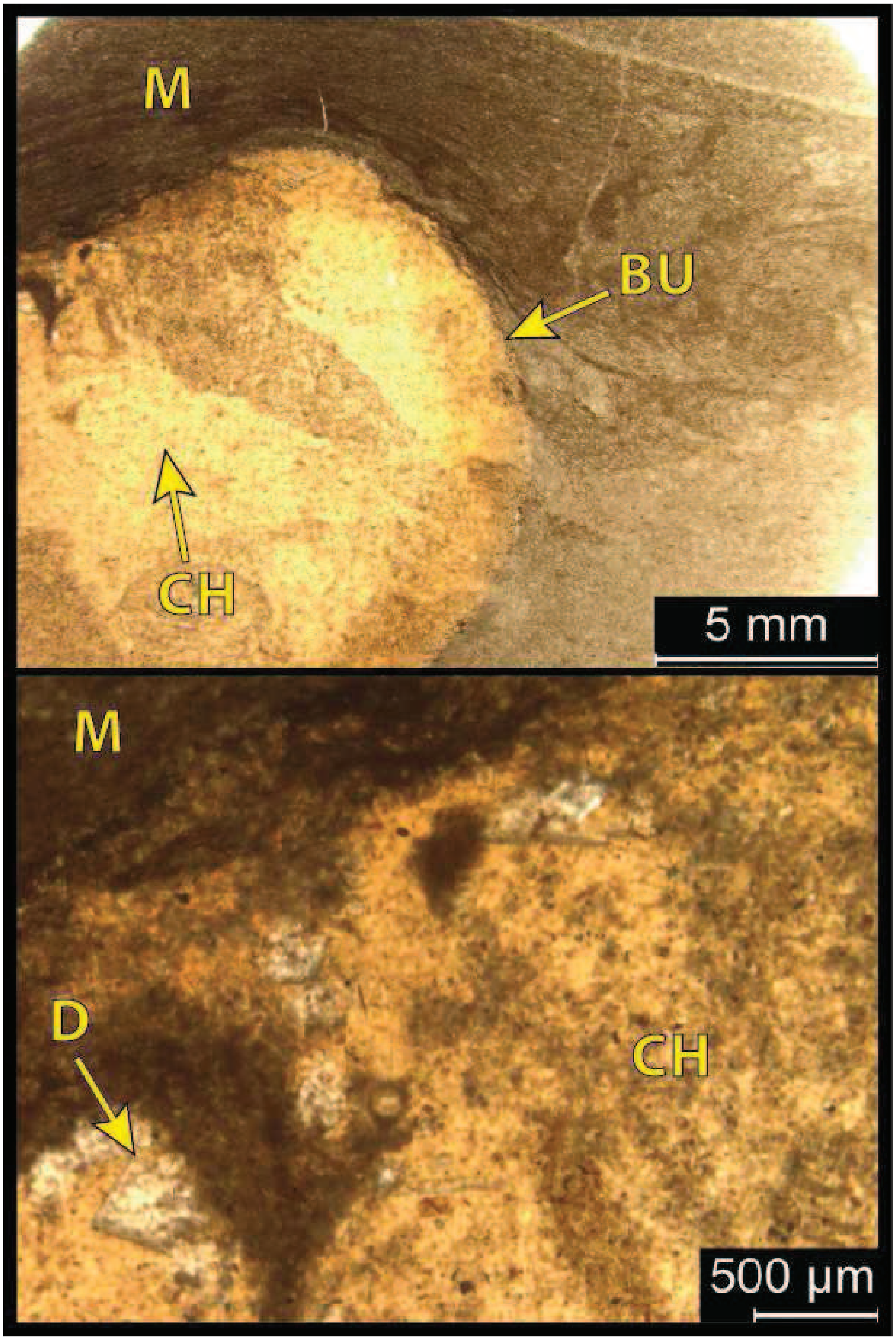

8,396': Siliceous mudstone. Facies 2. Top & Bottom: PPL. Porosity= <1%. B.I.: 3-4 (large cm-scale chert-replaced burrow). Mineralogy: 70% carbonates (65% calcite and 5% dolomite), 25% chert and 5% other minerals (2.5% pyrite). Matrix dominantly micritic (95%) with seldom (5%) undifferentiated silt-sized calcareous debris. Diagenesis: burrow replaced by chert, dolomite (~200-500 µm rhombs) and pyrite (~75 mic).

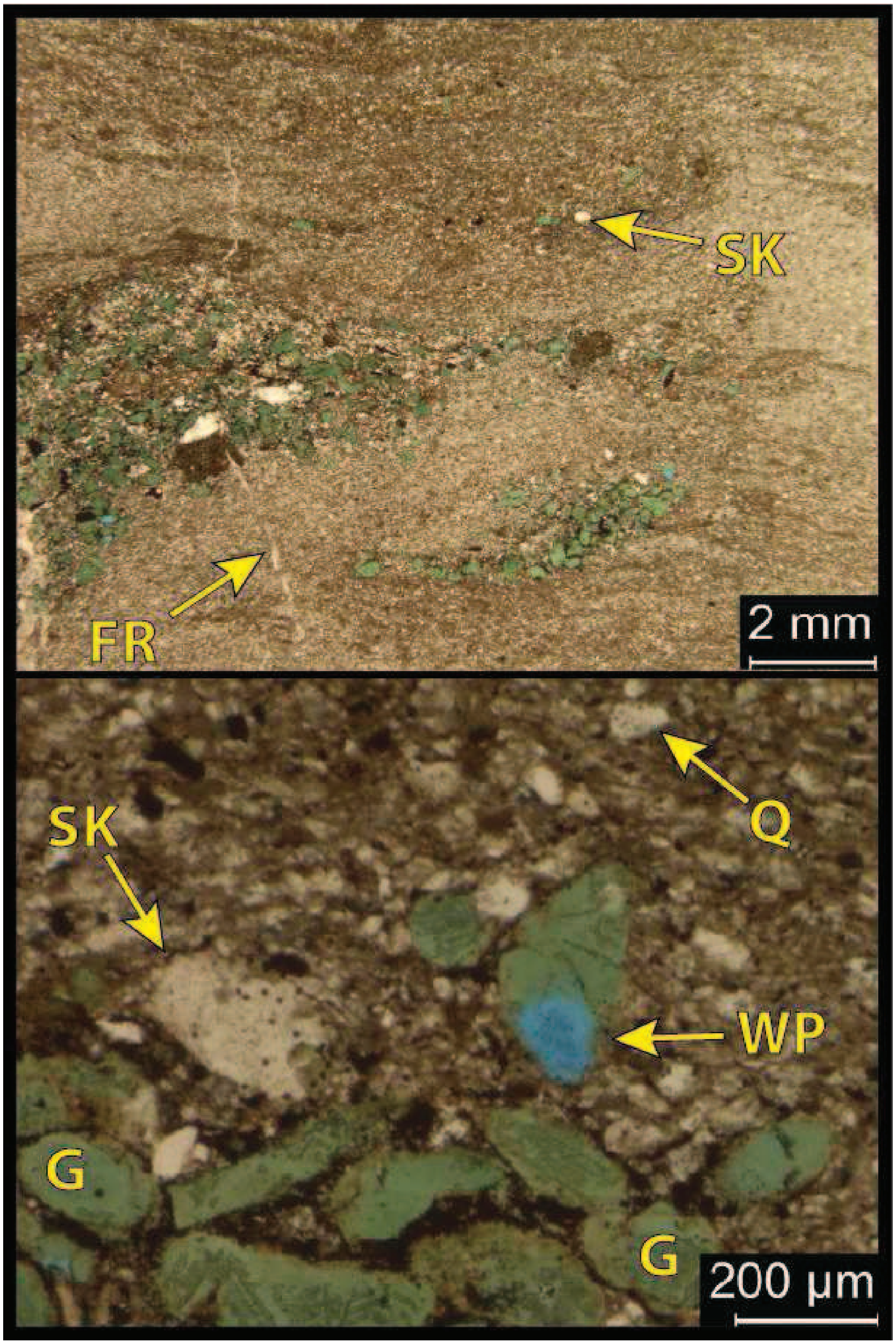

8,377.7': Glauconitic Sandstone. Facies 1. Top & Bottom: PPL. Porosity= 2-4%; variable intraparticle after glauconite; seldom fracture (<1%). B.I.: 1-2 (horizontal, mm-scale). Mineralogy: 75-80% calcite, 10-15% glauconite, 5% chert and 5% other minerals (2% pyrite, 1% quartz silt and 2% clays/feldspars). Grains: sub- to well-rounded glauconite grains (~75-375 μm) and silt-sized calcareous debris (crinoids among other undifferentiated grains).

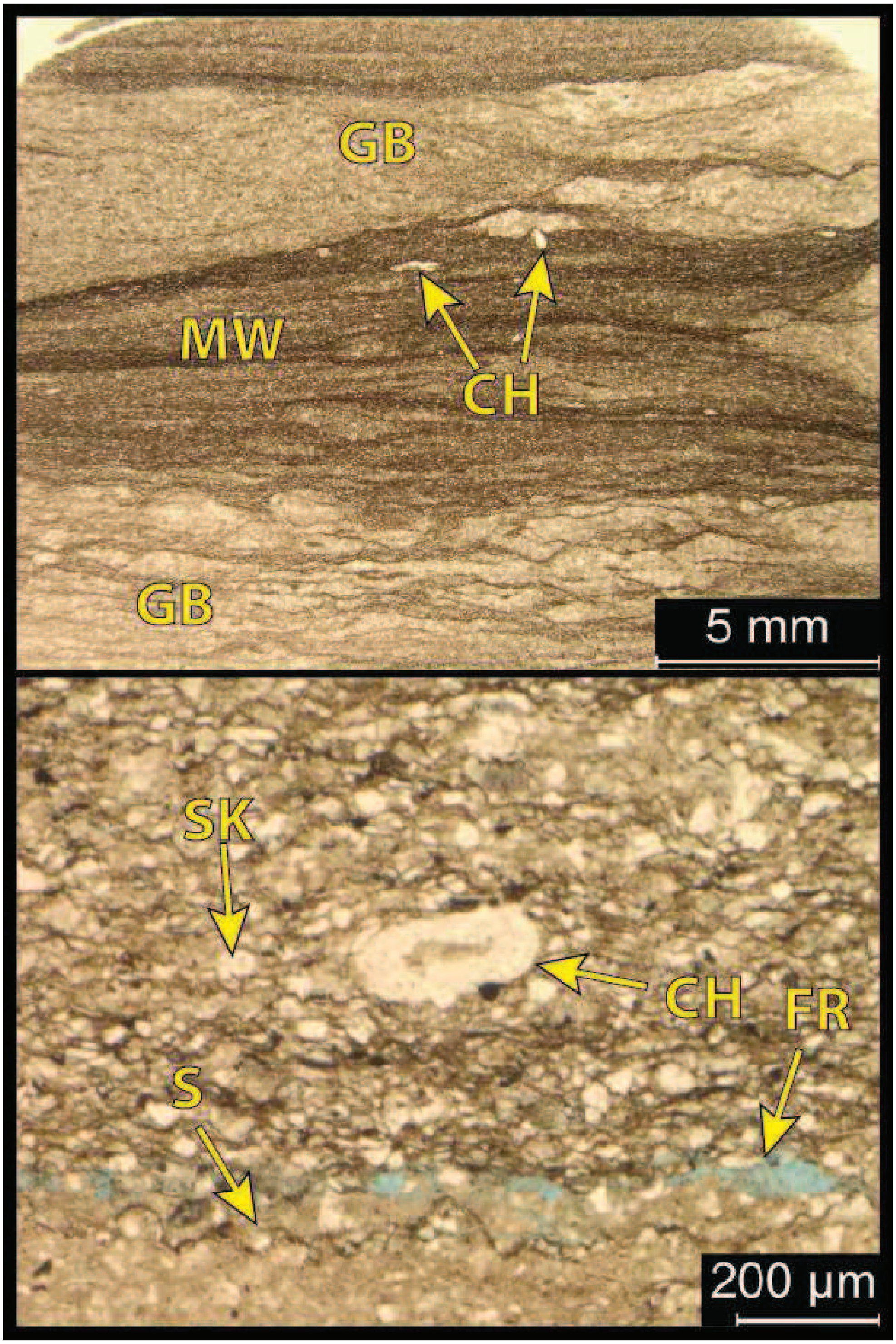

8,354.5': Silty, siliceous wackestone-packstone. Facies 4. Top & Bottom: PPL. Porosity= 2-4%; blue epoxy along stylolite/fracture and dead oil/vug in packstone portion. B.I.: 0-1 (horizontal, mm-scale). Mineralogy: 55% carbonate (54% calcite, 1% dolomite), 15% chert and 30% other minerals (10-15% quartz silt, 10-15% clays/feldspars and 1-2% pyrite). Grains: spicules (20% in packstone portion; 10-25 µm), quartz silt (10-15%), crinoidal debris (silt-sized) and undifferentiated grains (30%).

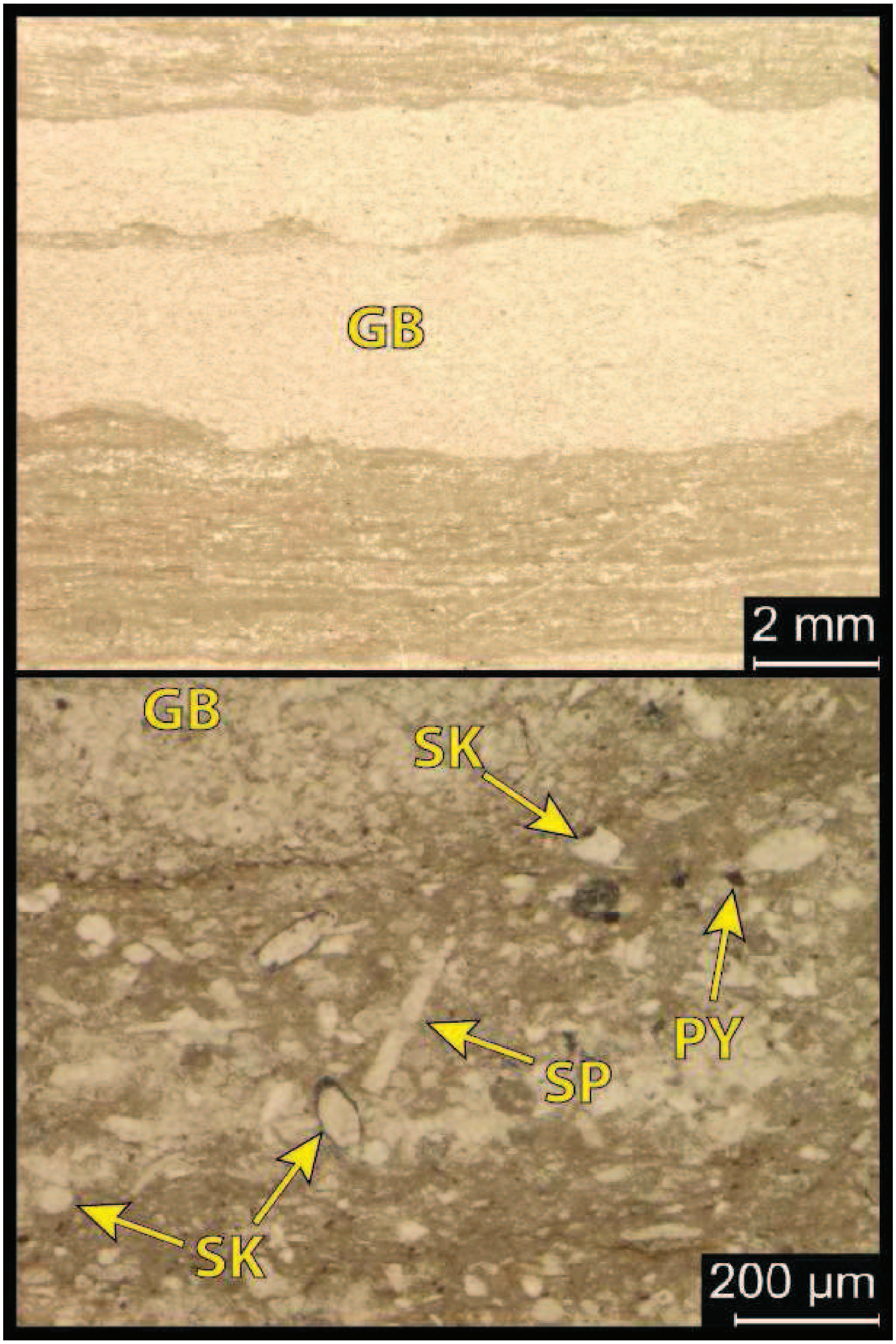

8,327.6': Mud-lean packstone/grainstone w/ wackestone interbeds. Facies 5. Top & Bottom: PPL. Porosity= 2%; no blue epoxy. B.I.: 0. Mineralogy: 85% carbonate (84% calcite, 1% dolomite), 5% chert and 10% other minerals (8% quartz silt-vf sand, 1% clays/feldspars and 1% pyrite). Grains: 5% spicules (biggest 25 x 225 µm and variably chert/calcite) and undifferentiated skeletal debris in poorly sorted wackestone interbed; well-sorted, fine-grained (~25-40 µm) grainstone interbeds.

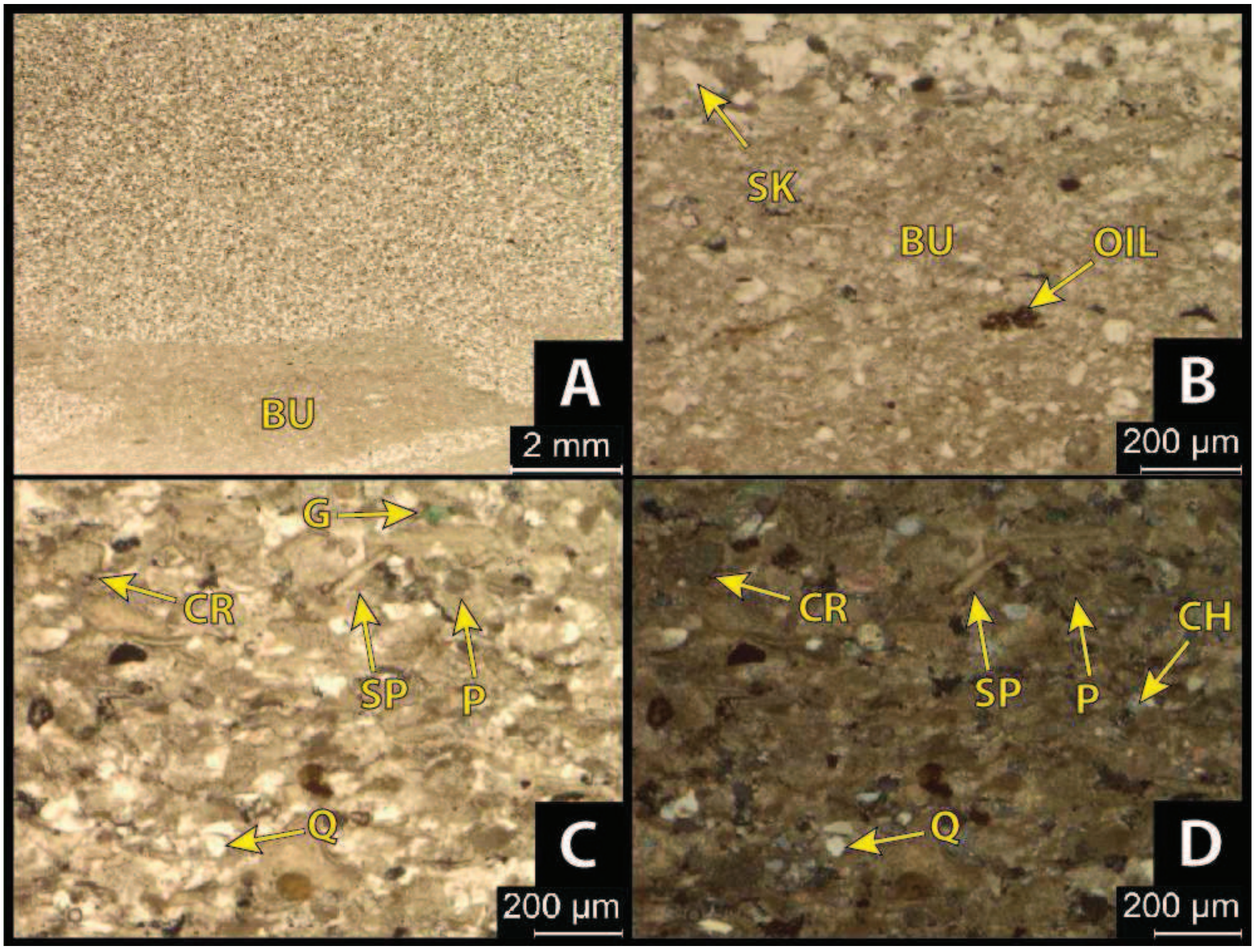

8,319': Mud-lean packstone/grainstone. Facies 5. A, B & C: PPL. D: XPL. Porosity= 2-4%; dead oil and 2-5 µm intergranular pores. B.I.: 1-2 (horizontal, cm-scale; fine-grained after). Mineralogy: 85% carbonate (84% calcite, 1% dolomite), 5-10% chert and 10% other minerals (15-20% quartz silt-vf sand, 1% clays/feldspars and 1% pyrite). Grains: Quartz silt and very fine sand; peloidal calcareous debris (silt-sized); crinoidal debris (5%; 150-250 µm); sponge spicules (5%); undifferentiated brachiopod and bryozoan debris.

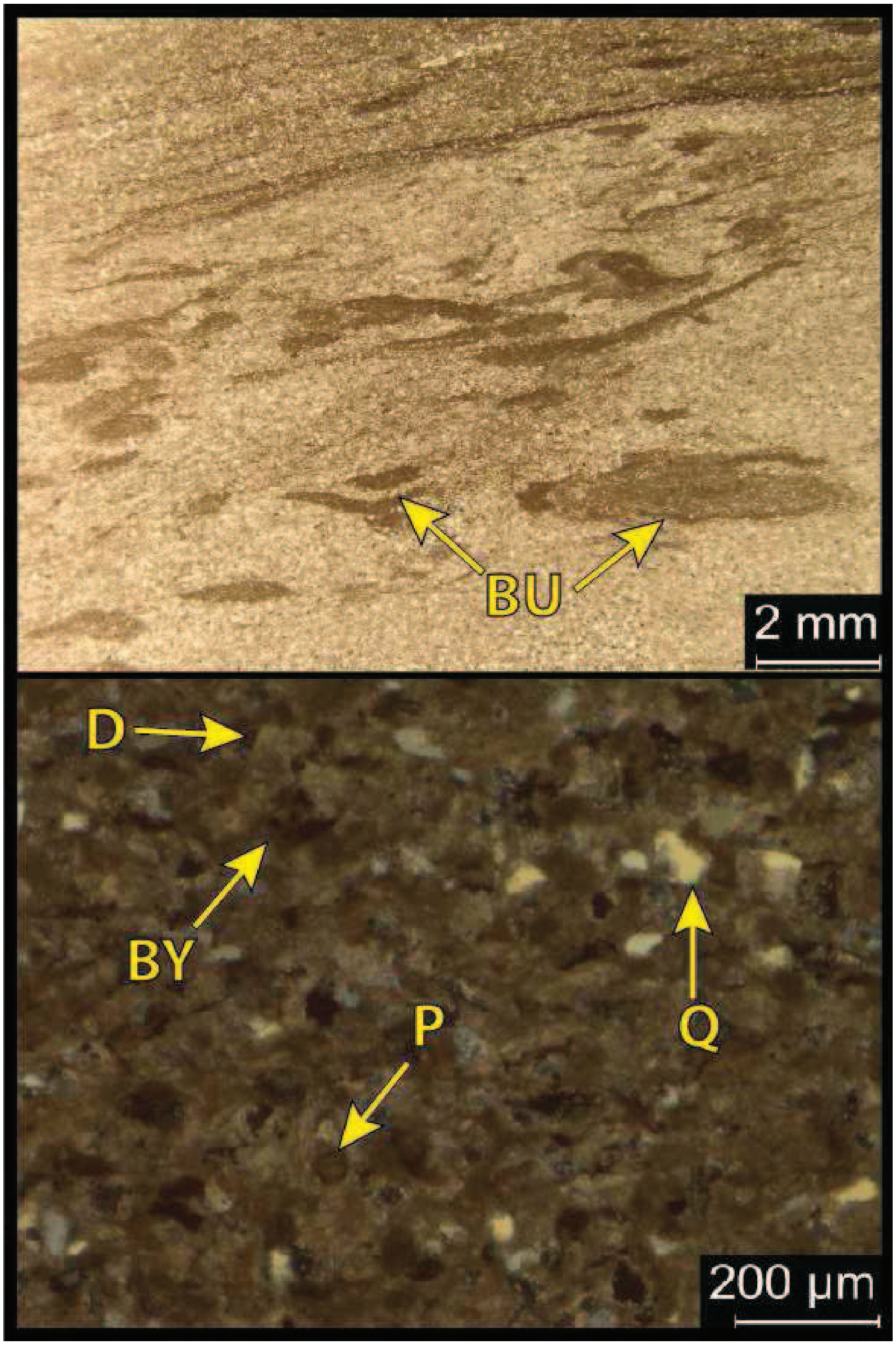

8,287.2': Silty mud-rich packstone/ mud-lean wackestone. Facies 4. Top: PPL. Bottom: XPL. Porosity= 2-4%. B.I.: 2-3 (horizontal, mm-scale; mud after). Mineralogy: 70% carbonate (68% calcite, 2% dolomite), 10% chert and 20% other minerals (15% quartz silt-vf sand, 2-4% clays/feldspars and 2% pyrite). Grains: peloidal silt-sized calcite grains and likely crinoidal fragments (70%); quartz silt to very fine sand (15%; preferential to wackestone portions); bryozoan rare (<1%).

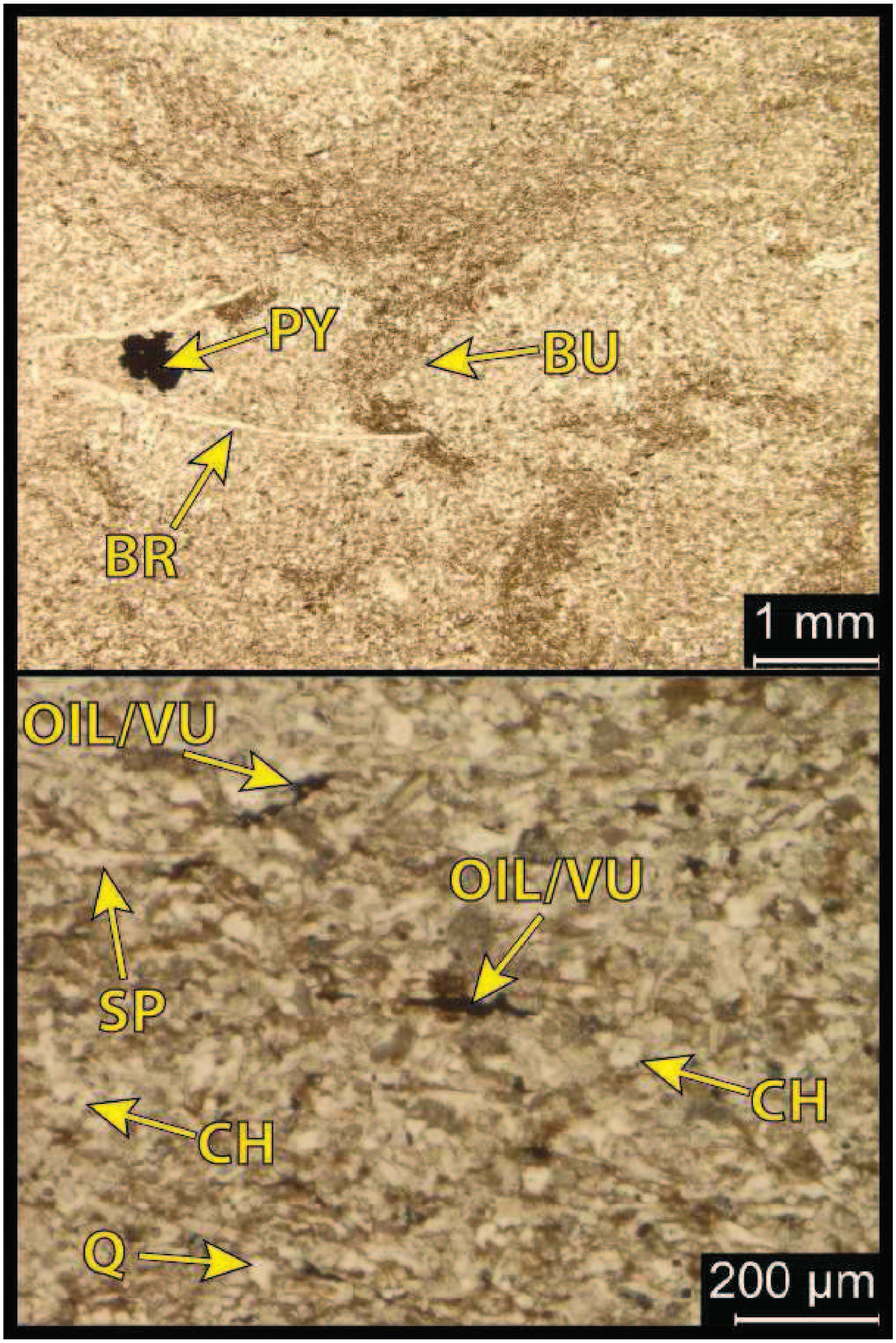

8,253.3': Silty packstone. Facies 5. Top & Bottom: PPL. Porosity= 2-4% (no blue epoxy; dead oil – 25-75 µm vugs). B.I.: 1-2 (horizontal/ vertical, mm-scale; mud after). Mineralogy: 70% carbonate (69% calcite, 1% dolomite), 10-15% chert and 17% other minerals (15% quartz silt, 1% clays/feldspars and 1-2% pyrite). Grains: Peloidal calcareous grains and undifferentiated skeletal fragments (65%); spicules (5%; ~25-50 x 200 µm); thin-shelled brachiopods (1%; 30 µm x 3mm). 5-10% calcite cementation throughout.

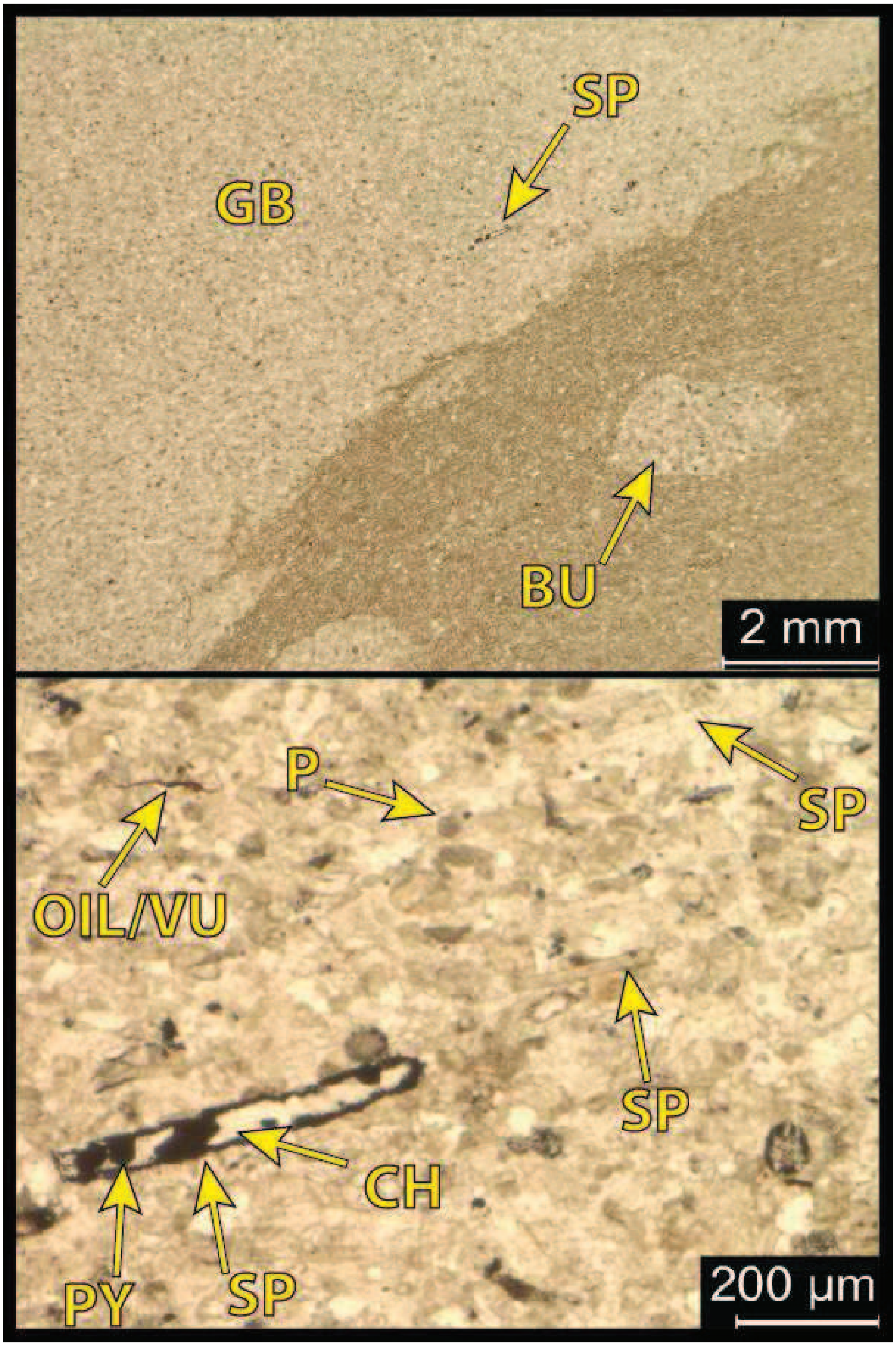

8,242.8': Silty mud-lean packstone. Facies 5. Top & Bottom: PPL. Porosity= 2% (dead oil; intergranular; fractures). B.I.: 1 (horizontal, mm-scale; coarse-grained after). Mineralogy: 60% carbonate (58% calcite, 2% dolomite), 15-20% chert and 20% other minerals (15-20% quartz silt, 1% clays/feldspars and 2% pyrite). Grains: crinoid debris (1%; ~200 µm); spicules (5%; biggest 50x500 µm); peloidal grains (2.5%; silt-sized); bryozoa (<1%; 100 µm); undifferentiated skeletal fragments. 20% calcite cementation in packstone portion (none in wackestone).

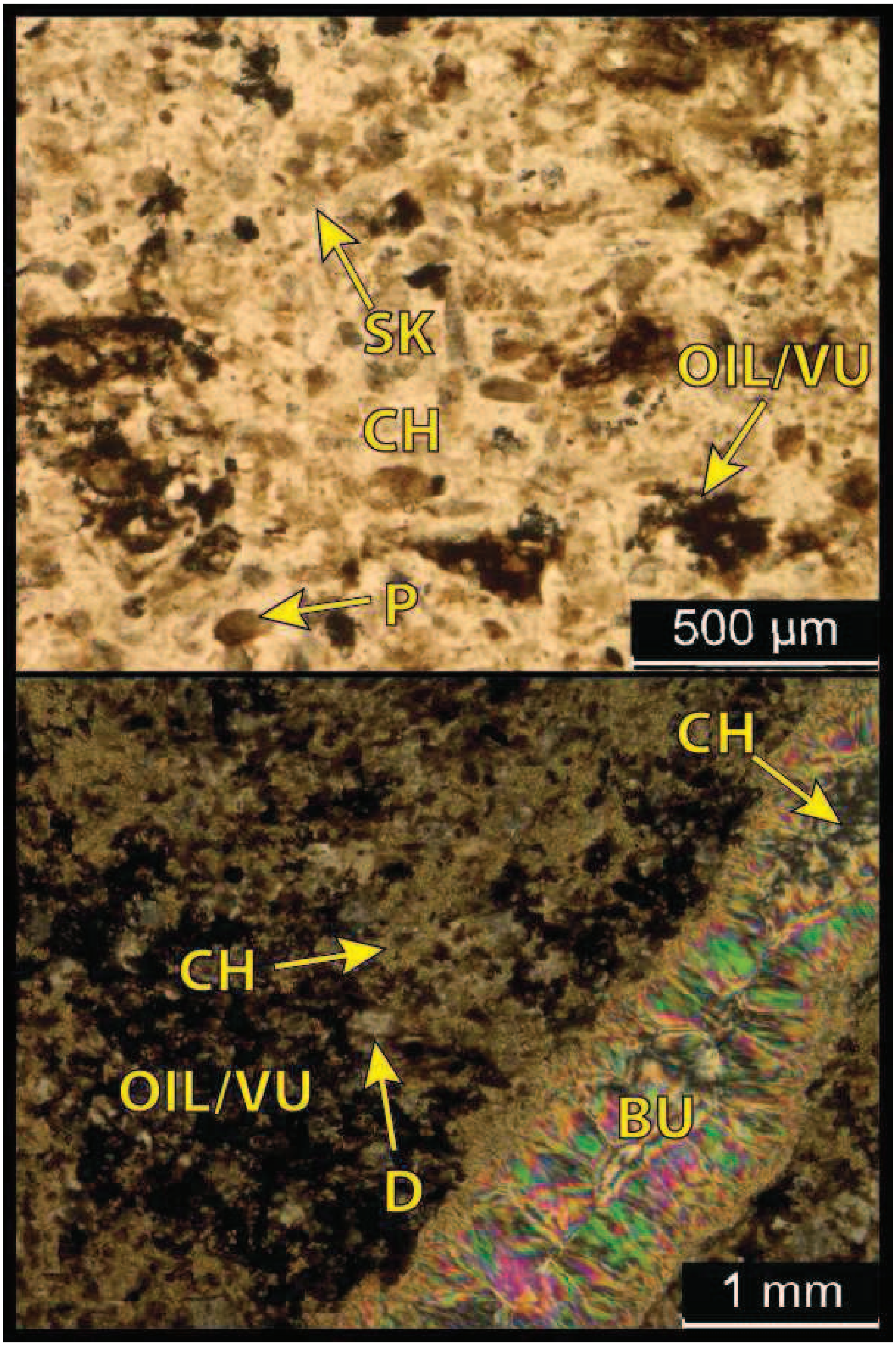

8,214.5': Siliceous, peloidal bearing dolomitic wackestone-packstone. Facies 5. Top: PPL. Bottom: XPL. Porosity= 4% (dead oil; intergranular oil staining). B.I.: 4 (vertical, mm-cm-scale). Mineralogy: 33% carbonate (25% calcite, 8% dolomite), 60% chert and 7% other minerals (1-2% quartz silt, 1% clays/feldspars and 4% pyrite). Grains: crinoidal debris (mostly 50-100 µm; variable calcitic/siliceous); undifferentiated calcareous fragments. Extensive diagenesis: 60% chert; 8% dolomite (most 50-100µm, few 350 µm rhombs); 2% calcite cementation (replacement of burrow/boring).

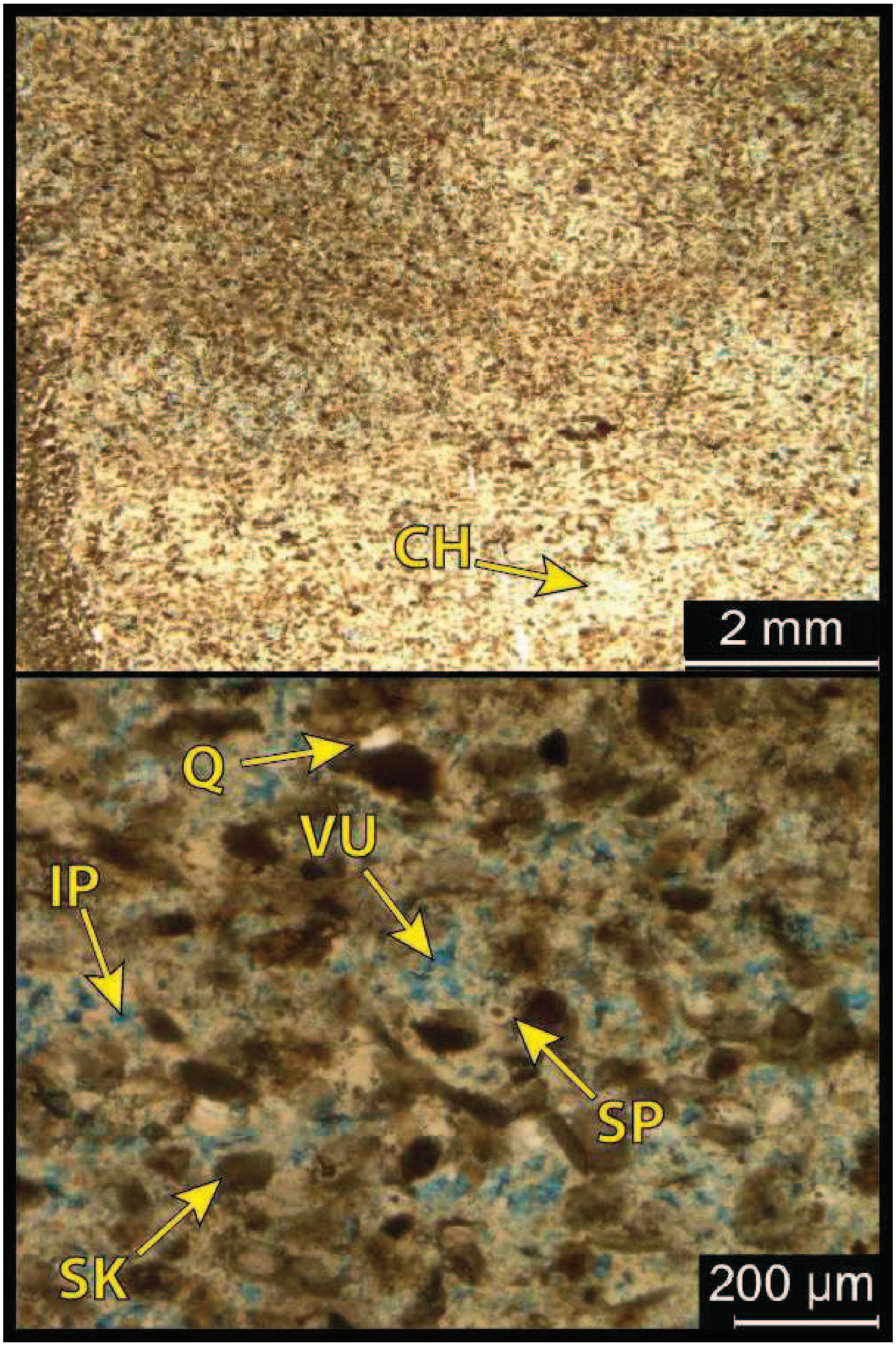

8,206': Siliceous, peloidal bearing packstone. Facies 5. Top & Bottom: PPL. Porosity=10% (dissolution-enhanced vugs and intergranular). B.I.: 1 (vertical, cm-scale). Mineralogy: 23% carbonate (21% calcite, 2% dolomite), 75% chert and 2% other minerals (1-2% quartz silt and <1% pyrite). Grains: peloidal and undifferentiated skeletal grains (20%; 100 µm) with rare remnant spicules (20 µm). Extensive diagenesis: 75% chert; 2% dolomite; <1% pyrite.

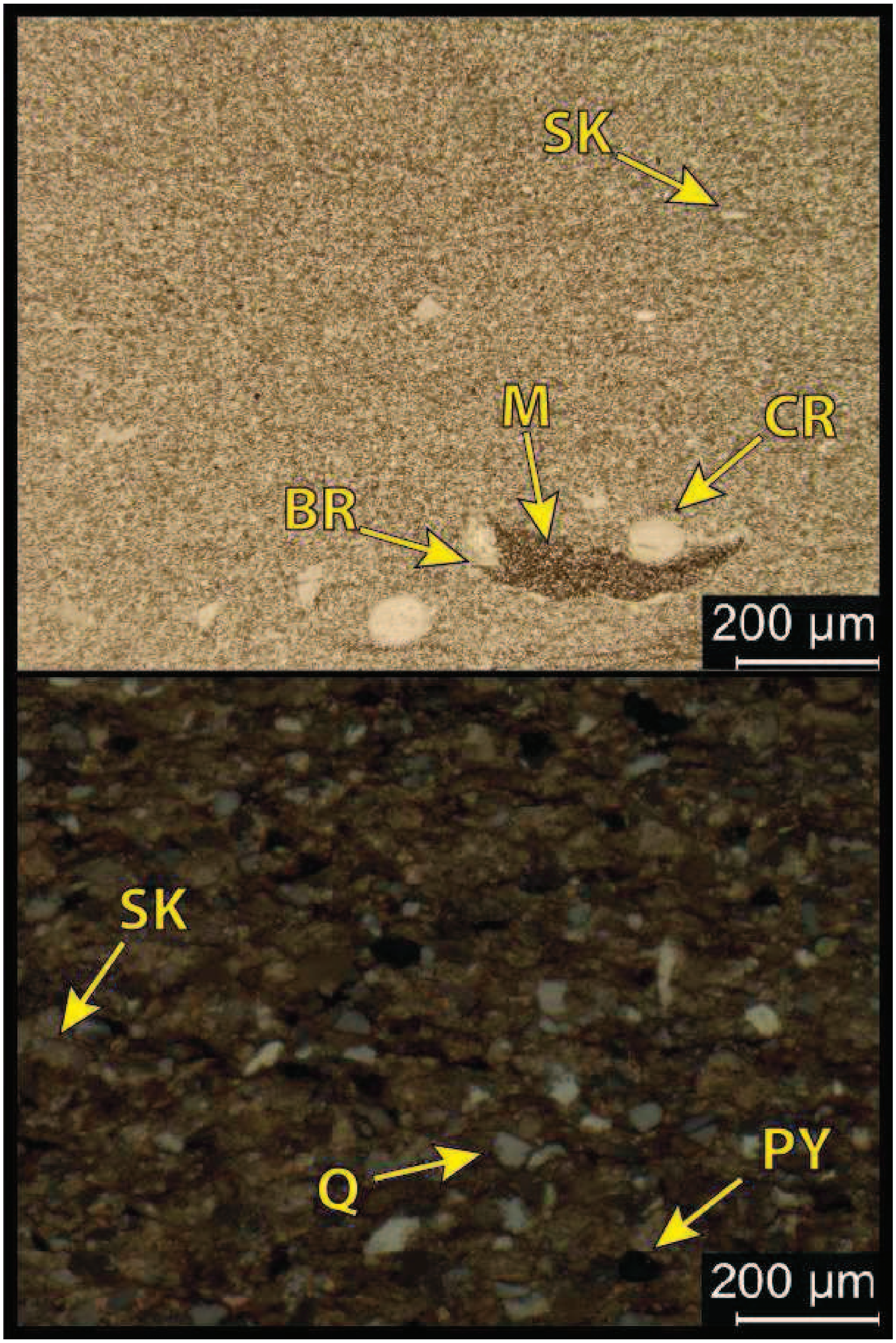

8,171.4': Arenitic mud-rich packstone/ mud-lean wackestone. Facies 4. Top-PPL. Bottom-XPL. Porosity= 1% (intergranular oil-stained). B.I.: 0. Mineralogy: 76% calcite, 2.5% chert and 21.5% other minerals (20% quartz silt and <2% pyrite). Grains: seldom (2.5%) crinoidal debris (<100 µm); seldom (<1%) brachiopods (400 µm; micritized and cemented); 20% quartz silt (most ~50 µm, biggest 80 µm); undifferentiated calcareous skeletal fragments (70%; silt-sized).

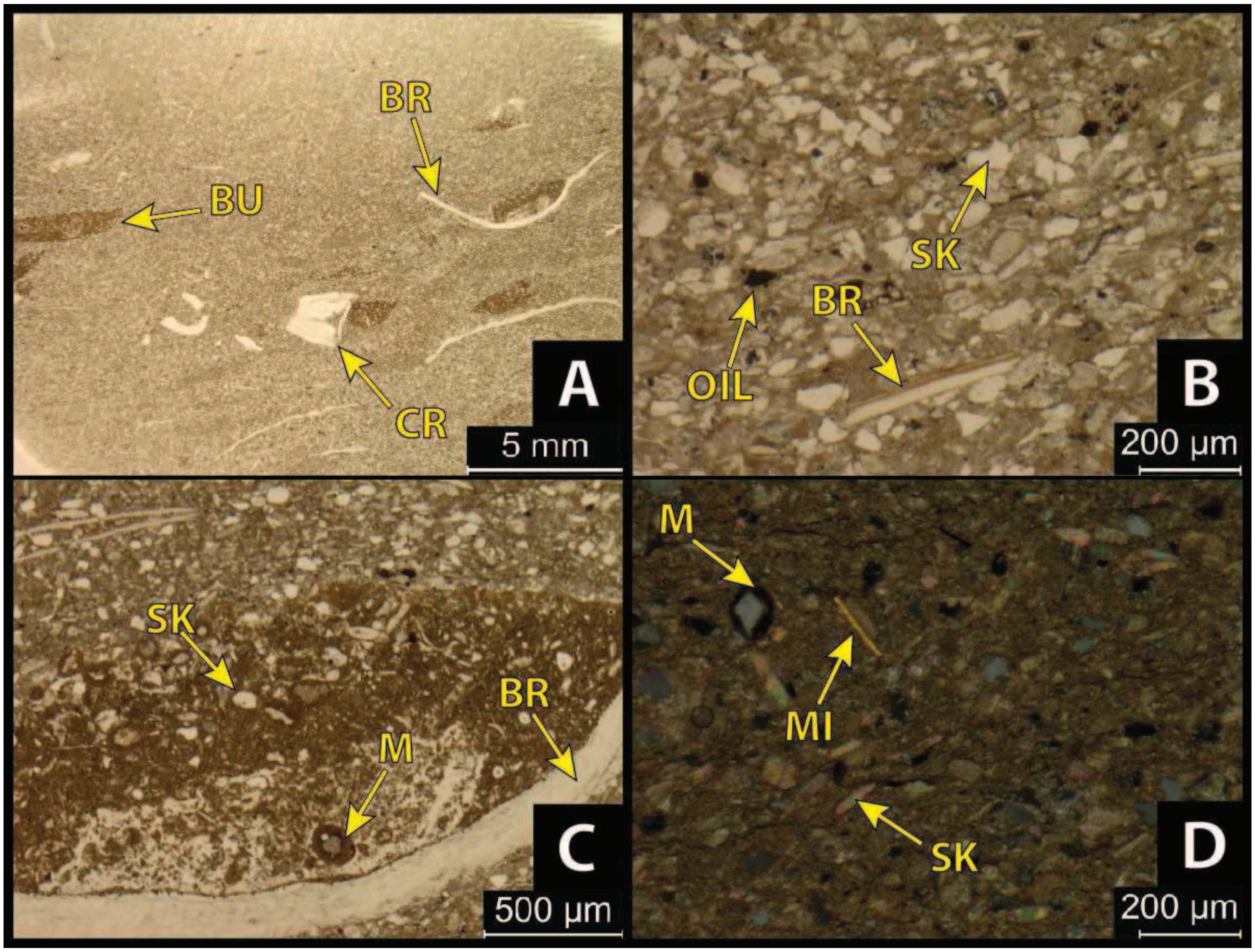

8,134.5': Mud-lean wackestone. Facies 4. A, B & C: PPL. D: XPL. Porosity= 1-2% (intergranular; biggest 50-70 µm). B.I.: 1 (horizontal, mm-scale; mud-after). Mineralogy: 88% calcite, 1-2% chert and 10% other minerals (1-2% quartz silt; 1-2% pyrite; 5% clays and feldspars). Grains: crinoids (2%; <100 µm – 3 mm); brachiopods (1%; thick-shelled); 1-2% quartz silt; undifferentiated calcareous skeletal fragments (70%; silt-sized; some micritized rims (C, D)).

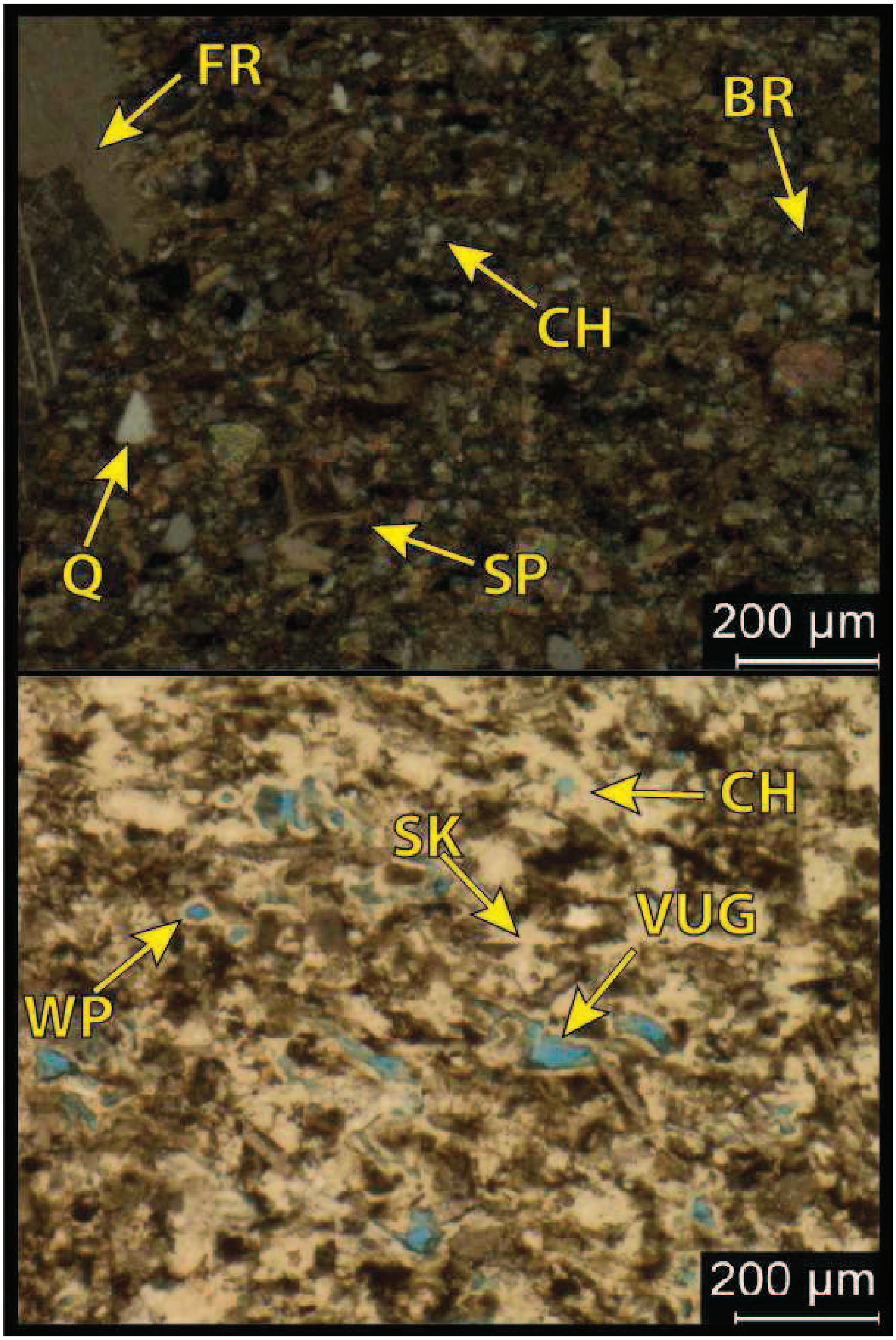

8,072.5': Spicule-bearing siliceous wackestone. Facies 4. Top: XPL. Bottom: PPL. Porosity= 5-7.5% (moldic, intercrystalline, intergranular; dissolution-enhanced; biggest 100 µm vugs). B.I.: 1. Mineralogy: 57% carbonate (53% calcite; 4% dolomite), 35% chert and 8% other minerals (2.5% quartz silt; <1% pyrite; 5% clays and feldspars). Grains: spicules (most 15 x <100 µm, biggest 25 x 150 µm; variably dissolved mold/ calcite/ chert); undifferentiated skeletal grains. Calcite cementation of fractures and variably throughout (5-10%).

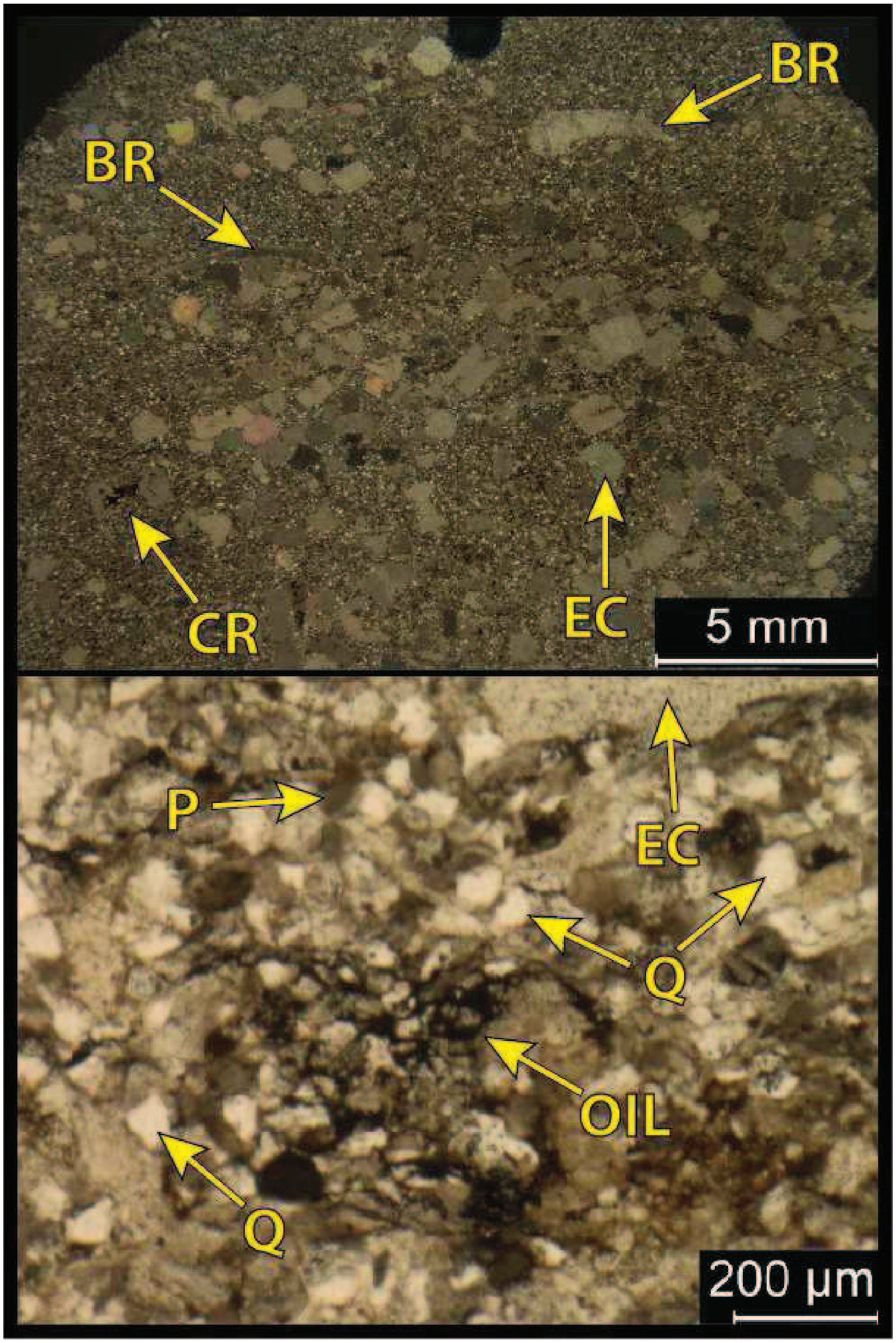

8,035.5': Silty fossiliferous packstone. Facies 6. Top: XPL. Bottom: PPL. Porosity= 1%. B.I.: 0. Mineralogy: 70% carbonate (68% calcite; 2% dolomite) and 30% other minerals (25% quartz silt- vf sand; <1% pyrite; 5% clays and feldspars). Grains: Crinoids (40%; most < 1mm; displaying dissolution features); brachiopods (<1%; biggest 3 x 0.5 mm; variably displaying microborings); well-rounded peloidal grains (40%; up to 60 µm); undifferentiated skeletal grains. 10-20% calcite cementation. Numerous low-amplitude stylolites.

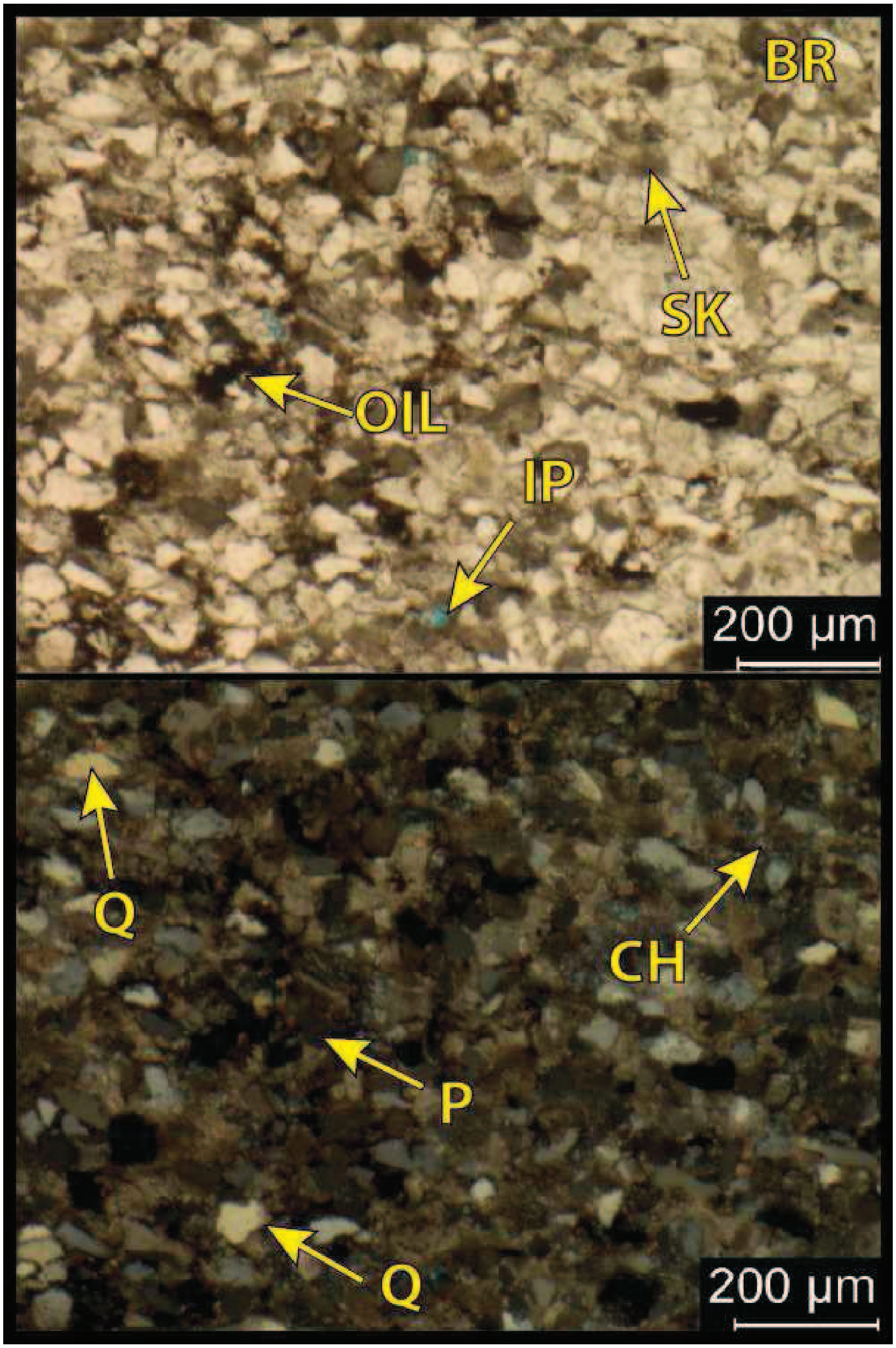

8,017.1’: Silty mud-lean wackestone/ calcareous siltstone. Facies 6. Top: PPL. Bottom: XPL. Porosity= 2% (intergranular, avg. 30 µm diameter). B.I.: 0. Mineralogy: 58% carbonate (56% calcite; 2% dolomite), 2% chert and 40% other minerals (30% quartz silt- vf sand; 3% pyrite; 7% clays and feldspars). Grains: Brachiopods (<1%; 400 x 800 µm; syntaxial cementation); well-rounded peloidal grains (25%; up to 60 µm); undifferentiated skeletal grains. 10% calcite cementation (syntaxial with calcareous debris).

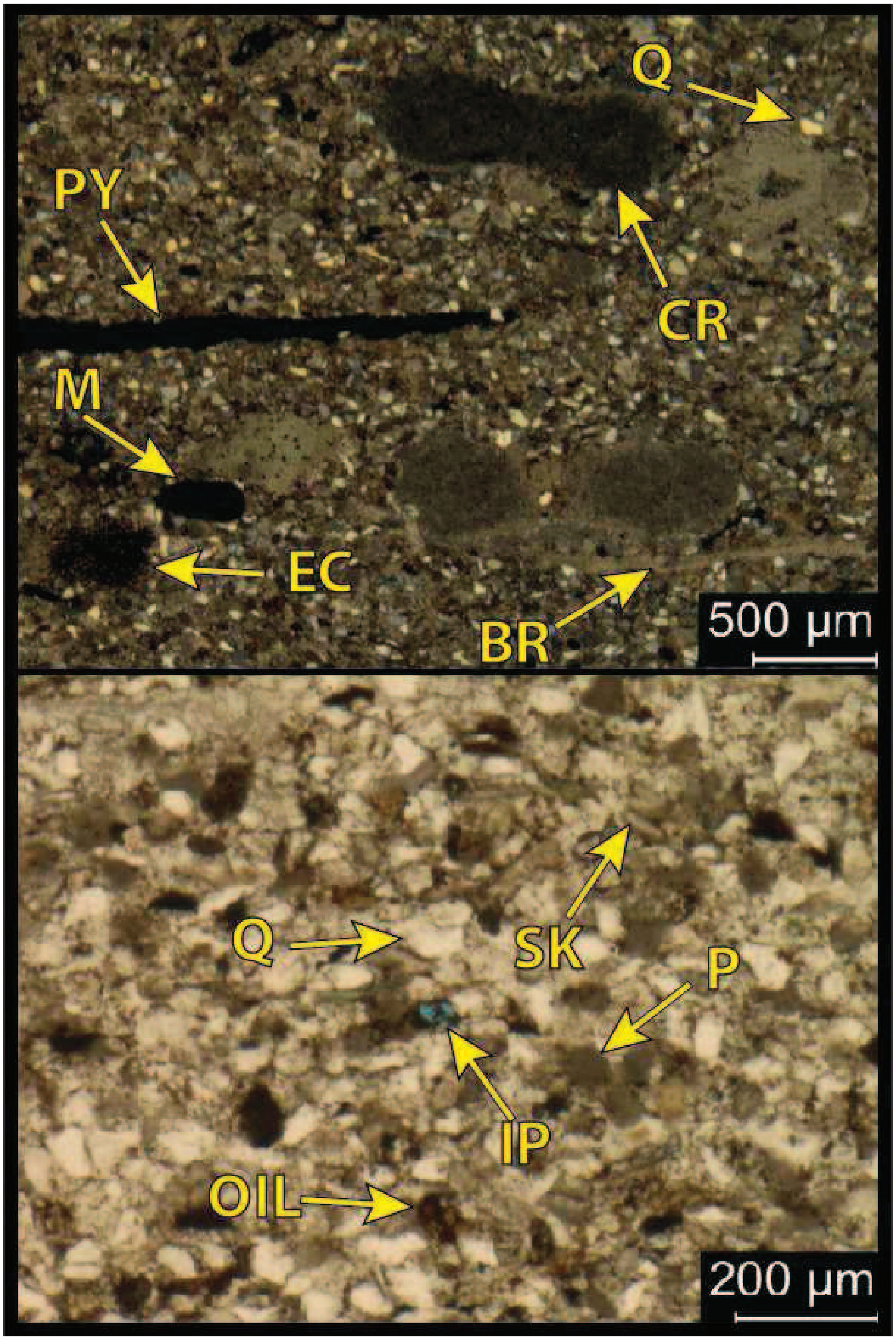

7,983.2’: Bioclastic silty mud-lean packstone. Facies 6. Top: XPL. Bottom: PPL. Porosity= 4% (intergranular, moldic after peloidal grains; 30-70 µm diam.). B.I.: 0. Mineralogy: 60% carbonate (59% calcite; 1% dolomite) and 40% other minerals (35% quartz silt- vf sand; 1% pyrite; 4% clays and feldspars). Grains: Bioclasts (10%); crinoids (0.5-1 mm); echinoid (~300 µm; micritized); brachiopods (1 - 800 µm; variably phosphatic); bryozoa; ostracodes (25 x 200 µm); peloidal grains (silt- vf sand); undifferentiated skeletal grains. 5% calcite cementation (syntaxial with crinoids and variably throughout).

III. Effie B York Unit #1 Core Descriptions

Preliminary Core Descriptions

Cores were described using the Dunham classification method. Tracts display (from left to right): thin section description (preliminary), Depth (ft.), oil staining, thin section location, Sedimentary structures/ Notes, Facies Type (color coded), Lithology (overprinted by symbols to indicate features (burrowing, stylolites, fractures, HCS and chert)), Textural classification (Dunham), Bioturbation (mm-scale horizontal, cm-scale horizontal, mm-scale vertical, cm-scale vertical), Bioturbation Index (using the Bann et al. (2008) classification method), Grain Types, Lamination (Suspension, traction, mottled), Color, Photograph & depth taken, Depositional Environment

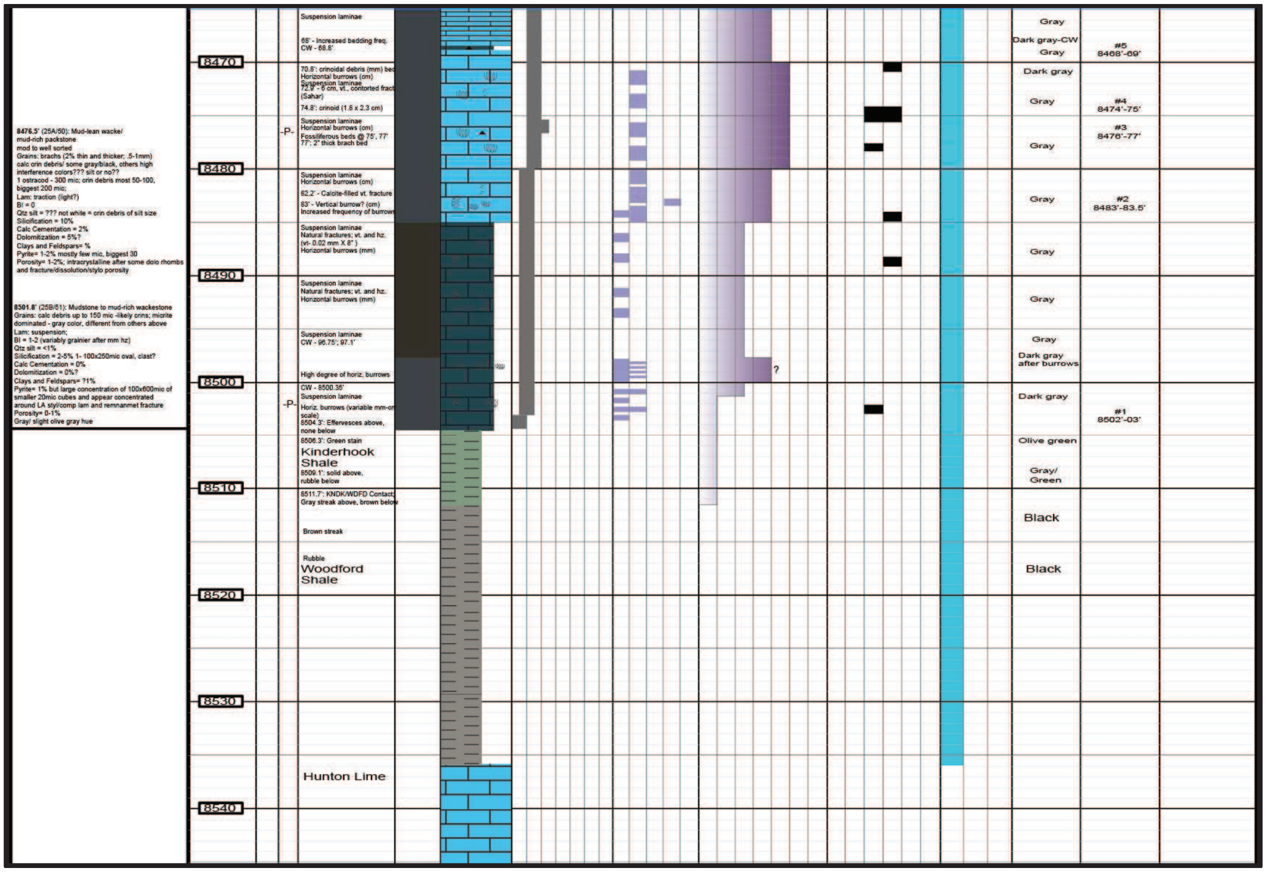
8476.5' (25A/50): Mud-lean wacke/
mud-rich packstone
mod to well sorted
Grains: brachs (2% thin and thicker; .5-1mm)
calc crin debris/ some gray/black, others high
interference colors??? silt or no??
1 ostracod - 300 mic; crin debris most 50-100,
biggest 200 mic;
Lam: traction (light?)
BI = 0
Qtz silt = ??? not white = crin debris of silt size
Silicification = 10%
Calc Cementation = 2%
Dolomitization = 5%?
Clays and Feldspars= %
Pyrite= 1-2% mostly few mic, biggest 30
Porosity= 1-2%; intracrystalline after some dolo rhombs
and fracture/dissolution/stylo porosity
8501.8' (25B/51): Mudstone to mud-rich wackestone
Grains: calc debris up to 150 mic -likely crins; micrite
dominated - gray color, different from others above
Lam: suspension;
BI = 1-2 (variably grainier after mm hz)
Qtz silt = <1%
Silicification = 2-5% 1- 100x250mic oval, clast?
Calc Cementation = 0%
Dolomitization = 0%?
Clays and Feldspars= ?1%
Pyrite= 1% but large concentration of 100x600mic of
smaller 20mic cubes and appear concentrated
around LA styl/comp lam and remnanmet fracture
Porosity= 0-1%
Gray/ slight olive gray hue
8470
8480
8490
8500
8510
8520
8530
8540
-P-
-P-
Suspension laminae
68' - Increased bedding freq.
CW - 68.8'
70.8': crinoidal debris (mm) bed
Horizontal burrows (cm)
Suspension laminae
72.9' - 6 cm, vt., contorted fract
(Sahar)
74.8': crinoid (1.8 x 2.3 cm)
Suspension laminae
Horizontal burrows (cm)
Fossiliferous beds @ 75', 77'
77': 2" thick brach bed
Suspension laminae
Horizontal burrows (cm)
82.2' - Calcite-filled vt. fracture
83' - Vertical burrow? (cm)
Increased frequency of burrows
Suspension laminae
Natural fractures; vt. and hz.
(vt- 0.02 mm X 8")
Horizontal burrows (mm)
Suspension laminae
Natural fractures; vt. and hz.
Horizontal burrows (mm)
Suspension laminae
CW - 96.75'; 97.1'
High degree of horiz. burrows
CW - 8500.35'
Suspension laminae
Horiz. burrows (variable mm-cm
scale)
8504.3': Effervesces above,
none below
8506.3': Green stain
Kinderhook
Shale
8509.1': solid above,
rubble below
8511.7': KNDK/WDFD Contact;
Gray streak above, brown below
Brown streak
Rubble
Woodford
Shale
Hunton Lime
?
Gray
Dark gray-CW
Gray
#5
8468'-69'
Dark gray
Gray
#4
8474'-75'
#3
8476'-77'
Gray
Gray
#2
8483'-83.5'
Gray
Gray
Gray
Dark gray
after burrows
Dark gray
#1
8502'-03'
Olive green
Gray/
Green
Black
Black

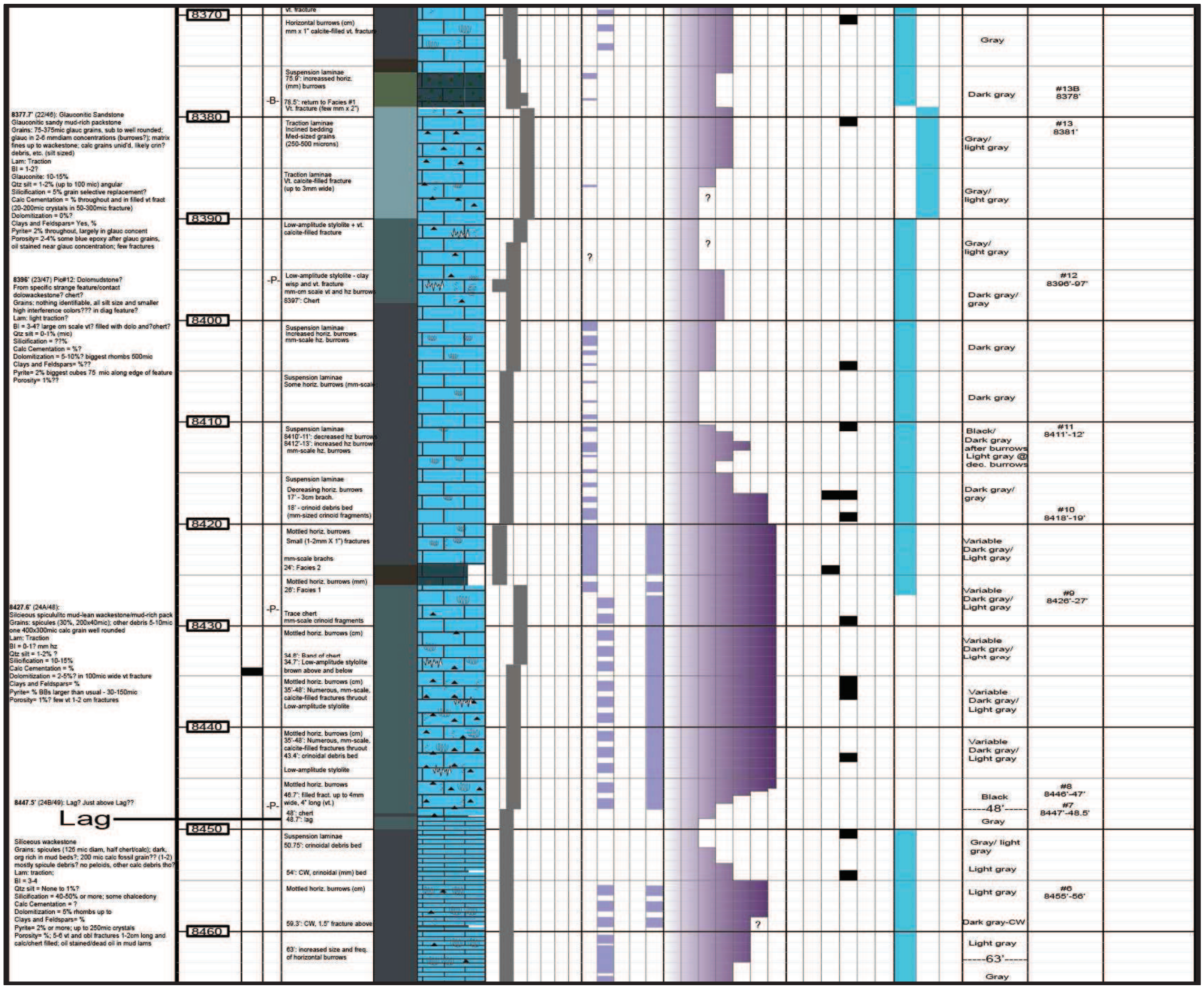
8370
8380
8390
8400
8410
8420
8430
8440
8450
8460
Lag
Gray
Dark gray
Gray/ light gray
Dark gray/ gray
Black
Light gray

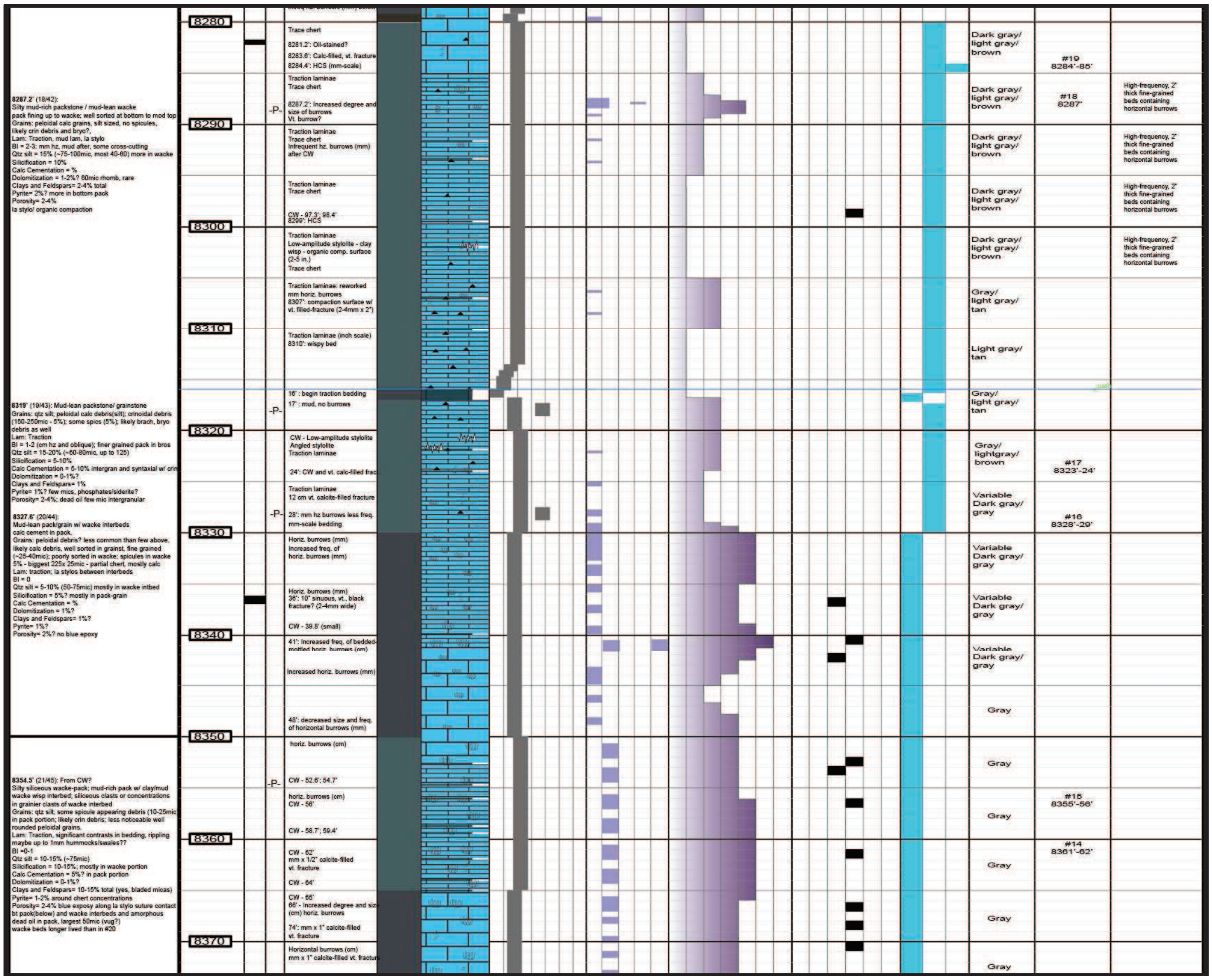
8287.2' (18/42):
Silty mud-rich packstone / mud-lean wacke
pack fining up to wacke; well sorted at bottom to mod top
Grains: peloidal calc grains, silt sized, no spicules,
likely crin debris and bryo?,
Lam: Traction, mud lam, la stylo
BI = 2-3; mm hz, mud after, some cross-cutting
Qtz silt = 15% (~75-100mic, most 40-60) more in wacke
Silicification = 10%
Calc Cementation = %
Dolomitization = 1-2%? 60mic rhomb, rare
Clays and Feldspars= 2-4% total
Pyrite= 2%? more in bottom pack
Porosity= 2-4%
la stylo/ organic compaction
8319' (19/43): Mud-lean packstone/ grainstone
Grains: qtz silt; peloidal calc debris(silt); crinoidal debris
(150-250mic - 5%); some spics (5%); likely brach, bryo
debris as well
Lam: Traction
BI = 1-2 (cm hz and oblique); finer grained pack in bros
Qtz silt = 15-20% (~60-80mic, up to 125)
Silicification = 5-10%
Calc Cementation = 5-10% intergran and syntaxial w/ crin
Dolomitization = 0-1%?
Clays and Feldspars= 1%
Pyrite= 1%? few mics, phosphates/siderite?
Porosity= 2-4%; dead oil few mic intergranular
8327.6' (20/44):
Mud-lean pack/grain w/ wacke interbeds
calc cement in pack.
Grains: peloidal debris? less common than few above,
likely calc debris, well sorted in grainst, fine grained
(~25-40mic); poorly sorted in wacke; spicules in wacke
5% - biggest 225x 25mic - partial chert, mostly calc
Lam: traction; la stylos between interbeds
BI = 0
Qtz silt = 5-10% (50-75mic) mostly in wacke intbed
Silicification = 5%? mostly in pack-grain
Calc Cementation = %
Dolomitization = 1%?
Clays and Feldspars= 1%?
Pyrite= 1%?
Porosity= 2%? no blue epoxy
8354.5' (21/45): From CW?
Silty siliceous wacke-pack; mud-rich pack w/ clay/mud
wacke wisp interbed; siliceous clasts or concentrations
in grainier clasts of wacke interbed
Grains: qtz silt; some spicule appearing debris (10-25mic
in pack portion; likely crin debris; less noticeable well
rounded peloidal grains.
Lam: Traction, significant contrasts in bedding, rippling
maybe up to 1mm hummocks/swales??
BI =0-1
Qtz silt = 10-15% (~75mic)
Silicification = 10-15%; mostly in wacke portion
Calc Cementation = 5%? in pack portion
Dolomitization = 0-1%?
Clays and Feldspars= 10-15% total (yes, bladed micas)
Pyrite= 1-2% around chert concentrations
Porosity= 2-4% blue exposy along la stylo suture contact
bt pack(below) and wacke interbeds and amorphous
dead oil in pack, largest 50mic (vug?)
wacke beds longer lived than in #20
8280
8290
8300
8310
8320
8330
8340
8350
8360
8370
-P-
-P-
-P-
-P-
Trace chert
8281.2': Oil-stained?
8283.6': Calc-filled, vt. fracture
8284.4': HCS (mm-scale)
Traction laminae
Trace chert
8287.2': Increased degree and size of burrows
Vt. burrow?
Traction laminae
Trace chert
Infrequent hz. burrows (mm) after CW
Traction laminae
Trace chert
CW - 97.3'; 98.4'
8299': HCS
Traction laminae
Low-amplitude stylolite - clay wisp - organic comp. surface (2-5 in.)
Trace chert
Traction laminae: reworked mm horiz. burrows
8307': compaction surface w/ vt. filled-fracture (2-4mm x 2")
Traction laminae (inch scale)
8310': wispy bed
16': begin traction bedding
17': mud, no burrows
CW - Low-amplitude stylolite
Angled stylolite
Traction laminae
24': CW and vt. calc-filled frac
Traction laminae
12 cm vt. calcite-filled fracture
28': mm hz burrows less freq. mm-scale bedding
Horiz. burrows (mm)
Increased freq. of horiz. burrows (mm)
Horiz. burrows (mm)
36': 10" sinuous, vt., black fracture? (2-4mm wide)
CW - 39.6' (small)
41': Increased freq. of bedded-mottled horiz. burrows (cm)
Increased horiz. burrows (mm)
48': decreased size and freq. of horizontal burrows (mm)
horiz. burrows (cm)
CW - 52.6'; 54.7'
horiz. burrows (cm)
CW - 56'
CW - 58.7'; 59.4'
CW - 62'
mm x 1/2" calcite-filled vt. fracture
CW - 64'
CW - 65'
66': increased degree and size (cm) horiz. burrows
74': mm x 1" calcite-filled vt. fracture
Horizontal burrows (cm)
mm x 1" calcite-filled vt. fracture
Dark gray/ light gray/ brown
#19 8284'-85'
Dark gray/ light gray/ brown
#18 8287'
High-frequency, 2" thick fine-grained beds containing horizontal burrows
Dark gray/ light gray/ brown
High-frequency, 2" thick fine-grained beds containing horizontal burrows
Dark gray/ light gray/ brown
High-frequency, 2" thick fine-grained beds containing horizontal burrows
Dark gray/ light gray/ brown
High-frequency, 2" thick fine-grained beds containing horizontal burrows
Gray/ light gray/ tan
Light gray/ tan
Gray/ light gray/ tan
Gray/ lightgray/ brown
#17 8323'-24'
Variable Dark gray/ gray
#16 8328'-29'
Variable Dark gray/ gray
Variable Dark gray/ gray
Variable Dark gray/ gray
Gray
Gray
Gray
#15 8355'-56'
Gray
#14 8361'-62'
Gray
Gray

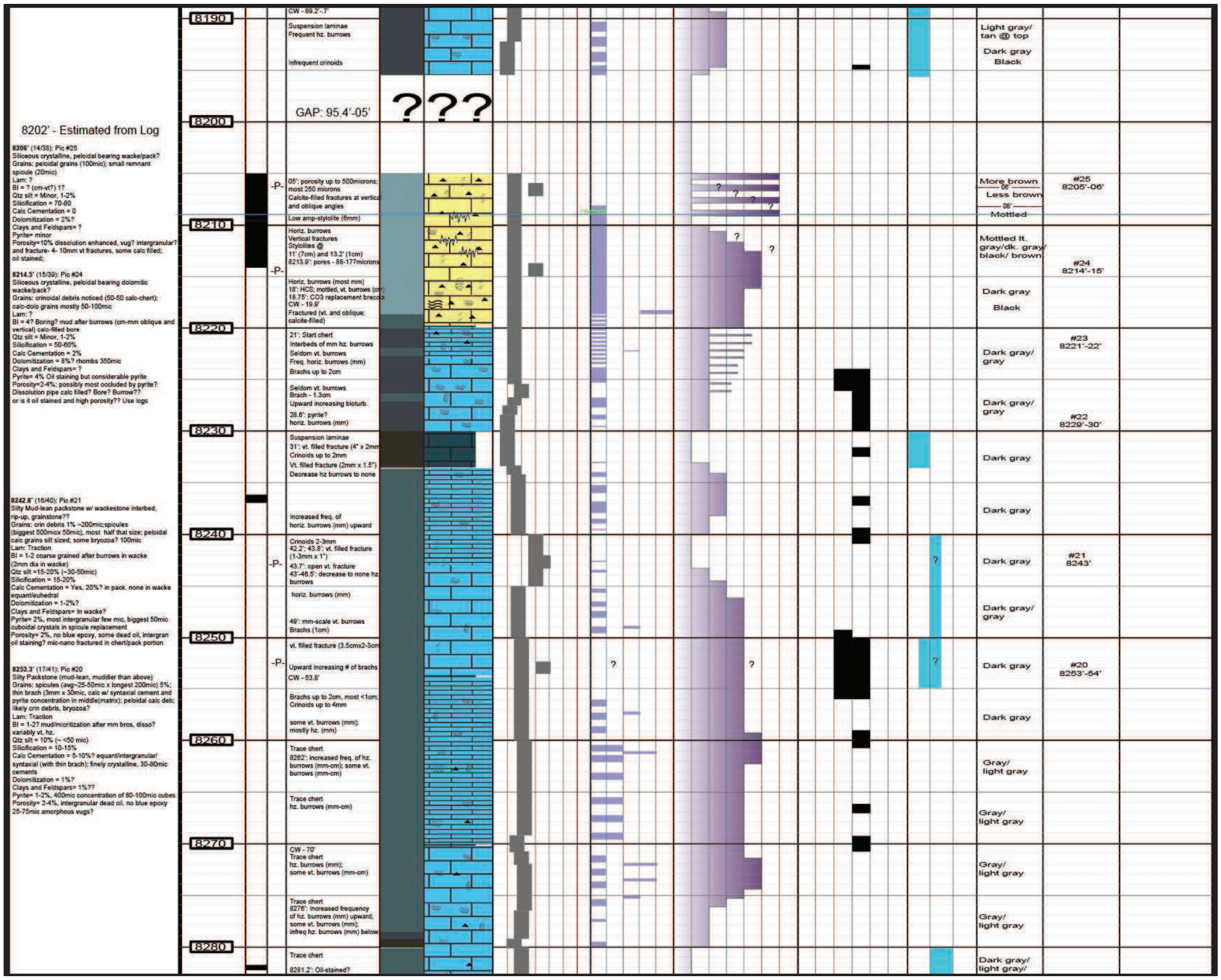
8202' - Estimated from Log
8206' (14/38): Pic #25
Siliceous crystalline, peloidal bearing wacke/pack?
Grains: peloidal grains (100mic); small remnant spicule (20mic)
Lam: ?
BI = ? (cm-vt?) 1?
Qtz silt = Minor, 1-2%
Silicification = 70-80
Calc Cementation = 0
Dolomitization = 2%?
Clays and Feldspars= ?
Pyrite= minor
Porosity=10% dissolution enhanced, vug? intergranular? and fracture- 4- 10mm vt fractures, some calc filled; oil stained;
8214.5' (15/39): Pic #24
Siliceous crystalline, peloidal bearing dolomitic wacke/pack?
Grains: crinoidal debris noticed (50-50 calc-chert); calc-dolo grains mostly 50-100mic
Lam: ?
BI = 4? Boring? mud after burrows (cm-mm oblique and vertical) calc-filled bore
Qtz silt = Minor, 1-2%
Silicification = 50-60%
Calc Cementation = 2%
Dolomitization = 8%? rhombs 350mic
Clays and Feldspars= ?
Pyrite= 4% Oil staining but considerable pyrite
Porosity=2-4%; possibly most occluded by pyrite? Dissolution pipe calc filled? Bore? Burrow?? or is it oil stained and high porosity?? Use logs
8242.8' (16/40): Pic #21
Silty Mud-lean packstone w/ wackestone interbed, rip-up, grainstone??
Grains: crin debris 1% ~200mic;spicules (biggest 500micx 50mic), most half that size; peloidal calc grains silt sized; some bryozoa? 100mic
Lam: Traction
BI = 1-2 coarse grained after burrows in wacke (2mm dia in wacke)
Qtz silt =15-20% (~30-50mic)
Silicification = 15-20%
Calc Cementation = Yes, 20%? in pack, none in wacke equant/euhedral
Dolomitization = 1-2%?
Clays and Feldspars= In wacke?
Pyrite= 2%, most intergranular few mic, biggest 50mic cuboidal crystals in spicule replacement
Porosity= 2%, no blue epoxy, some dead oil, intergran oil staining? mic-nano fractured in chert/pack portion
8253.3' (17/41): Pic #20
Silty Packstone (mud-lean, muddier than above)
Grains: spicules (avg~25-50mic x longest 200mic) 5%; thin brach (3mm x 30mic, calc w/ syntaxial cement and pyrite concentration in middle(matrix); peloidal calc deb; likely crin debris, bryozoa?
Lam: Traction
BI = 1-2? mud/micritization after mm bros, disso? variably vt. hz.
Qtz silt = 10% (~ <50 mic)
Silicification = 10-15%
Calc Cementation = 5-10%? equant/intergranular/ syntaxial (with thin brach); finely crystalline, 30-80mic cements
Dolomitization = 1%?
Clays and Feldspars= 1%??
Pyrite= 1-2%, 400mic concentration of 80-100mic cubes
Porosity= 2-4%, intergranular dead oil, no blue epoxy 25-75mic amorphous vugs?
8190
8200
8210
8220
8230
8240
8250
8260
8270
8280
-P-
CW - 89.2'-.7'
Suspension laminae
Frequent hz. burrows
Infrequent crinoids
GAP: 95.4'-05'
???
05': porosity up to 500microns; most 250 microns
Calcite-filled fractures at vertical and oblique angles
Low amp-stylolite (6mm)
Horiz. burrows
Vertical fractures
Stylolites @ 11' (7cm) and 13.2' (1cm)
8213.9': pores - 88-177microns
Horiz. burrows (most mm)
18': HCS; mottled, vt. burrows (cm)
18.75': CO3 replacement breccia
CW - 19.9'
Fractured (vt. and oblique; calcite-filled)
21': Start chert
Interbeds of mm hz. burrows
Seldom vt. burrows
Freq. horiz. burrows (mm)
Brachs up to 2cm
Seldom vt. burrows
Brach - 1.3cm
Upward increasing bioturb.
28.6': pyrite?
horiz. burrows (mm)
Suspension laminae
31': vt. filled fracture (4" x 2mm)
Crinoids up to 2mm
Vt. filled fracture (2mm x 1.5")
Decrease hz burrows to none
Increased freq. of horiz. burrows (mm) upward
Crinoids 2-3mm
42.2'; 43.8': vt. filled fracture (1-3mm x 1")
43.7': open vt. fracture
43'-46.5': decrease to none hz. burrows
horiz. burrows (mm)
49': mm-scale vt. burrows
Brachs (1cm)
vt. filled fracture (3.5cmx2-3cm)
Upward increasing # of brachs
CW - 53.8'
Brachs up to 2cm, most <1cm;
Crinoids up to 4mm
some vt. burrows (mm); mostly hz. (mm)
Trace chert
8262': increased freq. of hz. burrows (mm-cm); some vt. burrows (mm-cm)
Trace chert
hz. burrows (mm-cm)
CW - 70'
Trace chert
hz. burrows (mm); some vt. burrows (mm-cm)
Trace chert
8276': increased frequency of hz. burrows (mm) upward; some vt. burrows (mm); infreq hz. burrows (mm) below
Trace chert
8281.2': Oil-stained?
Light gray/ tan @ top
Dark gray
Black
More brown
Less brown
Mottled
#25
8205'-06'
Mottled lt. gray/dk. gray/ black/ brown
#24
8214'-15'
Dark gray
Black
#23
8221'-22'
Dark gray/ gray
Dark gray/ gray
#22
8229'-30'
Dark gray
Dark gray
Dark gray
#21
8243'
Dark gray/ gray
Dark gray
#20
8253'-54'
Dark gray
Gray/ light gray
Gray/ light gray
Gray/ light gray
Gray/ light gray
Dark gray/ light gray/

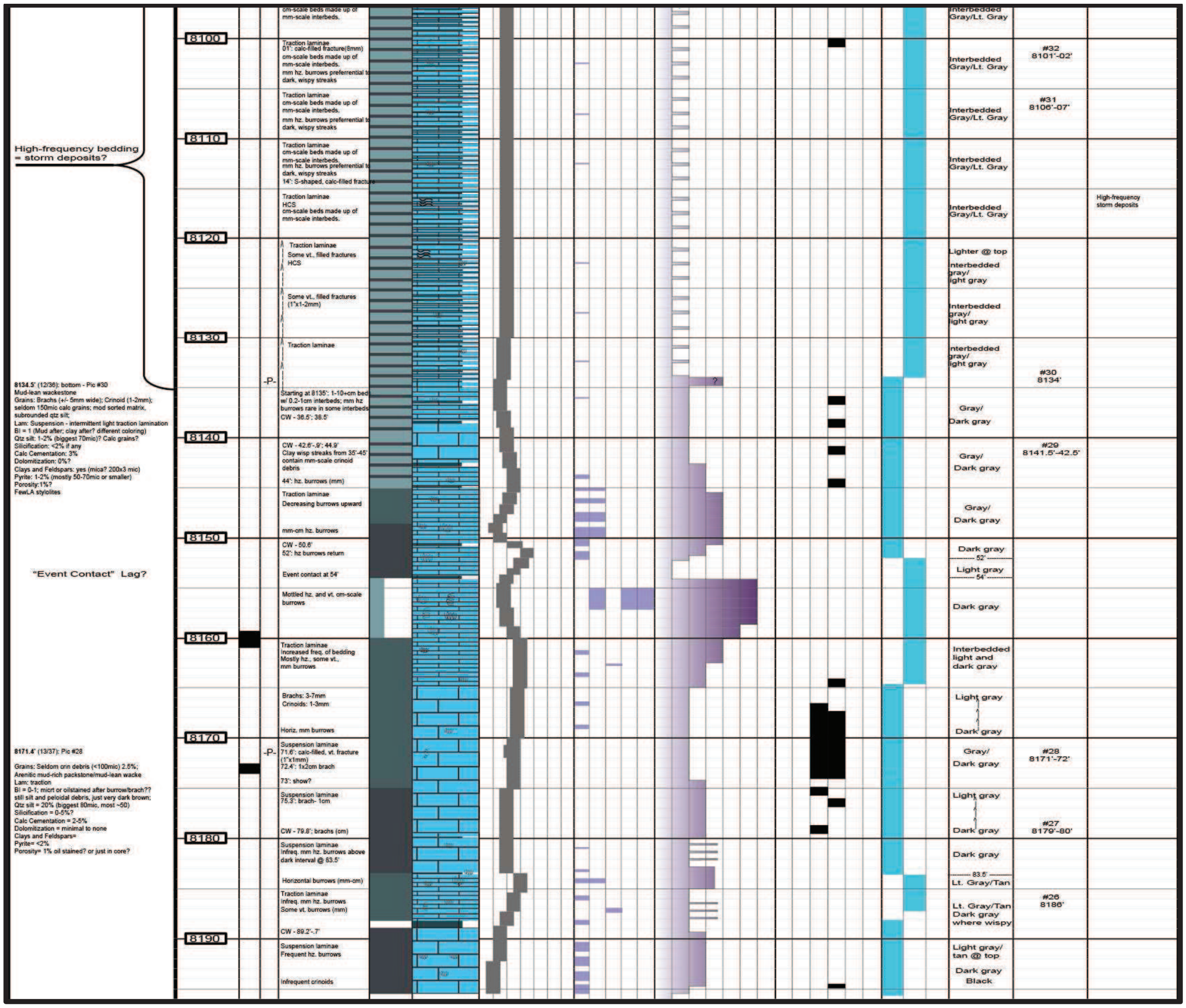
High-frequency bedding = storm deposits?
8134.5' (12/36): bottom - Pic #30
Mud-lean wackestone
Grains: Brachs (+/- 5mm wide); Crinoid (1-2mm); seldom 150mic calc grains; mod sorted matrix, subrounded qtz silt;
Lam: Suspension - intermittent light traction lamination
BI = 1 (Mud after; clay after? different coloring)
Qtz silt: 1-2% (biggest 70mic)? Calc grains?
Silicification: <2% if any
Calc Cementation: 3%
Dolomitization: 0%?
Clays and Feldspars: yes (mica? 200x3 mic)
Pyrite: 1-2% (mostly 50-70mic or smaller)
Porosity:1%?
FewLA stylolites
"Event Contact" Lag?
8171.4' (13/37): Pic #28
Grains: Seldom crin debris (<100mic) 2.5%;
Arenitic mud-rich packstone/mud-lean wacke
Lam: traction
BI = 0-1; micrt or oilstained after burrow/brach??
still silt and peloidal debris, just very dark brown;
Qtz silt = 20% (biggest 80mic, most ~50)
Silicification = 0-5%?
Calc Cementation = 2-5%
Dolomitization = minimal to none
Clays and Feldspars=
Pyrite= <2%
Porosity= 1% oil stained? or just in core?
8100
8110
8120
8130
8140
8150
8160
8170
8180
8190
-P-
-P-
Interbedded Gray/Lt. Gray
Interbedded Gray/Lt. Gray
#32 8101'-02'
Interbedded Gray/Lt. Gray
#31 8106'-07'
Interbedded Gray/Lt. Gray
Interbedded Gray/Lt. Gray
High-frequency storm deposits
Lighter @ top
Interbedded gray/ light gray
Interbedded gray/ light gray
Interbedded gray/ light gray
#30 8134'
Gray/ Dark gray
Gray/ Dark gray
#29 8141.5'-42.5'
Gray/ Dark gray
Dark gray
52'
Light gray
54'
Dark gray
Interbedded light and dark gray
Light gray
Dark gray
Gray/ Dark gray
#28 8171'-72'
Light gray
Dark gray
#27 8179'-80'
Dark gray
83.5'
Lt. Gray/Tan
Lt. Gray/Tan Dark gray where wispy
#26 8186'
Light gray/ tan @ top
Dark gray
Black

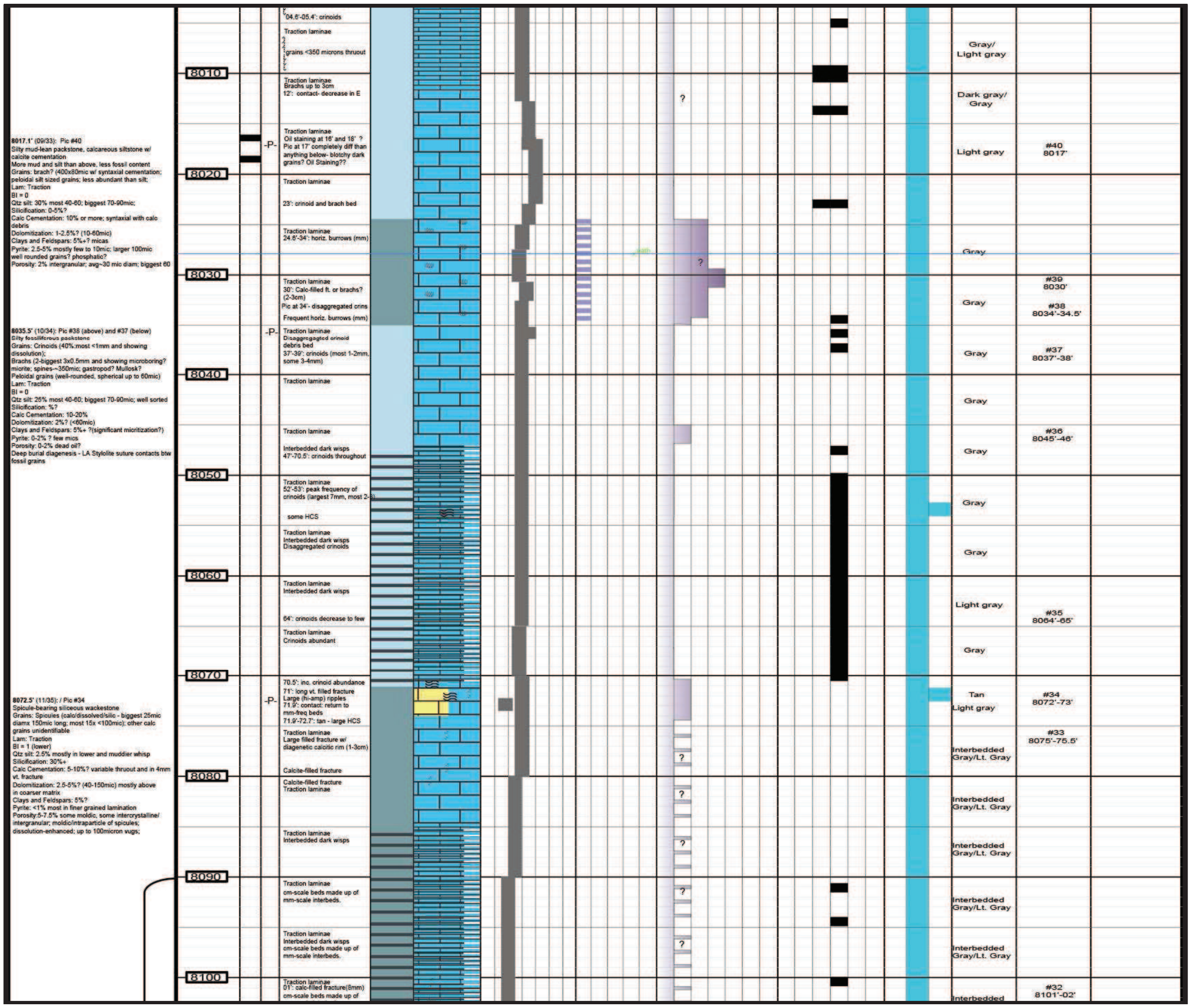
8017.1' (09/33): Pic #40
Silty mud-lean packstone, calcareous siltstone w/ calcite cementation
More mud and silt than above, less fossil content
Grains: brach? (400x80mic w/ syntaxial cementation; peloidal silt sized grains; less abundant than silt;
Lam: Traction
BI = 0
Qtz silt: 30% most 40-60; biggest 70-90mic;
Silicification: 0-5%?
Calc Cementation: 10% or more; syntaxial with calc debris
Dolomitization: 1-2.5%? (10-60mic)
Clays and Feldspars: 5%+? micas
Pyrite: 2.5-5% mostly few to 10mic; larger 100mic well rounded grains? phosphatic?
Porosity: 2% intergranular; avg~30 mic diam; biggest 60
8035.5' (10/34): Pic #38 (above) and #37 (below)
Silty fossiliferous packstone
Grains: Crinoids (40%:most <1mm and showing dissolution);
Brachs (2-biggest 3x0.5mm and showing microboring? micrite; spines-~350mic; gastropod? Mullosk?
Peloidal grains (well-rounded, spherical up to 60mic)
Lam: Traction
BI = 0
Qtz silt: 25% most 40-60; biggest 70-90mic; well sorted
Silicification: %?
Calc Cementation: 10-20%
Dolomitization: 2%? (<60mic)
Clays and Feldspars: 5%+ ?(significant micritization?)
Pyrite: 0-2% ? few mics
Porosity: 0-2% dead oil?
Deep burial diagenesis - LA Stylolite suture contacts btw fossil grains
8072.5' (11/35): / Pic #34
Spicule-bearing siliceous wackestone
Grains: Spicules (calc/dissolved/silic - biggest 25mic diamx 150mic long; most 15x <100mic); other calc grains unidentifiable
Lam: Traction
BI = 1 (lower)
Qtz silt: 2.5% mostly in lower and muddier whisp
Silicification: 30%+
Calc Cementation: 5-10%? variable thruout and in 4mm vt. fracture
Dolomitization: 2.5-5%? (40-150mic) mostly above in coarser matrix
Clays and Feldspars: 5%?
Pyrite: <1% most in finer grained lamination
Porosity:5-7.5% some moldic, some intercrystalline/ intergranular; moldic/intraparticle of spicules; dissolution-enhanced; up to 100micron vugs;
8010
8020
8030
8040
8050
8060
8070
8080
8090
8100
-P-
-P-
-P-
04.6'-05.4': crinoids
Traction laminae
grains <350 microns thruout
Traction laminae
Brachs up to 3cm
12': contact- decrease in E
Traction laminae
Oil staining at 16' and 18' ?
Pic at 17' completely diff than anything below- blotchy dark grains? Oil Staining??
Traction laminae
23': crinoid and brach bed
Traction laminae
24.6'-34': horiz. burrows (mm)
Traction laminae
30': Calc-filled ft. or brachs? (2-3cm)
Pic at 34'- disaggregated crins
Frequent horiz. burrows (mm)
Traction laminae
Disaggregagted crinoid debris bed
37'-39': crinoids (most 1-2mm, some 3-4mm)
Traction laminae
Traction laminae
Interbedded dark wisps
47'-70.5': crinoids throughout
Traction laminae
52'-53': peak frequency of crinoids (largest 7mm, most 2-3)
some HCS
Traction laminae
Interbedded dark wisps
Disaggregated crinoids
Traction laminae
Interbedded dark wisps
64': crinoids decrease to few
Traction laminae
Crinoids abundant
70.5': inc. crinoid abundance
71': long vt. filled fracture
Large (hi-amp) ripples
71.9': contact: return to mm-freq beds
71.9'-72.7': tan - large HCS
Traction laminae
Large filled fracture w/ diagenetic calcitic rim (1-3cm)
Calcite-filled fracture
Calcite-filled fracture
Traction laminae
Traction laminae
Interbedded dark wisps
Traction laminae
cm-scale beds made up of mm-scale interbeds.
Traction laminae
Interbedded dark wisps
cm-scale beds made up of mm-scale interbeds.
Traction laminae
01': calc-filled fracture(8mm)
cm-scale beds made up of
?
?
?
?
?
?
?
Gray/ Light gray
Dark gray/ Gray
Light gray
Gray
Gray
Gray
Gray
Gray
Gray
Gray
Light gray
Gray
Tan
Light gray
Interbedded Gray/Lt. Gray
Interbedded Gray/Lt. Gray
Interbedded Gray/Lt. Gray
Interbedded Gray/Lt. Gray
Interbedded Gray/Lt. Gray
Interbedded
#40 8017'
#39 8030'
#38 8034'-34.5'
#37 8037'-38'
#36 8045'-46'
#35 8064'-65'
#34 8072'-73'
#33 8075'-75.5'
#32 8101'-02'

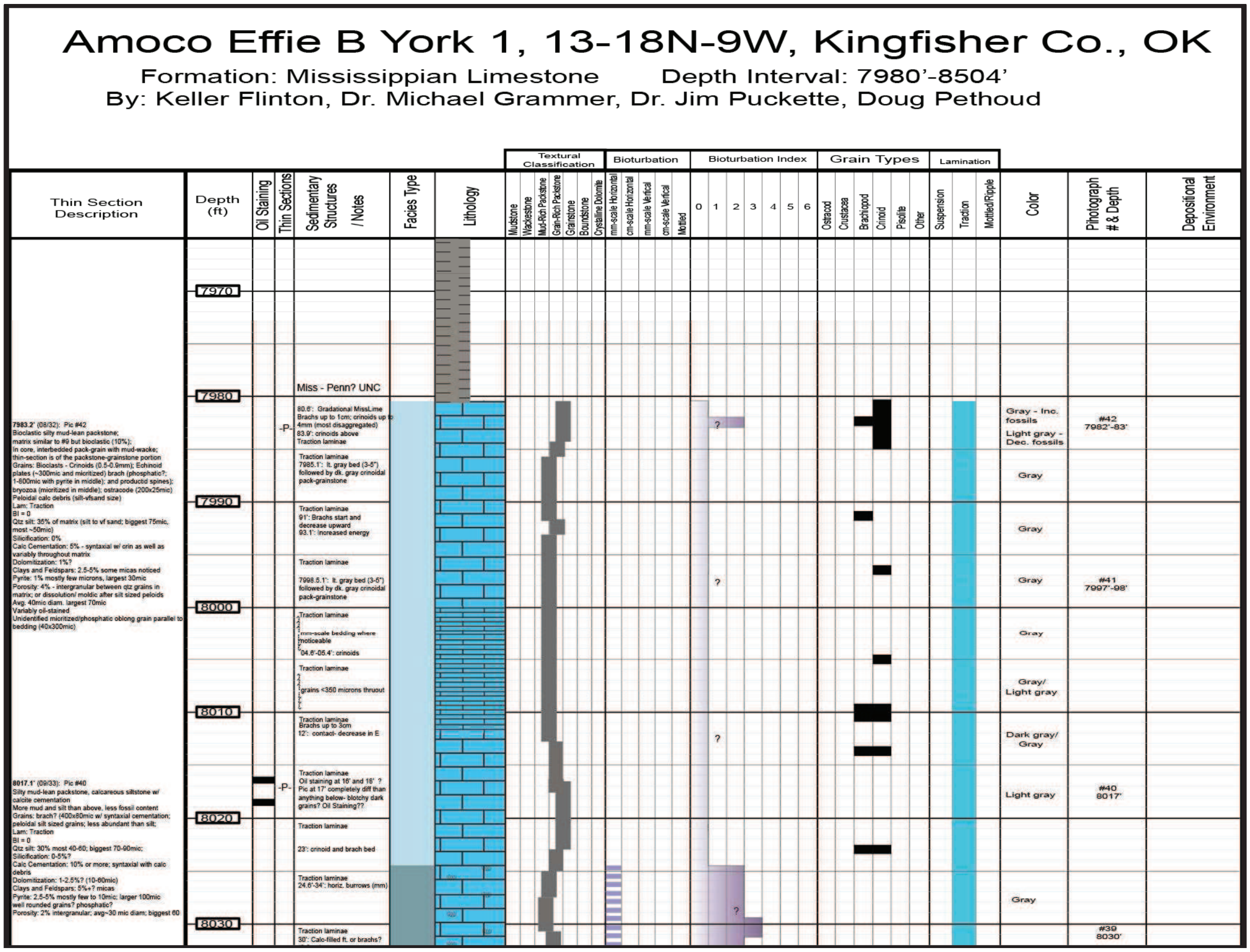

Amoco Effie B York 1, 13-18N-9W, Kingfisher Co., OK
Formation: Mississippian Limestone
Depth Interval: 7980'-8504'
By: Keller Flinton, Dr. Michael Grammer, Dr. Jim Puckette, Doug Pethoud
Textural Classification
Bioturbation
Bioturbation Index
Grain Types
Lamination
Thin Section Description
Depth (ft)
Oil Staining
Thin Sections
Sedimentary Structures / Notes
Facies Type
Lithology
Mudstone
Wackestone
Mud-Rich Packstone
Grain-Rich Packstone
Grainstone
Boundstone
Crystalline Dolomite
mm-scale Horizontal
cm-scale Horizontal
mm-scale Vertical
cm-scale Vertical
Mottled
0
1
2
3
4
5
6
Ostracod
Crustacea
Brachiopod
Crinoid
Pisolite
Other
Suspension
Traction
Mottled/Ripple
Color
Photograph # & Depth
Depositional Environment
7970
7980
7990
8000
8010
8020
8030
Miss - Penn? UNC
7983.2' (08/32): Pic #42
Bioclastic silty mud-lean packstone;
matrix similar to #9 but bioclastic (10%);
In core, interbedded pack-grain with mud-wacke;
thin-section is of the packstone-grainstone portion
Grains: Bioclasts - Crinoids (0.5-0.9mm); Echinoid
plates (~300mic and micritized) brach (phosphatic?;
1-800mic with pyrite in middle); and productid spines);
bryozoa (micritized in middle); ostracode (200x25mic)
Peloidal calc debris (silt-vfsand size)
Lam: Traction
BI = 0
Qtz silt: 35% of matrix (silt to vf sand; biggest 75mic,
most ~50mic)
Silicification: 0%
Calc Cementation: 5% - syntaxial w/ crin as well as
variably throughout matrix
Dolomitization: 1%?
Clays and Feldspars: 2.5-5% some micas noticed
Pyrite: 1% mostly few microns, largest 30mic
Porosity: 4% - intergranular between qtz grains in
matrix; or dissolution/ moldic after silt sized peloids
Avg. 40mic diam. largest 70mic
Variably oil-stained
Unidentified micritized/phosphatic oblong grain parallel to
bedding (40x300mic)
8017.1' (09/33): Pic #40
Silty mud-lean packstone, calcareous siltstone w/
calcite cementation
More mud and silt than above, less fossil content
Grains: brach? (400x80mic w/ syntaxial cementation;
peloidal silt sized grains; less abundant than silt;
Lam: Traction
BI = 0
Qtz silt: 30% most 40-60; biggest 70-90mic;
Silicification: 0-5%?
Calc Cementation: 10% or more; syntaxial with calc
debris
Dolomitization: 1-2.5%? (10-60mic)
Clays and Feldspars: 5%+? micas
Pyrite: 2.5-5% mostly few to 10mic; larger 100mic
well rounded grains? phosphatic?
Porosity: 2% intergranular; avg~30 mic diam; biggest 60
-P-
80.6': Gradational MissLime
Brachs up to 1cm; crinoids up to
4mm (most disaggregated)
83.9': crinoids above
Traction laminae
Traction laminae
7985.1': lt. gray bed (3-5")
followed by dk. gray crinoidal
pack-grainstone
Traction laminae
91': Brachs start and
decrease upward
93.1': Increased energy
Traction laminae
7998.5.1': lt. gray bed (3-5")
followed by dk. gray crinoidal
pack-grainstone
Traction laminae
mm-scale bedding where
noticeable
04.6'-05.4': crinoids
Traction laminae
grains <350 microns thruout
Traction laminae
Brachs up to 3cm
12': contact- decrease in E
Traction laminae
Oil staining at 16' and 18' ?
Pic at 17' completely diff than
anything below- blotchy dark
grains? Oil Staining??
Traction laminae
23': crinoid and brach bed
Traction laminae
24.6'-34': horiz. burrows (mm)
Traction laminae
30': Calc-filled ft. or brachs?
?
Gray - Inc. fossils
Light gray - Dec. fossils
#42
7982'-83'
Gray
Gray
Gray
#41
7997'-98'
Gray
Gray/ Light gray
Dark gray/ Gray
Light gray
#40
8017'
Gray
#39
8030'

Core-to-Wireline Log Tie

From left to right: Gamma Ray curve (0-120 API Units), RILD Resistivity curve (logarithmic 10-100), Sequence stratigraphic hierarchy, Depth (ft.) Dunham erosional profile, Diagenetic effects.

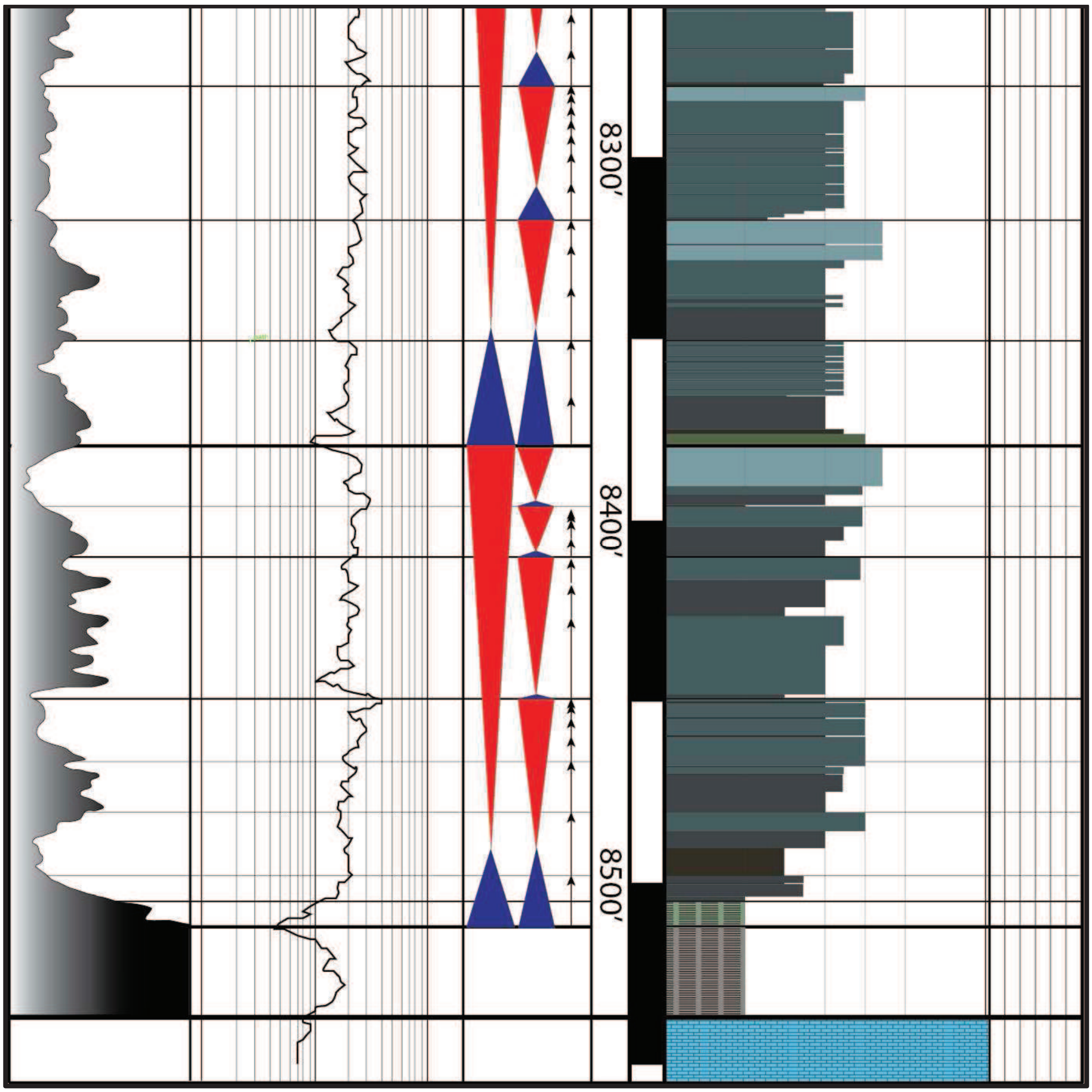

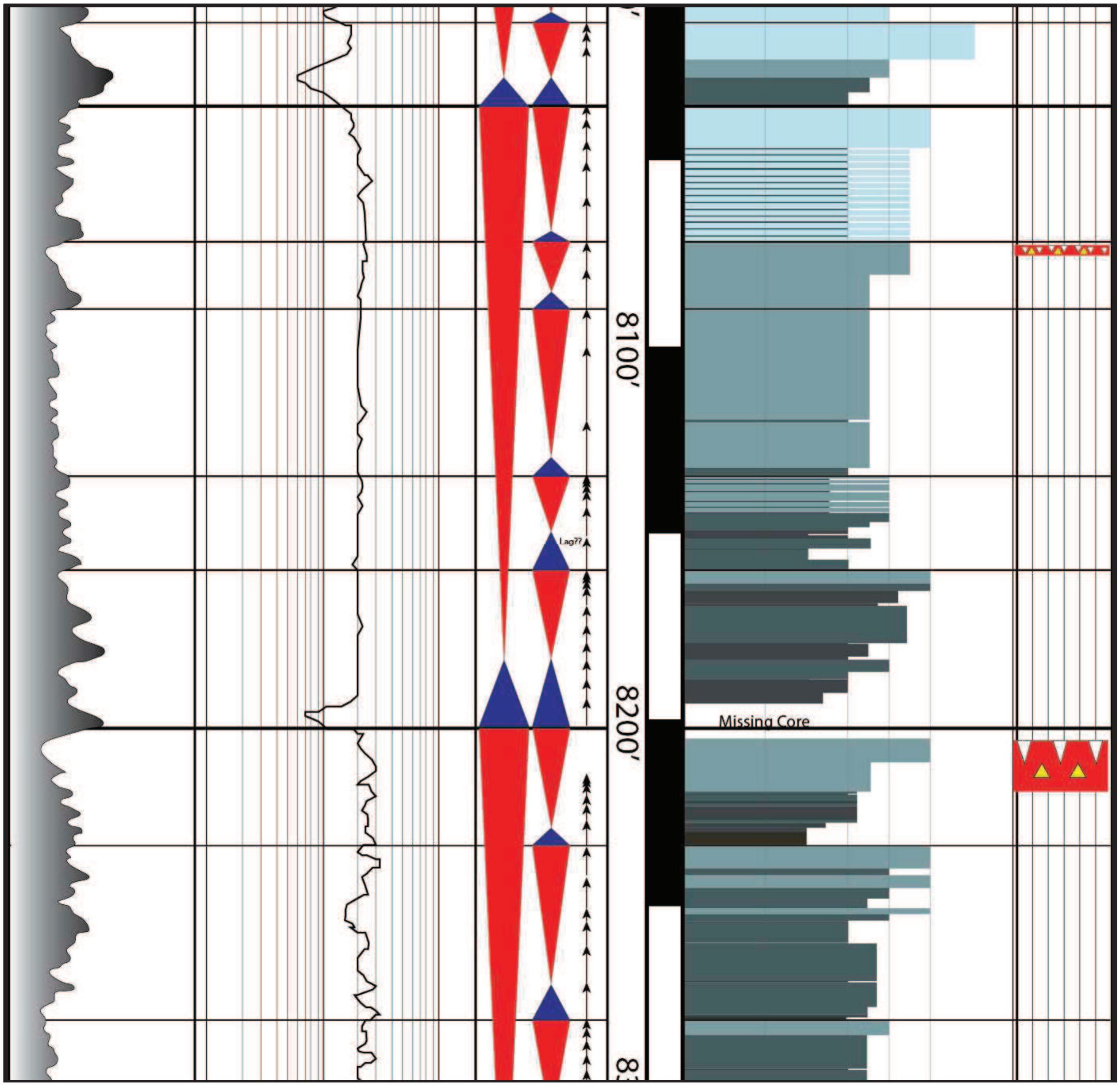

8100'
Lag??
8200'
Missing Core

Effie B York Unit #1

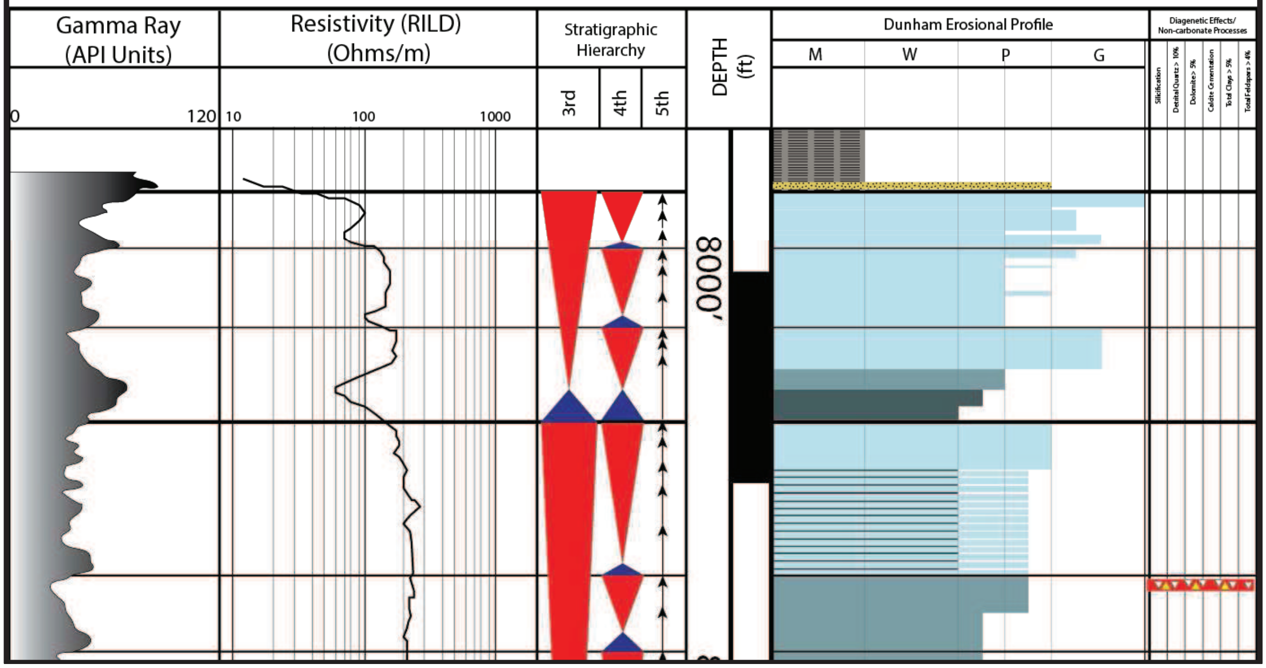

APPENDIX B

Moore Unit D #1
Sec. 12 – T. 18N – R. 9W

I. Moore Unit D #1 Core Slab Photographs

Core slab photographs were taken by the Oklahoma Petroleum Information Center. They are oriented top ("younger") up and were taken wet unless otherwise indicated. Please refer to Table 6 for abbreviations.


8420′
Pan American / Moore Un D1
35073503490000
kingfisher Co, Oklahoma
"Mississippian limestone"
8,437′
"Kinderhook" Shale
8,442′
Woodford Shale
8458′


8406.5′
Pan American / Moore Un D1
35073503490000
kingfisher Co, Oklahoma
F2
8,414′
F3
8420′

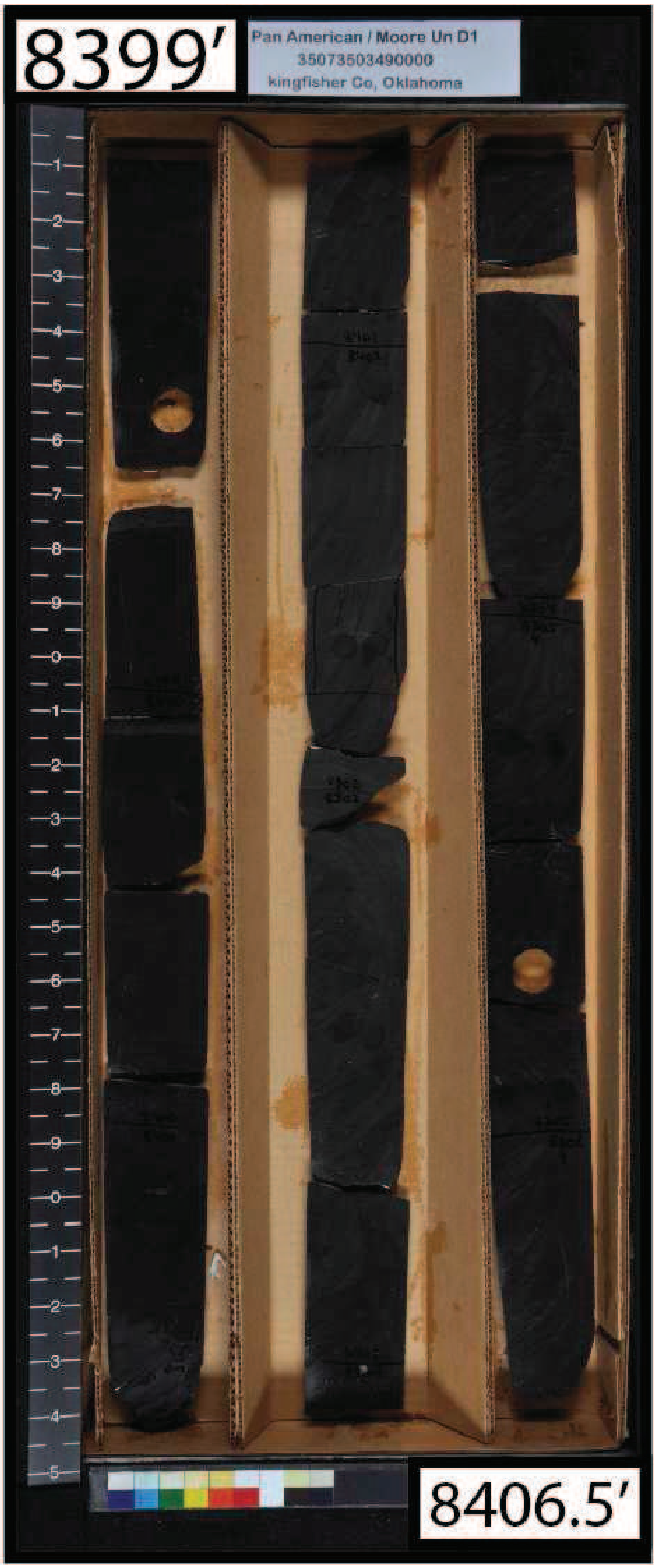
8399′
Pan American / Moore Un D1
35073503490000
kingfisher Co, Oklahoma
8406.5′

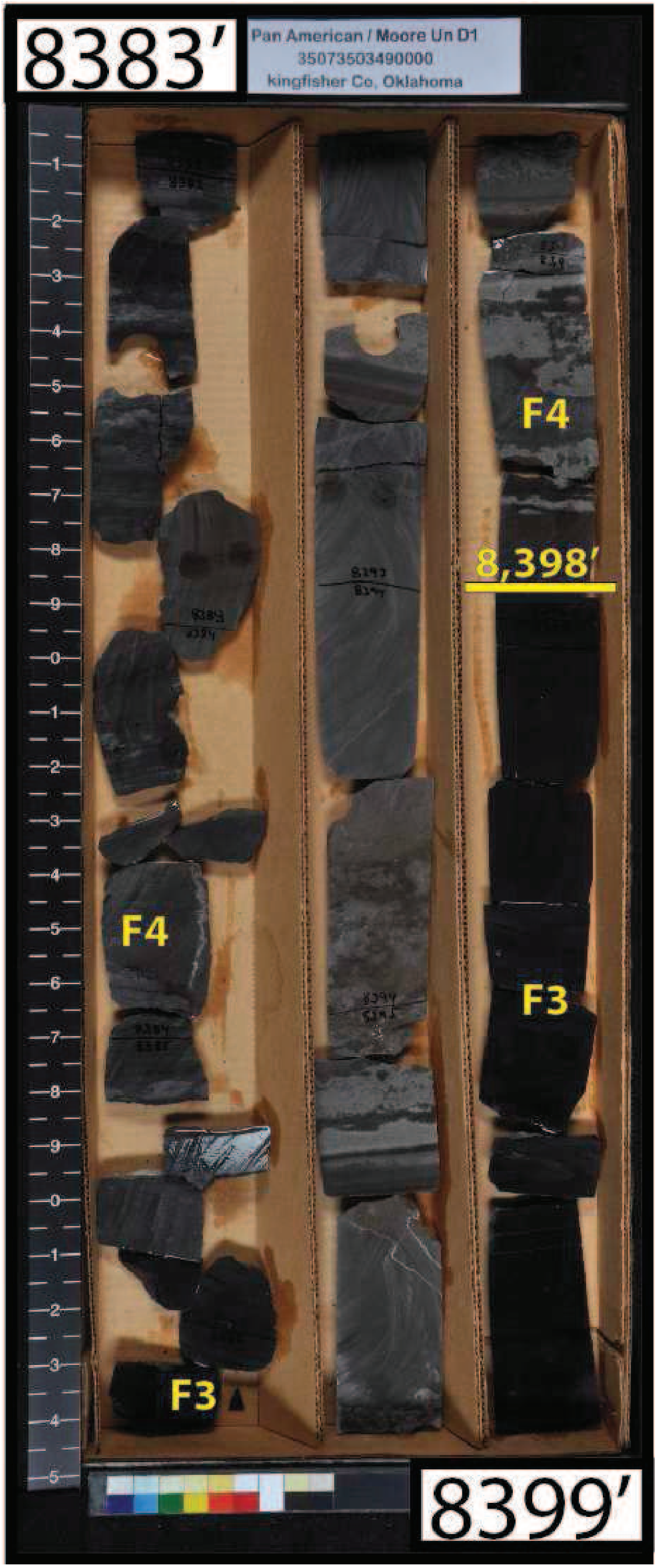
8383′
Pan American / Moore Un D1
35073503490000
kingfisher Co, Oklahoma
F4
8,398′
F4
F3
F3
8399′

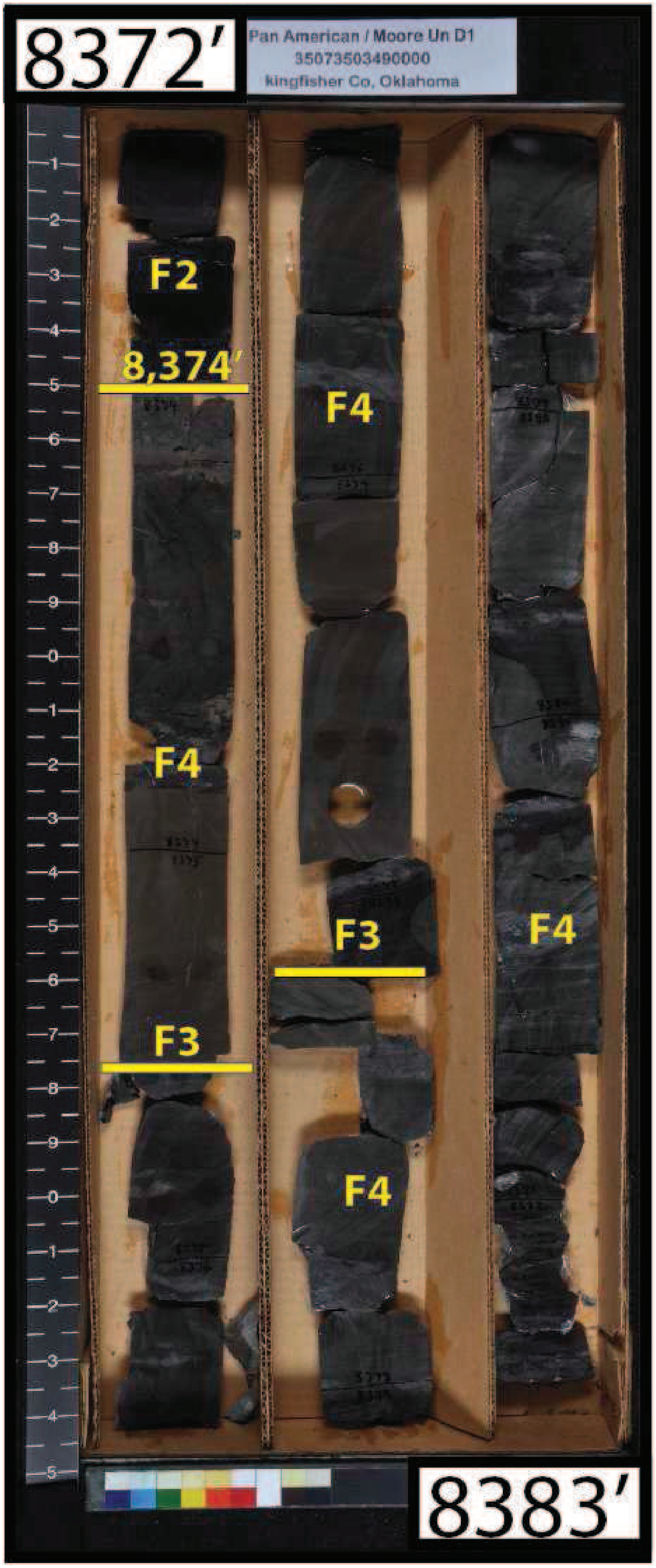
8372′
Pan American / Moore Un D1
35073503490000
kingfisher Co, Oklahoma
F2
8,374′
F4
F4
F3
F3
F4
F4
8383′

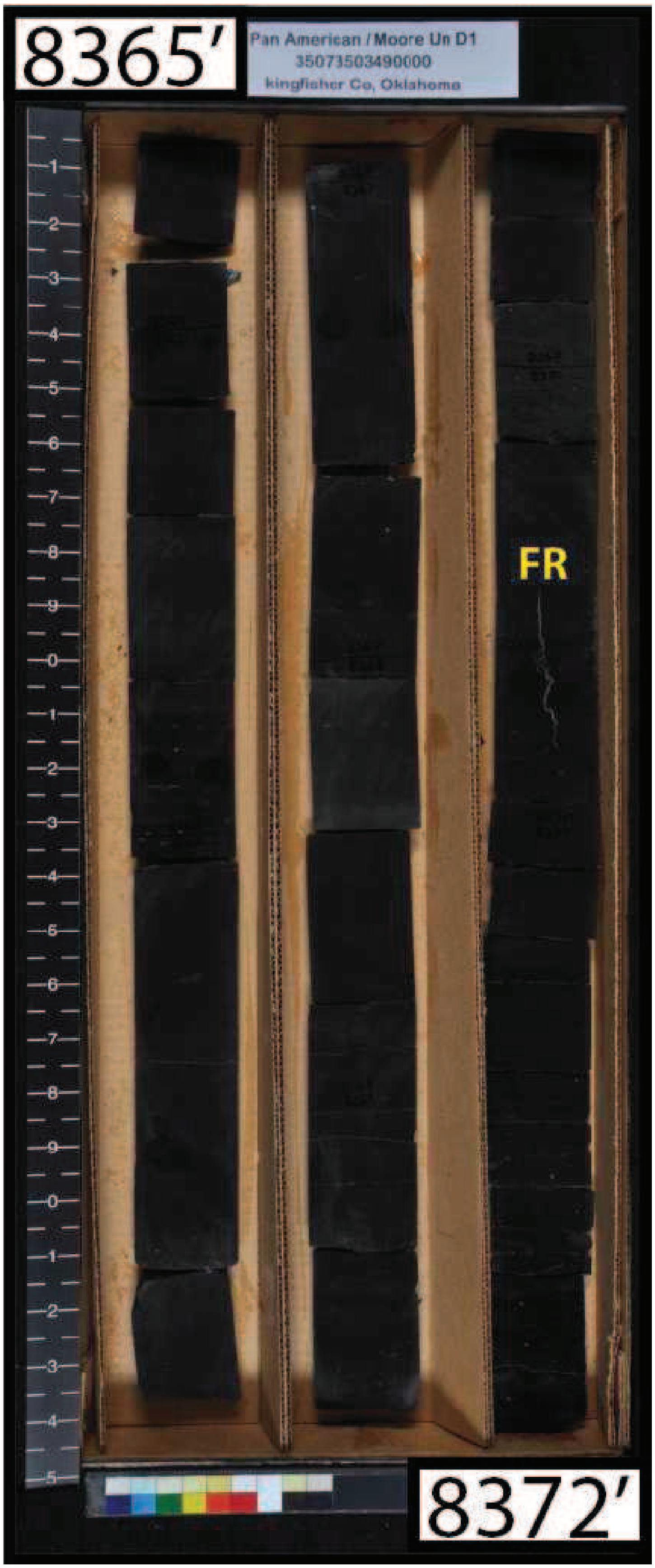
8365′
Pan American / Moore Un D1
35073503490000
kingfisher Co, Oklahoma
FR
8372′

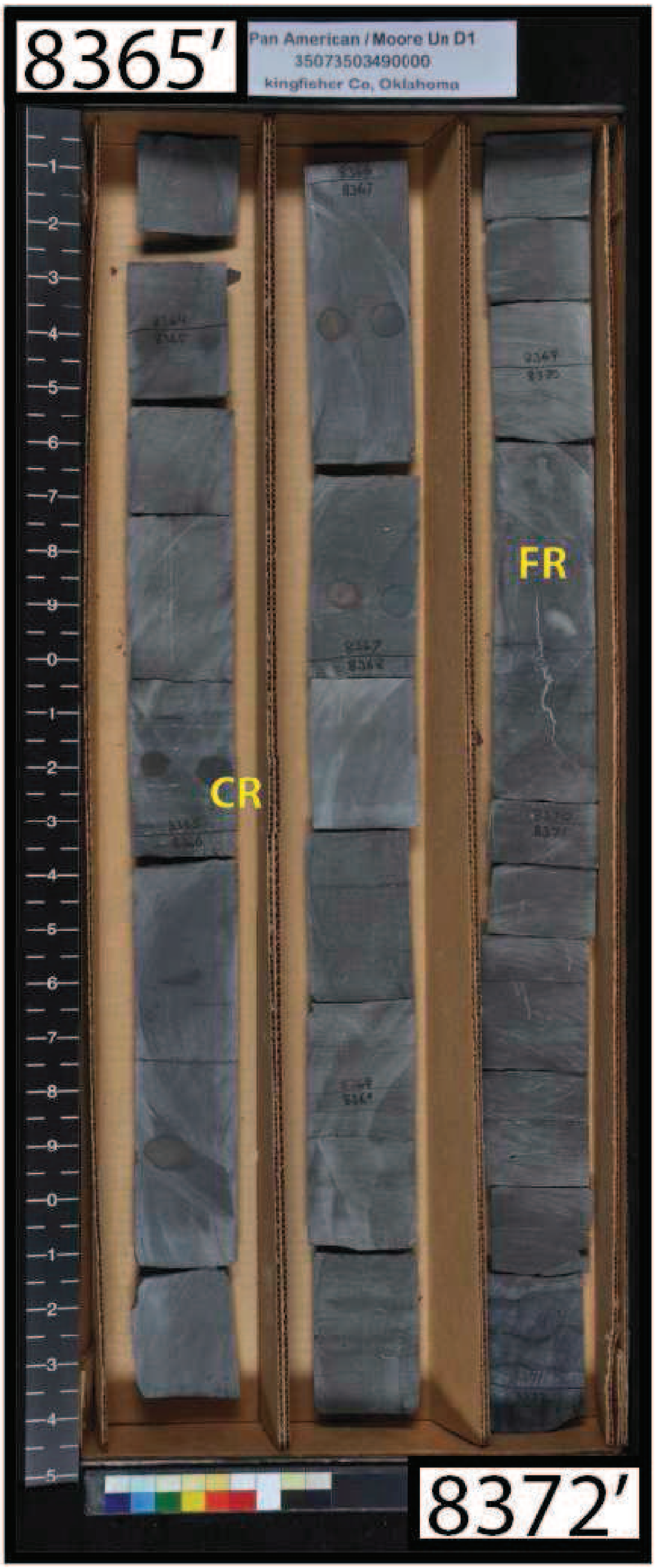
8365′
Pan American / Moore Un D1
35073503490000
kingfisher Co, Oklahoma
CR
FR
8372′


8357.3′
Pan American / Moore Un D1
35073503490000
kingfisher Co, Oklahoma
8365′


8350′
Pan American / Moore Us D1
35073503490000
kingfisher Co, Oklahoma
F4
F3
8357.3′

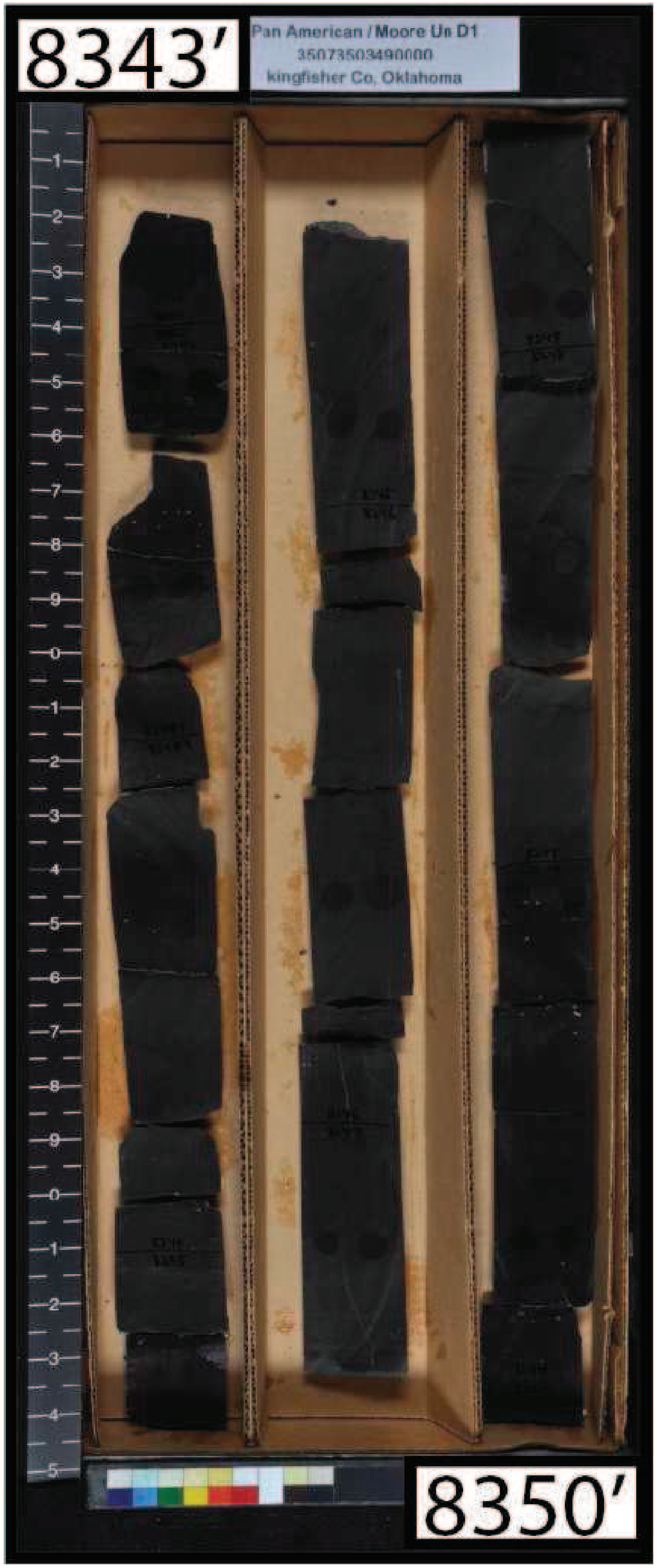
8343′
Pan American / Moore Un D1
35073503490000
kingfisher Co, Oklahoma
8350′

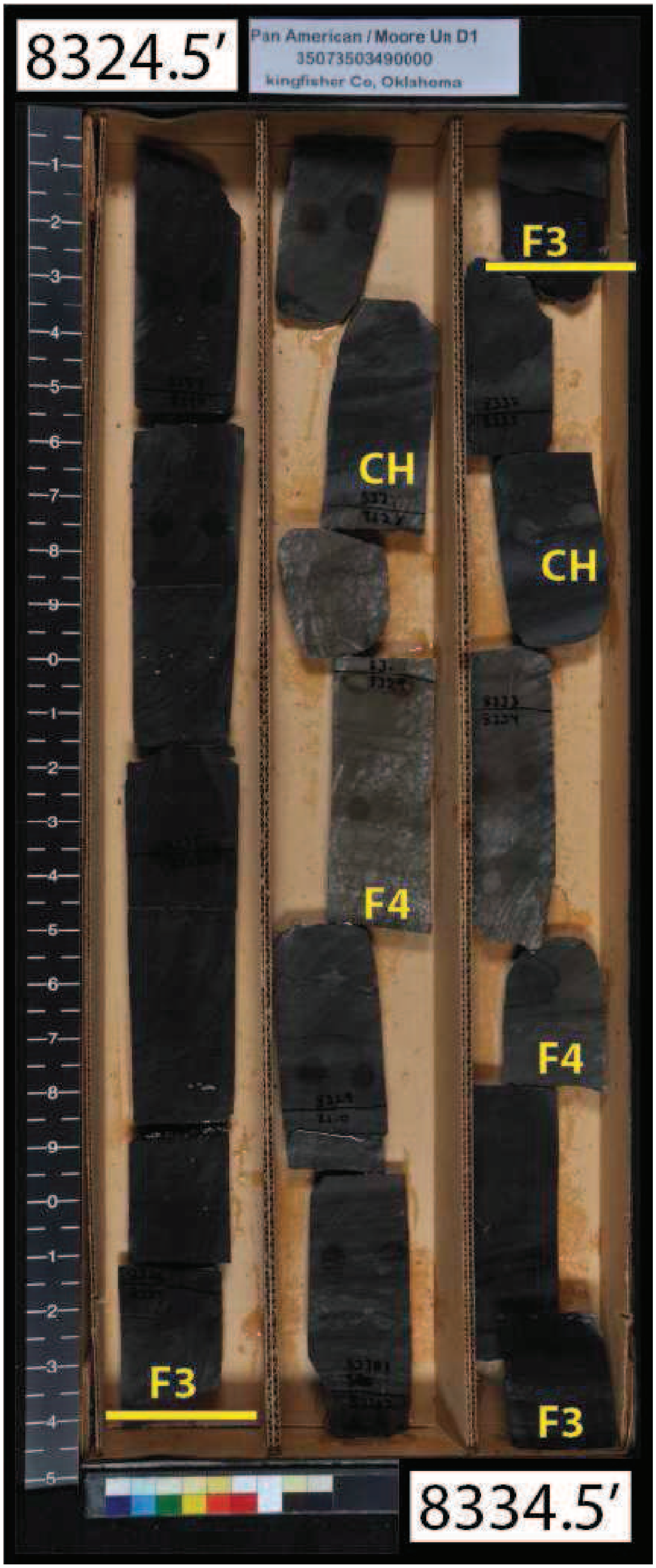
8324.5′
Pan American / Moore Un D1
35073503490000
kingfisher Co, Oklahoma
F3
CH
CH
F4
F4
F3
F3
8334.5′

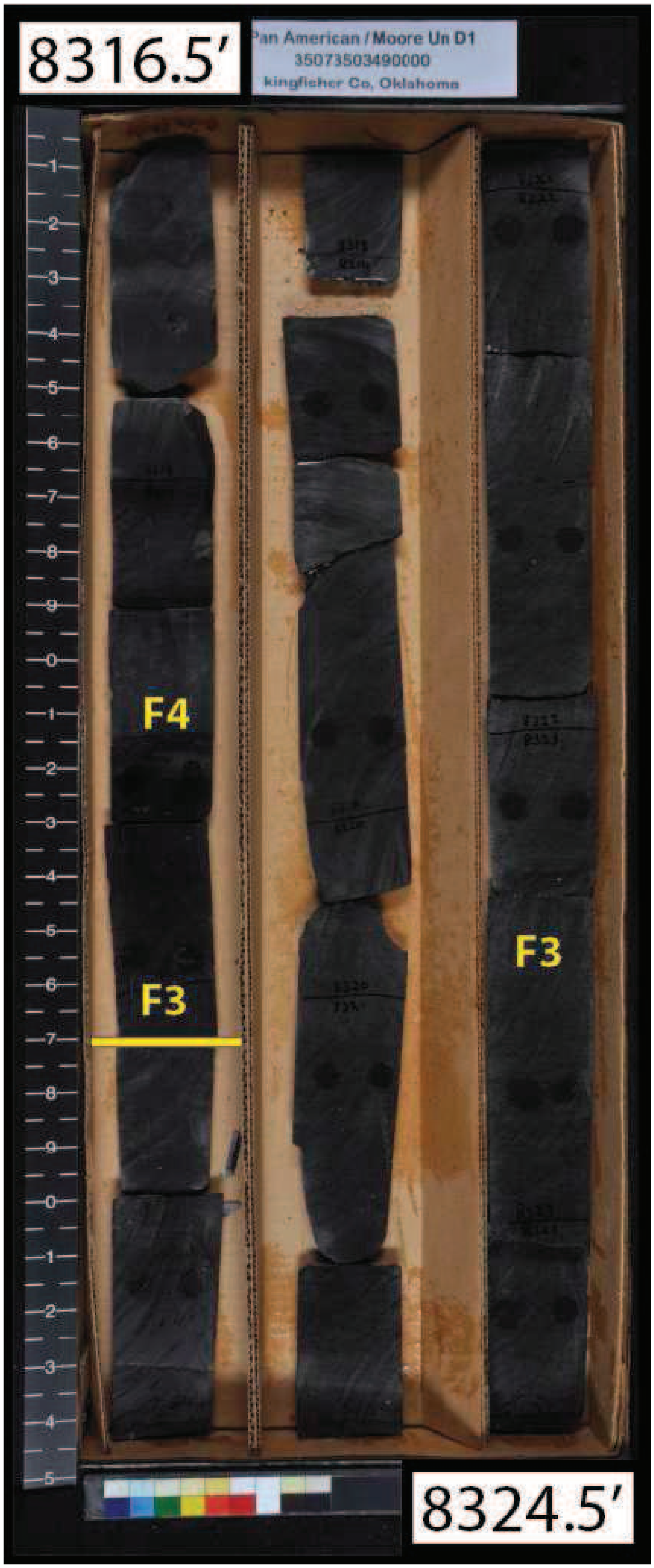
8316.5′
Pan American / Moore Un D1
35073503490000
kingfisher Co, Oklahoma
F4
F3
F3
8324.5′

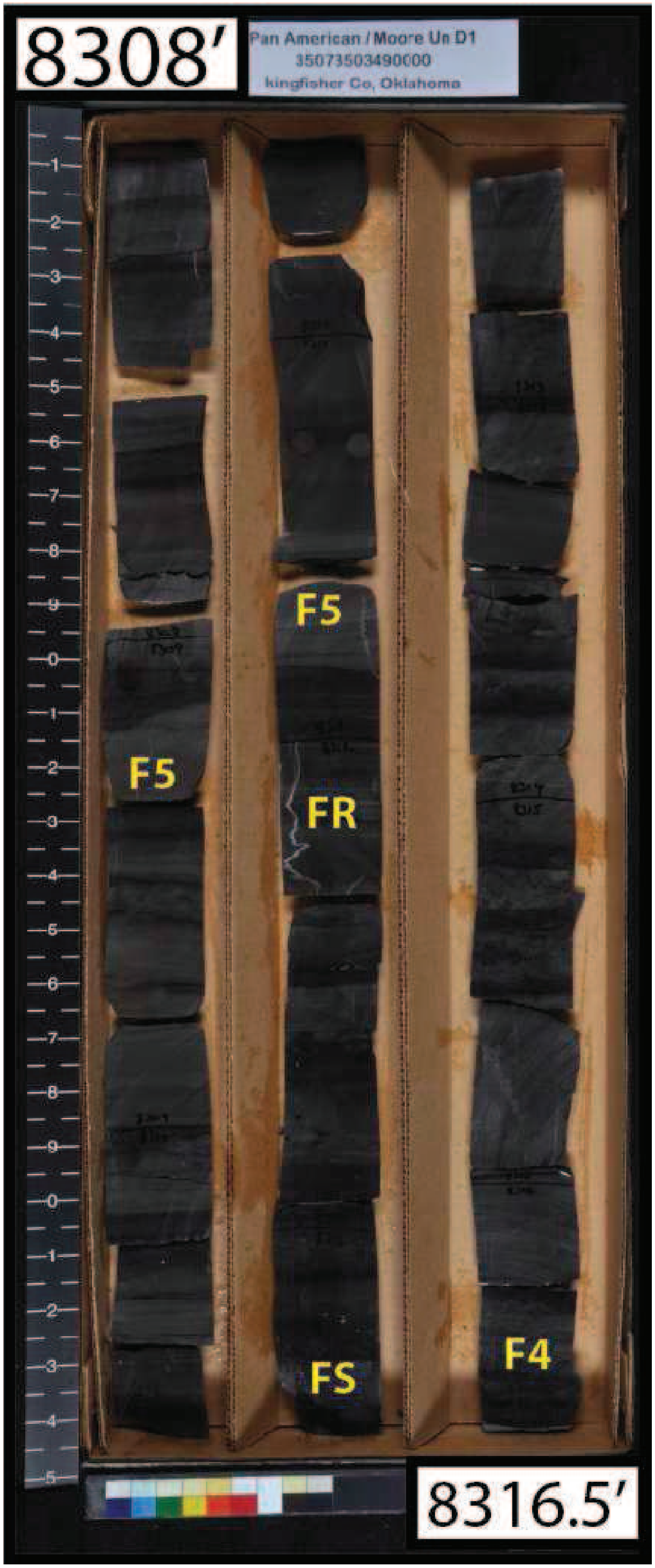
8308′
Pan American / Moore Un D1
35073503490000
kingfisher Co, Oklahoma
F5
F5
FR
FS
F4
8316.5′

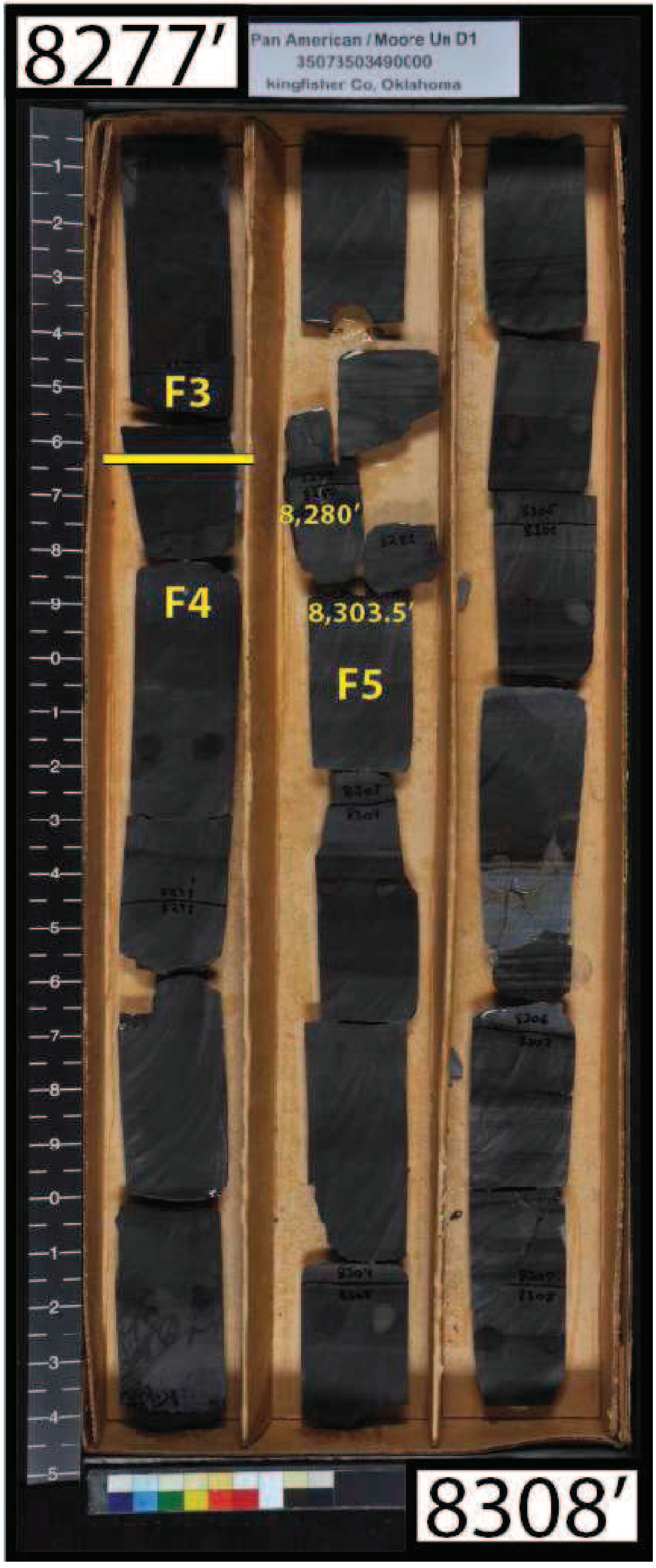
8277′
Pan American / Moore Un D1
35073503490000
kingfisher Co, Oklahoma
F3
8,280′
F4
8,303.5′
F5
8308′


8265.5′
Pan American / Moore Un D1
35073503490000
kingfisher Co, Oklahoma
BU
F4
F3
8277′

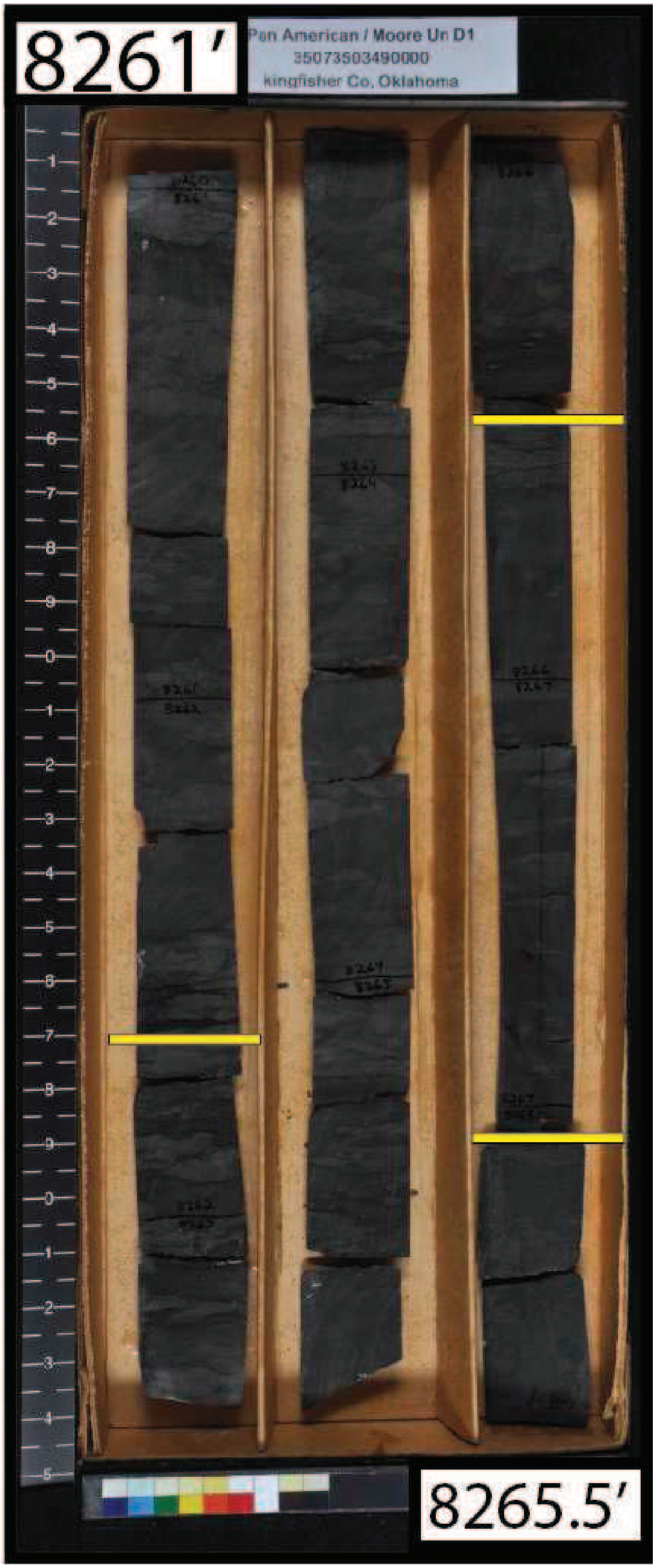
8261′
Pan American / Moore Un D1
35073503490000
kingfisher Co, Oklahoma
8265.5′


8252.5'
Pan American / Moore Un D1
35073503490000
kingfisher Co. Oklahoma
8261'


8246′
Pan American / Moore Un D1
35073503490000
kingfisher Co, Oklahoma
8253.5′

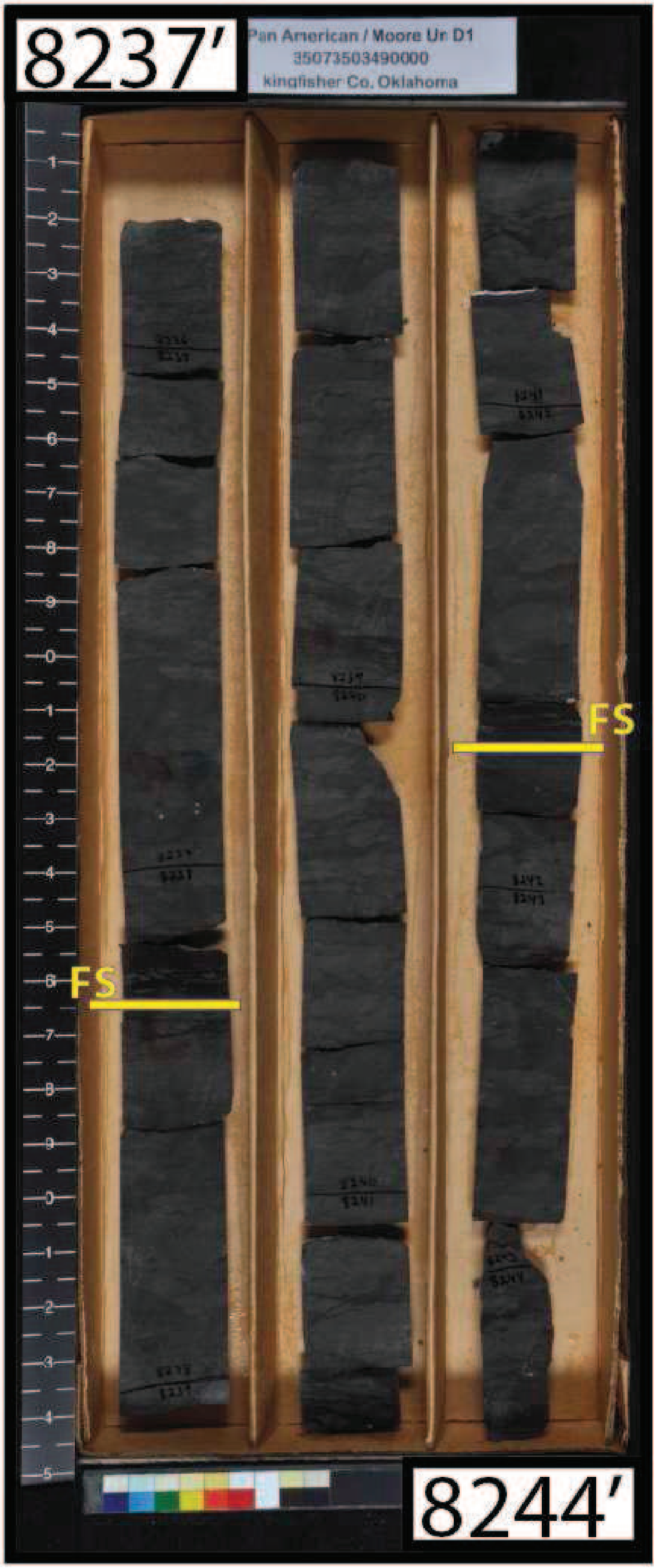
8237′
Pan American / Moore Ur D1
35073503490000
kingfisher Co. Oklahoma
FS
FS
8244′

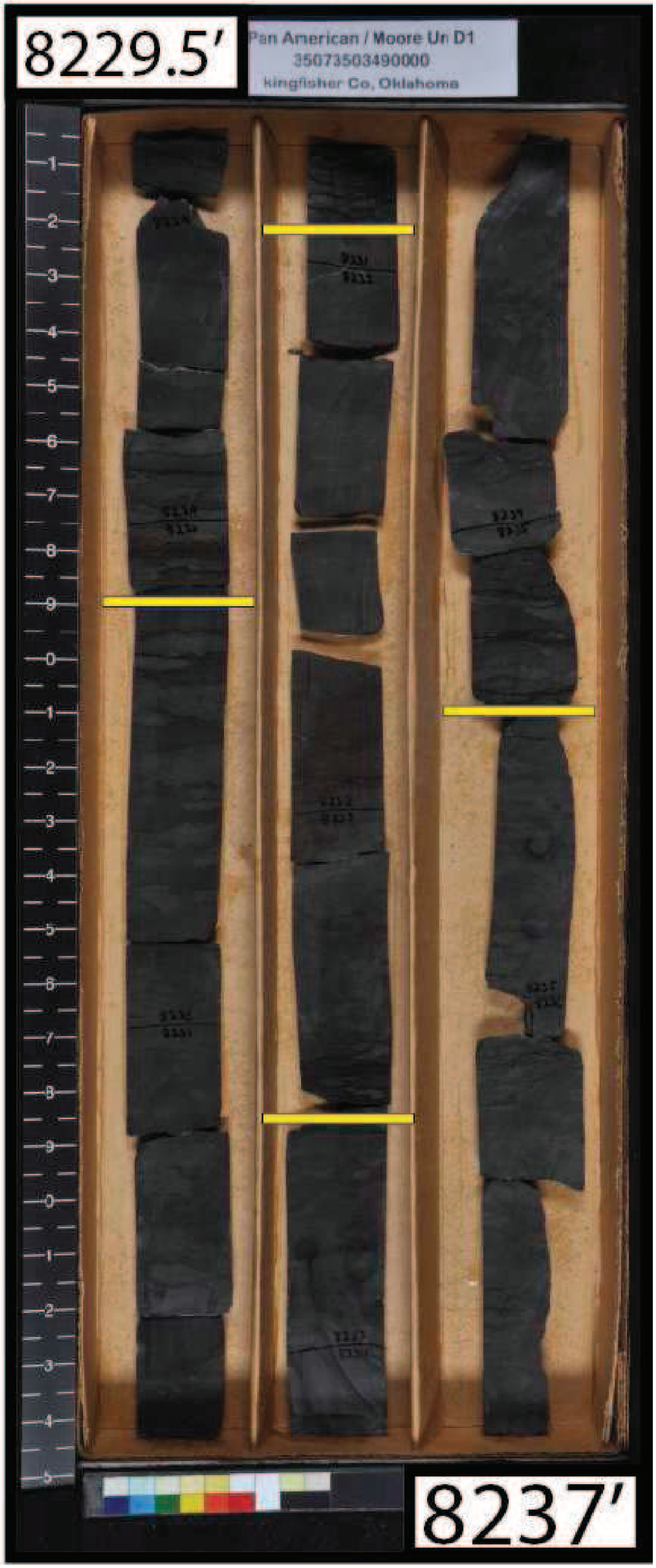
8229.5′
Pan American / Moore Un D1
35073503490000
kingfisher Co, Oklahoma
8237′

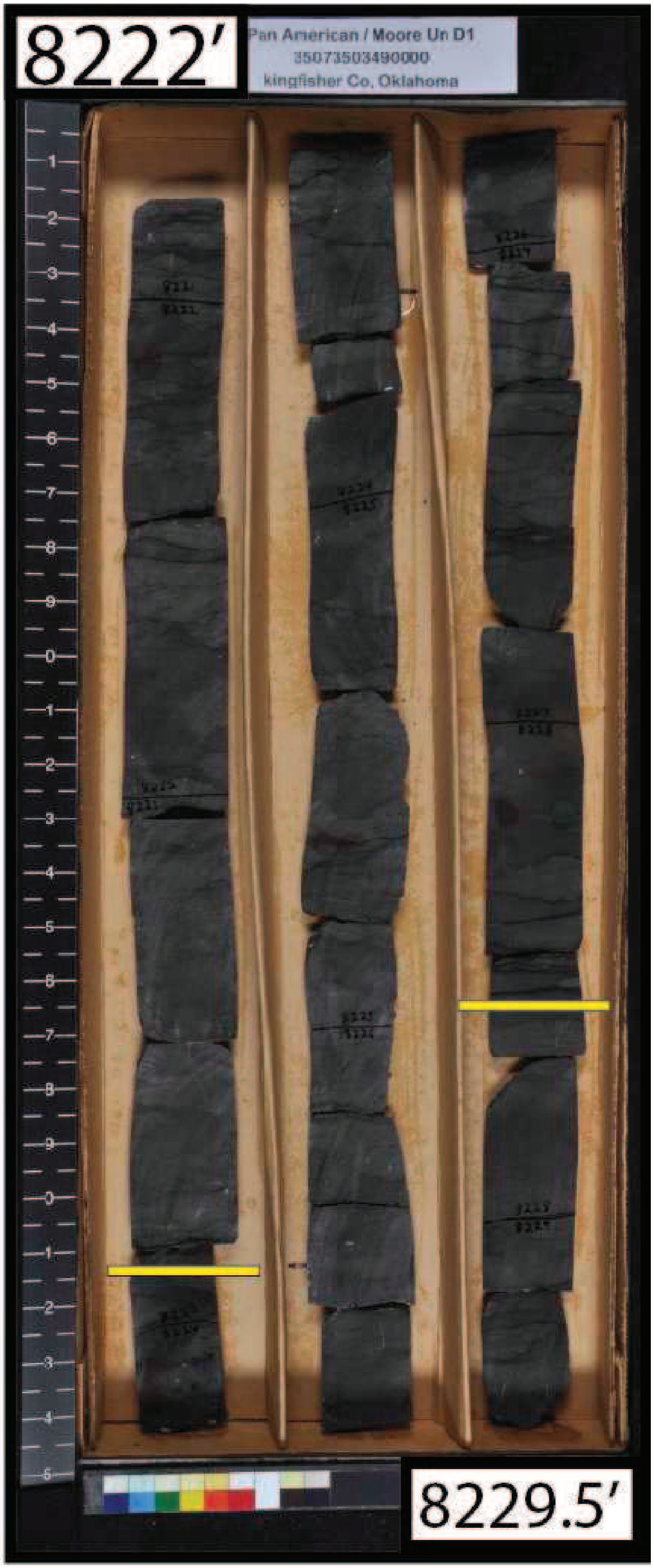
8222'
Pan American / Moore Un D1
35073503490000
kingfisher Co, Oklahoma
8229.5'


8214′
Pan American / Moore Un D1
35073503490000
kingfisher Co, Oklahoma
8222′

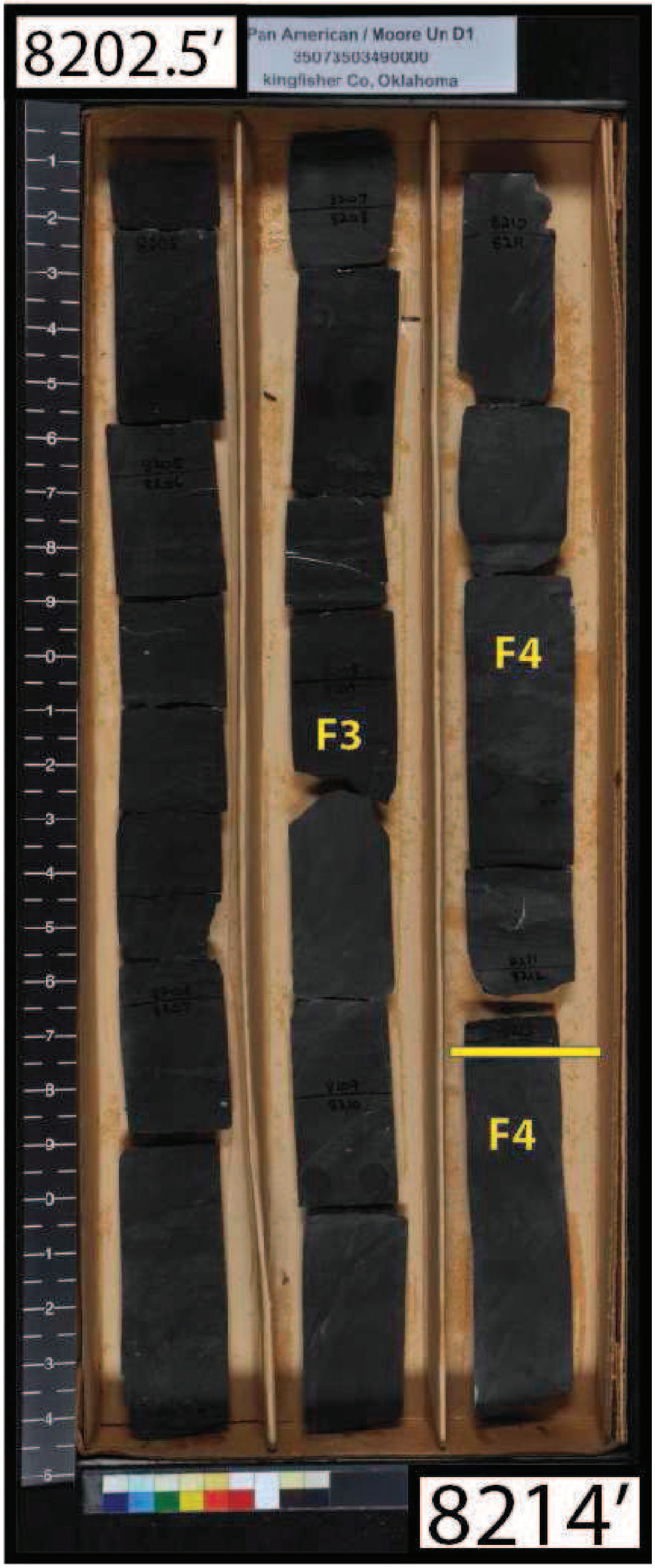
8202.5′
Pan American / Moore Un D1
35073503490000
kingfisher Co, Oklahoma
F3
F4
F4
8214′

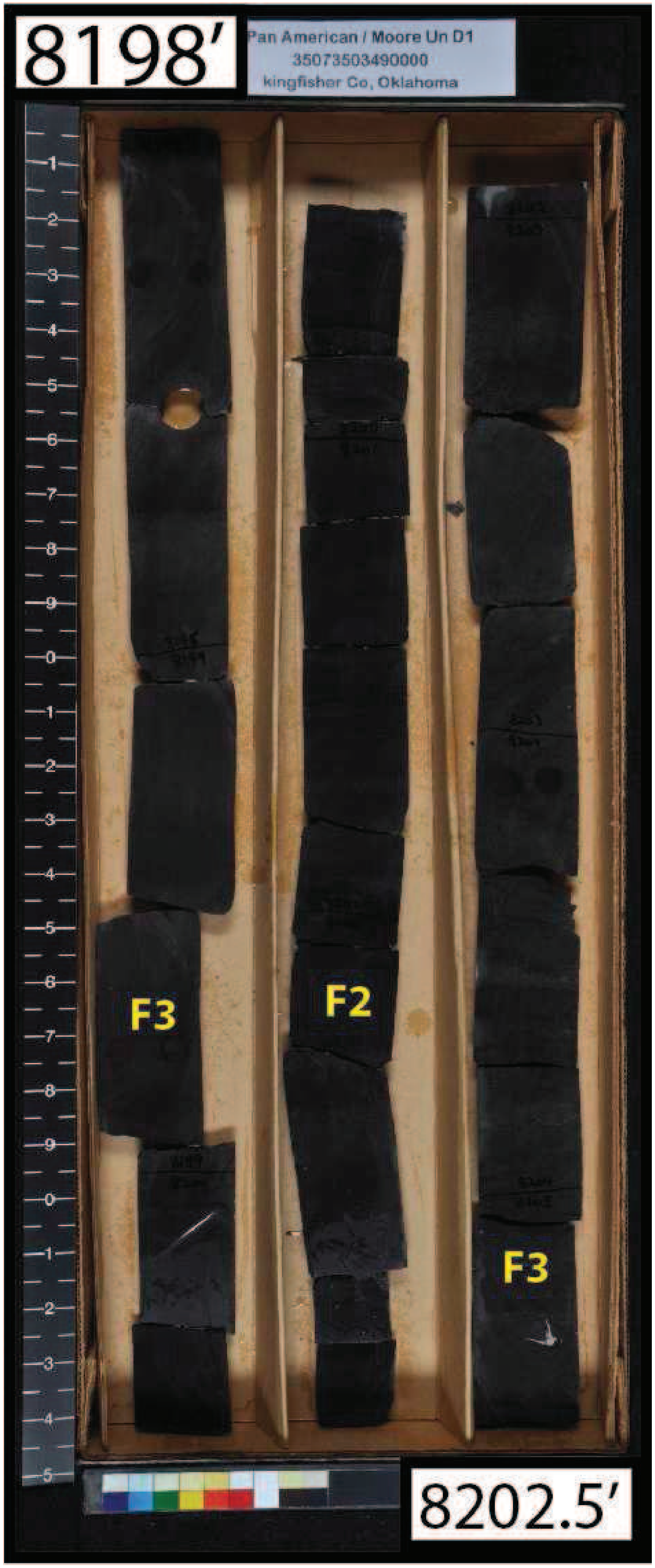
8198′
Pan American / Moore Un D1
35073503490000
kingfisher Co, Oklahoma
F3
F2
F3
8202.5′


8189′
Pan American / Moore Un D1
35073503490000
kingfisher Co. Oklahoma
8196.5′


8181′
Pan American / Moore Ur D1
35073503490000
kingfisher Co, Oklahoma
F4
F3
F4
8189′


8173′
Pan American / Moore Un D1
35073503490000
Kingfisher Co, Oklahoma
8181′


8166′
Pan American / Moore Un D1
35073503490000
kingfisher Co. Oklahoma
8173′


8157′
Pan American / Moore Un D1
35073503490000
kingfisher Co, Oklahoma
8165′


8145′
Pan American / Moore Ur. D1
35073503490000
Kingfisher Co. Oklahoma
F3
4′ gap
F3/4
8157′

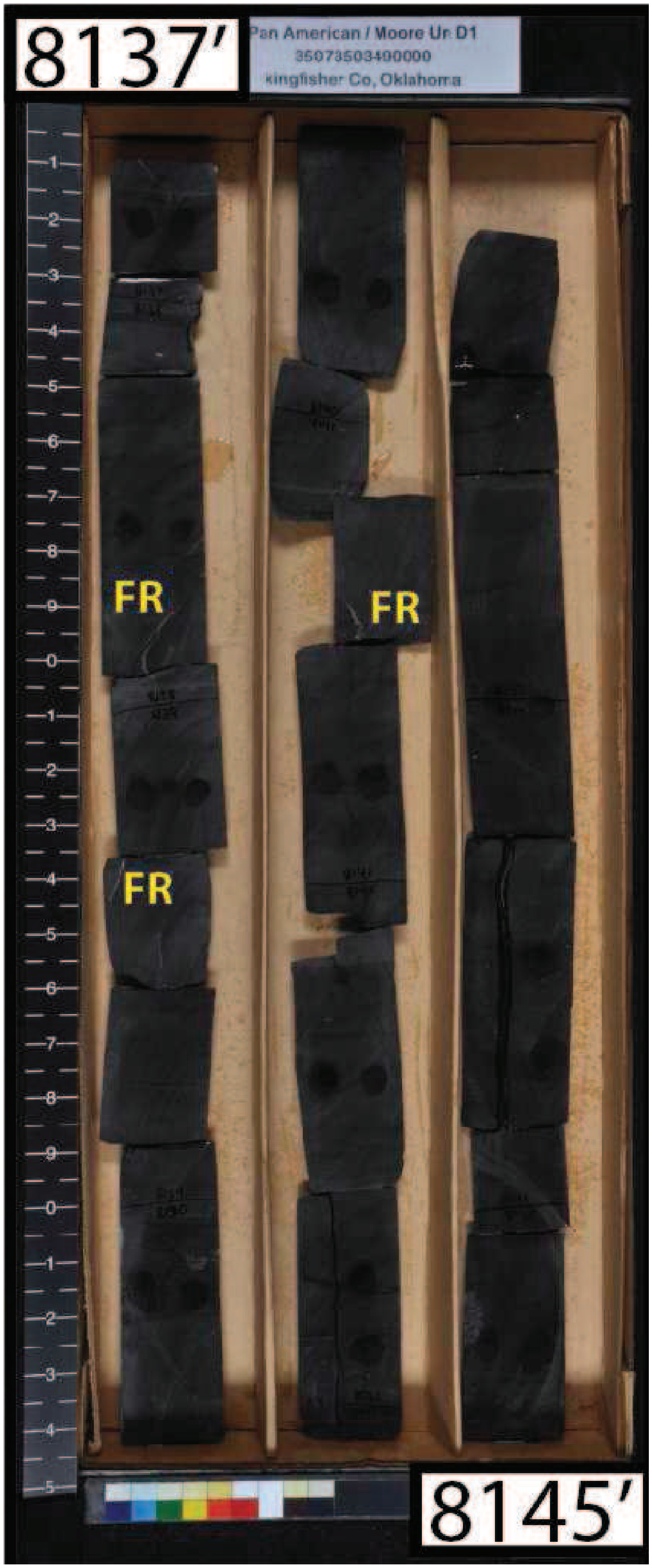
8137′
Pan American / Moore Ur D1
35073503400000
kingfisher Co, Oklahoma
FR
FR
FR
8145′


8130′
Pan American / Moore Un D1
35073503490000
kingfisher Co, Oklahoma
8137′


8123′
Pan American / Moore Ur D1
35073503490000
Kingfisher Co, Oklahoma
8130′


8111′
Pan American / Moore Ur D1
35073503490000
kinglisher Co. Oklahoma
F4
F3
8123′


8104′
Pan American / Moore Ur D1
35073503490000
kingfisher Co. Oklahoma
FS
8111′

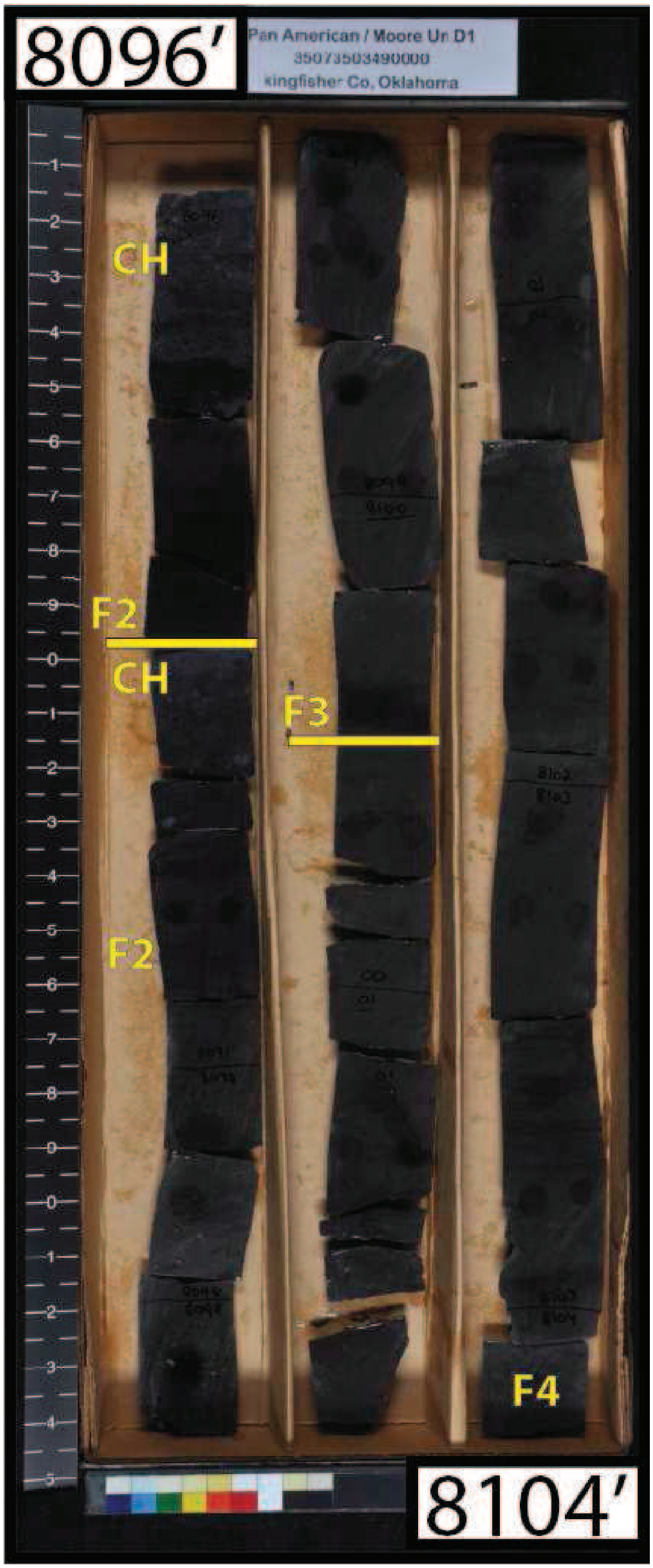
8096′
Pan American / Moore Ur D1
35073503490000
kingfisher Co, Oklahoma
CH
F2
CH
F2
F3
F4
8104′

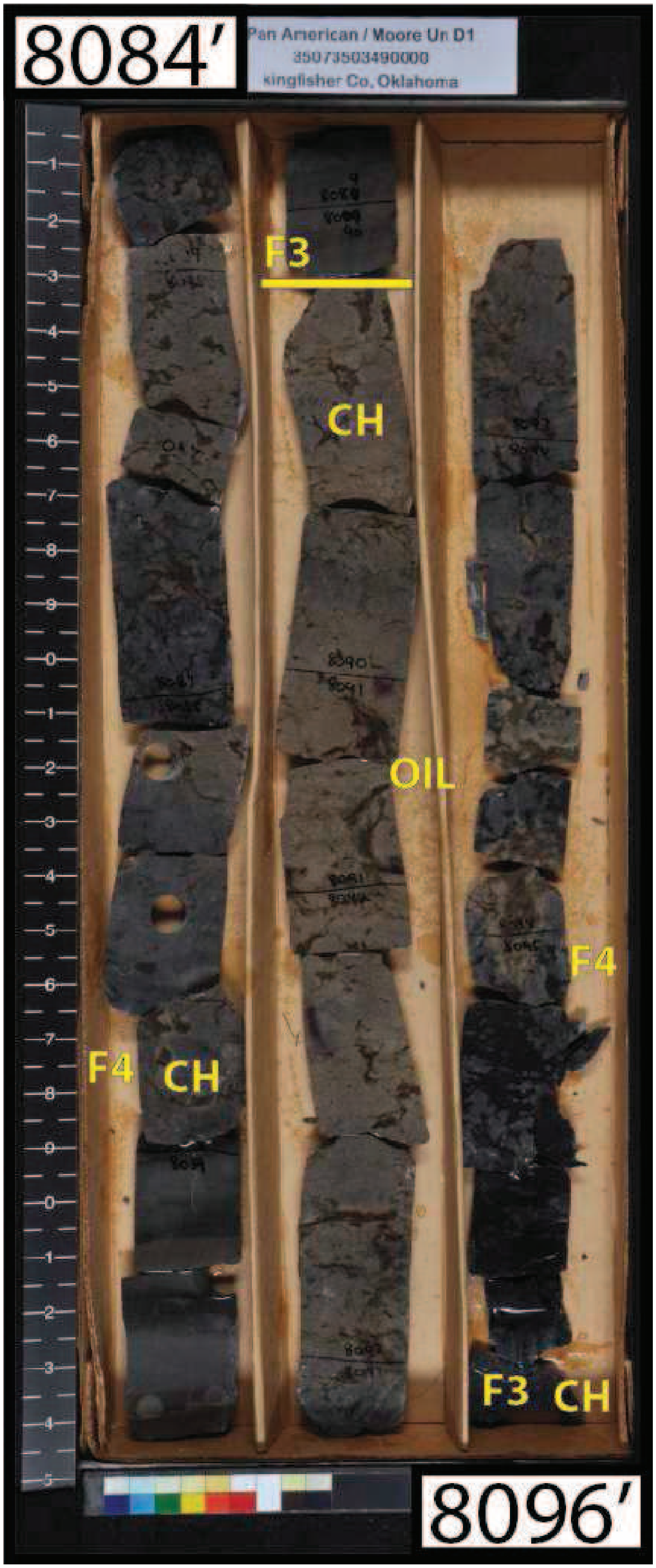
8084′
Pan American / Moore Un D1
35073503490000
kinglisher Co, Oklahoma
F3
CH
OIL
F4
F4
CH
F3
CH
8096′


8073′
Pan American / Moore Un D1
35073503490000
kingfisher Co, Oklahoma
8084′

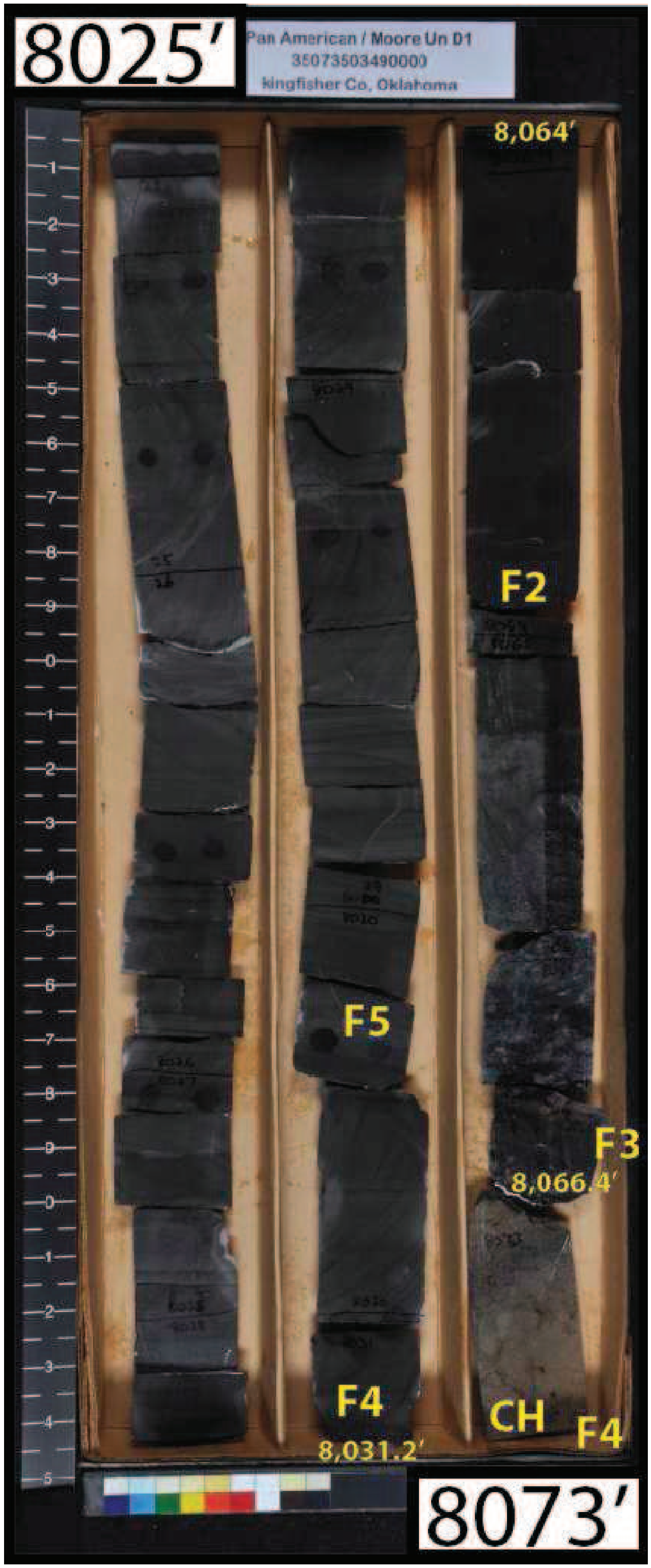

8025′
Pan American / Moore Un D1
35073503490000
kingfisher Co, Oklahoma
8,064′
F2
F5
F3
8,066.4′
F4
8,031.2′
CH
F4
8073′


8017′
Pan American / Moore Un D1
35073503490000
kingfisher Co, Oklahoma
8025′


8009′
Pan American / Moore Un D1
35073503490000
kingfisher Co, Oklahoma
8017′

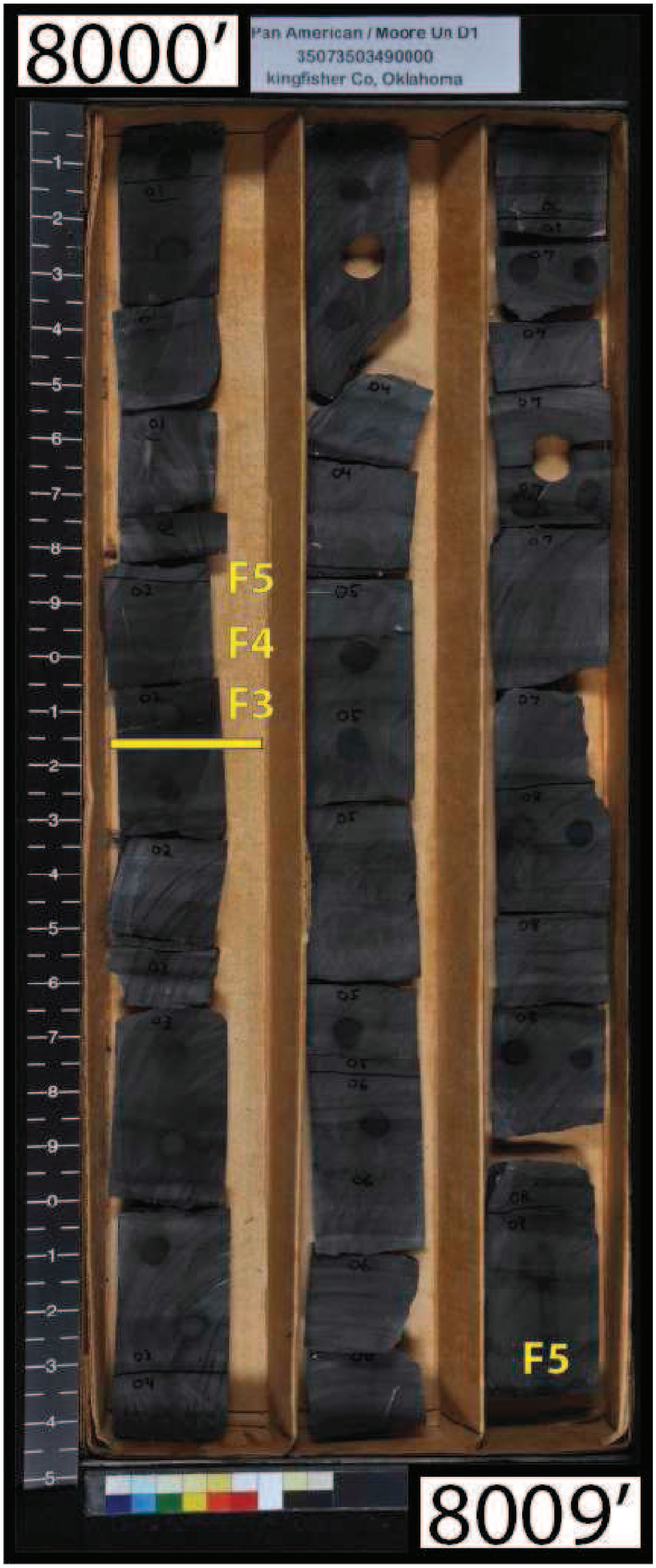
8000′
Pan American / Moore Un D1
35073503490000
kingfisher Co, Oklahoma
F5
F4
F3
F5
8009′


7992′
Pan American / Moore Un D1
35073503490000
kingfisher Co, Oklahoma
8000′


7984′
Pan American / Moore Un D1
35073503490000
kingfisher Co, Oklahoma
F6
F5
7992′

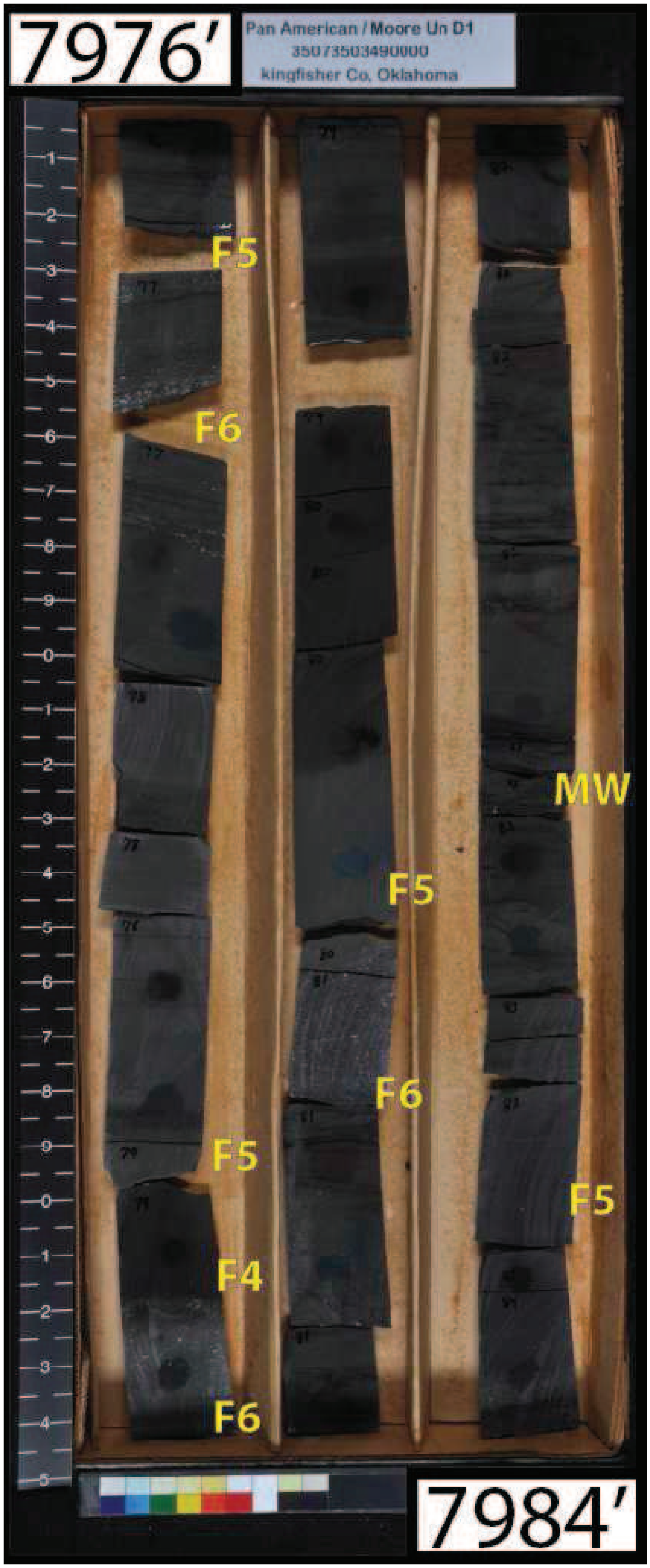
7976'
Pan American / Moore Un D1
35073503490000
kingfisher Co, Oklahoma
F5
F6
F5
F4
F6
F5
F6
MW
F5
7984'

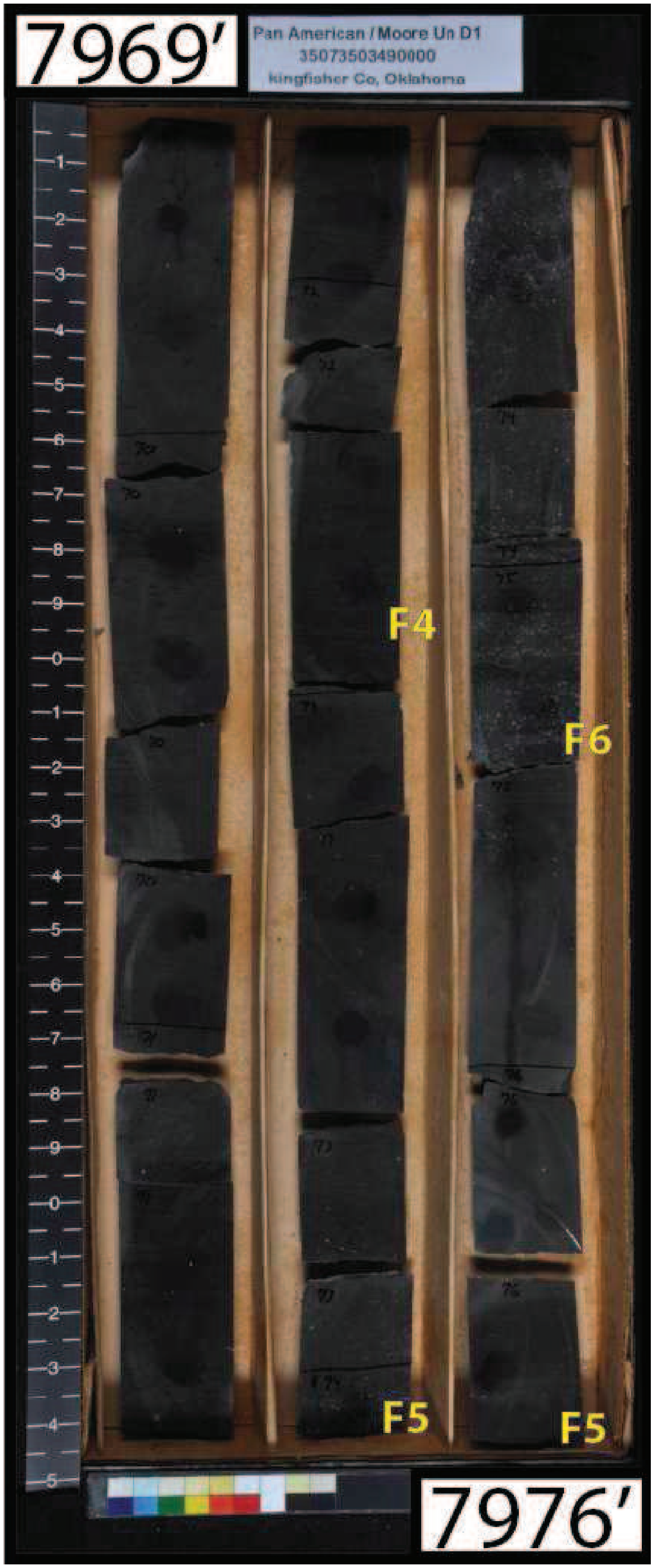
7969′
Pan American / Moore Un D1
35073503490000
kingfisher Co, Oklahoma
F4
F6
F5
F5
7976′

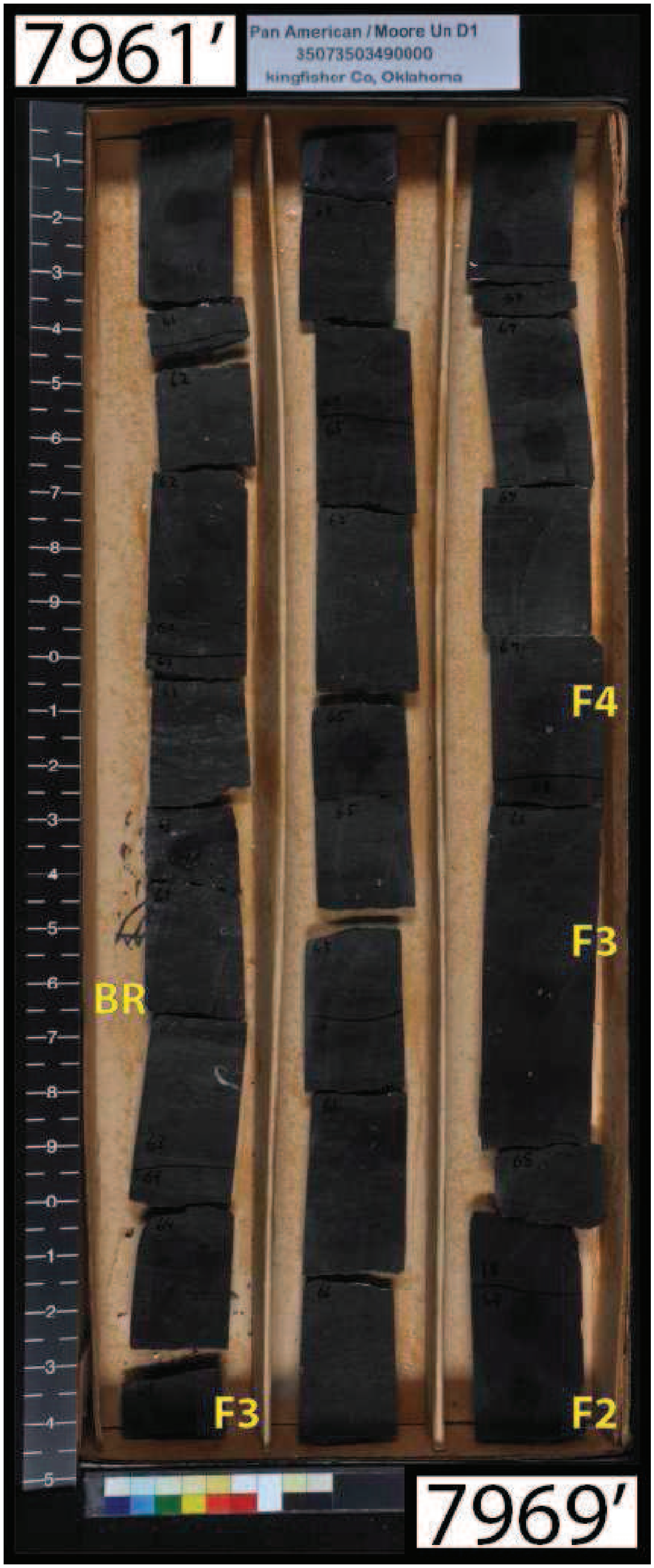
7961′
Pan American / Moore Un D1
35073503490000
kingfisher Co, Oklahoma
F4
F3
BR
F3
F2
7969′


7951'
Pan American / Moore Un D1
35073503490000
kingfisher Co, Oklahoma
7961'

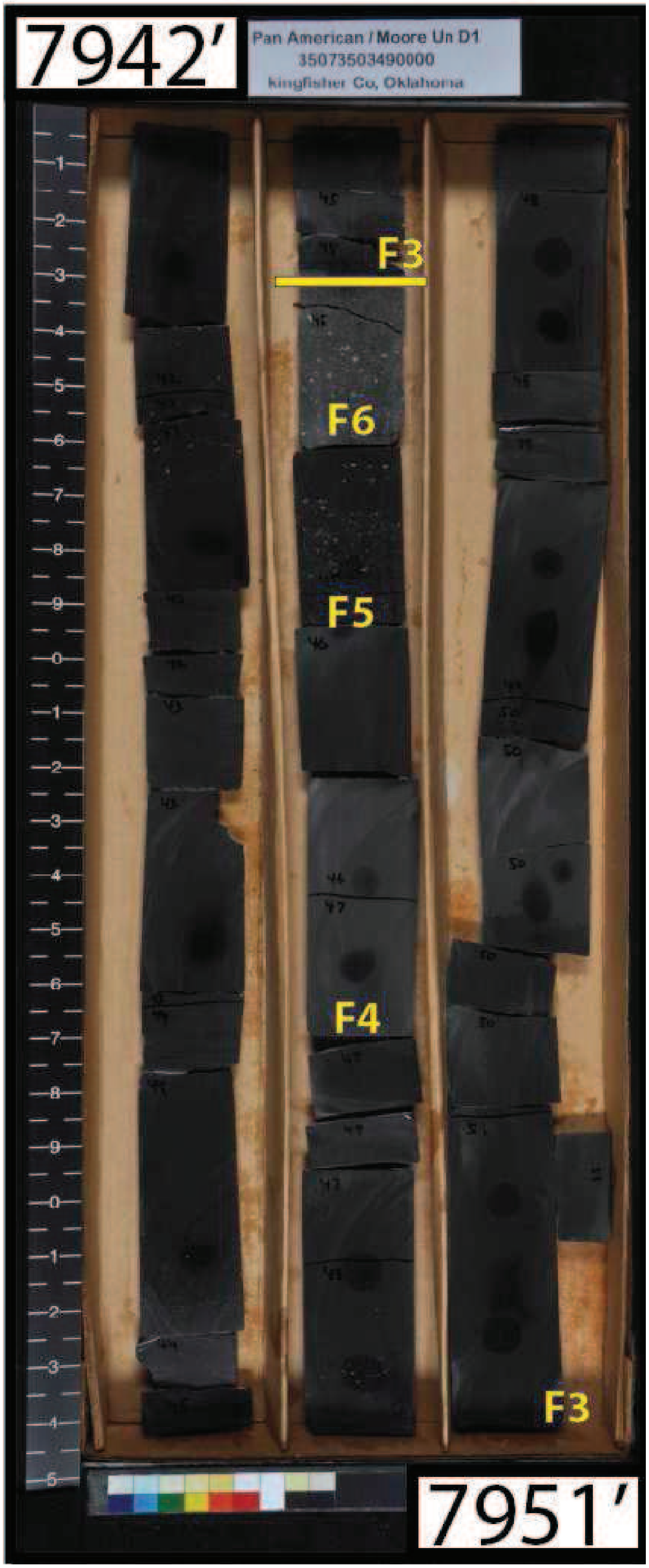
7942′
Pan American / Moore Un D1
35073503490000
kingfisher Co, Oklahoma
F3
F6
F5
F4
F3
7951′


7934′
Pan American / Moore Un D1
35073503490000
kingfisher Co, Oklahoma
F3
F4
F5
F3
7942′

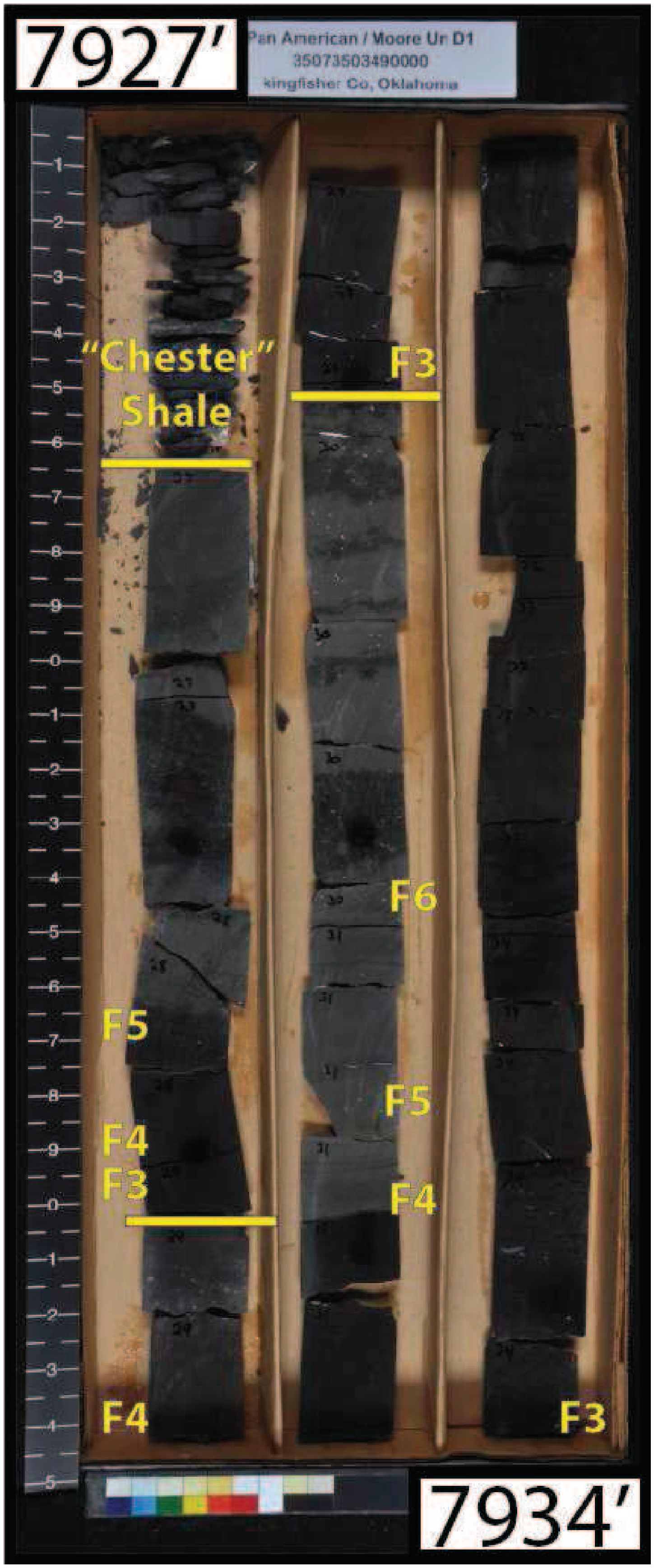
7927'
Pan American / Moore Ur D1
35073503490000
kingfisher Co, Oklahoma
"Chester"
Shale
F3
F6
F5
F5
F4
F3
F4
F4
F3
7934'

II. Moore Unit D #1 Thin Section Photomicrographs

Moore Unit D1 thin sections were prepared by Core Laboratories, Inc. through the financial assistance of Marathon Oil Corporation. All thin sections are alizarin red-S stained on the top (up) half and blue epoxy impregnated to show porosity. Please refer Table 6 for abbreviations.

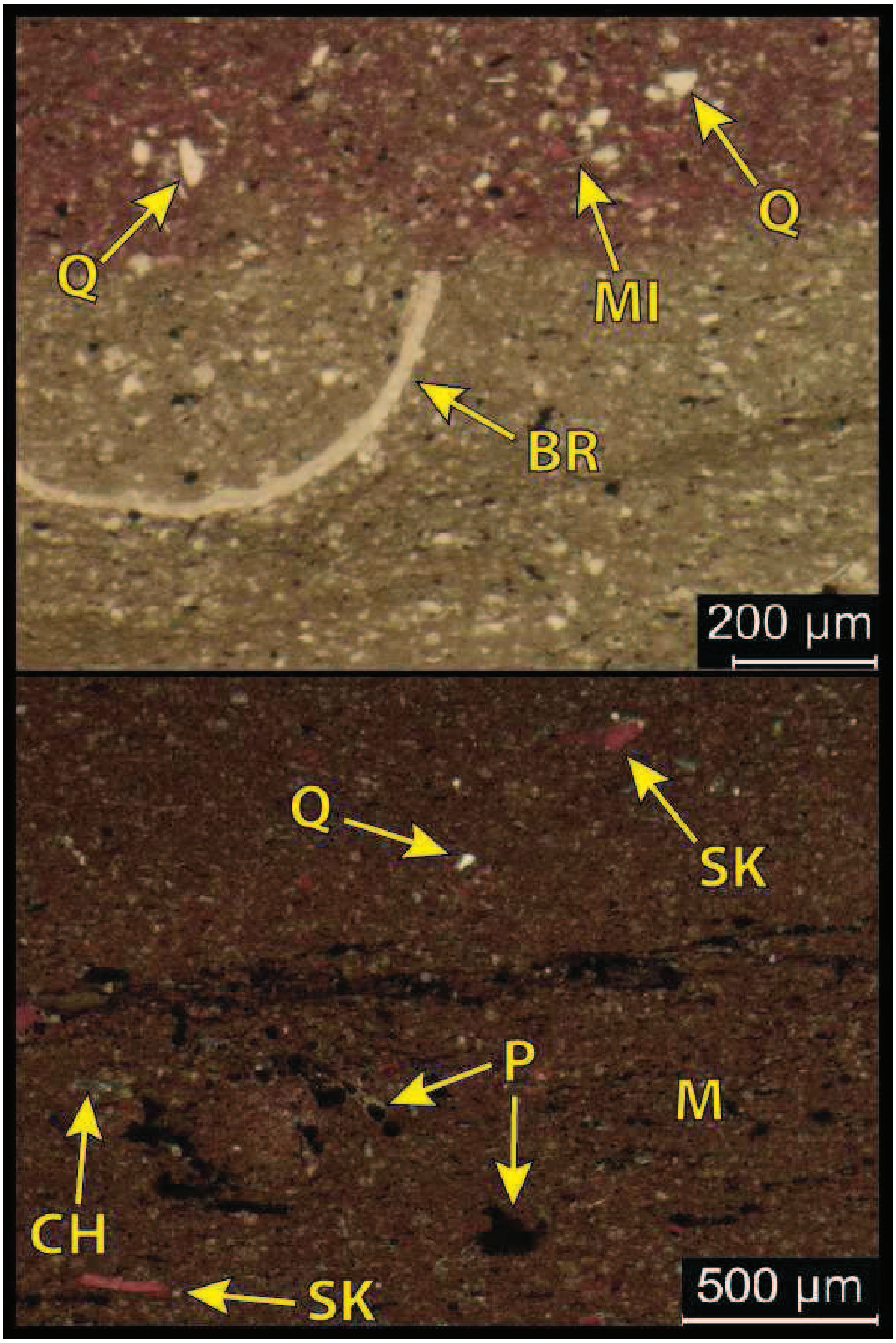

8,413.7': Mud-rich wackestone. Facies 2. Top: PPL; top1/2 alizarin red stained. Bottom: XPL; alizarin red stained. Porosity= 0.59%. B.I.: 1. Mineralogy: 48.6% carbonate (44.1% calcite; 4.5% dolomite), 5% chert and 46.4% other minerals (25% quartz silt; 2.3% pyrite; 3.3% feldspars; 15.4% Total Clays). Grains: ostracodes (~200 µm); thin-shelled brachiopod (25 x 600 µm); peloidal grains (<25 µm); sponge spicules (~100 µm; calcite); undifferentiated calcareous debris (up to 400 µm, most silt-sized or smaller). Pyrite (2.3%) concentrated along bedding and in 100-1000 µm clusters. Seldom (<1%) calcite-filled fractures.

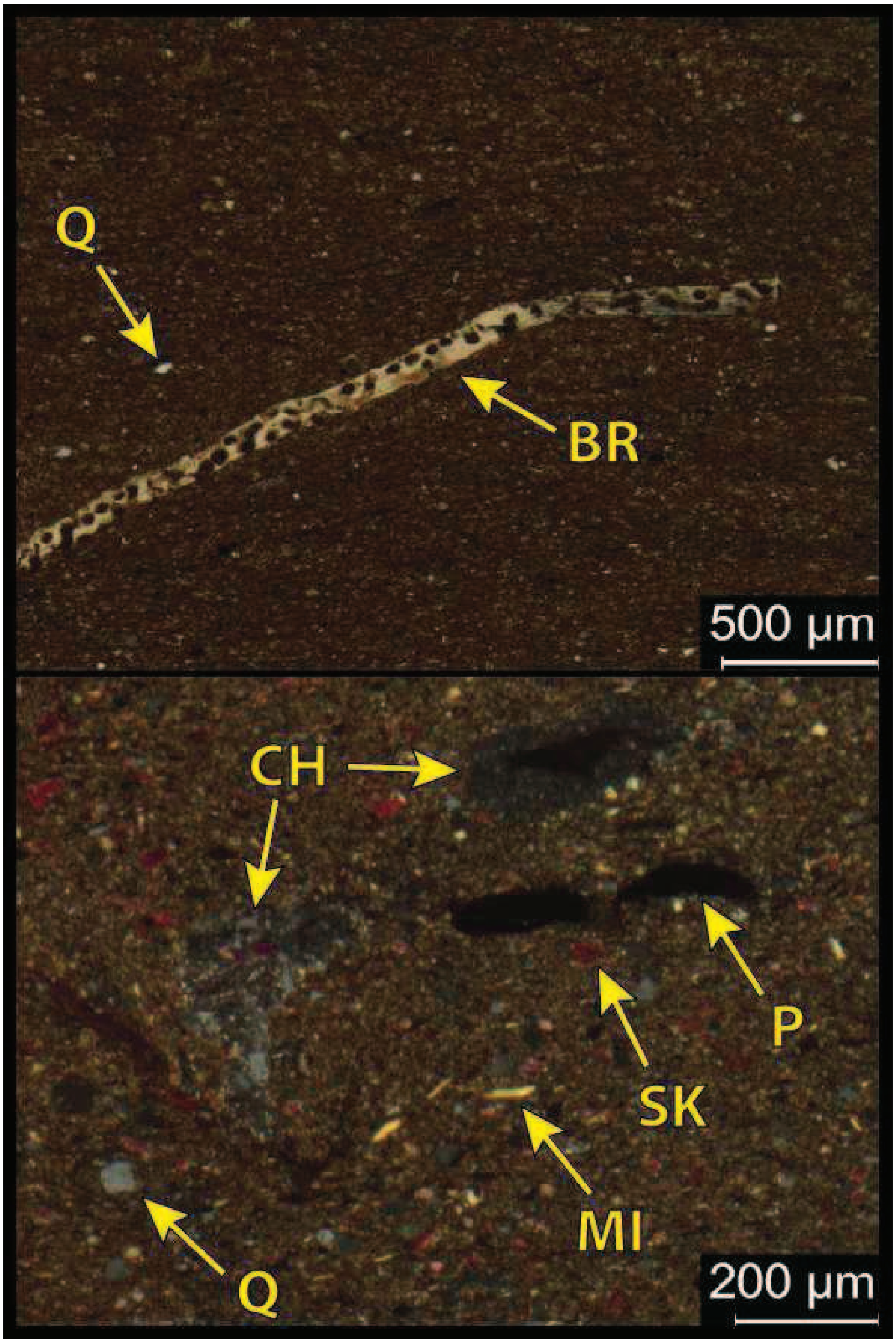

8,398.6': Silty siliceous mud-rich wackestone. Facies 2. Top: XPL. Bottom: PPL; alizarin red stained. Porosity= 1.3%. B.I.: 1. Mineralogy: 44.5% quartz (24.5% quartz silt; 20% chert), 26.2% carbonate (23.5% calcite; 2.7% dolomite), 22.1% total clay and 7.2% other minerals (2.9% pyrite; 4.3% feldspars). Grains: quartz silt, brachiopods (up to 150 µm x 2 mm; microbored) and undifferentiated skeletal grains (20-100 µm). Silicification after bioclasts and intergranular.

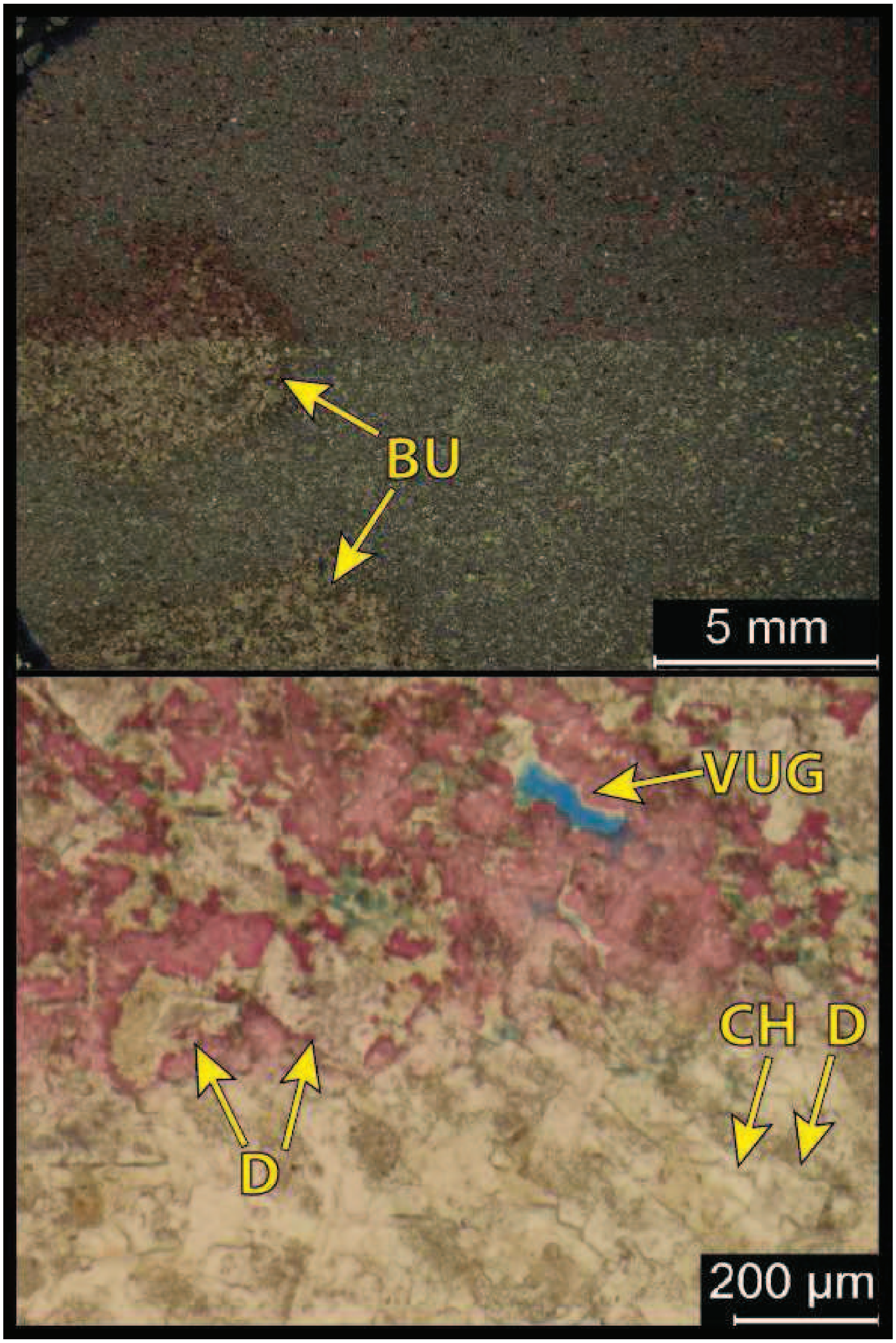

8,394.7': Siliceous dolomitic crystalline wackestone-packstone. Facies 4. Top: XPL/ ½ alizarin red stained. Bottom: PPL; ½ alizarin red stained. Porosity= 1.02%; intercrystalline and vugular (up to 200 µm). B.I.: 2 (hz, cm-scale). Mineralogy: 69.5% quartz (chert) and 30.6% carbonate (25.1% calcite; 5.5% dolomite). Grains: rare (1%) peloids. Diagenesis: calcite cementation concentrated in burrows. Highly siliceous (69.5%, chert with seldom chalcedony) and slightly dolomitic (5.5%, approx. 50-300 µm) throughout.

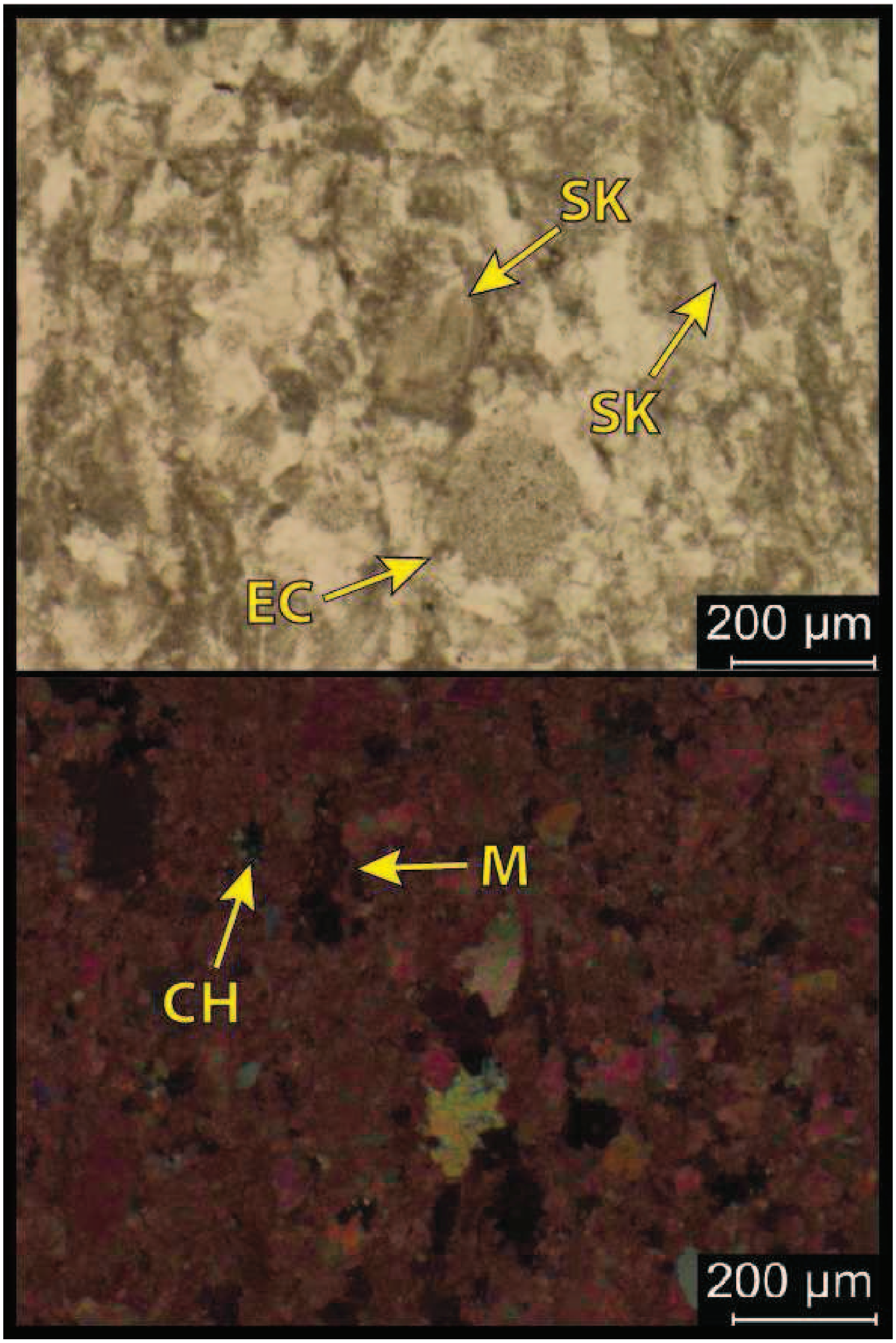

8,393.7': Crystalline packstone. Facies 4. Top: PPL. Bottom: XPL/ alizarin red stained. Porosity= 0.98%. B.I.: 0. Mineralogy: 96.6% carbonate (95.7% calcite; 0.9% dolomite) and 3.4% other minerals (1.8% quartz (50-50:chert-silt) and 1.6% total clay. Grains: Echinoids (5%; 50-250 µm) and undifferentiated skeletal fragments. Diagenesis: Abundant calcite cementation (~200 µm) and calcite-filled fracture of similar size (300 µm).

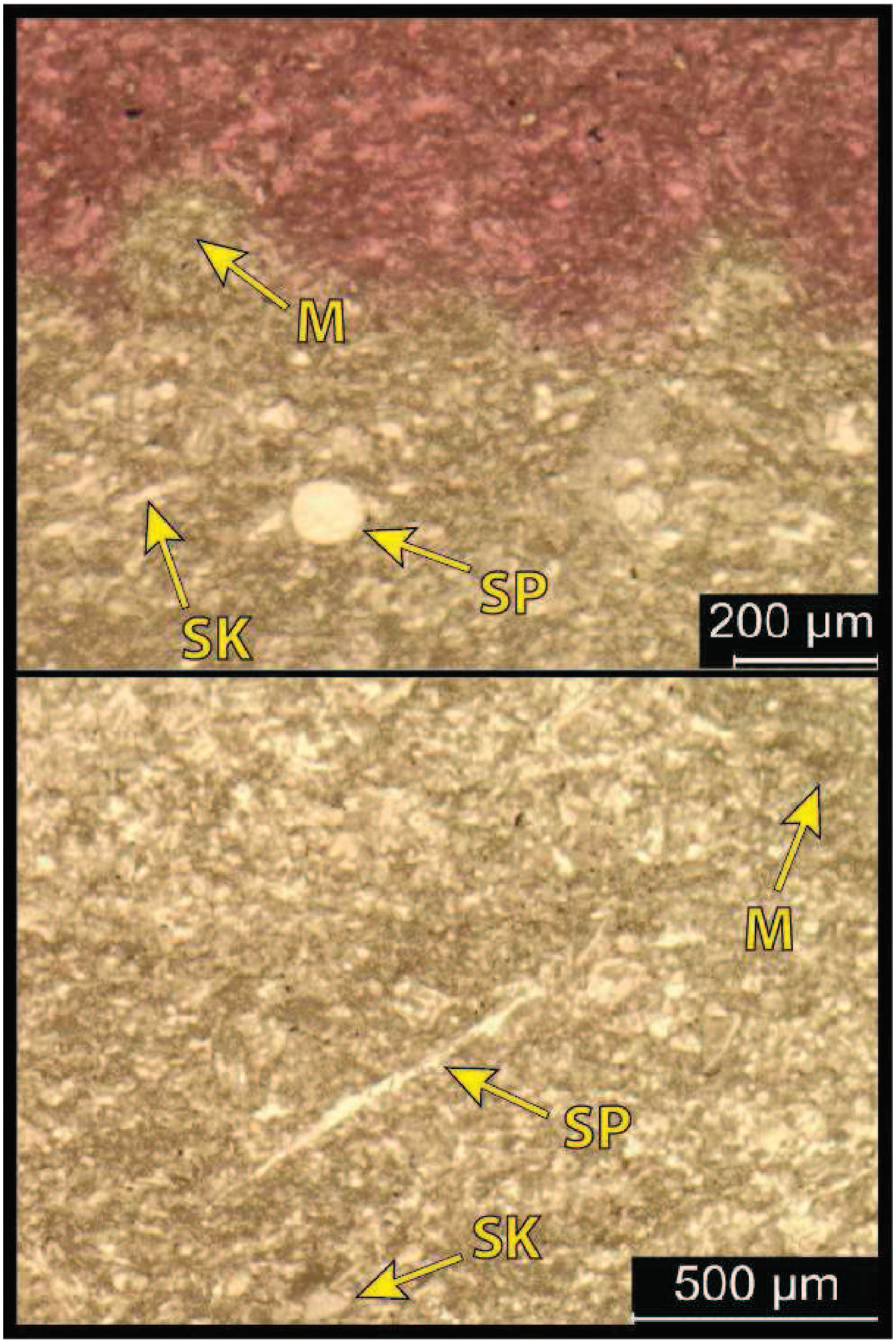

8,375.1': Mud-lean wackestone to mud-rich packstone. Facies 4. Top: PPL/ ½ alizarin red stained. Bottom: PPL. Porosity= 2.78%. B.I.: 3 (hz, mm-scale). Mineralogy: 92% carbonate (91.7% calcite; 0.3% dolomite), 5% quartz and 3% total clay. Grains: spicules (calcitic, 100x600 µm) and other undifferentiated calcareous debris (moderately sorted; 20-50 µm). 5% (visual estimation) calcite cementation in grain-supported portions.

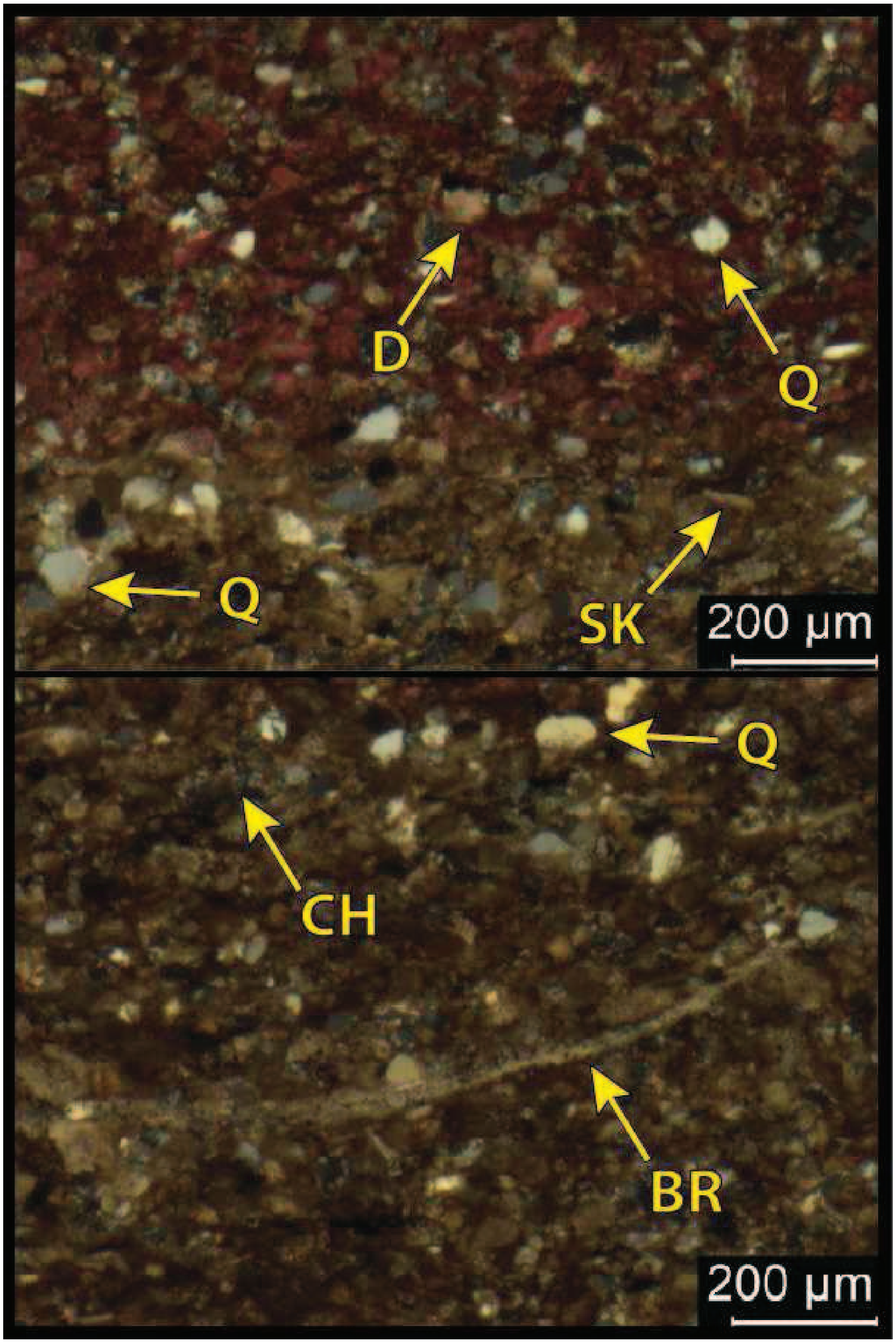

8,360.9': Slightly dolomitic, silty wackestone. Facies 4. Top: XPL/ ½ alizarin red stained. Bottom: XPL. Porosity= 2.11% (intergranular, <25 µm and oil-stained). B.I.: 2 (hz., mm-scale; mud-after). Mineralogy: 48.4% carbonate (41.3% calcite; 7.1% dolomite), 33.3% quartz (20% silt; 13.3% chert), 10.9% total clay, and 7.4% other minerals (5.7% feldspars; 1.75 pyrite). Grains: thin-shelled brachiopod (25 µm x 1mm); silt- to very fine sand- sized, undifferentiated, moderately-sorted calcareous debris (likely crinoids/brachiopods); seldom sponge spicules differentiated.

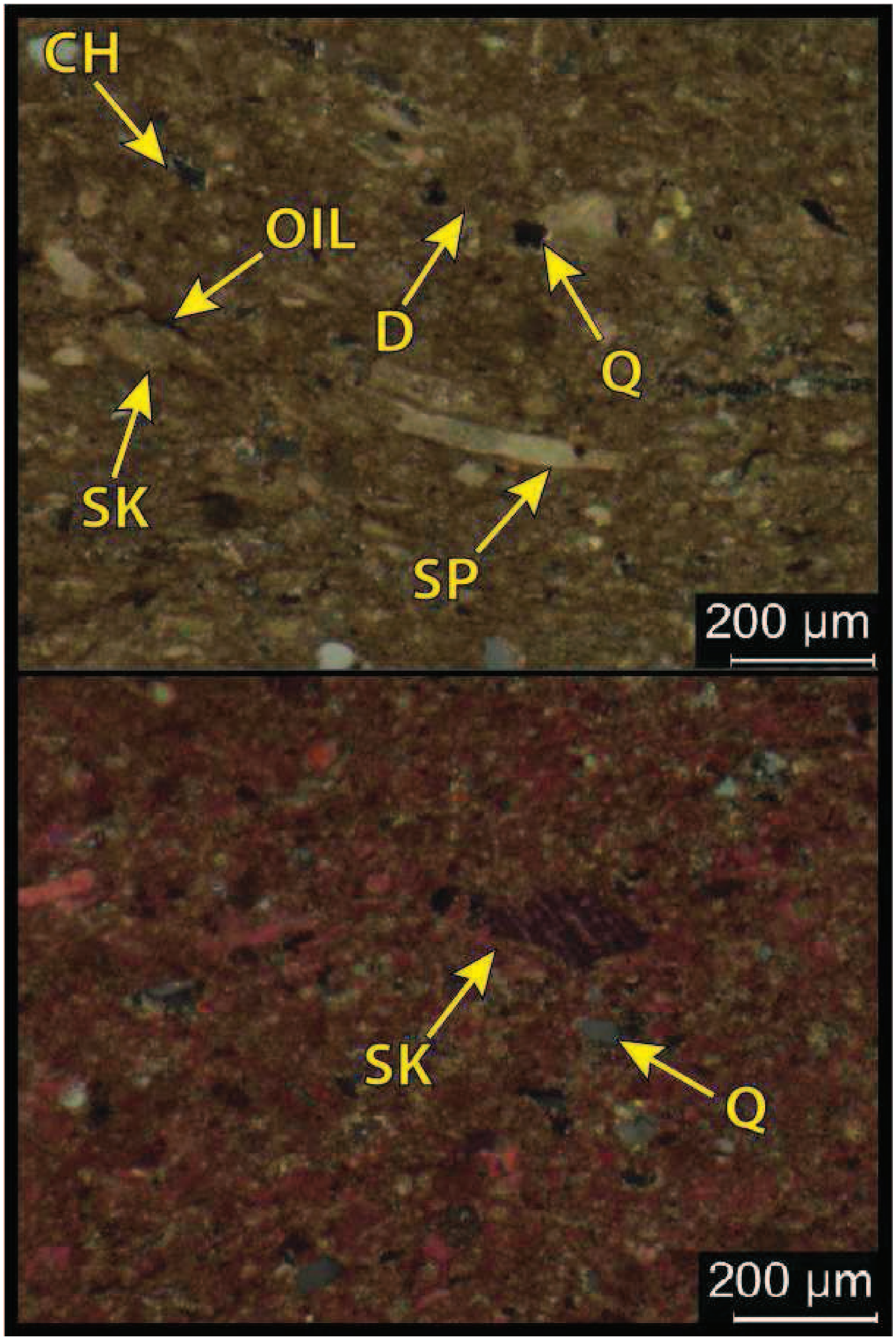

8,346.0': Silty, slightly siliceous mud-lean wackestone. Facies 4. Top: XPL. Bottom: XPL/ alizarin red stained. Porosity= 1.68% (amorphous dead oil – few microns by 100 µm). B.I.: 1. Mineralogy: 70% carbonate (63.6% calcite; 6.4% dolomite), 23.9% quartz (10% quartz silt- to v.f. sand; 13.9% chert), and 6.1% other minerals (3.9% total clay, 1.9% plagioclase, 0.3% pyrite). Grains: Echinoids (5%; biggest 500-600 µm), sponge spicules (2.5%; biggest 50x300 µm), and undifferentiated skeletal grains (silt- to v.f. sand-sized).

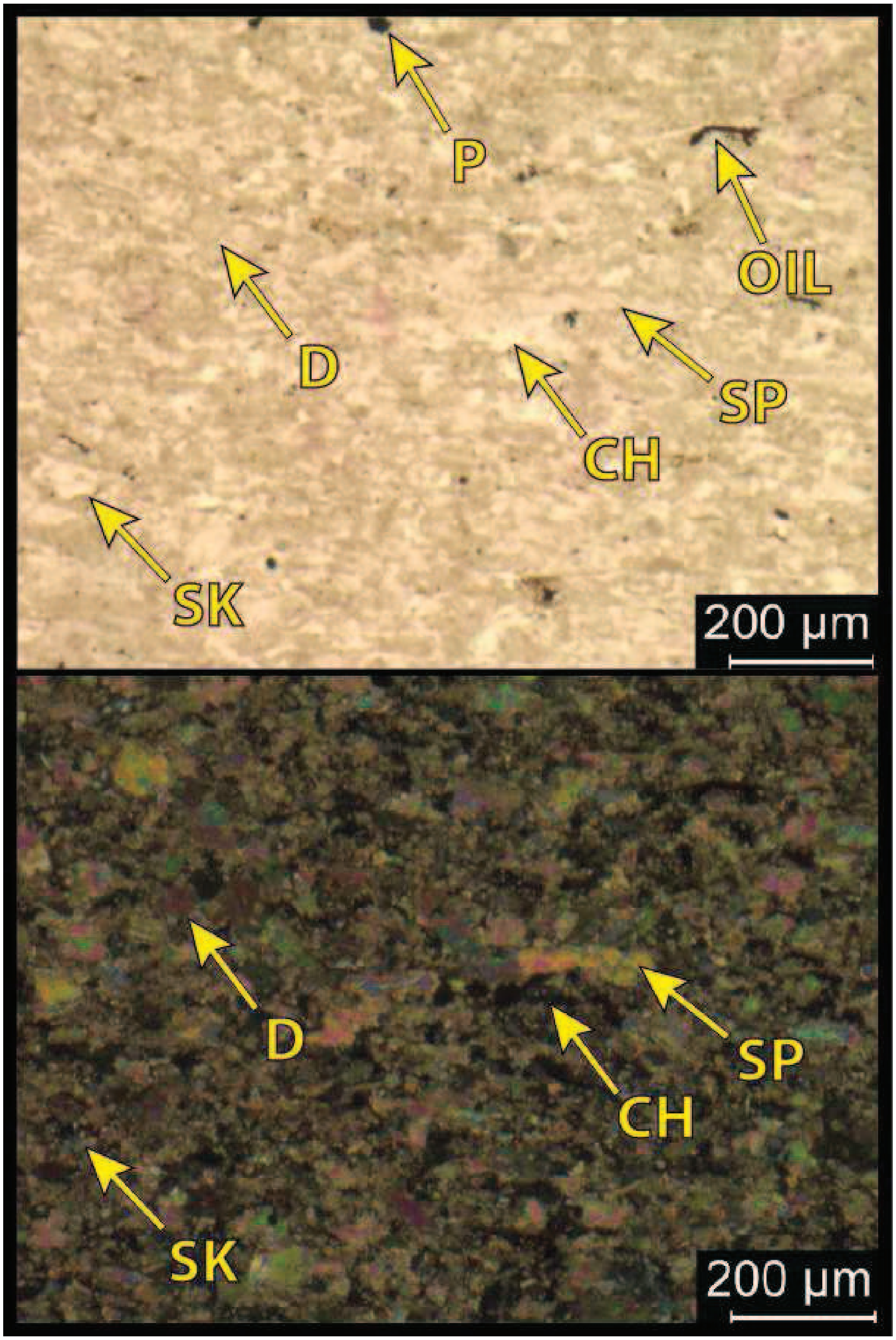

8,331.8': Siliceous, dolomitic crystalline packstone. Facies 4. Top & Bottom: PPL. Porosity= 0.95% (dead oil (few microns by 100 µm)). B.I.: 0. Mineralogy: 63% quartz (50% chert; 13% silt), 35.5% carbonate (23.6% calcite; 11.9% dolomite (40 µm rhombs)), and 1.5% other minerals (1.2% total clay, 0.2% plagioclase, 0.1% pyrite). Grains: crinoid fragments (5%; 50 µm), sponge spicules (2.5%; ~40 x 400 µm), and undifferentiated skeletal fragments (5%; most <25-50 µm, biggest 100 µm). Diagenesis: highly siliceous and dolomitic with abundant syntaxial calcite cementation.

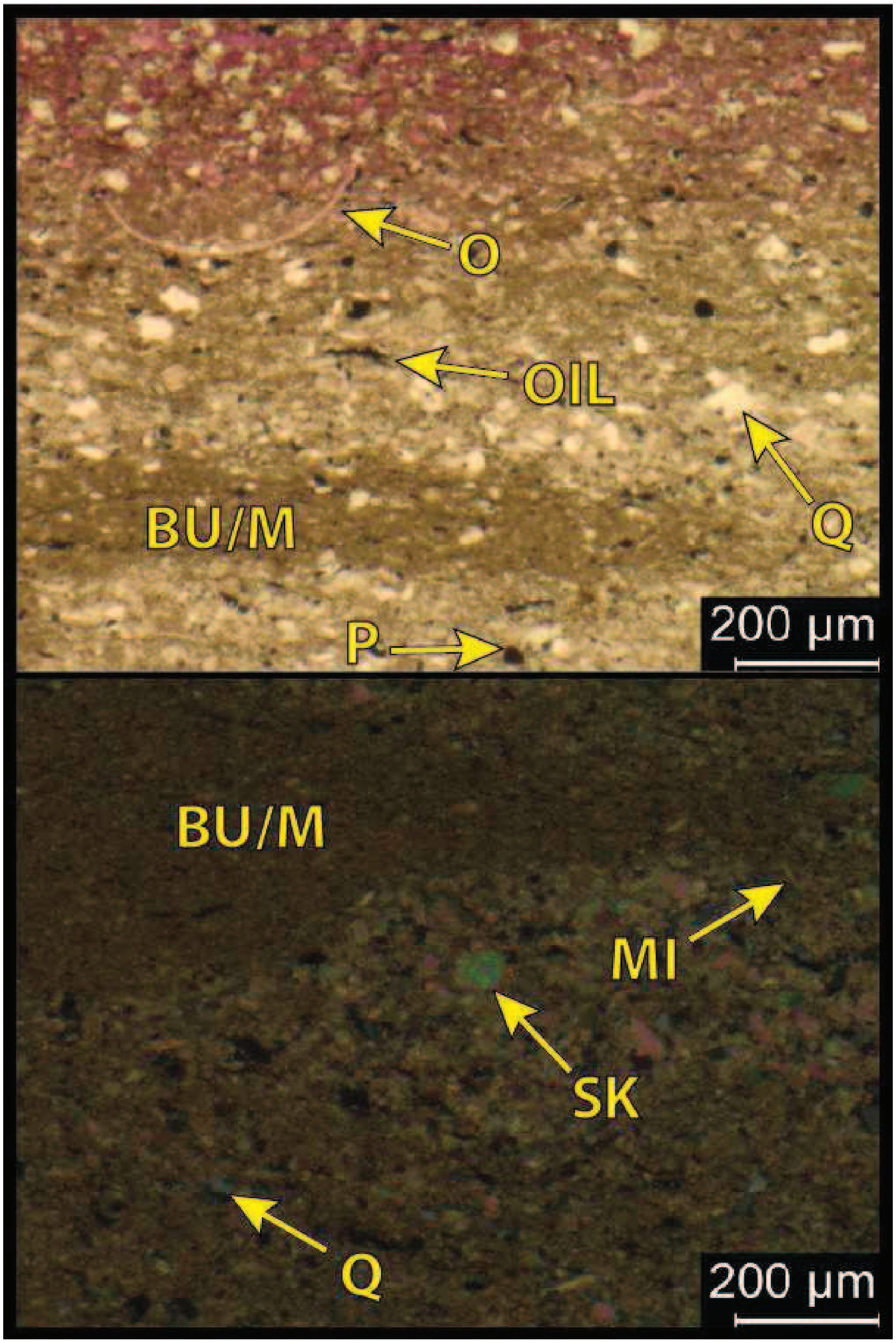

8,320.0': Silty mud-lean wackestone. Facies 3. Top: PPL/ top ¼ alizarin red stained. Bottom: XPL. Porosity= 1.91%. B.I.: 2. Mineralogy: 62.9% carbonate (60.7% calcite; 2.2% dolomite), 24% quartz (15% silt; 9% chert) and 13.1% other minerals (7.5% total clay, 4.2% plagioclase, 1.3% pyrite). Grains: Ostracodes (1%; 400 µm); undifferentiated skeletal debris (7.5%, likely crinoids; 10-90 µm). Silicification of grains (100-200 µm) and intergranular dolomitization and pyritization.

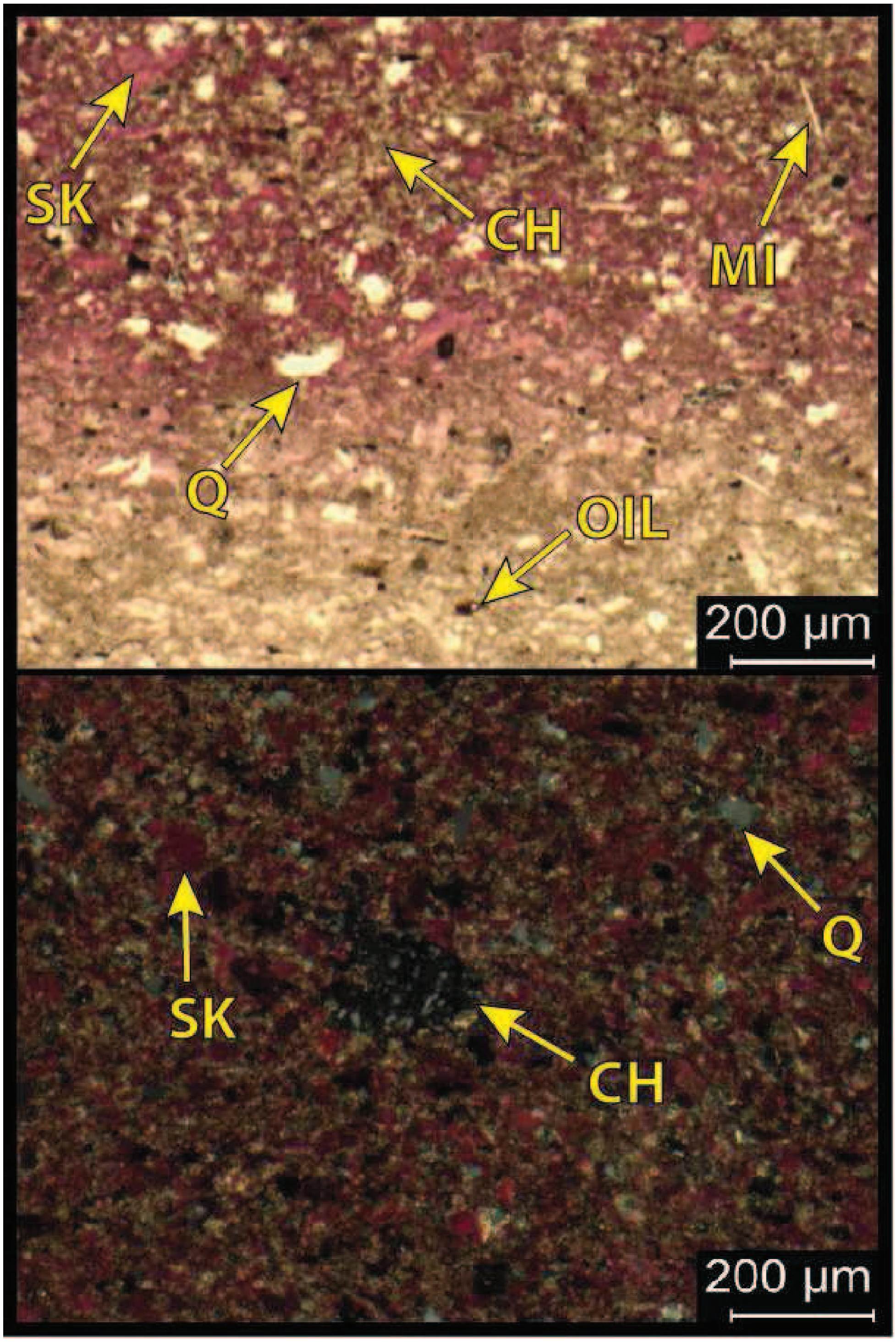

8,314.6': Silty, siliceous mud-lean wackestone. Facies 4. Top: PPL/ top ¼ alizarin red stained. Bottom: XPL and alizarin red stained. Porosity= 0.48%. B.I.: 1. Mineralogy: 66.2% quartz (58.7% chert; 7.5% silt), 30.2% carbonate (28% calcite; 2.2% dolomite) and 3.6% other minerals (3.1% total clay, 0.5% plagioclase). Grains: Crinoid, echinoid and undifferentiated skeletal fragments (~25%; 40-80 µm; well-sorted). Abundant silicification (interparticle and replacement after undifferentiated grains (~200 µm) - more common at top in grainier matrix with noticeable (2%) dolomitization.

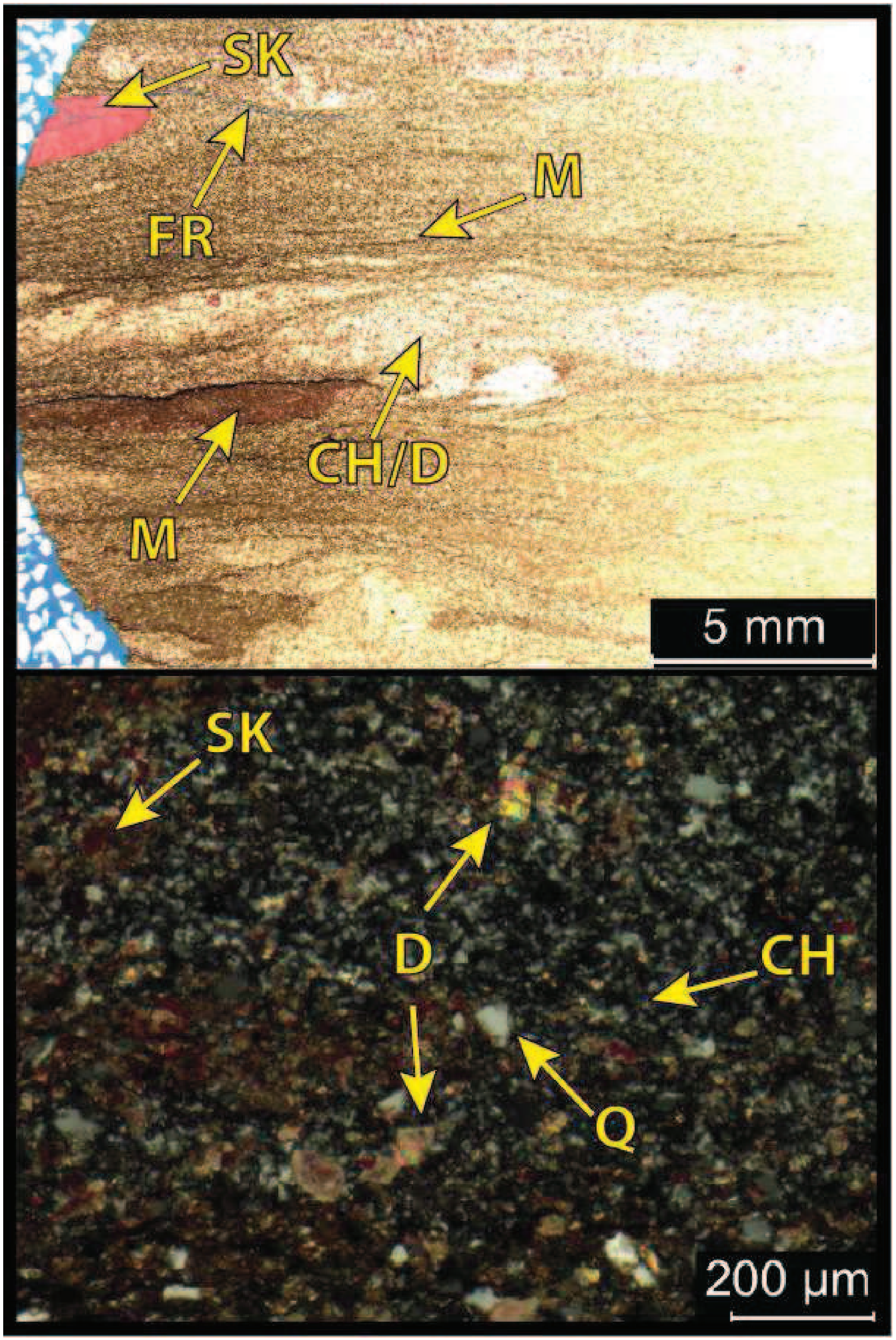

8,310.0': Dolomitic, siliceous wackestone-packstone. Facies 5. Top: PPL/ top ¼ alizarin red stained. Bottom: XPL and alizarin red stained. Porosity= 1.28% (fracture, intercrystalline and intraparticle). B.I.: 1-2. Mineralogy: 72.6% carbonate (62.3% calcite; 10.3% dolomite), 21.8% quartz (17.5% chert; 4.3% silt) and 5.6% other minerals (3.5% total clay, 1.9% plagioclase; 0.2% pyrite). Grains: Echinoid, undifferentiated skeletal fragments and detrital quartz (biggest 2-3mm; most 20-100 µm).

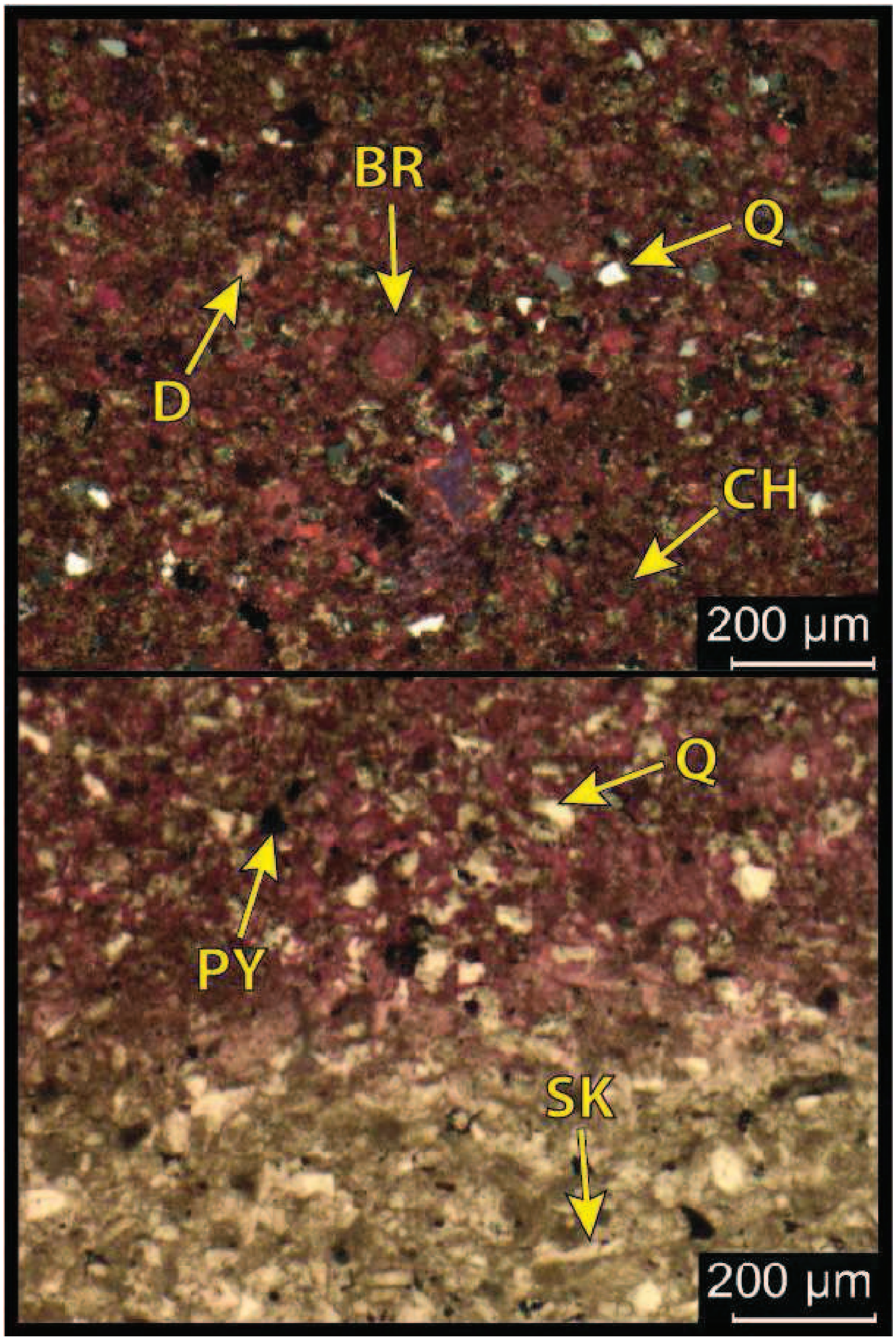

8,304.5': Dolomitic, silty packstone. Facies 5. Top: XPL/alizarin red stained. Bottom: XPL/top ½ alizarin red stained. Porosity= 0.95%. B.I.: 2. Mineralogy: 62.3% carbonate (51% calcite; 11.3% dolomite), 33.8% quartz (26.3% silt; 7.5% chert) and 3.9% other minerals (2.3% total clay; 1.0% plagioclase; 0.6% pyrite). Grains: crinoid, echinoderm and undifferentiated skeletal fragments (~40-100 µm) and quartz silt with seldom (1%) brachiopod spines. Diagenesis: 11.3% dolomitization (few µm-sized rhombs), approximately 10% calcite cementation, 7.5% silicification and 0.6% pyritization.

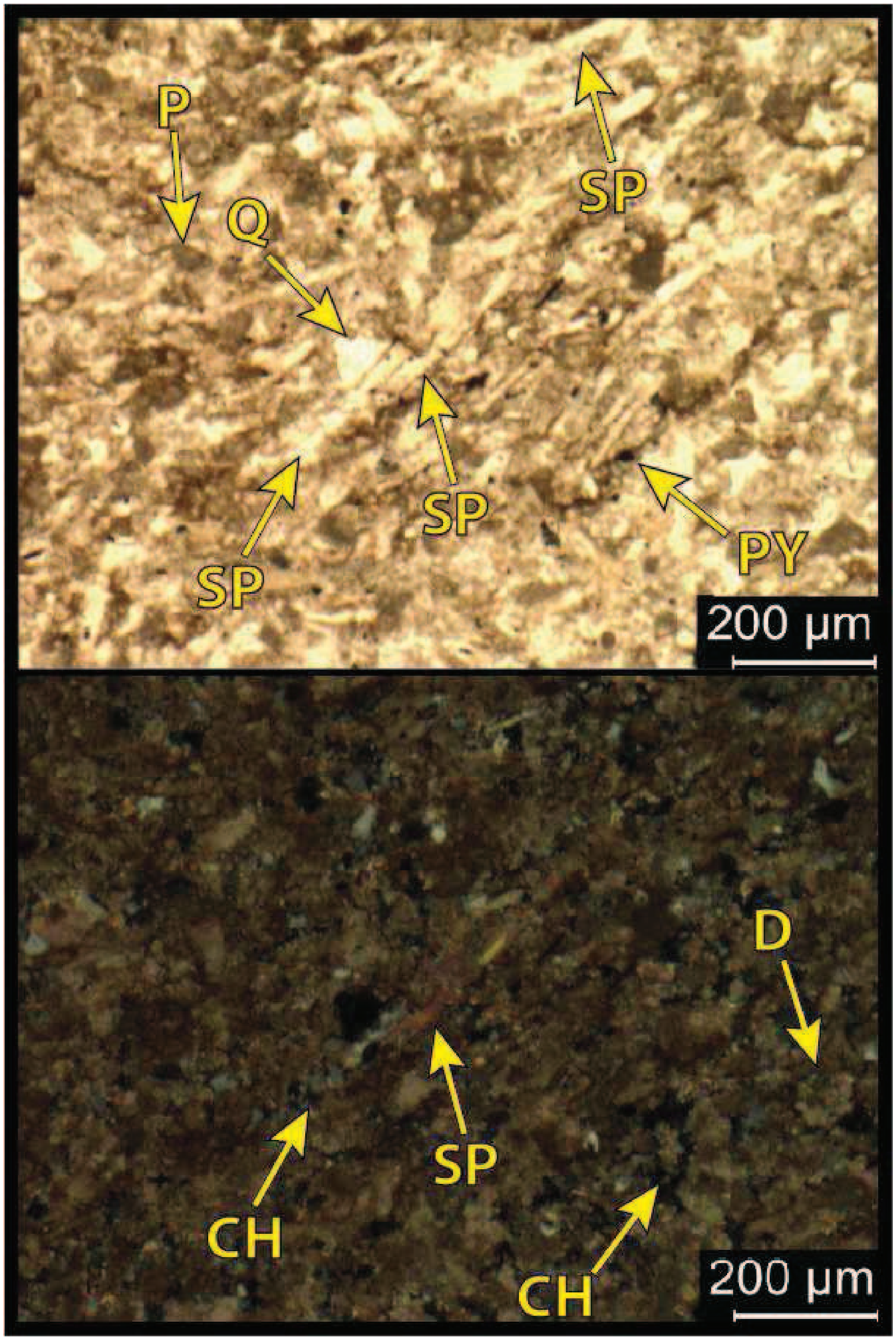

8,272.5': Dolomitic, siliceous and argillaceous spiculitic packstone. Facies 4. Top: PPL. Bottom: XPL. Porosity= 2.31%. B.I.: 1. Mineralogy: 49.6% carbonate (42.1% calcite; 7.5% dolomite), 33.9% quartz (25% silt; 8.9% chert) and 16.6% other minerals (11.9% total clay, 3.2% feldspar; 1.5% pyrite). Grains: moderately to well-sorted undifferentiated skeletal fragments (20%), sponge spicules (10%; variably calcitic/siliceous), peloidal grains (10-80 µm). Diagenesis: abundant calcite cementation (30%), 8.9% silicification, 7.5% dolomitization.

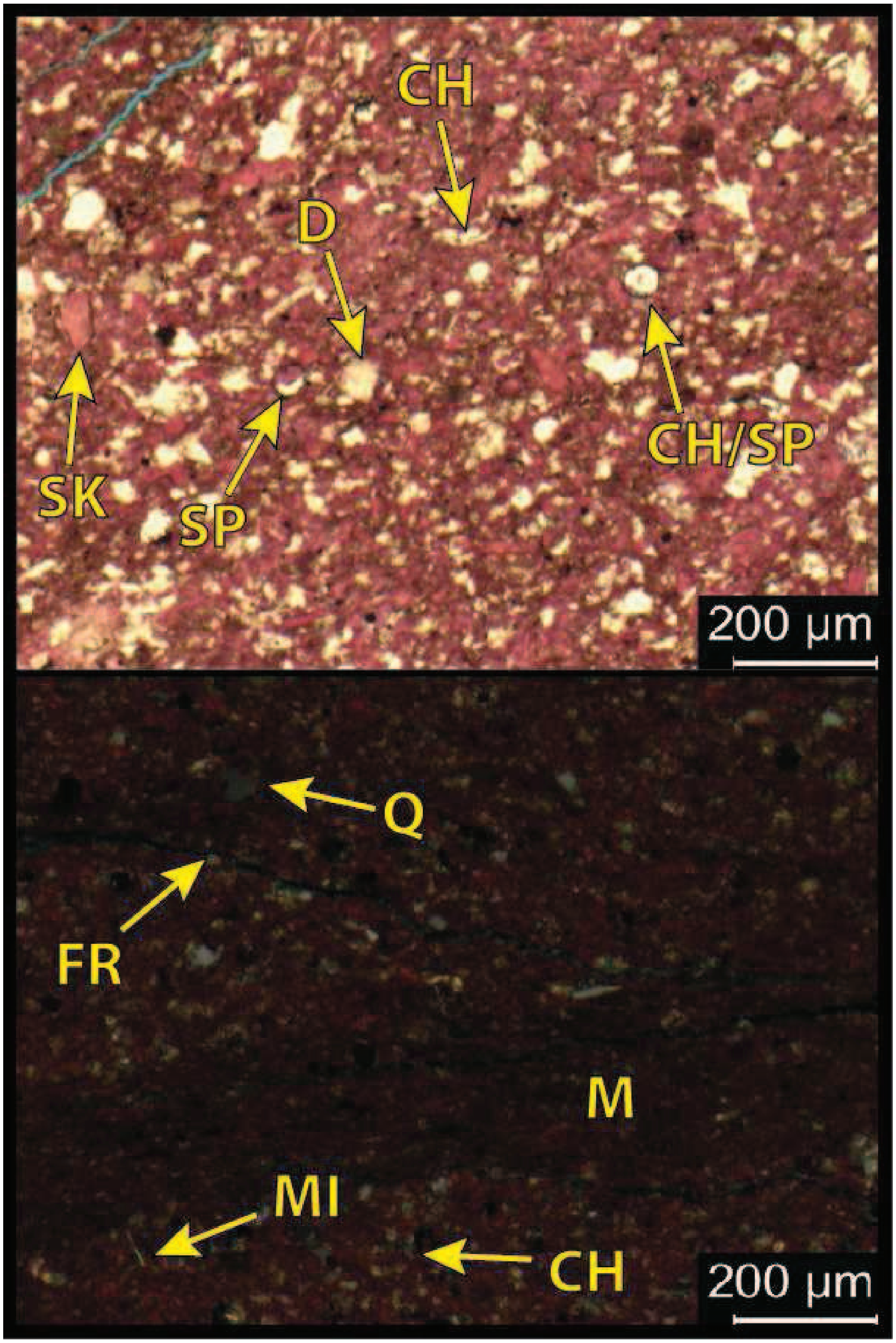

8,256.55': Slightly argillaceous silty mud-lean wackestone. Facies 4. Top: PPL/ alizarin red stained. Bottom: XPL/ alizarin red stained. Porosity= 1.45%. B.I.: 1. Mineralogy: 52% carbonate (48.4% calcite; 3.6% dolomite), 39.6% quartz (30% silt; 9.6% chert) and 8.4% other minerals (5.2% total clay, 2.7% feldspar; 0.4% pyrite). Grains: Brachiopod, crinoid and undifferentiated skeletal fragments (65%; 40-120 µm), quartz silt (30%) and sponge spicules (5%; ~50 µm and variably calcite/chert). Diagenesis: ~10% silicification, 5% calcite cementation and 3.6% dolomitization.

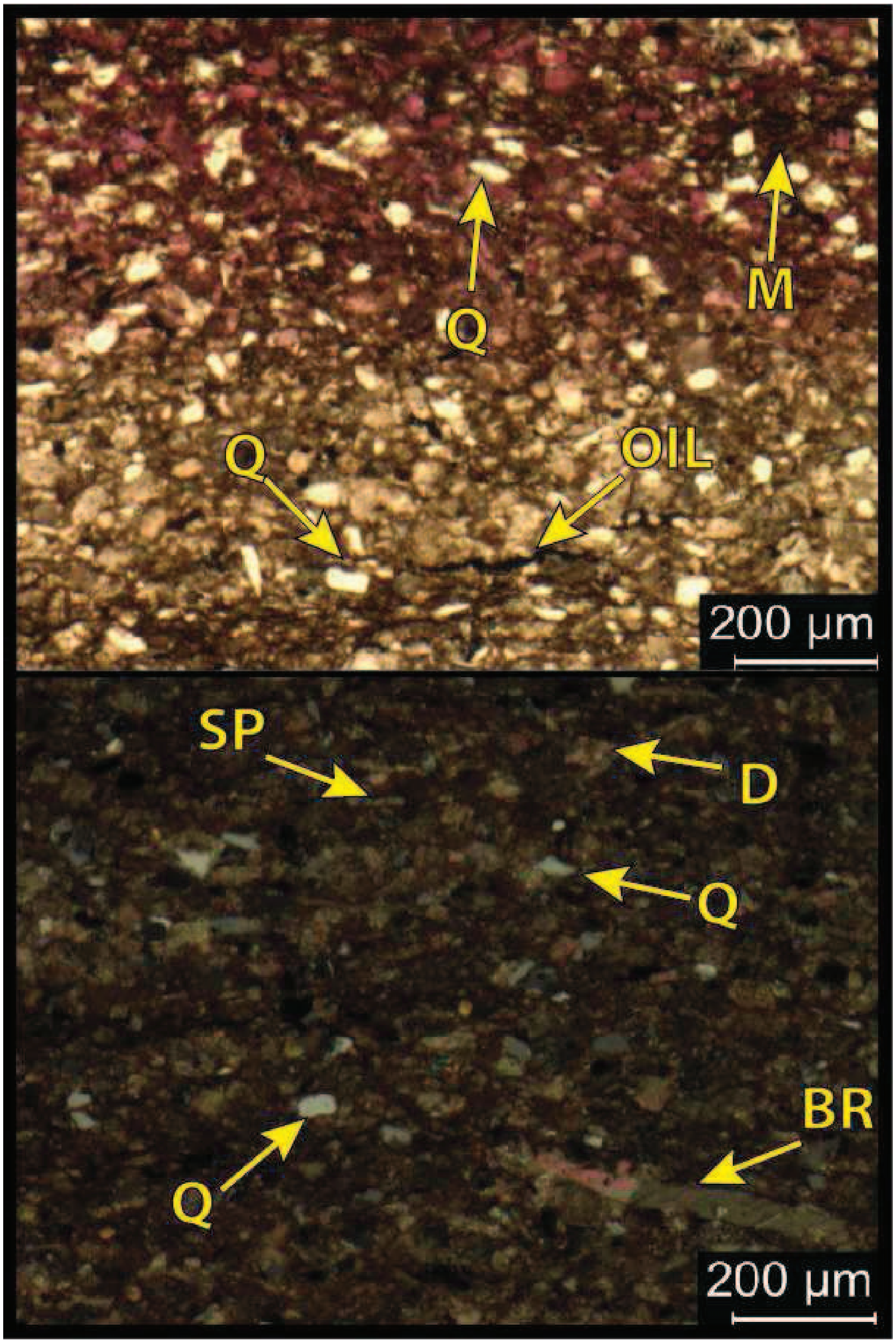

8,238.1': Argillaceous silty wackestone/ carbonaceous crystalline siltstone. Facies 4. Top: PPL/ ½ alizarin red stained. Bottom: XPL. Porosity= 1.85%. B.I.: 1. Mineralogy: 50% quartz (40% silt; 10% chert), 24.3% carbonate (17.5% calcite; 6.8% dolomitic) and 25.7% other minerals (13.9% total clay, 9.5% feldspar (7.6%Plag/1.9%K-Spar); 2.3% pyrite). Grains: quartz silt, brachiopods (some intact, some disarticulated), sponge spicules (silt-sized) and crinoids (most silt-sized, biggest 40μm). Diagenesis: 10% silicification; 6.8% dolomitization (rhombs approx.. 30μm).

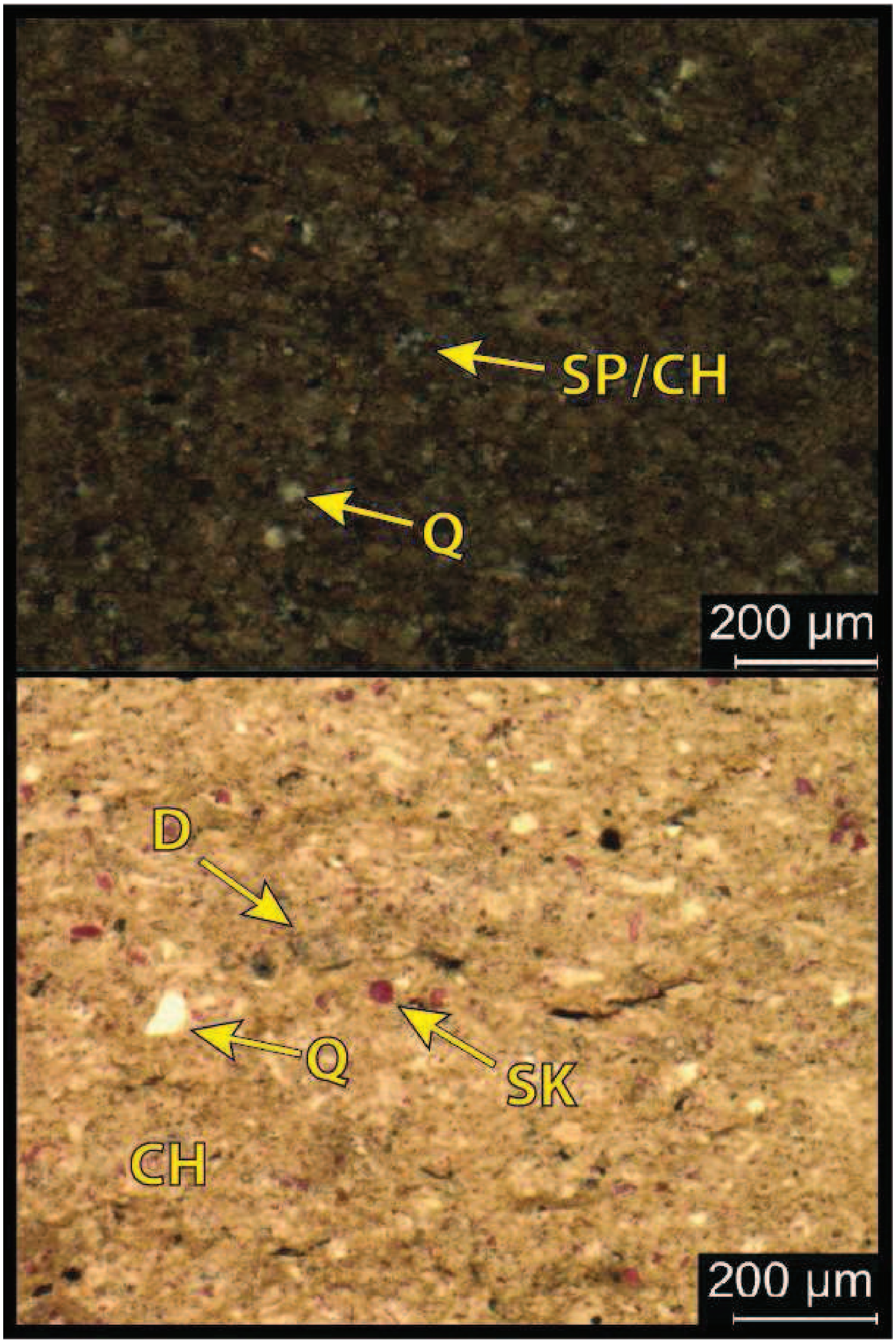

8,215.7': Silty packstone with interbedded silty wackestone. Facies 4. Top: XPL. Bottom: PPL/ alizarin red stained. Porosity= 0.59%. B.I.: 1-2. Mineralogy: 60.7% carbonate (58% calcite; 2.7% dolomite), 31.6% quartz (26.6% chert; 5% silt) and 7.7% other minerals (4.4% total clay; 3% feldspar; 0.3% pyrite). Grains: Sponge spicules (5%; 40 x 300 μm and preferential to packstone bed) and undifferentiated skeletal fragments. Diagenesis: 26.6% silicification, 2.7% dolomitization.

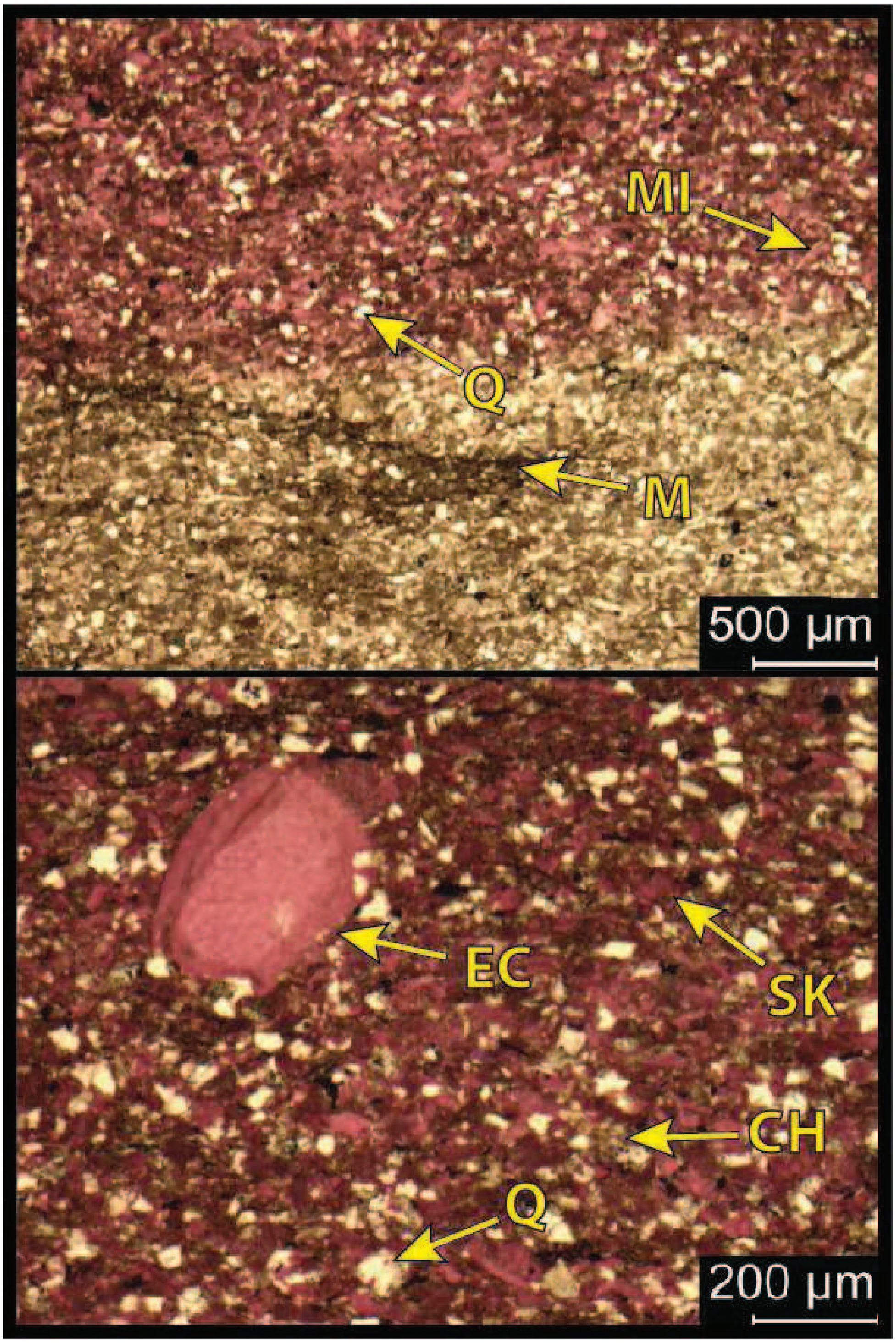

8,199.9': Silty mud-rich packstone. Facies 4. Top: PPL/ ½ alizarin red stained. Bottom: PPL/ alizarin red stained. Porosity= 1.44%. B.I.: 1. Mineralogy: 63.2% carbonate (60.5% calcite; 2.7% dolomite), 29.4% quartz (25% silt; 4.4%chert) and 7.4% other minerals (4.3% total clay; 2.9% feldspar; 0.3% pyrite). Grains: Ostracodes (40x400µm), bryozoan (150µm x 1.2mm), echinoids (400µm) and peloidal grains/ undifferentiated skeletal fragments (~40µm). Diagenesis: 4% silicification and 2.7% dolomitization.

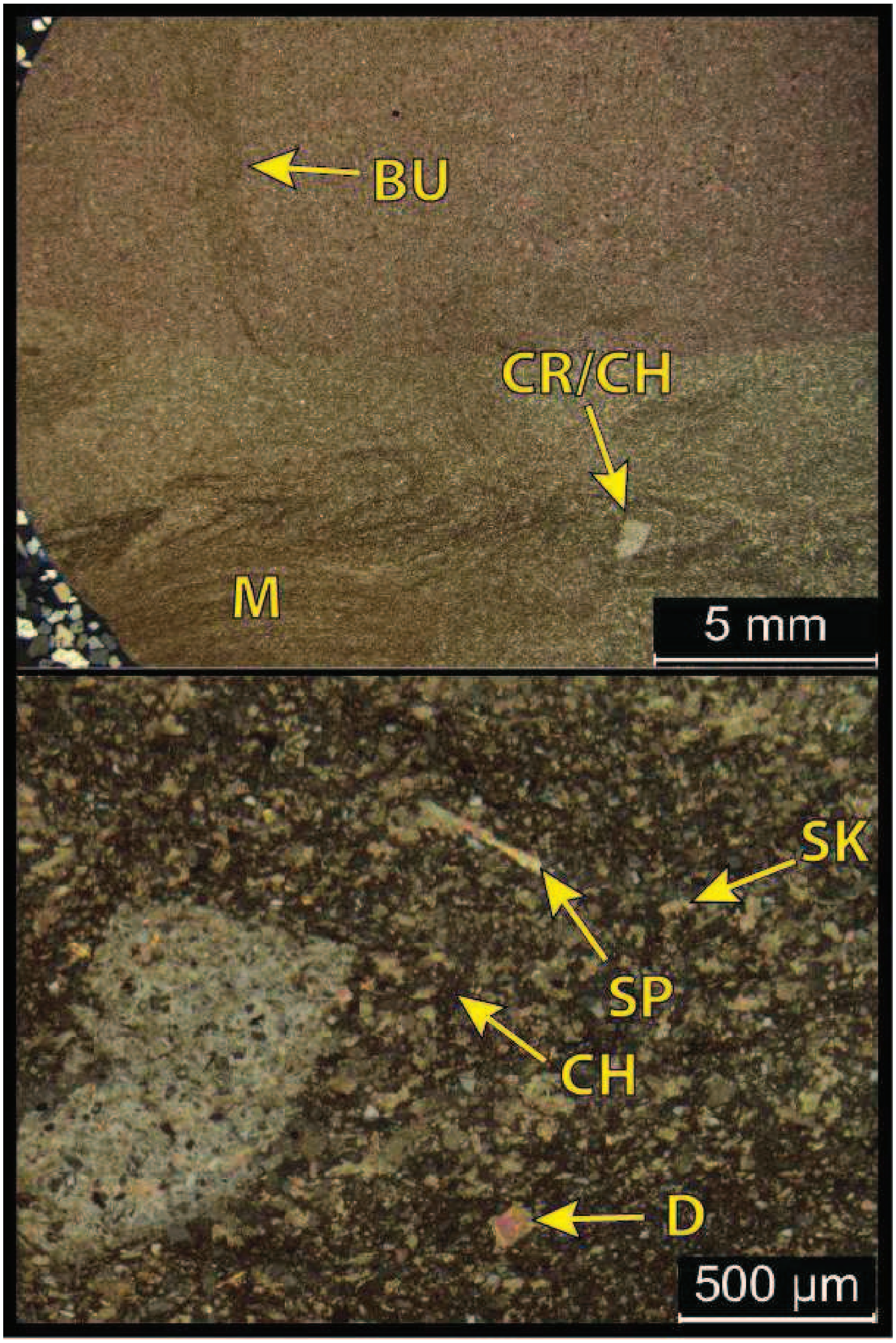

8,174.2': Siliceous packstone. Facies 4. Top: XPL/ ½ alizarin red stained. Bottom: XPL. Porosity= 1.32%. B.I.: 2. Mineralogy: 66.2% carbonate (62% calcite; 4.2% dolomite), 21% quartz (20% chert; 1% silt) and 12.8% other minerals (8.5% total clay; 3.4% plagioclase; 0.8% pyrite). Grains: crinoids (500x700µm; calcite replaced), disarticulated crinoid, bryozoa and echinoid debris (50-200µm), spicule? Diagenesis: 20% silicification; 5% calcite cementation; 4.2% dolomitization.

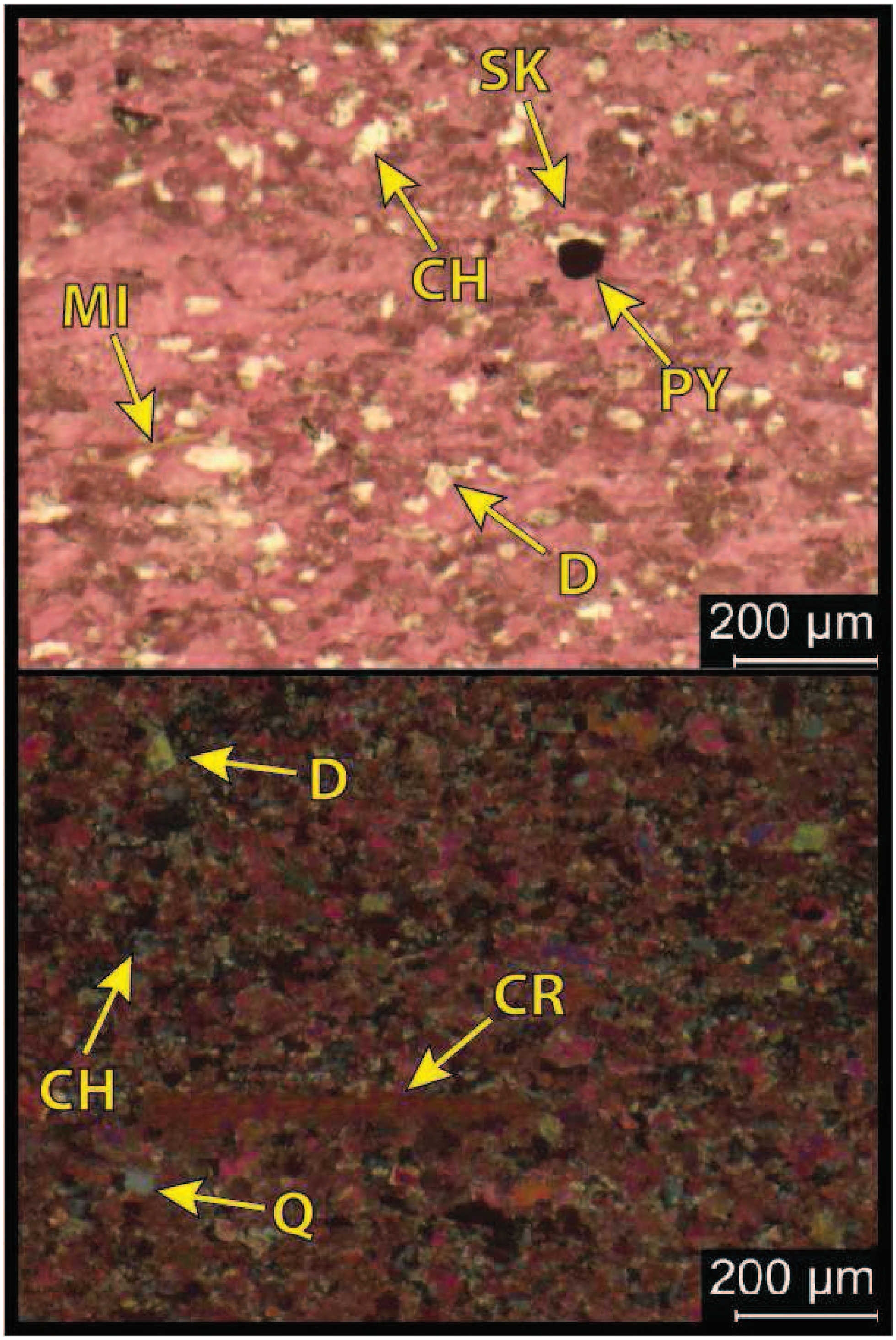

8,123.9': Slightly argillaceous and slightly dolomitic packstone. Facies 4. Top: PPL/ alizarin red stained. Bottom: XPL/ alizarin red stained. Porosity= 1.76%. B.I.: 0. Mineralogy: 55.4% carbonate (47% calcite; 8.4% dolomite), 28.7% quartz (25% chert; 3.7% silt) and 15.9% other minerals (9% total clay; 5.1% feldspar (4.4% plagioclase); 1.8% pyrite). Grains: Ostracodes (50-160µm), crinoid debris and peloidal grains (30-100µm). Diagenesis: 25% silicification; 8.4% dolomitization (max 50µm rhombs); 7.5% calcite cementation.

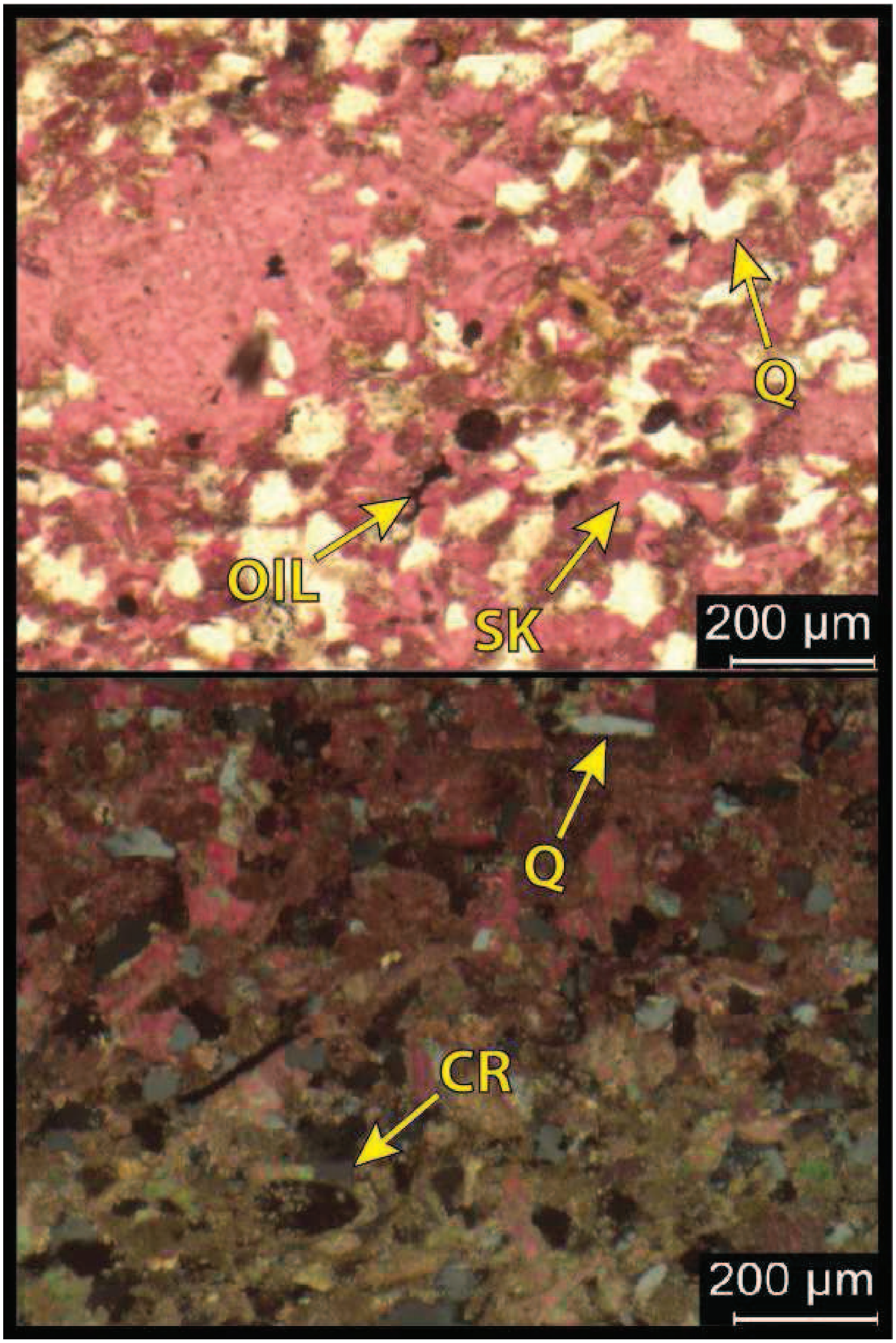

8,101.6': Arenitic mud-lean packstone. Facies 5. Top: PPL/ alizarin red stained. Bottom: XPL/ ½ alizarin red stained. Porosity= 0.84%. B.I.: 1. Mineralogy: 63.3% carbonate (62% calcite; 1.3% dolomite), 30.8% quartz (29.8% silt; 1% chert) and 5.9% other minerals (3.4% total clay; 2% plagioclase; 0.5% pyrite). Grains: Bryozoan (~200µm), foraminifera, echinoid, crinoid and peloidal fragments (30-100µm). Diagenesis: 15% calcite cementation; minor (1%) silicification and dolomitization.

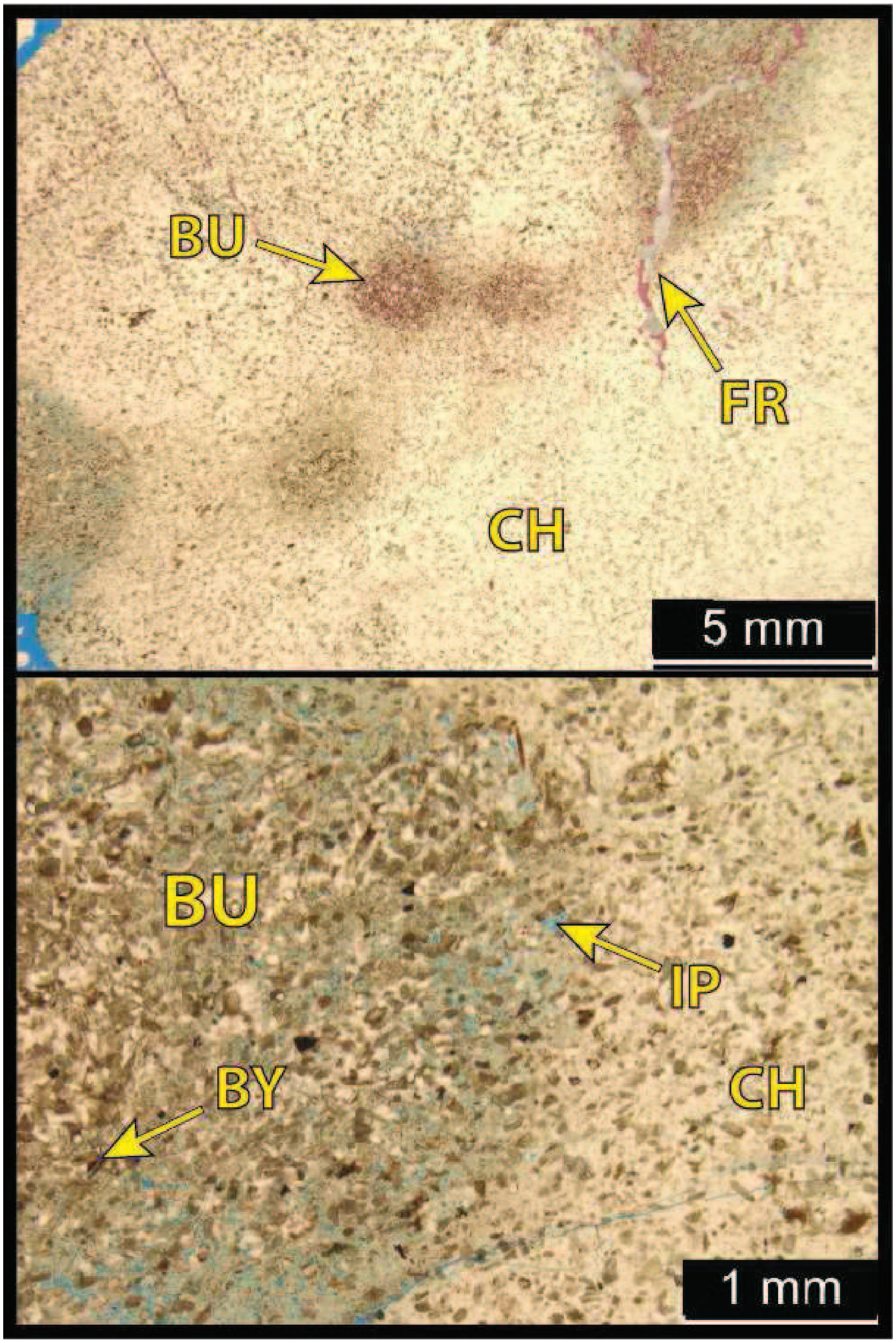

8,094.7': Siliceous, bryozoan-bearing crystalline limestone. Facies 5. Top: PPL/ ½ alizarin red stained. Bottom: PPL. Porosity= 2.22%. B.I.: 2-3. Mineralogy: 78.1% quartz (75% chert; 3.1% silt) and 21.9% carbonate (17.4% calcite; 4.5% dolomite). Grains: Peloidal (50-150µm) grains concentrated in burrows; bryozoan fragments (50-150µm) throughout and undifferentiated skeletal fragments. Diagenesis: 75% silicification; 4.5% dolomitization; calcite cementation in fractures.

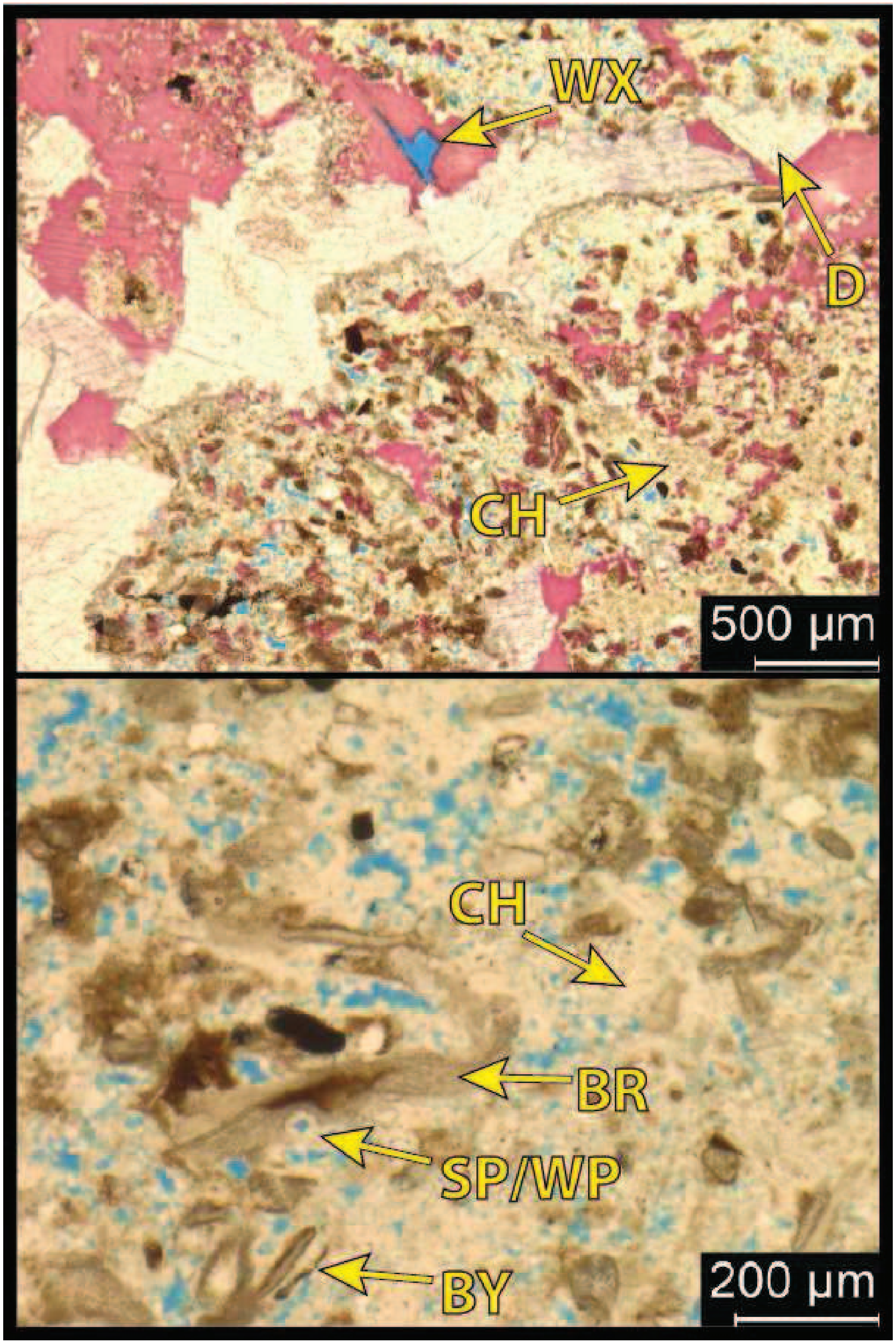

8,091.4': Siliceous, bryozoan-bearing crystalline limestone. Facies 5. Top: PPL/ alizarin red stained. Bottom: PPL. Porosity= 8.28%. B.I.: 0-1. Mineralogy: 81.5% quartz (78.5% chert ; 3% silt) and 18.5% carbonate (17.1% calcite; 1.4% dolomite). Grains: Peloidal and bryozoan fragments (50-150µm); micritized brachiopod (400µm); sponge spicules (<25µm). Diagenesis: 78.5% silicification; 1.4% dolomitization (primarily in large (1mm) fracture.

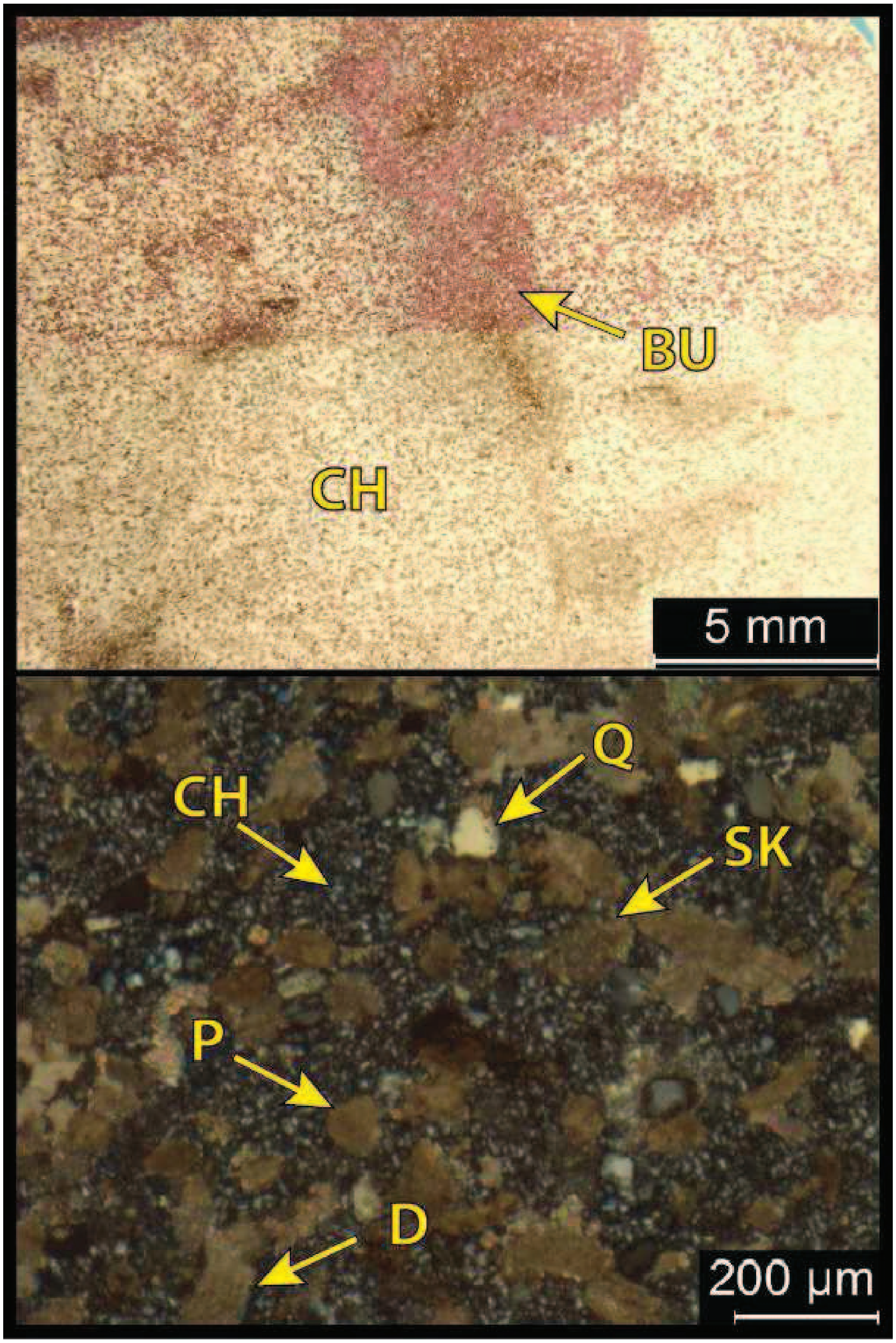

8,082.5: Siliceous, bryozoan-bearing crystalline limestone. Facies 5. Top: PPL/ ½ alizarin red stained. Bottom: XPL. Porosity= 4.49%. B.I.: 2-3. Mineralogy: 53.9% quartz (50% chert; 3.9% silt), 42.8% carbonate (40.7% calcite; 2.1% dolomite) and 3.3% other minerals (1.9% total clay; 1.4% feldspar). Grains: Peloidal and bryozoan fragments (50-150µm; variably micritized); sponge spicules (<25µm); crinoid and undifferentiated skeletal debris; peloidal debris in burrows. Diagenesis: Moderate silicification (50%); calcite cementation (20%; after burrows).

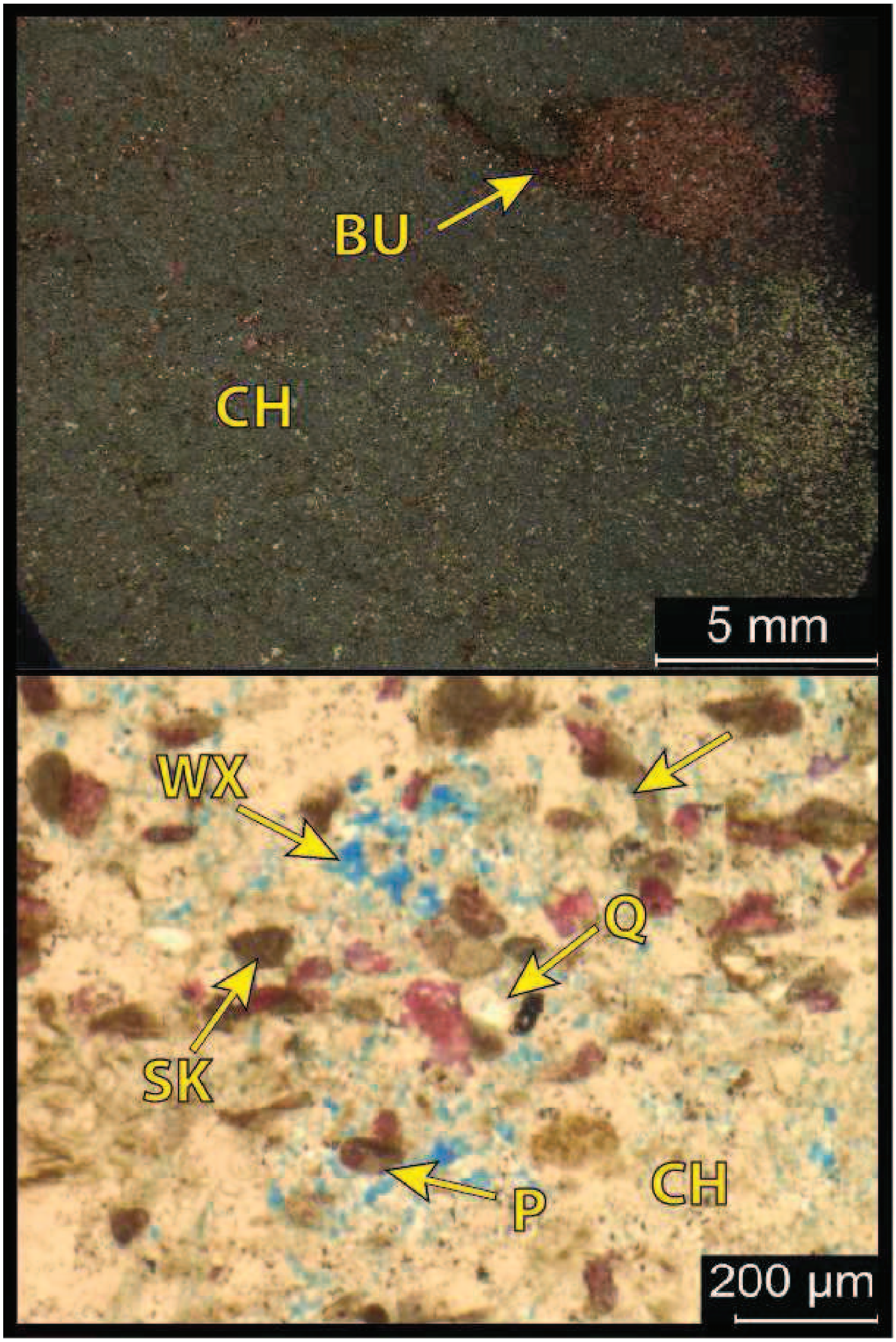

8,076.2': Siliceous, bryozoan-bearing crystalline limestone. Facies 5. Top: XPL/ ½ alizarin red stained. Bottom: PPL/ alizarin red stained. Porosity= 4.63%. B.I.: 2-3. Mineralogy: 87.3% quartz (84.8% chert; 2.5% silt), 12.3% carbonate (11.7% calcite; 0.6% dolomite) and 0.4% other minerals (K-feldspar). Grains: Sponge spicules, echinoid spines, bryozoan fragments (50-150µm); peloidal grains preferential to burrows. Diagenesis: Abundant silicification (84.8%).

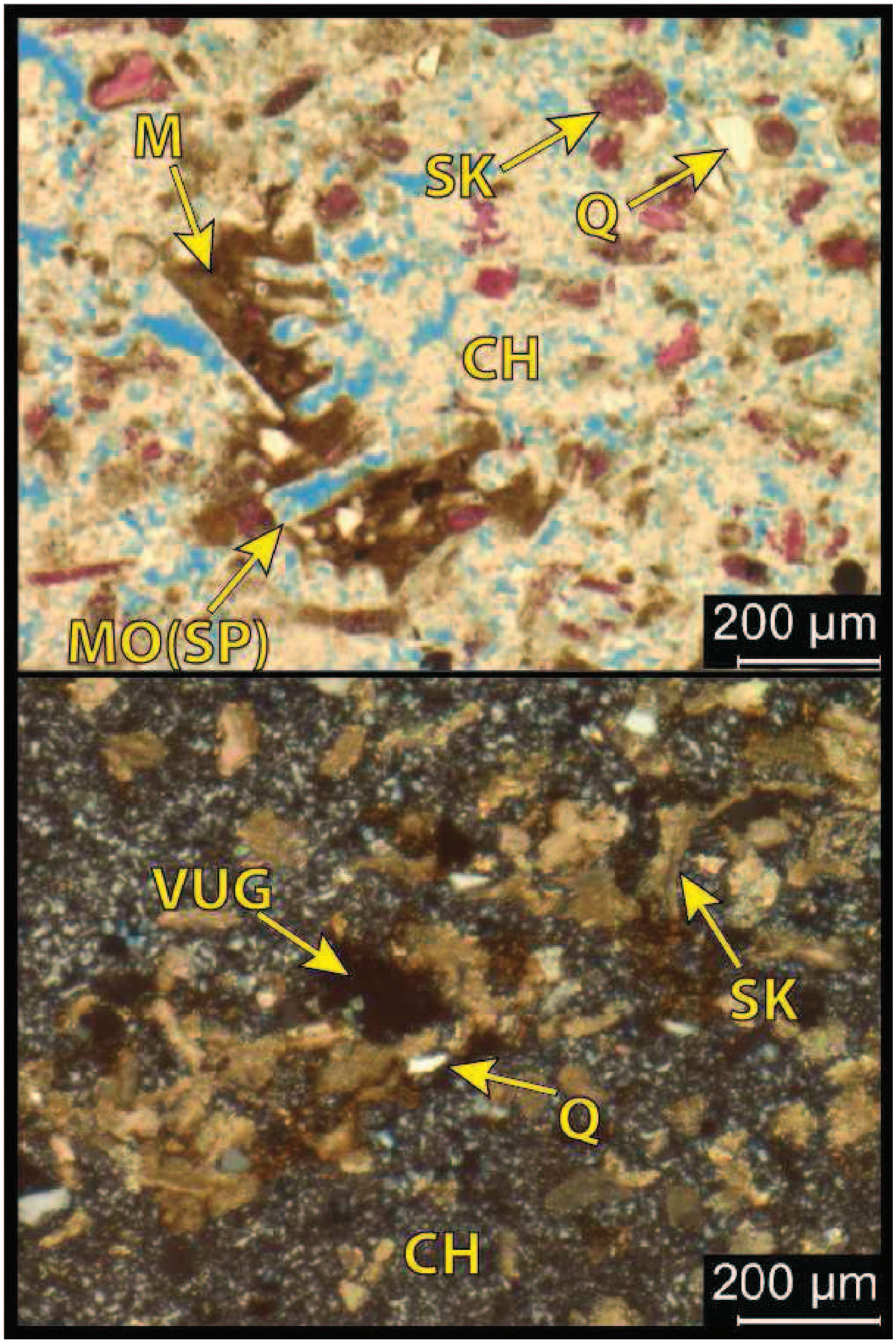

8,075.2': Siliceous, bryozoan-bearing crystalline limestone. Facies 5. Top: PPL/ alizarin red stained. Bottom: XPL. Porosity= 11.6% (moldic/vugular/interparticle/intercrystalline). B.I.: 2-3. Mineralogy: 84.2% quartz (81.7% chert; 2.5% silt), 13.9% carbonate (13.5% calcite; 0.4% dolomite) and 1.9% other minerals (1.6% total clay; 0.3% plagioclase). Grains: Sponge spicules (preferential dissolution), echinoid spines, bryozoan fragments (50-150µm). Abundant silicification (81.7%).

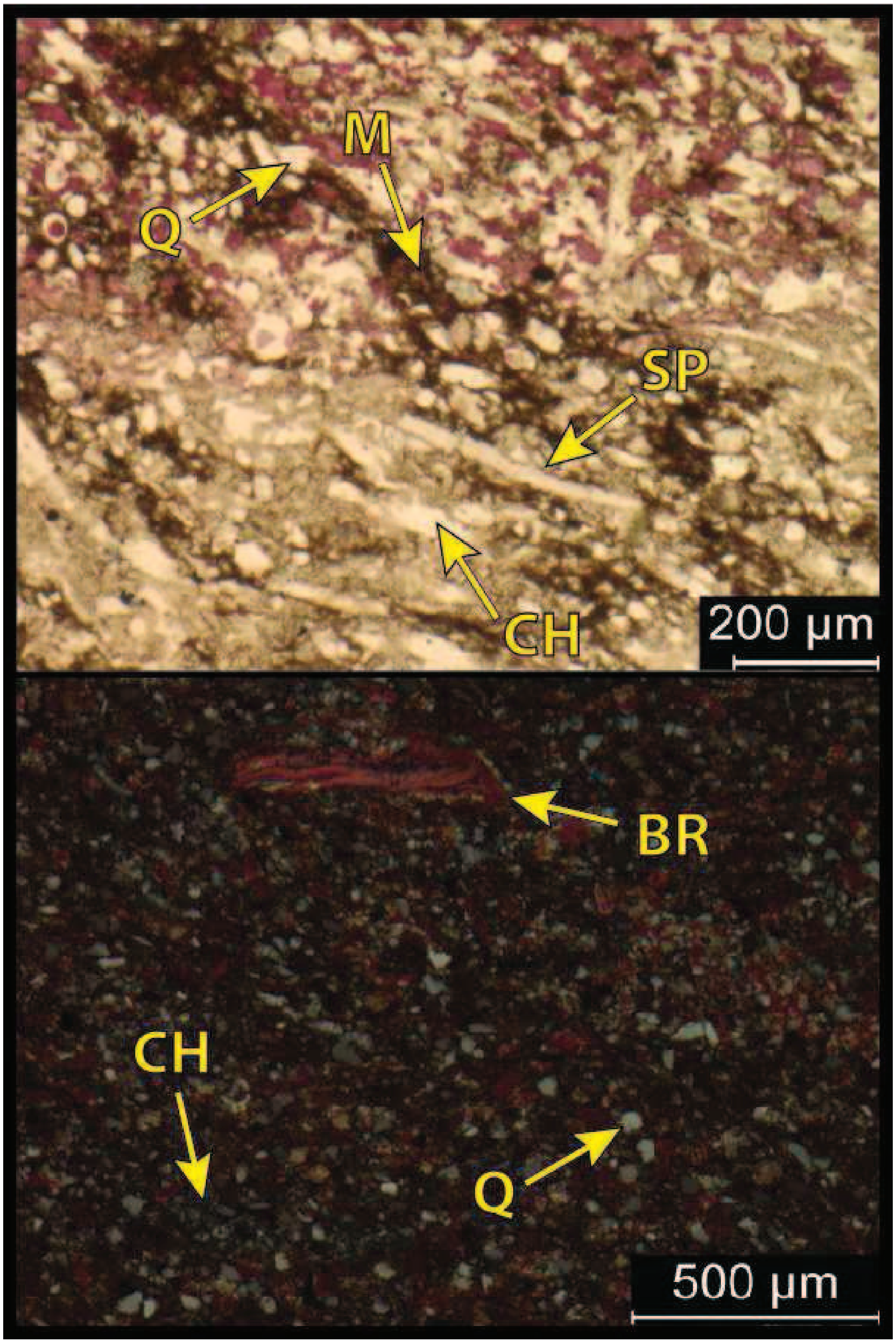

8,065.2': Siliceous mud-rich packstone. Facies 4. Top: PPL/ ½ alizarin red stained. Bottom: XPL alizarin red stained. Porosity= 1.8%. B.I.: 1. Mineralogy: 56.2% quartz (31.2% chert; 25% silt), 30.8% carbonate (28.6% calcite; 2.2% dolomite) and 13% other minerals (7.2% total clay; 5% fledpsar (4.3% plagioclase); 0.7% pyrite). Grains: Sponge spicules (30x300µm); brachiopods (~75µm x 1.5mm); benthic foraminifera; undifferentiated skeletal debris (20-40µm); poor to moderate sorting. Diagenesis: ~30% silicification, ~10% calcite cementation, 2.2% dolomitization.

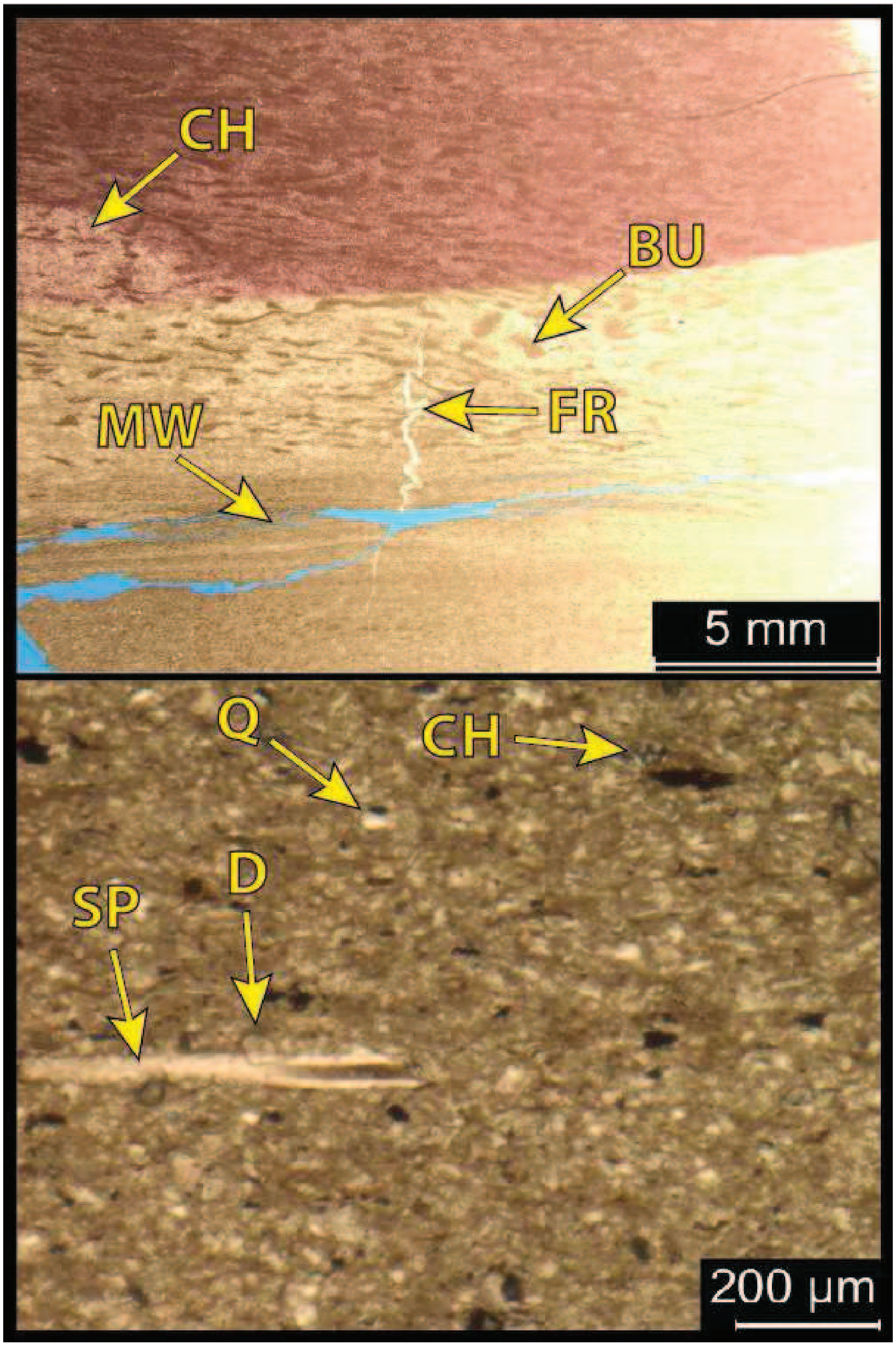

8,020.3’: Slightly silty, siliceous mud-lean wackestone. Facies 4. Top: PPL/ ½ alizarin red stained. Bottom: XPL. Porosity= 1.57%. B.I.: 2-3. Mineralogy: 56.7% carbonate (51.7% calcite; 5% dolomite), 33.2% quartz (22.2% chert; 10% silt) and 10.1% other minerals (7% total clay; 2.4% feldspar; 0.6% pyrite). Grains: peloidal/ undifferentiated skeletal fragments (silt-sized), sponge spicules (2.5%; biggest 400µm, most silt-sized). Diagenesis: ~20% silicification. 5% dolomitization, and ~2.5% calcite cementation.

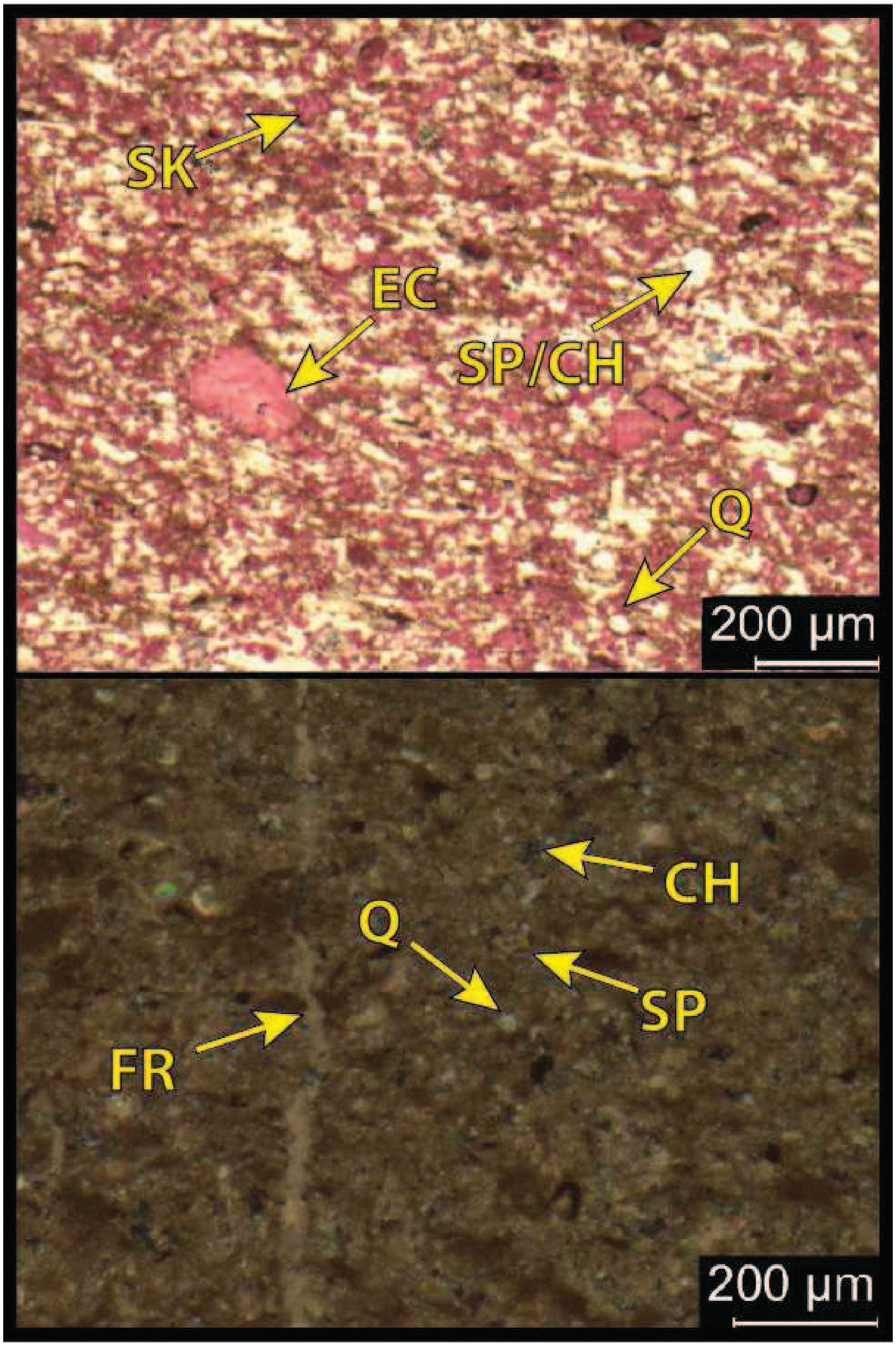

7,998.7': Siliceous packstone. Facies 4. Top: PPL/ alizarin red stained. Bottom: XPL. Porosity= 1.45%. B.I.: 0. Mineralogy: 50.2% carbonate (46.7% calcite; 3.5% dolomite), 42.2% quartz (37.2% chert; 5% silt) and 7.5% other minerals (5.5% total clay; 1.8% plagioclase; 0.4% pyrite). Grains: moderate to well-sorted sponge spicules (30x500µm), peloids, ostracodes, echinoderms. Diagenesis: ~35% silicification; ~5% calcite cementation; 3.5% dolomitization.

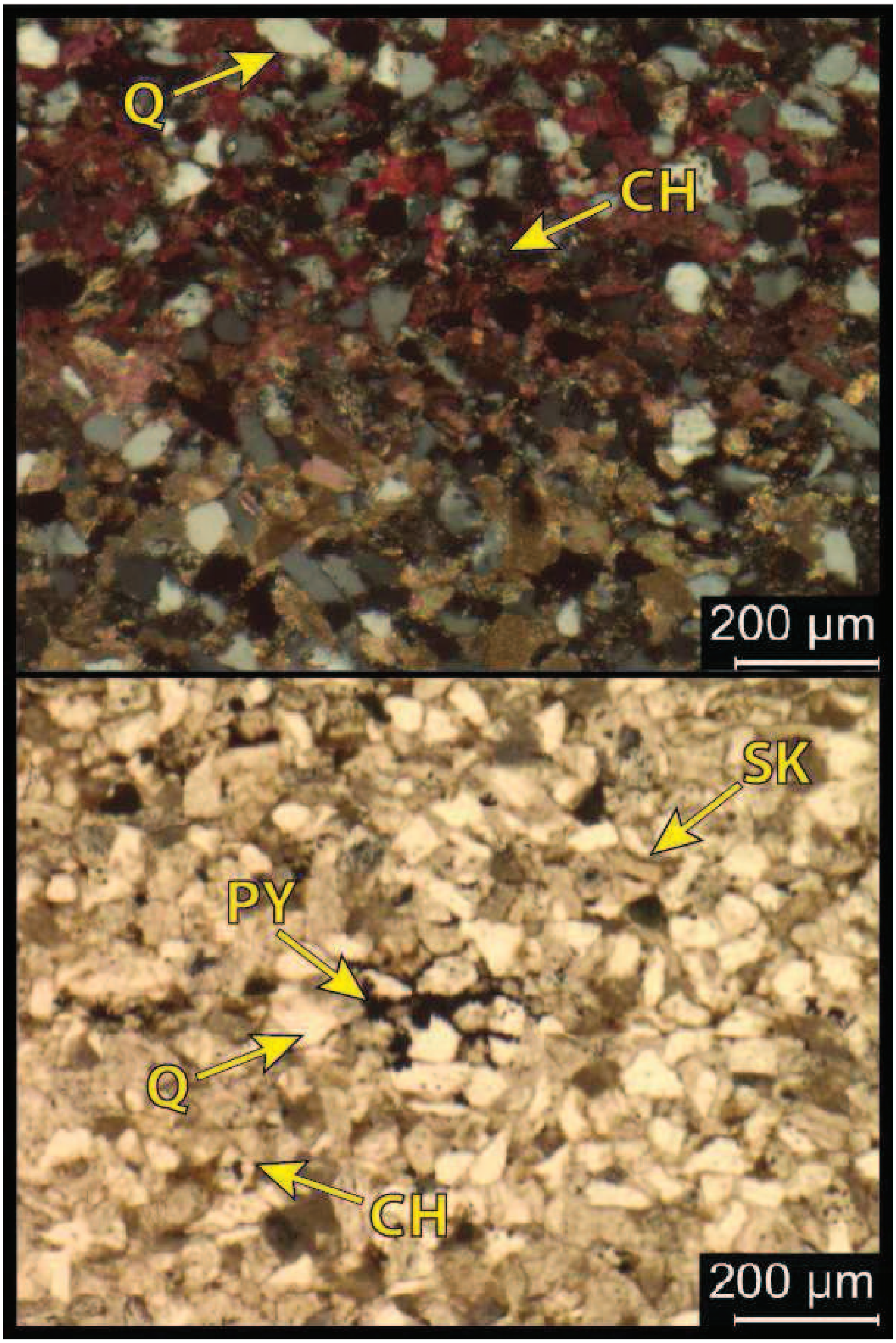

7,970.4': Arenitic packstone/ carbonaceous siltstone-v.f. sandstone. Facies 6. Top: XPL/ alizarin red staIned. Bottom: PPL. Porosity= 2.62%. B.I.: 0-1. Mineralogy: 50.4% quartz (40% silt; 10.4% chert), 32.8% carbonate (30.7% calcite; 2.1% dolomite) and 16.8% other minerals (9.4% feldpsar (8.7% plagioclase; 0.7% K-spar); 6.8% total clay; 0.7% pyrite). Grains: well-sorted quartz silt and undifferentiated skeletal fragments and echinoids of same size. Diagenesis: ~10% silicification; ~10% calcite cementation; 2.1% dolomitization.

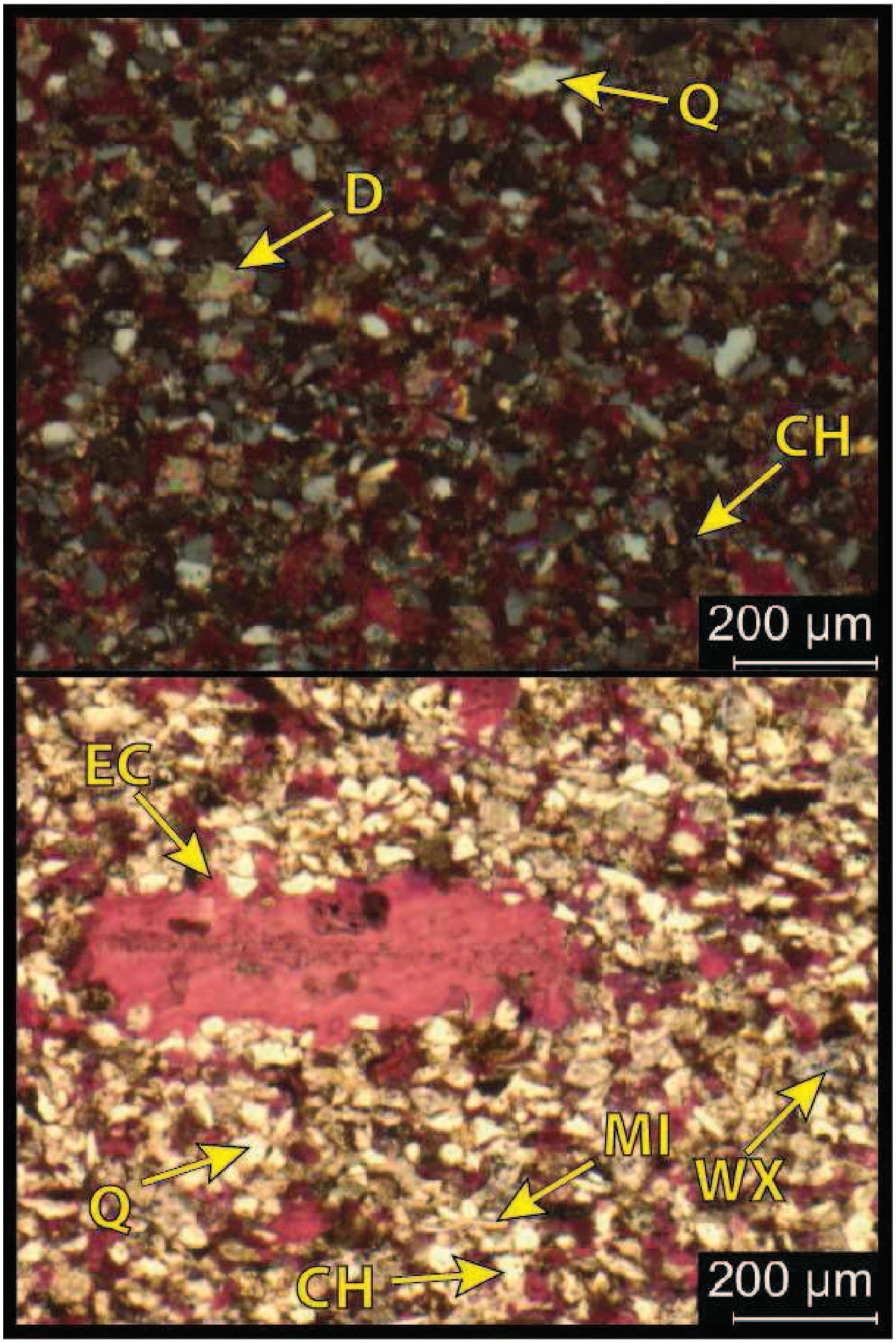

7,939.1': Calcareous, argillaceous siltstone/ Argillaceous silty packstone. Facies 6. Top: XPL/ alizarin red stained. Bottom: PPL/ alizarin red stained. Porosity= 4.1%. B.I.: 0. Mineralogy: 40% quartz (30% silt; 10% chert), 37.5% carbonate (31.8% calcite; 5.7% dolomite) and 22.5% other minerals (10.9% plagioclase; 10.6% total clay; 1% pyrite). Grains: well sorted quartz silt, peloids and undifferentiated skeletal fragments of same size; echinoids (plates up to 200x500µm); sponge spicules. Diagenesis: 10% silicification; 5.7% dolomitization; 5% calcite cementation.

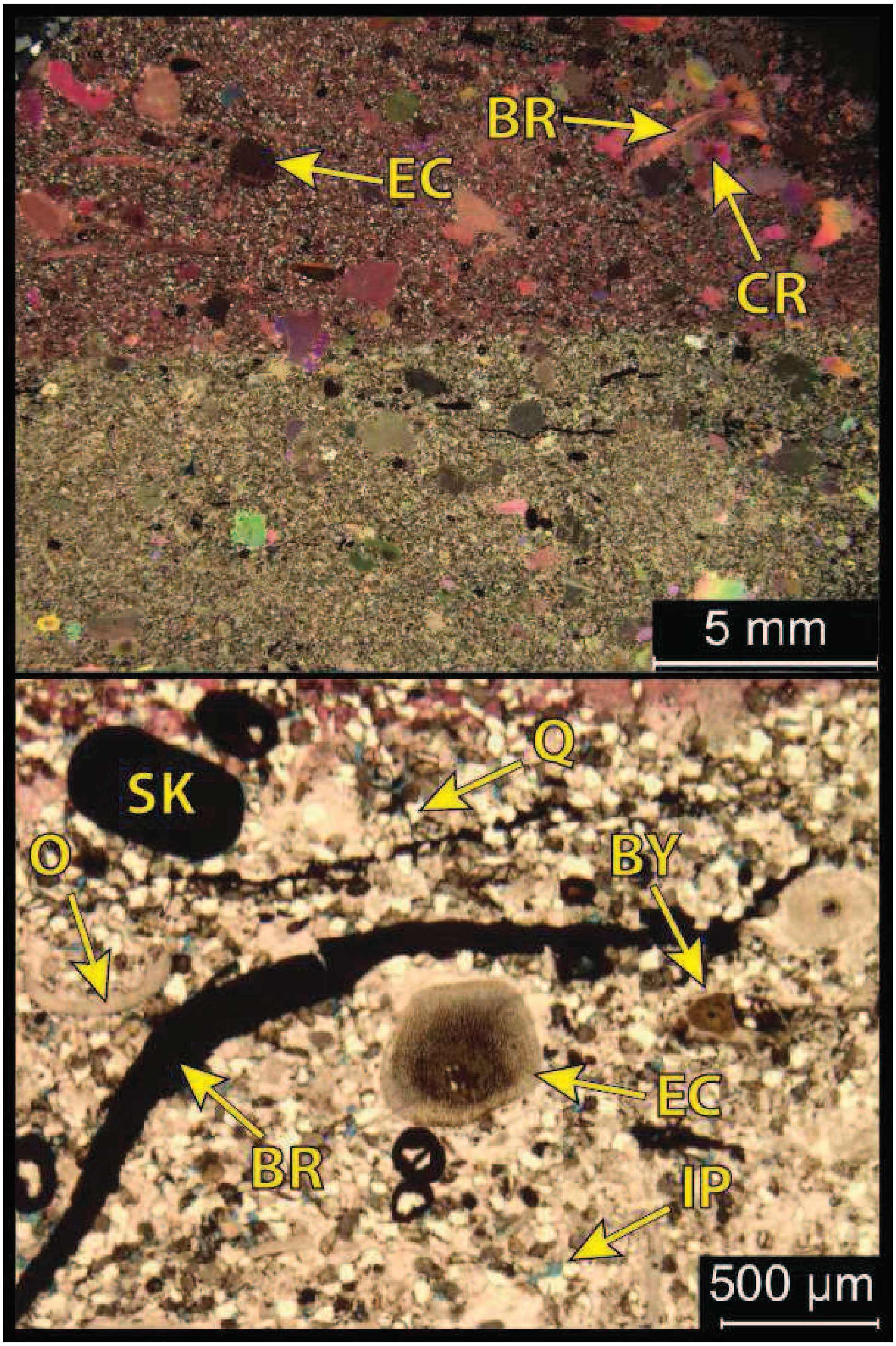

7,930.9': Silty fossiliferous packstone-grainstone. Facies 6. Top: XPL/ ½ alizarin red stained. Bottom: PPL. Porosity= 3.85% (interparticle). B.I.: 0. Mineralogy: 67.7% carbonate (65.9% calcite; 1.8% dolomite), 21.7% quartz (silt) and 10.6% other minerals (4.9% total clay; 4.5% plagioclase; 1.1% pyrite). Grains: quartz silt, peloids (silt-sized), ostracodes (up to 150µm), brachiopods (mm-scale; 200-300µm spines; some micritized/phosphatized), echinoid plates (0.5-1.5mm). Diagenesis: Syntaxial cementation (5%), minor dolomite and pyrite.

III. Moore Unit D #1 Scanning Electron Microscopy and X-Ray Diffraction Analyses on Conventional Core Samples

SEM and XRD analyses and descriptions were performed by Core Laboratories, Inc. through the financial assistance of Marathon Oil Corporation.

Image 1A

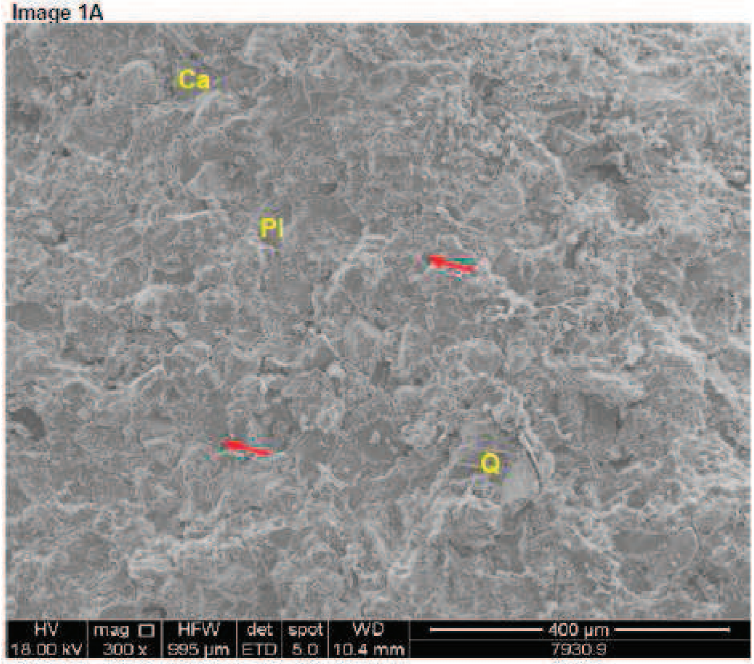

Image 1B

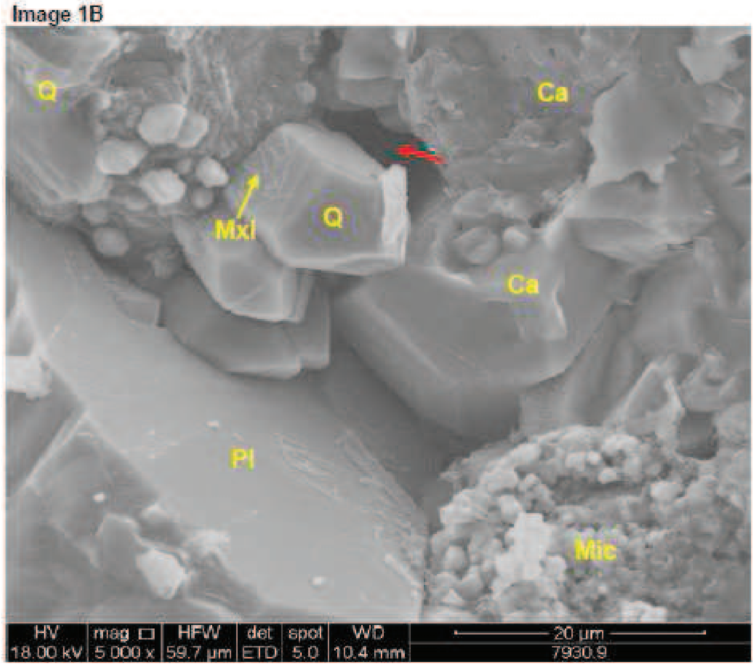

7,930.90': SEM analysis reveals that euhedral to anhedral quartz (Q), subhedral plagioclase (Pl), and calcite crystals (Ca) comprise most of the constituents for this sample. Micrite (mic) is locally observed as matrix for the calcite, plagioclase, and quartz grains. Authigenic mixed-layer illite/smectite (Mxl) is present. Intergranular pores (red arrows) between calcite crystals and quartz grains make up most of the porosity.

XRD-Whole Rock Mineralogy (Weight%): Quartz = 21.7 – K Feldspar = 0.0 – Plagioclase = 4.5 – Calcite = 65.9 – Dolomite & Fe = 1.8 – Pyrite = 1.1 – Total Clays = 4.9. Relative Clay Abundance (weight%): Illite = 2.1 – Chlorite = 1.2 – Kaolinite = 0.0 – Illite/Smectite = 1.6.

Image 2A

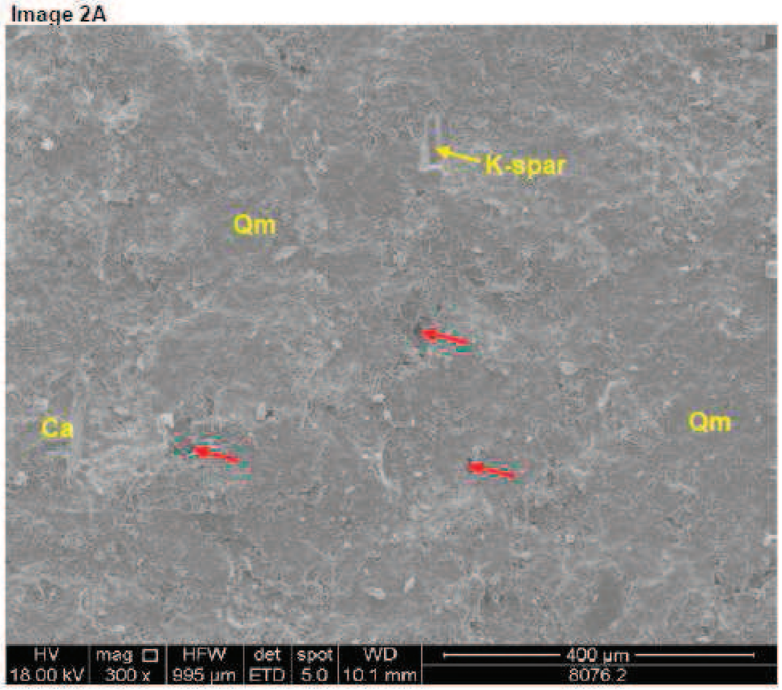

Image 2B

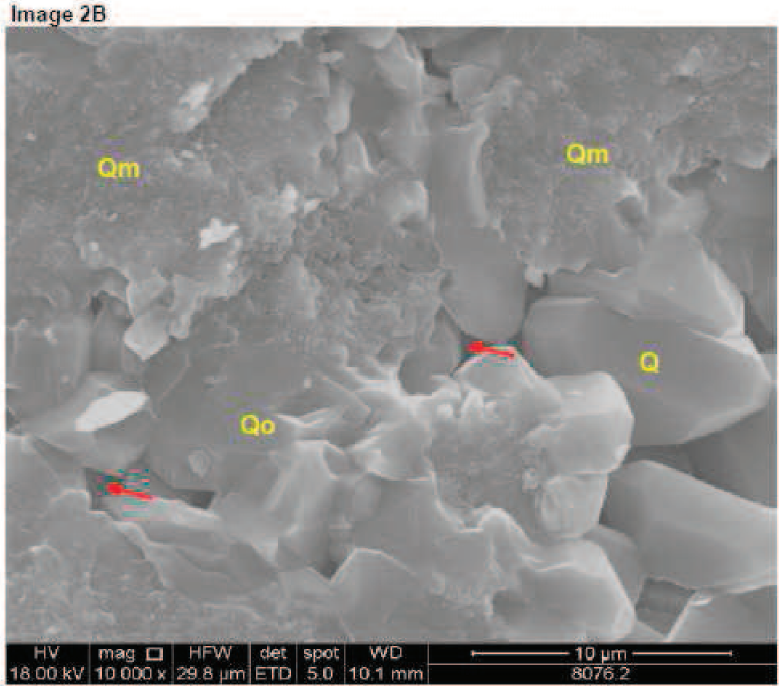

8,076.20’: Silica-rich matrix (Qm) is the predominant constituent in this SEM sample. Euhedral to anhedral quartz grains (Q) are locally observed within the silic-rich matrix. Subhedral calcite crystals (Ca) and potassium feldspar grains (K-spar) are noted in Image 2A. Intergranular pores (red arrows) between quartz grains are abundant throughout the sample.

XRD-Whole Rock Mineralogy (Weight%): Quartz = 87.3 – K Feldspar = 0.4 – Plagioclase = 0.0 – Calcite = 11.7 – Dolomite & Fe = 0.6 – Pyrite = 0.0 – Total Clays 0.0.

Image 3A

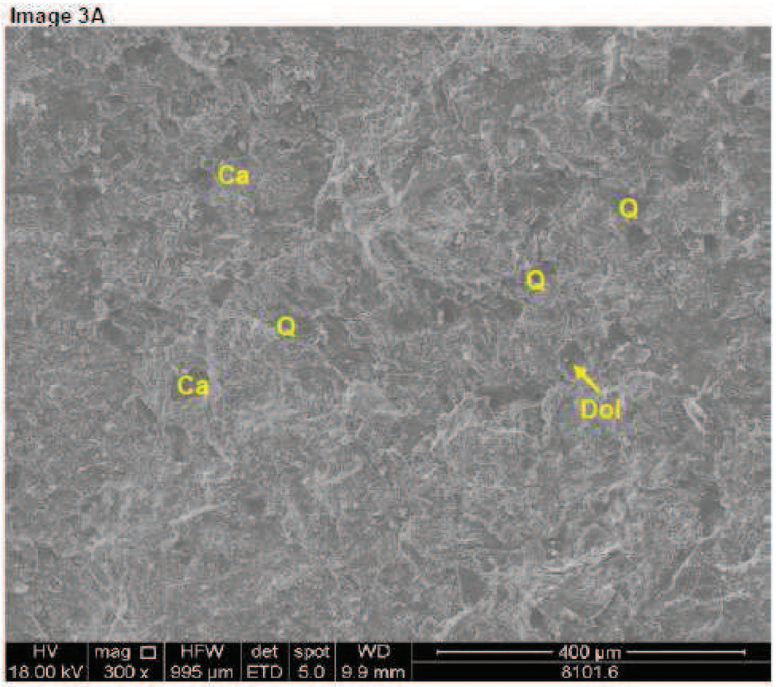

Image 3B

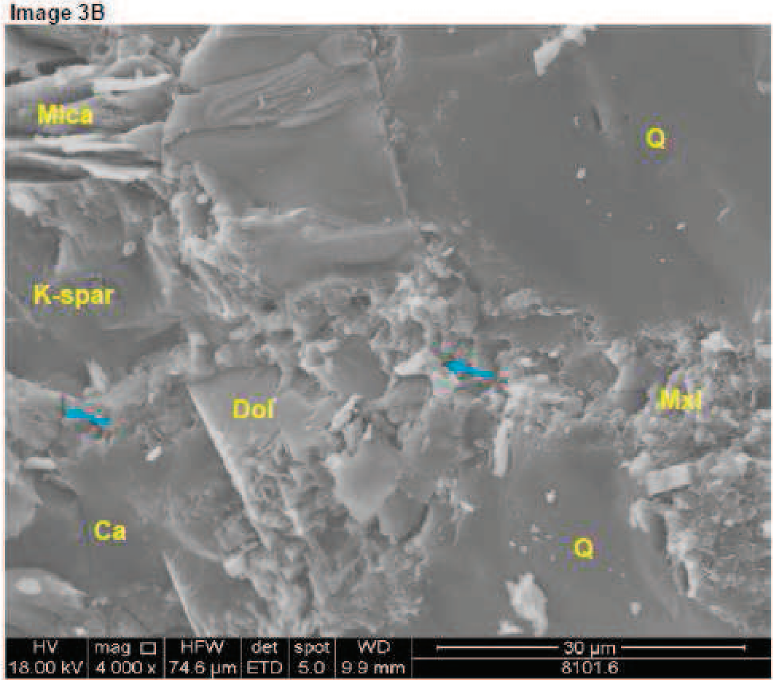

8,101.60': SEM analysis indicates a silica-rich authigenic mixed-layer illite/smectite matrix (Mxl) that surrounds subhedral to anhedral quartz (Q) grains comprise most of the sample constituents. A dolomite (Dol) rhombohedral crystal is observed in the images. A potassium feldspar grain (K-spar), calcite crystal (Ca), and mica are noted in Image 3B. Interparticle micropores (blue arrows) are rare within the mixed-layer illite/smectite.

XRD-Whole Rock Mineralogy (Weight%): Quartz = 30.8 – K Feldspar = 0.0 – Plagioclase = 2.0 – Calcite = 62 – Dolomite & Fe = 1.3 – Pyrite = 0.5 – Total Clays = 3.4. Relative Clay Abundance (weight%): Illite = 2.7 – Chlorite = 0.7 – Kaolinite = 0.0 – Illite/Smectite = 0.0.

Image 4A

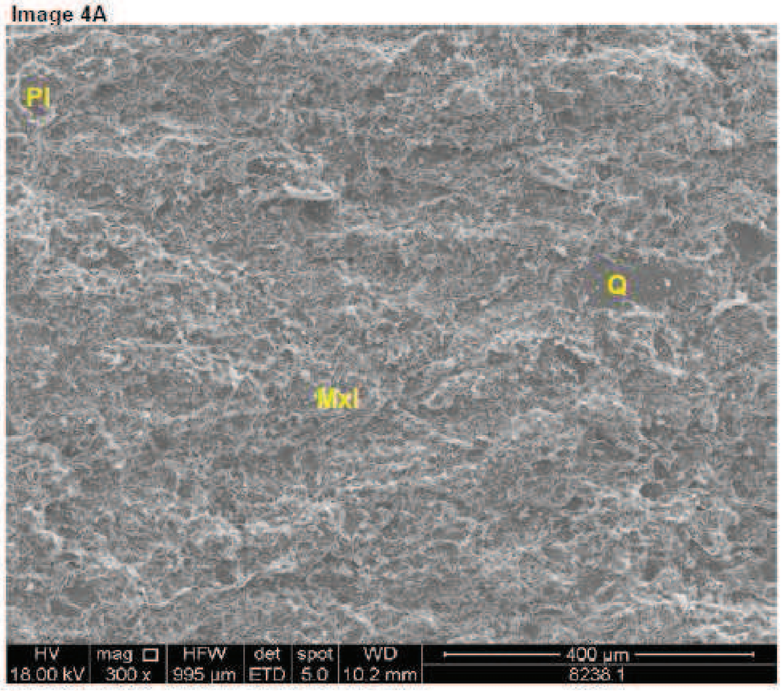

Image 4B

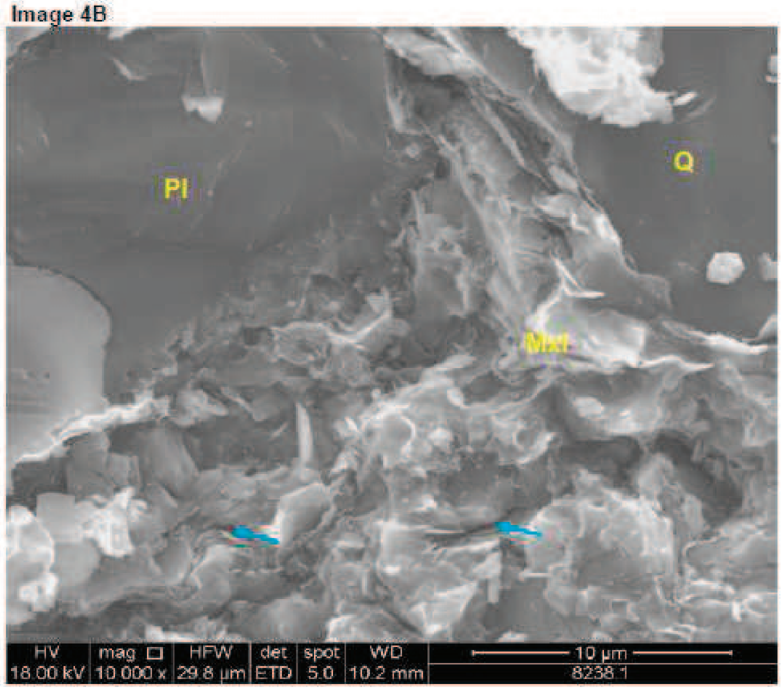

8,238.10': Silica-rich authigenic mixed-layer illite/smectite matrix (Mxl) and subhedral to anhedral quartz grains (Q) are the predominant constituents in this SEM sample. Subhedral plagioclase grains (Pl) are locally observed. Interparticle micropores (blue arrows) are noted between mixed-layer clay flakes and quartz grains within the matrix.
XRD-Whole Rock Mineralogy (Weight%): Quartz = 50 – K Feldspar = 1.9 – Plagioclase = 7.6 – Calcite = 17.5 – Dolomite & Fe = 6.8 – Pyrite = 2.3 – Total Clays = 13.9. Relative Clay Abundance (weight%): Illite = 8.2 – Chlorite = 2.1 – Kaolinite = 0.0 – Illite/Smectite = 3.6.

Image 5A

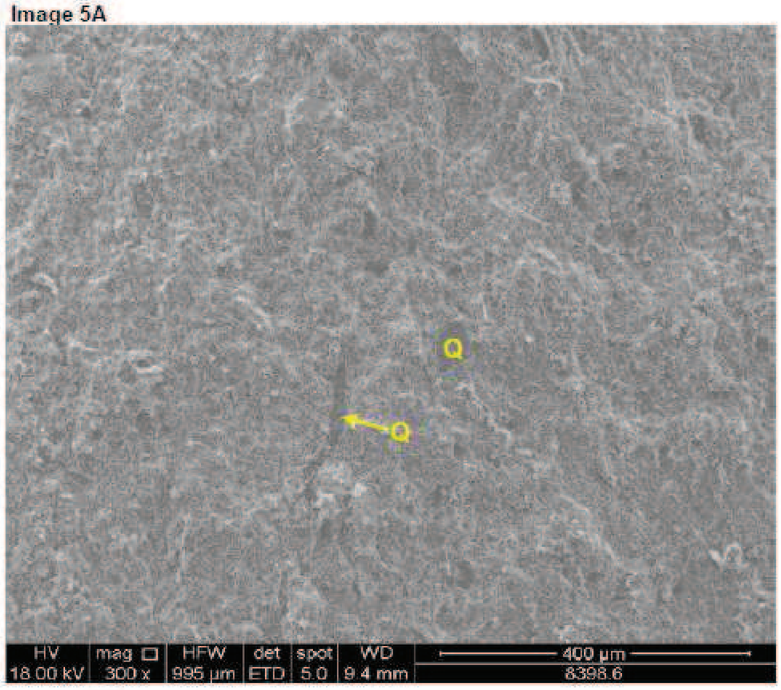

Image 5B

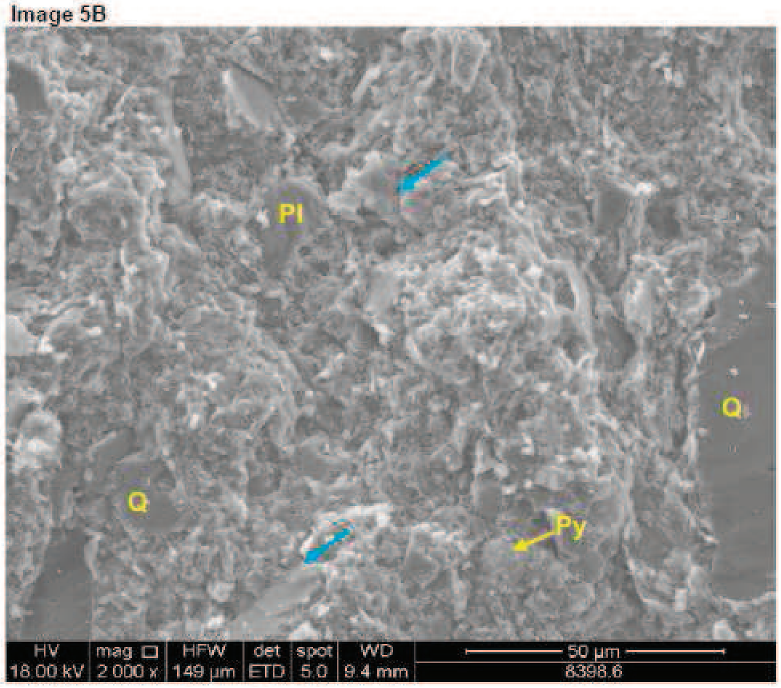

8,398.60': SEM analysis reveals that a silica-rich authigenic mixed-layer illite/smectite (Mxl) matrix is the predominant constituent in this sample. Subhedral to anhedral quartz (Q) are present throughout. Trace anhedral plagioclase (Pl) is locally observed. Framboidal pyrite (Py) is noted in Image 5B. Interparticle micropores (blue arrows) are rare, but indicated within the mixed-layer clay matrix.

XRD- Whole Rock Mineralogy (weight%): Quartz = 44.5 - K Feldspar = 1.0 – Plagioclase = 3.3 – Calcite = 23.5 – Dolomite & Fe = 2.7 – Pyrite = 2.9 – Total Clays = 22.1. Relative Clay Abundance (Weight%): Illite = 13.5 – Chlorite = 1.8 – Kaolinite = 0.0 – Illite/Smectite = 6.8

I. Moore Unit #1 Core Descriptions

Preliminary Core Descriptions

Cores were described using the Dunham classification method. Tracts display (from left to right): thin section description (preliminary), XRD Mineralogy % by Weight (color coded: yellow=silica, blue=calcite, green=dolomite, brown=total clays, pink=feldspars, white=remainder), Depth (ft.), oil staining, thin section location, Sedimentary structures/ Notes, Facies Type (color coded), Lithology (overprinted by symbols to indicate features (burrowing, stylolites, fractures, HCS and chert)), Textural classification (Dunham), Bioturbation (mm-scale horizontal, cm-scale horizontal, mm-scale vertical, cm-scale vertical), Bioturbation Index (using the Bann et al. (2008) classification method), Grain Types, Lamination (Suspension, traction, mottled), Color, Photograph & depth taken, Porosity and Permeabily measurements and Depositional Environment

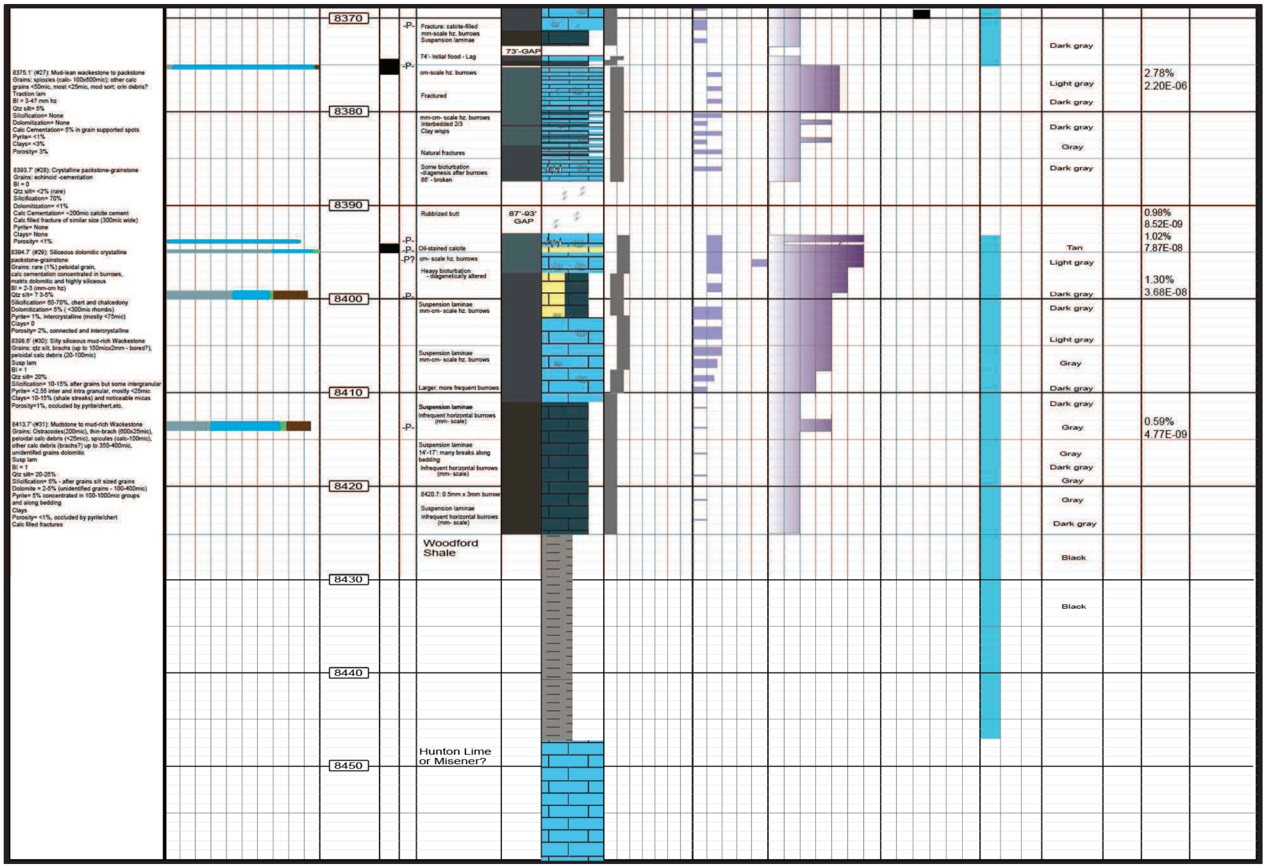

8375.1' (#27): Mud-lean wackestone to packstone
Grains: spicules (calc- 100x600mic); other calc grains <50mic, most <25mic, mod sort; crin debris?
Traction lam
BI = 3-4? mm hz
Qtz silt= 5%
Silicification= None
Dolomitization= None
Calc Cementation= 5% in grain supported spots
Pyrite= <1%
Clays= <3%
Porosity= 3%
8393.7' (#28): Crystalline packstone-grainstone
Grains: echinoid -cementation
BI = 0
Qtz silt= <2% (rare)
Silicification= 70%
Dolomitization= <1%
Calc Cementation= ~200mic calcite cement
Calc filled fracture of similar size (300mic wide)
Pyrite= None
Clays= None
Porosity= <1%
8394.7' (#29): Siliceous dolomitic crystalline packstone-grainstone
Grains: rare (1%) peloidal grain, calc cementation concentrated in burrows, matrix dolomitic and highly siliceous
BI = 2-3 (mm-cm hz)
Qtz silt= ? 3-5%
Silicification= 60-70%, chert and chalcedony
Dolomitization= 5% (<300mic rhombs)
Pyrite= 1%, intercrystalline (mostly <75mic)
Clays= 0
Porosity= 2%, connected and intercrystalline
8398.6' (#30): Silty siliceous mud-rich Wackestone
Grains: qtz silt, brachs (up to 150micx2mm - bored?), peloidal calc debris (20-100mic)
Susp lam
BI = 1
Qtz silt= 20%
Silicification= 10-15% after grains but some intergranular
Pyrite= <2.55 inter and intra granular, mostly <25mic
Clays= 10-15% (shale streaks) and noticeable micas
Porosity=1%, occluded by pyrite/chert,etc.
8413.7' (#31): Mudstone to mud-rich Wackestone
Grains: Ostracodes(200mic), thin-brach (600x25mic), peloidal calc debris (<25mic), spicules (calc-100mic), other calc debris (brachs?) up to 350-400mic, unidentifed grains dolomitic
Susp lam
BI = 1
Qtz silt= 20-25%
Silicification= 5% - after grains silt sized grains
Dolomite = 2-5% (unidentified grains - 100-400mic)
Pyrite= 5% concentrated in 100-1000mic groups and along bedding
Clays
Porosity= <1%, occluded by pyrite/chert
Calc filled fractures
8370
8380
8390
8400
8410
8420
8430
8440
8450
-P-
Fracture: calcite-filled
mm-scale hz. burrows
Suspension laminae
73'-GAP
74' - Initial flood - Lag
-P-
cm-scale hz. burrows
Fractured
mm-cm- scale hz. burrows
Interbedded 2/3
Clay wisps
Natural fractures
Some bioturbation
-diagenesis after burrows
88' - broken
Rubblized butt
87'-93' GAP
-P-
-P-
Oil-stained calcite
-P?
cm- scale hz. burrows
Heavy bioturbation
- diagenetically altered
-P-
Suspension laminae
mm-cm- scale hz. burrows
Suspension laminae
mm-cm- scale hz. burrows
Larger, more frequent burrows
Suspension laminae
Infrequent horizontal burrows (mm- scale)
-P-
Suspension laminae
14'-17': many breaks along bedding
Infrequent horizontal burrows (mm- scale)
8420.7: 0.5mm x 3mm burrow
Suspension laminae
Infrequent horizontal burrows (mm- scale)
Woodford Shale
Hunton Lime or Misener?
Dark gray
Light gray
Dark gray
Dark gray
Gray
Dark gray
Tan
Light gray
Dark gray
Dark gray
Light gray
Gray
Dark gray
Dark gray
Gray
Gray
Dark gray
Gray
Gray
Dark gray
Black
Black
2.78%
2.20E-06
0.98%
8.52E-09
1.02%
7.87E-08
1.30%
3.68E-08
0.59%
4.77E-09

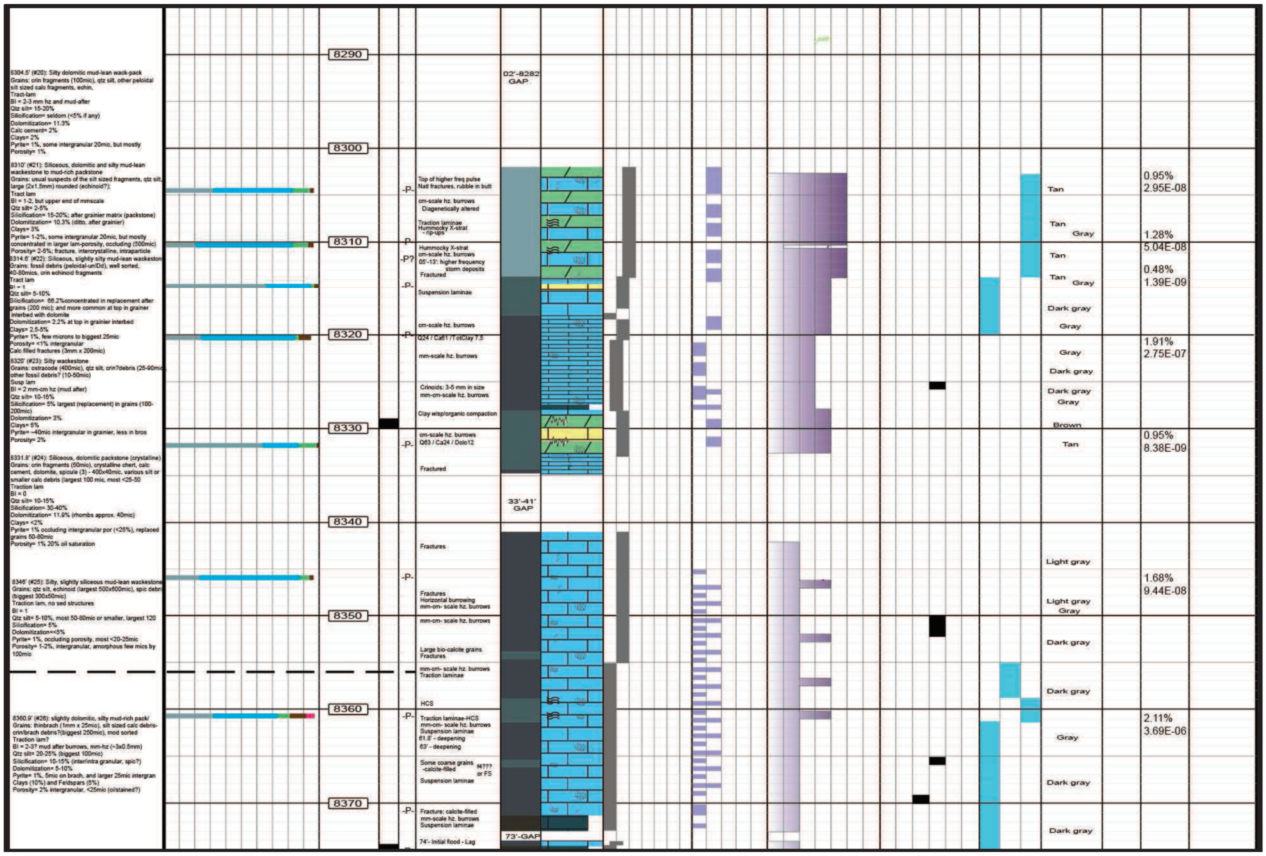
8290
8300
8310
8320
8330
8340
8350
8360
8370
02'-8282' GAP
33'-41' GAP
73'-GAP
Tan
Gray
Dark gray
Brown
Light gray
0.95%
2.95E-08
1.28%
5.04E-08
0.48%
1.39E-09
1.91%
2.75E-07
0.95%
8.38E-09
1.68%
9.44E-08
2.11%
3.69E-06

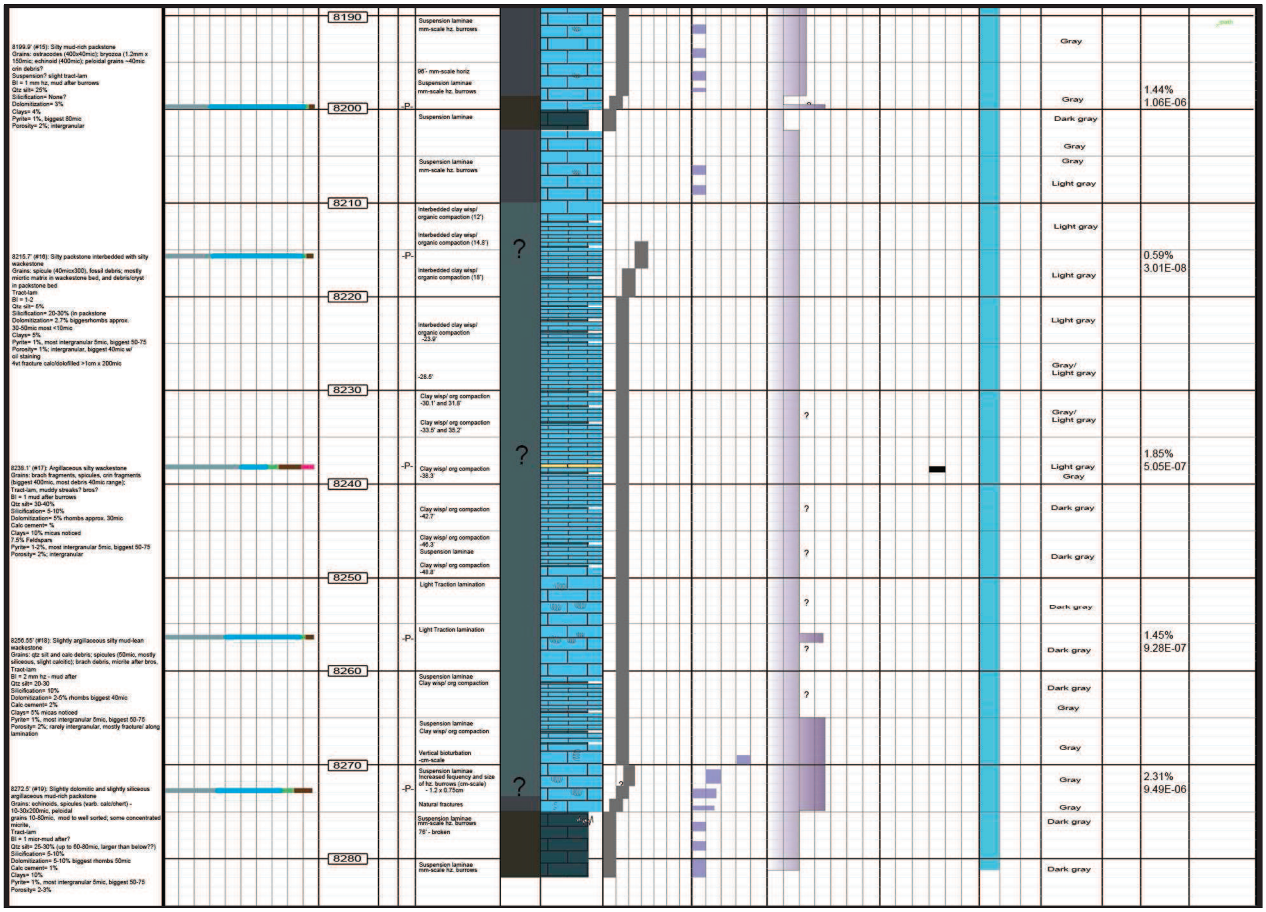
8190
8200
8210
8220
8230
8240
8250
8260
8270
8280
Gray
Gray
Dark gray
Gray
Gray
Light gray
Light gray
Light gray
Light gray
Gray/
Light gray
Gray/
Light gray
Light gray
Gray
Dark gray
Dark gray
Dark gray
Dark gray
Dark gray
Gray
Gray
Gray
Gray
Dark gray
Dark gray
1.44%
1.06E-06
0.59%
3.01E-08
1.85%
5.05E-07
1.45%
9.28E-07
2.31%
9.49E-06

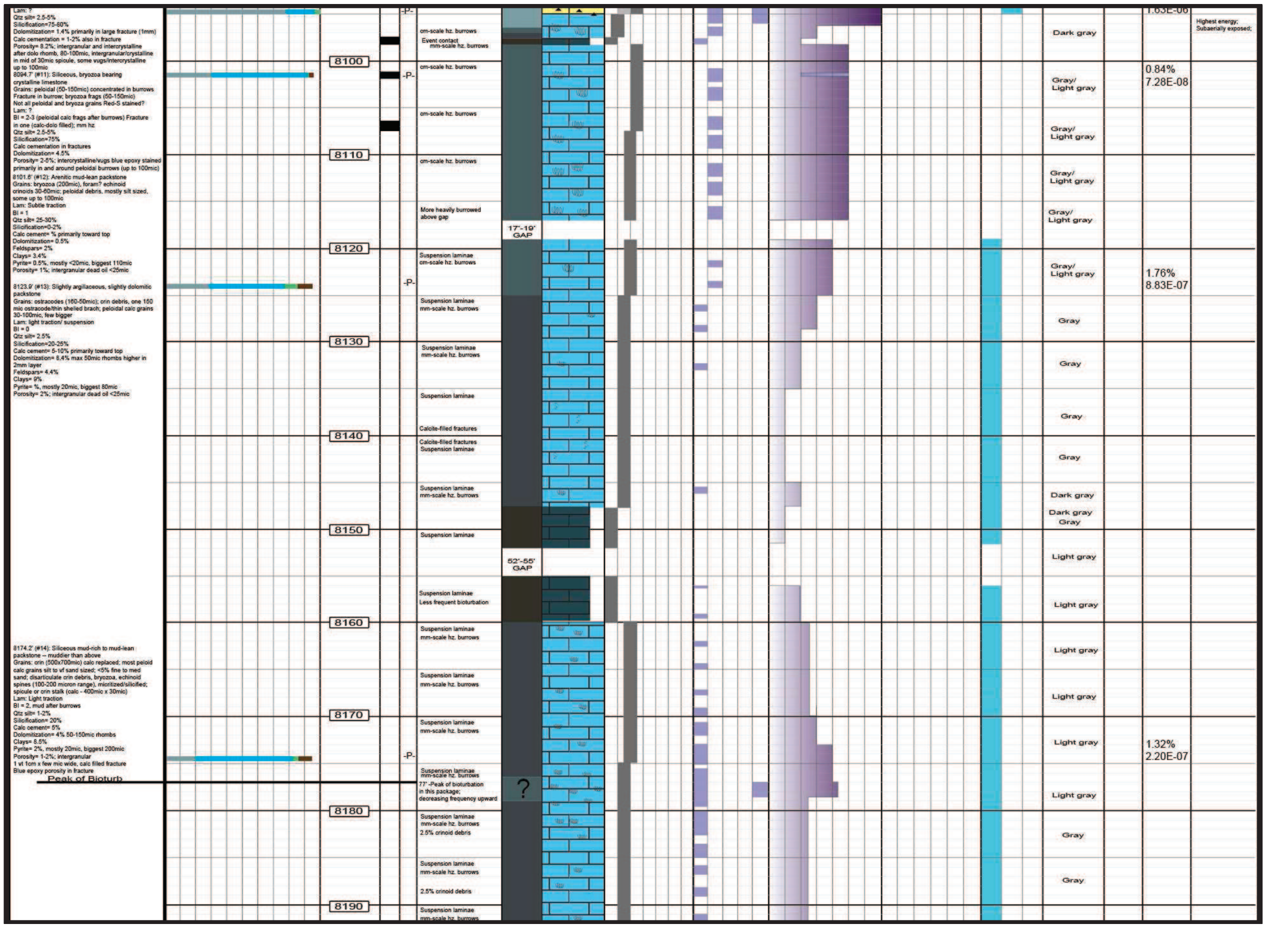

Lam: ?
Qtz silt= 2.5-5%
Silicification=75-80%
Dolomitization= 1.4% primarily in large fracture (1mm)
Calc cementation = 1-2% also in fracture
Porosity= 8.2%; intergranular and intercrystalline after dolo rhomb, 80-100mic, intergranular/crystalline in mid of 30mic spicule, some vugs/intercrystalline up to 100mic
8094.7' (#11): Siliceous, bryozoa bearing crystalline limestone
Grains: peloidal (50-150mic) concentrated in burrows
Fracture in burrow; bryozoa frags (50-150mic)
Not all peloidal and bryoza grains Red-S stained?
Lam: ?
BI = 2-3 (peloidal calc frags after burrows) Fracture in one (calc-dolo filled); mm hz
Qtz silt= 2.5-5%
Silicification=75%
Calc cementation in fractures
Dolomitization= 4.5%
Porosity= 2-5%; intercrystalline/vugs blue epoxy stained primarily in and around peloidal burrows (up to 100mic)
8101.6' (#12): Arenitic mud-lean packstone
Grains: bryozoa (200mic), foram? echinoid crinoids 30-60mic; peloidal debris, mostly silt sized, some up to 100mic
Lam: Subtle traction
BI = 1
Qtz silt= 25-30%
Silicification=0-2%
Calc cement= % primarily toward top
Dolomitization= 0.5%
Feldspars= 2%
Clays= 3.4%
Pyrite= 0.5%, mostly <20mic, biggest 110mic
Porosity= 1%; intergranular dead oil <25mic
8123.9' (#13): Slightly argillaceous, slightly dolomitic packstone
Grains: ostracodes (160-50mic); crin debris, one 150 mic ostracode/thin shelled brach; peloidal calc grains 30-100mic, few bigger
Lam: light traction/ suspension
BI = 0
Qtz silt= 2.5%
Silicification=20-25%
Calc cement= 5-10% primarily toward top
Dolomitization= 8.4% max 50mic rhombs higher in 2mm layer
Feldspars= 4.4%
Clays= 9%
Pyrite= %, mostly 20mic, biggest 80mic
Porosity= 2%; intergranular dead oil <25mic
8174.2' (#14): Siliceous mud-rich to mud-lean packstone -- muddier than above
Grains: crin (500x700mic) calc replaced; most peloid calc grains silt to vf sand sized; <5% fine to med sand; disarticulate crin debris, bryozoa, echinoid spines (100-200 micron range), micritized/silicified; spicule or crin stalk (calc - 400mic x 30mic)
Lam: Light traction
BI = 2, mud after burrows
Qtz silt= 1-2%
Silicification= 20%
Calc cement= 5%
Dolomitization= 4% 50-150mic rhombs
Clays= 8.5%
Pyrite= 2%, mostly 20mic, biggest 200mic
Porosity= 1-2%; intergranular
1 vt 1cm x few mic wide, calc filled fracture
Blue epoxy porosity in fracture
Peak of Bioturb
8100
8110
8120
8130
8140
8150
8160
8170
8180
8190
-P-
-P-
-P-
-P-
cm-scale hz. burrows
Event contact
mm-scale hz. burrows
cm-scale hz. burrows
cm-scale hz. burrows
cm-scale hz. burrows
More heavily burrowed above gap
17'-19' GAP
Suspension laminae
cm-scale hz. burrows
Suspension laminae
mm-scale hz. burrows
Suspension laminae
mm-scale hz. burrows
Suspension laminae
Calcite-filled fractures
Calcite-filled fractures
Suspension laminae
Suspension laminae
mm-scale hz. burrows
Suspension laminae
52'-55' GAP
Suspension laminae
Less frequent bioturbation
Suspension laminae
mm-scale hz. burrows
Suspension laminae
mm-scale hz. burrows
Suspension laminae
mm-scale hz. burrows
Suspension laminae
mm-scale hz. burrows
77' -Peak of bioturbation in this package; decreasing frequency upward
?
Suspension laminae
mm-scale hz. burrows
2.5% crinoid debris
Suspension laminae
mm-scale hz. burrows
2.5% crinoid debris
Suspension laminae
mm-scale hz. burrows
Dark gray
Gray/ Light gray
Gray/ Light gray
Gray/ Light gray
Gray/ Light gray
Gray/ Light gray
Gray
Gray
Gray
Gray
Dark gray
Dark gray
Gray
Light gray
Light gray
Light gray
Light gray
Light gray
Light gray
Gray
Gray
0.84%
7.28E-08
1.76%
8.83E-07
1.32%
2.20E-07
Highest energy; Subaerially exposed;

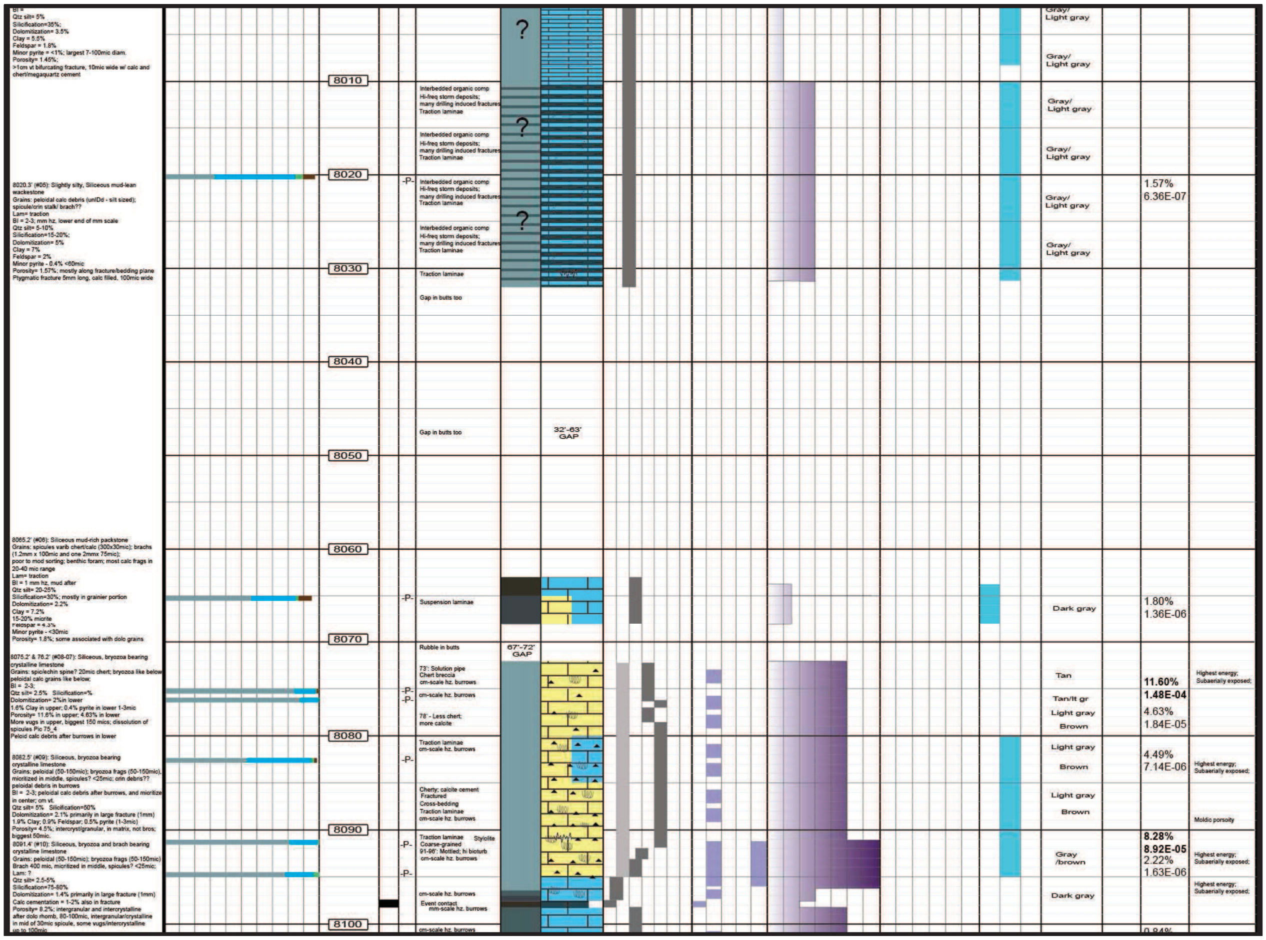

Qtz silt= 5%
Silicification=35%;
Dolomitization= 3.5%
Clay = 5.5%
Feldspar = 1.8%
Minor pyrite = <1%; largest 7-100mic diam.
Porosity= 1.45%;
>1cm vt bifurcating fracture, 10mic wide w/ calc and chert/megaquartz cement
8010
Interbedded organic comp
Hi-freq storm deposits;
many drilling induced fractures
Traction laminae
?
Gray/
Light gray
8020
-P-
8020.3' (#05): Slightly silty, Siliceous mud-lean wackestone
Grains: peloidal calc debris (unIDd - silt sized); spicule/crin stalk/ brach??
Lam= traction
BI = 2-3; mm hz, lower end of mm scale
Qtz silt= 5-10%
Silicification=15-20%;
Dolomitization= 5%
Clay = 7%
Feldspar = 2%
Minor pyrite - 0.4% <60mic
Porosity= 1.57%; mostly along fracture/bedding plane
Ptygmatic fracture 5mm long, calc filled, 100mic wide
1.57%
6.36E-07
8030
Traction laminae
Gap in butts too
8040
32'-63'
GAP
8050
8060
8065.2' (#06): Siliceous mud-rich packstone
Grains: spicules varib chert/calc (300x30mic); brachs (1.2mm x 100mic and one 2mmx 75mic);
poor to mod sorting; benthic foram; most calc frags in 20-40 mic range
Lam= traction
BI = 1 mm hz, mud after
Qtz silt= 20-25%
Silicification=30%; mostly in grainier portion
Dolomitization= 2.2%
Clay = 7.2%
15-20% micrite
Feldspar = 4.3%
Minor pyrite - <30mic
Porosity= 1.8%; some associated with dolo grains
Suspension laminae
Dark gray
1.80%
1.36E-06
8070
Rubble in butts
67'-72'
GAP
8075.2' & 76.2' (#08-07): Siliceous, bryozoa bearing crystalline limestone
Grains: spic/echin spine? 20mic chert; bryozoa like below peloidal calc grains like below;
BI = 2-3;
Qtz silt= 2.5% Silicification=%
Dolomitization= 2%in lower
1.6% Clay in upper; 0.4% pyrite in lower 1-3mic
Porosity= 11.6% in upper; 4.63% in lower
More vugs in upper, biggest 150 mics; dissolution of spicules Pic 75_4
Peloid calc debris after burrows in lower
73': Solution pipe
Chert breccia
cm-scale hz. burrows
78' - Less chert;
more calcite
Tan
Tan/lt gr
Light gray
Brown
11.60%
1.48E-04
4.63%
1.84E-05
Highest energy;
Subaerially exposed;
8080
8082.5' (#09): Siliceous, bryozoa bearing crystalline limestone
Grains: peloidal (50-150mic); bryozoa frags (50-150mic), micritized in middle, spicules? <25mic; crin debris??
peloidal debris in burrows
BI = 2-3; peloidal calc debris after burrows, and micritize in center; cm vt.
Qtz silt= 5% Silicification=50%
Dolomitization= 2.1% primarily in large fracture (1mm)
1.9% Clay; 0.9% Feldspar; 0.5% pyrite (1-3mic)
Porosity= 4.5%; intercryst/granular, in matrix, not bros; biggest 50mic.
Traction laminae
cm-scale hz. burrows
Cherty; calcite cement
Fractured
Cross-bedding
Light gray
Brown
4.49%
7.14E-06
Moldic porsoity
8090
8091.4' (#10): Siliceous, bryozoa and brach bearing crystalline limestone
Grains: peloidal (50-150mic); bryozoa frags (50-150mic)
Brach 400 mic, micritized in middle, spicules? <25mic;
Lam: ?
Qtz silt= 2.5-5%
Silicification=75-80%
Dolomitization= 1.4% primarily in large fracture (1mm)
Calc cementation = 1-2% also in fracture
Porosity= 8.2%; intergranular and intercrystalline after dolo rhomb, 80-100mic, intergranular/crystalline in mid of 30mic spicule, some vugs/intercrystalline up to 100mic
Traction laminae
Stylolite
Coarse-grained
91-96': Mottled; hi bioturb
Gray
/brown
8.28%
8.92E-05
2.22%
1.63E-06
Event contact
mm-scale hz. burrows
Dark gray
8100

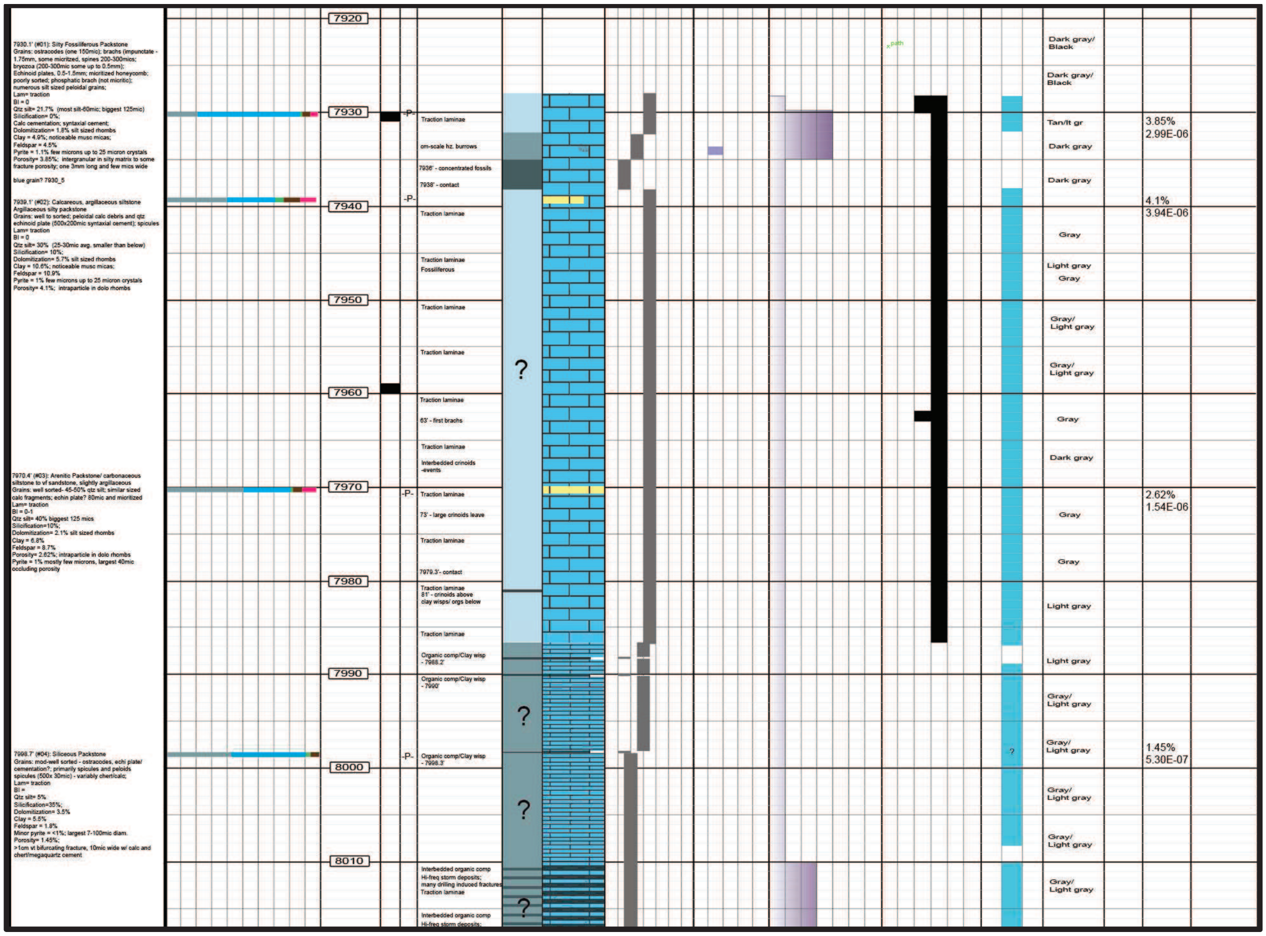
7920
7930
7940
7950
7960
7970
7980
7990
8000
8010
Dark gray/ Black
Dark gray/ Black
Tan/lt gr
Dark gray
Dark gray
Gray
Light gray
Gray
Gray/ Light gray
Gray/ Light gray
Gray
Dark gray
Gray
Gray
Light gray
Light gray
Gray/ Light gray
Gray/ Light gray
Gray/ Light gray
Gray/ Light gray
Gray/ Light gray
3.85%
2.99E-06
4.1%
3.94E-06
2.62%
1.54E-06
1.45%
5.30E-07

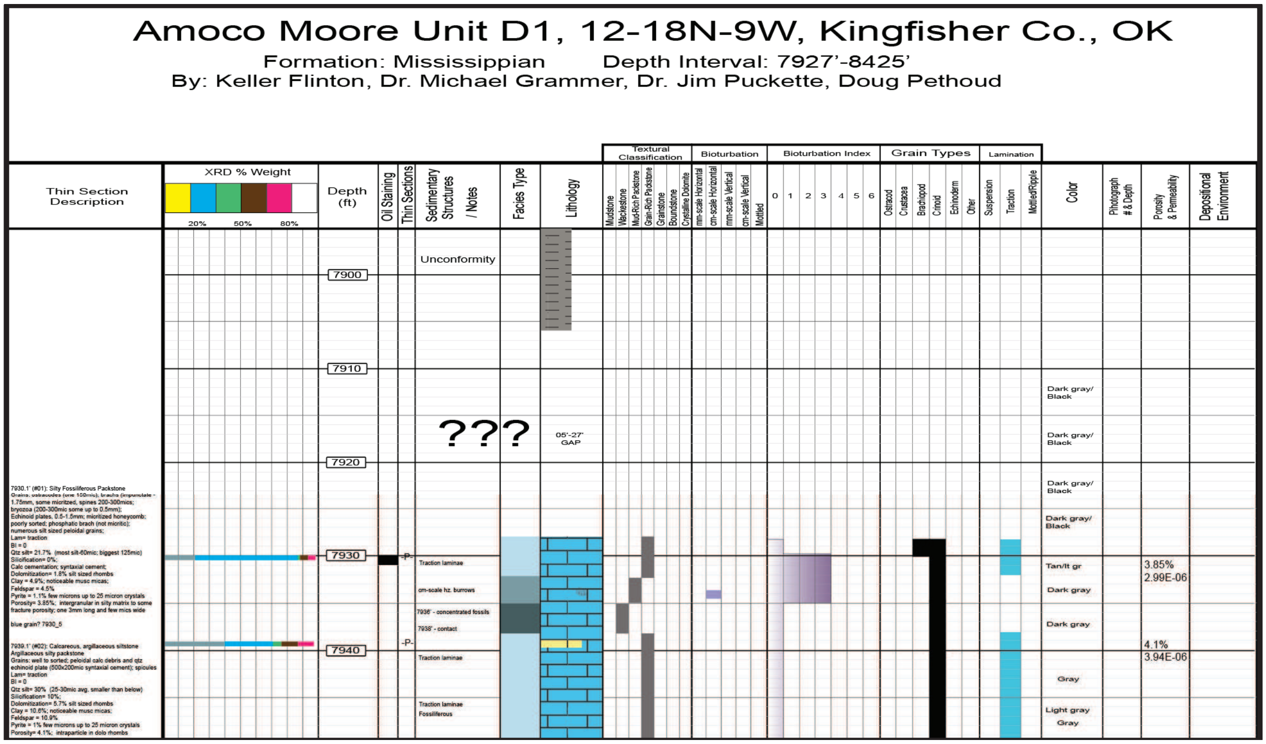

Amoco Moore Unit D1, 12-18N-9W, Kingfisher Co., OK
Formation: Mississippian
Depth Interval: 7927'-8425'
By: Keller Flinton, Dr. Michael Grammer, Dr. Jim Puckette, Doug Pethoud
Thin Section Description
XRD % Weight
20%
50%
80%
Depth (ft)
Oil Staining
Thin Sections
Sedimentary Structures / Notes
Facies Type
Lithology
Textural Classification
Mudstone
Wackestone
Mud-Rich Packstone
Grain-Rich Packstone
Grainstone
Boundstone
Crystalline Dolomite
Bioturbation
mm-scale Horizontal
cm-scale Horizontal
mm-scale Vertical
cm-scale Vertical
Mottled
Bioturbation Index
0 1 2 3 4 5 6
Grain Types
Ostracod
Crustacea
Brachiopod
Crinoid
Echinoderm
Other
Lamination
Suspension
Traction
Mottled/Ripple
Color
Photograph # & Depth
Porosity & Permeability
Depositional Environment
7900
7910
7920
7930
7940
Unconformity
???
05'-27' GAP
Traction laminae
cm-scale hz. burrows
7936' - concentrated fossils
7938' - contact
Traction laminae
Traction laminae
Fossiliferous
-P-
-P-
Dark gray/ Black
Dark gray/ Black
Dark gray/ Black
Dark gray/ Black
Tan/lt gr
Dark gray
Dark gray
Gray
Light gray
Gray
3.85%
2.99E-06
4.1%
3.94E-06
7930.1' (#01): Silty Fossiliferous Packstone
Grains: ostracodes (one 150mic); brachs (impunctate - 1.75mm, some micritzed, spines 200-300mics; bryozoa (200-300mic some up to 0.5mm); Echinoid plates, 0.5-1.5mm; micritized honeycomb; poorly sorted; phosphatic brach (not micritic); numerous silt sized peloidal grains;
Lam= traction
BI = 0
Qtz silt= 21.7% (most silt-60mic; biggest 125mic)
Silicification= 0%;
Calc cementation; syntaxial cement;
Dolomitization= 1.8% silt sized rhombs
Clay = 4.9%; noticeable musc micas;
Feldspar = 4.5%
Pyrite = 1.1% few microns up to 25 micron crystals
Porosity= 3.85%; intergranular in silty matrix to some fracture porosity; one 3mm long and few mics wide
blue grain? 7930_5
7939.1' (#02): Calcareous, argillaceous siltstone
Argillaceous silty packstone
Grains: well to sorted; peloidal calc debris and qtz echinoid plate (500x200mic syntaxial cement); spicules
Lam= traction
BI = 0
Qtz silt= 30% (25-30mic avg. smaller than below)
Silicification= 10%;
Dolomitization= 5.7% silt sized rhombs
Clay = 10.6%; noticeable musc micas;
Feldspar = 10.9%
Pyrite = 1% few microns up to 25 micron crystals
Porosity= 4.1%; intraparticle in dolo rhombs

Core-to-Wireline Log Tie

From left to right: Gamma Ray curve (0-110 API Units), Guard Resistivity curve (black = 0-50, blue = 0-500, red = 0-5,000 Ohms/m), Sequence stratigraphic hierarchy, Depth (ft.) Dunham erosional profile, Diagenetic effects.

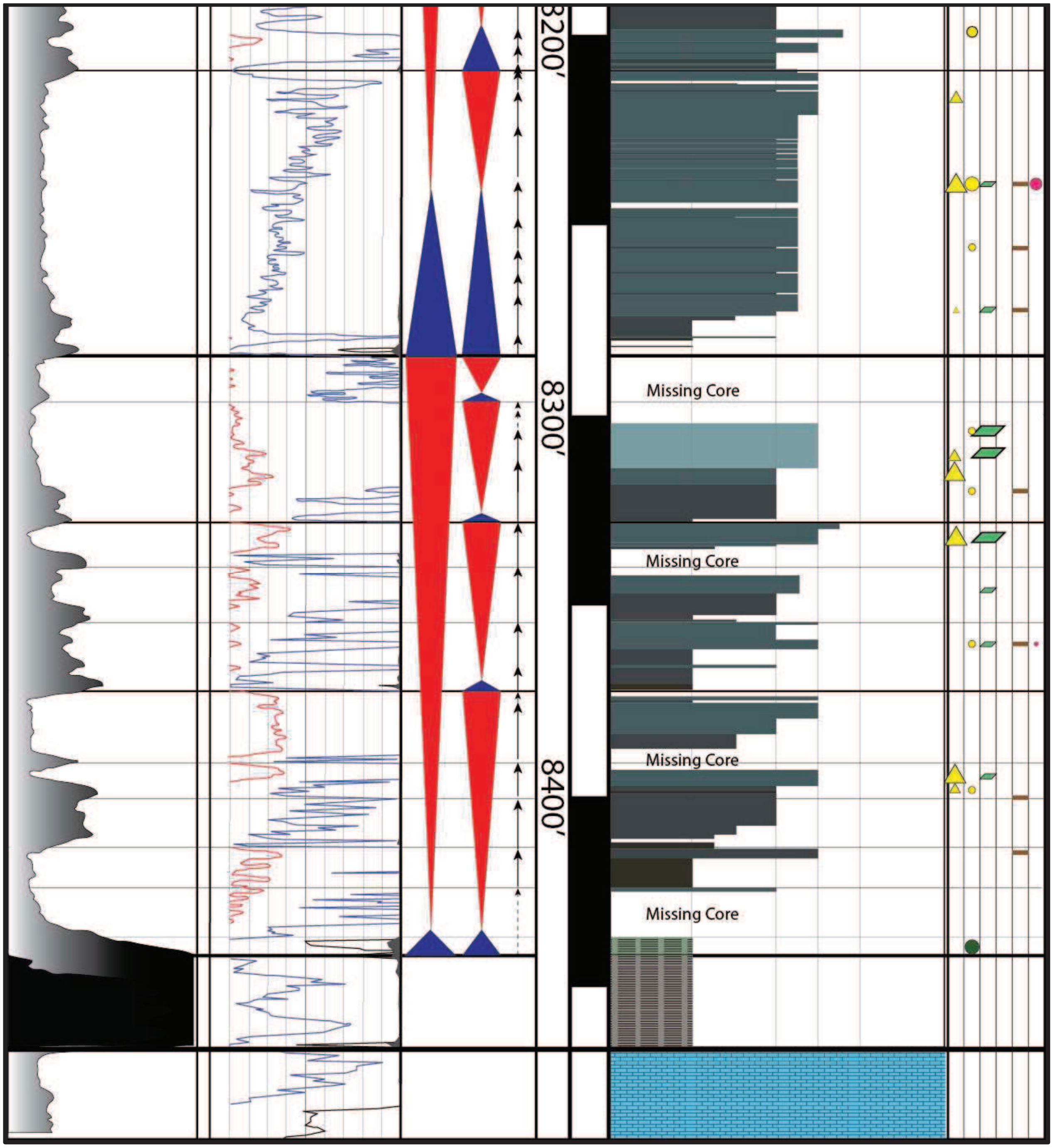
8200'
8300'
8400'
Missing Core
Missing Core
Missing Core
Missing Core

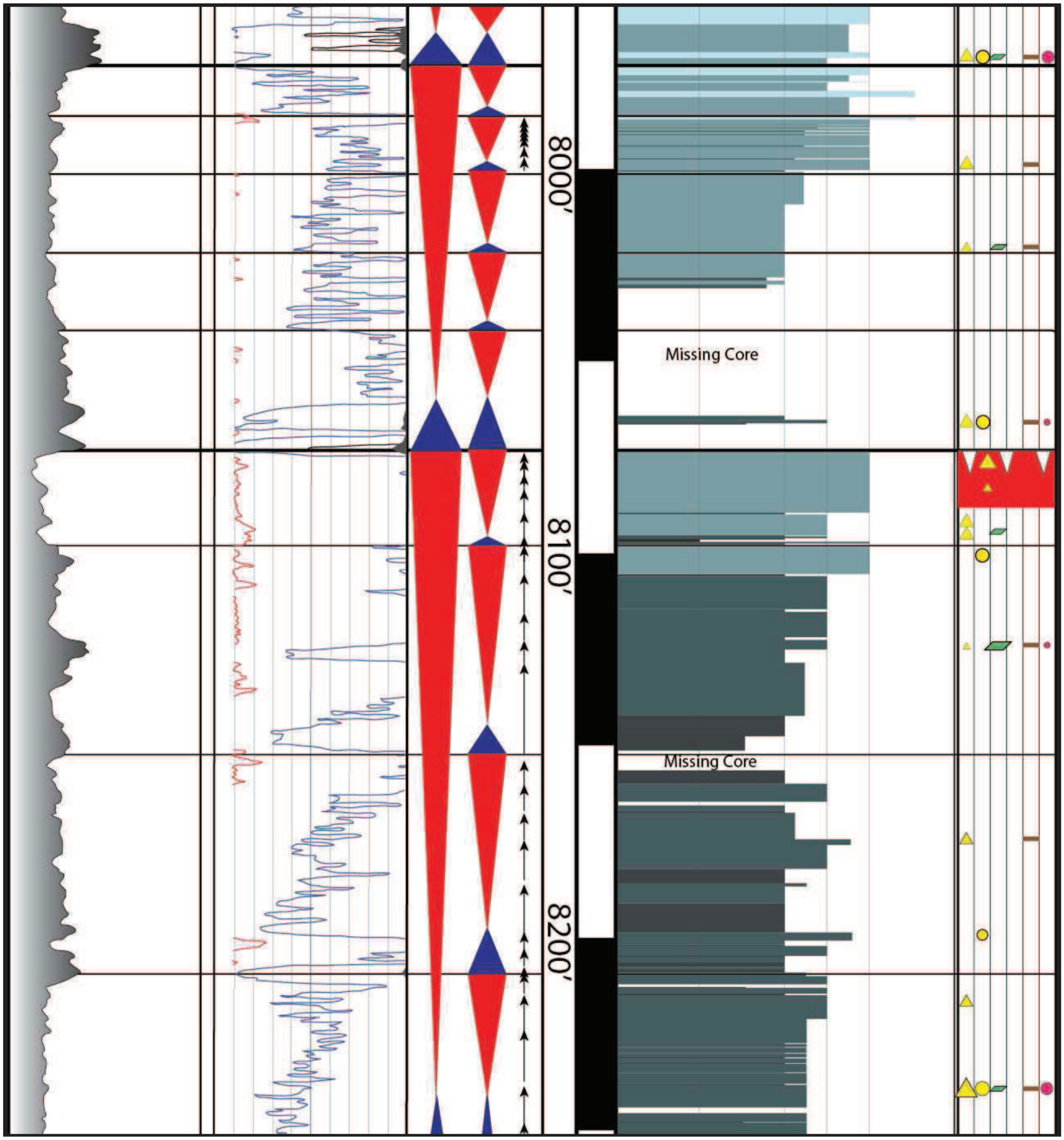
8000'
8100'
8200'
Missing Core
Missing Core

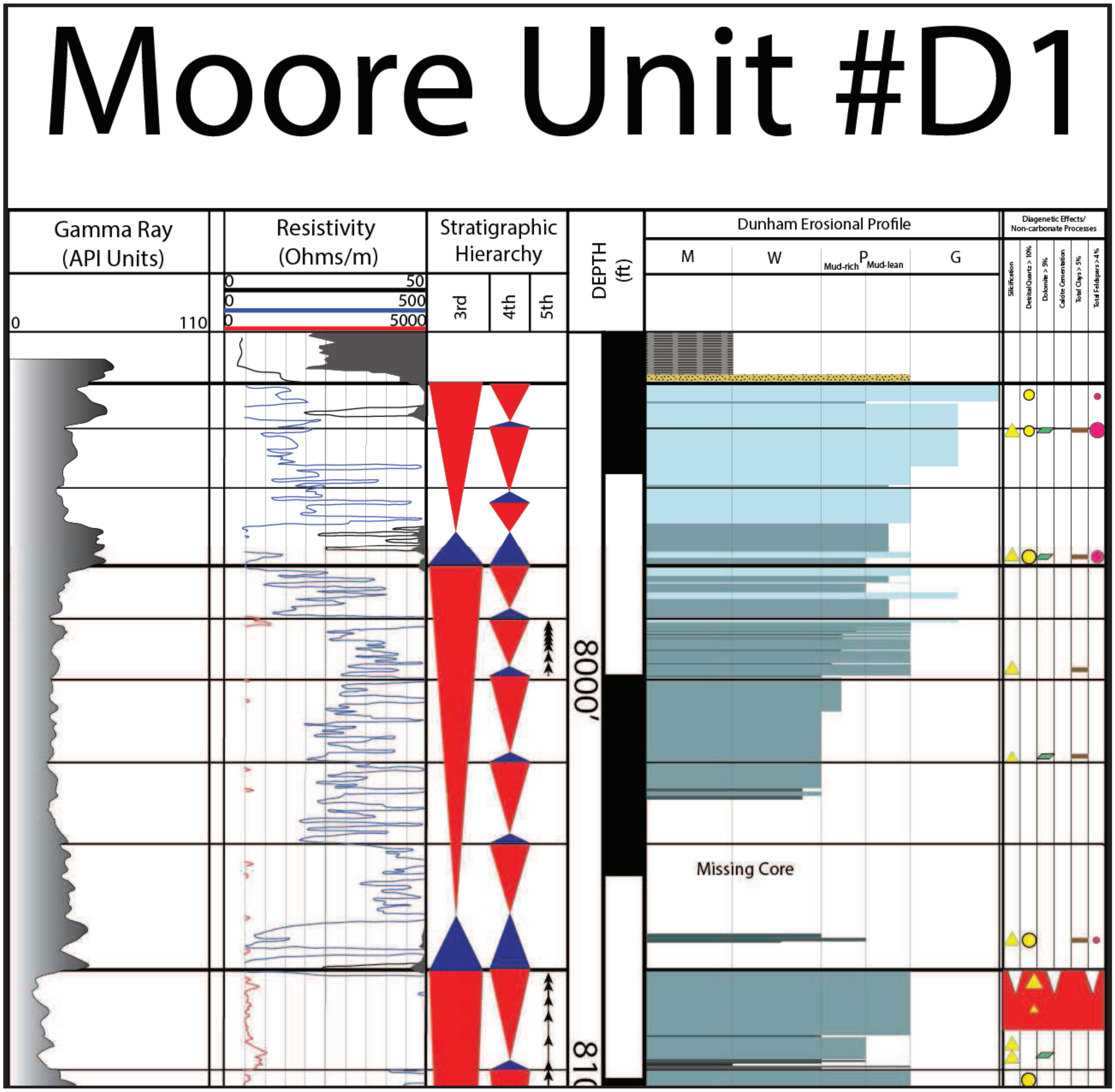
Moore Unit #D1
Gamma Ray
(API Units)
0
110
Resistivity
(Ohms/m)
0 50
0 500
0 5000
Stratigraphic
Hierarchy
3rd
4th
5th
DEPTH
(ft)
8000'
810
Dunham Erosional Profile
M
W
P
Mud-rich
Mud-lean
G
Missing Core
Diagenetic Effects/
Non-carbonate Processes

APPENDIX C

Droke Unit #1
Sec. 4 – T. 18N – R. 9W

I. Droke Unit #1 Core Photographs

Core butts of the Droke Unit #1 are 3.5 inches in width and are oriented with the top ("younger") up. Please refer to Table 6 for abbreviations.

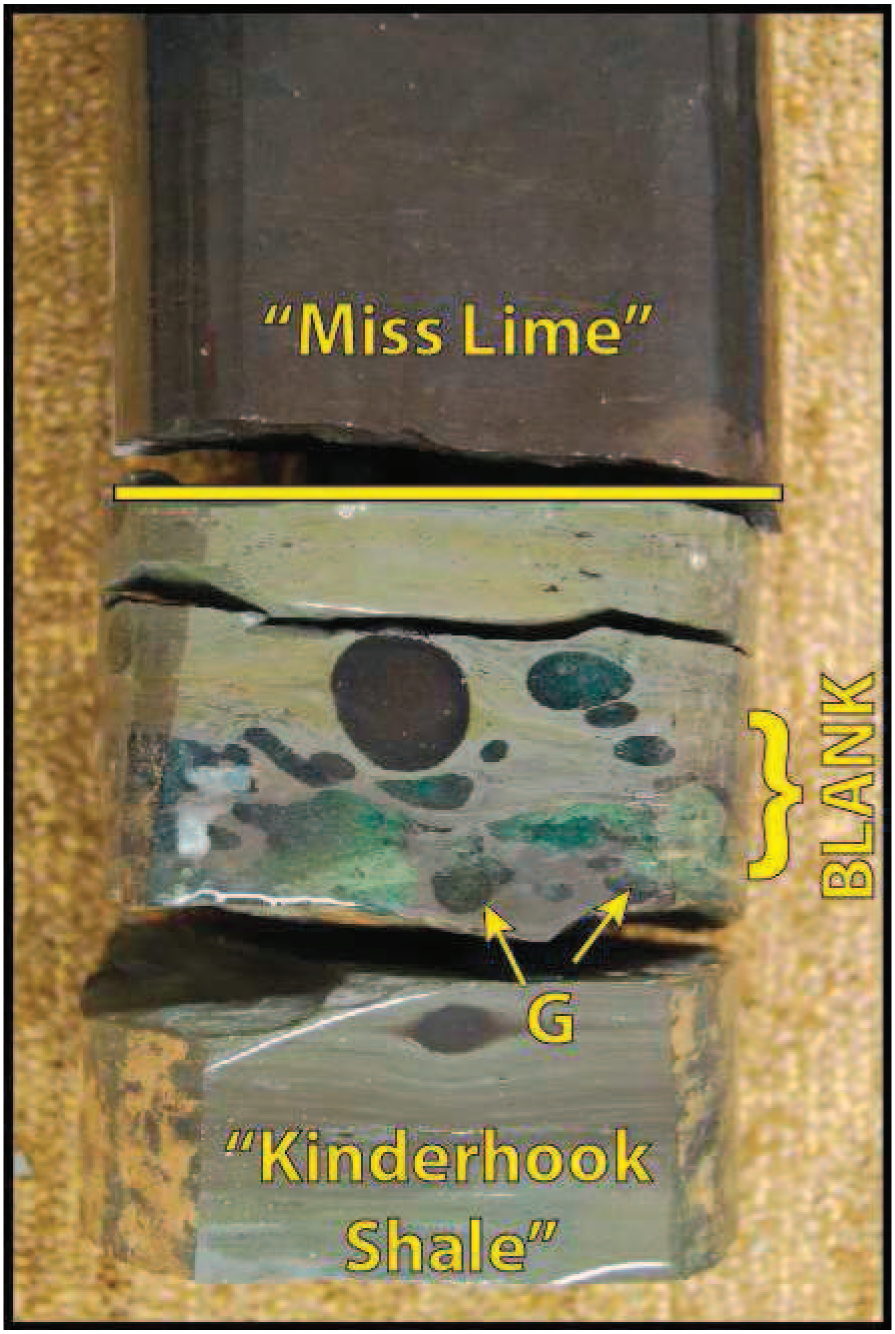

8,449-8,450': Facies 1 "Kinderhook" Shale (bottom) and Facies 2 (top)

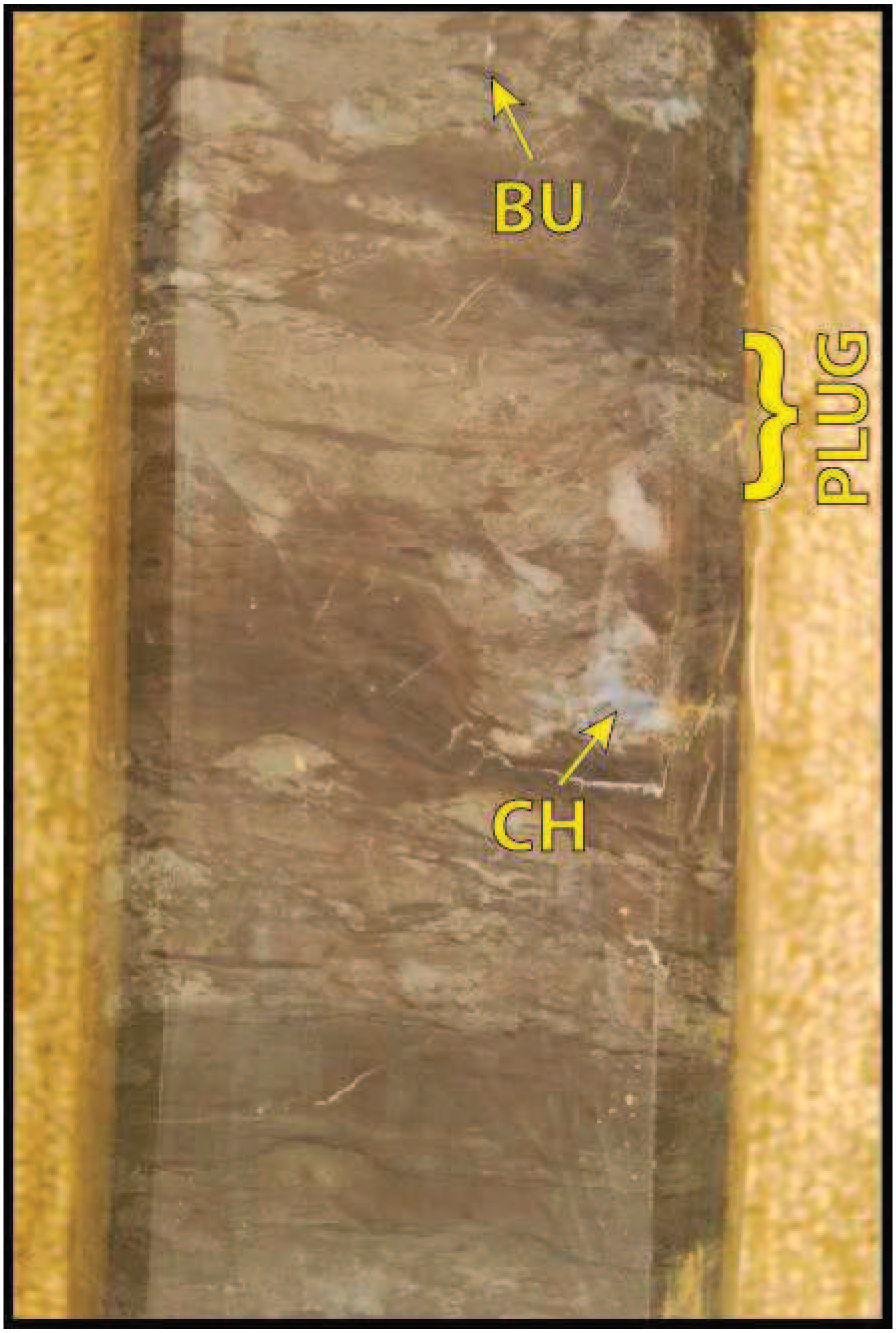

8,437-8,438’: Facies 4.

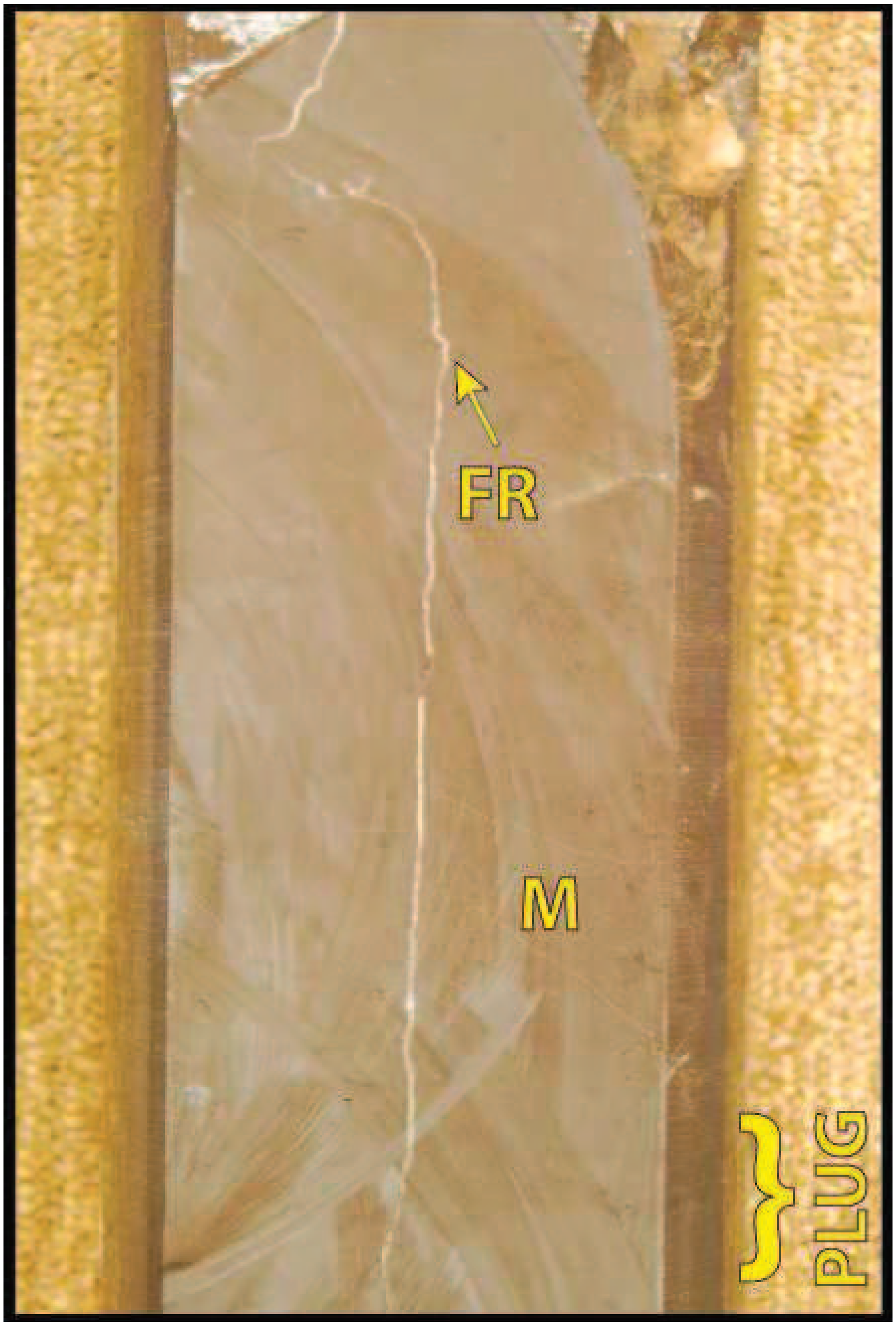

8,427-8,428’: Facies 2.

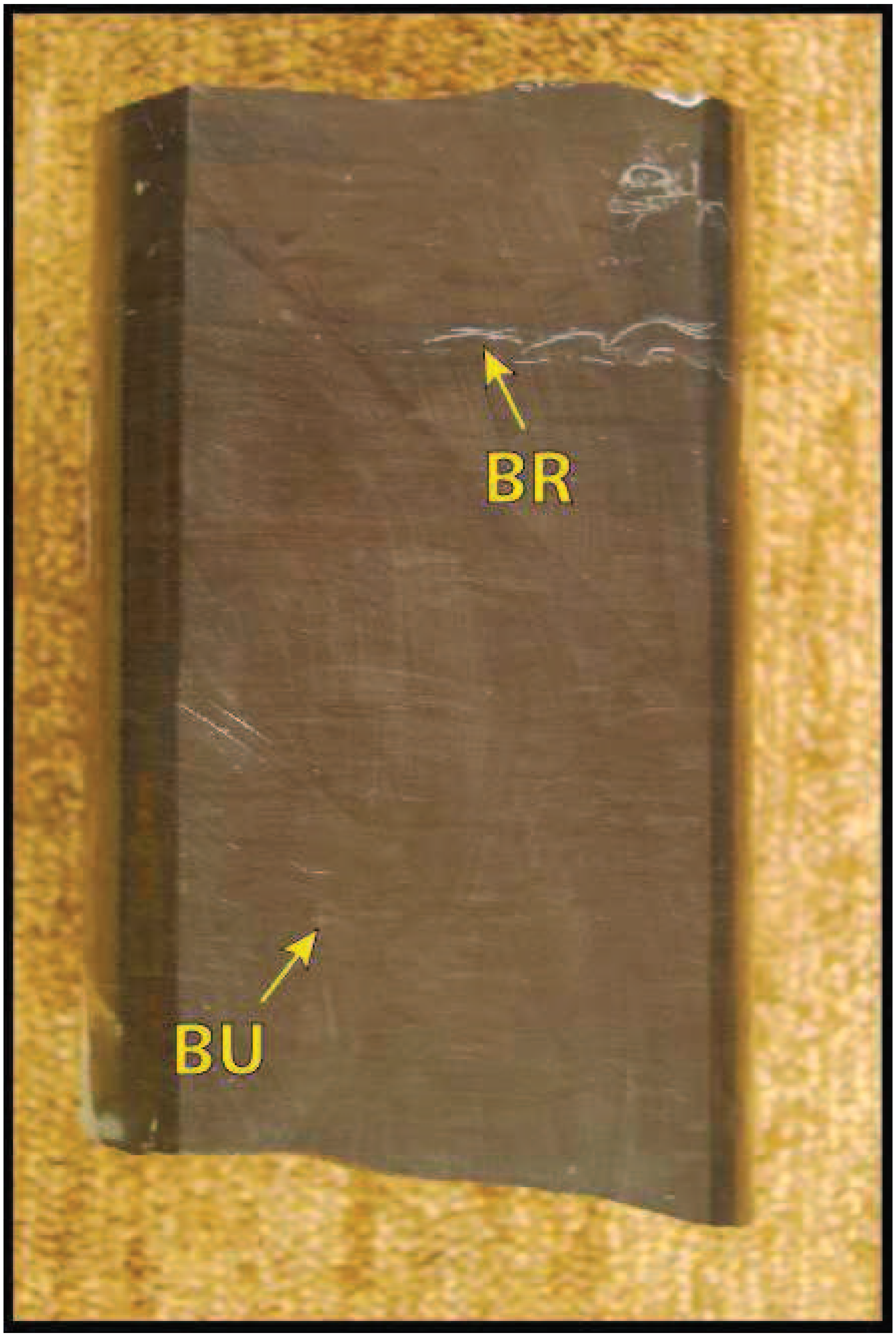

8,415-8,416’: Facies 3.

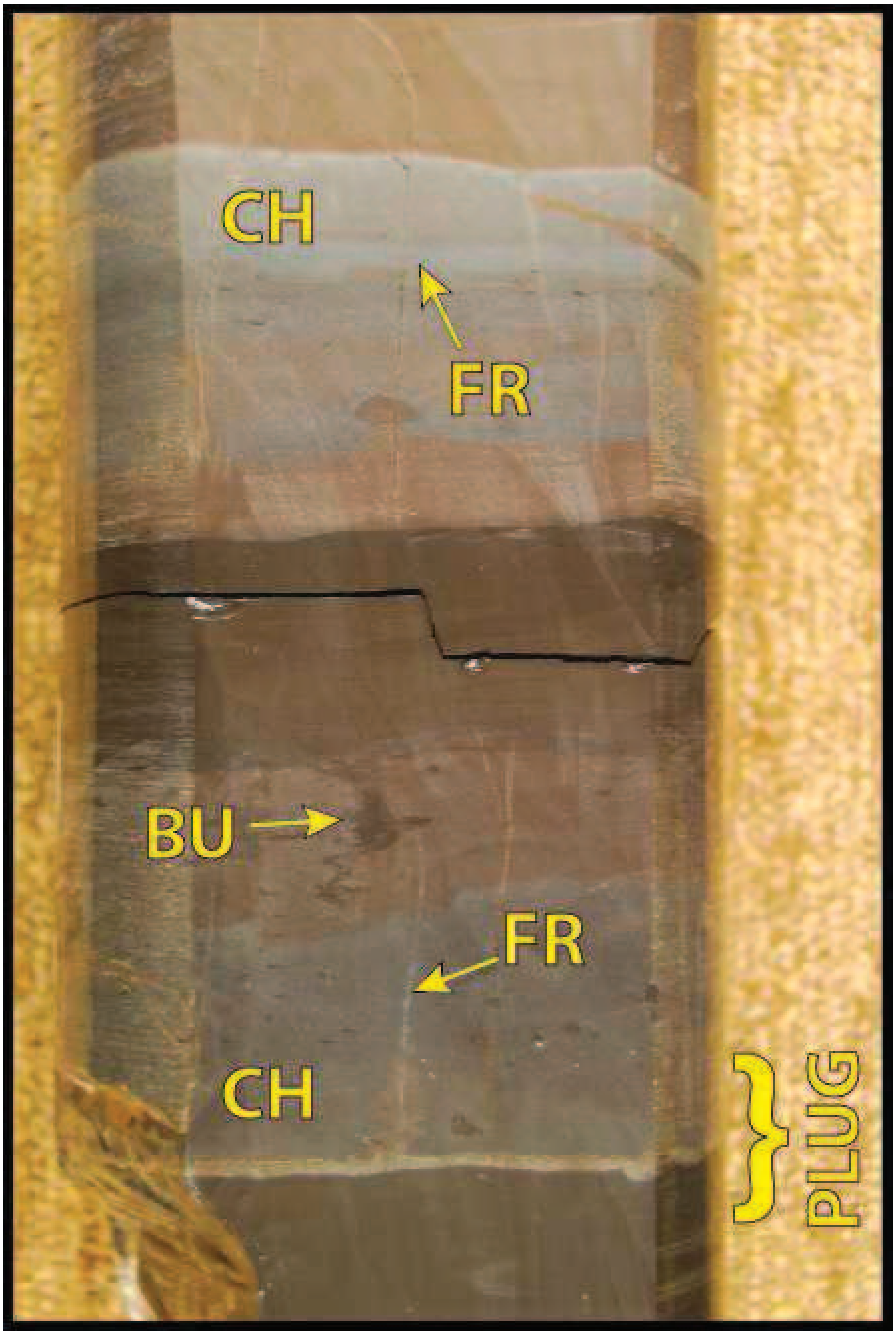

8,397-8,398': Facies 4.

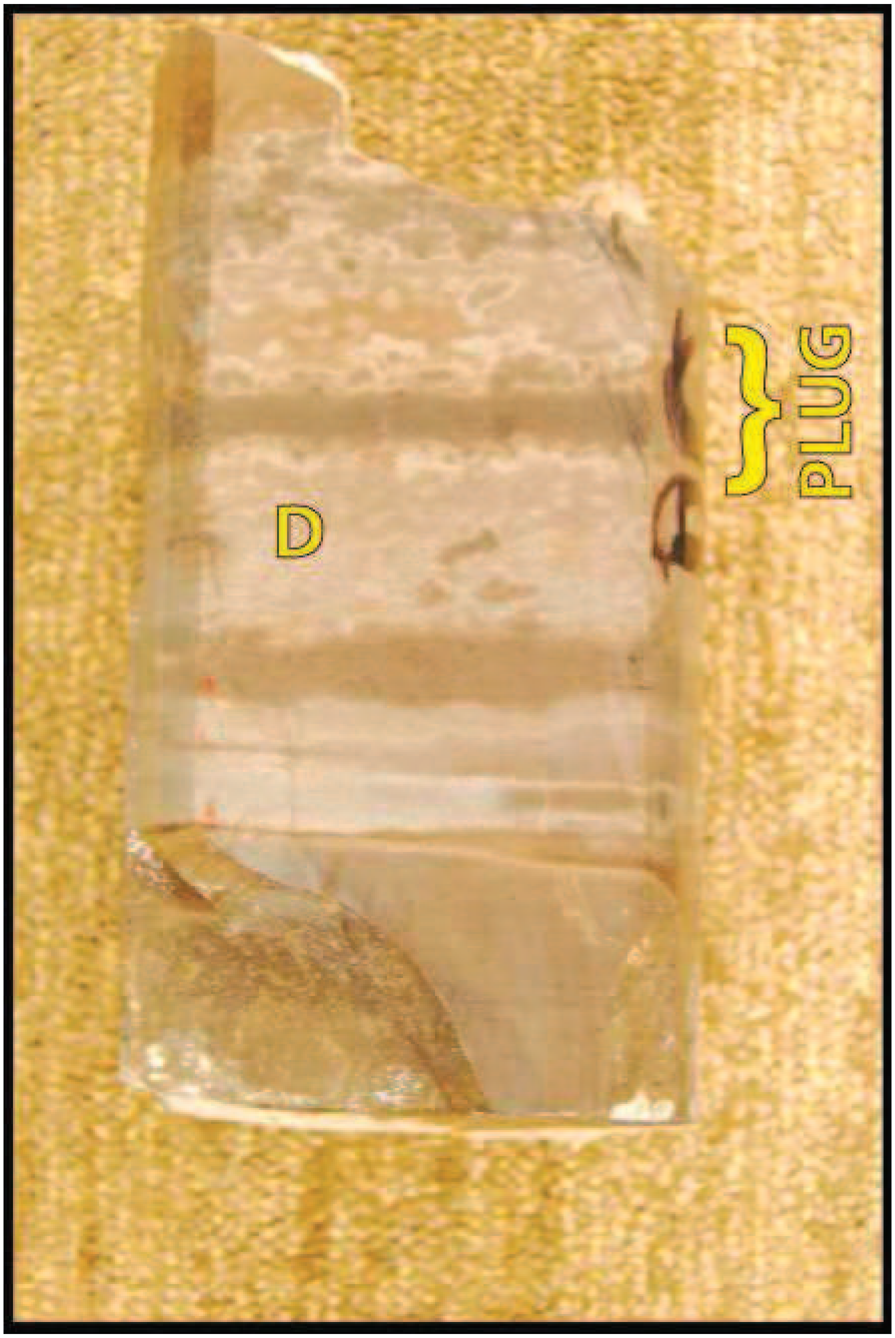

8,395-9,395.5’: Facies 5.

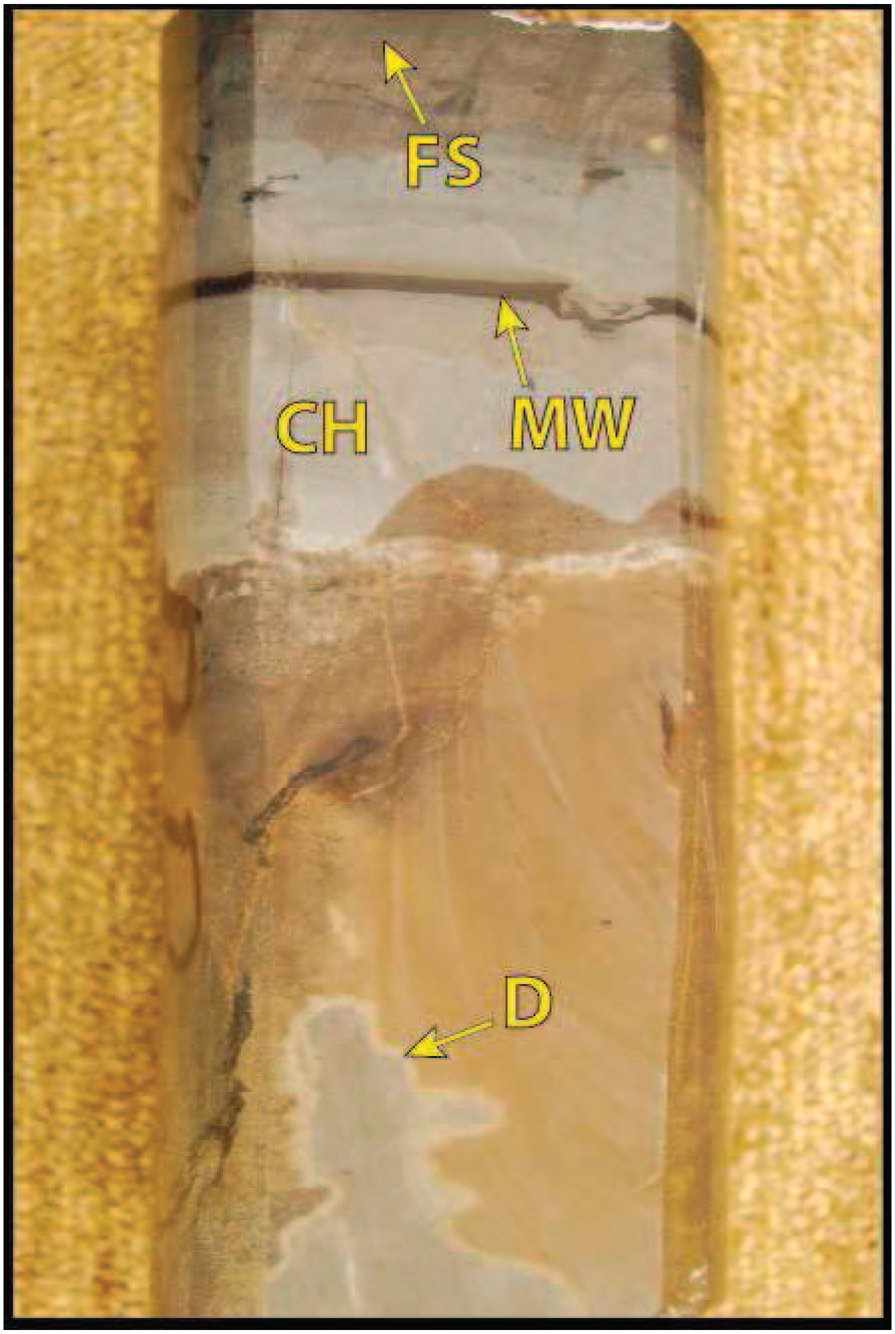

8,392-8,393’: Facies 5.

8,391-8,392’: Facies 2.

8,358-8,358.5’: Facies 3.

8,352-8,353’: Facies 4.

8,342-8,343’: Facies 4.

8,339.5-8,340’: Facies 5.

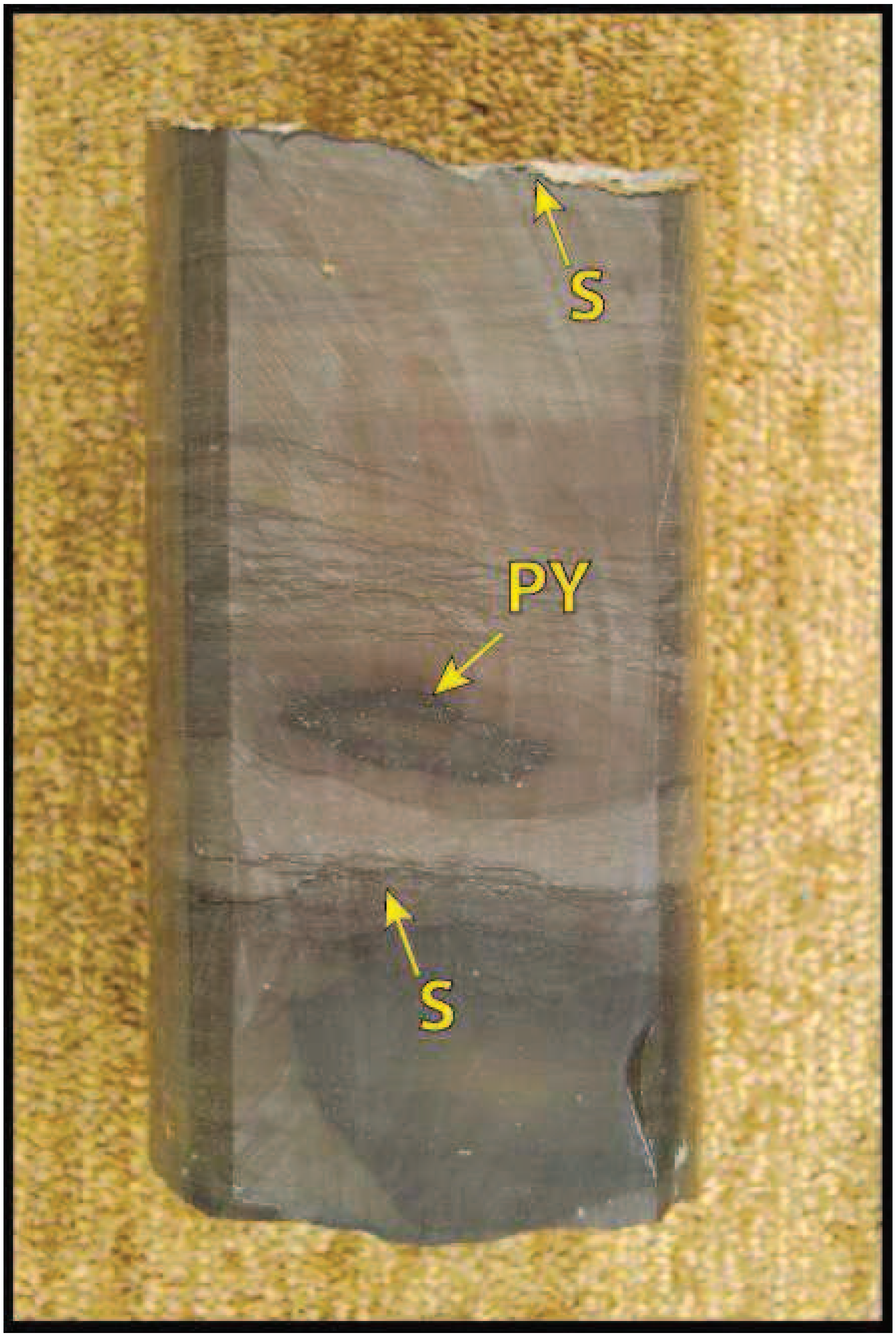

8,322-8,323’: Facies 4.

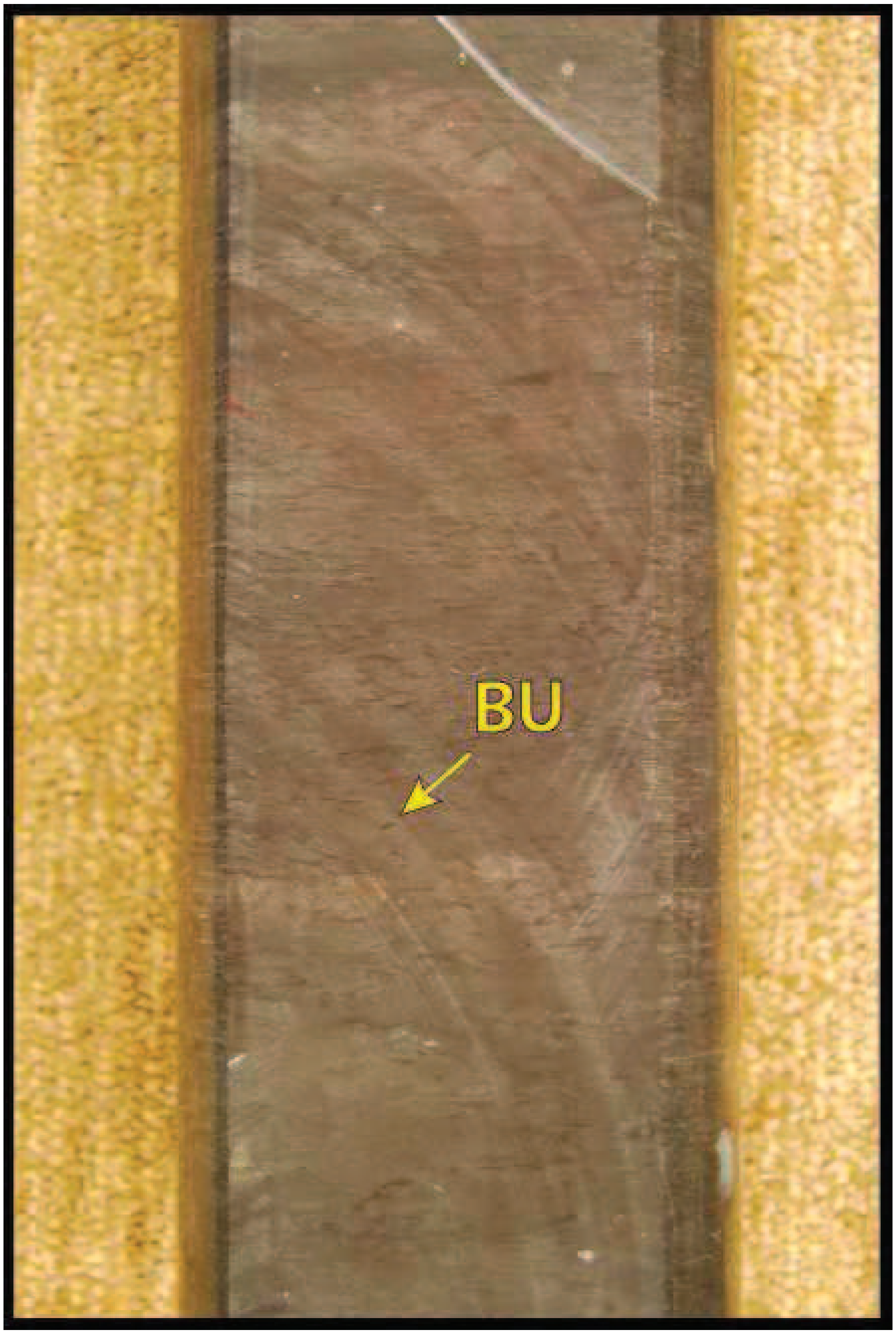

8,310-8,311': Facies 3.

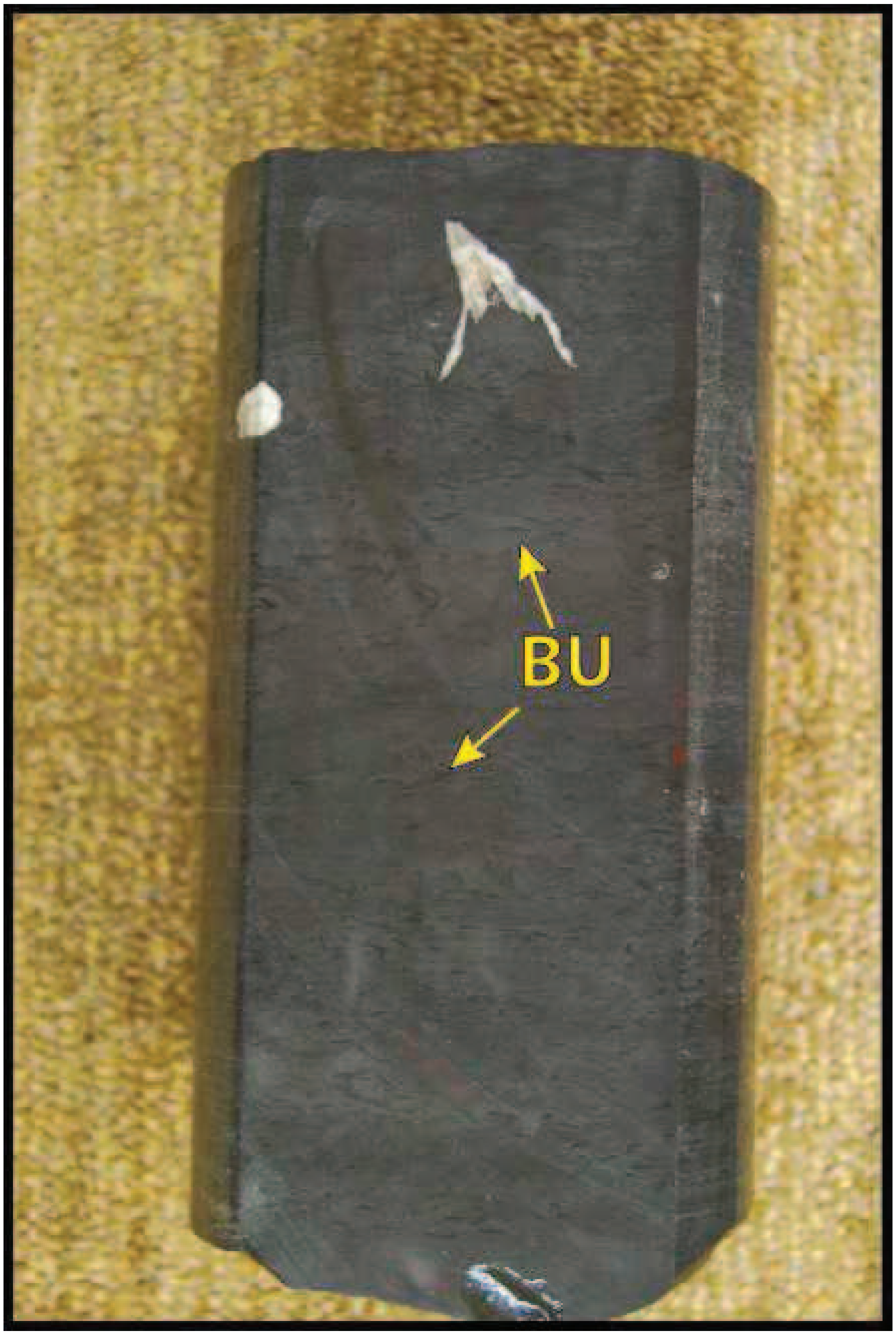

8,305.5-8,306’: Facies 3.

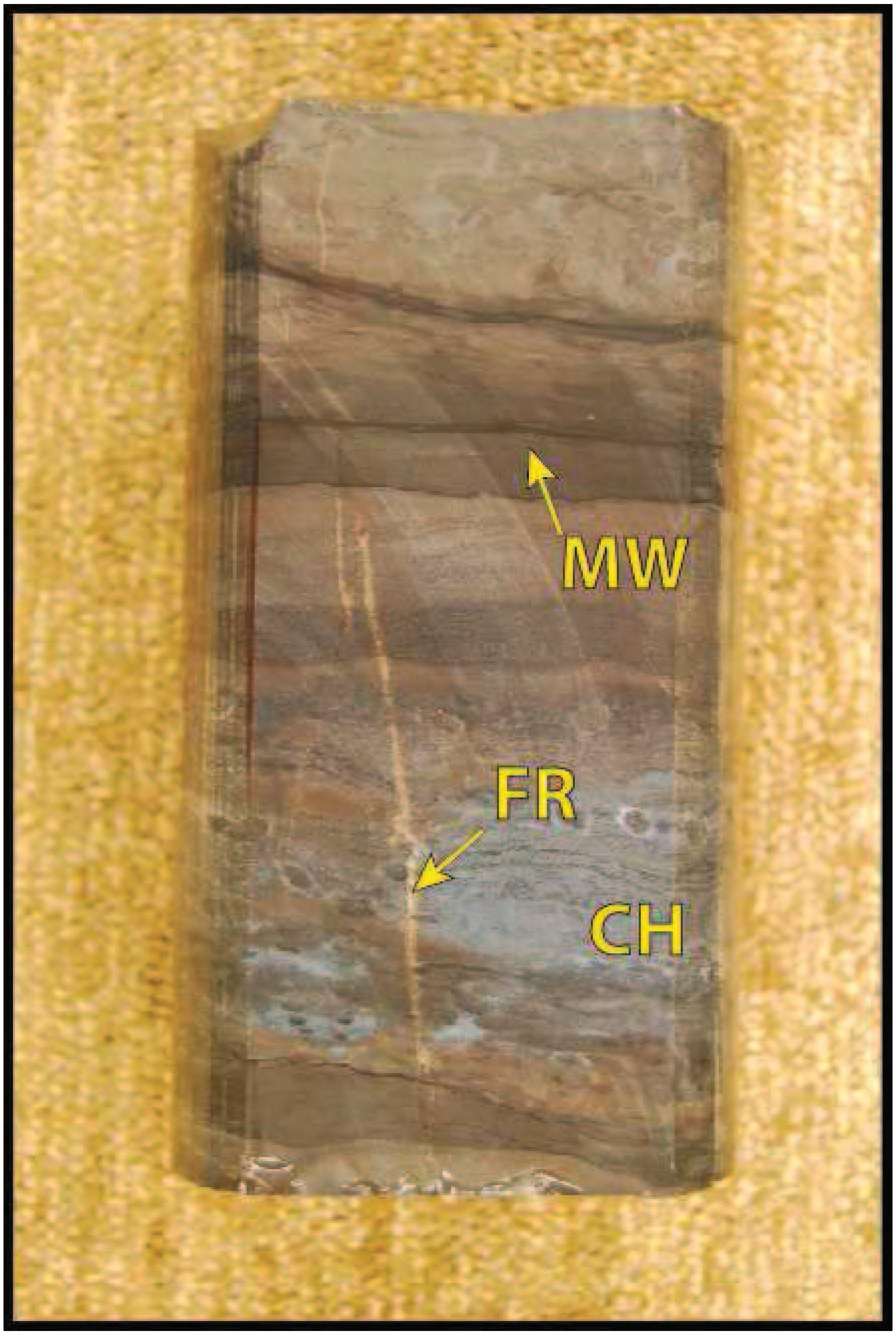

8,299-8,300’: Facies 4.

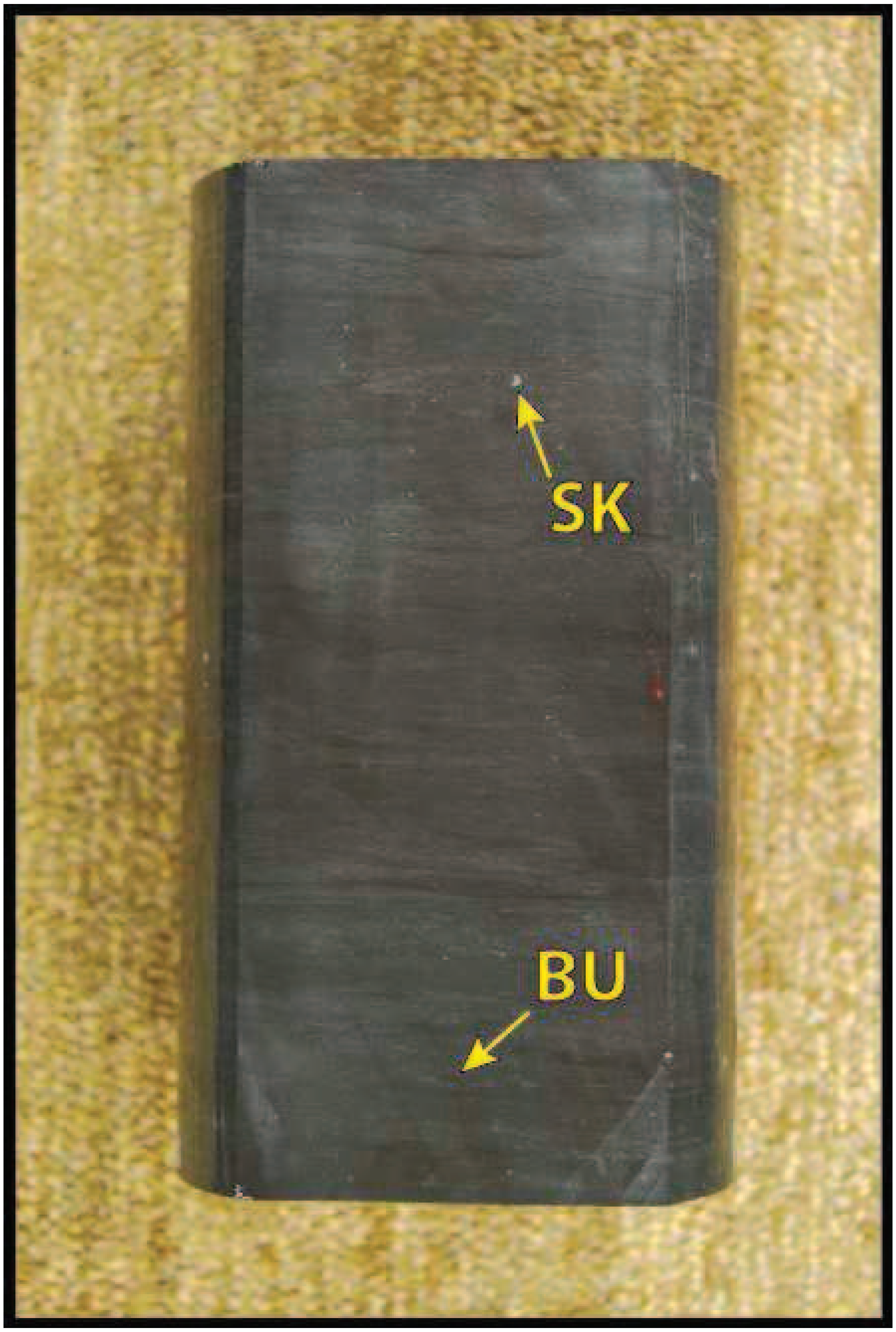

8,291-8,292’: Facies 3.

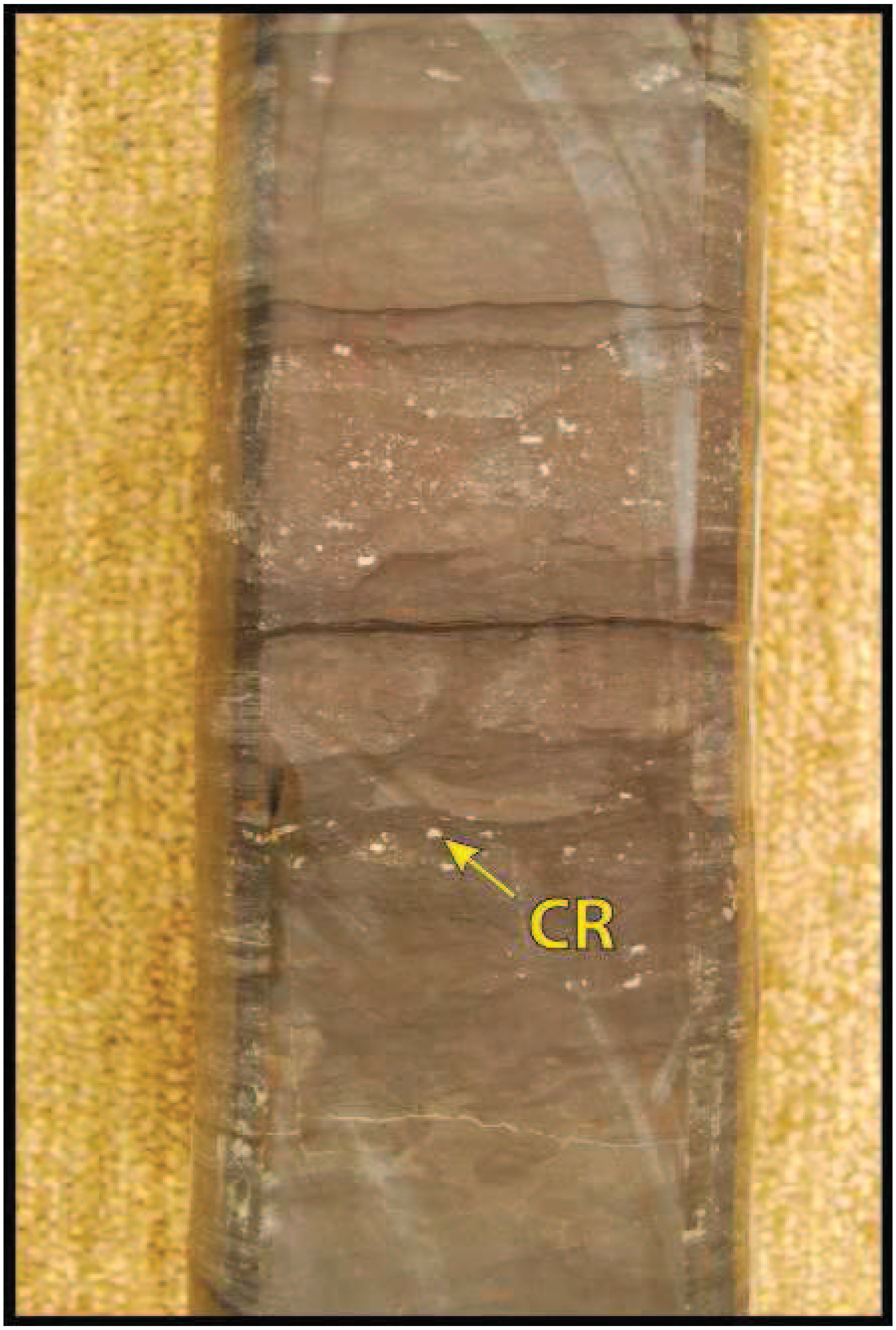

8,283-8,284': Facies 4.

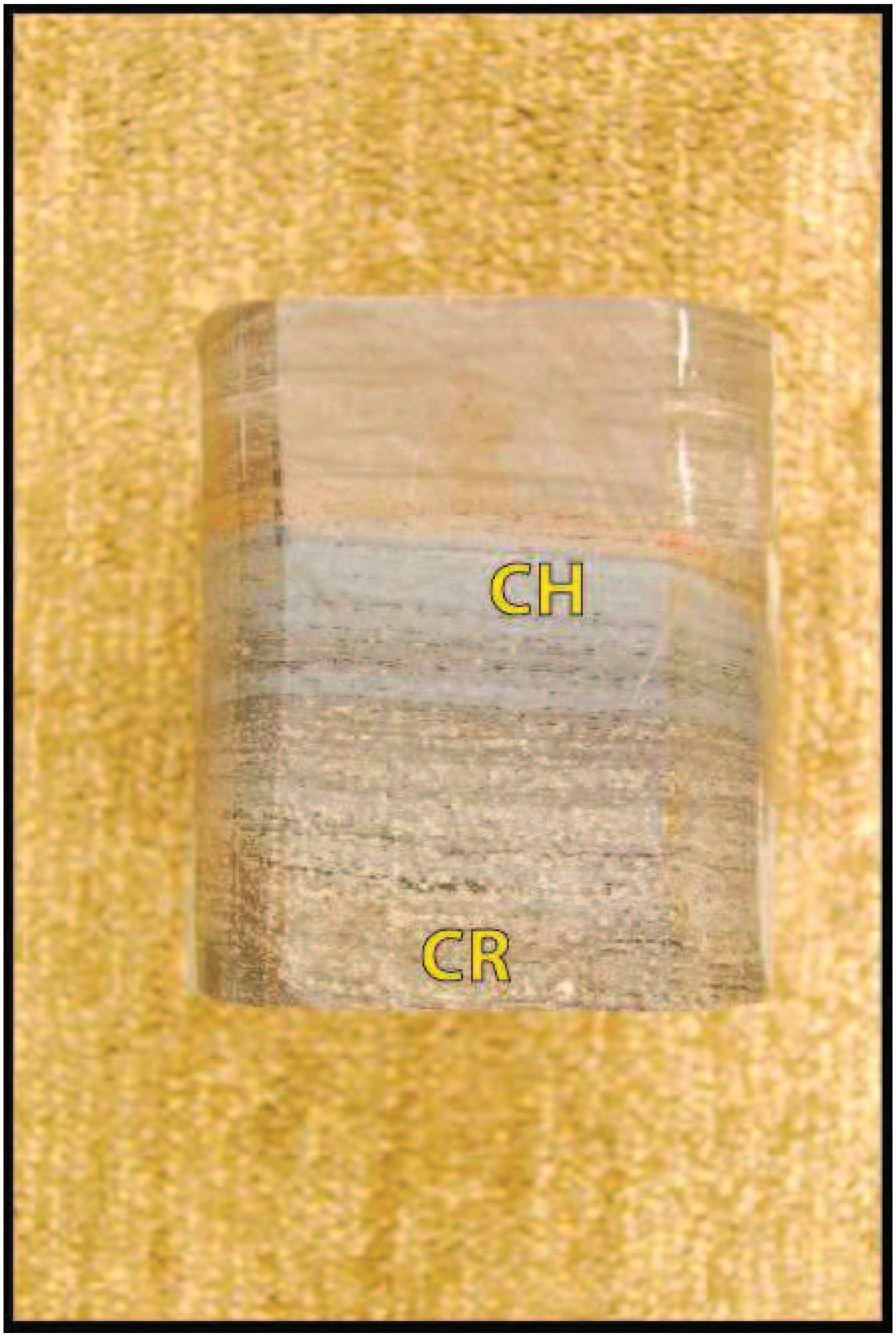

8,268-8,268.4’: Facies 5.

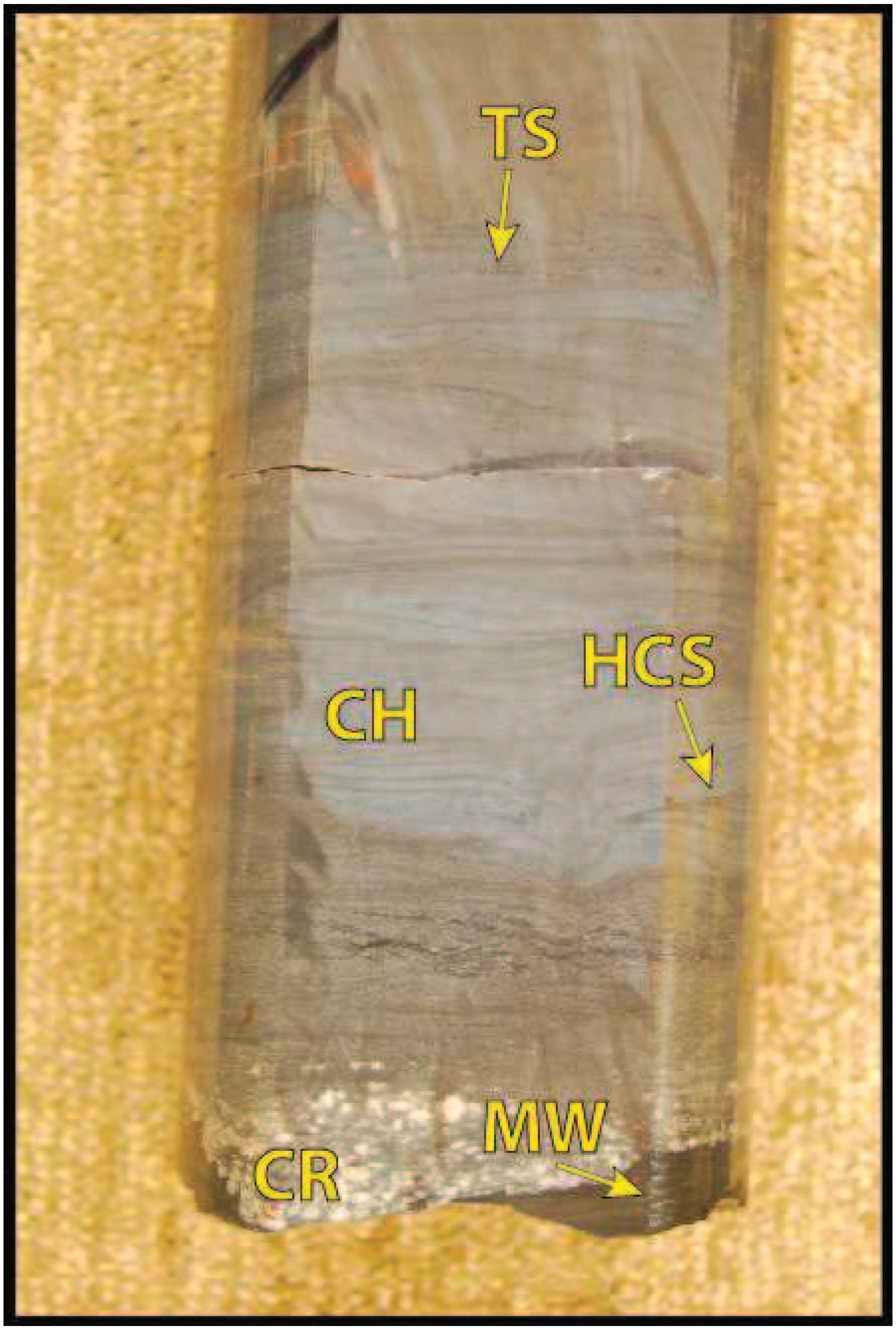

8,263-8,264’: Facies 5.

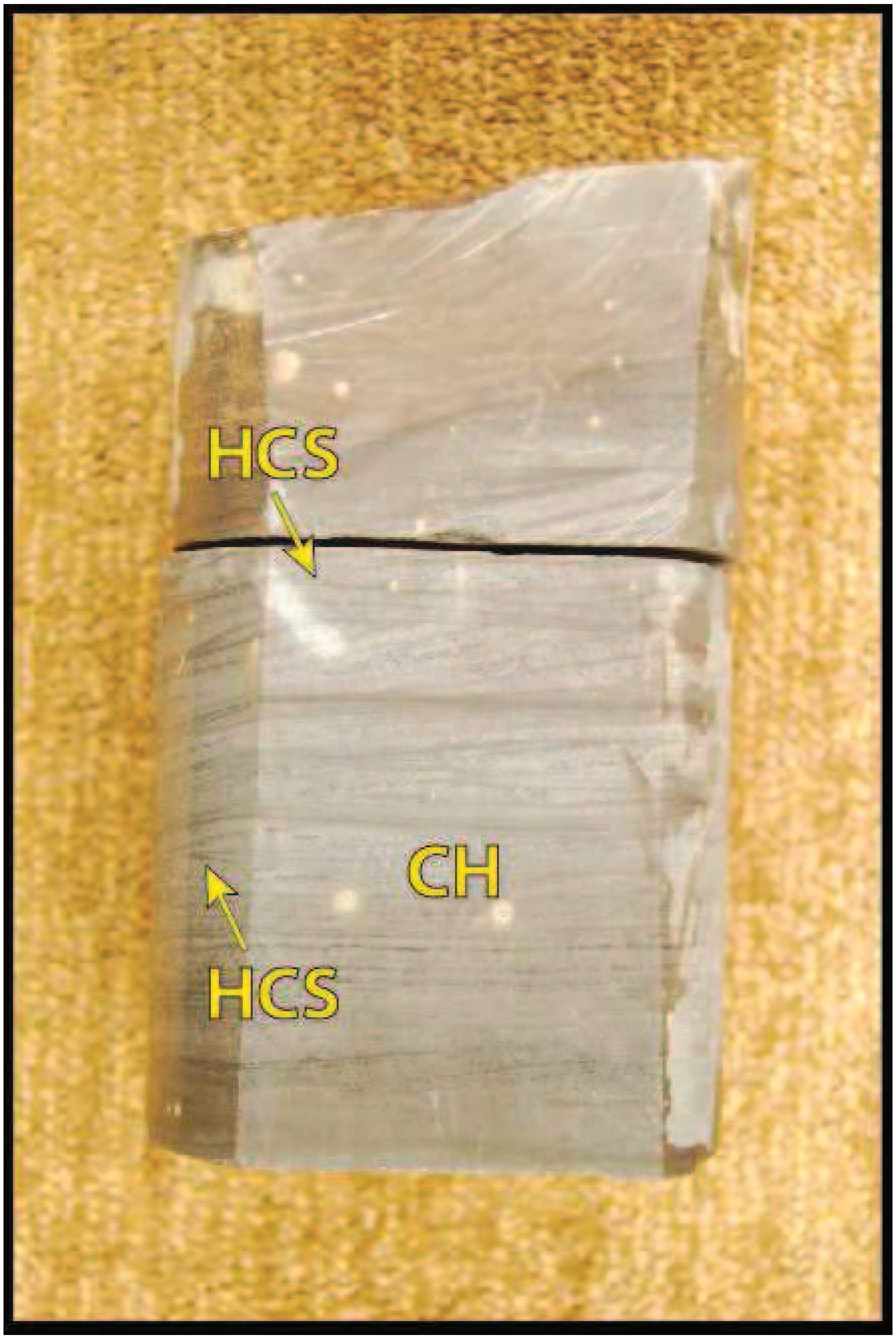

8,257-8,258’: Facies 5.

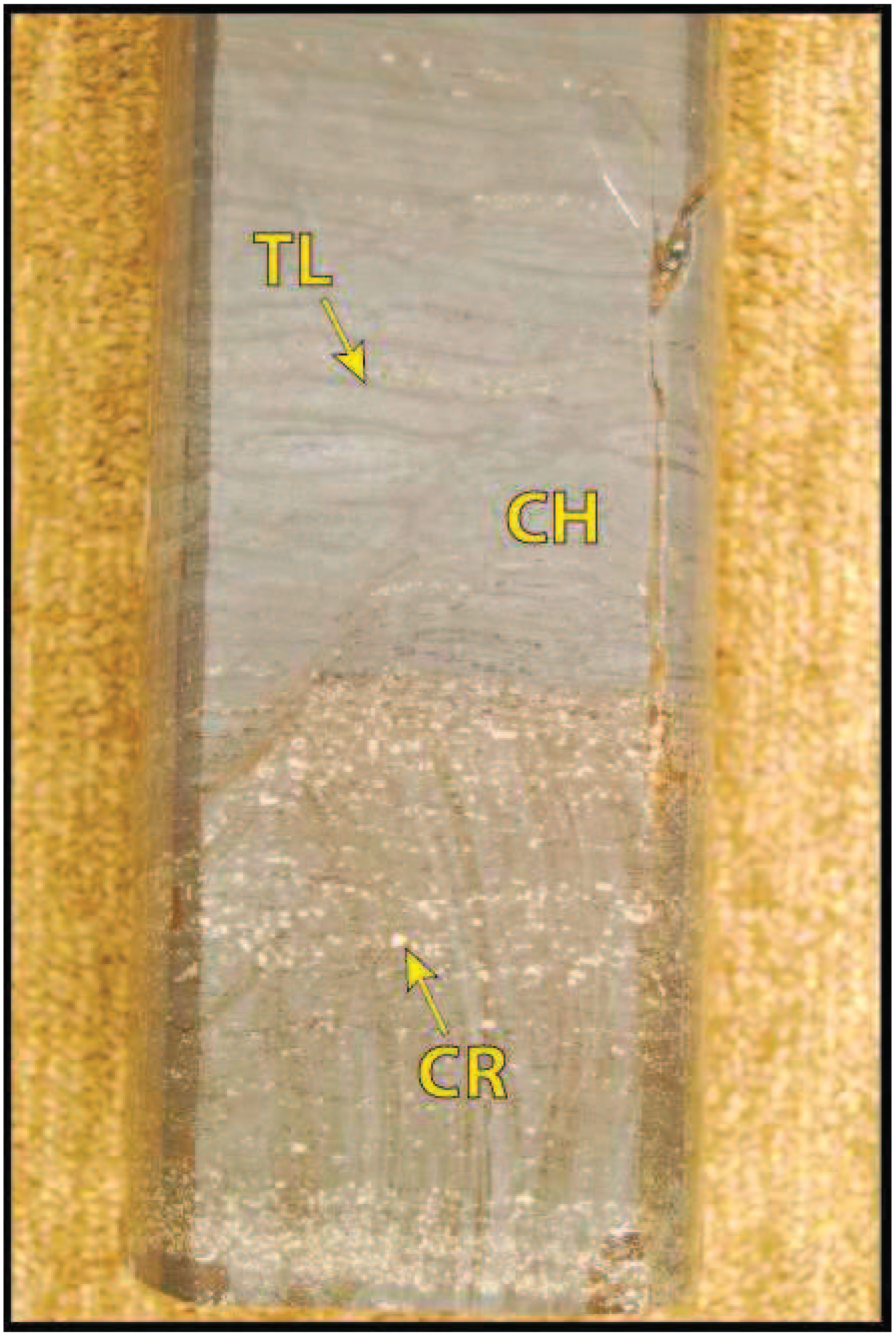

8,254-8,255': Facies 5.

8,246-8,247': Facies 5.

8,226-8,227’: Facies 1.

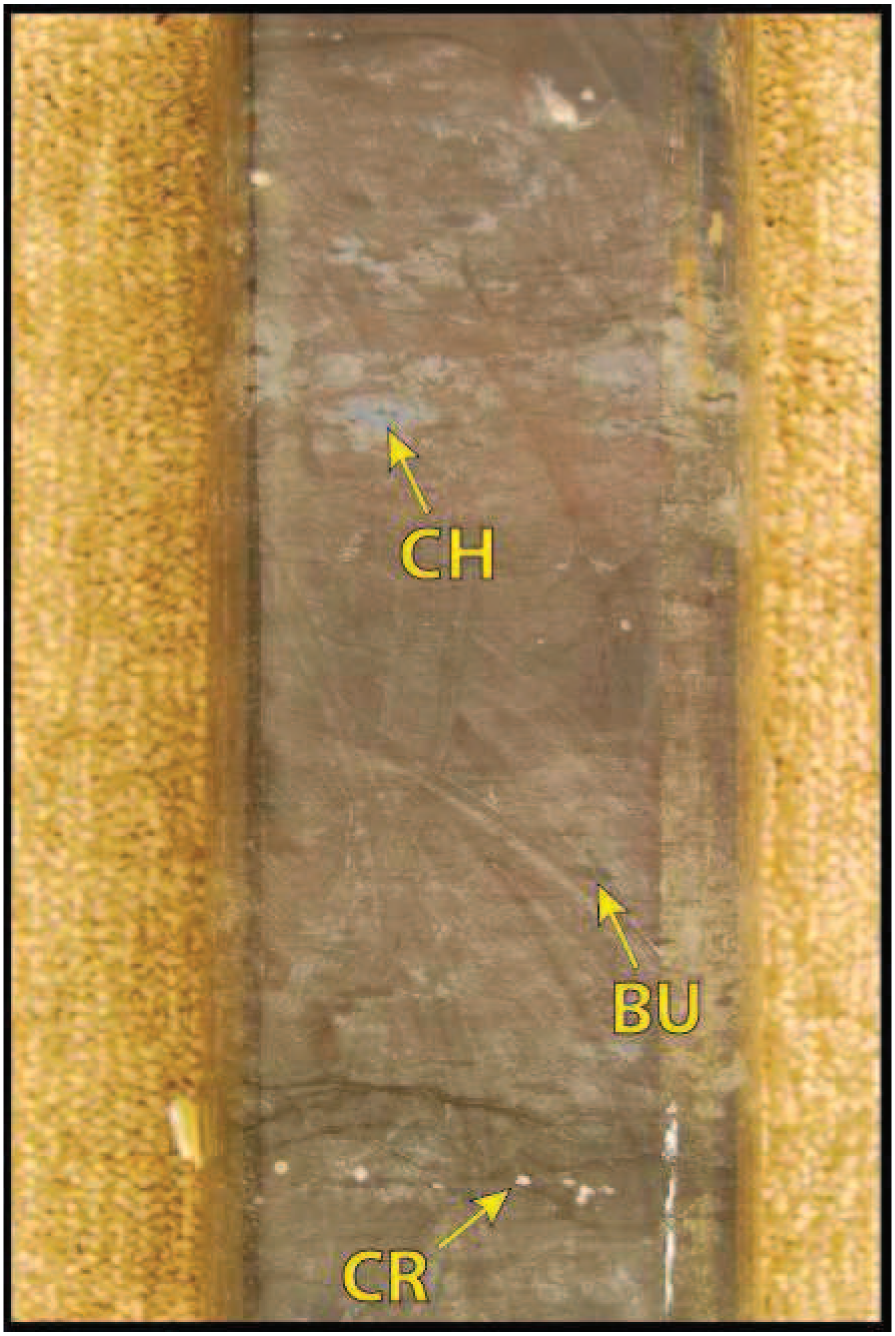

8,217-8,218’: Facies 3.

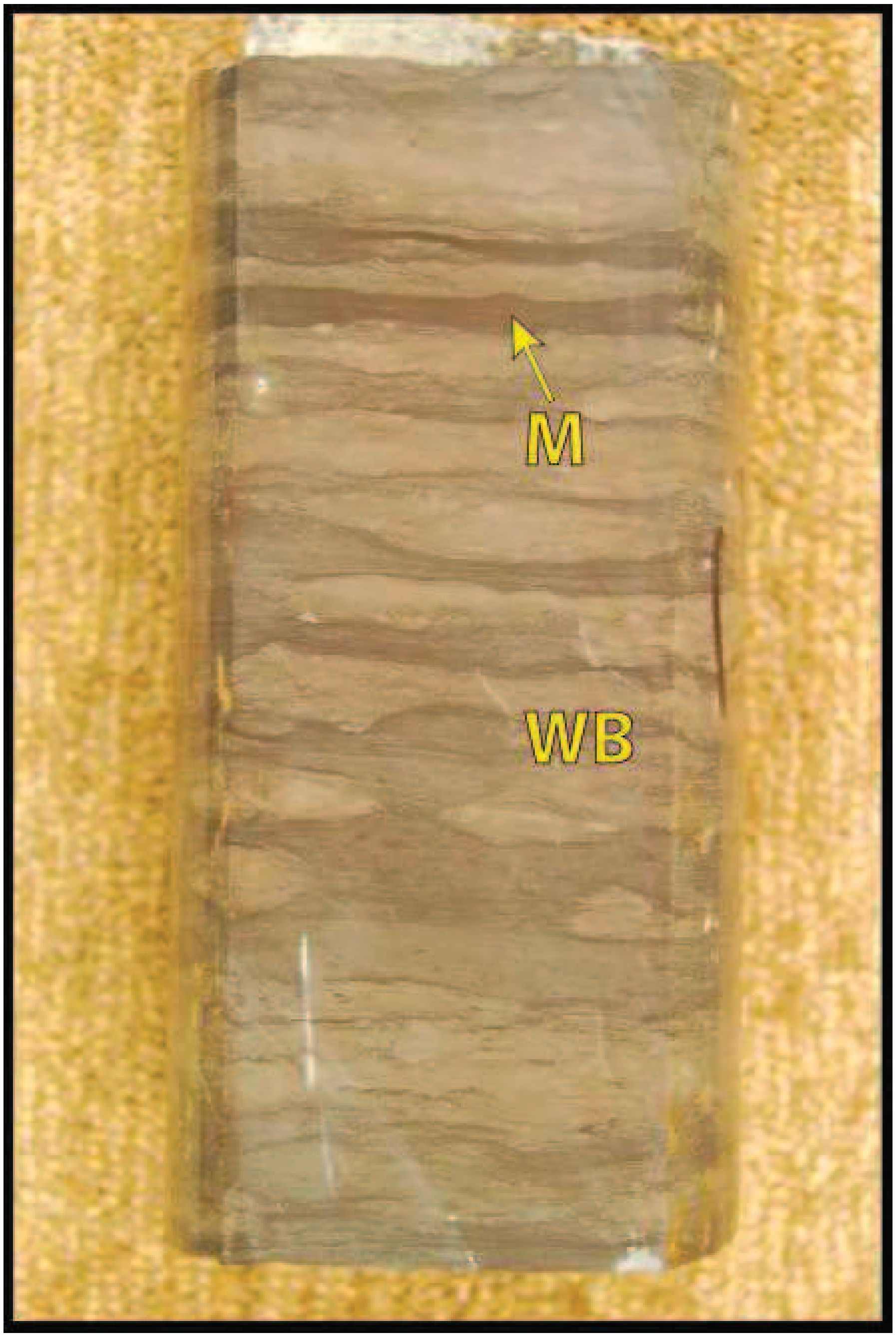

8,199-8,200’: Facies 5.

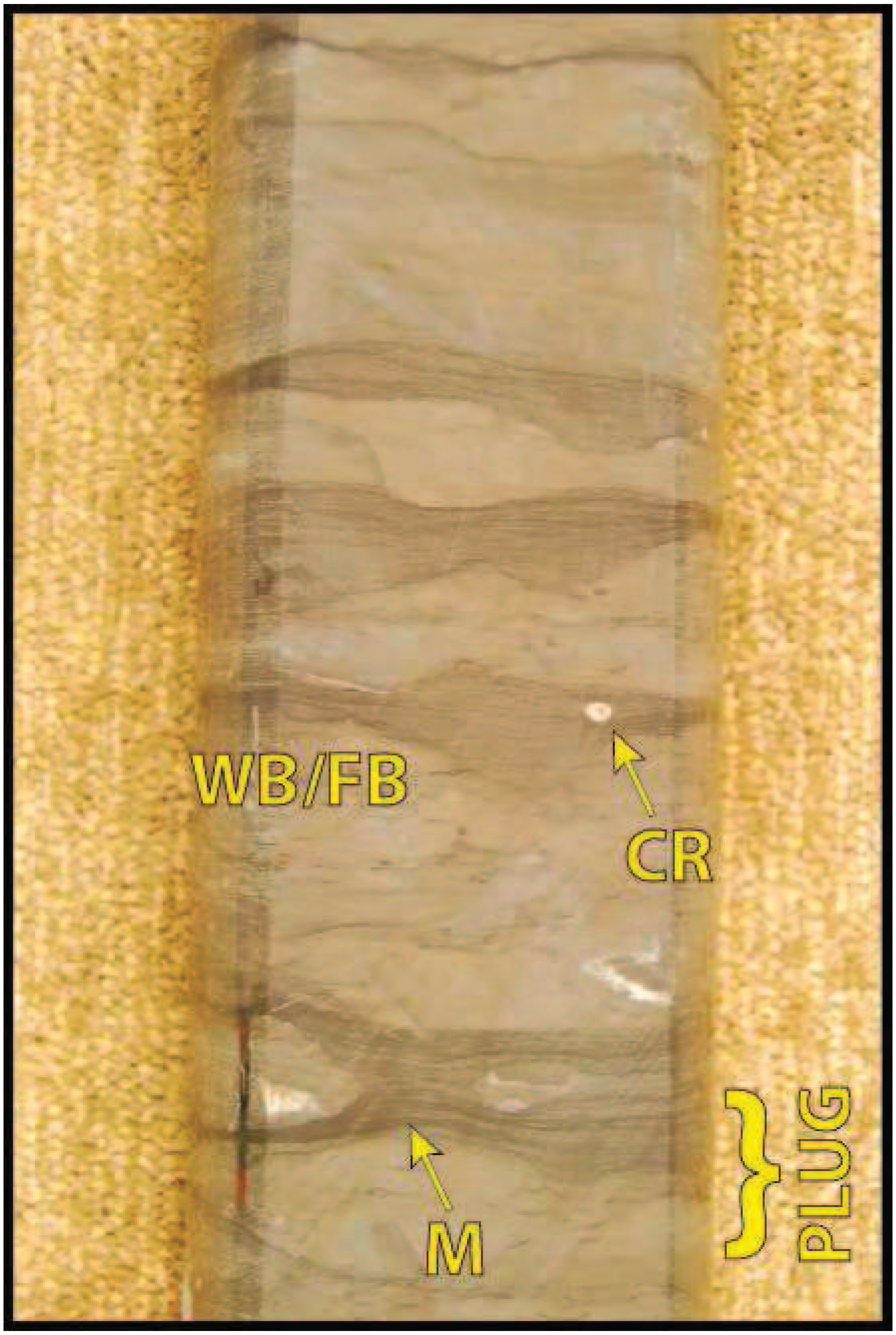

8,193-8,194': Facies 4.

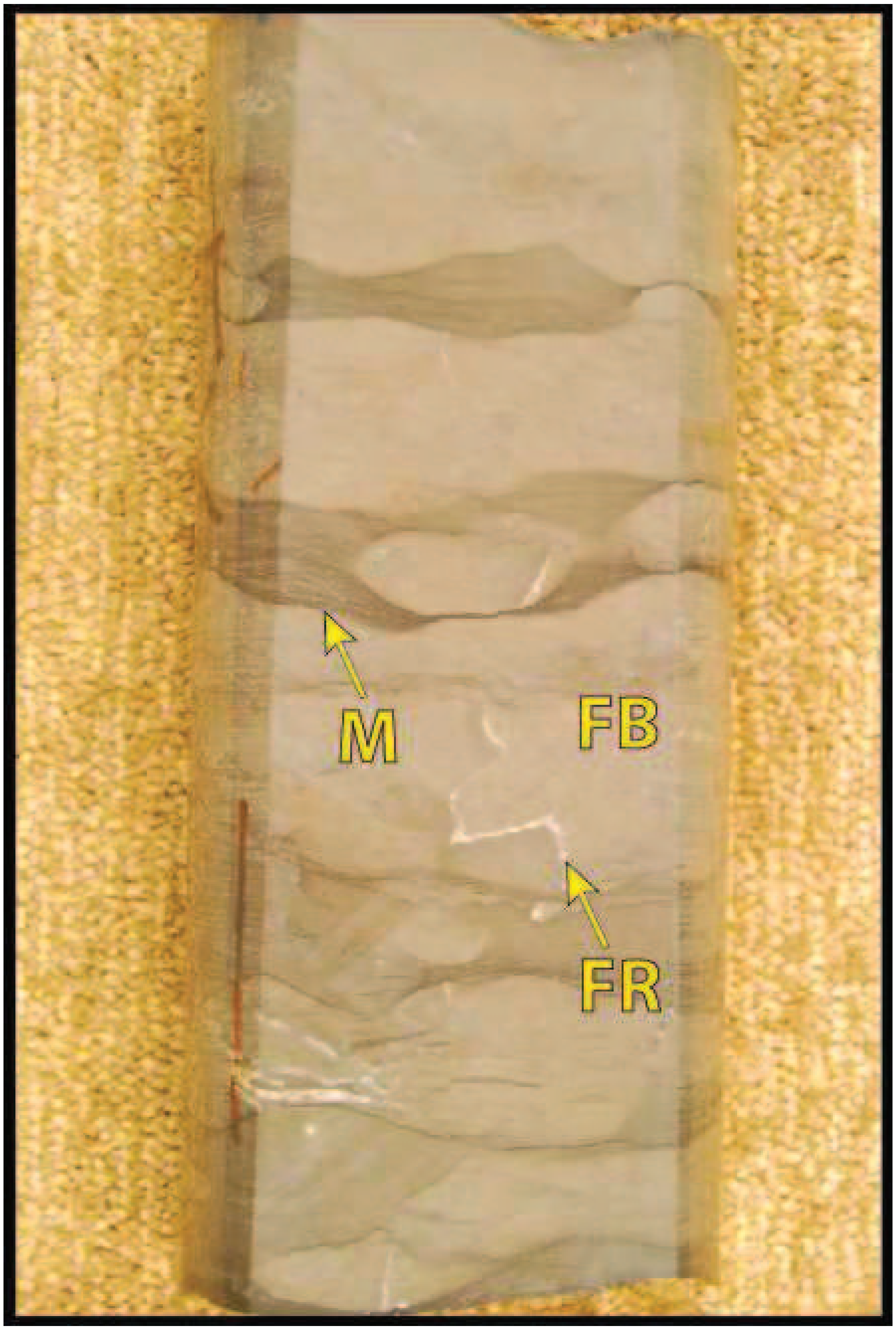

8,184-8,185': Facies 5.

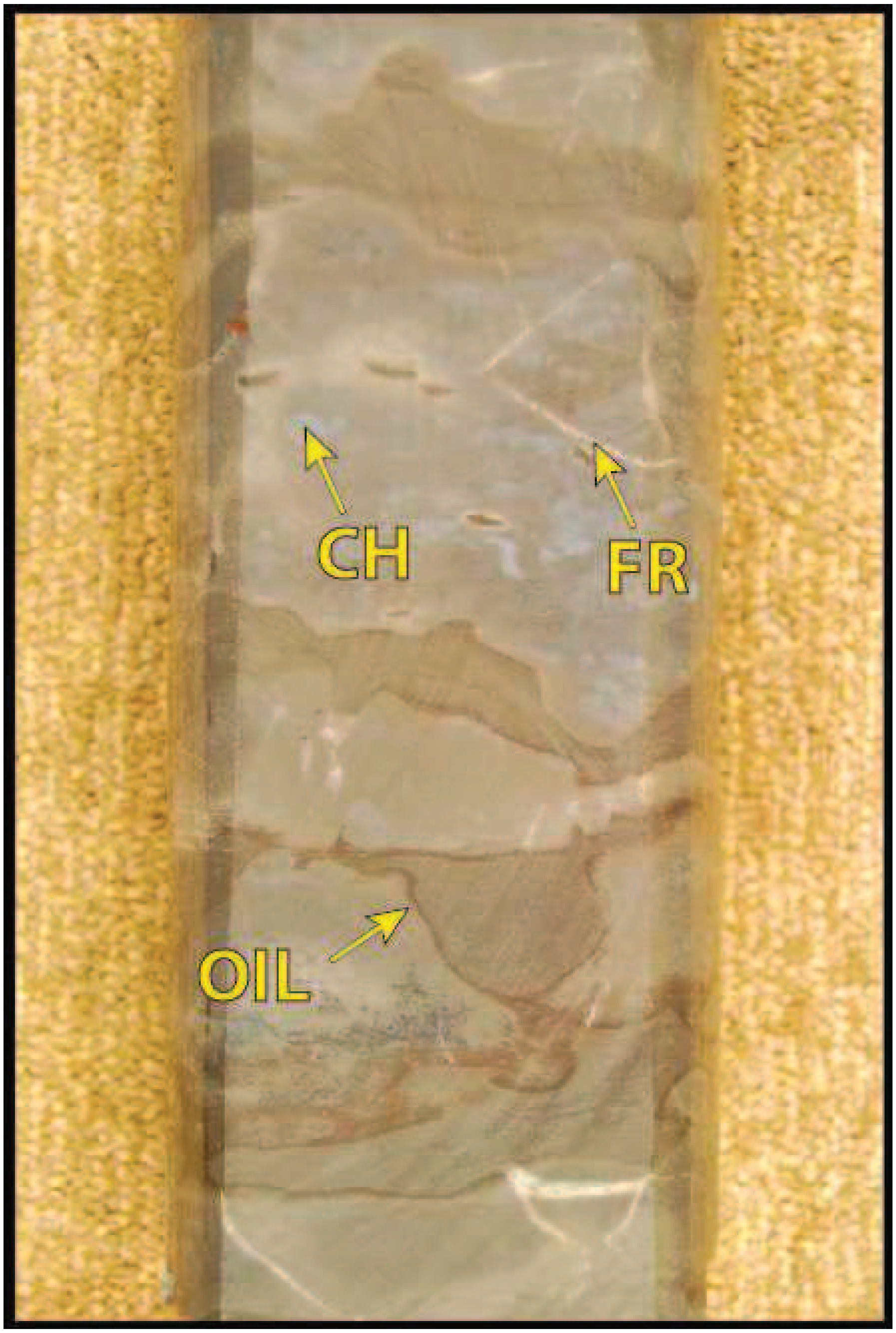

8,172-8,173’: Facies 5.

8,153-8,154’: Facies 5.

8,127-8,128’: Facies 5.

8,098-8,099’: Facies 5.

8,056-8,057’: Facies 4.

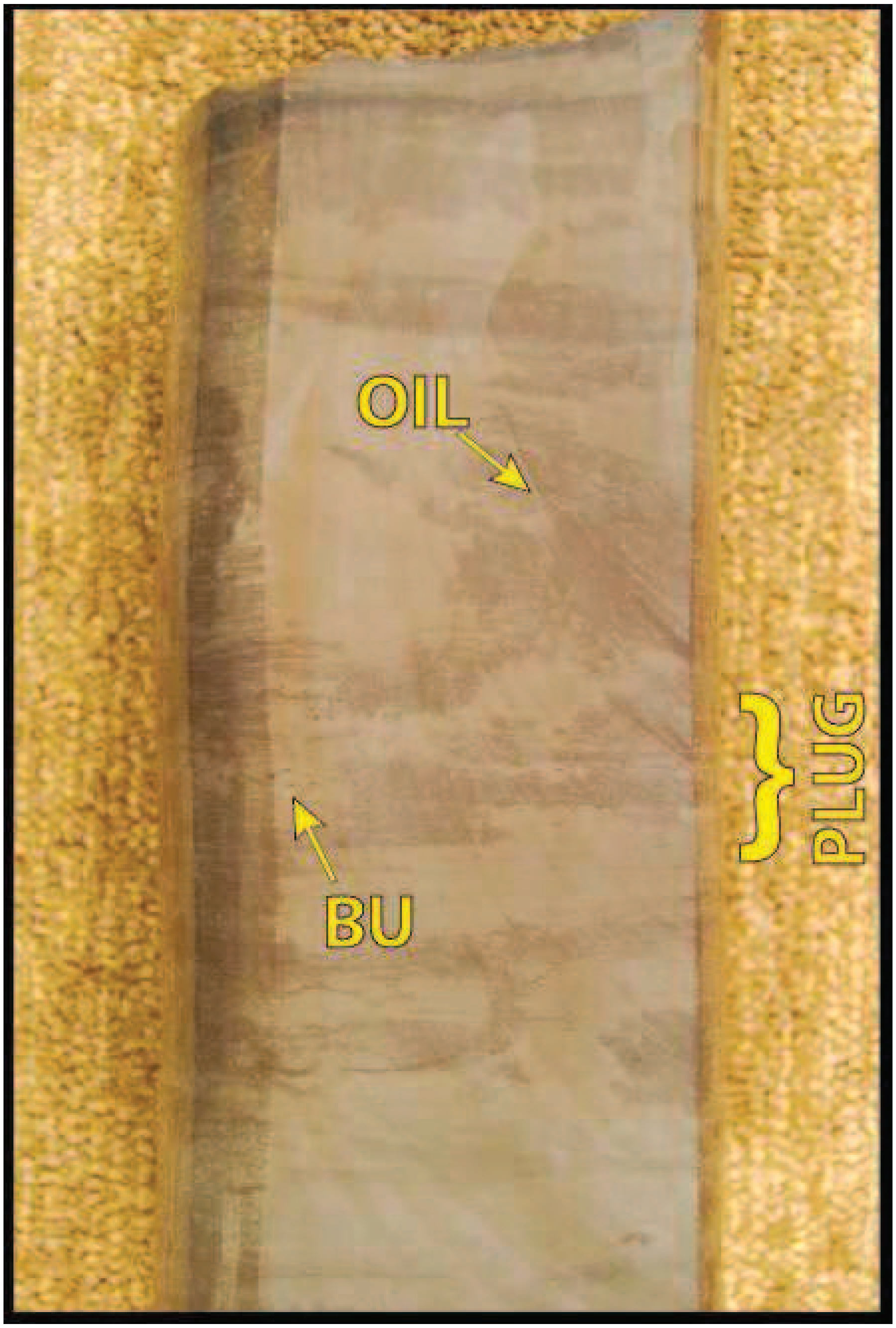

8,034-8,035’: Facies 3.

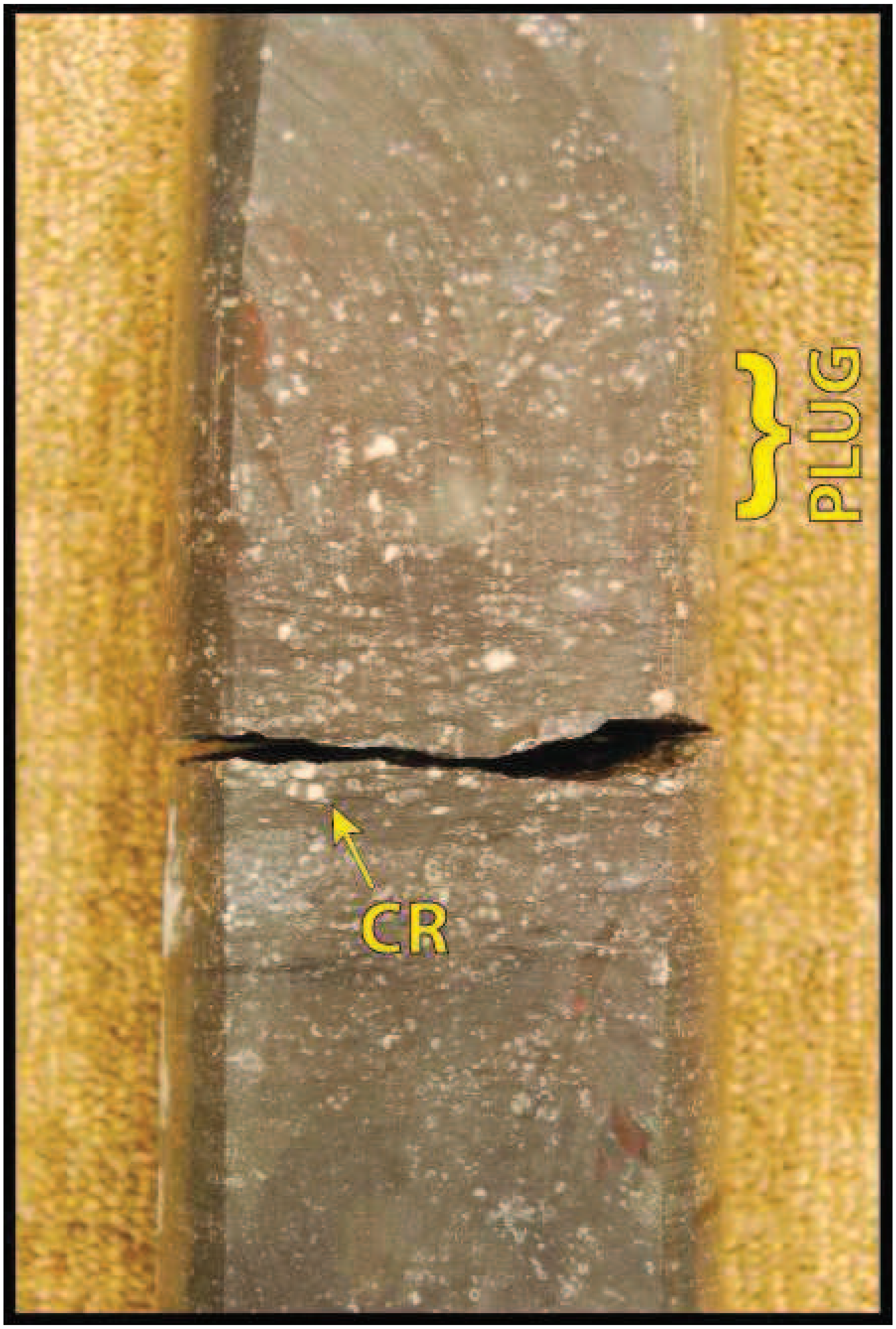

8,000-8,001’: Facies 5.

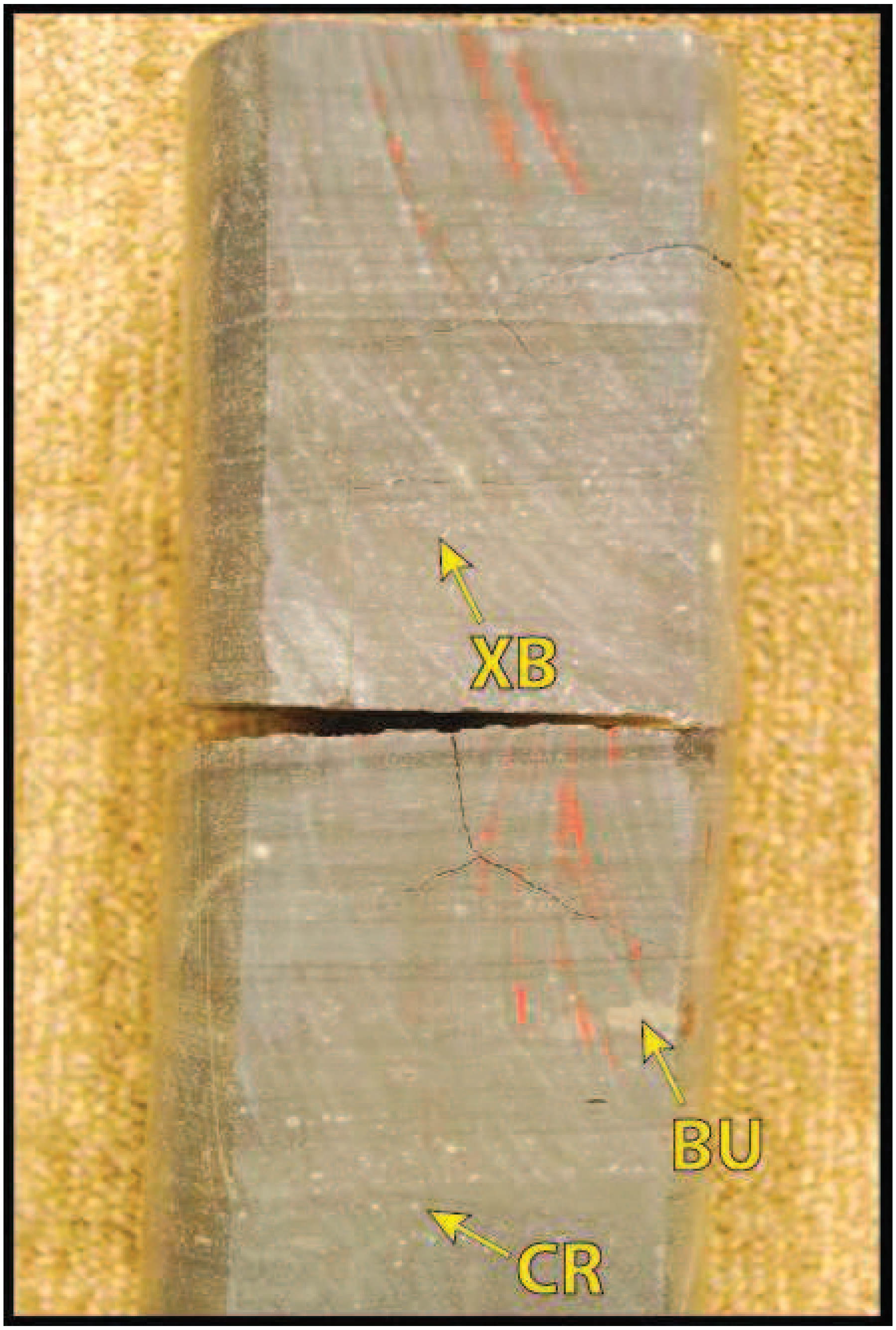

7,995-7,996': Facies 6.

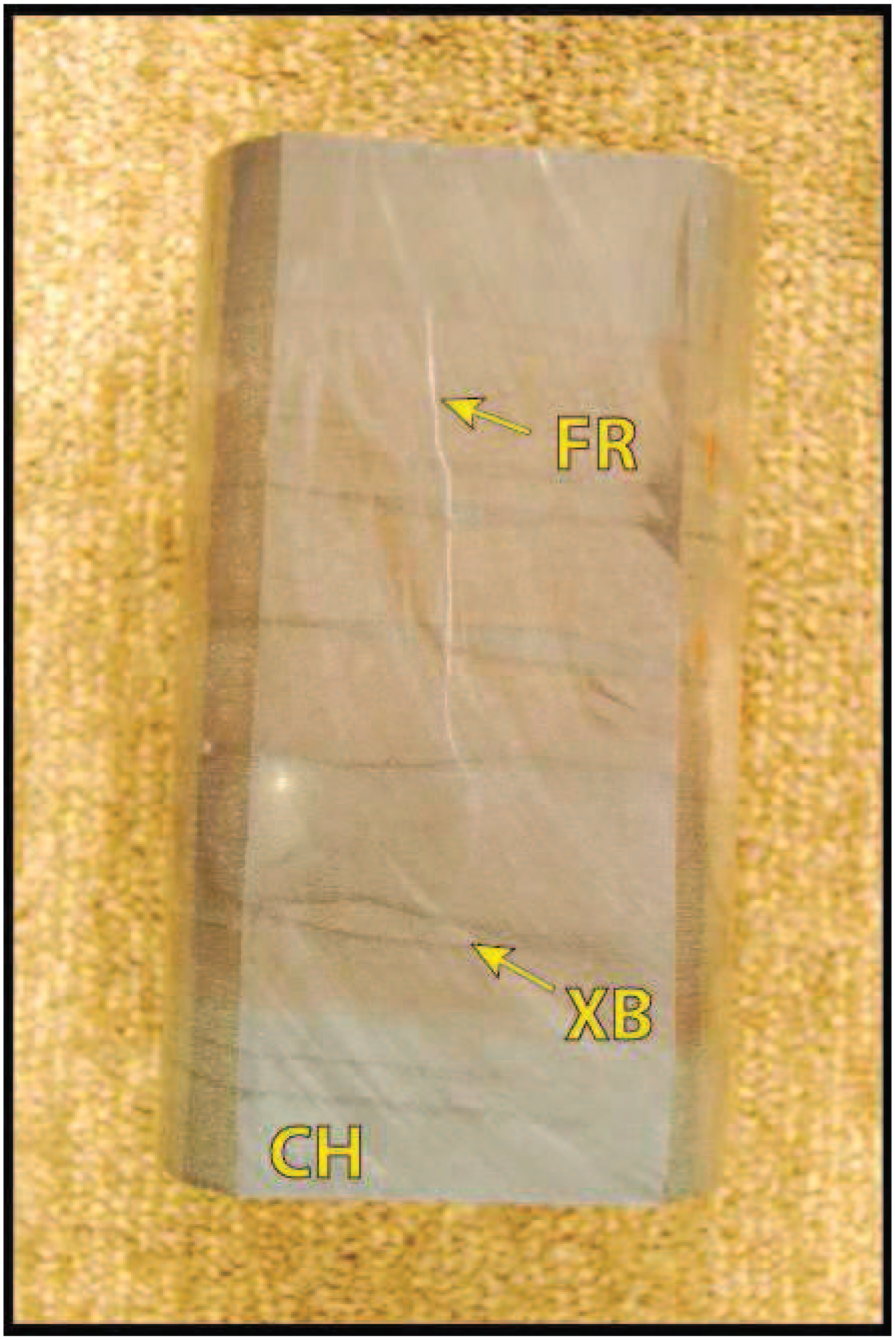

7,985-7,986’: Facies 5.

7,978-7,979’: Facies 2.

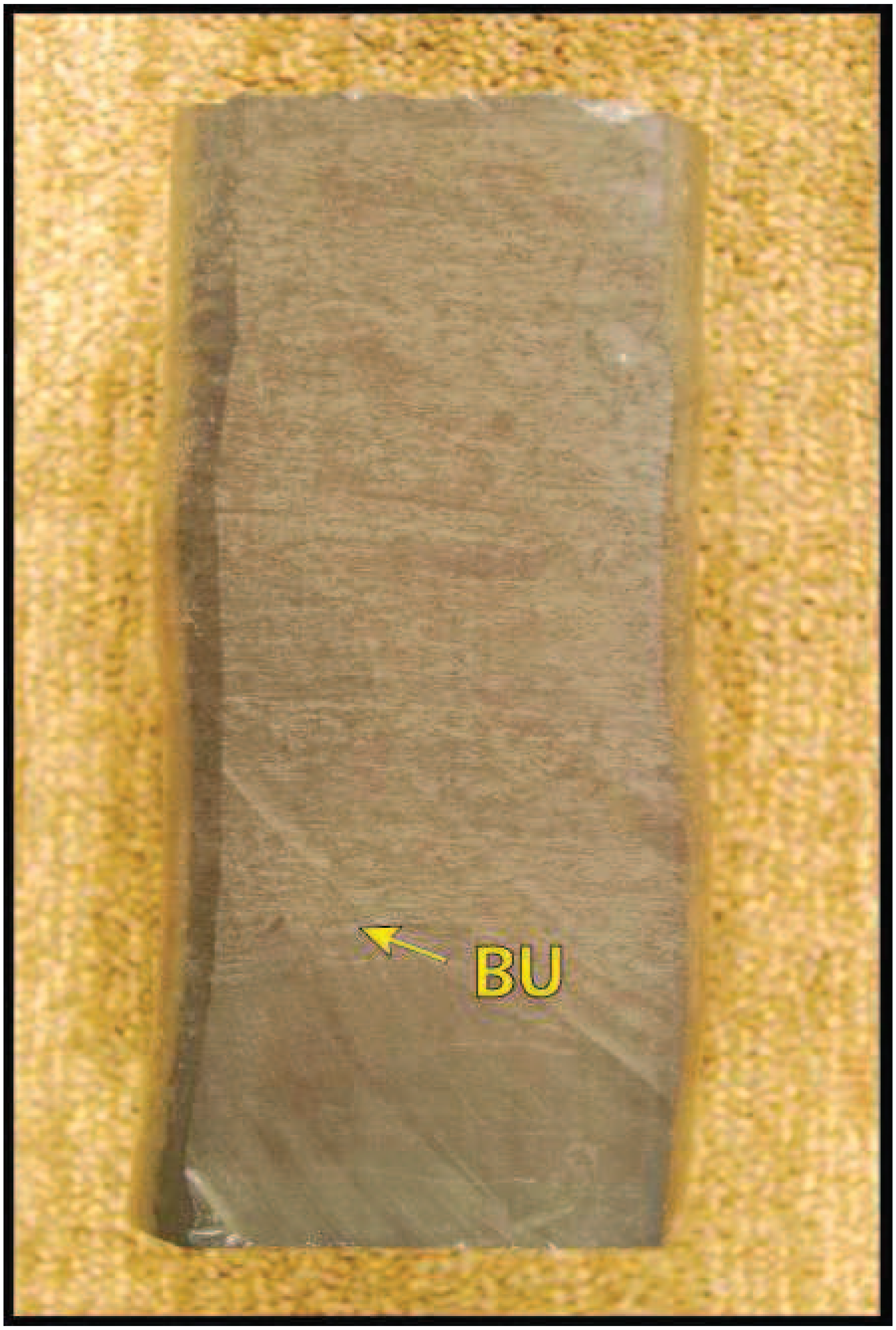

7,972-7,973’: Facies 3.

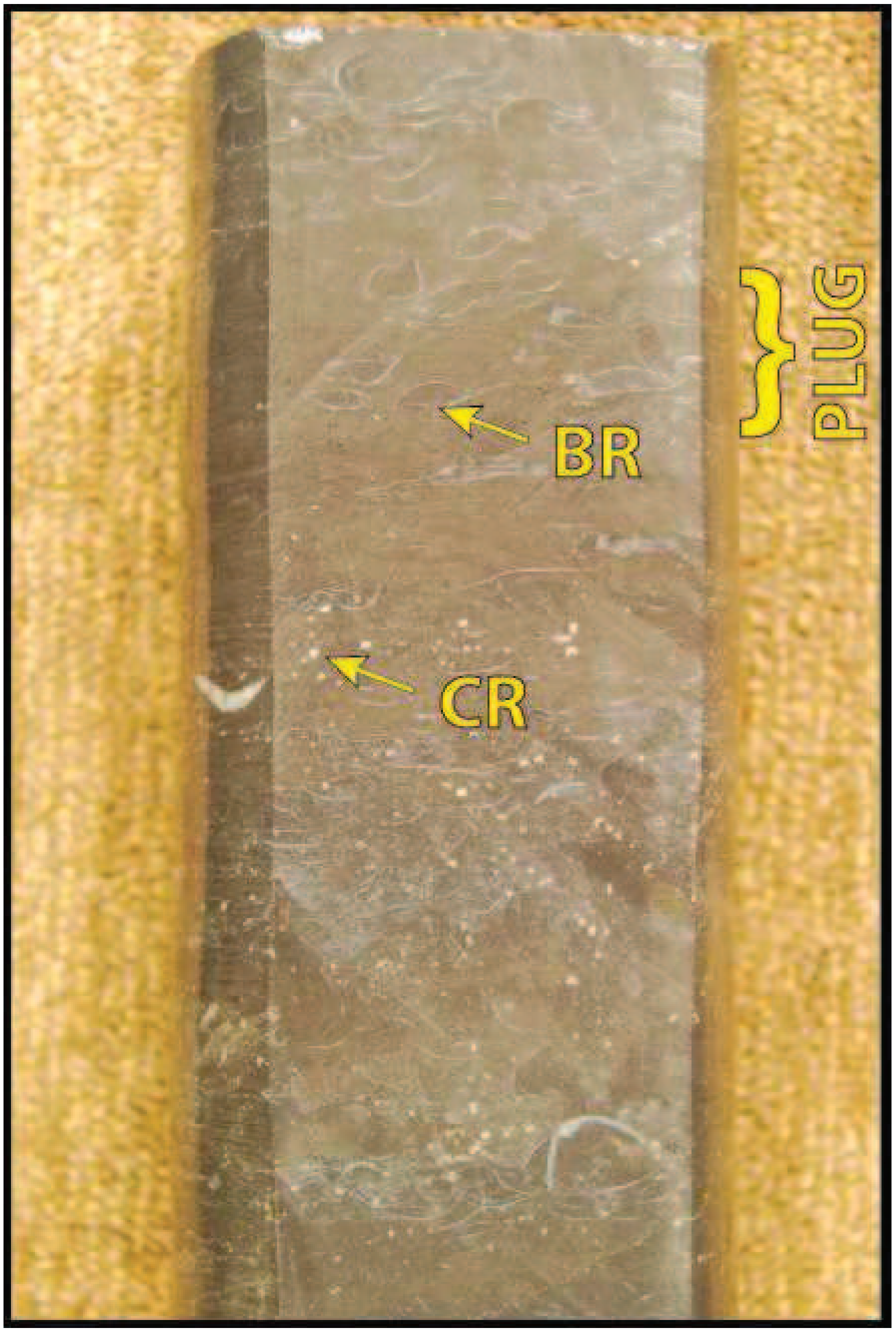

7,970-7,971’: F6

7,962-7,963’: Facies

7,946-7,947’: F6.

7,944-7,945: F6.

7,938.5-7,939.5': Top of "Mississippian Limestone".

II. Droke Unit #1 Thin Section Photomicrographs

Droke Unit #1 thin sections were prepared by Tulsa Sections, Inc. and were blue epoxy impregnated to show porosity. Please refer to Table 6 for abbreviations.

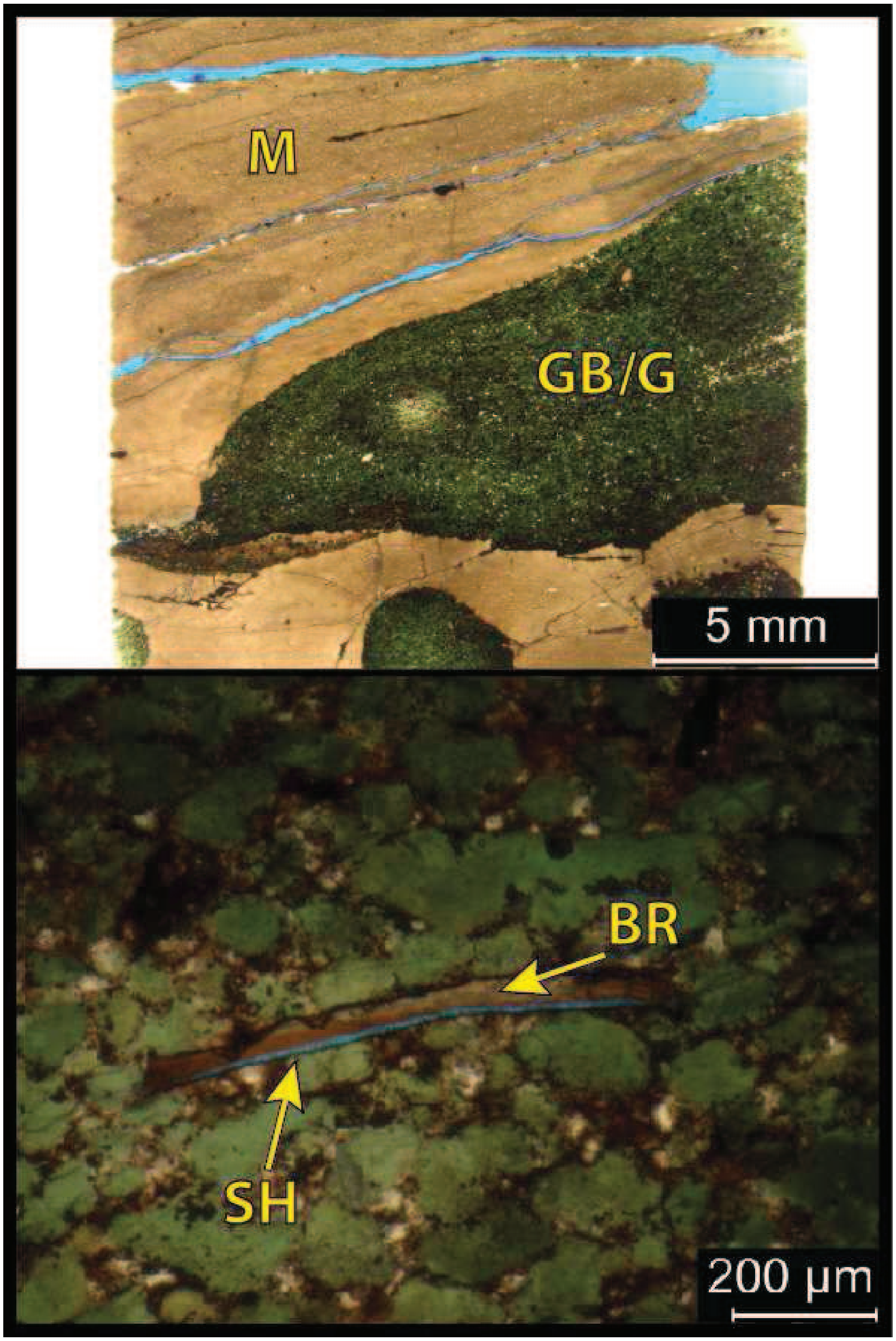

8,450.0': Glauconitic Sandy Shale. "Kinderhook" Shale. Facies 1. Top: XPL. Bottom: PPL. Porosity= 2% (shelter w/ brachiopods in glauconitic portion/ fractured in mud matrix). B.I.: 0. Mineralogy: 75% carbonate, 15% quartz and 10% other minerals. Grains: glauconitic sand grains (25%; 50-400 µm; avg. 200 µm; poor to moderately sorted), brachiopods (<1%; shelter porosity) and trace <1% angular quartz silt in mud matrix.

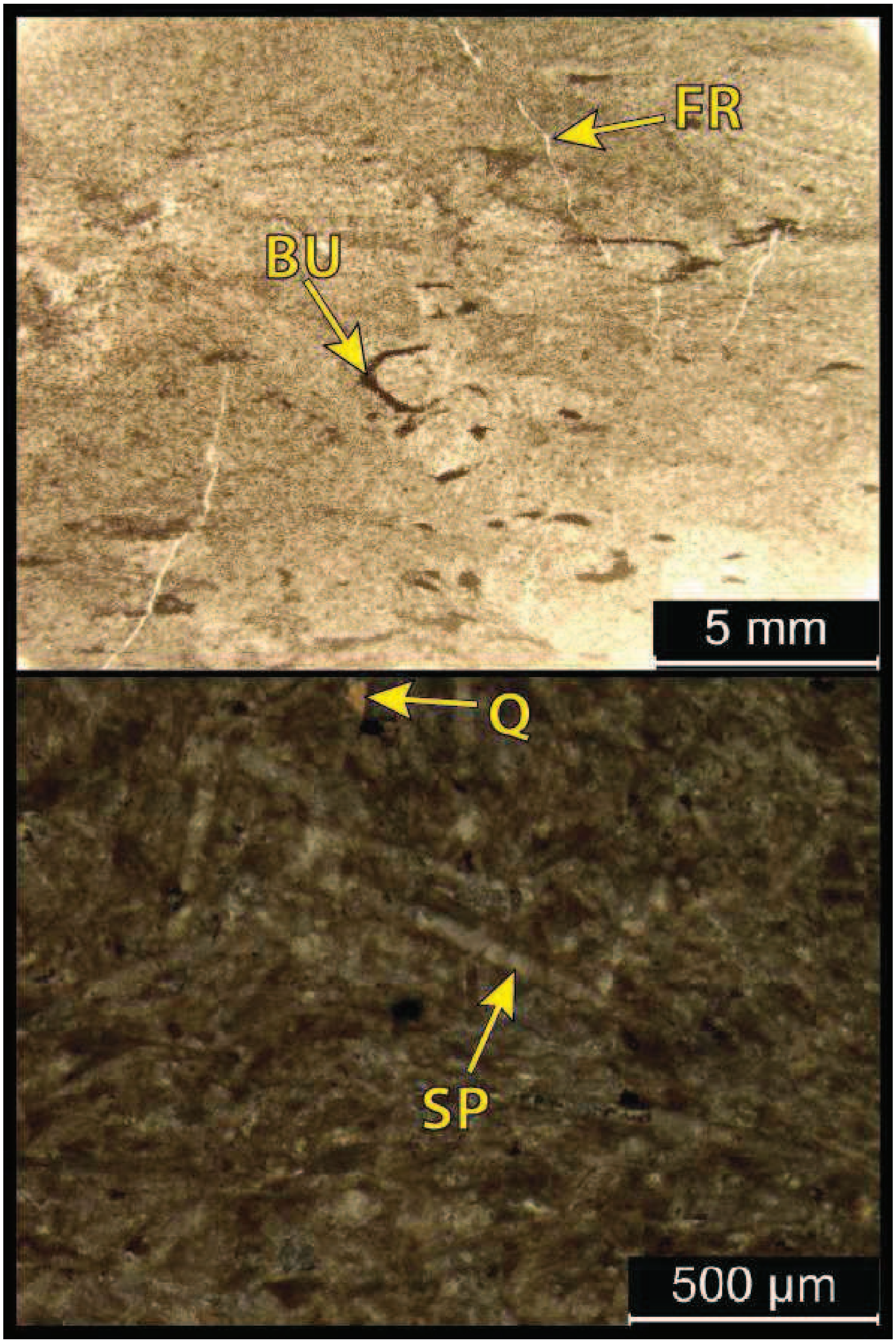

8,437.6': Siliceous and dolomitic mud-rich packstone. Facies 4 Top: XPL. Bottom: PPL. Porosity= 2-4%. B.I.: 1-2 (hz/mm; mud after). Mineralogy: 80% carbonate (65% calcite; 15% dolomite), 15% quartz (14% chert; 1% silt) and ~5% other minerals (clays; feldspars; ~1% pyrite). Grains: Sponge spicules (5%; variably calcitic/siliceous/pyritized; few microns by 500-750 µm blades. Diagenesis: 15% dolomitization, 15% calcite cementation and ~14% silicification (preferential to grainier matrix).

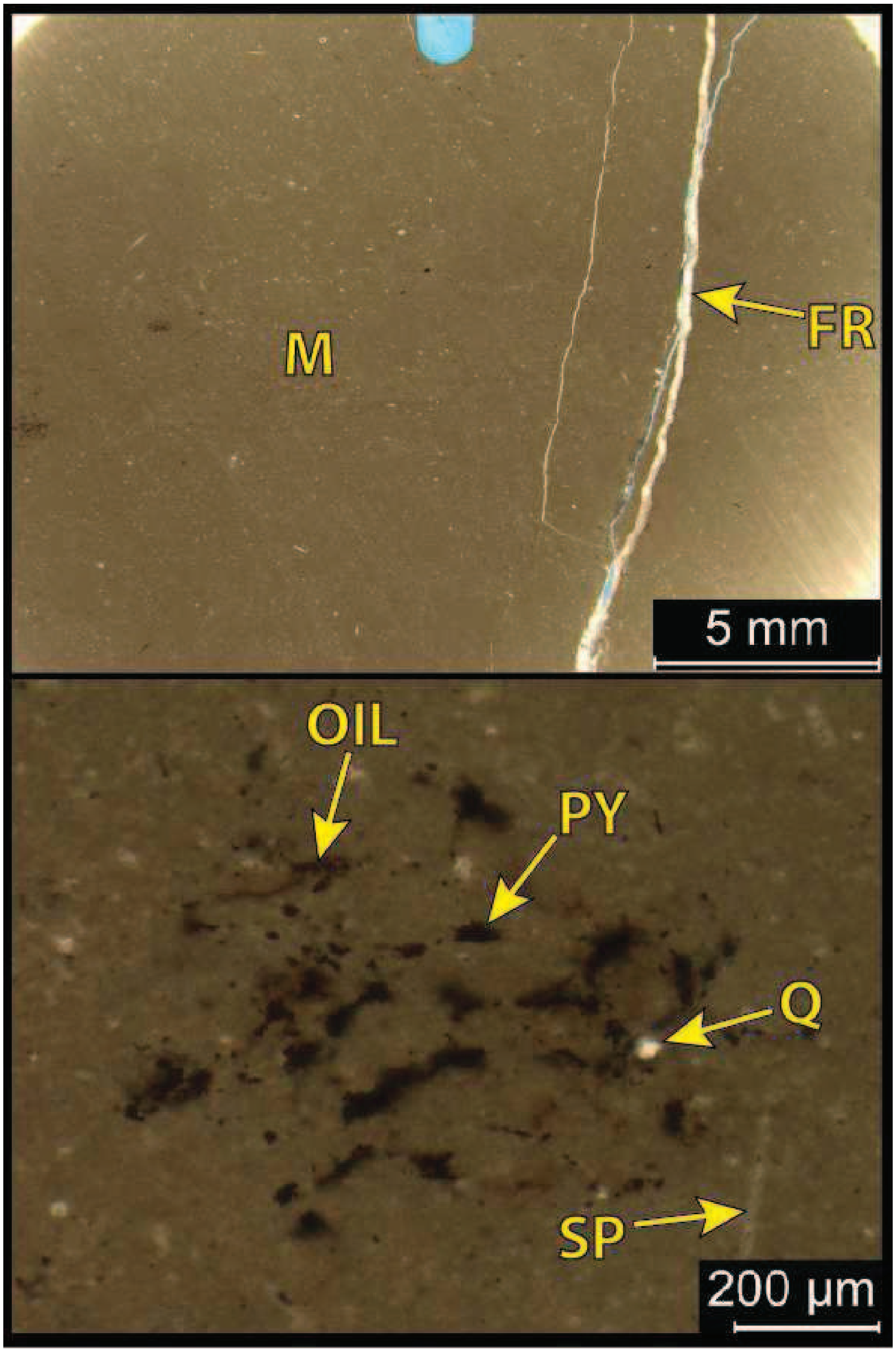

8,426.6': Mudstone. Facies 2. Top: XPL. Bottom: PPL. Porosity= 1% (fracture and dissolution after calcite; dead oil). B.I.: 1 (hz/mm). Mineralogy: 94% carbonate (90% micrite; 4% grains), 2% quartz (1% chert; 1% silt) and 4% other minerals (clays; feldspars; ~2% pyrite). Grains: Sponge spicules (2.5%; calcitic, 4x200 μm blades) and undifferentiated skeletal grains (2%; 10-40μm).

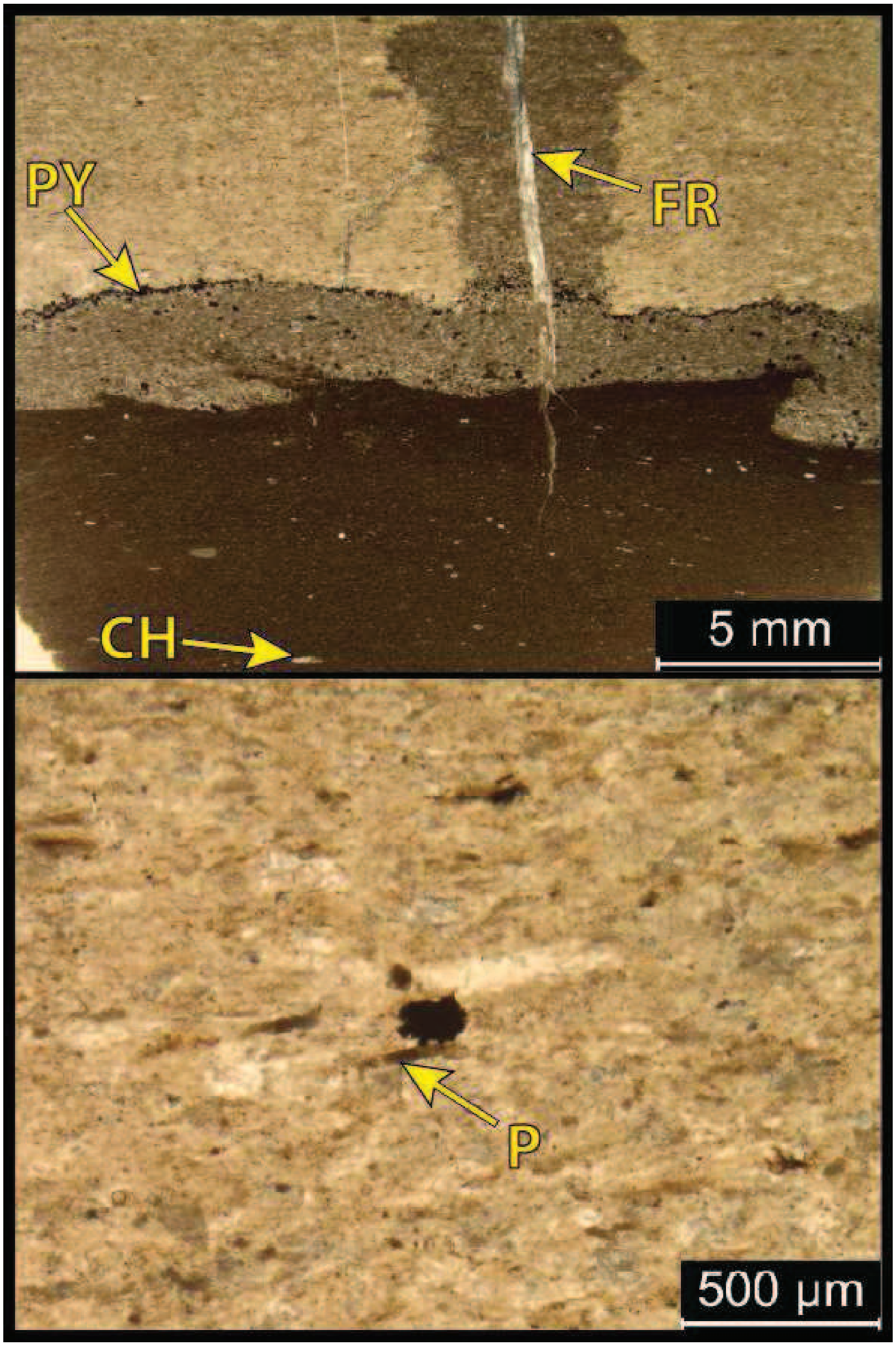

8,397.7': Contact – Mudstone (M) below, mud-lean packstone (P) above. Facies 4. Top: XPL. Bottom: PPL. Porosity= 5% (fracture, 10-40 µm intergranular dead oil). B.I.: 0. Mineralogy: 87% carbonate (79.5% calcite; 7.5% dolomite), 3% quartz (2.5% chert; <1% silt) and 10% other minerals (5% clays/feldspars; 5% pyrite). Grains: 5% -Sponge spicules (2.5%; P; calcitic; ~150µm), 2.5% bioclasts up to 100x500µm parallel to bedding in M (undifferentiated skeletal fragments, benthic foraminifera, echinoderms). Diagenesis: 20% calcite cementation (P), 7.5% dolomitization (P), 5% pyritization (concentrated at contact) and 2.5% silicification (nodules in M).

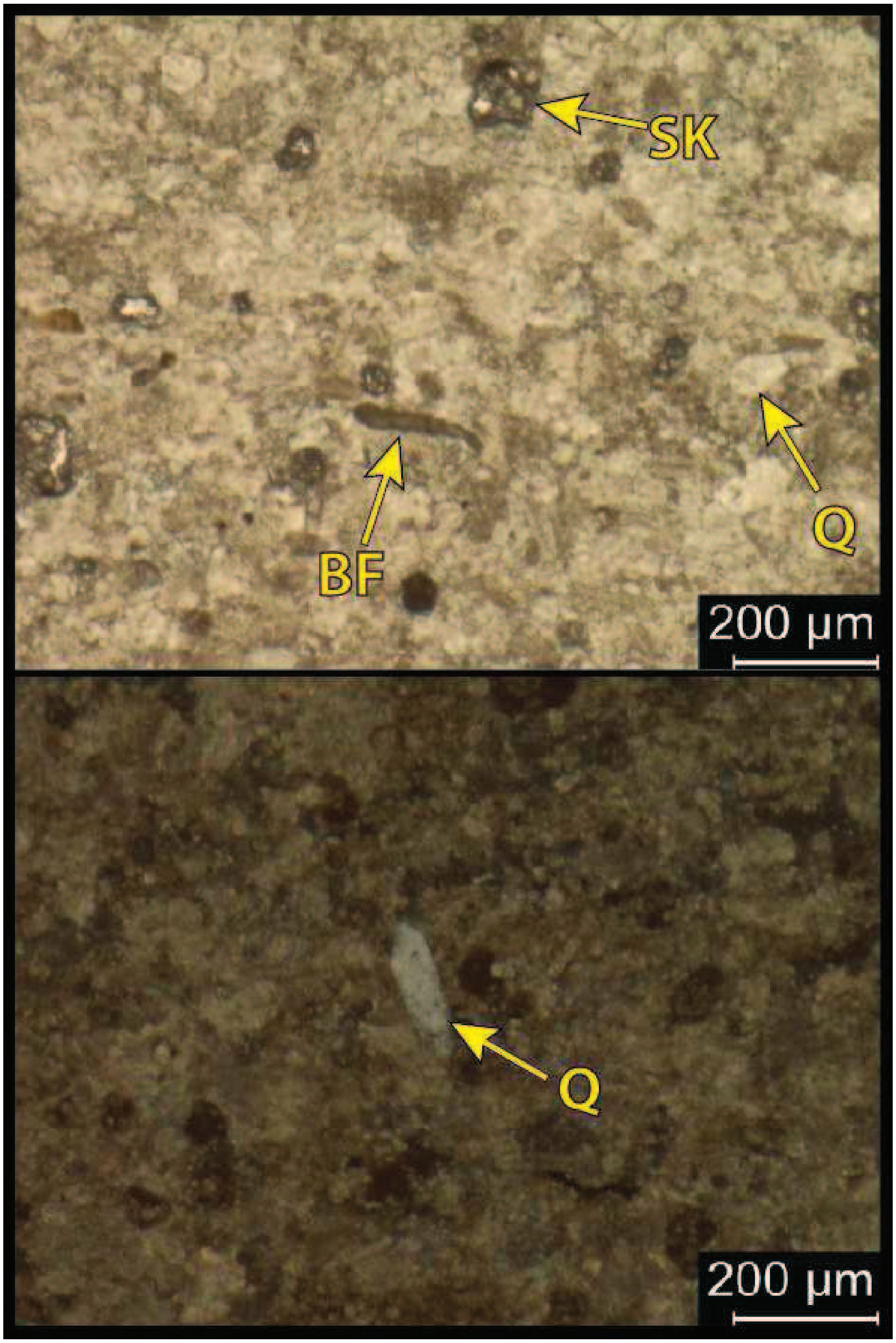

8,395.5': Dolomitic mud-lean packstone. Facies 5 Top: XPL. Bottom: PPL. Porosity= 4% (intergranular). B.I.: 0. Mineralogy: 96% carbonate (86% calcite; 10% dolomite), 3% quartz (2% silt; 1% chert) and 1% other minerals. Grains: very well-sorted peloidal, brachiopod and crinoid fragments, benthic foraminifera and undifferentiated skeletal fragments (all ~80-160µm). Common abrasion of undifferentiated grains during polishing. Diagenesis: 15-20% calcite cementation and 10% dolomitization.

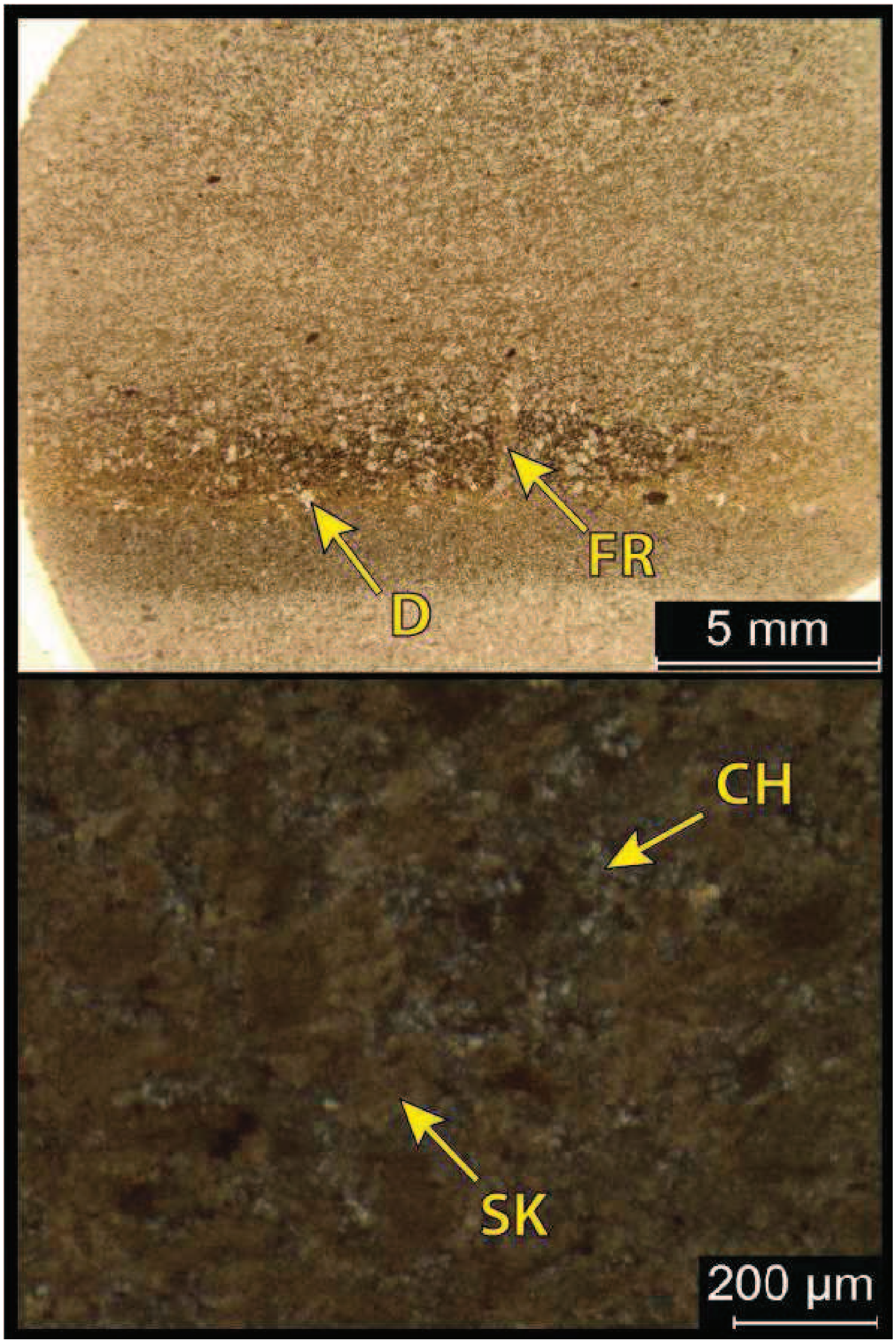

8,394.0': Dolomitic and siliceous wackestone-packstone. Facies 5 Top: XPL. Bottom: PPL. Porosity= 5-7.5% (intergranular and fracture). B.I.: 0. Mineralogy: 71.5% carbonate (56.5% calcite; 15% dolomite), 21% quartz (20% chert; 1% silt) and 7.5% other minerals (5% clays/feldspars; 2.5% pyrite). Grains: peloidal/ undifferentiated skeletal fragments (50-200µm) and seldom (<1%) thin-shelled brachiopods (150µm x 3mm). Diagenesis: 20% silicification, 10% dolomitization (100-300µm and concentrated in muddier bed/fracture), 2.5% calcite cementation and 2.5% pyritization.

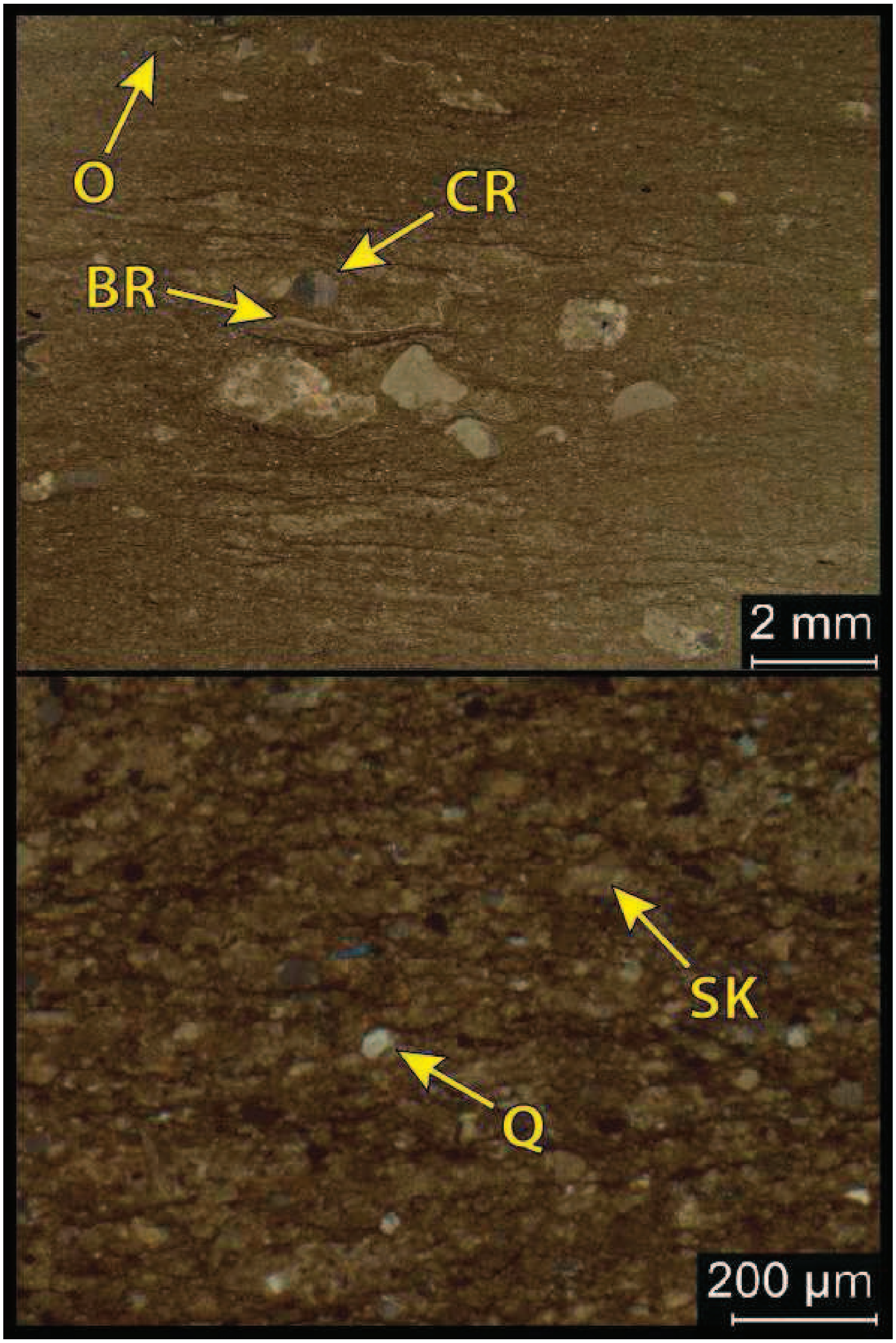

8,358.0': Bioclastic crinoidal wackestone. Facies 3. Top: XPL. Bottom: PPL. Porosity= 2% (intergranular). B.I.: 0. Mineralogy: 84% carbonate (79% calcite; 5% dolomite), 6% quartz (5% silt; 1% chert) and 10% other minerals (8% clays/feldspars; 2% pyrite). Grains: Crinoids (15%; up to 1.5mm), ostracodes (1%; 300-500µm) and undifferentiated skeletal debris (5%; 40-160µm). Diagenesis: 10% calcite cementation (after bioclasts); 5% dolomitization (after bioclasts); 1% silicification.

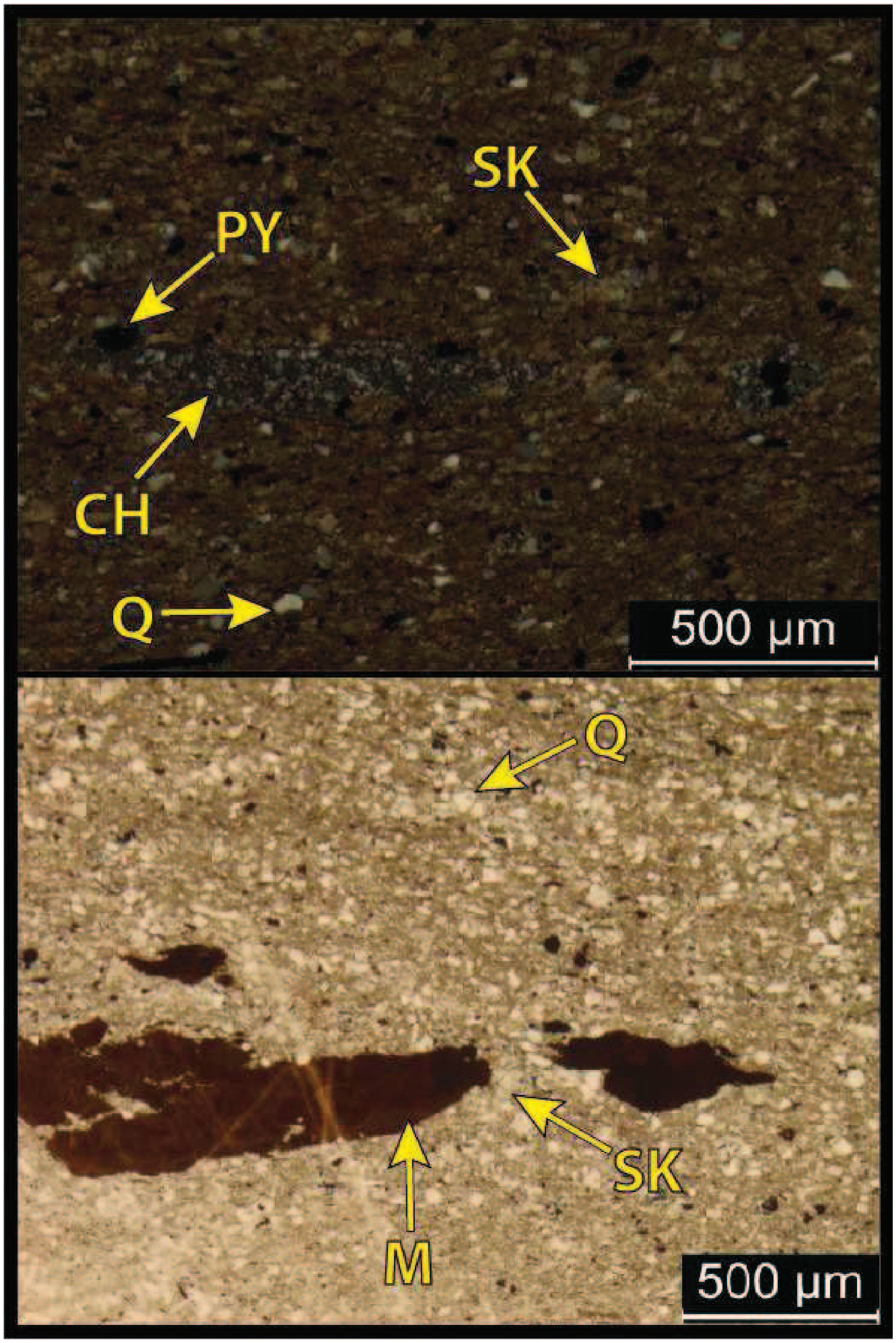

8,330.6': Silty mud-lean wackestone. Facies 4. Top: XPL. Bottom: PPL. Porosity= 2% (intergranular). B.I.: 1. Mineralogy: 65.5% calcite, 22.5% quartz (10% silt; 12.5% chert) and 12% other minerals (9% clays/feldspars; 3% pyrite). Grains: few bioclasts (<1%; 200-500µm); Sponge spicules (2.5%; up to 70µm x 1mm); crinoid and undifferentiated skeletal fragments (5%; avg. 50-100µm). Diagenesis: 5% calcite cementation; 12.5% silicification (nodular).

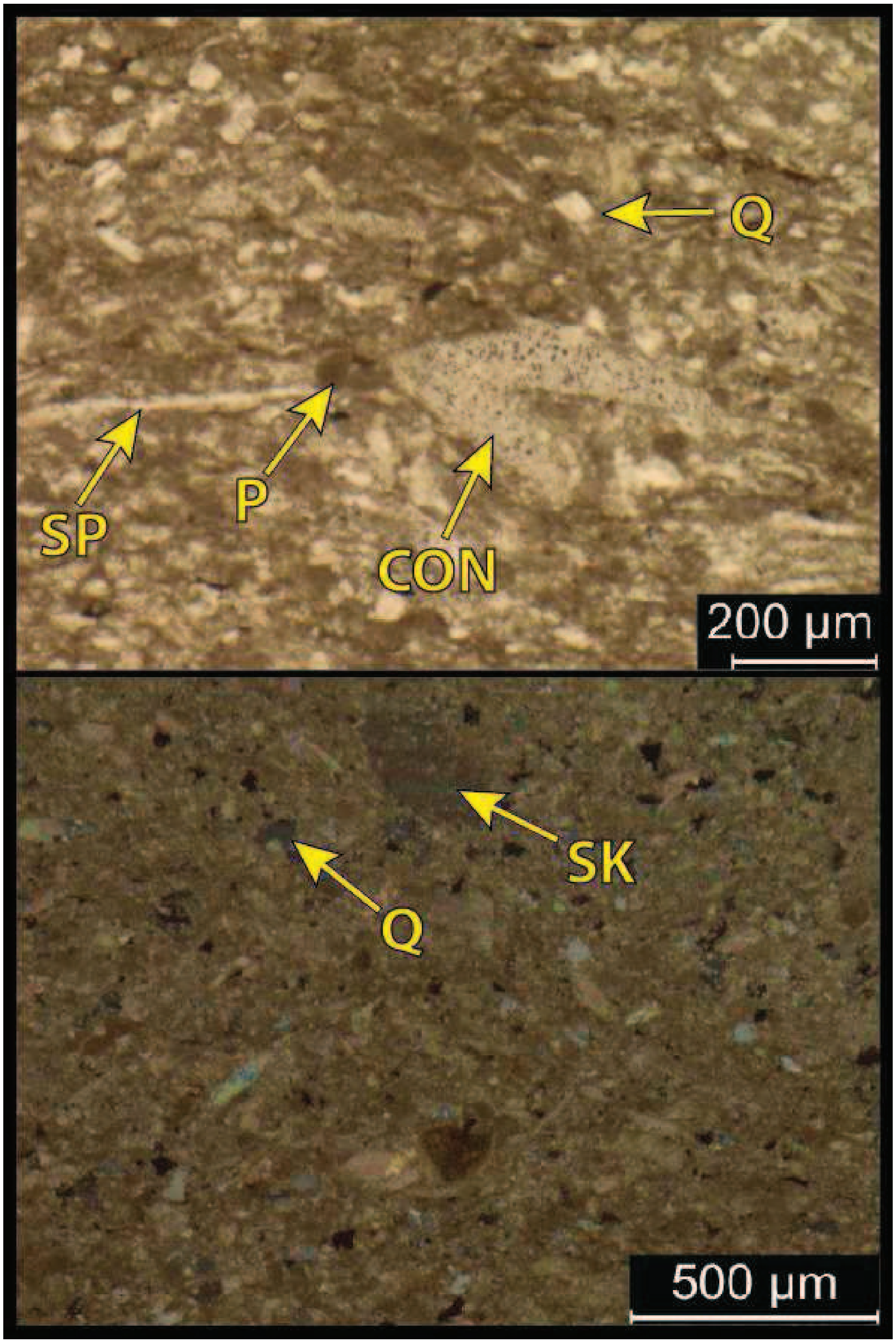

8,325.0': Silty, siliceous mud-rich packstone. Facies 4. Top: XPL. Bottom: PPL. Porosity= 4% (intergranular; some oil-stained). B.I.: 2. Mineralogy: 84.5% carbonate (82.5% calcite; 2% dolomite), 7% quartz (5% silt; 2% chert) and 8.5% other minerals (7.5% clays/feldspars; 1% pyrite). Grains: Poorly sorted; few bioclasts (0.25-0.75mm); crinoid, brachiopod, peloidal and undifferentiated skeletal fragments (~50-100µm); sponge spicules (up to 1mm; most <500µm). Diagenesis: 10% calcite cementation; 2% dolomitization (~100µm rhombs); 2% silicification.

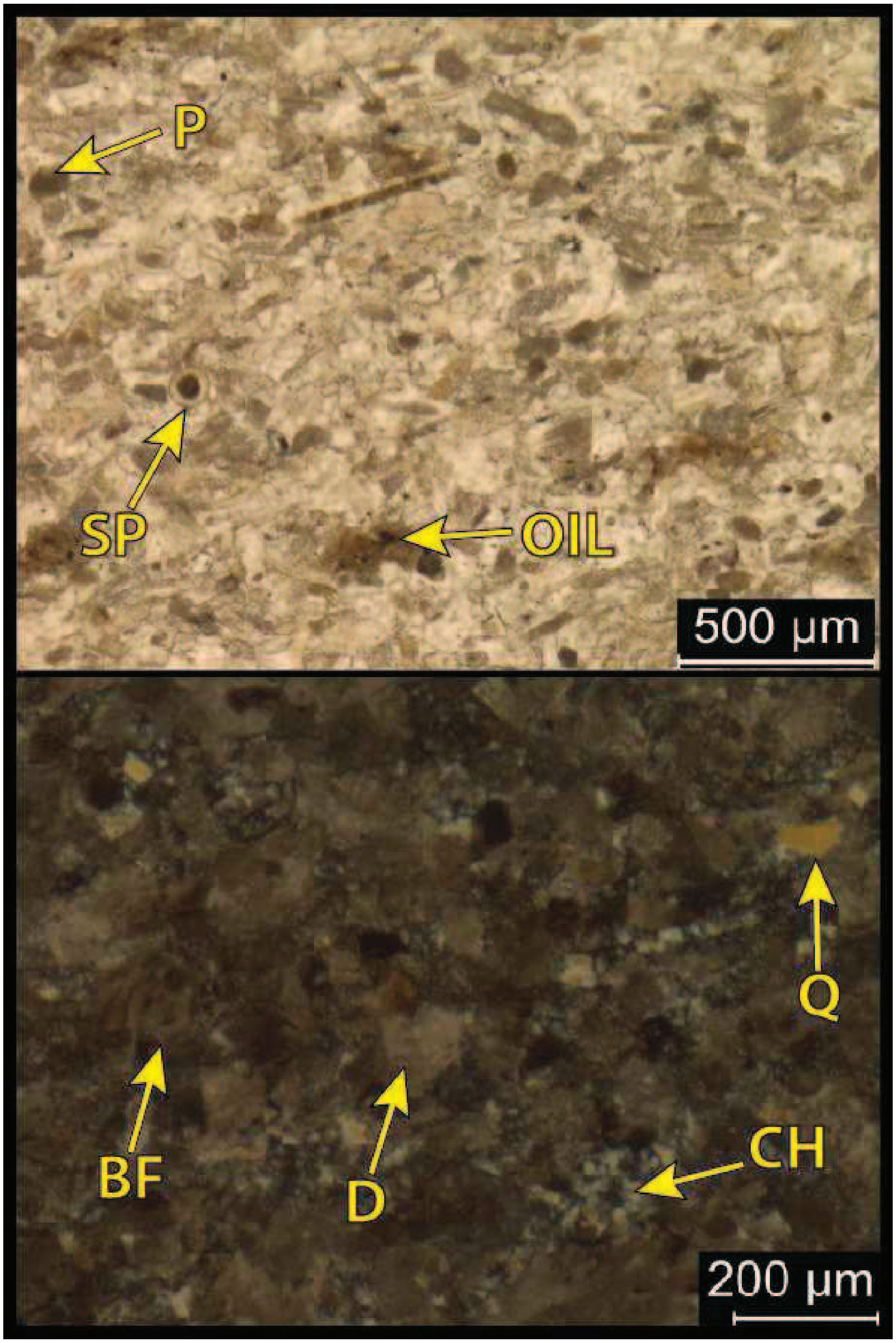

8,260.0': Dolomitic fossiliferous mud-lean packstone. Facies 5. Top: XPL. Bottom: PPL. Porosity= 5% (intergranular/intercrystalline; oil-staining). B.I.: 0. Mineralogy: 88.5% carbonate (76% calcite; 12.5% dolomite), 7.5% quartz (5% chert; 2.5% silt) and 4% other minerals (2% clays/feldspars; 2% pyrite). Grains: well-sorted peloid, crinoid, brachiopod, bryozoa and undifferentiated skeletal fragments (50-100µm) with rare (<1%) sponge spicules. Diagenesis: 15% calcite cementation; 12.5% dolomitization (~100µm rhombs); 5% silicification; micritized fossil grains.

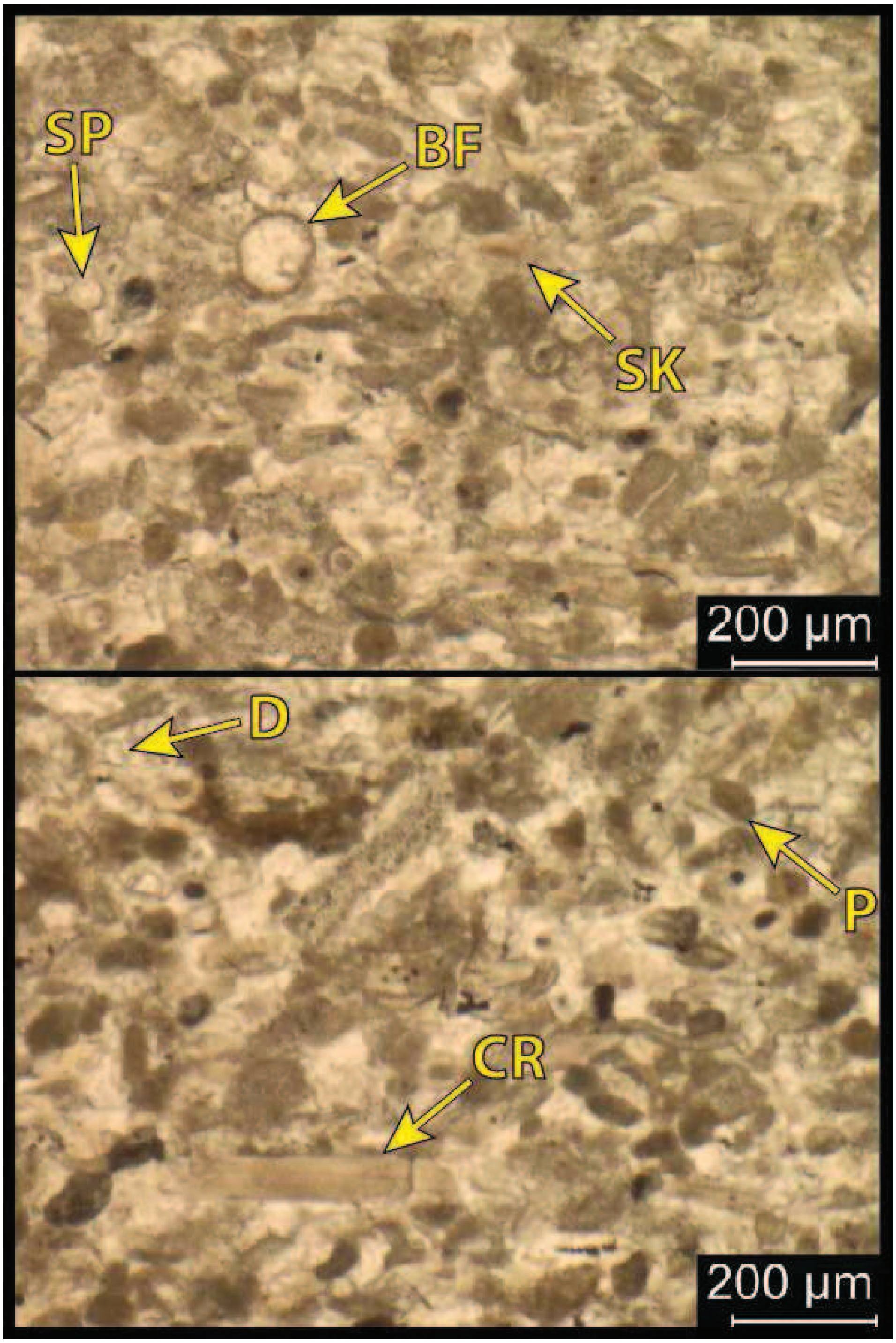

8,236.5': Slightly dolomitic fossiliferous mud-lean packstone. Facies 5. Top: XPL. Bottom: PPL. Porosity= 2%. B.I.: 0. Mineralogy: 93.5% carbonate (86% calcite; 7.5% dolomite), 4.5% quartz (2.5% chert; 2% silt) and 2% other minerals (1% pyrite). Grains: well-sorted foraminifera, peloids, crinoids, brachiopods, bryozoa and undifferentiated skeletal fragments (max 300µm; avg. 40-120µm) with rare (<1%) sponge spicules. Diagenesis: 15% calcite cementation; 7.5% dolomitization (~10-40µm rhombs); 2.5% silicification; micritized fossil grains.

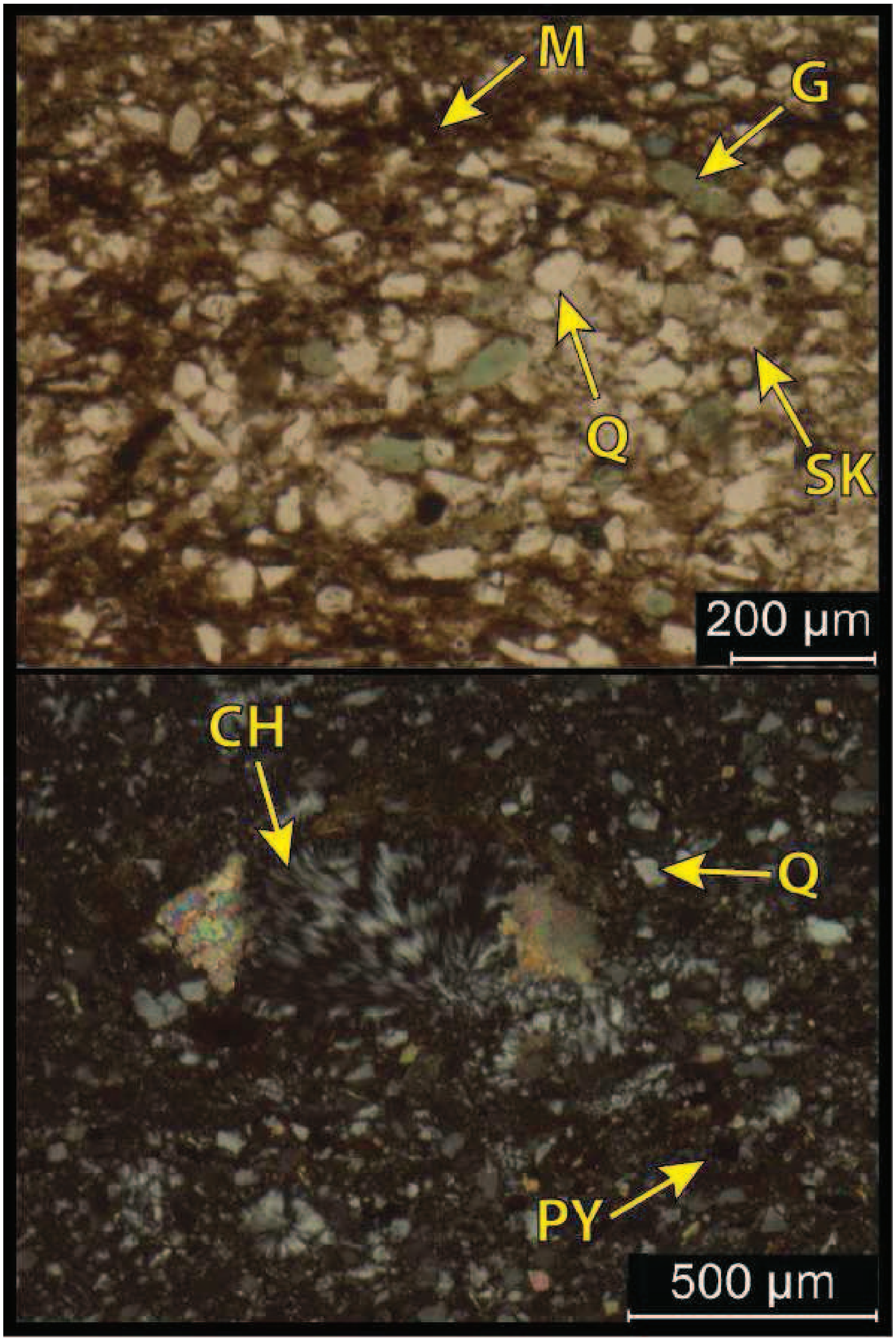

8,226.4': Glauconitic siltstone. Facies 1. Top: XPL. Bottom: PPL. Porosity= 2-4%. B.I.: 2. Mineralogy: 65% quartz (35% silt-vf sand; 30% chert); 15% carbonate (14% calcite; 1% dolomite) 10% glauconite and 10% other minerals (7% clays/feldspars; 3% pyrite). Grains: undifferentiated skeletal fragments (50-100µm); silicified crinoid/echinoid grains (2.5%; 0.5-1mm). Diagenesis: 30% silicification (chert to some chalcedony); 3% pyritization (most few microns, up to 75µm cuboidal crystals within highly siliceous portions/spicules).

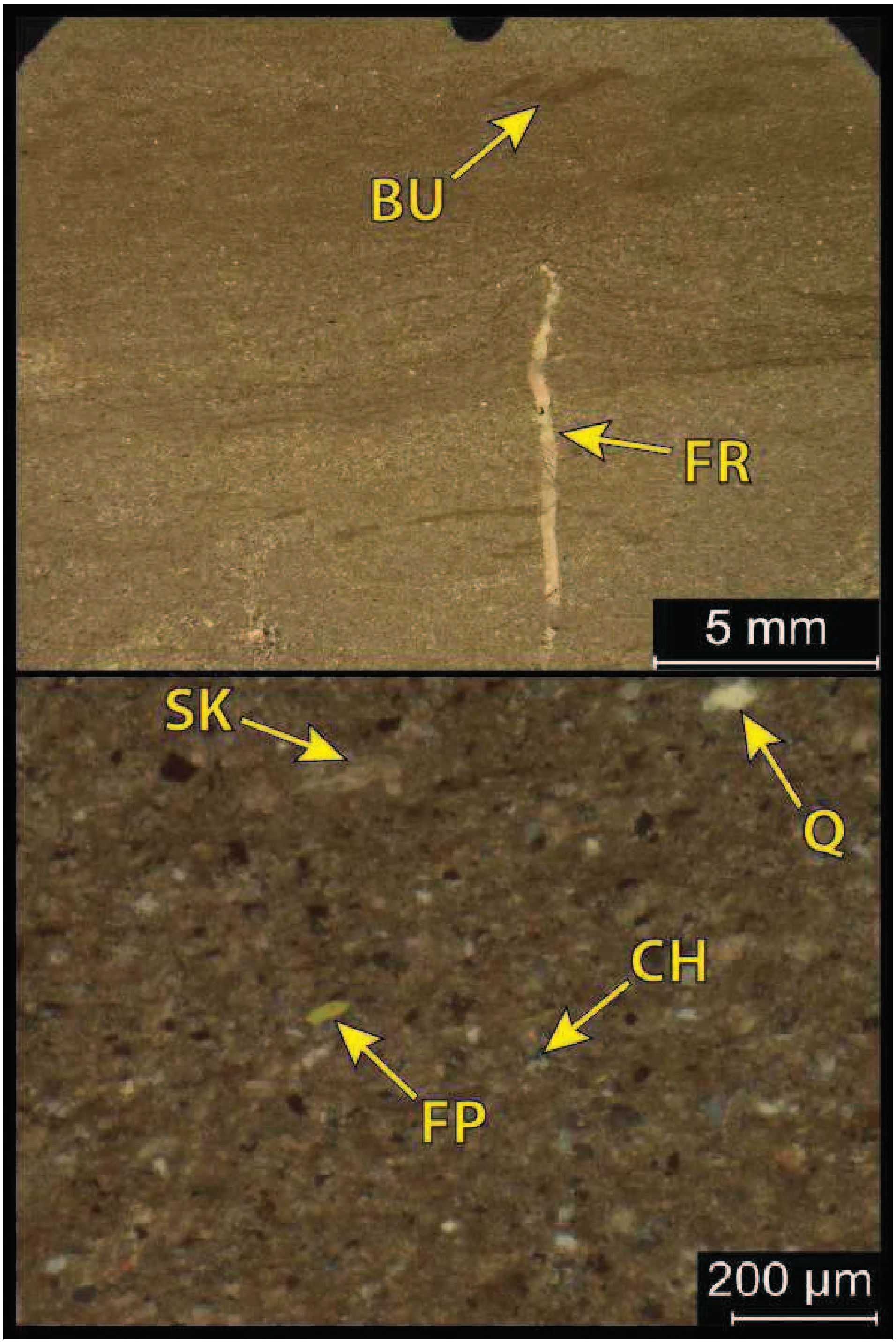

8,201.5': Mud-lean wackestone/ mud-rich packstone. Facies 4. Top: XPL. Bottom: XPL. Porosity= 2%. B.I.: 3. Mineralogy: 71% carbonate (70% calcite; 1% dolomite), 17.5% quartz (10% chert; 5% silt) and 11.5% other minerals (10% clays/feldspars; 1.5% pyrite). Grains: crinoidal, peloidal and undifferentiated skeletal fragments (avg. 60µm; biggest 125µm); 2% sponge spicules (variably calc/chert; 40x200µm). Diagenesis: 10% silicification; 2.5% calcite cementation.

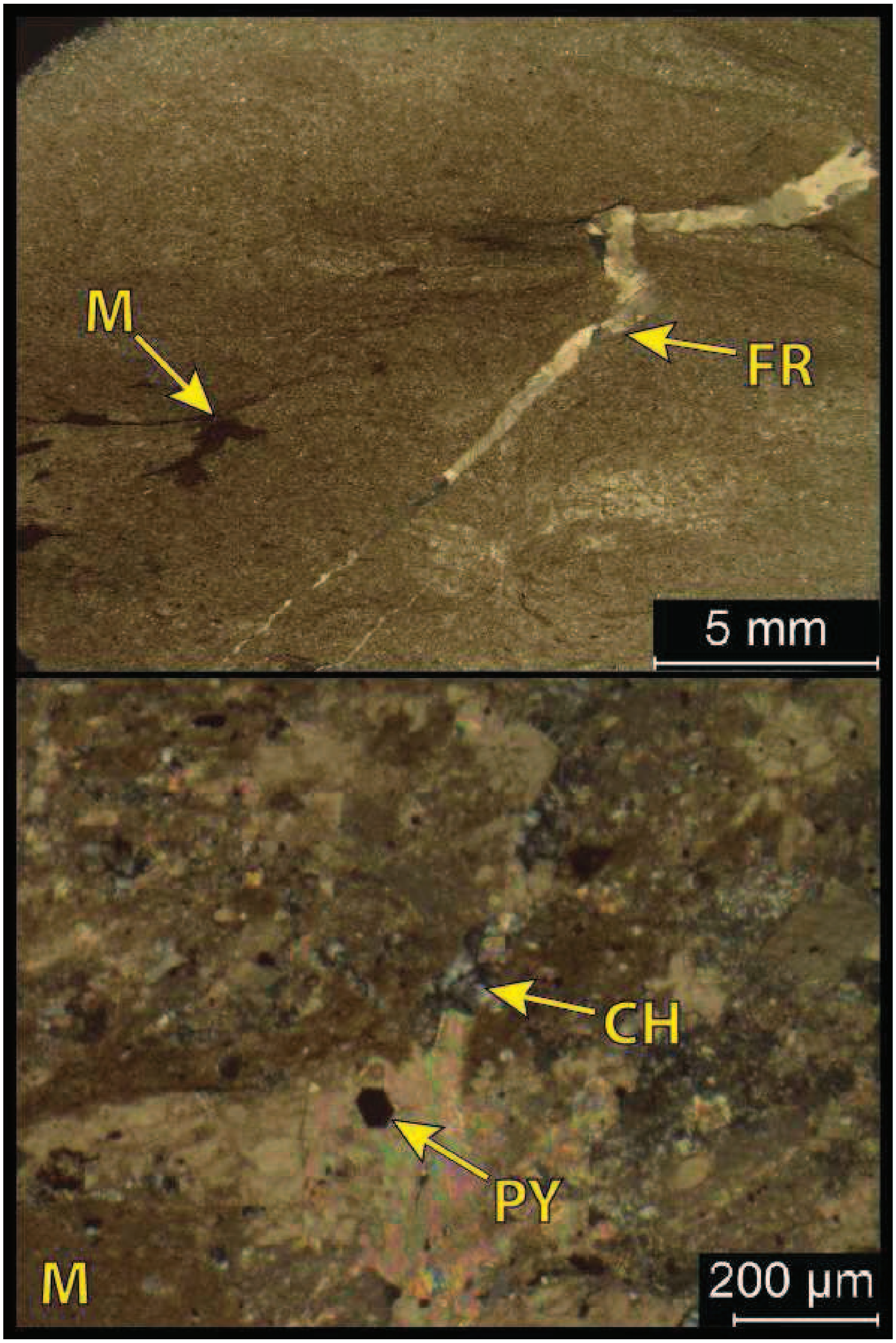

8,193.0': Siliceous and silty mud-lean wackestone. Facies 4. Top: XPL. Bottom: XPL. Porosity= 4%. B.I.: 2 (mud-after). Mineralogy: 55.5% carbonate (50.5% calcite; 5% dolomite), 32.5% quartz (25% chert; 7.5% silt) and 12% other minerals (10% clays/feldspars; 2% pyrite). Grains: crinoidal/peloidal/undifferentiated skeletal fragments (10-50µm); sponge spicules (10-25µm) Diagenesis: 25% silicification; 5% dolomitization (preferential to grainier matrix); 5% calcite cementation. Cm-scale vertical fractures (chert & dolomite-filled).

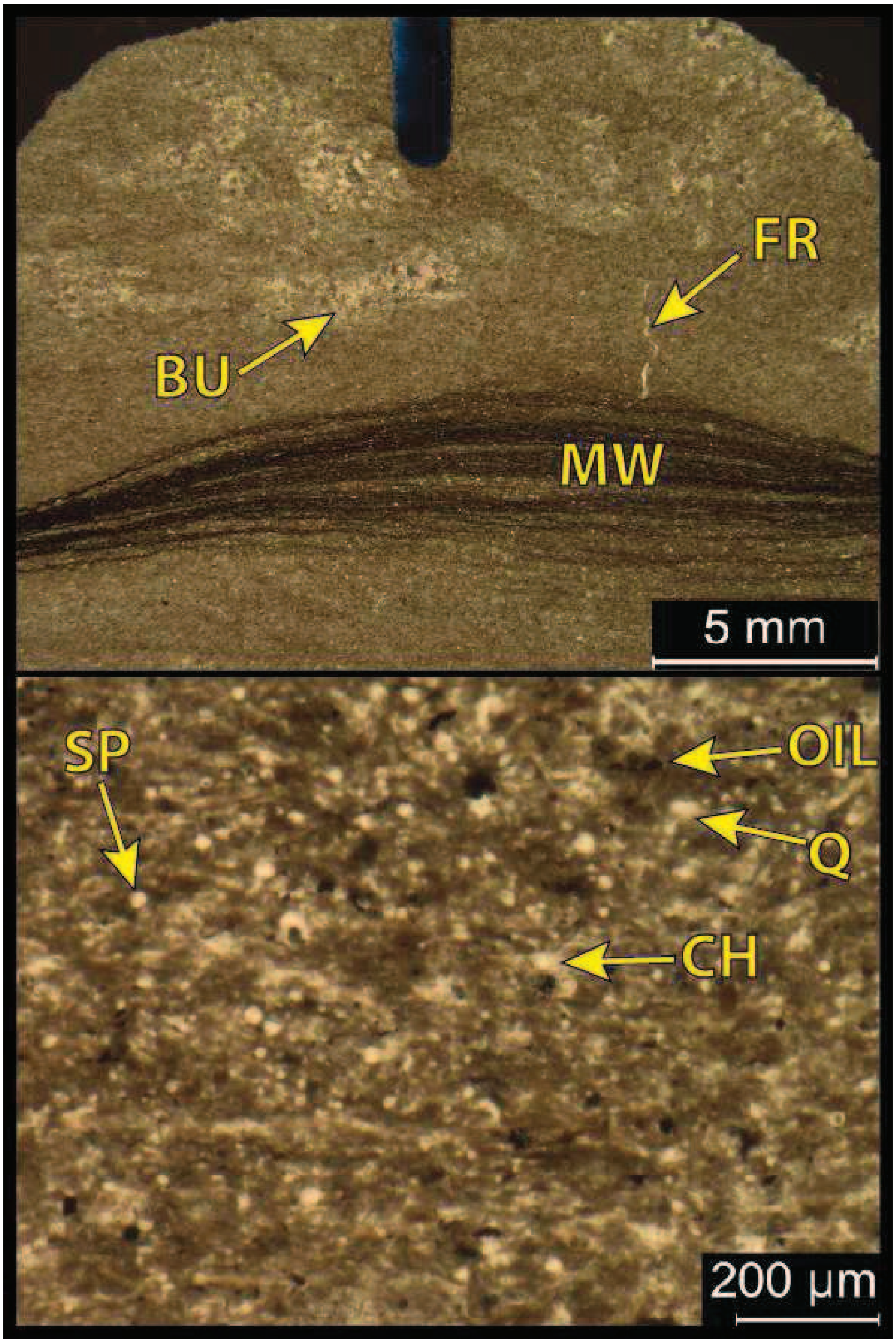

8,179.0': Siliceous silty packstone (w/ mud wisp interbed). Facies 4. Top: XPL. Bottom: PPL. Porosity= 4% (nano/ 100µm vug in dolomitic burrow). B.I.: 3 (mm-scale; preferential chert/hi-Mg calcite/dolomite). Mineralogy: 54% carbonate (46.5% calcite; 7.5% dolomite), 30% quartz (20% chert; 10% silt) and 16% other minerals (15% clays/feldspars; 1% pyrite). Grains: crinoidal/peloidal/undifferentiated skeletal fragments (biggest 350µm; most 10-50µm); sponge spicules (10-25µm). Diagenesis: 20% silicification, 7.5% dolomitization and 5% calcite cementation (preferential to burrows).

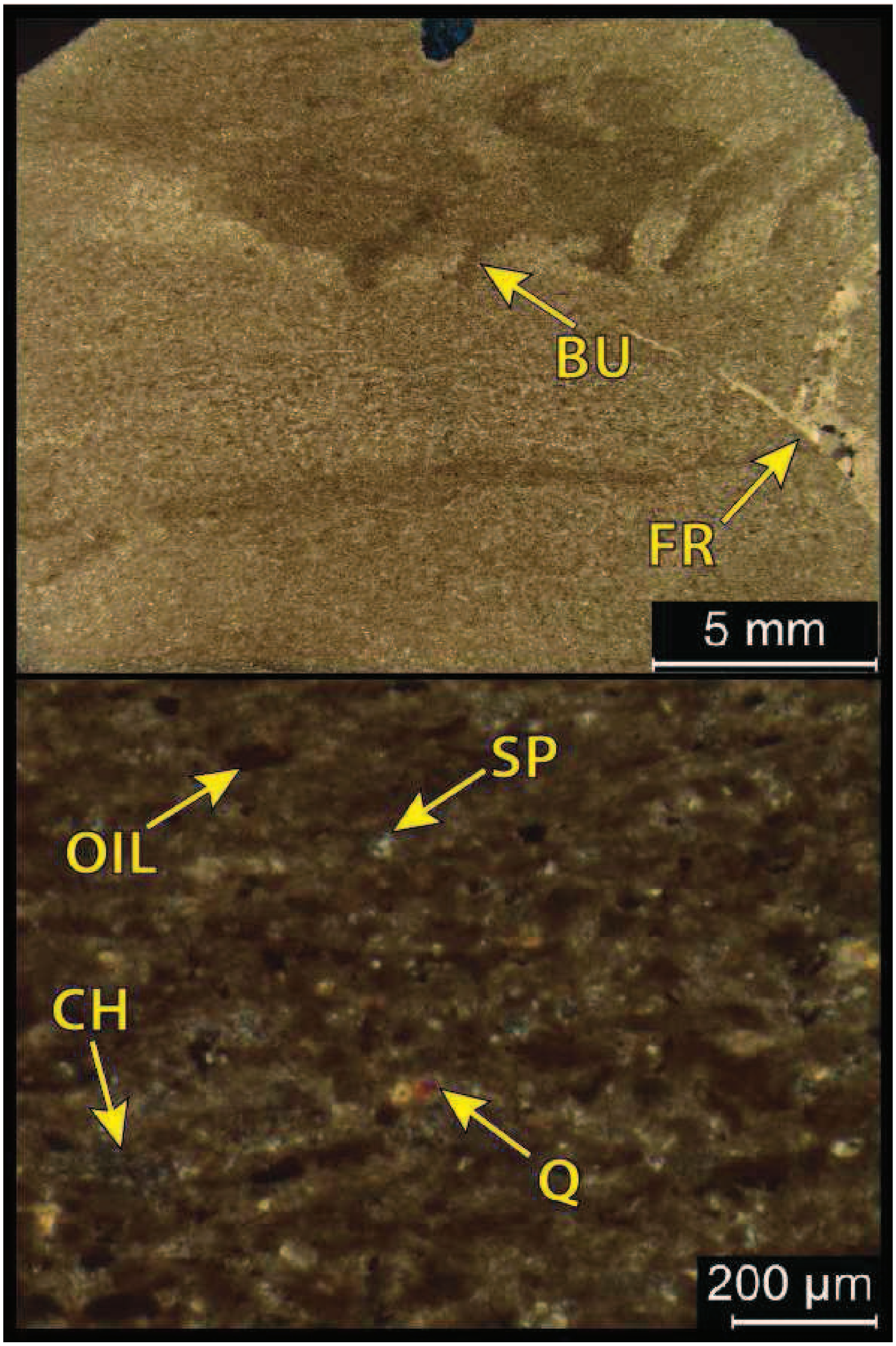

8,178.3': Siliceous silty packstone. Facies 4. Top: XPL. Bottom: XPL. Porosity= 1%. B.I.: 2-3. Mineralogy: 52.5% carbonate (48.5% calcite; 4% dolomite), 35% quartz (30% chert; 5% silt) and 12.5% other minerals (10% clays/feldspars; 2.5% pyrite). Grains: well-sorted peloidal/ undifferentiated skeletal fragments (20-40µm); sponge spicules (10x500µm). Diagenesis: 30% silicification; 5% calcite cementation; 4% dolomitization (filling fracture).

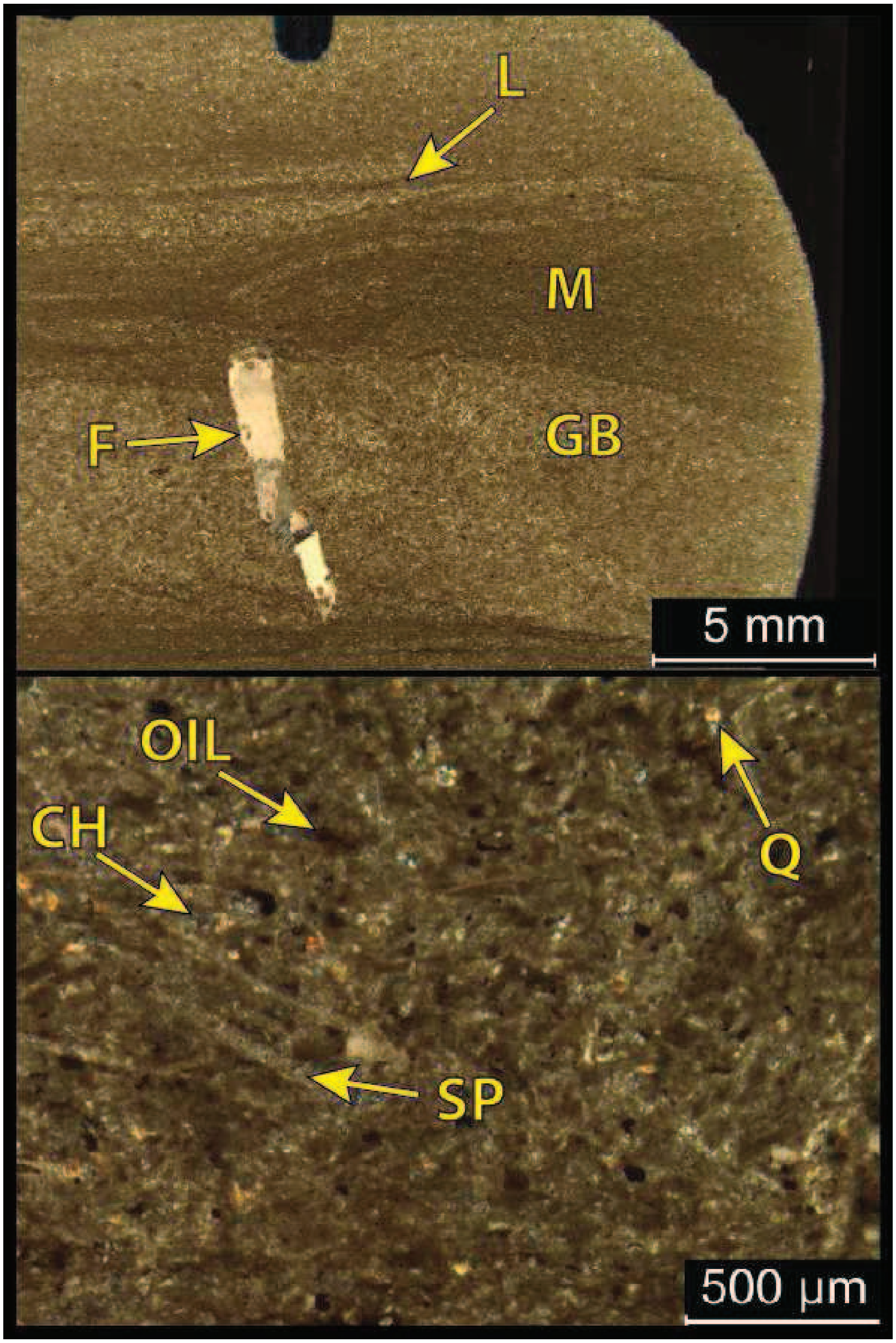

8,127.7': Slightly siliceous wackestone/packstone (interbeds). Facies 5. Top: XPL. Bottom: XPL. Porosity= 1%. B.I.: 1-2. Mineralogy: 77.5% carbonate (75.5% calcite; 2% dolomite), 12.5% quartz (7.5% chert; 5% silt) and 10% other minerals (7.5% clays/feldspars; 2.5% pyrite). Grains: moderately-sorted sponge spicules (10%; variably calcite/chert; 50x500μm) and peloidal/ undifferentiated skeletal fragments (20%; 20-50μm). Diagenesis: 7.5% silicification; 7.5% calcite cementation (deep burial fracture-fill). 1mm-wide fracture preferential to grain-rich bed.

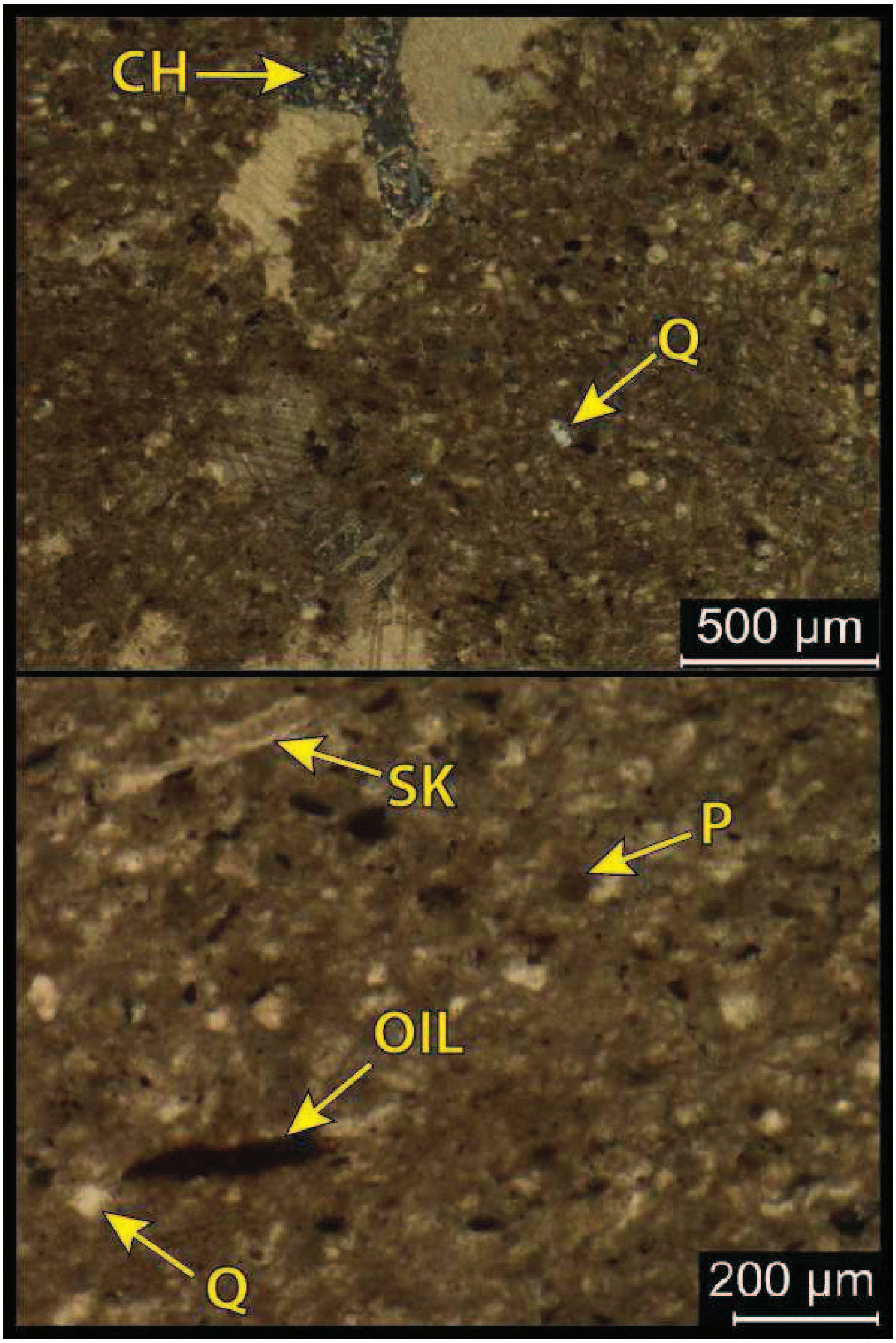

8,121.0': Slightly siliceous wackestone. Facies 4. Top: XPL. Bottom: PPL. Porosity= 1-2%. B.I.: 2 (mud after). Mineralogy: 76.5% carbonate (75.5% calcite; 1% dolomite), 12.5% quartz (7.5% chert; 5% silt) and 11% other minerals (7.5% clays/feldspars; 3.5% pyrite). Grains: peloidal grains (<40µm); undifferentiated skeletal fragments (20-75µm); sponge spicules (50-250µm; variably calcite/chert). Diagenesis: 10% calcite cementation throughout (multiple generations in fracture); 7.5% silicification.

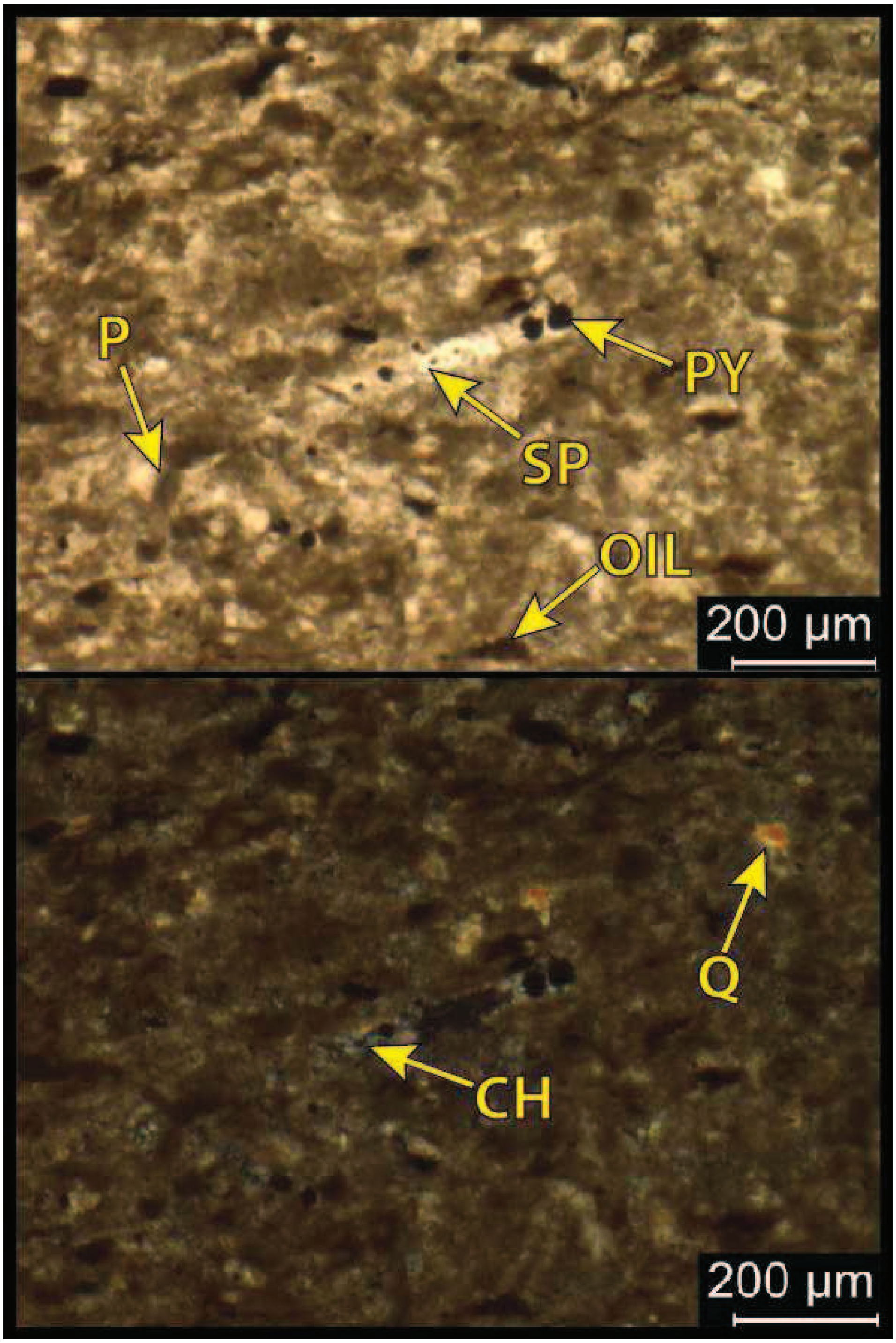

8,103.9': Slightly siliceous mud-lean wackestone. Facies 3. Top: PPL. Bottom: XPL. Porosity= <1%. B.I.: 1-2 (mud after). Mineralogy: 76.5% carbonate (75.5% calcite; 1% dolomite), 12.5% quartz (7.5% chert; 5% silt) and 11% other minerals (7.5% clays/feldspars; 3.5% pyrite). Grains: peloidal grains (<40µm); undifferentiated skeletal fragments (20-75µm); sponge spicules (50-250µm; variably calcite/chert/minor pyrite). Diagenesis: 10% calcite cementation throughout; 7.5% silicification.

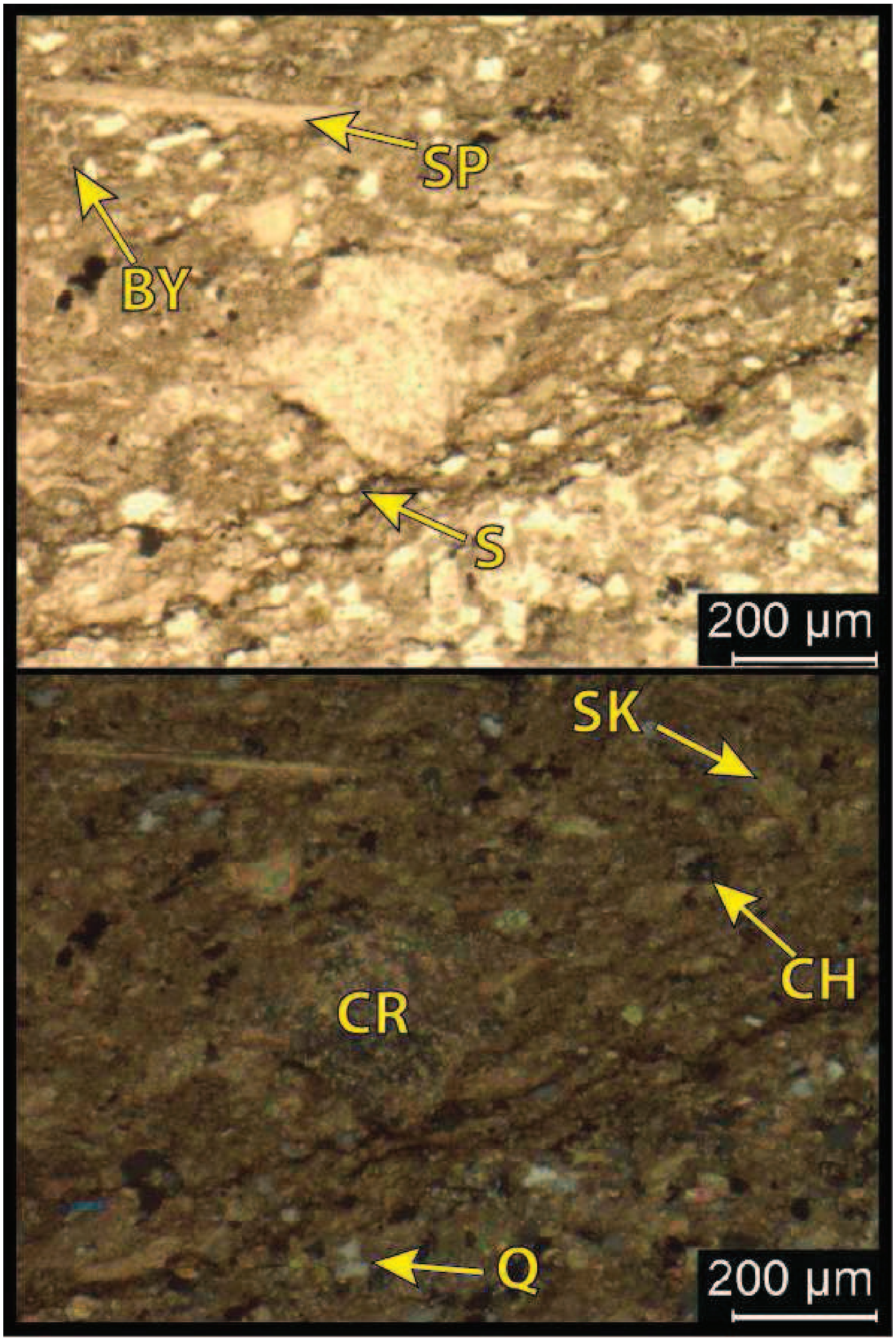

8,054.0': Slightly siliceous, silty mud-lean wackestone/ mud-rich packstone. Facies 4. Top: PPL. Bottom: XPL. Porosity= 1%. B.I.: 2 (mud after). Mineralogy: 82.5% carbonate, 7.5% quartz (2.5% silt-vf sand; 5% chert) and 10% other minerals (7% clays/feldspars; 3% pyrite). Grains: Peloidal grains/ undifferentiated skeletal fragments (20-50µm); crinoid, brachiopod and bryozoa fragments (biggest 275µm; more prevalent in muddier matrix); sponge spicules (~40x400µm). Diagenesis: 5% calcite cementation throughout; 5% silicification.

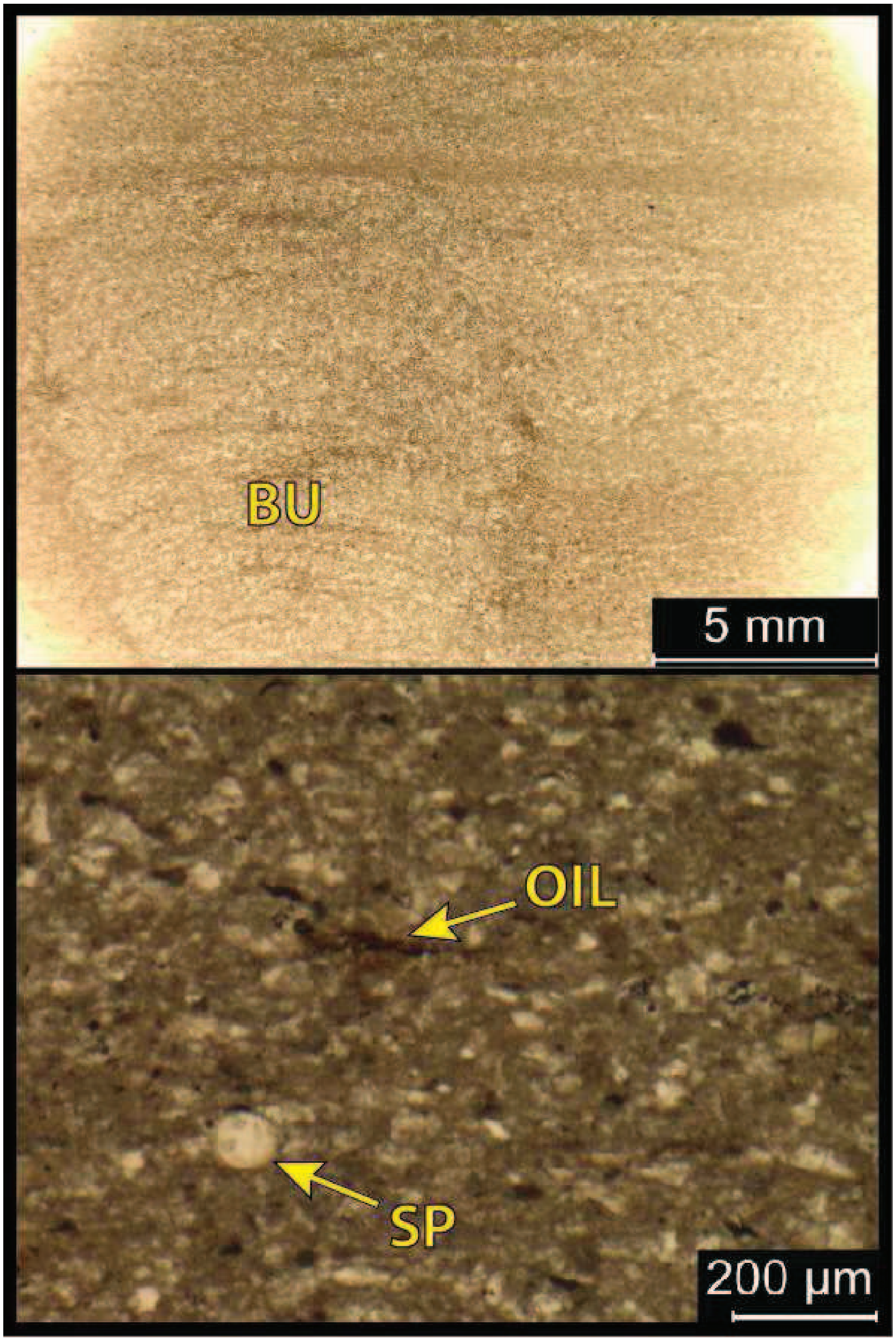

8,034.7': Slightly siliceous, silty mud-lean wackestone. Facies 4. Top: PPL. Bottom: PPL. Porosity= 3%. B.I.: 2 (grain-rich after). Mineralogy: 80% carbonate (79% calcite; 1% dolomite), 10% quartz (7.5% chert; 2.5% silt) and 10% other minerals (8% clays/feldspars; 2% pyrite). Grains: peloidal grains (15%; <40µm); crinoid/undifferentiated skeletal fragments (5%; 20-100µm); sponge spicules (<1%; 20-100µm). Diagenesis: 7.5% silicification; 5% calcite cementation.

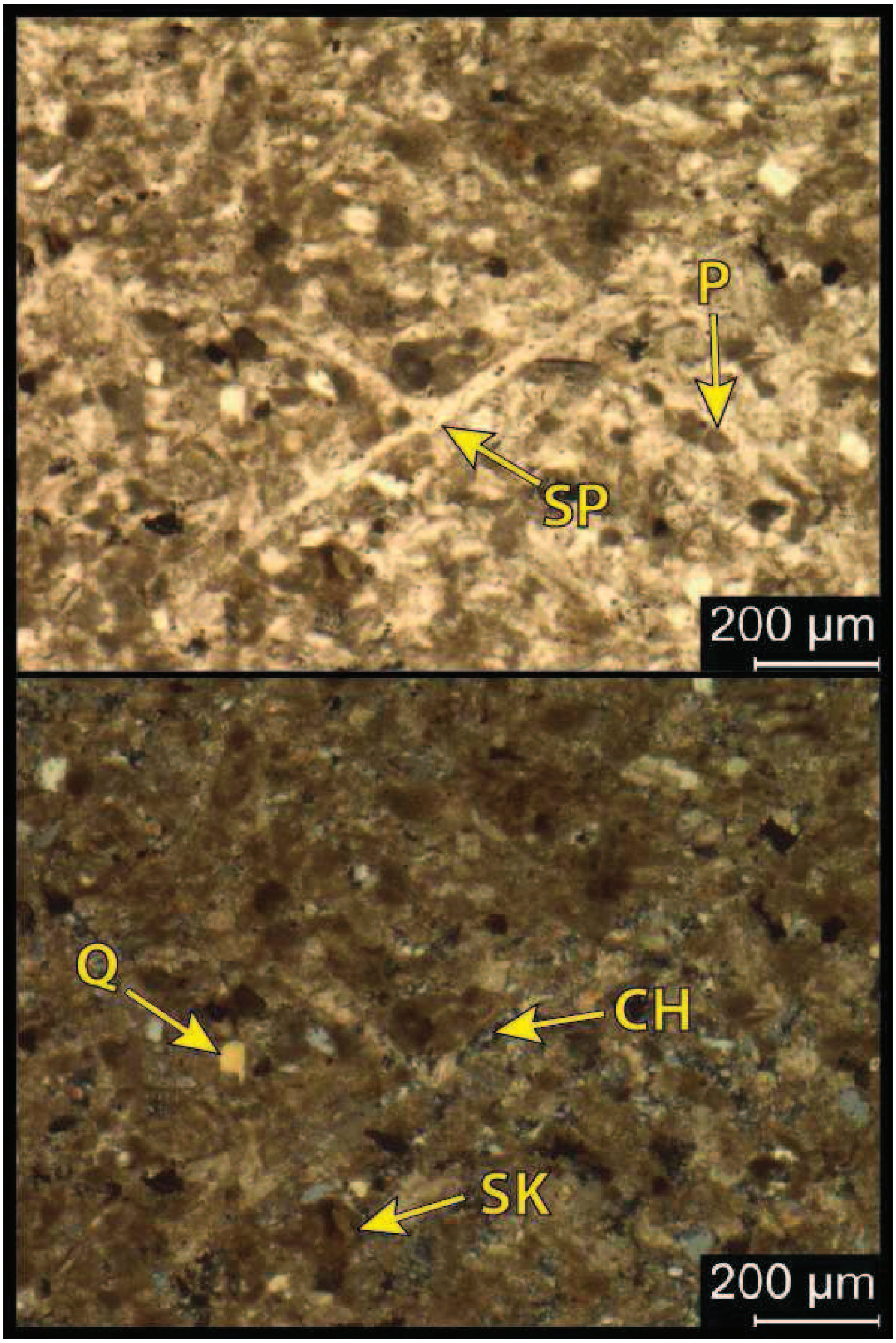

8,014.0': Siliceous, silty mud-lean packstone. Facies 5. Top: PPL. Bottom: XPL. Porosity= 1%. B.I.: 1 (mud-after). Mineralogy: 69% carbonate (67% calcite; 2% dolomite), 25% quartz (20% chert; 5% silt) and 6% other minerals (4% clays/feldspars; 2% pyrite). Grains: well-sorted peloidal/undifferentiated skeletal fragments (70%; 20-60µm) and sponge spicules (1%; 20-100µm; variably calcitic/chert). Diagenesis: 20% silicification; 5% calcite cementation.

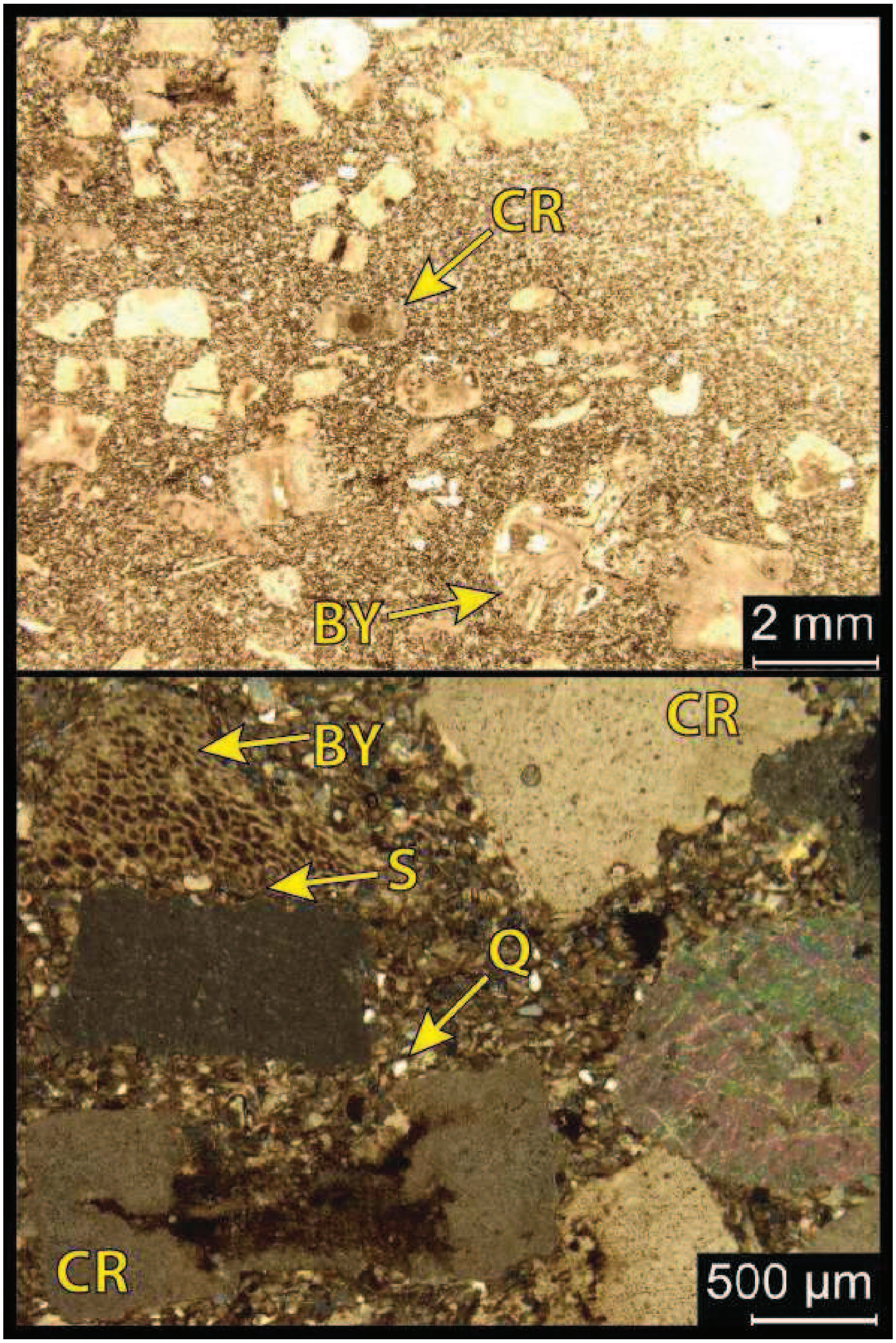

8,001.0': Slightly siliceous, bioclastic packstone. Facies 6. Top: PPL. Bottom: XPL. Porosity= 2%. B.I.: 0. Mineralogy: 67.5% carbonate (65.5% calcite; 2% dolomite), 17.5% quartz (10% chert; 7.5% silt) and 15% other minerals (14% clays/feldspars; 1% pyrite; <.01% glauconite). Grains: Crinoids (25%; 20-60µm in matrix; clasts 1-2mm); bryozoa (2%; clasts ~1-2mm; one rhomboporoid bryozoa w/ microboring/micritization); silt-sized undifferentiated skeletal fragments/seldom sponge spicules in matrix. Diagenesis: 10% silicification of matrix. Low-amplitude stylolites between bioclasts throughout.

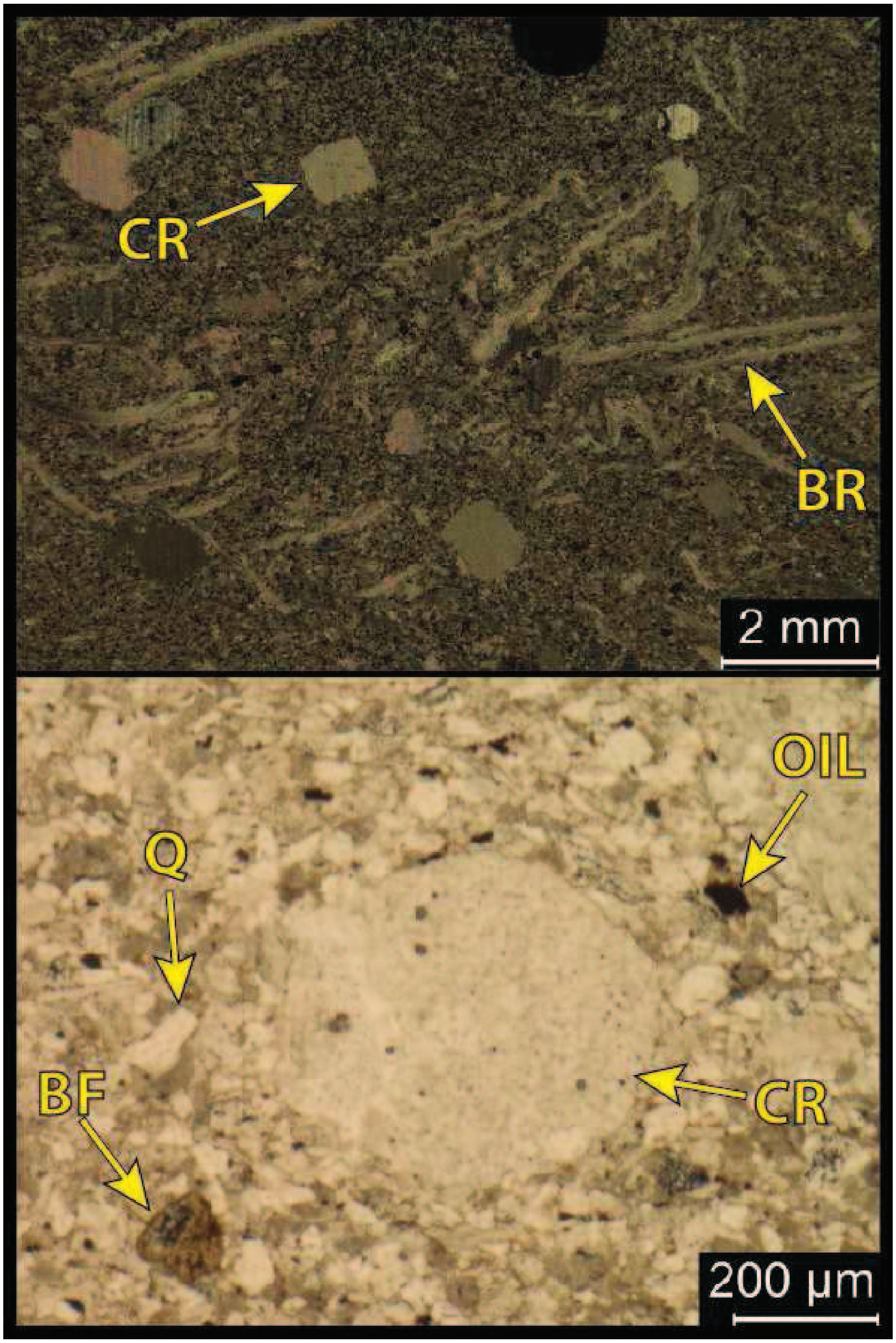

7,970.2': Silty bioclastic packstone-grainstone. Facies 6. Top: XPL. Bottom: PPL. Porosity= 2%. B.I.: 0. Mineralogy: 60.5% calcite, 30% quartz (25% silt-vf sand; 5% chert) and 9.5% other minerals (8% clays/feldspars; 1.5% pyrite). Grains: Brachiopods (20%; 1-4mm x 200µm); crinoids (5%; 0.5-1.5mm); benthic foraminifera (<1%; 60-100µm); peloidal grains in matrix with quartz silt (50:50; 40-100µm). Diagenesis: 5% silicification and 5% calcite cementation.

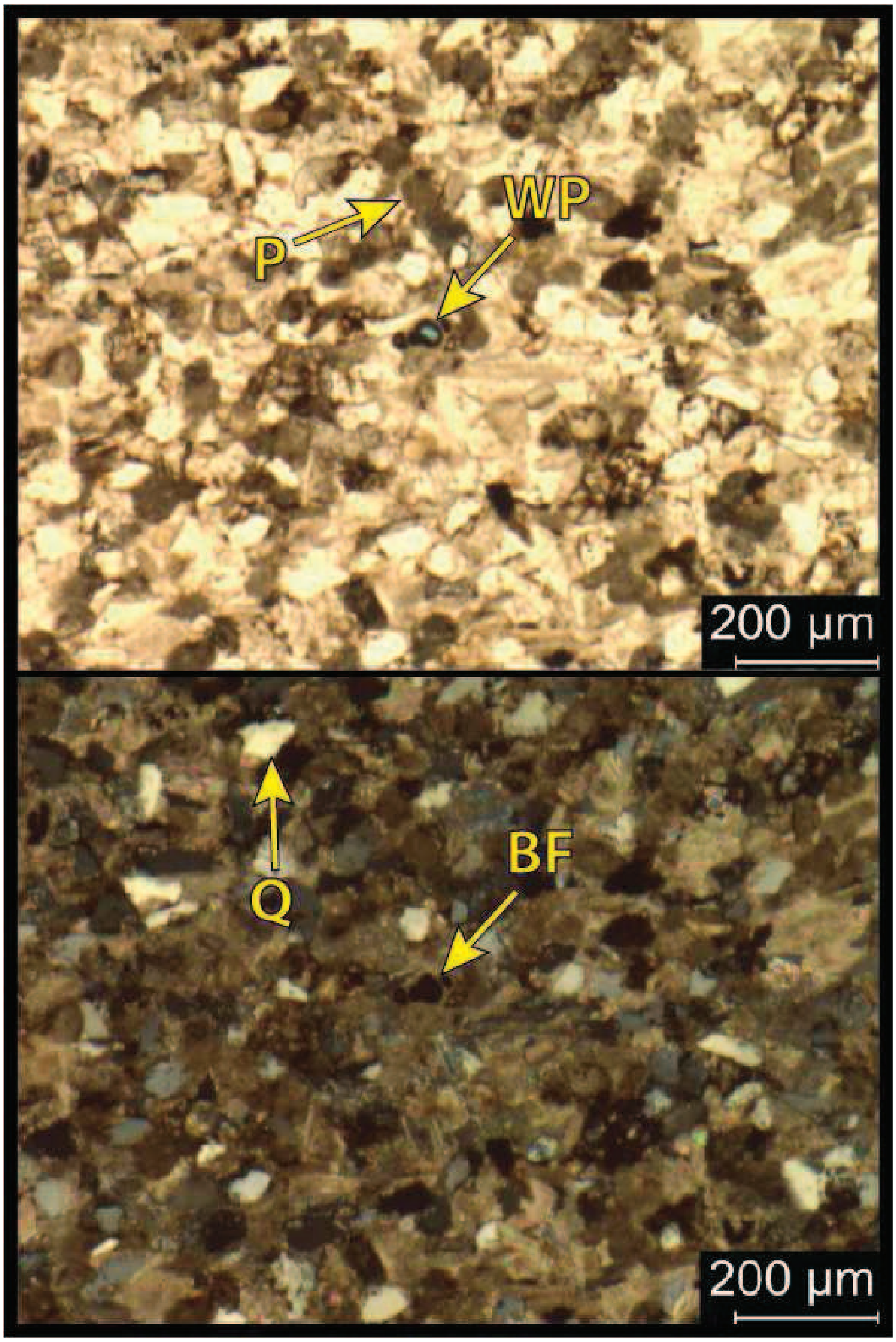

7,966.0': Silty peloidal packstone-grainstone. Facies 6. Top: PPL. Bottom: XPL. Porosity= 4% (inter/intragranular). B.I.: 0. Mineralogy: 46.5% carbonate (42.5% calcite; 4% dolomite), 42% quartz (40% silt-vf sand; 2% chert) and 11.5% other minerals (10% clays/feldspars; 1.5% pyrite). Grains: Peloidal grains in matrix with quartz silt and undifferentiated skeletal fragments (40%silt: 40%calc-grains; v.well-sorted; 40-100µm); benthic foraminifera (1%; 80µm). Diagenesis: 10% calcite cementation; 2% silicification.

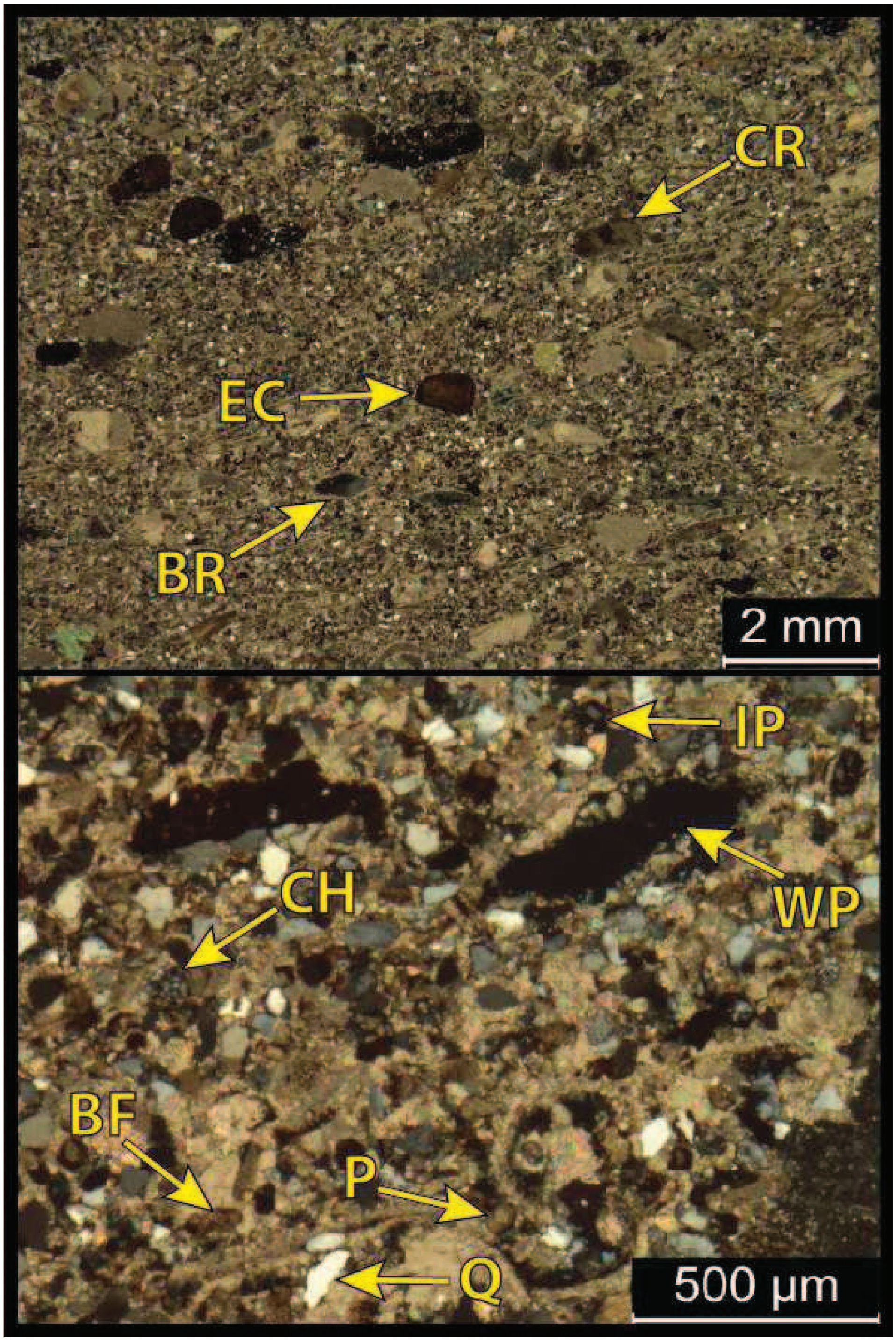

7,941.0': Silty fossiliferous mud-lean packstone/grainstone. Facies 6. Top: XPL. Bottom: XPL. Porosity= 5% (inter/intragranular). B.I.: 0. Mineralogy: 57% carbonate (54% calcite; 3% dolomite), 40% quartz (35% silt-vf sand; 5% chert) and 3% other minerals (2.5% clays/feldspars; 1% pyrite). Grains: Peloids in matrix (~30%; 40-100µm; v.well-sorted; variably micritized); brachiopods (15%; 0.5-1.5mm; internally cemented; echinoderms (15%; ~1mm; variably micritized); benthic foraminifera (10%; ~80µm; variably micritized/silicified). Diagenesis: 10% calcite cementation; 5% silicification.

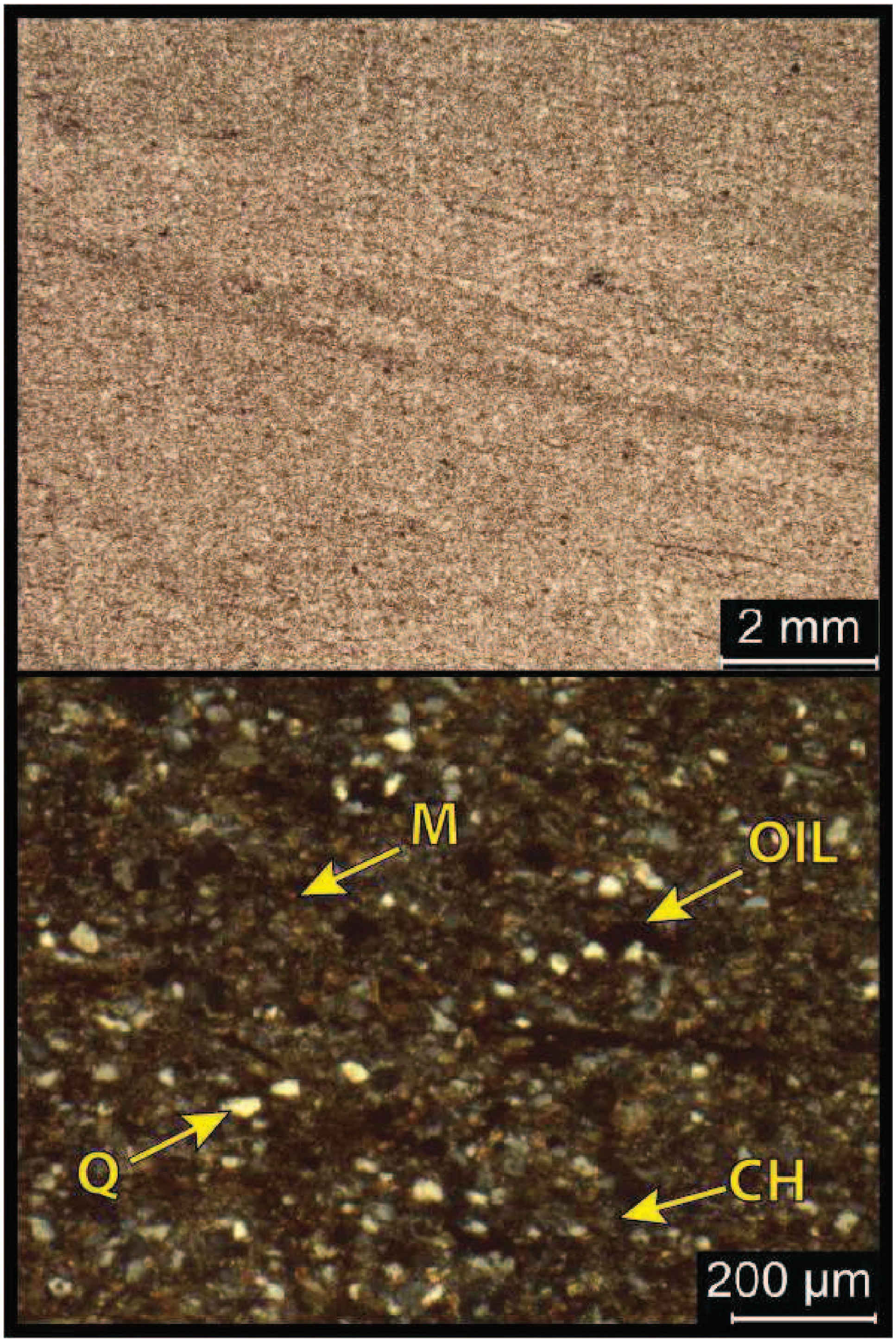

7,938.0': Slightly siliceous siltstone. "Chester". Top: PPL. Bottom: XPL. Porosity= 4% (intergranular; oil-staining/dead oil). B.I.: 0. Mineralogy: 70% quartz (65% silt; 5% chert); 25% other minerals (12.5% clays; 12.5% feldspars); 5% calcite (cementation). Grains: v.well-sorted quartz silt (20-60µm); no carbonate grains. Diagenesis: 5% silicification.

III. Moore Unit #1 Core Descriptions

Preliminary Core Descriptions

Cores were described using the Dunham classification method. Tracts display (from left to right): thin section description (preliminary), Depth (ft.), oil staining, thin section location, Sedimentary structures/ Notes, Facies Type (color coded), Lithology (overprinted by symbols to indicate features (burrowing, stylolites, fractures, HCS and chert)), Textural classification (Dunham), Bioturbation (mm-scale horizontal, cm-scale horizontal, mm-scale vertical, cm-scale vertical), Bioturbation Index (using the Bann et al. (2008) classification method), Grain Types, Lamination (Suspension, traction, mottled), Color, Photograph & depth taken and Depositional Environment

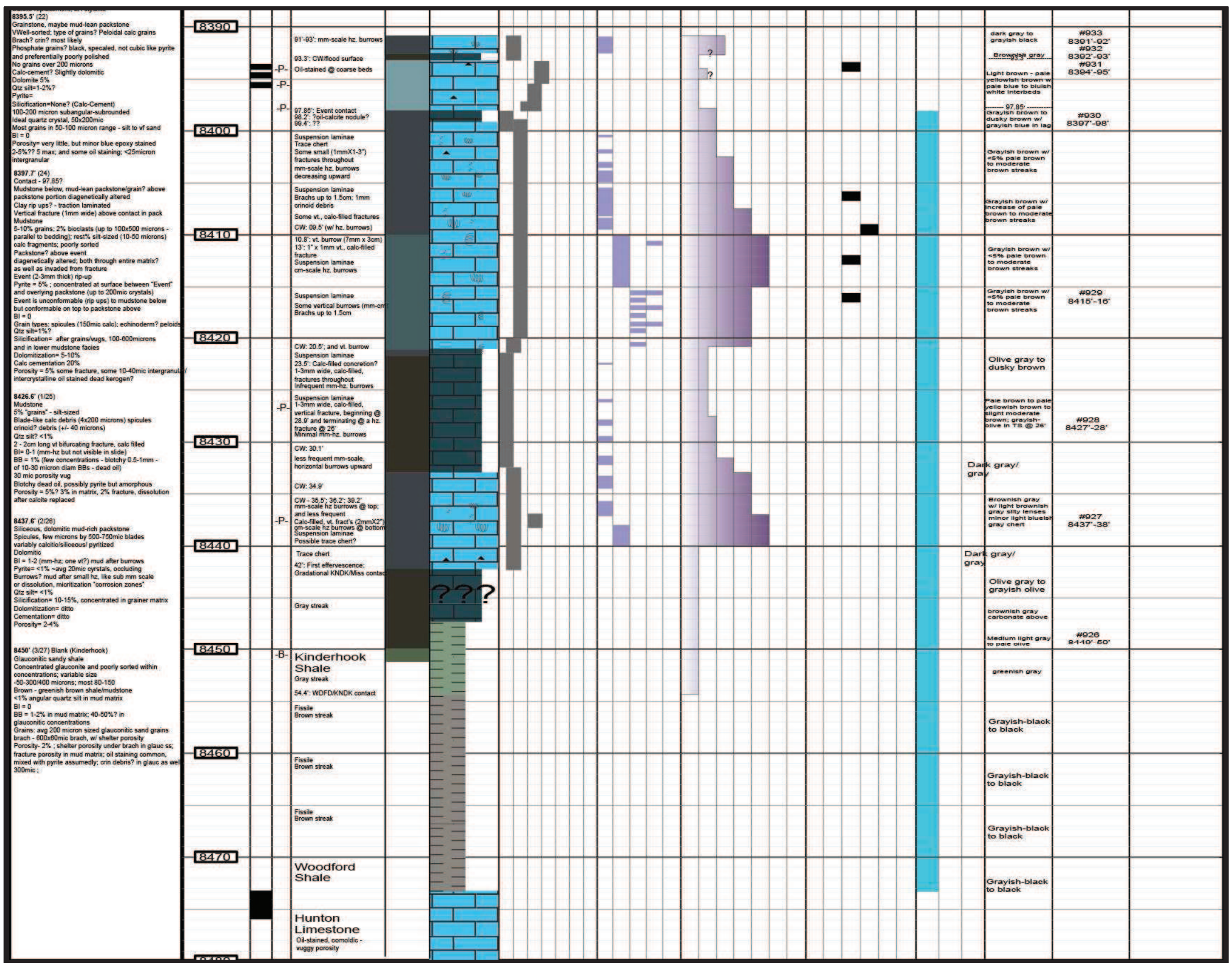

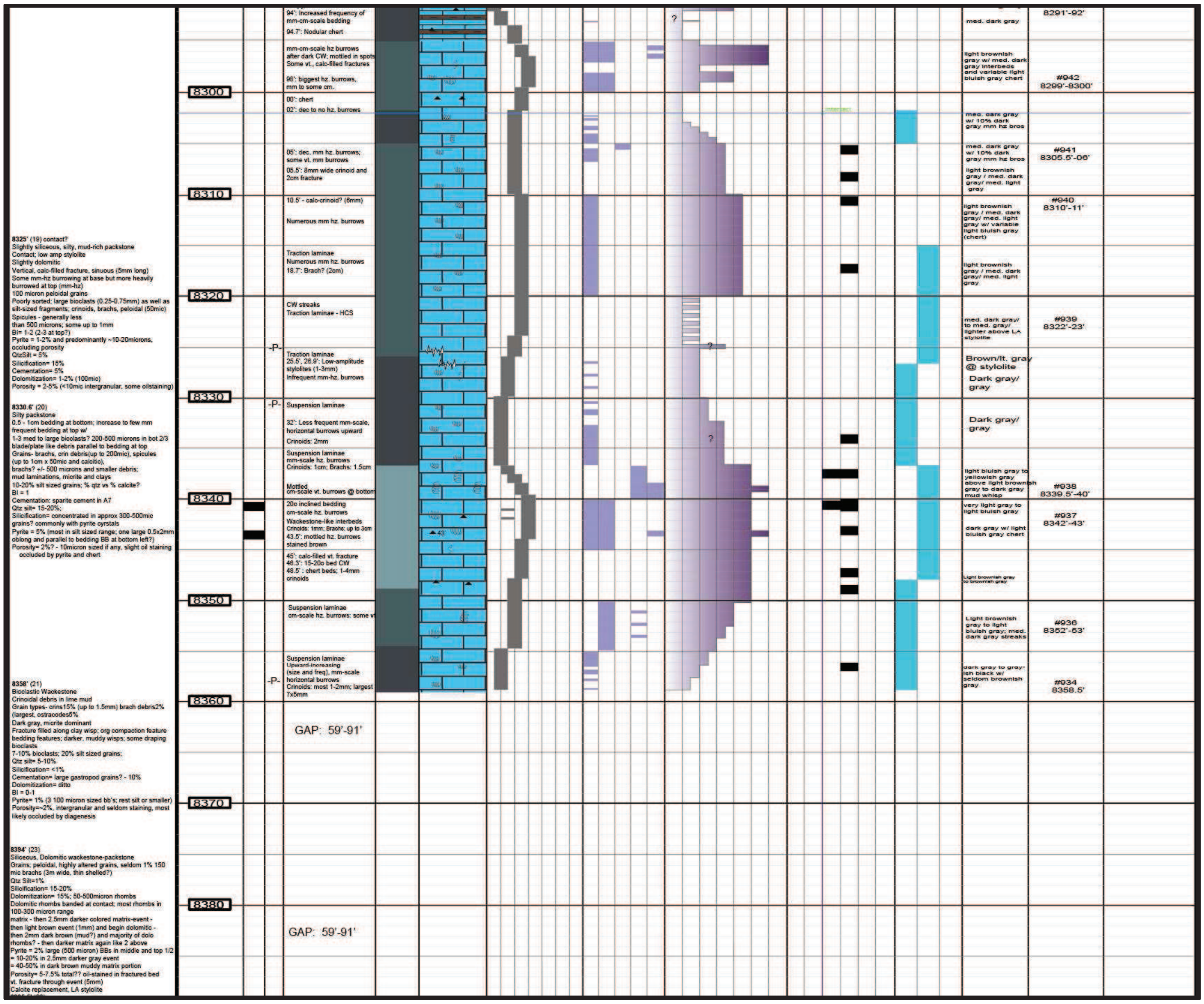
8325' (19) contact?
Slightly siliceous, silty, mud-rich packstone
Contact; low amp stylolite
Slightly dolomitic
Vertical, calc-filled fracture, sinuous (5mm long)
Some mm-hz burrowing at base but more heavily burrowed at top (mm-hz)
100 micron peloidal grains
Poorly sorted; large bioclasts (0.25-0.75mm) as well as silt-sized fragments; crinoids, brachs, peloidal (50mic)
Spicules - generally less than 500 microns; some up to 1mm
BI= 1-2 (2-3 at top?)
Pyrite = 1-2% and predominantly ~10-20microns, occluding porosity
QtzSilt = 5%
Silicification= 15%
Cementation= 5%
Dolomitization= 1-2% (100mic)
Porosity = 2-5% (<10mic intergranular, some oilstaining)
8330.6' (20)
Silty packstone
0.5 - 1cm bedding at bottom; increase to few mm frequent bedding at top w/
1-3 med to large bioclasts? 200-500 microns in bot 2/3
blade/plate like debris parallel to bedding at top
Grains- brachs, crin debris(up to 200mic), spicules (up to 1cm x 50mic and calcitic),
brachs? +/- 500 microns and smaller debris;
mud laminations, micrite and clays
10-20% silt sized grains; % qtz vs % calcite?
BI = 1
Cementation: sparite cement in A7
Qtz silt= 15-20%;
Silicification= concentrated in approx 300-500mic grains? commonly with pyrite cyrstals
Pyrite = 5% (most in silt sized range; one large 0.5x2mm oblong and parallel to bedding BB at bottom left?)
Porosity= 2%? - 10micron sized if any, slight oil staining occluded by pyrite and chert
8358' (21)
Bioclastic Wackestone
Crinoidal debris in lime mud
Grain types- crins15% (up to 1.5mm) brach debris2% (largest, ostracodes5%
Dark gray, micrite dominant
Fracture filled along clay wisp; org compaction feature bedding features; darker, muddy wisps; some draping bioclasts
7-10% bioclasts; 20% silt sized grains;
Qtz silt= 5-10%
Silicification= <1%
Cementation= large gastropod grains? - 10%
Dolomitization= ditto
BI = 0-1
Pyrite= 1% (3 100 micron sized bb's; rest silt or smaller)
Porosity=~2%, intergranular and seldom staining, most likely occluded by diagenesis
8394' (23)
Siliceous, Dolomitic wackestone-packstone
Grains; peloidal, highly altered grains, seldom 1% 150 mic brachs (3m wide, thin shelled?)
Qtz Silt=1%
Silicification= 15-20%
Dolomitization= 15%; 50-500micron rhombs
Dolomitic rhombs banded at contact; most rhombs in 100-300 micron range
matrix - then 2.5mm darker colored matrix-event - then light brown event (1mm) and begin dolomitic - then 2mm dark brown (mud?) and majority of dolo rhombs? - then darker matrix again like 2 above
Pyrite = 2% large (500 micron) BBs in middle and top 1/2
= 10-20% in 2.5mm darker gray event
= 40-50% in dark brown muddy matrix portion
Porosity= 5-7.5% total?? oil-stained in fractured bed
vt. fracture through event (5mm)
Calcite replacement, LA stylolite
8300
8310
8320
8330
8340
8350
8360
8370
8380
-P-
-P-
-P-
94': increased frequency of mm-cm-scale bedding
94.7': Nodular chert
mm-cm-scale hz burrows after dark CW; mottled in spots
Some vt., calc-filled fractures
98': biggest hz. burrows, mm to some cm.
00': chert
02': dec to no hz. burrows
05': dec. mm hz. burrows; some vt. mm burrows
05.5': 8mm wide crinoid and 2cm fracture
10.5' - calc-crinoid? (6mm)
Numerous mm hz. burrows
Traction laminae
Numerous mm hz. burrows
18.7': Brach? (2cm)
CW streaks
Traction laminae - HCS
Traction laminae
25.5', 26.9': Low-amplitude stylolites (1-3mm)
Infrequent mm-hz. burrows
Suspension laminae
32': Less frequent mm-scale, horizontal burrows upward
Crinoids: 2mm
Suspension laminae
mm-scale hz. burrows
Crinoids: 1cm; Brachs: 1.5cm
Mottled
cm-scale vt. burrows @ bottom
20o inclined bedding
cm-scale hz. burrows
Wackestone-like interbeds
Crinoids: 1mm; Brachs: up to 3cm
43.5': mottled hz. burrows stained brown
45': calc-filled vt. fracture
46.3': 15-20o bed CW
48.5' : chert beds; 1-4mm crinoids
Suspension laminae
cm-scale hz. burrows; some vt
Suspension laminae
Upward-increasing (size and freq), mm-scale horizontal burrows
Crinoids: most 1-2mm; largest 7x5mm
GAP: 59'-91'
GAP: 59'-91'
?
?
?
med. dark gray
8291'-92'
light brownish gray w/ med. dark gray interbeds and variable light bluish gray chert
#942
8299'-8300'
med. dark gray w/ 10% dark gray mm hz bros
med. dark gray w/ 10% dark gray mm hz bros
#941
8305.5'-06'
light brownish gray / med. dark gray/ med. light gray
#940
8310'-11'
light brownish gray / med. dark gray/ med. light gray w/ variable light bluish gray (chert)
light brownish gray / med. dark gray/ med. light gray
med. dark gray/ to med. gray/ lighter above LA stylolite
#939
8322'-23'
Brown/lt. gray @ stylolite
Dark gray/ gray
Dark gray/ gray
light bluish gray to yellowish gray above light brownish gray to dark gray mud whisp
#938
8339.5'-40'
very light gray to light bluish gray
dark gray w/ light bluish gray chert
#937
8342'-43'
Light brownish gray to brownish gray
Light brownish gray to light bluish gray; med. dark gray streaks
#936
8352'-53'
dark gray to grayish black w/ seldom brownish gray
#934
8358.5'

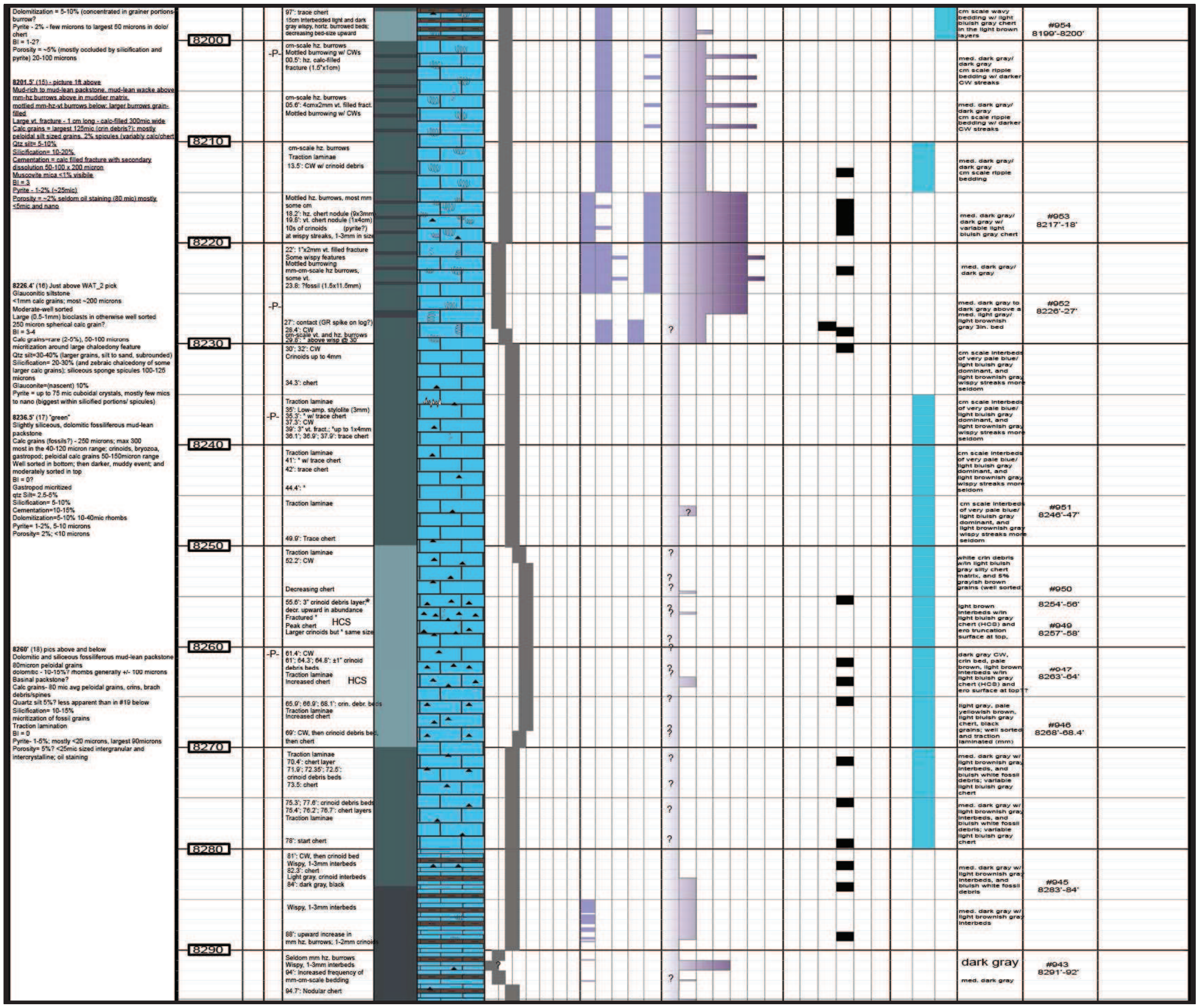

8200
8210
8220
8230
8240
8250
8260
8270
8280
8290
HCS
HCS
dark gray
#954 8199'-8200'
#953 8217'-18'
#952 8226'-27'
#951 8246'-47'
#950
8254'-56'
#949 8257'-58'
#947 8263'-64'
#946 8268'-68.4'
#945 8283'-84'
#943 8291'-92'

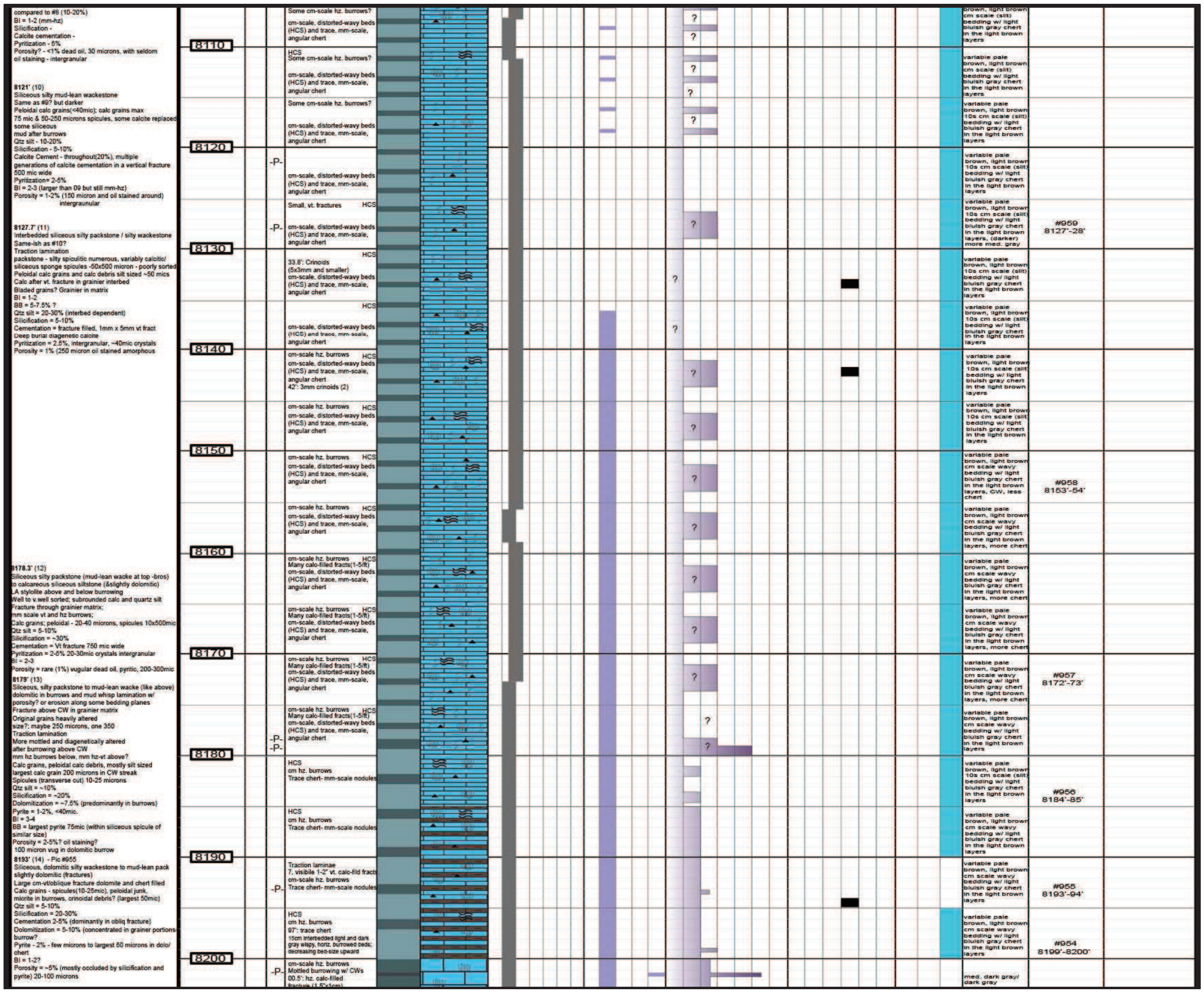
compared to #8 (10-20%)
BI = 1-2 (mm-hz)
Silicification -
Calcite cementation -
Pyritization - 5%
Porosity? - <1% dead oil, 30 microns, with seldom oil staining - intergranular
8121' (10)
Siliceous silty mud-lean wackestone
Same as #9? but darker
Peloidal calc grains(<40mic); calc grains max 75 mic & 50-250 microns spicules, some calcite replaced some siliceous mud after burrows
Qtz silt - 10-20%
Silicification - 5-10%
Calcite Cement - throughout(20%), multiple generations of calcite cementation in a vertical fracture 500 mic wide
Pyritization= 2-5%
BI = 2-3 (larger than 09 but still mm-hz)
Porosity = 1-2% (150 micron and oil stained around) intergraunular
8127.7' (11)
Interbedded siliceous silty packstone / silty wackestone
Same-ish as #10?
Traction lamination
packstone - silty spiculitic numerous, variably calcitic/ siliceous sponge spicules -50x500 micron - poorly sorted
Peloidal calc grains and calc debris silt sized ~50 mics
Calc after vt. fracture in grainier interbed
Bladed grains? Grainier in matrix
BI = 1-2
BB = 5-7.5% ?
Qtz silt = 20-30% (interbed dependent)
Silicification = 5-10%
Cementation = fracture filled, 1mm x 5mm vt fract
Deep burial diagenetic calcite
Pyritization = 2.5%, intergranular, ~40mic crystals
Porosity = 1% (250 micron oil stained amorphous
8178.3' (12)
Siliceous silty packstone (mud-lean wacke at top -bros) to calcareous siliceous siltstone (&slightly dolomitic)
LA stylolite above and below burrowing
Well to v.well sorted; subrounded calc and quartz silt
Fracture through grainier matrix;
mm scale vt and hz burrows;
Calc grains; peloidal - 20-40 microns, spicules 10x500mic
Qtz silt = 5-10%
Silicification = ~30%
Cementation = Vt fracture 750 mic wide
Pyritization = 2-5% 20-30mic crystals intergranular
BI = 2-3
Porosity = rare (1%) vugular dead oil, pyritic, 200-300mic
8179' (13)
Silceous, silty packstone to mud-lean wacke (like above) dolomitic in burrows and mud whisp lamination w/ porosity? or erosion along some bedding planes
Fracture above CW in grainier matrix
Original grains heavily altered
size?; maybe 250 microns, one 350
Traction lamination
More mottled and diagenetically altered after burrowing above CW
mm hz burrows below, mm hz-vt above?
Calc grains, peloidal calc debris, mostly silt sized
largest calc grain 200 microns in CW streak
Spicules (transverse cut) 10-25 microns
Qtz silt = ~10%
Silicification = ~20%
Dolomitization = ~7.5% (predominantly in burrows)
Pyrite = 1-2%, <40mic.
BI = 3-4
BB = largest pyrite 75mic (within siliceous spicule of similar size)
Porosity = 2-5%? oil staining?
100 micron vug in dolomitic burrow
8193' (14) - Pic #955
Siliceous, dolomitic silty wackestone to mud-lean pack slightly dolomitic (fractures)
Large cm-vt/oblique fracture dolomite and chert filled
Calc grains - spicules(10-25mic), peloidal junk, micrite in burrows, crinoidal debris? (largest 50mic)
Qtz silt = 5-10%
Silicification = 20-30%
Cementation 2-5% (dominantly in obliq fracture)
Dolomitization = 5-10% (concentrated in grainer portions-burrow?
Pyrite - 2% - few microns to largest 50 microns in dolo/ chert
BI = 1-2?
Porosity = ~5% (mostly occluded by silicification and pyrite) 20-100 microns
8110
8120
8130
8140
8150
8160
8170
8180
8190
8200
#959 8127'-28'
#958 8153'-54'
#957 8172'-73'
#956 8184'-85'
#955 8193'-94'
#954 8199'-8200'

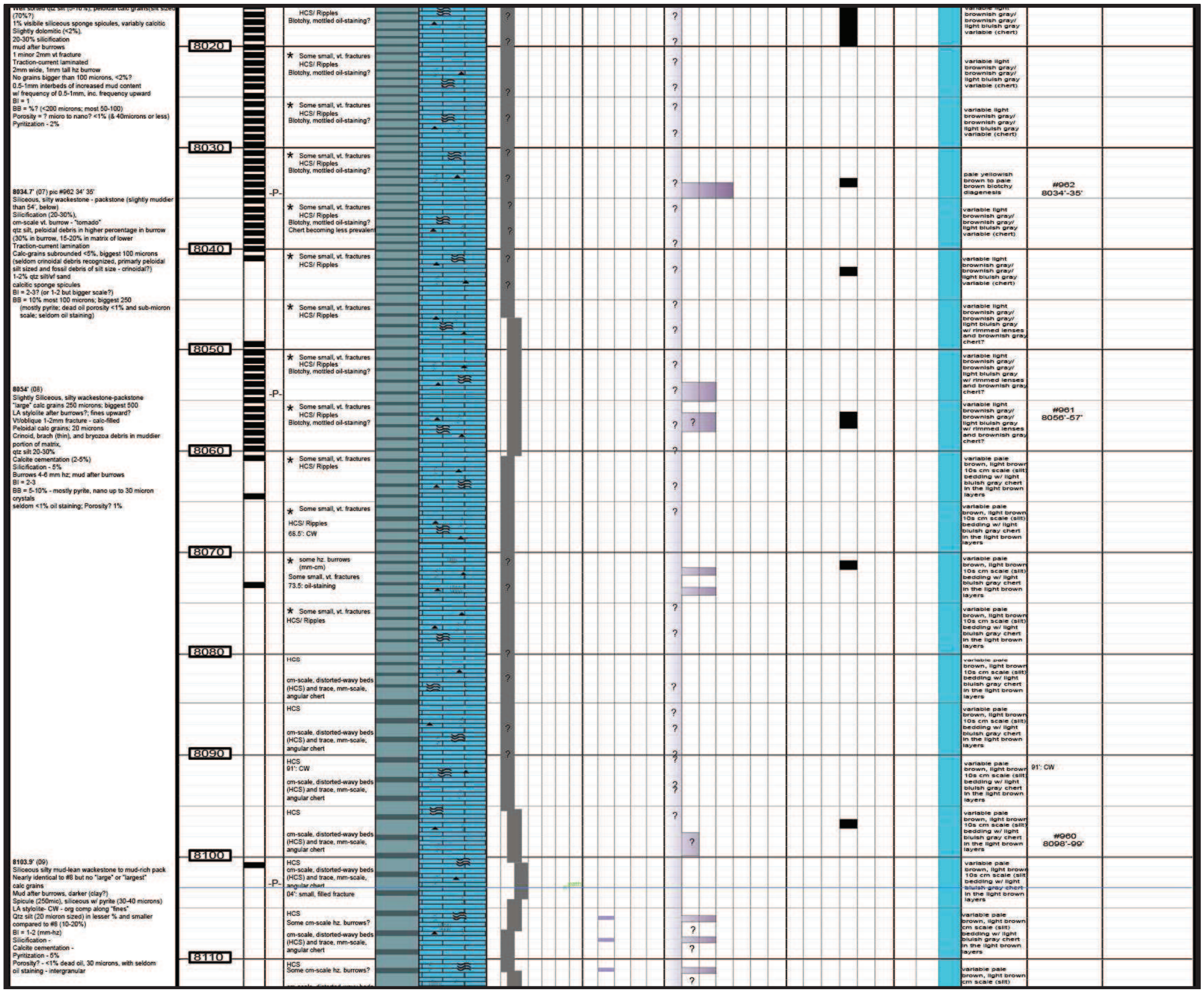
Well sorted qtz silt (5-10%), peloidal calc grains(silt sized (70%?)
1% visibile siliceous sponge spicules, variably calcitic
Slightly dolomitic (<2%),
20-30% silicification
mud after burrows
1 minor 2mm vt fracture
Traction-current laminated
2mm wide, 1mm tall hz burrow
No grains bigger than 100 microns, <2%?
0.5-1mm interbeds of increased mud content
w/ frequency of 0.5-1mm, inc. frequency upward
BI = 1
BB = %? (<200 microns; most 50-100)
Porosity = ? micro to nano? <1% (& 40microns or less)
Pyritization - 2%
8034.7' (07) pic #962 34' 35'
Siliceous, silty wackestone - packstone (slightly muddier than 54', below)
Silicification (20-30%),
cm-scale vt. burrow - "tornado"
qtz silt, peloidal debris in higher percentage in burrow
(30% in burrow, 15-20% in matrix of lower
Traction-current lamination
Calc-grains subrounded <5%, biggest 100 microns
(seldom crinoidal debris recognized, primarly peloidal silt sized and fossil debris of silt size - crinoidal?)
1-2% qtz silt/vf sand
calcitic sponge spicules
BI = 2-3? (or 1-2 but bigger scale?)
BB = 10% most 100 microns; biggest 250
(mostly pyrite; dead oil porosity <1% and sub-micron scale; seldom oil staining)
8054' (08)
Slightly Siliceous, silty wackestone-packstone
"large" calc grains 250 microns; biggest 500
LA stylolite after burrows?; fines upward?
Vt/oblique 1-2mm fracture - calc-filled
Peloidal calc grains; 20 microns
Crinoid, brach (thin), and bryozoa debris in muddier portion of matrix,
qtz silt 20-30%
Calcite cementation (2-5%)
Silicification - 5%
Burrows 4-6 mm hz; mud after burrows
BI = 2-3
BB = 5-10% - mostly pyrite, nano up to 30 micron crystals
seldom <1% oil staining; Porosity? 1%
8103.9' (09)
Siliceous silty mud-lean wackestone to mud-rich pack
Nearly identical to #8 but no "large" or "largest" calc grains
Mud after burrows, darker (clay?)
Spicule (250mic), siliceous w/ pyrite (30-40 microns)
LA stylolite- CW - org comp along "fines"
Qtz silt (20 micron sized) in lesser % and smaller compared to #8 (10-20%)
BI = 1-2 (mm-hz)
Silicification -
Calcite cementation -
Pyritization - 5%
Porosity? - <1% dead oil, 30 microns, with seldom oil staining - intergranular
8020
8030
8040
8050
8060
8070
8080
8090
8100
8110
-P-
#962
8034'-35'
#961
8056'-57'
91': CW
#960
8098'-99'

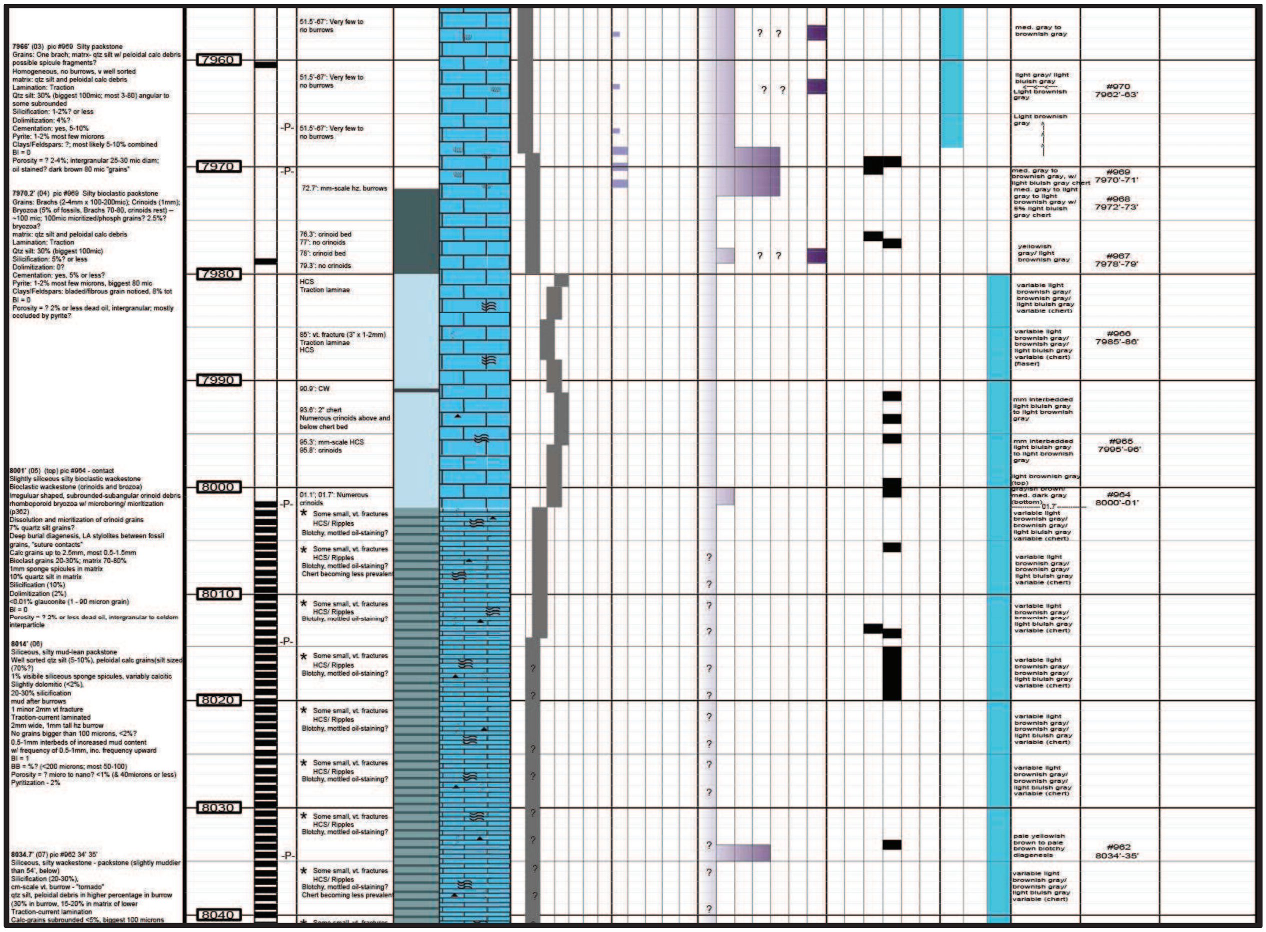
7966' (03) pic #969 Silty packstone
Grains: One brach; matrx- qtz silt w/ peloidal calc debris
possible spicule fragments?
Homogeneous, no burrows, v well sorted
matrix: qtz silt and peloidal calc debris
Lamination: Traction
Qtz silt: 30% (biggest 100mic; most 3-80) angular to some subrounded
Silicification: 1-2%? or less
Dolimitization: 4%?
Cementation: yes, 5-10%
Pyrite: 1-2% most few microns
Clays/Feldspars: ?; most likely 5-10% combined
BI = 0
Porosity = ? 2-4%; intergranular 25-30 mic diam; oil stained? dark brown 80 mic "grains"
7970.2' (04) pic #969 Silty bioclastic packstone
Grains: Brachs (2-4mm x 100-200mic); Crinoids (1mm); Bryozoa (5% of fossils, Brachs 70-80, crinoids rest) -- ~100 mic; 100mic micritized/phosph grains? 2.5%? bryozoa?
matrix: qtz silt and peloidal calc debris
Lamination: Traction
Qtz silt: 30% (biggest 100mic)
Silicification: 5%? or less
Dolimitization: 0?
Cementation: yes, 5% or less?
Pyrite: 1-2% most few microns, biggest 80 mic
Clays/Feldspars: bladed/fibrous grain noticed, 8% tot
BI = 0
Porosity = ? 2% or less dead oil, intergranular; mostly occluded by pyrite?
8001' (05) (top) pic #964 - contact
Slightly siliceous silty bioclastic wackestone
Bioclastic wackestone (crinoids and brozoa)
Irreguluar shaped, subrounded-subangular crinoid debris
rhomboporoid bryozoa w/ microboring/ micritization (p362)
Dissolution and micritization of crinoid grains
7% quartz silt grains?
Deep burial diagenesis, LA stylolites between fossil grains, "suture contacts"
Calc grains up to 2.5mm, most 0.5-1.5mm
Bioclast grains 20-30%; matrix 70-80%
1mm sponge spicules in matrix
10% quartz silt in matrix
Silicification (10%)
Dolimitization (2%)
<0.01% glauconite (1 - 90 micron grain)
BI = 0
Porosity = ? 2% or less dead oil, intergranular to seldom interparticle
8014' (06)
Siliceous, silty mud-lean packstone
Well sorted qtz silt (5-10%), peloidal calc grains(silt sized (70%?)
1% visibile siliceous sponge spicules, variably calcitic
Slightly dolomitic (<2%),
20-30% silicification
mud after burrows
1 minor 2mm vt fracture
Traction-current laminated
2mm wide, 1mm tall hz burrow
No grains bigger than 100 microns, <2%?
0.5-1mm interbeds of increased mud content
w/ frequency of 0.5-1mm, inc. frequency upward
BI = 1
BB = %? (<200 microns; most 50-100)
Porosity = ? micro to nano? <1% (& 40microns or less)
Pyritization - 2%
8034.7' (07) pic #962 34' 35'
Siliceous, silty wackestone - packstone (slightly muddier than 54', below)
Silicification (20-30%),
cm-scale vt. burrow - "tornado"
qtz silt, peloidal debris in higher percentage in burrow (30% in burrow, 15-20% in matrix of lower
Traction-current lamination
Calc-grains subrounded <5%, biggest 100 microns
7960
7970
7980
7990
8000
8010
8020
8030
8040
-P-
51.5'-67': Very few to no burrows
51.5'-67': Very few to no burrows
51.5'-67': Very few to no burrows
72.7': mm-scale hz. burrows
76.3': crinoid bed
77': no crinoids
78': crinoid bed
79.3': no crinoids
HCS
Traction laminae
85': vt. fracture (3" x 1-2mm)
Traction laminae
HCS
90.9': CW
93.6': 2" chert
Numerous crinoids above and below chert bed
95.3': mm-scale HCS
95.8': crinoids
01.1'; 01.7': Numerous crinoids
★ Some small, vt. fractures
HCS/ Ripples
Blotchy, mottled oil-staining?
Chert becoming less prevalent
med. gray to brownish gray
light gray/ light bluish gray
Light brownish gray
Light brownish gray
med. gray to brownish gray, w/ light bluish gray chert
med. gray to light gray to light brownish gray w/ 5% light bluish gray chert
yellowish gray/ light brownish gray
variable light brownish gray/ brownish gray/ light bluish gray variable (chert)
variable light brownish gray/ brownish gray/ light bluish gray variable (chert) [flaser]
mm interbedded light bluish gray to light brownish gray
light brownish gray (top)
grayish brown/ med. dark gray (bottom)
01.7'
pale yellowish brown to pale brown blotchy diagenesis
#970
7962'-63'
#969
7970'-71'
#968
7972'-73'
#967
7978'-79'
#966
7985'-86'
#965
7995'-96'
#964
8000'-01'
#962
8034'-35'

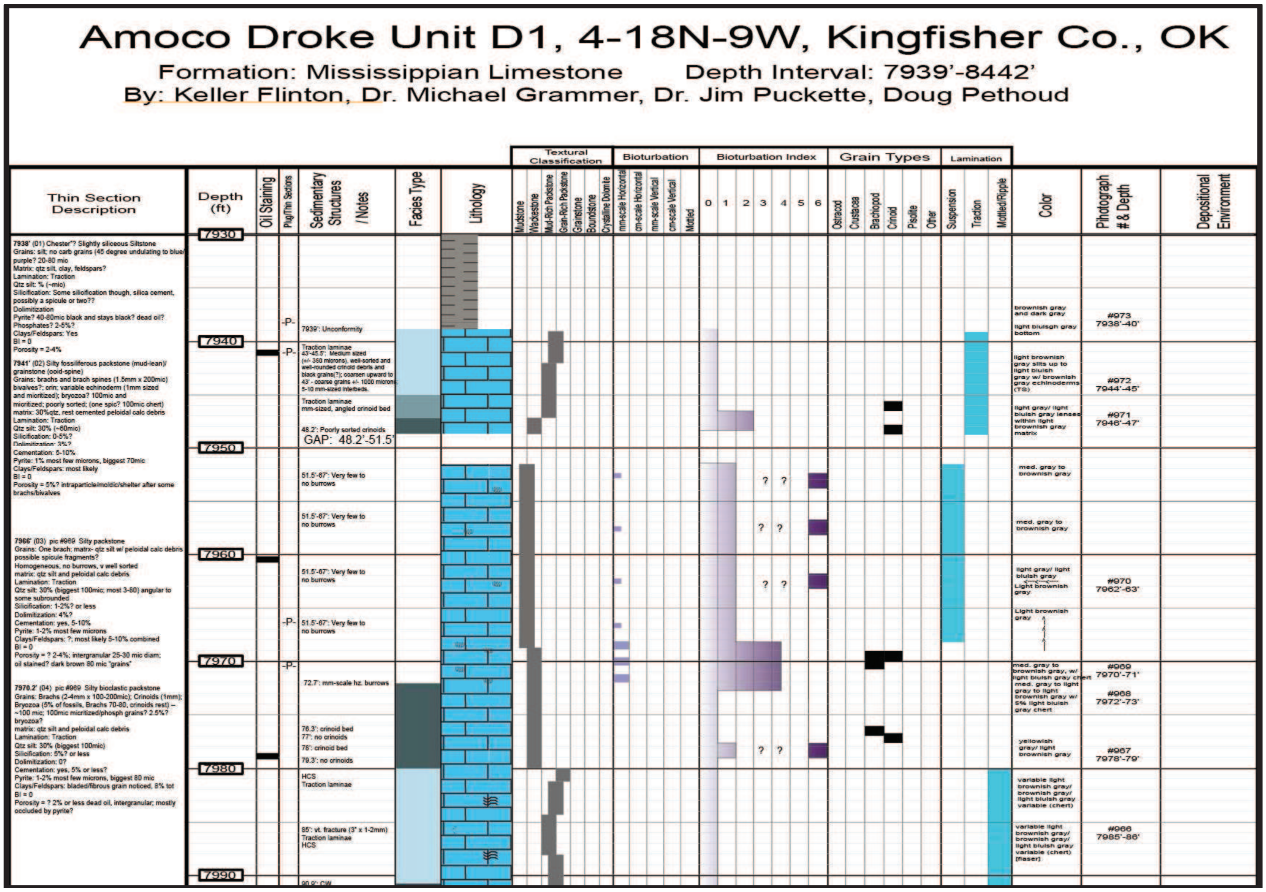

Amoco Droke Unit D1, 4-18N-9W, Kingfisher Co., OK
Formation: Mississippian Limestone
Depth Interval: 7939'-8442'
By: Keller Flinton, Dr. Michael Grammer, Dr. Jim Puckette, Doug Pethoud
Thin Section Description
Depth (ft)
Oil Staining
Plug/Thin Sections
Sedimentary Structures /Notes
Facies Type
Lithology
Textural Classification
Mudstone
Wackestone
Mud-Rich Packstone
Grain-Rich Packstone
Grainstone
Boundstone
Crystalline Dolomite
Bioturbation
mm-scale Horizontal
cm-scale Horizontal
mm-scale Vertical
cm-scale Vertical
Mottled
Bioturbation Index
0 1 2 3 4 5 6
Grain Types
Ostracod
Crustacea
Brachiopod
Crinoid
Pisolite
Other
Lamination
Suspension
Traction
Mottled/Ripple
Color
Photograph # & Depth
Depositional Environment
7930
7940
7950
7960
7970
7980
7990
7938' (01) Chester"? Slightly siliceous Siltstone
Grains: silt; no carb grains (45 degree undulating to blue/purple? 20-80 mic
Matrix: qtz silt, clay, feldspars?
Lamination: Traction
Qtz silt: % (~mic)
Silicification: Some silicification though, silica cement, possibly a spicule or two??
Dolimitization
Pyrite? 40-80mic black and stays black? dead oil?
Phosphates? 2-5%?
Clays/Feldspars: Yes
BI = 0
Porosity = 2-4%
7941' (02) Silty fossiliferous packstone (mud-lean)/ grainstone (ooid-spine)
Grains: brachs and brach spines (1.5mm x 200mic) bivalves?; crin; variable echinoderm (1mm sized and micritized); bryozoa? 100mic and micritized; poorly sorted; (one spic? 100mic chert)
matrix: 30%qtz, rest cemented peloidal calc debris
Lamination: Traction
Qtz silt: 30% (~60mic)
Silicification: 0-5%?
Dolimitization: 3%?
Cementation: 5-10%
Pyrite: 1% most few microns, biggest 70mic
Clays/Feldspars: most likely
BI = 0
Porosity = 5%? intraparticle/moldic/shelter after some brachs/bivalves
7966' (03) pic #969 Silty packstone
Grains: One brach; matrx- qtz silt w/ peloidal calc debris possible spicule fragments?
Homogeneous, no burrows, v well sorted
matrix: qtz silt and peloidal calc debris
Lamination: Traction
Qtz silt: 30% (biggest 100mic; most 3-80) angular to some subrounded
Silicification: 1-2%? or less
Dolimitization: 4%?
Cementation: yes, 5-10%
Pyrite: 1-2% most few microns
Clays/Feldspars: ?; most likely 5-10% combined
BI = 0
Porosity = ? 2-4%; intergranular 25-30 mic diam; oil stained? dark brown 80 mic "grains"
7970.2' (04) pic #969 Silty bioclastic packstone
Grains: Brachs (2-4mm x 100-200mic); Crinoids (1mm); Bryozoa (5% of fossils, Brachs 70-80, crinoids rest) – ~100 mic; 100mic micritized/phosph grains? 2.5%? bryozoa?
matrix: qtz silt and peloidal calc debris
Lamination: Traction
Qtz silt: 30% (biggest 100mic)
Silicification: 5%? or less
Dolimitization: 0?
Cementation: yes, 5% or less?
Pyrite: 1-2% most few microns, biggest 80 mic
Clays/Feldspars: bladed/fibrous grain noticed, 8% tot
BI = 0
Porosity = ? 2% or less dead oil, intergranular; mostly occluded by pyrite?
-P-
7939': Unconformity
-P-
Traction laminae
43'-45.5": Medium sized (+/- 350 microns), well-sorted and well-rounded crinoid debris and black grains(?); coarsen upward to 43' - coarse grains +/- 1000 microns; 5-10 mm-sized interbeds.
Traction laminae
mm-sized, angled crinoid bed
48.2': Poorly sorted crinoids
GAP: 48.2'-51.5'
51.5'-67': Very few to no burrows
51.5'-67': Very few to no burrows
51.5'-67': Very few to no burrows
-P-
51.5'-67': Very few to no burrows
-P-
72.7': mm-scale hz. burrows
76.3': crinoid bed
77': no crinoids
78': crinoid bed
79.3': no crinoids
HCS
Traction laminae
85': vt. fracture (3" x 1-2mm)
Traction laminae
HCS
90.9': CW
? ?
? ?
? ?
? ?
brownish gray and dark gray
light bluisgh gray bottom
#973 7938'-40'
light brownish gray silts up to light bluish gray w/ brownish gray echinoderms (TS)
#972 7944'-45'
light gray/ light bluish gray lenses within light brownish gray matrix
#971 7946'-47'
med. gray to brownish gray
med. gray to brownish gray
light gray/ light bluish gray
Light brownish gray
#970 7962'-63'
Light brownish gray
med. gray to brownish gray, w/ light bluish gray chert
#969 7970'-71'
med. gray to light gray to light brownish gray w/ 5% light bluish gray chert
#968 7972'-73'
yellowish gray/ light brownish gray
#967 7978'-79'
variable light brownish gray/ brownish gray/ light bluish gray variable (chert)
variable light brownish gray/ brownish gray/ light bluish gray variable (chert) [flaser]
#966 7985'-86'

Core-to-Wireline Log Tie

From left to right: Gamma Ray curve (0-120 API Units), RILD Resistivity curve (logarithmic 10-100), Sequence stratigraphic hierarchy, Depth (ft.) Dunham erosional profile, Diagenetic effects.

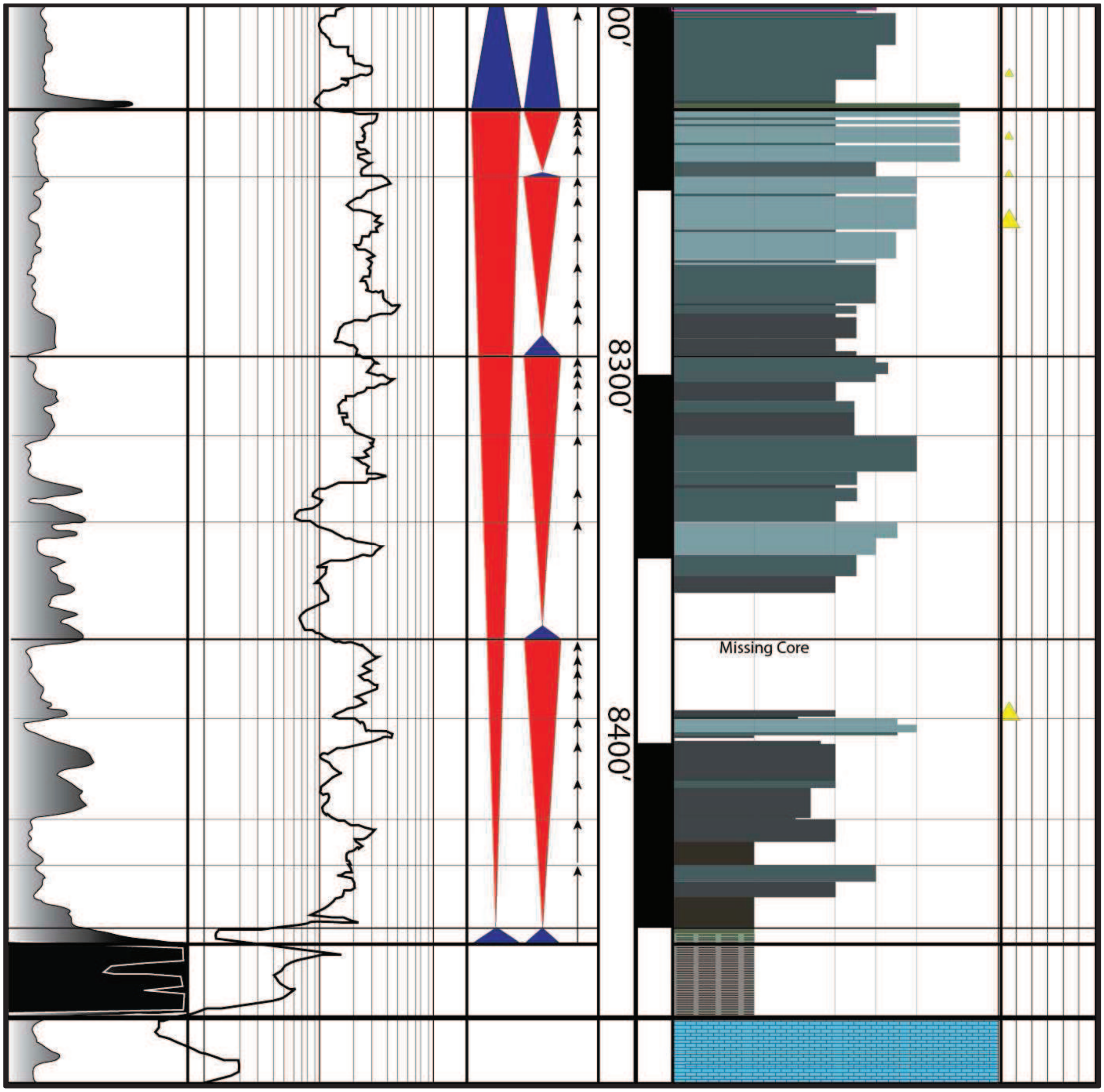

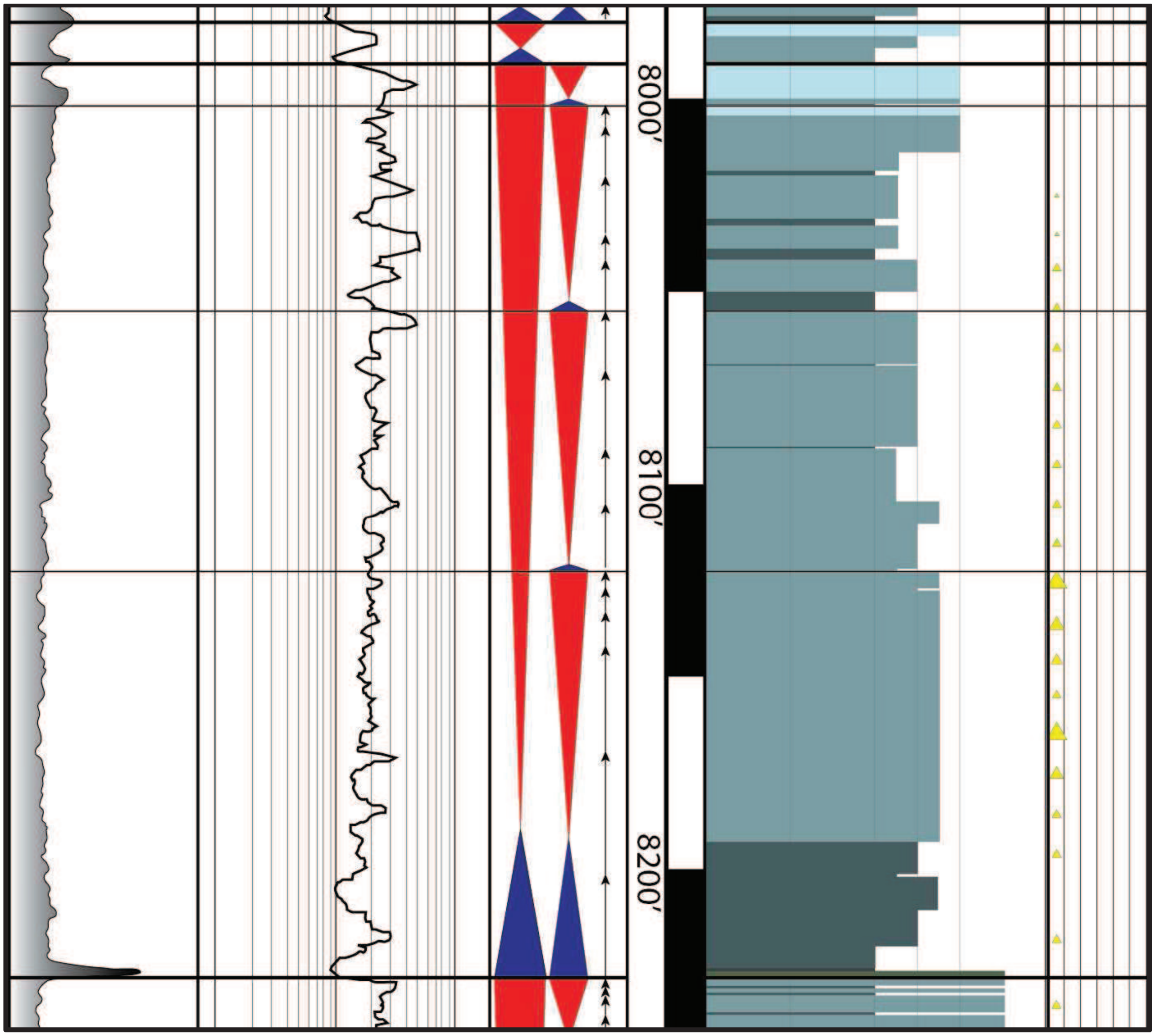
8000'
8100'
8200'

Droke Unit #1

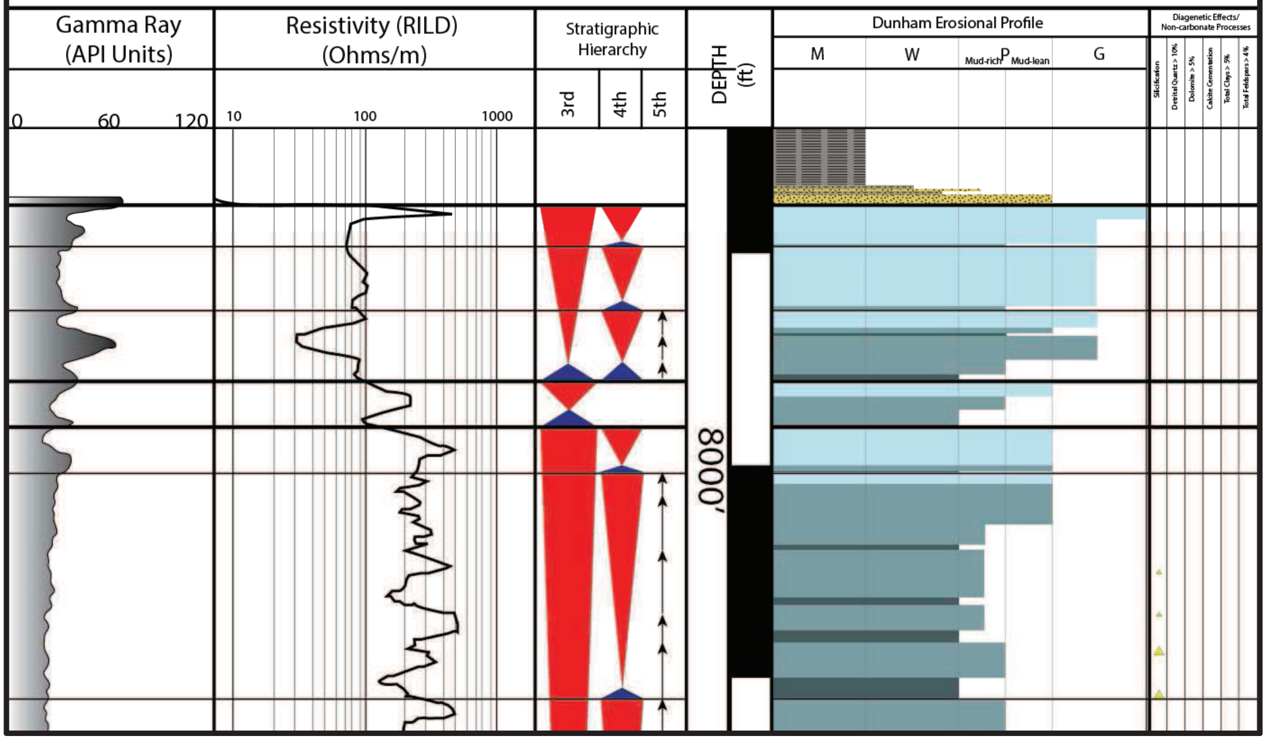
Gamma Ray
(API Units)
0
60
120
Resistivity (RILD)
(Ohms/m)
10
100
1000
Stratigraphic Hierarchy
3rd
4th
5th
DEPTH
(ft)
8000'
Dunham Erosional Profile
M
W
Mud-rich
P
Mud-lean
G
Diagenetic Effects/
Non-carbonate Processes
Silicification
Detrital Quartz > 10%
Dolomite > 5%
Calcite Cementation
Total Clays > 5%
Total Feldspars > 4%

Appendix D: Stratigraphic Architecture/ Subsurface Mapping

Subsurface maps and cross sections were created using Petra geological software, a product of IHS, Inc.

I. 3rd-Order Gross Isopach Maps

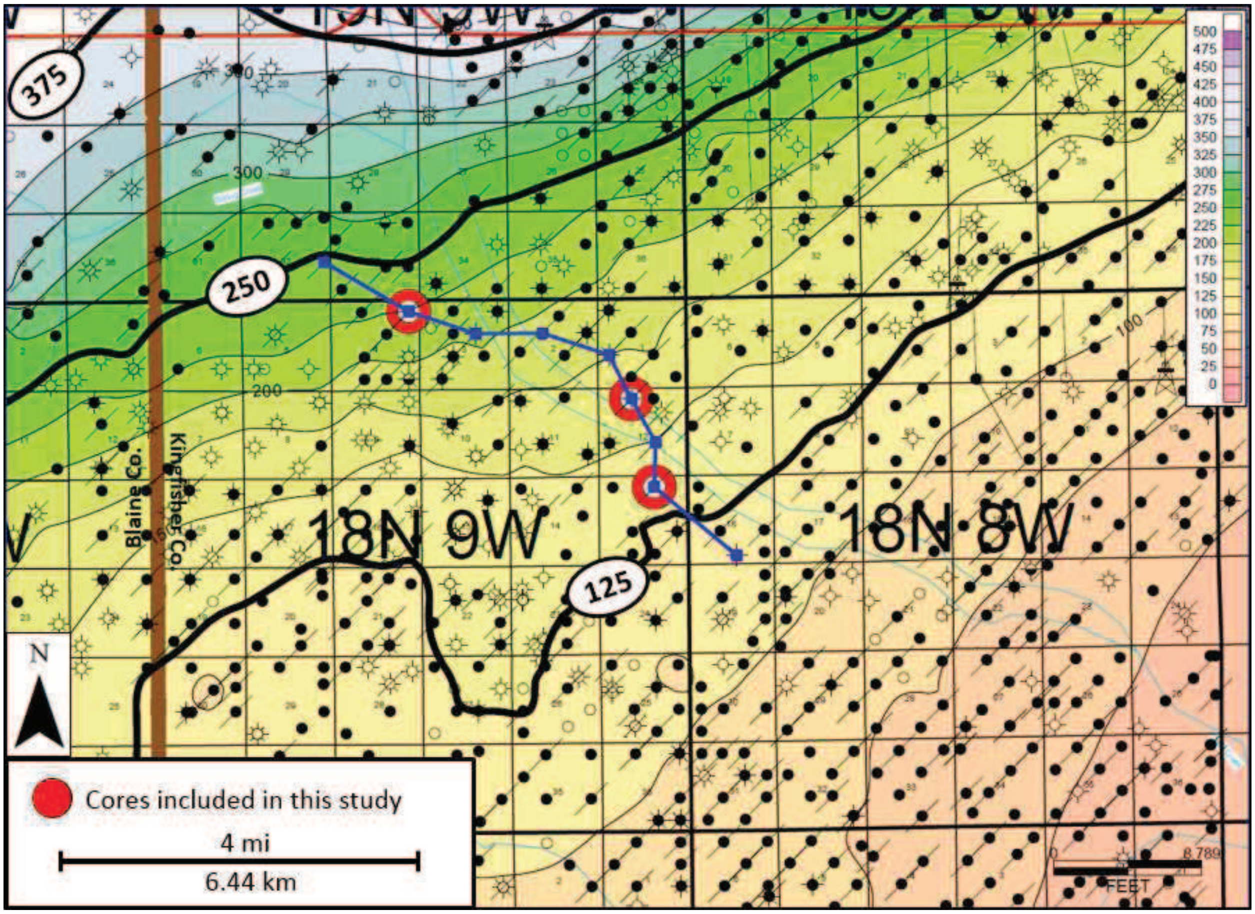

D-I-a. 3rd-Order Sequence #1 (S1) Gross Isopach. Contour interval = 25 ft. Color bar displays pink and yellow hues thinner than green and purple hues. 3 cores researched indicated by red well symbols. Cross section (Appendix D-II-b) denoted by blue lines. Note the consistent distribution parallel to depositional strike (NE-SW) with minor dip-oriented variability and thickening to the northwest, perpendicular to depositional strike.

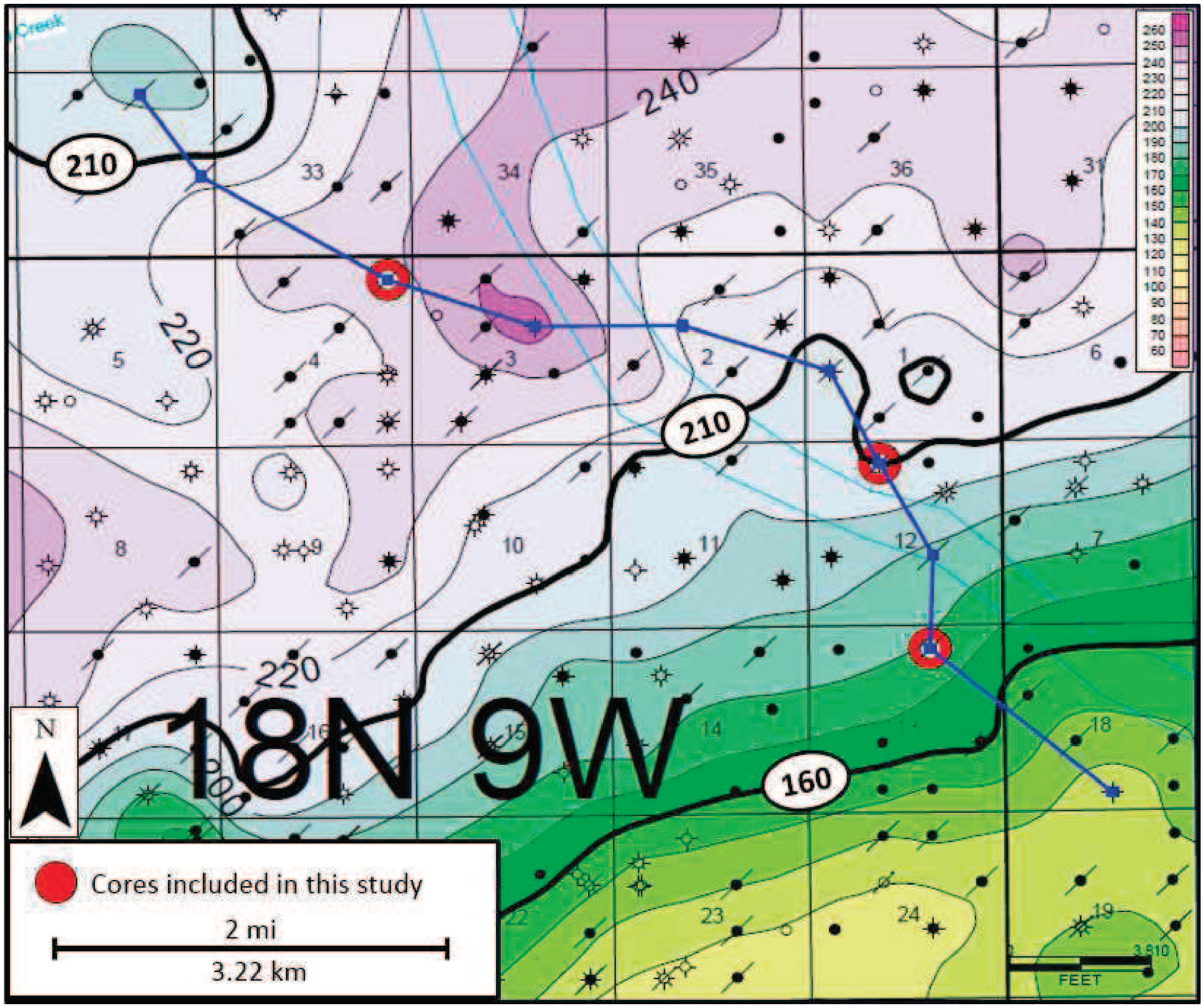

D-I-b. 3rd-Order Sequence #2 (S2) Gross Isopach. Contour interval = 10 ft. Color bar displays yellow and green hues thinner than purple hues. 3 cores researched indicated by the red well symbols. Cross section (Appendix D-II-b) denoted by blue lines. Note the distribution parallel to depositional strike (NE-SW) with minor dip-oriented variability. Also note the thinning to the northwest of the Droke Unit #1 core in Section 4 of T.18N R.9W hypothesized to be attributed to the geometrical nature of the S2 clinoform or erosion during exposure.

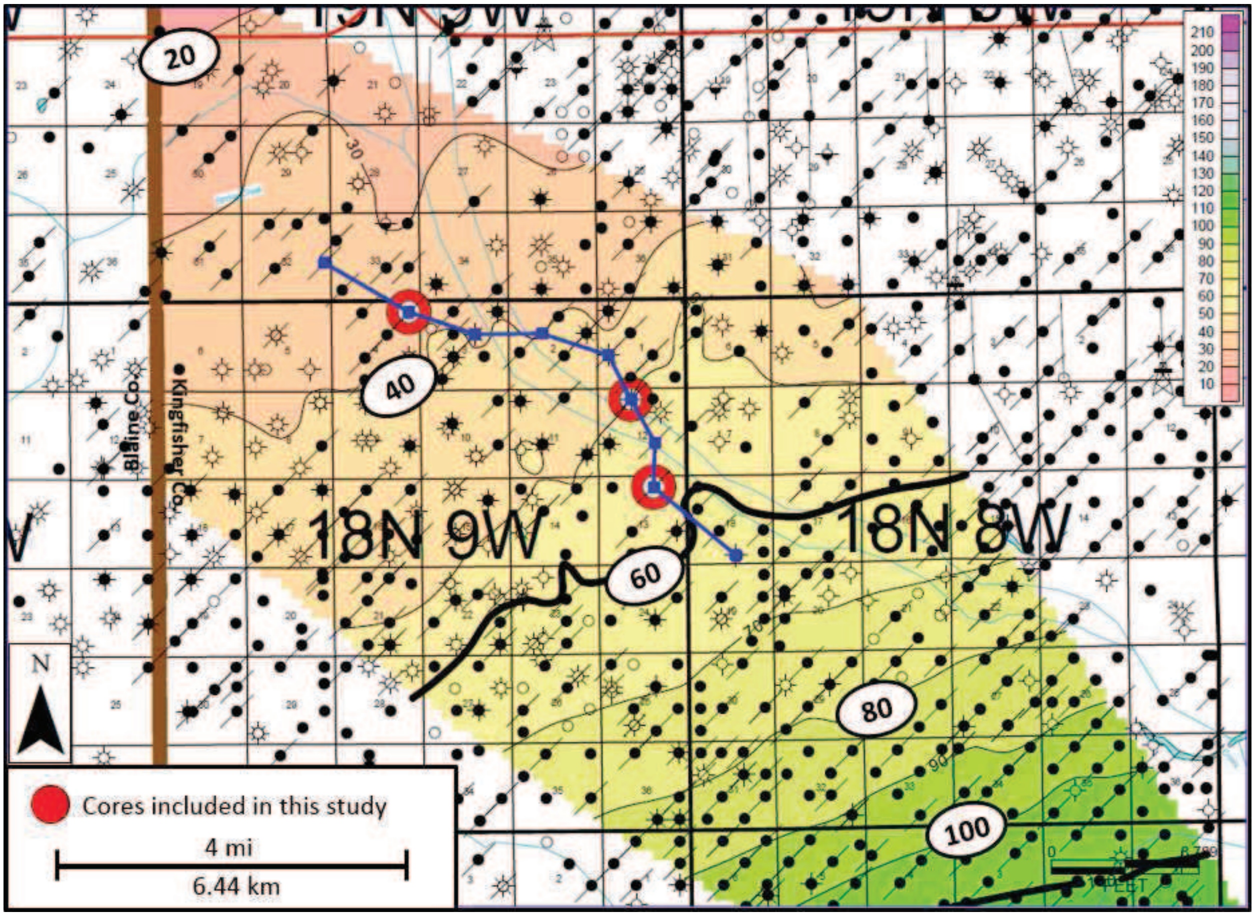

D-I-c. 3rd-Order Sequence #4 (S4) Gross Isopach. Contour interval = 10 ft. Color bar displays pink and yellow hues thinner than green hues. 3 cores researched indicated by the red well symbols. Cross section (Appendix D-II-b) denoted by blue lines. Note the distribution parallel to depositional strike (NE-SW) with minor dip-oriented variability. Also note the thickening in a basinward (SE) direction interpreted to be due to progradation of the S4 clinoform due to long-term sea level fall.

II. Reservoir Distribution

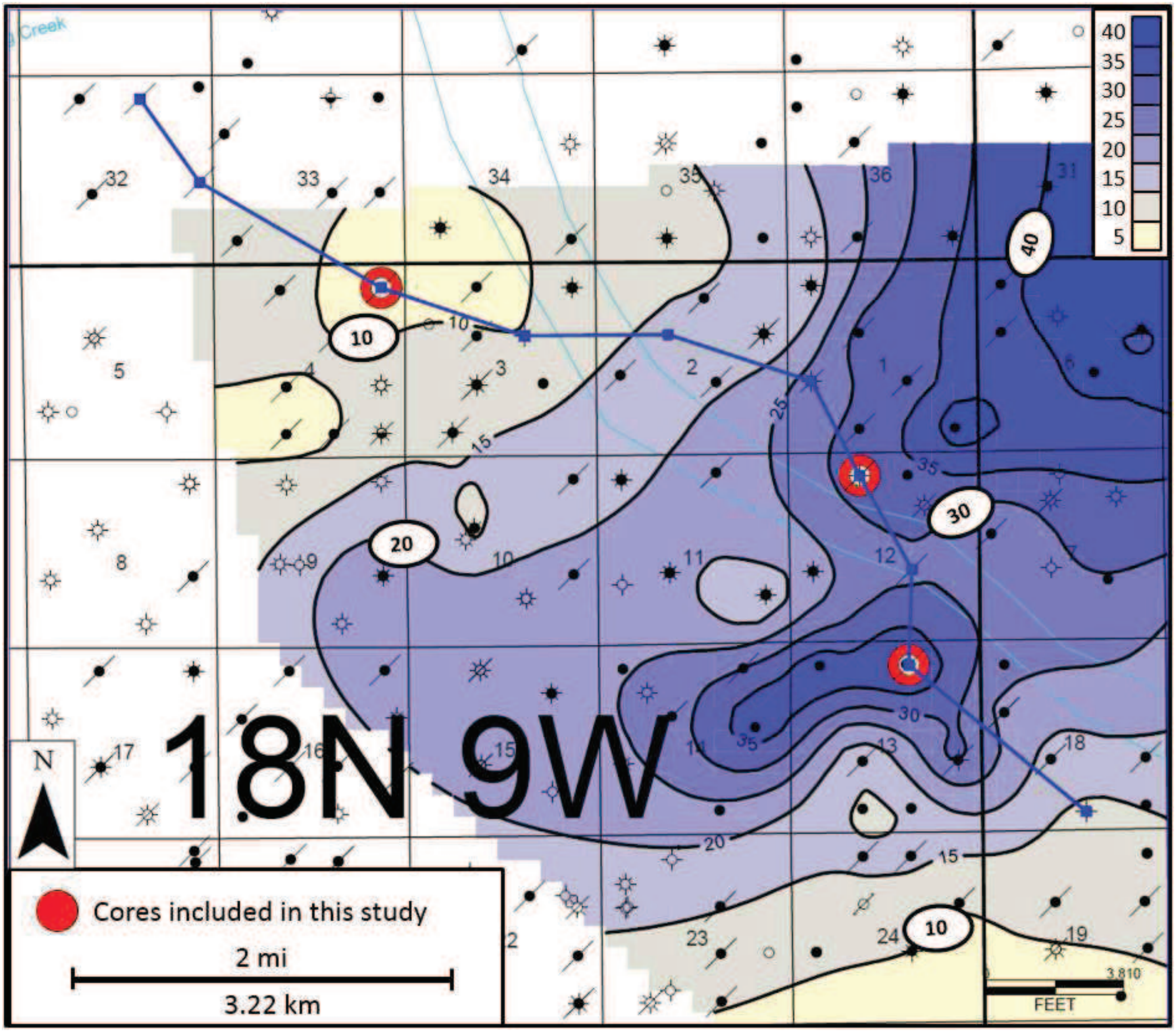

D-II-a. S2-HFS4 Gross Isopach (Chert Reservoir Distribution). Contour interval = 5 ft. (1.52 m). Color fill displays thinner units in tan and thicker units in blue. 3 cores researched indicated by the red well symbols. Cross section (Appendix D-II-b) denoted by blue lines. Note the distribution oriented perpendicular to depositional strike and thinning both to the SE and NW. Also note the lack of control to the SW due to inconsistent wireline log signatures attributed to a lateral facies change.

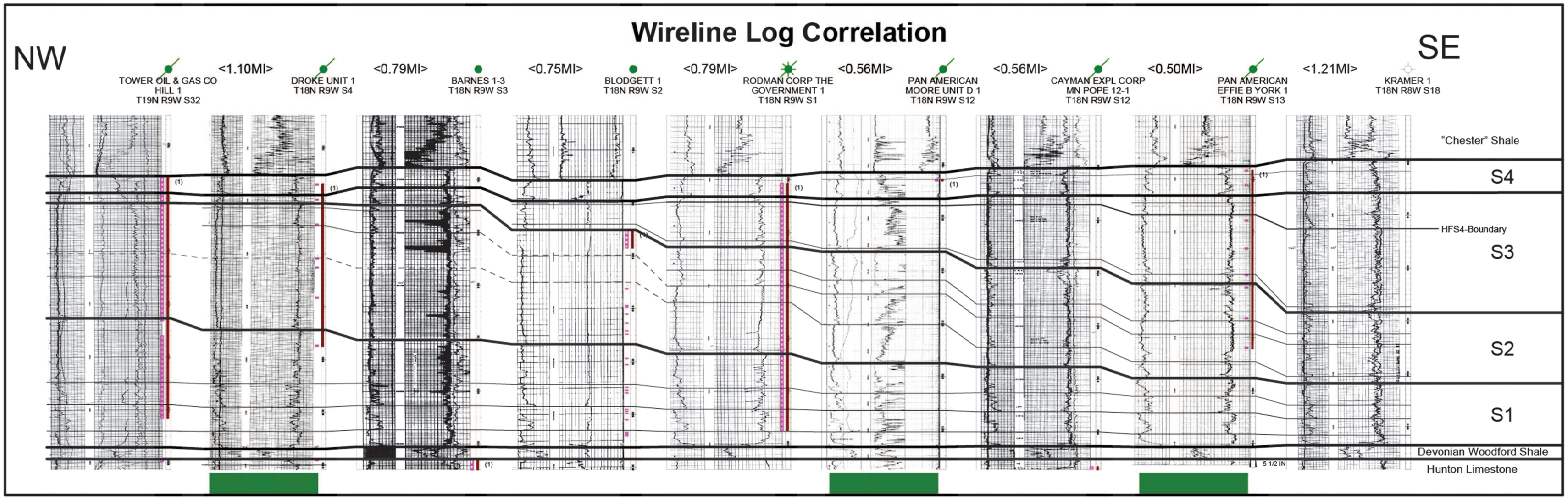

D: II. b. Subsurface Wireline Log Correlation. Cross section is oriented nearly perpendicular to depositional strike (NW-SE) through the study area (See Figure 28). Green boxes indicate researched core. Datum is the top of the Hunton Limestone/ base of the Devonian Woodford Shale. Bold Correlations indicate sequence boundaries. Thin correlations indicate variably correlative HFS and HFC boundaries. Note the high-frequency sequence boundary within S3 (S3-HFS4) corresponding to a secondary reservoir (chert) associated with an exposure horizon.

VITA

Keller Charles Flinton

Candidate for the Degree of

Master of Science

Thesis: THE EFFECTS OF HIGH-FREQUENCY CYCLICITY ON RESERVOIR CHARACTERISTICS OF THE "MISSISSIPPIAN LIMESTONE", ANADARKO BASIN, KINGFISHER COUNTY, OKLAHOMA

Major Field: Geology

Biographical:

Education:

Completed the requirements for the Master of Science in Geology at Oklahoma State University, Stillwater, Oklahoma in May, 2016.

Completed the requirements for the Bachelor of Science in Geology at Oklahoma State University, Stillwater, Oklahoma in 2012.

Experience:

Geology Intern: Strat Land Exploration, Tulsa, OK
Geology Intern: SandRidge Energy, Oklahoma City, OK
Geology Intern: Maverick Brothers Resources, Enid, OK
Associate Geologist: Permian Resources, LLC, formerly American Energy Partners, LP, Oklahoma City, OK

Professional Memberships: AAPG, OCGS